THÈSE DE DOCTORAT
D'AIX-MARSEILLE UNIVERSITÉ

Spécialité : Microbiologie

École doctorale nº062: Sciences de la vie et de la santé

réalisée

à l'Institut des Sciences Moléculaires de Marseille - Equipe BiosCiences et Adisseo

sous la direction de Josette Perrier, Michael Lafond, Estelle Devillard

présentée par

Clarisse ROBLIN

pour obtenir le grade de :

DOCTEUR D'AIX-MARSEILLE UNIVERSITÉ

Sujet de la thèse :

Les Ruminococcines C, une nouvelle famille de sactipeptides comme alternatives aux antibiotiques conventionnels

Thesis subject :

Ruminococcins C, a new family of sactipeptides as alternatives to conventional antibiotics

soutenue le 14 Septembre 2020

devant le jury composé de :

M.	Marc FONTECAVE	Président du jury
Mme	Sylvie REBUFFAT	Rapportrice
M.	Lhousseine TOUQUI	Rapporteur
M.	Patrice POLARD	Examinateur
Mme	Josette PERRIER	Directrice de thèse
Mme	Estelle DEVILLARD	Directrice de thèse
M.	Michael LAFOND	Directeur de thèse
M.	Victor DUARTE	Invité

Acknowledgements

First, I would like to express my deepest appreciation to all the jury members, Sylvie Rebuffat, Lhousseine Touqui, Marc Fontecave and Patrice Polard for accepting to read and evaluate this work and I would like to thank them in advance for their presence at the defense.

I would also like to thank my committee members, Delphine Destoumieux-Garzon and Aurélie Tasiemski for accepting to review my work along the project and for giving me their helpful insights.

I express my gratitude to the head of BiosCiences, Thierry Tron, and the head of the Institute des Sciences Moléculaires de Marseille, Jean Rodriguez, for giving me the opportunity to do research in this lab. In addition, I would like to thank Adisseo for their participation in a CIFRE convention and for financing my thesis project.

I would like to express my deepest gratitude to my thesis advisors: Estelle Devillard, Josette Perrier and Mickael Lafond. Estelle, it was always a pleasure to work with you and I learn from you skills that I wouldn't have been exposed to in a "purely academic PhD", for that I am thankful. Josette and Mickael, I am glad I joined you on this great RumC project and I am grateful for the journey we took together. It took us some time to find our pace, but once we did, I enjoyed every moment we worked together. Thank you for the trust you put in me everyday and for your support. In particular, I want to emphasize my gratitude to Mickael for his constant involvement in this project and for helping me to reach my full potential.

Through this project I had the opportunity to discover how competitive research can be and how it can sometimes be an obstacle to our field but above all this project brought to light the best that collaborative work has to offer. It is amazing to see what we can achieve when people from different backgrounds truly work together. Thus, I would like to thank our many collaborators.

First, the people from Grenoble: Victor, Hamid, Christian, Sylvie, Yohann and Steve, it was a pleasure to work with you and share this wonderful RumC project with you all these years. It was also a pleasure to travel with you, visit you in Grenoble or welcome you in Marseille and spend time together outside of the frame of work. To Steve, in particular, I am grateful, we had the opportunity to "share" a PhD, never in competition but always supporting each other's. I hope our professional paths will cross again! Victor, I am thankful you accepted to be in my jury too. You already know most of the content of this manuscript so it might be a little long to read but you might find a few surprises at the end.

Then, I would like to thank the people from IMM: Françoise, Olivier and Matthieu. Thank you for your dedication to the resolution of RumC1's structure and to Olivier,

thanks for the coffee whenever I was at the IMM microscopy platform. Speaking of the microscopy platform, I would like to address a huge thanks to Artemis and Hugo for always welcoming me, with a special mention to Hugo who, not only welcomed me at the platform, but also at the apéro at the end of the day! Many thanks to Gael too, for those long days doing flow cytometry, the great conversations during those days and for your curiosity and your interest in our project.

I also want to thank the people from Toulouse for welcoming us for our experiments. I would like to express my gratitude to Leo, Michèle and AJ for letting us use their facilities. To Nathalie, Mathieu and Patrice thank you for the warm welcome and I am glad you jumped on board and are now part of the RumC project as well. I would like to thank Patrice for his sharp insight and the interesting discussions on the project, I am sure we will have a lot more during the defense. Nathalie, we clearly have in common the love for fluorescent microscopy and it was a pleasure to spend all these hours visualizing the effects of RumC1 on bacteria with you.

Finally, I also want to thank Michel F. for his help on the project and Cédric for his reactivity.

I also want to thank all the people from the lab and former members of the lab. Marc and Hamza, it was a pleasure to work with you guys. We did not always agree on everything but at the end we improved each other's projects and my time in the lab wouldn't have been the same without you. Cendrine, it was always a pleasure to work with you as well and it was never boring, thank you for all the laughs during the hours spending at staring at the shape of pencil stains under the microscope. In addition, thank you for everything you do for this lab. Agnès, thank you for your help during those last months but above all thank you for your pleasant presence in the lab and for feeding me cakes and crepes. Thank you to Elise, Yolande, Olga, Thierry G. for their help on my project. I also want to thank Yasmina, Christophe, Katia and Marius for the interest they took in my progress and globally our project. A special thanks to Pierre for his involvement, although he was not supposed to be a member of our project he ended up being one of the person who helped me the most in the lab. Finally, thanks to all the PhD students and post-doc: Alex, Hugo, David, Julie, Maxime, Raul, Quim, Alessia, Bernadette, Rogelio, Stefani, Mike, Claudio, Robert... I am glad I got to share some parts of this experience with you. My thoughts go to Sybille, as well, I am glad I started this project with you and I wish you the best for your new MCU position.

On a more personal note, I would like to thank all my friends who have been with me all along this project and who have been supporting me. A special thanks to those who had to listen daily to my lab stories: my sisters, Lulu and Chloé, and Juju H. before them. Thanks to Juju P. (the voice of reason in the final moments), Lilice, Léon, Etienne for always being here for me. My deepest gratitude goes to Lucas, writing this thesis would have been way more painful without his help. Thanks to all my friends from Paris, Moustakhs and affiliates for the distracting week-ends and holidays. I would also like to thank "La team Marseillaise" for the weekly distraction and JP for his presence when I was writing and for the change of scenery during that period. In addition, I thank two of my friends from the US for always believing in me: Dana and Lindsey. Lindsey, may we always find a way to meet when we're travelling in each other's countries for work. Finally, I'd like to thank Lisa and Marie. Lisa, your faith in me never stops to amaze me. Marie, thank you for listening to me almost everyday.

Finally, I would like to thank my family for supporting me all these years, even though my academic cursus was not always easy to follow and was paved with a few detours. I would like to address a huge thanks to my parents for their advice whenever I was facing an obstacle during this PhD. To my brother, just thank you, for everything.

List of abbreviations

ABC	ATP-Binding Cassette
AMP	AntiMicrobial Peptide
AMU	Aix-Marseille University
ATP	Adenosine TriPhosphate
BGC	Biosynthetic Genetic Cluster
CBD	Cell wall Binding Domain
CCK	Cylic Cystine Knot
CDI	*Clostridium difficile* infection
CERN	Centre of Expertise and Research in Nutrition
CTAB	Cetyltrimethylammonium bromide
Dha	Didehydroalanine
Dhb	Didehydrobutyrine
FMT	Fecal Matter Transplant
GI	Gastro-Intestinal
GlcNAc	N-acetylglucosamine
HAI	Hopistal-Acquired infection
HIV	Human Immunodeficiency Virus
IBD	Inflammatory Bowel Disease
IMM	Mediterranean Microbiology Institute
ISM2	Institute of Molecular Sciences of Marseille
LAB	Lactic Acid Bacteria
Lan	Lanthionine
LAP	Linear Azol(in)e-containing Peptide
LC	Liquid Chromatography
LCBM	Laboratory of Metal Chemistry and Biology
LPS	LipoPolySaccharide
LTA	LipoTeiochic Acid
mAb	Mono-clonal Antibody
MBC	Minimum Bactericidal Concentration
MDR	Multi-Drug Resistant
MeLan	Methyl-Lanthionine
MIC	Minimum Inhibitory Concentration
mRNA	Messenger Ribonucleic Acid
MRSA	Methicillin-Resistant *Staphylococcus aureus*
MS	Mass Spectrometry
MS/MS	Tandem Mass Spectrometry
MurNAc	N-acetylmuramic acid

NMR	Nuclear Magnetic Resonance
NRP	NonRibosomal Peptide
NRPS	NonRibosomal Peptide Synthetase
ORF	Open Reading Frame
PBP	Penicillin-Binding Protein
PBS	Phosphate-Buffered Saline
PCAT	Peptidase-Containing ATP-binding Cassette
PDB	Protein Data Bank
PDR	Pan-Drug Resistant
PI	Propidium Iodide
PTM	Post-Translational Modification
QS	Quorum Sensing
RiPP	Ribosomally synthesized and Post-translationally modified Peptide
RIT	RadioImmunoTherapy
RRE	RiPP precursor peptide Recognition Element
rRNA	Ribosomal Ribonucleic Acid
RumA	Ruminococcin A
RumC	Ruminococcin C
Sacti	Sulfur to α Carbon Thioether
SAM	S-Adenosyl-Methionine
SCFA	Short Chain Fatty Acid
SCIFF	Six Cysteine In Forty-Five residue
SKF	Sporulation Killing Factor
SPPS	Solid-Phase Peptide Synthesis
TEM	Transmission Electron Microscopy
VAPGH	Virion-Associated PeptidoGlycan Hydrolase
VRE	Vancomycin-Resistant *Enterococcus faecalis*
WHO	World Health Organization
5'-Ado•	5-deoxyadenosyl

List of Figures

1.1 Timeline of antibiotic discovery . . . 2
1.2 Examples from each class of antibiotics . . . 6
1.3 Mechanisms of antibiotic resistance . . . 12
1.4 Timeline of clinical introduction of antibiotics and first identifications of resistant bacteria . . . 15
1.5 Main causes of deaths worldwide and estimated annual numbers . . . 17
1.6 Phage infection of bacterial cells through lytic or lysogenic cycles . . . 19
1.7 Mechanisms of peptidoglycan cleavage by phage lysins . . . 21
1.8 Roles of antibodies in bacterial infections . . . 23
1.9 Action of commensal bacteria or probiotics against pathogens in mammalian host . . . 25
1.10 Common characteristics and differences of proteinaceous substances active against microorganisms . . . 28
1.11 Biosynthesis of NRPS . . . 29

2.1 Classification of bacteriocins . . . 33
2.2 Structure of class II bacteriocins . . . 34
2.3 Structure of the bacteriolysin lysostaphin . . . 35
2.4 Sequences and disulfide networks of class IIa microcins MccV and MccL . . . 36
2.5 Structure of colicins . . . 37
2.6 RiPP biosynthesis pathway . . . 39
2.7 RRE of several RiPP maturation enzymes . . . 41
2.8 Hybrid RiPP biosynthetic pathway strategy for novel RiPPs generation . . . 42
2.9 Structure of the lanthipeptide nisin A . . . 45
2.10 Structure of the LAP plantazolicin . . . 45
2.11 Structure of the proteusin polytheonamide B . . . 47
2.12 Structure of the linaridin cypemycin . . . 47
2.13 Structure of the bottromycin A2 . . . 47
2.14 Structure of the thiopeptide thiostrepton A . . . 49
2.15 Structure of the class IIb microcin E492 . . . 49
2.16 Structure of the cyanobactin patellamide A . . . 51
2.17 Structure of the circular bacteriocin acidocin B . . . 51
2.18 Structure of the microviridin B . . . 53
2.19 Structure of the glycocin sublancin 168 . . . 53
2.20 Structure of the copper methanobactin produced by *Methylocystis* sp. LW4 53
2.21 Structure of the class I lasso peptide specialicin . . . 55
2.22 Structure of the autoinducing peptide AIP-1 . . . 55
2.23 Structure of the streptide StrA . . . 55

2.24 Structures of the amatoxin α-amanatin and the phallotoxin phalloidin . . . 57
2.25 Structure of the borosin omphalotin A . . . 57
2.26 Structure of dikaritins . . . 57
2.27 Structure of the epichloëcyclin A . . . 59
2.28 Structure of the cyclotide kalata B1 . . . 59
2.29 Structure of the orbitide pohlianin A . . . 61
2.30 Structure of the conopeptide contulakin-G . . . 61
2.31 Sequences and thioether networks of sactipeptides . . . 65
2.32 Three-dimensional structure of sactipeptides . . . 66
2.33 Biosynthetic genetic clusters of sactipeptides . . . 67
2.34 Radical SAM-based chemistry . . . 68
2.35 Radical based mechanism of thioether formation in sactipeptides . . . 69
2.36 Sactipeptide versus ranthipeptide thioether linkages . . . 73
2.37 Sequences and thioether networks of ranthipeptides . . . 74
2.38 Chemical structures of GE2270A and its analogs . . . 77

3.1 *R. gnavus* E1 . . . 81
3.2 Kinetics of elimination of *C. perfringens* CpA in rats feces after inoculation with *R. gnavus* E1 . . . 82
3.3 Sequence and putative PTMs of RumA . . . 83
3.4 Genetic regulon of RumA . . . 84
3.5 Actualized PTMs of RumA . . . 85
3.6 Expression of genes from the RumA and RumC regulons . . . 86
3.7 Regulon of RumC . . . 87
3.8 Amino acid sequences of the 5 isoforms of RumC . . . 88

4.1 Objectives, strategies and partners . . . 92

5.1 Ruminococcin C purification protocol developed by Crost et al., 2011 . . . 94

6.1 Spectra of thermal denaturation of RumC1 . . . 183
6.2 Incorporation of a fluorescent precursor of peptidoglycan . . . 184

List of Tables

1.1 Examples of generalist definitions of antibiotic and antimicrobial 5

3.1 Molecular weights (Da) of the RumC isoforms isolated from cecal contents of *R. gnavus* E1 mono-associated rats 89

Contents

Acknowledgements **i**

List of abbreviations **v**

Preamble **xiii**

1 The arms race for new antibiotics **1**
1.1 Antibiotics: from the discovery of magic bullets to the return to the Dark Ages of Medicine . . . 1
1.1.1 Antibiotics discovery . . . 1
1.1.2 Definition of antibiotic . . . 4
1.1.3 Classification of antibiotics . . . 5
1.1.4 Emergence of resistance . . . 11
1.1.5 Projections for the future . . . 15
1.2 Alternatives to conventional antibiotics . . . 18
1.2.1 Phages . . . 18
1.2.2 Phage lytic proteins . . . 21
1.2.3 Antibodies . . . 23
1.2.4 Alterations of the microbiome . . . 25
1.2.5 Bacteriocins and Antimicrobial Peptides . . . 27

2 Ribosomal proteinaceous substances as novel antimicrobial agents **31**
2.1 Bacteriocins . . . 32
2.1.1 Generalities and classification . . . 32
2.1.2 Unmodified peptides from Gram positive bacteria . . . 32
2.1.3 Proteins from Gram positive bacteria . . . 35
2.1.4 Microcins: peptides from Gram negative bacteria . . . 36
2.1.5 Colicins: proteins from Gram negative bacteria . . . 37
2.2 Ribosomally synthesized and post-translationally modified peptides (RiPPs) 38
2.2.1 Definition of RiPPs and generalities . . . 38
2.2.2 Roles of the leader peptide . . . 39
2.2.3 Classification . . . 44
2.2.4 Sactipeptides . . . 65
2.2.5 Ranthipeptides . . . 72
2.3 Current clinical application . . . 75
2.3.1 In humans . . . 76
2.3.2 In poultry . . . 78

3 RiPPs of *Ruminococcus gnavus* E1 **81**
3.1 *Ruminococcus gnavus* E1 vs. *Clostridium perfringens* 81
3.2 Ruminococcin A 82
3.3 Ruminococcins C 86

4 Thesis objectives **91**

5 Ruminococcin C, a promising antibiotic produced by a human gut symbiont **93**
5.1 Context 93
5.2 Published paper 94
5.3 Summary and comments 122

6 The unusual structure of Ruminococcin C1 antimicrobial peptide confers clinical properties **127**
6.1 Context 127
6.2 Accepted paper 128
6.3 Summary and comments 181

7 Ruminococcin C1, a multifunctional antibacterial sactipeptide **185**
7.1 Context 185
7.2 Publication in preparation 186
7.3 Summary and comments 216

8 Mechanism of antibacterial action of Ruminococcin C1 **219**
8.1 Context 219
8.2 Preliminary data 219
8.3 Material and Methods 234
8.4 Summary and comments 236

9 General conclusion and perspectives **239**

References **243**

Appendix 1: Book soon to be published **263**

Appendix 2: Patent FR 19 01896 - Fungal cyclic peptides as antibacterial agents active against *Clostridium perfringens* **267**

Preamble

One of the major concerns in Public Health nowadays is antibiotic resistant bacteria, it has been estimated that millions of people will perish from infections caused by multi-drug resistant (MDR) bacteria in the decades to come. Each time a new class of antibiotics has been introduced to the clinic, the bacterial populations with an intrinsic or acquired resistance mechanism have an advantage for survival, leading to the emergence of an increasing number of resistant bacteria and to their spreading. Moreover, only two new classes of antibiotics have been discovered since the 1960s. Therefore, it is essential and urgent to find new antibiotics. Most antibiotics currently used in the clinic were isolated from soil microorganisms or are chemical derivatives of these natural products. Lately lots of researchers have shown the major role of the gut microbiome and taught us about its high diversity. The human body carries more microorganism cells than human cells and the abnormal regulation, or dysbiosis, of the gut microbiome can be linked to any type of diseases from inflammatory bowel disease (IBD) to depressive behaviors. Therefore the gut microbiome is a potential treasure trove of new natural drugs including antibiotics. However, because of its high complexity and because of the difficulties to culture most of the related species in laboratory conditions, it remains under-explored.

Previous work showed that one of the dominant members of the human gut microbiome, *Ruminococcus gnavus* is able to produce such antibacterial molecules. *R. gnavus* is a Gram positive bacterium, strictly anaerobic, present in the digestive tract of 90% healthy human adults. The strain E1 that was isolated from the feces of a healthy adult produces active antibacterial molecules against *Clostridium perfringens*. *C. perfringens* is Gram positive bacterium, anaerobic and ubiquitous. In humans, it is an opportunistic pathogen responsible for food-borne gastro-intestinal infections, whereas in animals it is one of the main pathogens affecting poultry resulting in an estimated economic loss of 6 billions dollars per year worldwide. The antibacterial substances produced by *R. gnavus* E1 are Ribosomally synthesised and Post-translationally modified Peptides (RiPPs), a promising category of bio-active peptides. Although nisin, one of this antibacterial RiPPs, was discovered the same year as penicillin, and hundreds of RiPPs have been identified since then, no RiPPs have been introduced to the clinic yet.

The aim of my thesis project was to purify and characterize the Ruminococcins C (RumCs), which are antibacterial peptides belonging to the RiPPs family produced by *R. gnavus* E1. Moreover, my project was also aiming at demonstrating the therapeutic potential of RumCs to fight infections caused by *C. perfringens* but also by other pathogens of relevance for human or animal health and especially MDR bacteria. My work was part of the French National Research Agency (ANR) project RUMBA 2016-2020 ANR-15-CE21-0020 and was carried out in partnership between the Institute of Molecular Sciences of Marseille (ISM2) at Aix-Marseille University (AMU) and the Centre of Expertise and Research in Nutrition (CERN) of Adisseo (Industrial Agreement of

Training through Research CIFRE-2016/0657).

This thesis manuscript is presenting bibliographic research divided in three chapters: one demonstrating in further details the need for new antibiotics and where will they come from; the second one focusing on peptides and in particular RiPPs as alternatives to conventional antibiotics; and the last one introducing the different types of RiPPs produced by *R. gnavus* E1. The fourth chapter is a descriptive list of the objectives of my project. Then, the results accumulated during my thesis are presented in three chapters based on scientific publications respectively published, accepted or to be shortly submitted in high ranking journals. The first publication displays the production and purification of RumC, its attribution to the RiPPs classification thanks to a structural characterization, its complex maturation process and finally preliminary data on the biological activity and safety. The second one exposes the solved three-dimensional structure of RumC which was undescribed in RiPPs so far and explores deeper the therapeutic potential of RumC as well as its mode of action. The third publication, in preparation, presents the efficacy of RumC as an alternative to antibiotics to rescue an animal model from a lethal infection but also a scope of other possible clinical applications of RumC based on its biological activities on both prokaryotic and eukaryotic cells. Finally, a fourth chapter of results includes preliminary data on the antibacterial mechanism of action of RumC that will be further studied in the near future and that are expected to be published as well.

Chapter 1

The arms race for new antibiotics

1.1 Antibiotics: from the discovery of magic bullets to the return to the Dark Ages of Medicine

1.1.1 Antibiotics discovery

At the beginning of the XXth century, Paul Ehlrich noticed that some synthetic dyes such as aniline selectively stained some bacteria while other bacteria remained free of dye. This observation led to one of the most common and applied tool in microbiology: the Gram staining technique. Though above all, this observation contributed to another major scientific breakthrough: it made Ehlrich conceptualized the idea of antibiotics. He hypothesized that infectious diseases caused by bacteria could be treated if "*substances have been discovered which have an exclusive affinity for these bacteria and act deleteriously or lethally on these alone, while at the same time they possess no affinity for the normal constituents of the body and can therefore have the least harmful, or other, effect on that body. Such substances would then be able to exert their full action exclusively on the parasite harboured within the organism and would represent, so to speak, magic bullets, which seek their target of their own accord*". Therefore, in 1904, Ehlrich started a massive synthesis and screening program to find such "magic bullets". He synthesized hundreds of organoarsenic compounds and assayed their efficacy to cure rabbits suffering from Syphilis caused by infection by the *Treponema pallidum* bacterium. In 1909, Ehlrich found that the 6th molecules of the 600e serie was able to cure the infected rabbits. This molecule was then commercialized as Salvarsan and was clinically used as soon as in 1910 (Aminov, 2010; Zanders, 2015). Ehlrich's approach was then widely used by the pharmaceutical industry to discover new antibiotics. Mass synthesis and screening of chemical drugs was launched as well as attempts to translate the drugs in a clinical context. In 1932, the chemists Joseph Klarer and Fritz Mietzch achieved the synthesis of a new antibiotic: sulfonamidochrysoidine also named Prontosil. Further studies revealed that sulfonamidochrysoidine was actually the precursor of sulfanilamide, the active molecule. Chemical derivatives of sulfanilamide were then synthesized and screened for the antibacterial activity, giving birth to the sulfonamides class of antibiotics (**Figure 1.1**) (Aminov, 2010).

A few years earlier in 1928, Alexander Fleming observed an area of growth inhibition on a plate inoculated with a *Staphylococcus* strain where another organism had contaminated the plate and grown. This organism was identified as the fungus *Penicillium notatum* and was shown to produce in liquid or jellified cultures an active substance against Staphylococci. Whereas Ehlrich showed that "magic bullets" able to cure bacterial infections

could be chemically synthesized, Fleming found that such "magic bullets" also already existed in nature and could be isolated from living organisms. Howard Florey and Ernest Chain begun to develop in 1940 a purification protocol of this substance from cultures of *P. notatum*, later named penicillin. A few years later in 1945, mass production and commercialization of penicillin started. To sum up, thanks to Ehlrich and Fleming's discoveries, an era of mass screening of chemical or natural products begun to find molecules able to inhibit the growth of bacteria or to kill them (Aminov, 2010; Lewis, 2013; Singh et al., 2017).

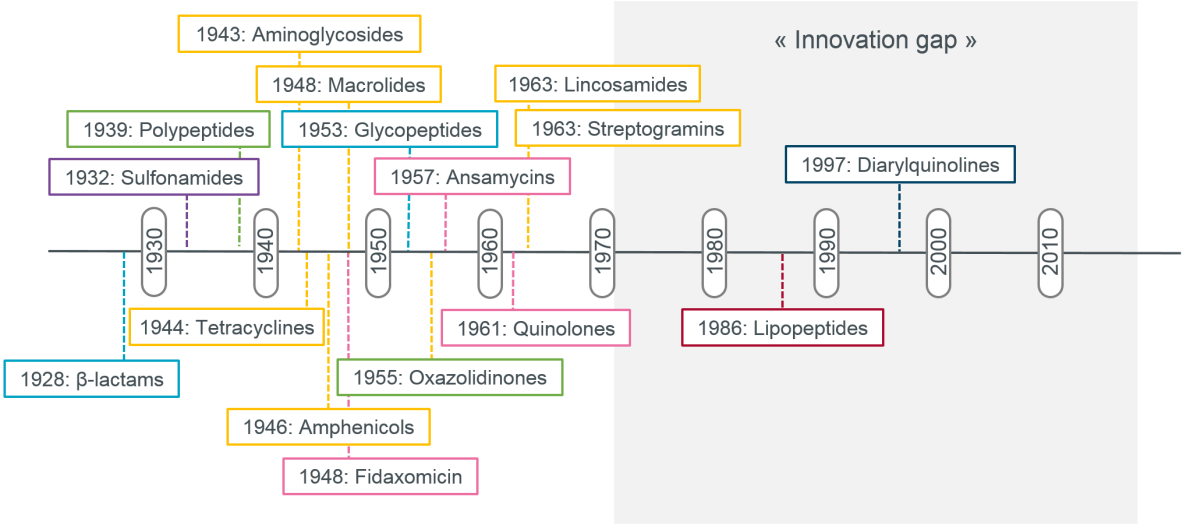

Figure 1.1: Timeline of antibiotic discovery

Colors indicate the main pathways inhibited by the different classes of antibiotics: clear blue=cell wall synthesis; purple=folate metabolism; yellow=protein translation; pink=nucleic acids replication; red=membrane polarization; dark blue=ATP synthesis; green=various.

Most antibiotics used still nowadays were discovered between 1940 and 1970 during the "Golden Age" of antibiotic discovery (**Figure 1.1**), first thanks to the screening of natural molecules. Scientists started to look for microbes producing antibiotics from soil samples coming from all over the world with the help of Christian missionaries bringing back samples from their travels (Gould, 2016). In 1939, René Dubos had the idea to incubate soil on a mixture of pathogenic bacteria including Staphylococci, Pneumococci and hemolytic Streptococci. From this soil sample, he isolated a strain of *Brevibacillus brevis* (formerly known as *Bacillus brevis*) producing a mixture of polypeptides able to kill Gram positive bacteria. Analysis of this mixture, named thyrothricin, revealed that it was composed of a cyclic decapeptide (tyrocidine) and a linear pentadecapeptide (gramicidin). Because of its hemolytic effect, thyrothricin wasn't commercialized as a systemic antibiotic but was still one of the first antibiotic commercialized and was widely used for topic applications (Van Epps, 2006). In the 1940s, the microbiologist Selman Waksman worked on the elaboration of a systematic protocol for antibiotic discovery from soil samples. Basically, isolated soil-derived microorganisms were cultured in overlay plates of different target bacteria and selected upon their ability to inhibit the growth of the targets. The soil microbes producing active substances were then produced in liquid cul-

tures in several media and filtrates were collected from each cultures. The antibacterial activity of these filtrates were then assayed against a panel of target bacteria typically including *Escherichia coli*, *Bacillus subtilis* and *Staphylococcus aureus*. This systematic protocol for antibiotic discovery led to the discovery of streptomycin in 1943 (Schatz et al., 1944; Lewis, 2013). Streptomycin was the first antibiotic identified as effective for the treatment of tuberculosis and was the first member of a new chemical class of antibiotics: the aminoglycosides.

This platform for antibiotic discovery developed by Waksman was used by the pharmaceutical industry between the 1940s and the 1960s leading to the identification of many new classes of antibiotics such as tetracyclines (e.g. chlortetracycline), amphenicols (e.g. chloramphenicol), macrolides (e.g. erythromycin), glycopeptides (e.g. vancomycin), fidaxomicin, oxazolidinones (e.g. cycloserine), ansamycins (e.g. rifampicin), streptogramins (e.g. streptogramin B), lincosamides (e.g. lincomycin). However soil microorganisms were not an unlimited source of new antibiotics and after about 20 years of screening, the "Waksman platform" stopped being efficient as only already known compounds could be identified. Only one novel class of natural antibiotics was found after the 1960s: the lipopeptides (e.g. daptomycin) (Lewis, 2013; Aminov, 2017).

To override this lack of new natural products, scientist started to design semi-synthetic molecules by modifying the known natural molecules using enzymes or chemical techniques, leading to the expansion of the above-mentioned class of antibiotics. Moreover, scientists in the pharmaceutical industry implemented a new platform for antibiotic discovery from synthetic molecules. The idea was to identify the essential proteins for bacterial growth and survival by detecting the most conserved proteins throughout species thanks to the development of genomics tools and then to design rational drugs that would inhibit these targets. However this platform failed to yield new antibiotics. Although inhibitors of the protein targets were identified in vitro, they were not necessarily able to cross the bacterial membrane in vivo or had a toxic activity toward host cells as well (Lewis, 2013). Except for the sulfonamides, only two other classes of antibiotics came from a synthetic origin. In the late 1950s the pharmaceutical company Sterling Drug was studying the by-products of the synthesis of chloroquine, an antimalarial drug. In that context, George Lesher isolated 7-chloro-1-ethyl-1,4-dihydro-4-oxo-3-quinolinecarboxylic acid, a molecule that showed antibacterial activity. The latter was used as a scaffold for the design of analogs with improved activity and led to the discovery in 1962 of nalidixic acid, the first antibiotic of the quinolones family (Bisacchi, 2015). Years later, in the 1990s, diarylquinolines were discovered through the screening program of two pharmaceutical companies, Janssen Pharmaceutica NV and TiboTech, of drugs active against *Mycobacterium tuberculosis*. Unfortunately, the company didn't release information about the rational of the types of molecules that were screened, although they released the information than 70 000 compounds were screened in that program for their activity against *Mycobacterium smegmatis*, a non pathogenic specie of *Mycobacterium*. This screening revealed 23 clusters of active molecules that were tested for potential uses as antibiotics. Finally, one molecule, bedaquiline, was retained for clinical trials and is currently used for the treatment of tuberculosis (Guillemont et al., 2011; Barry, 2011). After the "Golden era" where many antibiotics were discovered in a few decades, despite the efforts to screen microorganisms first and then synthetic molecules, the research for new antibiotics reached an "innovation gap".

1.1.2 Definition of antibiotic

Selman Waksman who isolated streptomycin and developed the platform for antibiotic discovery from soil microbes, wrote a paper called "What is an Antibiotic or Antibiotic substance?" in 1947 and proposed a definition of the word antibiotic as: "*a chemical substance, produced by microorganisms, which has the capacity to inhibit the growth of and even to destroy bacteria and other microorganisms*. He also specified that "*the action of an antibiotic against microorganisms is selective in nature* [...] *each antibiotic is thus characterized by a specific antimicrobial spectrum. The selective action of an antibiotic is also manifested against microbial vs. host cells*" (Waksman, 1947). Therefore Waksman included in his definition of antibiotic the notion of selectivity that Ehlrich discovered while studying synthetic dyes, however he left out of his definition the synthetic molecules active against bacteria like salvasaran that was synthesized by Ehlrich and is nowadays considered as the first commercialized antibiotic.

Since Waksman published a definition of antibiotic in 1947 many scientists have been trying to improve it. In 2003, Bentley and Bennett carried on Waksman's work by publishing a paper entitled "What is an antibiotic? Revisited" (Bentley & Bennett, 2003). They compared dozens of definitions proposed since 1947. They noticed that many definitions in scientific papers still limit antibiotics to natural products even though most scientists and physicians consider as antibiotics both natural and synthetic products. Similarly, there is no consensus about the origin of molecules (natural or synthetic) that are considered as antibiotics in the definitions from generalists sources such as dictionaries or official and regulatory organisms like the World Health Organization (WHO) or the European Parliament (Table 1.1). Many of the latest definitions collected in Bentley and Bennett's paper narrow down the activity of antibiotics to antibacterial activity whereas Waksman's definition considered natural molecules able to inhibit the growth or kill any type of microorganisms. Therefore, most recent definitions distinguish antibiotics which exhibit activity restricted toward bacteria from antimicrobial molecules which are active against one or multiple types of microorganisms including bacteria but also fungi, parasites and viruses. Likewise, in generalist definitions, there is a distinction between antibiotic and antimicrobial (Table 1.1.). Most of the scientific definitions mention "selective toxicity" which is the concept that the molecule considered as an antibiotic inhibits the growth or kill the infecting organisms without deleterious effects for the host cells, while that concept is totally left out of the generalist definitions. Based on all these considerations we will consider the following criteria to define an antibiotic for the rest of this expose:

- A natural or synthetic molecule;
- Inhibiting the growth of bacteria or killing them;
- With selective toxicity towards bacteria vs. host cells.

An antimicrobial is defined with the same criteria but the spectrum of action extends to any type of microorganisms including viruses, fungi or parasites.

Table 1.1: Examples of generalist definitions of antibiotic and antimicrobial

Source	Antibiotic	Antimicrobial
Larousse Dictionary	"Substance, natural or synthetic, used against infections caused by bacteria"	"Which fights microbes"
World Health Organization	"Medicines used to prevent and treat bacterial infections"	Includes "antibiotics, antifungals, antivirals, antimalarials, and anthelmintics"
Regulation (EC) No 1831/2003 of the European Parliament	"Antimicrobials produced by, or derived from, a microorganism, which destroys or inhibits the growth of other microorganisms"	"Substances produced either synthetically or naturally, used to kill or inhibit the growth of microorganisms, including bacteria, viruses or fungi, or of parasites"

1.1.3 Classification of antibiotics

Antibiotics are classified based on their chemical structures, alternatively they can also be clustered based on their mode of action (**Figure 1.1**). Additionally, antibiotics can be characterized by their impacts on bacteria: they can be bacteriostatic, meaning they inhibit the growth and multiplication of bacteria, or they can be bactericidal and cause cell death. Here, antibiotics that have been introduced to the clinic are presented based on their chemical structures (**Figure 1.2**).

1. β-Lactams: β-Lactam was the first class of antibiotic to be identified with the discovery of penicillin. Currently four sub-classes belong to β-lactams antibiotics: penicillin, carbapenem, cephalosporin and monobactam. They all contain a β-lactam ring. Except for the monobactams, they harbor a second ring fused to the β-lactam ring. Cephalosporins have a 6-membered second ring carrying a sulfur atom whereas penicillins and carbapenems have a 5-membered second ring. The presence of a sulfur atom on the 5-membered second ring discriminates penicillins from carbapenems. β-Lactams are broad-spectrum bactericidal antibiotics inhibiting cell wall synthesis by binding to the penicillin-binding proteins (PBPs), a family of enzymes involved in the synthesis, maturation and recycling of peptidoglycan. Syntheses of derivatives of natural β-lactam molecules have allowed this family to expand to over 100 molecules (Singh et al., 2017).

2. Sulfonamides: Sulfonamides belong to one of the few classes of antibiotics originated from chemical synthesis. They are synthesized by replacing the hydroxyl group of sulfonic acid with an amino group. Sulfonamides are composed of the functional group R-SO_2-NH_2 in which R is either an alkyl, aryl or hetero aryl moiety. In particular antibacterial sulfonamides are composed of the sulfonamide group (SO_2-NH_2) and an amino group in the *para* position of a benzene ring. The free amino group is essential for antibacterial activity. They can carry additional hydrogen, alkyl, aryl or hetero aryl groups on the sulfonamide group. Sulfonamides have a broad spectrum of activity and a bacteriostatic effect coming from the inhibition of folic acid synthesis. Specifically they prevent the first step of folic acid synthesis which is the

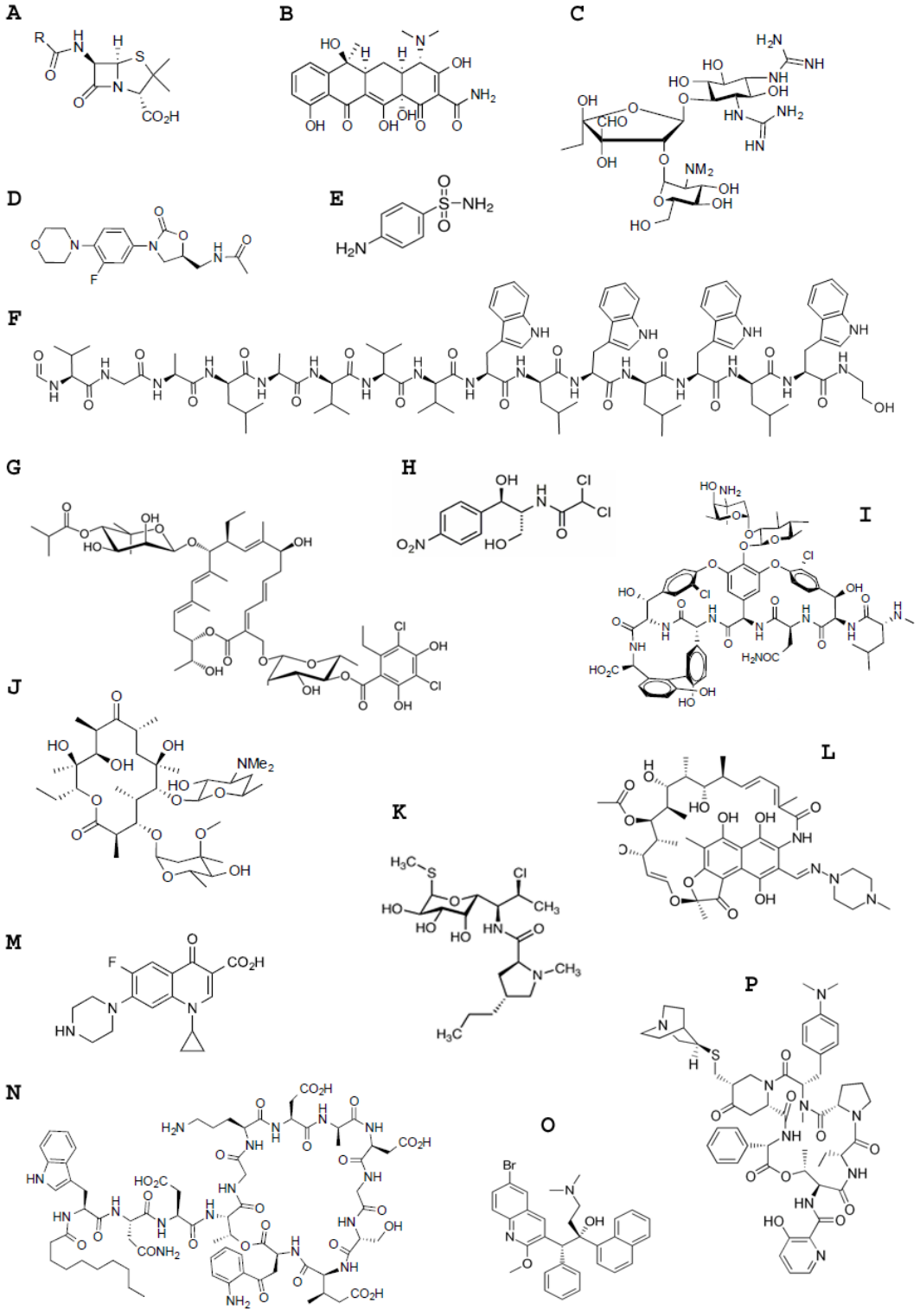

Figure 1.2: Examples from each class of antibiotics

A=Penicillin (β-lactam), B=Tetracycline (Tetracycline), C=Streptomycin (Aminoglycoside), D=Linezolid (Oxazolidinone), E=Sulfanilamide (Sulfonamide), F=Gramicidin A (Polypeptide), G=Fidaxomicin, H=Chloramphenicol (Amphenicol), I=Vancomycin (Glycopeptide), J=Erythromycin (Macrolide), K=Clindamycin (Lincosamide), L=Rifampicin (Ansamycin), M=Ciprofloxacin (Quinolone), N=Daptomycin (Lipopetide), O=Bedaquiline (Diarylquinoline), P=Quinupristin (Streptogramin)

formation of dihydropteroate obtained by the reaction of *p*-aminobenzoic acid and dihydropteroate pyrophosphate in the presence of the enzyme dihydropteroate synthase. Sulfonamides are competitive antagonists of *p*-aminobenzoic acid, thus the dihydropteroate synthase binds to sulfonamides preventing the formation of dihydropteroate. Folic acid is essential for the synthesis of purine and pyrimidine bases among others and therefore for DNA synthesis (Sonu et al., 2017; Fernández-Villa et al., 2019).

3. Aminoglycosides: The common chemical structure of aminoglycosides is composed of amino-sugars linked by glycosidic bonds to an aminocyclitol. Aminoglycosides differ by the nature of their aminocyclitol component. Moreover, different amino or hydroxyl groups on their core structure impact the antibacterial potency. Therefore derivatives of natural molecules have been designed by addition or modification of functional groups by chemical or enzymatic synthesis. Aminoglycosides are broad spectrum bactericidal antibiotics that inhibit protein synthesis by binding to the A-site of the 16S rRNA of the 30S ribosome subunit, resulting in either elongation blockage or mistranslation (Krause et al., 2016).

4. Tetracyclines: Tetracyclines have a backbone of 4 hydrocarbon rings with different functional groups like alkyl, hydroxyl and amine on the lower and upper part of the rings. Modification or addition of functional groups led to the expansion of this class of antibiotics originally identified from natural products. While some functional groups can be modified without loosing a specific biological activity, some others are essential. For example the dimethylamine group on the carbon at position 4 (C4) is essential for antibacterial activity whereas tetracycline lacking this group can have an antifungal or an antitumor effect. Like aminoglycosides, tetracycline have a broad spectrum and inhibit protein synthesis by binding to the 30S ribosome subunit. However, their mechanisms of action is different: they prevent the binding of the aminoacyl-tRNA to the ribosome-mRNA complex. They have a bacteriostatic effect most likely because their interactions with ribosomes are reversible (Tariq et al., 2018; Chopra & Roberts, 2001).

5. Macrolides: Macrolides are characterized by the presence of a macrocyclic lactone ring. The size of the ring varies between 12-, 14-, 15- or 16-membered ring. Additionally, most macrolides contained amino sugars or sugars linked to the macrocyclic lactone ring by glycosolic bonds. Semi-synthetic derivatives of natural macrolides were designed to improve their poor bioavaibility. They have a broad-spectrum bacteriostatic activity against Gram positive bacteria but limited activity against Gram negative bacteria. They inhibit protein synthesis by binding reversibly to the nascent peptide exit tunnel (Site E) on the 23S rRNA of the 50S ribosomal subunit and prevent peptide chain elongation (Dinos, 2017).

6. Polypeptides: Polypeptides regroup linear and cyclic nonribosomal peptides (NRPs) meaning peptides that are produced in a RNA independent manner by specific NRP synthetases (NRPSs). These peptides vary in length, amino acid composition, structure and mechanism of action. The first polypeptides identified were tyrocidine and Gramicidin D. Tyrocidin is a cyclic β-sheet decapeptide acting as a membrane lysin active on both Gram positive and negative bacteria whereas Gramicidin D in only active against Gram positive bacteria. Gramicidin D is actually a mix of Gramicidin A, B and C. Gramicidin A, B and C are pentadecapeptides differing

only at their 11th amino acid residue (respectively a tryptophan, phenylalanine, or tyrosine). The amino acids alternate D- and L-configurations which mediates the formation of a β-helix structure. Gramicidins can be homodimeric and form a head to head single stranded helical structure or heterodimeric with a double stranded β-helical structure. Unlike tyrocidine and Gramidicin S, another polypeptide similar to tyrocidine, Gramicidin G acts by binding to bacterial membrane causing ions loss and hence loss of membrane potential, inhibition of the respiratory chain and macromolecule synthesis, decrease in ATP and eventually cell death. Polymyxin and bacitracin are other notorious examples of polypeptides. Due to their hemolytic activity most polypeptide antibiotics are restricted to topical use (Aminov, 2017; Wenzel et al., 2018; Pavithrra & Rajasekaran, 2020).

7. Amphenicols: The first amphenicol to be discovered was chloramphenicol, it is composed of a *p*-nitrobenzene ring linked to a dichloroacetyl moiety through a 2-amino-1,3-propanediol group. Only the *D-threo* isomer has antibacterial activity. Modifications of any moiety of chloramphenicol has been attempted to generate derivatives with antibacterial activity and fewer toxicity for host cells. The first strategy was to replace the nitro group of the *p*-nitrobenzene ring with other functional groups or to modify the entire ring. The only clinically approved antibiotic yielded from that strategy is thiamphenicol which has a methyl sulfone instead of the nitro group. A few derivatives were also synthesized from substitutions in the 2-amino-1,3-propanediol moiety. However every attempted modifications of the dichloroacetyl moiety resulted in loss of bactericidal activity, showing the crucial role of this group. Amphenicols have a broad-spectrum and bacteriostatic activity and such as macrolides they inhibit protein elongation. Amphenicols bind to the 23S rRNA of the 50S ribosomal unit inhibiting the peptidyltransferase activity and thus preventing the peptide bond formation (Dinos et al., 2016).

8. Oxazolidinones: The common chemical features of oxazolidinones include a 5-member heterocyclic ring composed of a carbon carrying a ketone group, a nitrogen and an oxygen atom. Oxazolidinones can be separated in two main groups: natural products such as D-cycloserine and synthetic molecules such as linezolid. D-cycloserine also contains a carbon with a amino group in the heterocyclic ring. Synthetic oxazolidinones were discovered 20 years after the identification of D-cycloserine and were not derived from this natural product. These synthetic molecules have their carbon with a ketone group located between the nitrogen and oxygen atoms. D-cycloserine inhibits cell wall synthesis and in particular the two sequential enzymes alanine (Ala) racemase and D-Ala:D-Ala ligase that synthesize the D-Ala dipeptide essential for transpeptidation of the peptidoglycan (Prosser & de Carvalho, 2013; Batson et al., 2017). Synthetic oxazolidinones have a different mode of action and inhibit protein synthesis by preventing the formation of the 70S initiation complex by binding to the 23S rRNA of the 50S ribosome subunit. D-cycloserine has a broad-spectrum activity whereas synthetic oxazolidinones have limited activity toward Gram negative bacteria. They both have a bacteriostatic effect (Bozdogan & Appelbaum, 2004; Pandit et al., 2012).

9. Fidaxomicin: Fidaxomicin is a class of antibiotic constituted so far by only one member related to macrolides. It is composed of a 18-membered macrocyclic lactone ring with a 7-carbon sugar moiety at carbon 12 and a 6-deoxy sugar group at carbon

21. Fidaxomicin has a bactericidal activity with a very narrow-spectrum composed only of Gram positive anaerobes. This antibiotic inhibits transcription initiation by binding to the DNA-RNA polymerase complex and preventing the opening of the DNA strands (Zhanel et al., 2015).

10. Glycopeptides: Glycopeptides are NRPs like polypeptides. They are highly modified heptapeptides. Two natural glycopeptides are currently used in the clinic: vancomycin and teicoplanin. Their amino acid residues are subjected to oxidative cross-linking and carry different types of moieities, such as sugars residues, lipid chains and chlorine atoms. Screening of natural products or metagenomic analysis based on the NRPSs sequences of vancomycin and teicoplanin revealed that lots of other natural glycopeptides could be developed as antibiotics and potentially undergo many more modifications including halogenation, methylation, sulfation and sugar acylation. Derivatives of glycopeptides have been synthesized and so far three reached the clinic. For example, dalbavancin was obtained by addition of a lipophilic side chain and an amidated carboxyl side group on teicoplanin. Glycopeptides are active against Gram positive bacteria with a bactericidal activity. They bind to the D-Ala-D-Ala terminus of the pentapeptide of the peptidoglycan preventing its transpeptidation and therefore inhibiting cell wall synthesis and remodelling (Binda et al., 2014; Zeng et al., 2016).

11. Ansamycins: Ansamycins are divided in two groups: they can be either composed by a naphtalenic or benzoic chromophore ring and a aliphatic polyketide chain linking both sides of the ring, named "ansa" chain because of it resemblance with the grip of a basket. Rifamycin was the first natural antibacterial ansamycin discovered. Most semi-synthetic derivatives were generated by modifying the functional group of the 3rd carbon (C3) of the naphtalenic ring of rifamycin. Ansamycins inhibit transcription by binding to RNA polymerase and have a bactericidal action against Gram positive and negative bacteria (Wehrli, 1977; Watanabe et al., 2003; Floss & Yu, 2005).

12. Lincosamides: The common chemical feature of lincosamides is a amino acid residue linked to a sugar moiety. The first lincosamide identified was lincomycin which is composed of the non proteogenic propylhygric amino acid associated by a peptide bond to the sugar 6-amino-6,8-dideoxy-1-thio-D erythro-α-D-galactopyranoside. Other natural lincosamides such as celesticetins or desalicetin have been isolated and many chemical derivatives have been synthesized. So far, the only semi-synthetic lincosamide used in the clinic is a clindamycin, a chlorinated derivative of lincomycin. Lincosamides have a bacteriostatic activity against Gram positive bacteria similar to macrolides and amphenicols: they bind to the 50S ribosome subunit and prevent peptide chain formation. Unlike macrolides though they are direct peptidyltransferase inhibitors (Spížek & Řezanka, 2017).

13. Streptogramins: This class of antibiotics is divided in two groups: streptogramins A and B. Group A are polyunsaturated cyclo-peptidic mactolactones whereas group B are NRP cyclic hexadepsipeptides. Natural streptogramins are poorly soluble in water therefore semi-synthetic derivatives were generated with multiple modifications of functional groups to obtain soluble antibiotics. Streptogramins are active against Gram positive bacteria but have a limited activity against Gram negative bacteria. Both groups have a bacteriostatic activity resulting from the inhibition

of protein synthesis associated with binding of the 50S ribosome subunit, however the combination of the two groups produce a bactericidal activity. The group A has an action similar to lincosamides and inhibit the peptidyltransferase, whereas the group B is closer to macrolides and prevent the peptide chain elongation by binding to the nascent peptide exit tunnel. The binding of group A streptogramins on the 23S rRNA alters the conformation of the ribosome leading to a more stable interaction with group B streptogramins (Bonfiglio & Furneri, 2001; Mast & Wohlleben, 2014).

14. Diarylquinolines: This class of antibiotics originates from synthetic chemistry. Diarylquinolines are composed of a quinoline core, i.e. a double-ring composed of a benzene and a pyridine ring, fused to a functionalized lateral chain. Modulation of the length of the lateral chain as well as substitution of the basic moieties or the phenyl rings of the lateral chain and substitutions on the quinoline core have been used to generate derivatives of diarylquinolines and reached the development of bedaquiline, the only antibiotic from this class approved in clinic so far. Bedaquiline inhibits the C subunit of the ATP synthase resulting in a bactericidal activity, selective against Mycobacteria (Guillemont et al., 2011; Salfinger & Migliori, 2015).

15. Quinolones: This family of synthetic antibiotics is composed of a bicyclic core structure with a nitrogen atom at position 1 (N1). Some chemical features are essential for antibacterial activity like a carboxyl group at carbon 3 (C3) and an oxygen atom at carbon 4 (C4) because these positions directly interact with DNA which is the target of quinolones. In that sens, a hydrogen atom is optimal at carbon 2 (C2) because any larger moiety could cause steric hindrance at C3 and C4. Other lateral chains can be modified to modulate the activity. In particular, addition of a fluorine atom at carbon 6 (C6) led to the opening of a subclass of quinolones, the fluoroquinolones, which exerts drastically improved potency compared to quinolones. Quinolones have a bactericidal activity on Gram positive and negative bacteria. They bind to the DNA replication complex formed by the DNA strand and topoisomerase IV and DNA gyrase resulting in both inhibition of DNA synthesis and chromosome breakages (Tillotson, 1996; Pham et al., 2019).

16. Lipopeptides: Lipopeptides are another class of antibiotic NRPs, consisting in cyclic depsipeptides bearing at least one ester bond and a fatty acid chain. The first lipopeptide identified were daptomycin and its natural derivatives. Studies on this family of lipopeptides revealed that the length of the fatty acid chain has an impact on antimicrobial activity but also on selectivity towards bacterial cells versus host cells. Daptomycin with its linear decanoyl chain was found to have the optimal balance between activity and toxicity compared to the other derivatives carrying *anteiso*-undecanoyl or *anteiso*-tridecanoyl for example. Other natural lipopeptides have been discovered with variations of the length of the amino acid sequence and the fatty acid chain. Some antibiotics like ramoplanins are classified in the subclass glycolipopeptides as they also bear a sugar moiety. Lipopeptides have a bactericidal activity against Gram positive bacteria and interact with cell membrane. In the case of daptomycin, it inserts into the bilayer of phospholipids causing loss of potassium ions and therefore loss of membrane potential (Bionda et al., 2013).

1.1.4 Emergence of resistance

Antibiotics are not active against all bacteria. One of the main reasons is explained by the nature of the bacterial membrane and its role as a barrier. As we have seen in the classification section, many antibiotics are only active against Gram positive bacteria which is due to their inability to cross the outer membrane of Gram negative bacteria. Nonetheless, the difference in bacterial membrane composition and permeability doesn't account for all the variations in antibiotic susceptibility. If bacteria are lacking the target of the antibiotic or the metabolic pathways for activation of the antibiotic, they have intrinsic resistance. For example the peptidoglycan of some species of lactobacilli has a pentapeptide ending in D-serine (Ser) instead of D-Ala the binding site of vancomycin, thus preventing the activity of vancomycin (Delcour et al., 1999). As another example, the antibiotic metronidazole is only effective when reduced, yet this reduction only happens in anaerobic bacteria, therefore aerobic bacteria have a intrinsic resistance to metronidazole (Laws et al., 2019). Other mechanisms like the expression of efflux pumps or enzymes able to modify antibiotics also result in intrinsic resistance (Cox & Wright, 2013) and will be discussed below.

Furthermore, resistance to antibiotics can also be acquired from vertical or horizontal evolution. Vertical evolution is the result of a spontaneous mutation resulting in the loss of sensitivity to an antibiotic transferred by a bacterium to its progeny. Vertical evolution can be a multi-step process with heritage of series of spontaneous mutations. On the other hand, horizontal evolution arise from gene transfer between a bacterium carrying a resistance gene to a susceptible bacterium (Laws et al., 2019). Gene transfer can be accomplished by 3 mechanisms: conjugation, transduction and transformation. Conjugation involves cell to cell contact for the transfer of a plasmid bearing the resistant gene through a conjugative pilus. To the contrary, transduction doesn't require cell to cell contact, as gene transfer is accomplished by infection with a phage integrating DNA from a bacterium and releasing it to another bacterium at a following cycle of infection. Finally, transformation is a process in which a bacterium uptake free extracellular foreign DNA and incorporate it into its genome. For transformation to happen, the cell must be in a state of competency which is regulated by environmental conditions. These mechanisms of genetic material transfer allow resistance gene transfer across bacterial species (Trevors, 1999).

The 6 main mechanisms of antibiotic resistance (Coates et al., 2002; Alanis, 2005; Lewis, 2013) are summarized on **Figure 1.3**.

1. First the target of the antibiotic can be modified, resulting in lack of antibiotic binding to its target. For example amino acid substitutions in the GyrA subunit of DNA gyrase was identified in quinolones-resistant *Escherichia coli* (Jacoby, 2005).

2. Instead of modifying the target, bacteria can also overproduce it to overcome the antibiotic inhibition. Overexpression of *alr* and *ddl*, the genes encoding the Ala racemase and D-Ala:D-Ala ligase targeted by D-cycloserine, has been measured in *Streptococcus challis* strains resistant to this antibiotic (Chopra, 1998). However this mechanism doesn't always result in resistance and can even lead to increased susceptibility. Overexpression of *gyrA* and *gyrB* the genes encoding the two subunits of DNA gyrase in *E. coli* resulted in resistance to coumermycin A1 but increased sensitivity to ciprofloxacin. Coumermycin A1 competes with ATP for binding on the GyrB domain, resulting in lack of activity of DNA gyrase, whereas ciprofloxacin

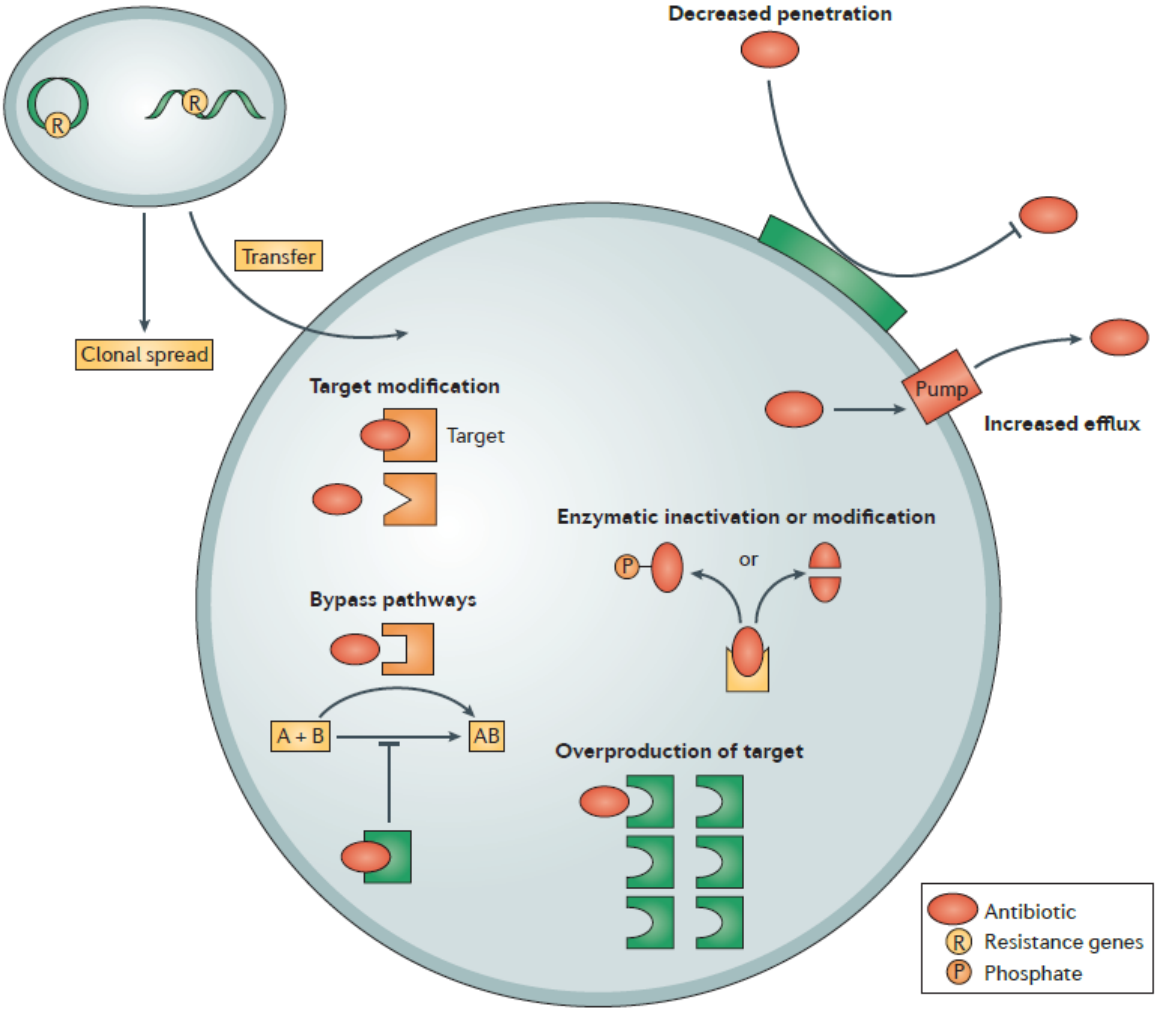

Figure 1.3: Mechanisms of antibiotic resistance
Figure From Lewis, 2013.

binds to DNA and the GyrA subunit and inhibits the DNA re-ligation activity of the gyrase but not its DNA cleavage activity while stabilizing the DNA-gyrase complex. Therefore in the case of coumermycin, overexpression helps to restore the full activity of DNA gyrase while treatment with ciprofloxacin associated with overexpression leads to increased DNA breakages that are toxic to the cells (Palmer & Kishony, 2014).

3. Otherwise instead of acting on the target to achieve resistance, the antibiotic itself can be cleaved or modified into an inactive form by enzymes. A major example of such mechanisms is the hydrolysis of the lactam ring of β-lactams by β-lactamases that can occur in both Gram positive and Gram negative bacteria (Poole, 2004).

4. Just like the level of target can be increased, the level of antibiotic can also be decreased to escape its action by modulating membrane permeability or expressing efflux pumps. Gram negative bacteria are protected by two bilayers of lipids. The second layer or outer membrane, contains porins which are transmembrane proteins allowing the passage of small and hydrophilic molecules like nutriments. Antibiotics can use these porins to cross the outer membrane. Loss or modification of porins, like the loss of OmpC in *Salmonella enterica*, can result in antibiotic resistance and in this example to cephalosporins (Nikaido, 2003).

5. Whereas porins allow the entry of molecules from the extracellular compartment, efflux pumps permit the release of molecules from the bacteria to the extracellular compartment. Efflux pumps have several roles and can be involved for example in bacterial communications or detoxifying of the bacterial cell. Antibiotics can be pushed out by such pumps specific or not to the antibiotic. Efflux pumps can be constitutive and therefore be implicated in an intrinsic resistance or overexpressed in a transient or stable manner by a acquired resistance arising from a mutation in the regulatory components of the pump (Blanco et al., 2016). As an example, MDR clinical isolates of *Pseudomonas aeruginosa* were identified with mutations in the genes encoding the regulators of the *mexXY* and *mexAB-OprM* operons and resulting in the operon overexpression and therefore the overprodution of the efflux pumps MexXY and MexAB-OprM (Llanes et al., 2004).

6. The last strategy to achieve resistance is to develop a new pathway to accomplish a biological function bypassing the original pathway targeted by an antibiotic. The most notorious example of this mechanism is the emergence of Methicillin-Resistant *Staphylococcus aureus* (MRSA). *S. aureus* is sensitive to methicillin, a semi-synthetic derivative of penicillin that is not susceptible to staphylococci β-lactamases and inhibits cell wall synthesis by binding to PBPs. Horizontal transfer of the *mecA* gene encoding PBP2a in *S. aureus* conferred resistance to methicillin as PBP2a replaces the functions of some PBPs and has very low affinity for β-lactams (Munita & Arias, 2016).

Development of resistance is promoted by exposure to antibiotics. Indeed antibiotic exposure creates a selective pressure: bacteria with an acquired or intrinsic resistance have an advantage for survival and for spreading on sensitive bacteria. As most antibiotics come from natural origins and in particular from microorganisms, bacteria have been exposed to them and started developing resistance long before their discovery by humans. For example, phylogenetic analysis revealed that β-lactamases encoding genes appeared two

billion years ago and might have been horizontally transferred by conjugation for millions of years (Aminov, 2010). However, the industrialization of antibiotics has accelerated this phenomenon and every introduction of an antibiotic in the clinic has been followed by the emergence of resistant bacteria a couple years later or sometimes even the same year (**Figure 1.4**). Some bacteria have evolved so much in the last decades that they became resistant to several classes of antibiotics or to all of them, they are respectively designated as Multi-Drug and Pan-Drug Resistant (MDR and PDR) bacteria (Ventola, 2015). The main causes that led to such a critical situation are: overpopulation, increased migration, poor sanitation, enhanced usages in clinic and for animal production and misuse of antibiotics (Aslam et al., 2018; Chokshi et al., 2019). Although Fleming publicly expressed his concerns about misuse of antibiotics as early as 1945, history mostly retained the story of his discovery of penicillin and his warning was forgotten for a long time. His exact words when he received the Nobel price for the discovery of penicillin were: *"It is not difficult to make microbes resistant to penicillin in the laboratory by exposing them to concentrations not sufficient to kill them, and the same thing has occasionally happened in the body. The time may come when penicillin can be bought by anyone in the shops. Then there is the danger that the ignorant man may easily underdose himself and by exposing his microbes to non-lethal quantities of the drug make them resistant"* (Fleming, 1945). He also stated that same year in an interview published in the New-York times: *"The thoughtless person playing with penicillin treatment is morally responsible for the death of the man who succumbs to infection with the penicillin-resistant organism"*(Sillankorva et al., 2019). Yet, following their discovery, antibiotics were widely used and misused. Recent studies suggest that, in the United-States of America (US), the decision to use antibiotics to treat an infection, or the choice of antibiotic and finally the duration of the treatment are inappropriate in 30 to 50% of cases (Aslam et al., 2018). While in developed countries antibiotics are often used more than necessary, in developing countries ineffective treatments arising from bad quality of drugs enhance the selective pressure on bacteria and distressed sanitation associated with lack of diagnosis facilitate their spreading (Chokshi et al., 2019). However, among all the causes behind rising of resistance, the most detrimental is probably the use of antibiotics for agricultural purpose. Antibiotics are added in animal feed not only for treating diseases but for preventing them and increase animal growth. In the US, it is estimated that around 80% of the national's annual consumption of antibiotics is destined to livestock (Van Boeckel et al., 2015). This proportion was only 40% in the 1980's (Feeds, National Research Council (US) Committee to Study the Human Health Effects of Subtherapeutic Antibiotic Use in Animal, 1980) and is expecting to keep growing. In 2006, the European Union banned the use of antibiotics as growth promoters and for the prevention of disease in animals (Regulation [EC] No 1831/2003 of the European Parliament) but there is still almost no regulation or weak regulation in most of the world (Maron et al., 2013).

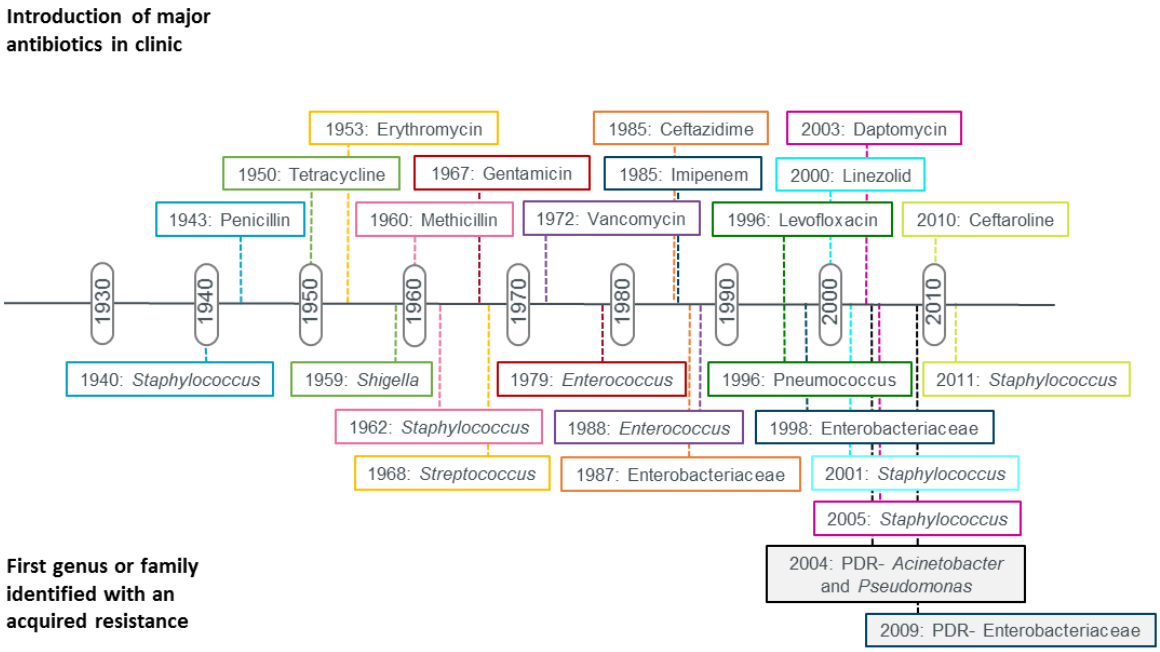

Figure 1.4: Timeline of clinical introduction of antibiotics and first identifications of resistant bacteria

PDR=Pan-Drug Resistant. Figure adapted from Ventola, 2015.

1.1.5 Projections for the future

Currently, in the US, it is estimated that almost 100,000 deaths are caused each year because of antibiotic-resistant pathogen-associated hospital-acquired infections (HAIs). Moreover, the total economic loss that can be credited to antibiotic resistance in the US is estimated at 55 billion of dollars a year (Aslam et al., 2018). Efforts have been made to obtain such estimations worldwide but poor surveillance and lack of reporting complicate this task. Still, the lowest evaluation of the number of deaths caused by drug-resistant bacterial infections but also human immunodeficiency viruses (HIV) and malaria is set at 700,000. Tuberculosis caused by MDR *M. tuberculosis* alone is responsible of 200,000 deaths a year (O'Neill, 2016).

Resistance to antibiotics is not slowing down and is even expected to rise as consumption of antibiotics is still increasing. In particular, uses of antibiotics for livestock have already increased by 26% between 2009 and 2015 in the US (Chokshi et al., 2019) and is expected to rise by 67% worldwide by 2030 (Van Boeckel et al., 2015). Moreover, we are currently going through an "innovation gap" and no new class of antibiotics has been discovered since 1997 that could help fighting the MDR or PDR strains (**Figure 1.1**). Therefore, it might be impossible in the future to treat bacterial infections. Currently some PDR bacteria are already associated with a 50% mortality rate such as some strains of *Klebsiella* (Centers for Disease Control and Prevention (CDC), 2013). Moreover, effective antibiotics are also necessary for many more medical procedures than treating declared infections. For example, procedures that require or provoke depression of the immune system such as organs transplantation or chemotherapy could be too dangerous to perform if no effective antibiotics are available. Common surgery such as joint replacements or cesearian section could also be lethal in case of postoperative infections (Dadgostar,

2019). Therefore the rise of resistance associated with the lack of new drugs is expected to lead to the return to "the Dark Ages of Medicine" which designate the era of medicine before antibiotic discovery. Deaths attributable to antibiotic, and more broadly to antimicrobial, resistance are thought to drastically increased up to 10 millions worldwide by 2050, making antimicrobial resistance the first cause of death (**Figure 1.5**).

This projection comes from the work of the economist Jim O'Neill who was commissioned by the government of the United Kingdom to review the threats caused by antimicrobial resistance and to propose solutions to answer those threats (O'Neill, 2016). The report proposes 5 measures to tackle the antimicrobial crisis, that were also adopted by WHO (WHO, 2015):

1. Raise global awareness about antibiotic resistance to educate the public about unnecessary uses of antibiotics and create a climate for behavioral changes;

2. Improve hygiene to reduce the numbers of cases of infection and therefore the use of antibiotics as well as preventing the dissemination of MDR and PDR strains;

3. Enhance and promote global surveillance to contain the expansion of MDR and PDR strains;

4. Reduce antibiotics uses to limit development of resistance: first in humans by implementing diagnosis methods to prescribe antibiotics only when necessary and secondly by limiting and eventually banning their preventive use and usage as growth promoters in animals;

5. Find new antibiotics and alternatives to antibiotics to treat infections and especially infections caused by MDR and PDR strains.

It is worth noting than these 5 guidelines are in accordance with the One Health approach which encourages researchers and physicians to improve collaboratively human, animal and environmental health care worldwide for a better global health. Indeed, human health is ineluctably linked to animal and environmental health. For example, it is estimated than more than half of the infectious cases in humans come from contamination by animals through direct contacts or environment and food contamination. Therefore, in the case of antibiotic resistant bacteria, it is crucial to reduce their spreading in humans but also in animals (McEwen & Collignon, 2018). While the 5 guidelines are all equally crucial to overcome the resistance crisis and prevent the beginning of a post-antibiotic era, most of them cover public health and political topics. Only the 5th proposition will be further discussed in this manuscript.

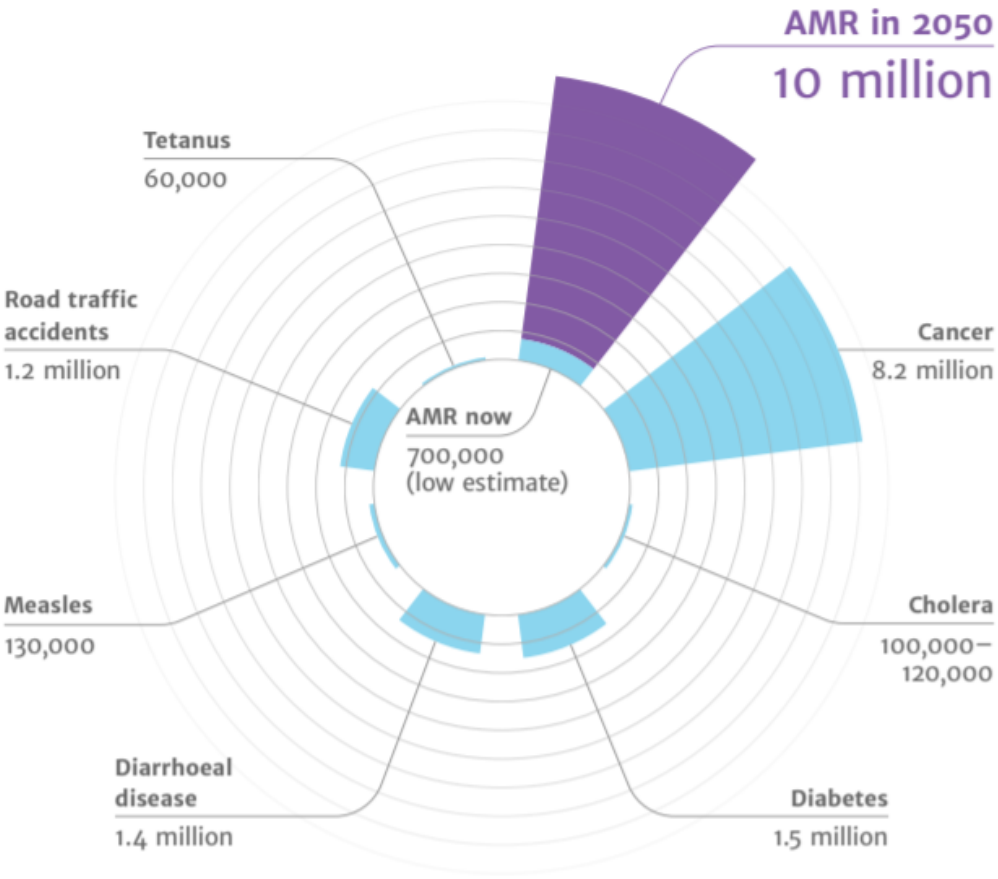

Figure 1.5: Main causes of deaths worldwide and estimated annual numbers
The blue color represents the estimated numbers of deaths in 2016, whereas purple shows projection for 2050. AMR = Antimicrobial Resistance, it includes infections caused by resistant strains of bacteria but also other microorganisms such as parasites, viruses or fungi. Figure from O'Neill, 2016.

1.2 Alternatives to conventional antibiotics

As bacteria are becoming more and more resistant to antibiotics, it is urgent do develop therapeutic alternatives. These alternatives must be active against MDR and PDR strains and ideally limit the emergence of resistant strains. Another desirable traits for an optimal antibiotic is specificity. Indeed, although broad-spectrum antibiotics came as handy as they could be used to treat a wide range of infections, they also cause dysbiosis that can lead to secondary infections and they promote resistance development. Additionally, therapeutic agents with multi targets rather than a single target would be beneficial as bacteria would be less likely to achieve resistance through target mutation. Therapies with combination of antibiotics and/or alternative agents are also explored in that sense (Singh et al., 2017). Only novel therapeutic strategies will be discussed in this section and not preventive strategies such as vaccination (Theuretzbacher, Bush, et al., 2020; Theuretzbacher, Outterson, et al., 2020).

It is worth noting than most alternatives fit the definition of the term antibiotic (see subsection 1.1.2). However they are not considered as antibiotics yet as they are not currently employed in the clinic to treat infections. Only the two approaches using whole organisms instead of molecules, namely phage therapy and alterations of the microbiome, fall out of the definition of the term antibiotic.

1.2.1 Phages

Treatment of infection with phages is considered as an innovative strategy as it is not currently available in most parts of the world. However, phage therapy was actually carried out for the first time in 1919 before the discovery of penicillin and was widely developed and used until the 1940s. Several reasons, including scientific controversies as well as the beginning of mass production of penicillin but also the fact that science became an ideological tool during World War II, led to the abandon of phage research in the US and in Europe while it thrived in the Eastern bloc and in particular in the Soviet Union. Hence today, phage therapy is only approved in some of the former countries of the Eastern bloc but is getting a renewed interest worldwide as resistance to antibiotics is increasing (Fruciano & Bourne, 2007; Chanishvili, 2012; McCallin et al., 2019).

Phages are ubiquitous viruses that infect bacteria or achaea. Like any type of viruses, they carry genetic information on a single or double strands of DNA or RNA but are unable to translate it into proteins as they lack ribosomes. Moreover, they are not metabolically active. Therefore, these obligate parasites rely on the host machinery to reproduce. Phages recognize and attach to their host thanks to host cell surface receptors before injecting their nucleic acid into the cells. Some phages are designated as virulent as they systematically enter a lytic cycle after the genetic material is released in the cell. They hijack the host machinery to multiply and produce lytic proteins able to permeabilize the cell membrane and hydrolyze the peptidoglycan cell wall causing osmotic imbalance followed by cell lysis releasing the phage progeny. Other phages are qualified as temperate as they can also enter lysogenic cycles in which their genetic material is incorporated into the bacterial genome and is transferred to bacterial daughter cells along bacterial division. Variation of environmental conditions can trigger a shift to a lytic cycle (**Figure 1.6**). Research on phages as therapeutic agents is confined to virulent and strictly lytic phages that would

immediately kill their host as lysogenic phages participate in horizontal gene transfer in bacteria and could help spread resistance genes (Salmond & Fineran, 2015; Lin et al., 2017; Romero-Calle et al., 2019).

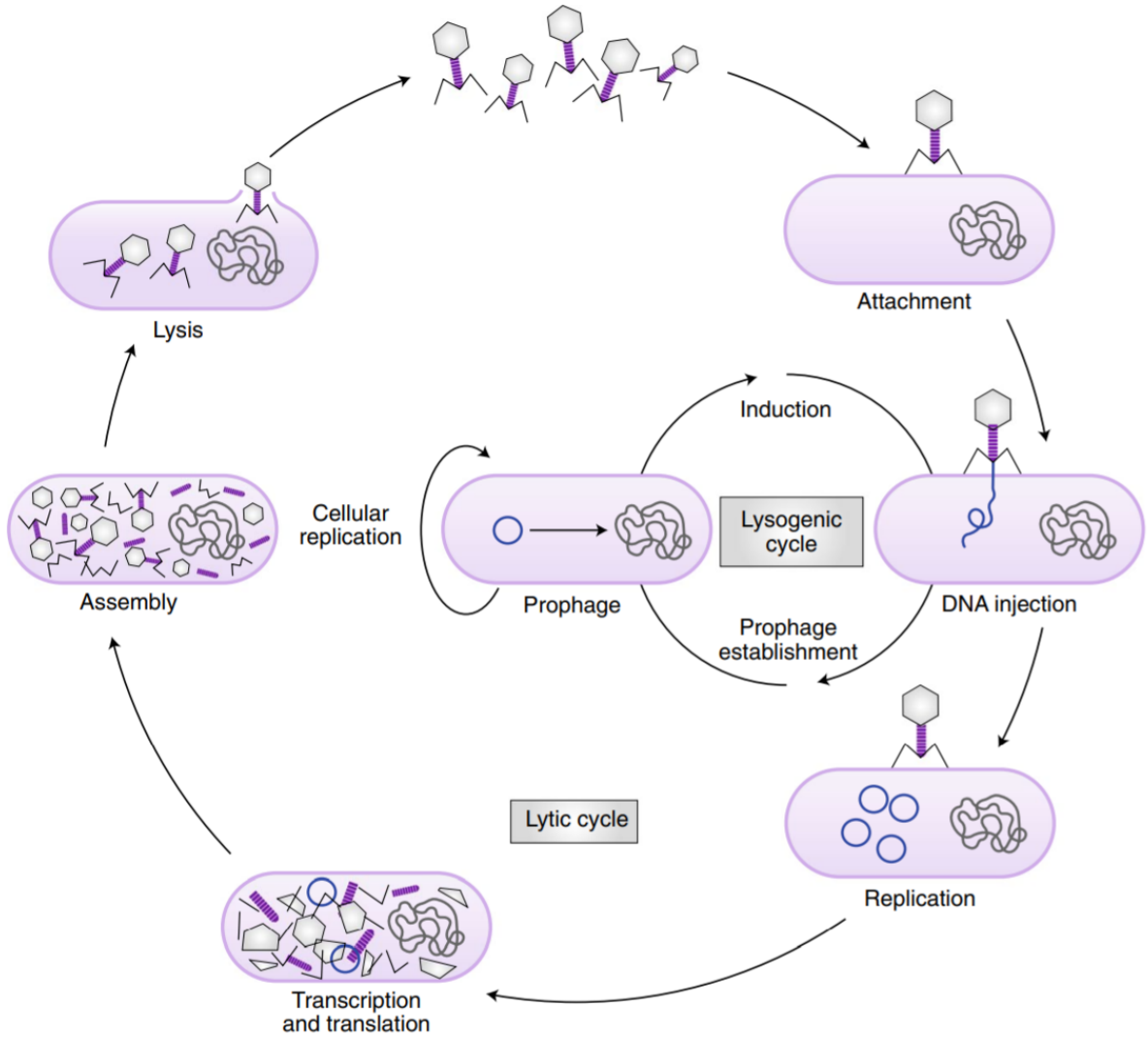

Figure 1.6: Phage infection of bacterial cells through lytic or lysogenic cycles
Figure adapted from Salmond & Finerand, 2015.

The primary advantage of phages is that they are safe for mammalian cells. Some studies report interactions between phages and mammalian cells but phages are unable to use the eukaryotic machinery to reproduce (Dabrowska et al., 2005). The safety of phage therapy for mammalian organisms is corroborated by nearly all clinical trials. Another advantage is that they can be administrated by most drug delivery routes and traverse mammalian barriers such as endotheliums or the blood-brain barrier and reach any tissues or organs (Huh et al., 2019). Finally, the last key advantage of phages compared to antibiotics is that they can be highly specific. Indeed specificity relies on host cell surface receptors recognition and therefore their distribution among bacterial species. Host cell surface receptors encompass different types of molecules exported to the cell surface such as membrane-bound proteins acting as bacterial receptors, transporters or constituting flagella; lipopolysaccharides (LPSs) of the outer membrane of Gram negative bacteria; and lipoteichoic acids (LTAs) that are element of the cell wall of Gram positive bacteria. LPSs

and LTAs vary among species and membrane-bound proteins can be widely distributed or very specific. As a result, phage specificity varies from one isolate to multiple species or genera. Studies report the efficient clearing of bacterial infections in challenged mice treated with phages with low impact on the commensal microbiota (Lin et al., 2017; Romero-Calle et al., 2019). For example, ShigActive^{TM}, a therapeutic phage-based agent was as effective as the antibiotic ampicillin to reduce the fecal and cecal loads of *Shigella sonnei* in challenged mice but high overall alterations of the gut microbiota were observed only after treatment with ampicillin (Mai et al., 2015).

Phages could also be used in combination with antibiotics to enhance their efficacy or overcome resistance. For example, the antibiotic chloramphenicol has been attached through a cleavable linker to the coating proteins of a engineered phage carrying antibodies specific to either *E. coli, S.aureus* and *Streptococcus pyogenes*. Linkage of the antibiotic to targeted phage particles resulted in an increase of potency by a factor of 20,000 against the 3 strains. This method could be used to deliver antibiotic to a specific targeted bacterium and therefore decrease microbiota perturbations. Moreover, it may also increase the antibiotic concentration reaching bacteria while reducing the free amount of antibiotic potentially harming mammalian tissues (Yacoby et al., 2007; Salmond & Fineran, 2015). Although lysogenic phages are not a suitable option for therapies restricted to phages, they could be highly useful tools to treat resistant bacteria in combination with antibiotics. The rational is to introduce in engineered lysogenic phages an antibiotic-sensitizing cassette that would be expressed in the bacterial cells and cancel the effects of the evolution that conferred them resistance. This strategy was successful to restore sensitivity to streptomycin in mutants of *E. coli* that had acquired resistance. Streptomycin resistance is associated in many cases to mutations in the *rspL* gene that encodes a highly conserved protein of the 30S ribosome subunit essential for streptomycin binding. Mutants of *E. coli* carrying mutations in the *rspL* gene conferring resistance to streptomycin were infected with a lysogenic phages encoding the wild-type *rspL* gene. After infection, these mutants were no longer resistant to streptomycin (Edgar et al., 2012).

Although phage therapy seems to offer many advantages as an alternative or a complement to antibiotics to treat bacterial infections, a few key points remain to be elucidated and challenges to be addressed before phage therapy can be routinely used. As for antibiotic, resistance can emerge to phages by mutation or lack of expression of host cell surface receptors. Such resistance to phages has been identified in multiple bacteria including *E. coli, S. aureus, Vibrio cholerae* and *Bordetella bronchiseptica* (Principi et al., 2019). Other mechanisms of resistance established so far consist in secretion of extracellular polymer to prevent phage attachment, blocking DNA entry, expression of endonuclease, premature cell lysis to prevent reproduction of phage particles and finally inhibition of phage assembly (Seed, 2015). A strategy to override these resistance mechanisms is the treatment with cocktails of various phages of different types and targeting different receptors rather than using a single phage. Phages can also be easily genetically engineer to attempt to modify their target and design phages active against any bacteria including resistant bacteria (Lin et al., 2017; Huh et al., 2019). One of the challenges with phage therapy concerns the amount of phage that need to be delivered to obtain an efficient therapy as their bioavailability and pharmacokinetics remain elusive. Phages can be eliminated by the mammalian immune system and their clearance rate as well as the overall immunological response of mammalian organisms to phage therapy remain unclear and to be investigated so far (Caflisch et al., 2019).

1.2.2 Phage lytic proteins

While phages can be used to kill bacteria and treat infections, another therapeutic strategy could be to exploit the lytic proteins that they encode rather than using the whole phage particles. Indeed, as we have seen in the previous section, the genetic material of phages encodes lytic proteins that are expressed at the end of the lytic cycle to lyse the bacterial host cell enabling the release of the replicated phage particles (**Figure 1.6**). These proteins are classified in two major classes: holins and endolysins. Holins are transmembrane proteins that form pores in the bacterial membrane allowing endolysins to access and hydrolyze the peptidoglycan cell wall. Moreover, some phage particles also carry another type of lysins called virion-associated peptidoglycan hydrolases (VAPGHs) that are essential for genetic material injection after phage attachment to the bacterial host cell. All these proteins exhibit high structural, biochemical and functional variability among phages. Since bacterial cell lysis can occur with the action of lysins (endolysins or VAPGHs) alone but not with holins alone, research on phage lytic proteins as therapeutic agents has been mainly focused on lysins so far. However, evidence of improved efficacy of lysins in the presence of holins suggest that they could be used together in combined therapies (Roach & Donovan, 2015; Rodríguez-Rubio et al., 2016; Lin et al., 2017).

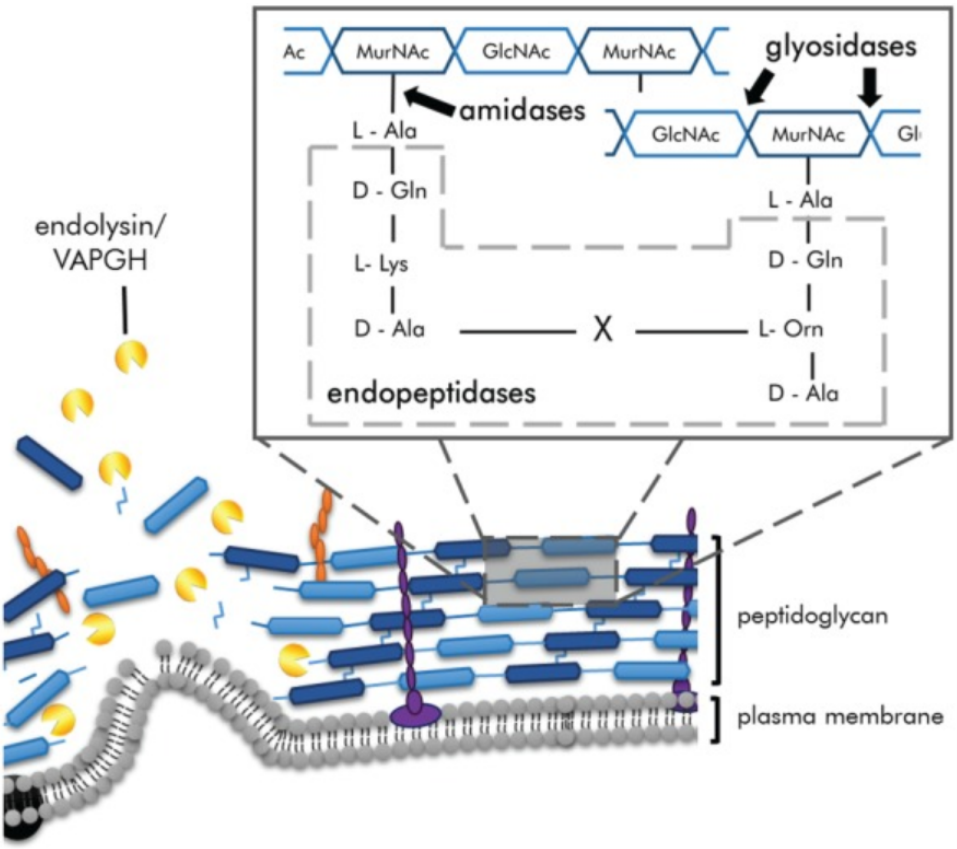

Figure 1.7: Mechanisms of peptidoglycan cleavage by phage lysins
Figure from Roach & Donovan, 2015.

The core common components of endolysins include at least one catalytic domain for endolysins from phage targeting Gram negative bacteria whereas endolysins targeting

Gram positive bacteria also carry at least one cell wall binding domain (CBD). In contrast, VAPGHs from both Gram positive and negative phages have no recognizable CBD and have respectively two and one catalytic domains. Endolysins and VAPGH can have a glycosidase, amidase or endopeptidase activity (Rodríguez-Rubio et al., 2016). Glycosidase lysins cleave the glycosolic bonds between the two alternating amino sugars N-acetylglucosamine (GlcNAc) and N-acetylmuramic acid (MurNAc). Lysins with amidase activity hydrolyze the amide bonds linking MurNAc to the peptide chain. Finally, endopeptidases cleave the peptide bonds within a peptide chain or cross-linking the peptide chains (**Figure 1.7**). Both purified VAPGH and endolysins have been shown to exert bacteriolytic activity on culture of bacterial cells. The activity of some lysins has also been confirmed in animal models (Roach & Donovan, 2015). For example, a study assayed the potency of 9 phage lysins to rescue mice from bacteremia caused by MRSA. Out of 9 lysins, 6 showed efficacies similar to vancomycin and were able to rescue 100% of animals (Schmelcher et al., 2015). The CBDs of endolysins can be specific to strains or species, therefore specific endolysins could be used for targeted therapies. Because endolysins target highly conserved and essential bonds in the peptidoglycan structure, bacteria are less prone to evolve as resistant to endolysins. As a result, no resistance to endolysins has been identified so far, although it can not be assured that resistance to endolysins is impossible and will never occur (Roach & Donovan, 2015; Gondil et al., 2020). Another advantage of lysins on antibiotics is that they have been shown to be active on vegetative cells and to disrupt biofilm (Lin et al., 2017).

One of the challenges arising from the use of lysins as alternatives to antibiotics is their limited action against Gram negative bacteria. Since endolysins naturally act from the inside of bacterial cells, most of them are ineffective against Gram negative bacteria when added exogenously because the bacterial outer membrane prevents the access to the peptidoglycan cell wall. Some lysins with highly positively charged terminal region have been identified as active against Gram negative strains, suggesting that these regions might interact with the anionic outer membrane (Lood et al., 2015; Roach & Donovan, 2015). Moreover, researchers have been developing engineered and chimeric lysins to overcome the limitation of lysins to Gram positive bacteria. A major example of chimeric lysins is the family of artilysins that are composed of a lysin fused to a cationic peptide. For example Art-175 is a fusion of the *Pseudomonas aeruginosa* phage KZ144 endolysin and SMAP-29, the sheep myeloid antimicrobial peptide of 29 amino acids. SMAP-29 is an antimicrobial peptide (AMP) that permeabilizes the membrane of broad-spectrum bacteria without causing cell lysis. The KZ144 endolysin was unable to kill cells of *P. aeruginosa* whereas Art-175 showed lytic activity. Moreover, although SMAP-29 fused to the KZ144 was successful to translocate the endolysin to the peptidoglycan, it lost its permeabilization activity and at the same time the cytotoxic activity toward eukaryotic cells that was limiting its use for the treatment of infections (Briers et al., 2014).

Such as phages, lysins could be used alone or in combined therapies with other lytic proteins, antibiotics or other alternatives to antibiotics to treat bacterial infections. However, currently there is a lack of data on the safety of lysins administration as a drug and the immune response to it in mammalian organisms. Some studies revealed that high level of pro-inflammatory cytokines can ensue in vivo administration of phage lysins. Therefore optimization of lysins might still be needed to obtain effective and safe drugs. Finally, as these lysins are proteinaceous in nature it remains challenging to find suitable routes of administration and efficient delivery (Gondil et al., 2020).

1.2.3 Antibodies

Such as phage therapy, bacterial infections were commonly treated with antibodies, or more precisely with antibodies-rich serum, before the discovery of antibiotics. In 1901, von Behring received the Nobel Prize in Medicine for the development of sheep serum therapy to treat diphtheria in humans. Other bacterial infections like pneumonia or meningitis were then treated with the serums of animals or humans who naturally recovered from the disease until the 1930s. However, as antibiotics offered many advantages compared to serum therapy, their discovery led to the abandon of serum therapy. Indeed, antibiotics were easier to produce on an industrial scale and with consistent activity compared to serums that were harvested on animals or humans with an inherent variability, they also exerted less toxicity and were more efficient than serum. Finally, as antibiotics were broad-spectrum they seemed more convenient at that time because they could be administrated without bacterial diagnosis, on the contrary to serum therapies that were specific to one pathogen (Saylor et al., 2009).

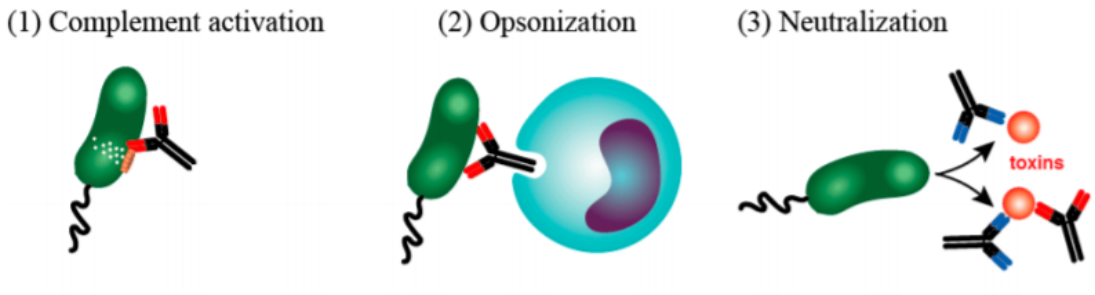

Figure 1.8: Roles of antibodies in bacterial infections
Figure from Sawa et al., 2019

Current strategies regarding the use of antibodies to treat bacterial, but also other types of infectious, diseases focus on mono-clonal antibodies (mAbs) instead of whole serum. While serum contains many type of immunoglobulins (also called antibodies) and other molecules, mAb corresponds to one type of immunoglobulin with a single isotype and targeting a specific epitope. The development of human or humanized immunoglobulins has been successful to overcome the toxicity issue that could be caused by antibody therapy. There are two strategies regarding the use of mAbs to treat bacterial infection: induction of bacterial cell death or inhibition of bacterial pathogenesis. Indeed, immunoglobulins can bind to targets situated on the surface of bacteria inducing mechanisms leading to their death (**Figure 1.8(1,2)**) or they can bind to toxins or virulence factors secreted by bacteria and causing pathogenesis (**Figure 1.8(3)**). Two mechanisms result in bacterial cell death: complement-associated immunolysis (**Figure 1.8(1)**) or opsonization (**Figure 1.8(2)**). In the first mechanism, the binding of immunoglobulins to bacterial cells results in recruitment of the complement that pierces the cell membrane leading to cell lysis, while in the second mechanism antibodies bound to the bacteria are recognized by neutrophils and macrophages. Then bacteria undergo phagocytosis, meaning that they are engulfed in the neutrophils or macrophages before being digested by lysosomal enzymes (Sawa et al., 2019). An example of immunoglobulin target that triggers immune system-mediated killing is the polysaccharide capsule of pneumococcus

(Saylor et al., 2009). Another example of surface target is the lipoteichoic acid (LTA) of *S. aureus*. Teichoic acids are produced by most Gram positive bacteria and can be linked to the peptidoglycan or the cytoplasmic membrane. Like lipopolysaccharides (LPS) from Gram negative bacteria, they are know to trigger an inflammatory response in mammalian hosts (Xia et al., 2010). LTA is highly conserved in Staphylococci and was therefore used to design a mAb. This mAb effectively rescued a murine model from *S. aureus* bacteremia. Binding of the mAb to the bacterial cells promoted their phagocytosis by the host immune system. This mAb, named pagibaximab, was also shown to be safe in both adults and neonates in clinical studies (Weisman, Fischer, et al., 2009; Weisman, Thackray, et al., 2009). Moreover, studies showed that some mAbs can have a direct and immediate bactericidal activity without stimulation of phagocytosis or complement activity. The bactericidal activity of an immunoglobulin and of a single chain variable fragment of this antibody were demonstrated on a clinical strain of *Borrelia*. The mechanisms leading to bacterial death involve disruption of the outer membrane (LaRocca et al., 2008). On the other hand, an example of the indirect approach resulting in pathogenesis inhibition, is the production of a mAb targeting the Shiga toxin produced by a strain of *E. coli*. Infection with shiga toxin-producing *E. coli* may cause hemorrhagic colitis or hemolytic uremic syndrome associated with sever complications including death. A set of mAbs were shown to neutralize shiga toxin and hence the toxicity of the bacterial cells on human cell lines in culture. Moreover, mice and piglets treated with mAb targeting the shiga toxin were rescued from lethal infection with shiga toxin-producing *E. coli* (Krautz-Peterson et al., 2008; Bitzan, 2009). Researchers working on antibodies as alternatives to antibiotics are also exploring RadioImmunoTherapy (RIT). RIT employs immunoglobulins coupled to radionucleides, it is already widely exploited in cancer therapy to deliver lethal doses of radiation to targeted cancer cells. This strategy could be applied to bacterial infections as well. Mice treated with the bismuth radiolabelled antibody 80 µCi^{123}Bi-D11 survived bacteremia induced by *Streptococcus pneumoniae* in 87 to 100% of cases whereas death happened in 1 to 3 days in the untreated control group. The treated mice showed no weight loss or clinical sign of adverse effects (Saylor et al., 2009).

More widely than RIT, antibodies have been extensively studies in other field of medicine like cancer therapy. The knowledge developed in these fields could be exploited to establish new therapeutic strategies for the treatment of infections with antibodies. Antibody therapies could even be easier to develop in the infectious field as antigens between bacteria and the host exhibit great variability whereas cancer therapy deals with antigens of cells coming from the same organism. However, there are also some limitations associated to antibody therapy. The cost of production of antibodies and thus the cost of treatment, even though reduced with the expansion of mAbs to replace serum, is high compared to antibiotics. Moreover, they are fragile macromolecules with low stability that are not easy to store. Beside the storage issue, their nature also make them hard to deliver. They have to be delivered by systemic route as they would be digested through the oral route. Antibodies, and especially mAbs, are very specific as they target one epitope, which can be an advantage as they won't affect commensals of the microbiota or trigger resistance in multiple bacteria, but therefore they also require very accurate diagnosis for efficient treatment. Moreover, bacteria can evolved by mutation of the epitope to achieve resistance. Resistance development and escape of treatment can be avoided by targeting highly conserved and essential epitopes or by using cocktails of mAbs designed against multiple epitopes or by developing mAbs with a bispecificity for two different epitopes. Another limitation of antibodies is that they are effective mostly in early treat-

ment. However, they can be combined to antibiotics or other alternatives to antibiotics to offer treatments effective throughout the time course of the disease and limiting the emergence of resistance (Saylor et al., 2009). As we have seen in the phage section, coupling antibodies, phage and antibiotics can be a possible approach to deliver broad-spectrum drugs to a specific bacteria (Yacoby et al., 2007; Salmond & Fineran, 2015).

1.2.4 Alterations of the microbiome

Bacteria live in communities and share their ecological niche with other species. While some species actually help and rely on each others to survive, others compete for the niche resources, mainly nutrients and space. This competition can be enforced by indirect mechanisms consisting in resource consumption or direct action by the production of active molecules inhibiting or killing competitors (Ghoul & Mitri, 2016). Lots of antibiotics are actually major examples of this direct mechanism used for competition between bacteria and more broadly microorganisms. One of the possible strategies to cure bacterial infection is to manipulate the composition of the infected communities, or microbiota, to trigger the competitive exclusion of the pathogens by commensal or harmless bacteria. Manipulation of the microbiome can be accomplished by the addition of a single bacterial strain, defined communities or transplantation of a whole foreign microbiome. The effects expected, summarized on **Figure 1.9**, are the inhibition or killing of the pathogens through direct or indirect bacterial competition mechanisms but also through enhancement of mucosal barriers and modulation of the host immune system (Ghosh et al., 2019).

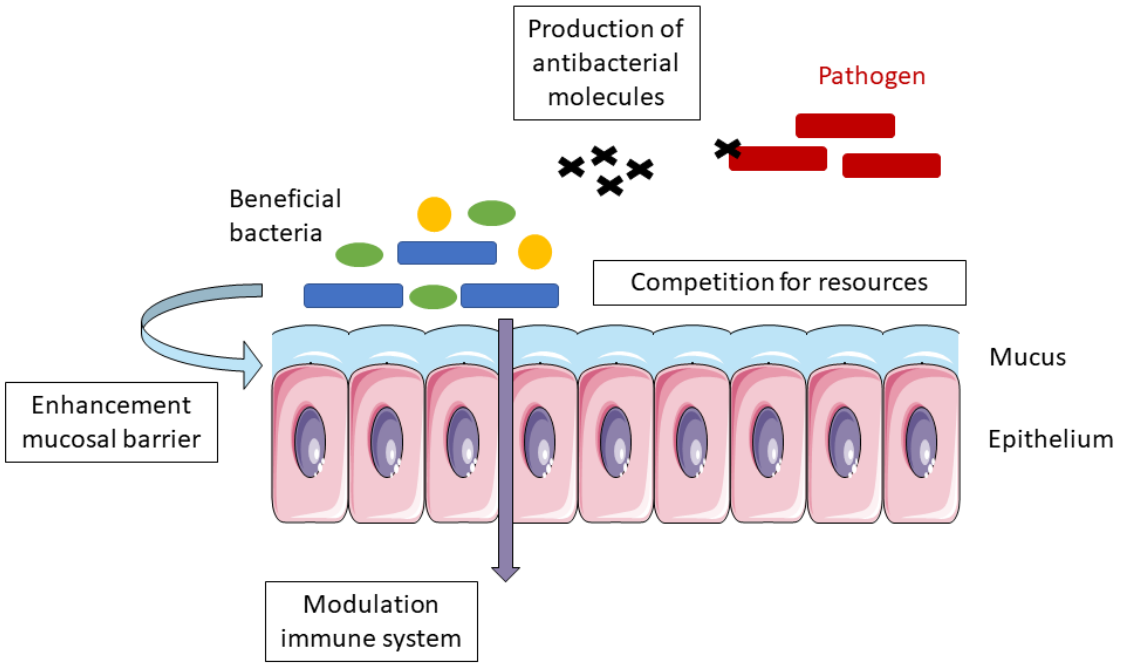

Figure 1.9: Action of commensal bacteria or probiotics against pathogens in mammalian host

The most successful and advanced therapy in that field is Fecal Matter Transplant (FMT) for the treatment of *Clostridium difficile* infections (CDIs). Infections with *C. dif-*

ficile don't occur in healthy individuals as their gut microbiome prevent the colonization by *C. difficile*. However individuals who suffer from dysbiosis, for example after a heavy treatment with broad-spectrum antibiotics, are prone to extreme gut colonization by *C. difficile*. As a result CDIs are the most frequent nosocomial infections in the US (Nowak et al., 2019). FMT consists in the transfer of stool contents and therefore fecal microbiota, from healthy to sick individuals by endoscopy, nasoenteric tubing, or ingestion of capsusles. CDIs patients treated with FMT loose clinical signs of the disease and are negative for fecal detection of *C. difficile* toxins in 90% of cases. The efficacy of FMT is superior than vancomycin for the treatment of CDIs and less likely to be followed by relapse. Moreover, FMTs have been shown to clinically cure 91% of patients who had failed to recover with antibiotic therapy (Kim & Gluck, 2019). As FMT has been proven to be an efficient therapy for CDIs, pre-clinical and clinical studies are under development for the treatment of other bacterial gut infections. For example, mice with a stable Vancomycin-Resistant *Enterococcus faecalis* (VRE) gut colonization showed reduction of VRE 7 days after FMT and no detectable VRE after 15 days (Ubeda et al., 2013). FMT was also able to cure gut infection caused by two conjoined MDR bacteria, namely *E. coli* and *K. pneumoniae*, in an immunocompromised patient. Both strains remained under detection level in fecal samples up to a month after the intervention (Biliński et al., 2016). So far the efficacy of FMTs to treat gut infections has been proven on a few models but the full scope of pathogens that could be excluded from sick individuals with FMTs remains to be characterized. Moreover, extensive studies are needed to determine a standardized protocol regarding the sample preparation and administration. Donor selection is also a tricky step of the procedure as thorough screening and analysis are necessary to avoid the transmission of other infectious pathogens to patients (Kim & Gluck, 2019). Characterization of the core bacteria from the samples that allow pathogens elimination could help to design defined synthetic communities of bacteria with less variability of transplants between patients and less risk of secondary infections. A team of researcher used a mouse model of CDI infection to look for such a bacterial consortium. Treatment with vancomycin failed to cure the mice whereas FMT from healthy mice cured them. From different preparations of fecal samples from healthy mice, they isolated a mixture of 6 bacteria that was also able to eradicate the infection. The mixture is composed of phylogenetically diverse bacteria including 3 known species (*Staphylococcus warneri, Enterococcus hirae, Lactobacillus reuteri*) and 3 novel species (*Anaerostipes sp. nov., Bacteroidetes sp. nov., Enterorhabdus sp. nov.*) (Lawley et al., 2012).

Probiotics are defined by WHO as "*live microorganisms which, when administrated in adequate amounts, confer a health benefit for the host*". Probiotics are distinct from prebiotics which are food compounds that promote the growth of bacteria beneficial for the host (Verna & Lucak, 2010). On the contrary to FMT, probiotics are administrated as single strains or cocktails of a few strains. However they can exert pathogen clearance through the same mechanisms than bacteria contained in FMT (**Figure 1.9**). The probiotics that are most used are Lactic Acid Bacteria (LAB) and *Bifidobacterium* (Patel & DuPont, 2015). Studies reported the efficient clearance of intestinal pathogens in murine models. For example, administration of *Bifidobacterium breve* significantly decreased fecal loads of *Salmonella enterica serovar Typhimurium* in mice (Asahara et al., 2001). However, so far there hasn't been consistent evidence of the efficacy of probiotics to cure gastro-intestinal (GI) infections in humans, although some probiotics have been identified for efficient prevention of such infections (Verna & Lucak, 2010). Nevertheless, the potent activity of probiotics have been shown in infections occurring in other human compart-

ments associated with complex microbiota, such as the oral cavity and the vagina. Bacterial vaginosis has a prevalence ranging respectively from 16 to 30% and up to 50% in the US and in Africa. Treatments with antibiotics fail in 20 to 30% of cases and are associated with 40 to 50% of relapse in the next year. Recently, a meta-analyse of 10 randomized clinical trials revealed that several strains of lactobacilli were effective and safe in short and long terms for the treatment of bacterial vaginosis (Wang et al., 2019). On the other hand, several studies reported that probiotics administrated in tablets, mouth rinse or directly in food significantly decreased oral pathogens responsible of peridonteal diseases and *Streptococcus mutans* the main pathogen causing dental carries, which affect both children and adult in large proportions (Saha et al., 2012).

1.2.5 Bacteriocins and Antimicrobial Peptides

Bacteriocins are ribosomally synthesized proteinaceous molecules produced by bacteria that kill or inhibit the growth of other bacteria. Bacteriocins can be proteins or peptides (Tagg et al., 1976; Jack et al., 1995). Antimicrobial peptides (AMPs) denominate peptides killing or inhibiting the growth of microorganisms. Therefore the first difference between bacteriocins and peptides lies in the size of the molecules. By convention peptides and proteins define proteinaceous substances smaller or bigger than 10 kDa, respectively (Sang & Blecha, 2008). Secondly, while bacteriocins are only produced by bacteria and target other bacteria, all type of living organisms produce AMPs targeting all kind of microorganisms including bacteria but also fungi, parasites and viruses. In higher organisms AMPs participate to the immunity of the host against infections, whereas in unicellular organisms AMPs and bacteriocins are mechanisms of direct competition (Mahlapuu et al., 2016). The last main difference between bacteriocins and AMPs is the synthesis pathway: while bacteriocins are strictly produced through ribosomal synthesis, AMPs can be produced by ribosomal or non ribosomal synthesis. The second category of AMPs are designated as NRPs and as we have seen in the antibiotic discovery section (section 1.1.), some NRPs like gramicidin have been used in the clinic for decades. To the contrary, bacteriocins and ribosomal AMPs have not been commercialized for the treatment of infections yet and will be discussed in more details in the second chapter. The ribosomally synthesized AMPs can be embodied in another class of biologically active peptides, namely the Ribosomally synthesized and Post-translationally modified Peptides (RiPPs) that will also be reviewed later in the second chapter. The common characteristics and main differences of bacteriocins, AMPs, RiPPs, NRPs are resumed in **Figure 1.10**. According to these, molecules that could be used as alternatives to antibiotics can belong to multiple classifications. For example, Ruminococcin A, a lanthipeptide that is ribosomally produced by the bacterium *R. gnavus* and active against the bacterium *C. perfringens* is a bacteriocin, a RiPP and an AMP (see subsection 3.2). Pinensins produced by *Chitinophaga pinensis* are antifungal ribosomal peptides and therefore belongs to AMPs and RiPPs but not bacteriocins (Mohr et al., 2015). Vancomycin, produced by *Amycolatopsis orientalis*, has a bactericidal activity and is included in NRPs and AMPs but not RiPPs and bacteriocins as it is not ribosomally synthesized (Okano et al., 2017).

	Bacteriocins	RiPPs	AMPs	NRPs
Size	No limitation	< 10 kDa		
Synthesis Pathway	Ribosomal		Ribosomal and non ribosomal	Non ribosomal
Activity	At least antibacterial	Antimicrobial, anticancer, allelopathic...	At least antimicrobial	
Producing organism	Bacteria only	Any organisms from the 3 domains of Life (i.e. archae, prokaryotes, eukaryotes)		

Figure 1.10: Common characteristics and differences of proteinaceous substances active against microorganisms

Ribosomally synthesized proteinaceous substances will be discussed in the second chapter, thus only a brief description of NRPs will be given here. Gramicidin D and tyrocidine, two NRPs, were discovered in 1939. However they were only qualified as peptides and not NRPs at that time. Studies of the biosynthesis of tyrocidine in 1963 revealed that it was independent of ribosomes as it wasn't affected by ribosome inhibitors (Mach et al., 1963). Since then, the discovery of NRPs and the elucidation of their biosynthesis have been extensively studied. NRPs are synthesized by Non Ribosomal Peptide Synthetases (NRPSs) in a mRNA- and ribosome-independent manner. NRPSs are multifunctional and modular enzymes, encoded in operons also frequently encoding building blocks and product decoration as well as resistance to and export of the NRP. Each module of the NRPS is responsible for the incorporation of a single building block, namely a proteinogenic or non proteinogenic amino acid, into the polypeptide chain (Winn et al., 2016; Süssmuth & Mainz, 2017). The modules of NRPSs are divided in 3 catalytic domains: an adenylation (A), a thiolation (T) or peptidyl carrier protein (PCP) and a condensation domain (C). The A domain selects the appropriate building block and transfers it to the T or PCP domain. Then, the C domain catalyzes the formation of a peptide bond between two building blocks carried by adjacent PCP or T domains. After all modules have incorporated and linked their building blocks, a thioesterase domain release the polypeptide (**Figure 1.11**). The polypeptide is synthesized from N to C terminus (Kittilä et al., 2016; Martínez-Núñez & López, 2016). After the peptide chain assembly, the polypeptide can be modified for example by the incorporation of branched fatty acids like in the case of daptomycin or decorated such as glycosylation of vancomycin. The final NRP can be either linear, cyclic or branched. One single and colossal NRPS can regroup all the modules necessary for synthesis of the polypeptide such as the NRPS of cyclosporin A that is produced by *Tolypocladium niveum* and weight 1.6 MDa or multiple protein subunits can be associated in a multi-enzymes system (Winn et al., 2016). NRPs are mainly produced by bacteria and fungi, although some NRPSs have been identified in higher organisms such as *Drosophila melanogaster* and *Caenorhabtidis elegans*. NRPs have been used to treat bacterial infections but also for other medical applications such as cancer treatment, pain management or immunosuppressive therapy. As seen in the subsection 1.1.3., the antibacterial modes of action and the spectra of activity differs among NRPs. Many NRPs are already widely used for the treatment of bacterial infections such as polypeptides, gly-

copeptides, lipopeptides but also β-lactams that are synthesized by NRPSs (Süssmuth & Mainz, 2017). Current research of NRPs for infectious diseases focus on expanding the known classes of NRPs and mining new ones with genomic tools. Novel NRPs can be generated by precursor directed biosynthesis which consists in providing a modified or synthetic amino acid as a substrate to the producer strain that could be incorporated thanks to substrate flexibility of the NRPs. Another strategy is the engineering of new NRPs by modifying or swapping their modules or catalytic domains (Winn et al., 2016).

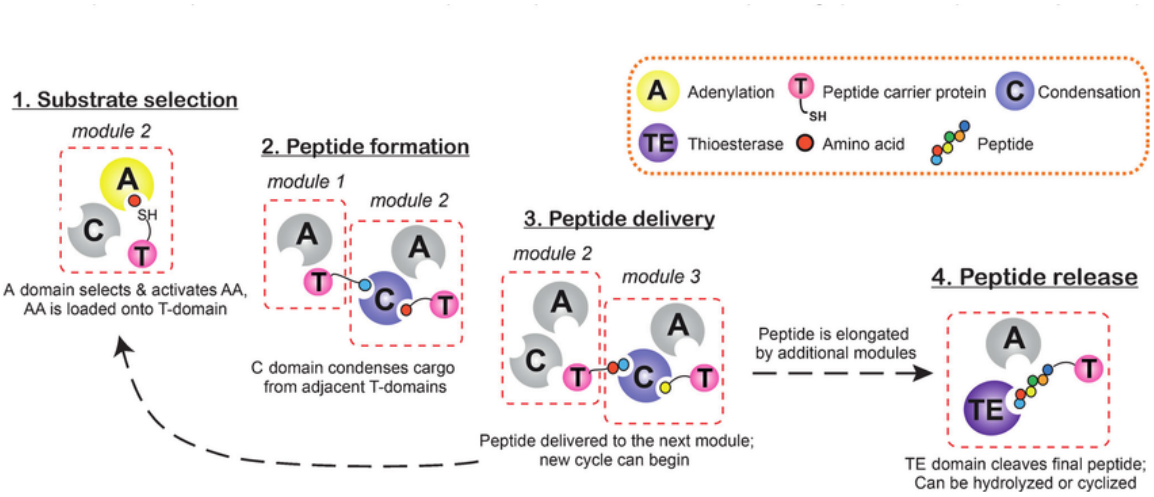

Figure 1.11: Biosynthesis of NRPS
Figure from Kittilä et al., 2016

Chapter 2

Ribosomal proteinaceous substances as novel antimicrobial agents

Ribosomal proteinaceous substances are peptides or proteins that are ribosomally translated in a mRNA-dependent manner. One of the major advantages of ribosomal proteinaceous substances compared to NRPs is that their amino acid sequences are directly related to genetic sequences. Therefore, the different classes of products can easily be expanded by site-mutations of the coding sequences or by fusions of domains of different products. Genetic manipulations of these sequences can lead to the generation of products with new functions, increased activity or improved stability. For example, the gene encoding the precursor of the RiPP MccB17 was mutated to integrate a 5th oxazole ring. The mutated RiPP has an antibacterial activity more potent by a factor of 1.5 compared to the native RiPP carrying 4 oxazole rings (Cotter et al., 2013). Another example concerns the well-known RiPP nisin. All natural variants of nisin exert antibacterial activity limited to Gram positive bacteria. Two single mutations in the sequence encoding the precursor of the variant nisin Z were sufficient to generate two novel variants of nisin exhibiting activity toward Gram negative bacteria. Furthermore, these biosynthetic variants also feature increased stability to heat (Yuan et al., 2004).

In this chapter, bacteriocins and RiPPs will be discussed. It should be mentioned that other ribosomally-synthesized peptides that are not produced by bacteria and that don't belong to RiPPs exist. These antimicrobial peptides can be produced for example by mammals, insects, amphibians, vertebrates, fungi, plants, arachnids and are classified as cationic peptides, defensins, cathelicidins, toxins (L.-j. Zhang & Gallo, 2016). Although these peptides have common features with bacteriocins and RiPPs as their synthesis is ribosome-dependent and as most of them are synthesized first as a precursor, sometimes even a larger protein with a distinct function, that undergo proteolytic cleavage, these peptides will not be discussed in this manuscript.

2.1 Bacteriocins

2.1.1 Generalities and classification

There are currently 230 bacteriocins referenced on the database Bactibase. Their sizes range from 7 to 688 amino acid residues although 75% of bacteriocins are comprised in the 20 to 60 amino acid residues length. Among these bacteriocins, 90% are produced by Gram positive bacteria (Hammami et al., 2007). Bacteriocins can be active against closely related or distant bacteria. The genes encoding the bacteriocin synthesis can be carried on the bacterial chromosome or on a plasmid. Bacteria possess genetically encoded immunity system to their own bacteriocins, however the release of some bacteriocins can lead to the death of the producer strain (Cascales et al., 2007). Bacteriocins cross the peptidoglycan wall and the outer membrane of Gram negative bacteria through electrostatic interactions and/or specific receptors. Then they can either form pores in the cytoplasmic membrane or enter in the cytoplasm. Pore formation can lead to the leaking of cytoplasmic content or the loss of membrane potential. Bacteriocins that enter the cytoplasm can have a nuclease activity (DNase or Rnase) or inhibit the macromolecules (DNA, RNA, proteins, cell wall) synthesis pathways (Cotter et al., 2013). Bacteriocins are classified according to the type of producing bacteria: Gram positive versus Gram negative and then can be subclassified in proteins, unmodified peptides and RiPPs (**Figure 2.1**). RiPPs will be further and extensively discussed in section 2.2 as the focus of my thesis, the Ruminococcins, falls into this category. Proteins and unmodified peptides will be briefly presented in this section.

2.1.2 Unmodified peptides from Gram positive bacteria

As previously mentioned, bacteriocins are ribosomally produced and most of them correspond to peptides with a molecular weight under 10 kDa. Most bacteriocins from that category are synthesized as a precursor peptide from which a leader domain is cleaved (Cotter et al., 2013; Alvarez-Sieiro et al., 2016). Class II bacteriocins are considered as "unmodified" - as opposed to RiPPs (class I) - since no post-translational modifications (PTMs) are introduced by enzymes on the amino acids residues contained in the sequence that remains after removal of the leader domain. However, it could be argue that they belong to the RiPPs classification if partial proteolysis of the precursor peptide is considered as a PTM (Rogers & Overall, 2013; Klein et al., 2018) and because these bacteriocins may harbor disulfide bonds or head-to-tail cyclization. Class II bacteriocins can be further divided in subclasses according to common structures or sequences (**Figure 2.1**).

Class IIa (**Figure 2.2A**) comprises peptides composed of a cationic N-terminal region harboring two Cys (cysteine) linked by a disulfide bond as well as a Tyr-Gly-Asp-Gly-Val (Tyr: tyrosine, Gly: glycine, Asp: asparagine, Val: valine) motif presumably involved in target interaction (Cui et al., 2012). Class IIa bacteriocin may carry a second disulfide bond (Bédard et al., 2018). Their C-terminal domain is variable and plays a role in bacterial cell target specificity. The leader domain of class IIa peptides as been shown to play a role as a secretion signal. It is recognized by adenosine triphosphate (ATP)-binding cassette (ABC) transporters that also perform the leader peptide removal. Class IIa bacteriocins often have a broad-spectrum action against Gram positive bacteria and

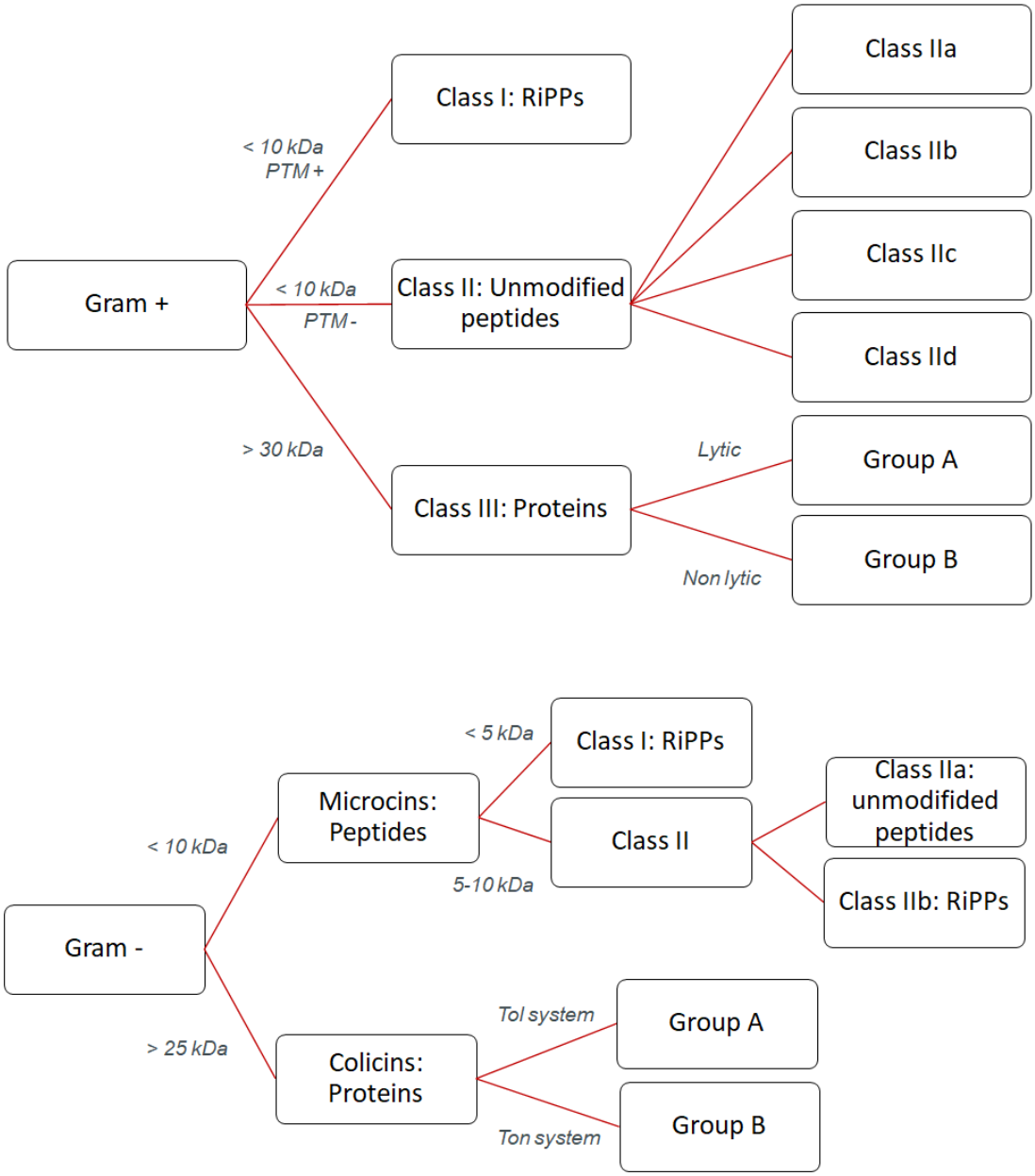

Figure 2.1: Classification of bacteriocins
PTM + and PTM - designate respectively the presence or the absence of post-translational modifications

form pores in the cytoplasmic membrane (Alvarez-Sieiro et al., 2016).

Class IIb bacteriocins are produced as two different peptides encoded in the same operon that both contain a Gly-X-X-X-Gly (X: any amino acid) motif involved in a helix-helix structure (**Figure 2.2B**). This specific structure allows penetration in the cytoplasmic membrane of Gram positive bacteria resulting in cell permeabilization. Although some peptides can exhibit antibacterial activity by themselves, both peptides are required for optimal activity. Such as class IIa peptides, the leader peptide of class IIb peptides is involved in secretion and cleaved by an ABC transporter, specifically after a Gly-Gly motif (Nissen-Meyer et al., 2010; Ekblad et al., 2016).

Peptides from class IIc are synthesized as precursor peptides and then circularized by an amide bond between their N- and C-termini after leader peptide removal (**Figure 2.2C**). The exact pathways leading to head-to-tail cyclization remain elusive for most class IIc bacteriocins. Circularization and secretion by ABC transporter can be coupled or independent steps (Perez et al., 2018). Their classification as unmodified peptides can be debated and some researchers classify them as class II bacteriocins whereas others classify them as RiPPs (Arnison et al., 2013; Cotter et al., 2013). These bacteriocins are mainly active against diverse Gram positive bacteria but some of them can also exert antibacterial activity against Gram negative strains. Like most class II bacteriocins from Gram positive bacteria, circular bacteriocins have a pore-forming activity (Belkum et al., 2011).

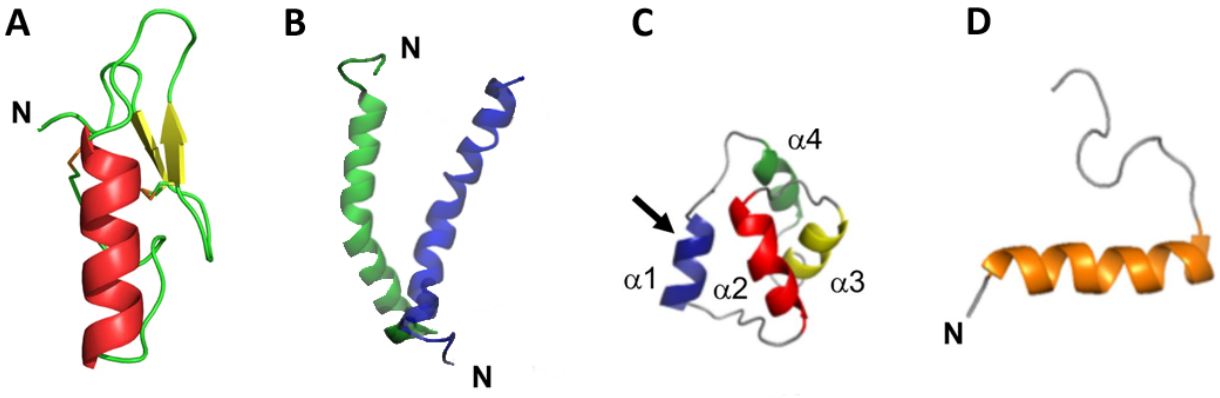

Figure 2.2: Structure of class II bacteriocins

*Representation of NMR structures of the synthetic pediocin PA-1 M31L analog (class IIa, **A**, PDB: 5UKZ); plantaricin EF (class IIb, **B**, PDB: 2RLW); acidocin B (class IIc, **C**, PDB: 2MWR); LsbB (class IId, **D**, PDB: 2MLU). N indicates N-termini whereas the arrow indicates N- to C-terminus cyclization. Figure adapted from Bédard* et al., *2018; Ekblad* et al., *2016; Perez* et al., *2018.*

Finally class IId regroups unmodified peptides that don't belong to subclasses IIa, b or c (Cotter et al., 2013). These bacteriocins can be composed of a single or two or even multi linear peptides and their modes and spectra of action, as well as secretion mechanisms differ. This group includes "leaderless peptides" that don't undergo proteolysis after peptide synthesis (**Figure 2.2D**). Most leaderless peptides are cationic and harbor a N-terminal formylated Met (Met: methionine). Little is known regarding the secretion of this leaderless peptides and the immunity of the cells against its own peptide (Perez et al., 2018). Indeed it has been proposed that the leader peptide is part of a protective strategy of the producer cell toward its own ribosomal antimicrobial peptide as it stays inactive while still attached to the leader peptide (cf subsection 2.2.2 Roles of the leader

peptide). In the absence of a leader peptide, the production of a ribosomal antimicrobial peptide can then be toxic for the cell or the cell must dispose of an intracellular immunity system.

2.1.3 Proteins from Gram positive bacteria

Class III bacteriocins of Gram positive bacteria are proteins with a size superior to 30 kDa. As shown of **Figure 2.1**, Class III bacteriocins are divided in Group A and B (Rea, Ross, et al., 2011; S.-C. Yang et al., 2014). Group A regroups enzymes also called bacteriolysins (**Figure 2.3**) that are able to digest the peptidoglycan cell wall inducing cell lysis. Most bacteriolysins have an endopeptidase activity similar to phage lysins (**Figure 1.7**). Their activity is specific of Gram positive bacteria as the outer membrane of Gram negative bacteria prevent them from reaching the cell wall. As their mode of action is specific to bacteria, they seem safe for mammalian organisms but they present inconvenient as alternatives to antibiotics as they are unstable and prompt to enzymatic digestion (Bastos et al., 2010; Alvarez-Sieiro et al., 2016; Tossavainen et al., 2018). On the other hand, bacteriocins belonging to Class III Group B are non lytic proteins that inhibit DNA or protein synthesis or sugar uptake in Gram positive bacteria. They harbor 3 distinct domains: the R domain recognizes and binds specific bacterial receptors; the T domain ensures translocation inside the bacterial target; the C domain has a cytotoxic activity (Alvarez-Sieiro et al., 2016).

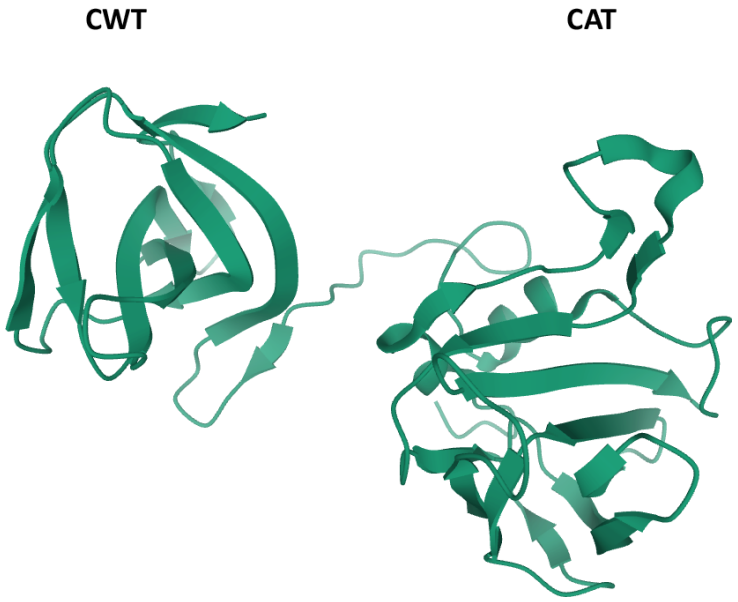

Figure 2.3: Structure of the bacteriolysin lysostaphin
Representation of NMR structure (PDB: 4LXC). CWT and CAT respectively indicates the Cell-Wall-Targeting and catalytic domains. Figure adapted from Tossaveinen et al., *2018.*

2.1.4 Microcins: peptides from Gram negative bacteria

Originally, the term microcins was proposed to distinguish the bacteriocins produced by Enterobacteriacea as opposed to colicins. Microcins refer to small antibacterial proteinaceous substances with a low molecular weight, resistant to proteases, pH and temperature whereas colicins regrouped bigger proteins with low stability (Rebuffat, 2011). Currently microcins regroup peptides ribosomally synthesized by Gram negative bacteria with a size up to 10 kDa. Like class I and most class II peptides from the Gram positive classification, microcins are produced as a precursor from which a leader peptide is removed after translation. Some microcins undergo PTMs and are therefore classified as RiPPs whereas other are unmodified, respectively such as class I and class II bacteriocins from Gram positive bacteria. However, microcins are a much smaller group of bacteriocins that class I and II from Gram positive bacteria and only 15 members have been identified so far with 8 chemically characterized (Baquero et al., 2019), compared to hundreds of RiPPs and unmodified peptides identified from Gram positive bacteria. Common features of microcins are found in their genetic cluster which are mainly carried on plasmids and all comprise at least genes encoding: the peptide precursor, one protein involved in self-immunity, several proteins involved in export. As shown of **Figure 2.1**, microcins are then subclassified in class I and II (Duquesne et al., 2007). Class I corresponds to peptides with a molecular weight inferior to 5 kDa that harbor PTMs. Therefore this class will be described in the RiPPs section (see 2.2.3 Classification). Class II regroups peptides with a molecular weight between 5 and 10 kDa. Class I microcins display long and diverse leader peptides (from 19 to 37 residues), whereas class II microcins exhibit short and conserved leader peptides (15 to 19 residues). For both class I and class II, in most cases the leader peptide is cleaved by an ABC transporter after a Gly-Gly or Gly-Ala motif (Arnison et al., 2013). Such as class IIa from Gram positive bacteria, class IIa microcins might harbor 1 or 2 or no disulfide bridges but no other PTMs (**Figure 2.4**). Class IIb regroups peptides with C-terminal PTMs and will be described in the RiPPs section (see 2.2.3 Classification). So far, 5 members have been identified in the class IIa microcins. These bacteriocins are active against Gram negative bacteria with variations in their spectra and their activity is dependent of receptors and proteins situated in the outer membrane of Gram negative bacteria. The mode of action of class IIa microcins has been identified for two members and for both it consists in disruption of membrane potential (Baquero et al., 2019).

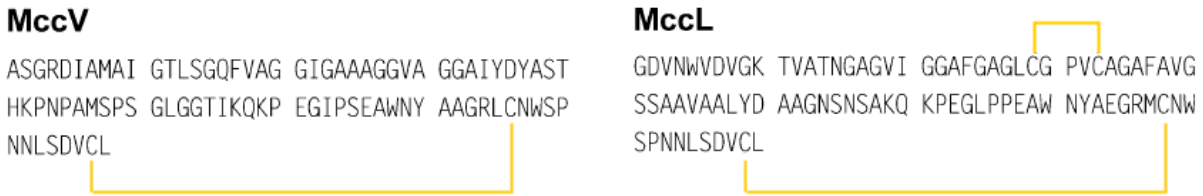

Figure 2.4: Sequences and disulfide networks of class IIa microcins MccV and MccL

Disulfide bridges are indicated by yellow lines. Figure adapted from Duquesnes et al., *2007.*

2.1.5 Colicins: proteins from Gram negative bacteria

Colicins are bacteriocins produced by Gram negative bacteria and are proteins ranging from 25 to 80 kDa. Colicins are mainly produced by *E. coli* although other Enterobacteriaceae like *Shigella*, *Salmonella* and *Citrobacter* have been found to produce them as well. Most colicins are encoded on plasmids and their production is lethal for the producer cells. Like class III bacteriocins from Gram positive bacteria, colicins harbor 3 distinct domains: the R or recognition domain; the T or translocation domain; the C or cytotoxic domain. The cytotoxic activity can be conveyed through membrane pore formation, inhibition of cell wall synthesis or digestion of DNA or RNA (**Figure 2.5**). The R domain can be specific for Tol or Ton receptors, classifying colicins in respectively Group A or Group B (**Figure 2.1**). Colicins target bacteria closely-related to the producer strain. They show low-toxicity toward mammalian cells, in accordance with their R domain being specific for bacterial receptors. Hence, colicins could be useful alternatives to antibiotics even though their delivery is challenging as they are relatively big and unstable proteins (Zakharov & Cramer, 2002; Cascales et al., 2007; Calcuttawala et al., 2015; Jin et al., 2018).

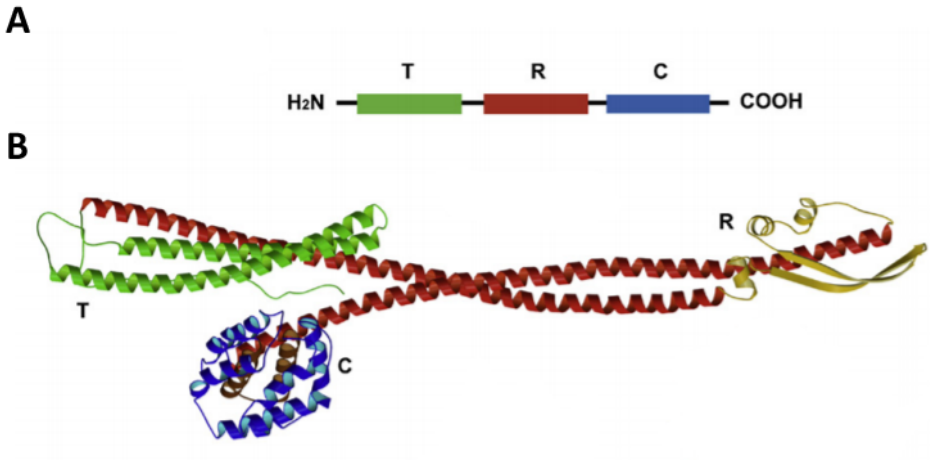

Figure 2.5: Structure of colicins

*General organization of colicin (**A**) and X-ray crystal structure of colicin Ia (**B**, PDB: 1CII). T (green), R (red) and C (blue) respectively indicate the translocation, recognition and cytotoxic domains. Figure adapted from Zakharov* et al., *2002.*

2.2 Ribosomally synthesized and post-translationally modified peptides (RiPPs)

The following section of my thesis is incorporated with slight modifications as a chapter named "Antimicrobial Ribosomally synthesized and Post-translationally modified Peptides as a source of alternatives to antibiotics: a focus on the sactipeptides and ranthipeptides subclasses" in the book entitled "Peptide and protein engineering for biotechnological ant therapeutical applications" soon to be published by World Scientific. The temporary table of content of the book is provided in Appendix 1, as well as the abstract of the chapter. The rest of the chapter is not joined to this manuscript as it is highly similar to this section. The main modifications between this section and the book chapter consist in the addition of data on Ruminococcin C acquired during my thesis project that are presented in the Chapter 5 and 6 of this manuscript.

2.2.1 Definition of RiPPs and generalities

RiPPs are peptides defined by a size limit of 10 kDa that are ribosomally translated in a mRNA-dependent manner and undergo various post-translational modifications (PTMs). They are produced by organisms from the 3 domains of Life (archaea, prokaryotes and eukaryotes) and exert multiple types of biological activities including antibacterial and antimicrobial activities but also insecticidal, nematoxic and anti-cancer effects among others (**Figure 1.10**). The PTMs carried by RiPPs and the structure of RiPPs are highly diverse and determine their classification that will be presented below. However, all RiPPs share a common biosynthesis pathway (Arnison et al., 2013; Luo & Dong, 2019). This pathway starts with the transcription and translation of a structural gene in a precursor peptide composed of 20 to 110 amino acid residues. The precursor peptide is composed of at least two distinct domains named leader peptide and core peptide. The core peptide defines the region that is subjected to PTMs whereas the leader peptide defines a region that is cleaved by proteolysis subsequently to the core peptide modification. In most RiPPs, the leader peptide is located at the N-terminus of the core peptide, but it can also be located at the C-terminus as in the case of bottromycins (Arnison et al., 2013). While most PTMs occur when the leader peptide is still attached to the core peptide, some modifications that require the free N-terminus of the core peptide, can happen after the excision of leader peptide. Such examples are found in the cyanobactin and lanthipeptide subclasses whose RiPPs might undergo head-to-tail cyclization and N-terminus alterations, respectively (X. Yang & van der Donk, 2013). Additionally, some RiPPs have a recognition sequence at the C-terminus that is required for cleavage and cyclization of the peptide such as amatoxins, phallotoxins, borosins or orbitides (Luo & Dong, 2019). In some cases, like cyanobactins, recognition sequences can be present at both N- and C-termini (Gu et al., 2018). In RiPPs produced by eukaryotes, such as cyclotides or conopeptides (Luo & Dong, 2019), a signal domain can be also found at the N-terminus that directs the precursor peptide to a specific cellular compartment where modifications of the core peptide occur. The fully mature and active RiPP corresponds to the modified core peptide excised from all the other domains, i.e. signal, recognition and leader (**Figure 2.6**).

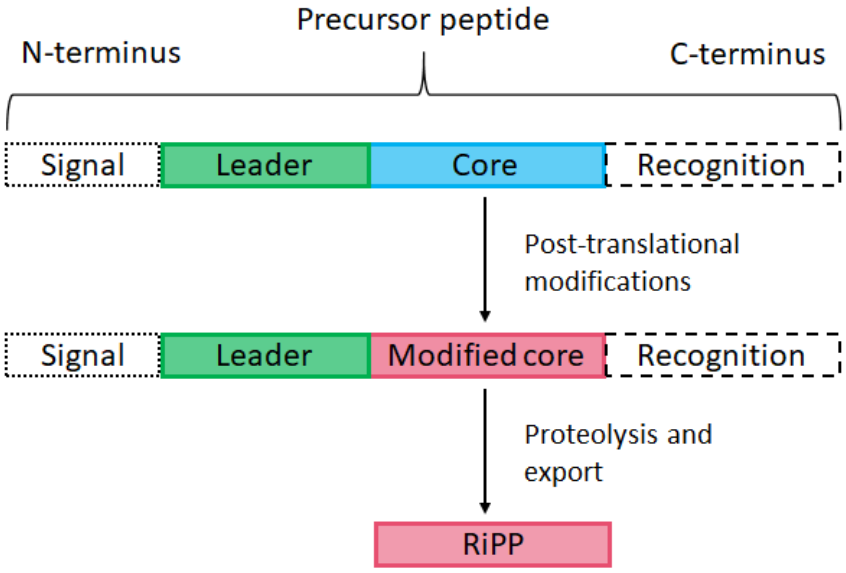

Figure 2.6: RiPP biosynthesis pathway

Common modular organization and maturation pathway of RiPPs. Solid lines indicate sequences found in all RiPPs whereas dashed lines represent optional sequences. In some cases the leader is found at the C-terminus of the core peptide rather than at the N-terminus.

The genes involved in the production and maturation of RiPPs are in most cases regrouped in genetic clusters. The number of genes composing these genetic clusters greatly vary but at least two Open Reading Frames (ORFs) are found for all RiPPs: the structural sequence and a sequence encoding a modification enzyme (also called maturation enzyme) (Truman, 2016). Multiple sequences encoding precursor peptides can be found instead of a single copy. Likewise, multiple maturation enzymes with similar activity or not can be encoded in RiPP biosynthesis genetic clusters (BGC). In some examples, the genes involved in RiPP biosynthesis are not clustered but rather distant in the genome. For example, in the genome of *Bacillus anthracis* the sequence encoding the precursor peptide of heterocycloanthracin is located 1.27 Mbases upstream of two clustered ORFs encoding distinct enzymes both involved in PTMs formation: a cyclodehydratase and a dehydrogenase (Haft, 2009). Another example is found in the genome of the cyanobacterium *Prochlorococcus*. A gene encoding a modification enzyme typical of the subclass lanthipeptide is clustered with 7 sequences encoding putative peptide precursors. However, 22 other similar structural sequences are found elsewhere in the bacterial genome (Li et al., 2010). Additionally, genes involved in the regulation of production, in proteolysis and export as well as in the cell immunity to its own RiPP are also commonly found in the RiPP BGC (Bartholomae et al., 2017).

2.2.2 Roles of the leader peptide

The leader peptides among RiPPs greatly vary in length as well as in amino acid composition. Several roles have been proposed for the leader peptide. First, the removal of the leader sequence in most RiPPs prevents or highly diminishes the incorporation of PTMs

on the core peptide (X. Yang & van der Donk, 2013). Therefore, it has been hypothesized that the leader peptide acts as a recognition sequence for the maturation enzymes or as an activator of these enzymes. This hypothesis was corroborated by the successful modification and export of non-natural peptides expressed as fusions with the leader peptide of the extensively studied lanthipeptide nisin in its natural producer strain *Lactococcus lactis* (Moll et al., 2010). Many RiPPs with high variability in the core peptide sequence exhibit the same PTMs. As it is unlikely that the enzyme could have such substrate tolerance, it has been proposed that the enzymes could recognized conserved motifs in the leader peptide of different RiPPs and exert their catalytic activities on the core peptide (Ortega & van der Donk, 2016). In fact some classes of RiPPs, such as lanthipeptides, exhibit conserved leader sequences but variable core sequences (Q. Zhang et al., 2014). In particular, in the case of prochlorosins cited earlier, the 29 putative peptide precursors share more than 90% of similarity in their leader sequence whereas no conserved motifs has been found in the core sequences. The single lanthipeptide modification enzyme is able to process the different precursors by incorporating the same type of PTMs, but at different positions resulting from the core sequence variability (Li et al., 2010; Tang & van der Donk, 2012; Q. Zhang et al., 2014). Moreover, a binding motif of the maturation enzyme to the leader peptide has been identified in some RiPPs such as for class I lanthipeptides. Their leader sequences almost all contain a Phe-Asp/Asn-Leu-Asn/Asp motif (with Phe: phenylalanine, Asp: aspartic acid, Leu: leucine). Mutation of this motif in NisA - the precursor of nisin - prevented binding to the dehydratase NisB which is the first enzyme catalyzing the two-steps modification of this lanthipeptide, suggesting that this motif is essential for substrate recognition (Mavaro et al., 2011). Co-crystallization of NisA with NisB provided more information on their interaction: the leader domain of NisA binds to NisB as an anti-parallel β-strand at a position ensuring that the core peptide is in contact with the catalytic site of NisB. The Phe-Asp/Asn-Leu-Asn/Asp conserved motif of the NisA leader peptide is involved in hydrophobic interactions with NisB (Ortega et al., 2015). Additional crystallization studies on other coupled precursor peptides and maturation enzymes, such as the cyanobactin heterocyclase LynD with an artificial precursor PatE' as well as the adenyltransferase MccB with MccA, the precursor of microcin C7, showed that the binding of the leader peptide to the enzyme involves similar interactions and structures (Regni et al., 2009; Koehnke et al., 2015). Specifically, the domain of the enzymes involved in leader peptide binding corresponds to a winged helix-turn-helix. It was then proposed that RiPP maturation enzymes harbor a specific RiPP precursor peptide Recognition Element (RRE). Analyses of known RREs revealed structural similarity with the small protein PqqD that is also involved in the multi-enzymes maturation of a RiPP - the pyrroloquinoline quinone (PQQ) - as a chaperone (**Figure 2.7**) (Evans et al., 2017). In silico analyses based on the structure of PqqD revealed that at least half of the prokaryotic subclasses of RiPPs are modified by enzymes containing a RRE (Burkhart et al., 2015). Interaction of the leader peptide and the maturation enzyme through a PqqD-like RRE were confirmed in 5 other subclasses of RiPPs: lasso peptides, linear azoline-containing peptides, thiopeptides, sactipeptides (see subsection 2.2.4) and ranthipeptides (see subsection 2.2.5) (Burkhart et al., 2015; Link, 2015; Wieckowski et al., 2015; Grove et al., 2017). For example, it was shown that the precursor of therbactin from the lasso peptides subclass binds to a PqqD-like RRE through hydrophobic interactions of a Tyr-X-X-Phe-X-Leu-X-X-X-Gly leader peptide motif that is essential and sufficient for the recognition by the maturation enzyme. Therefore, recognition of the leader peptide by the maturation enzyme is mediated through steric complementarity rather than

sequence specificity (Chekan et al., 2019). Notably, many RRE domains were identified in the family of radical-SAM enzymes involved in the maturation of several subclasses of RiPPs including bottromycin, proteusin, sactipeptide, ranthipeptide (Burkhart et al., 2015; Grove et al., 2017). Intriguingly, the elucidation of both structures of the streptide SuiA and its maturation enzyme belonging to the radical-SAM family SuiB revealed a binding of the leader peptide in a location that is distinct from the archetypal PqqD-like RRE domain (**Figure 2.7**) (Schramma et al., 2015; Davis et al., 2017; Schramma & Seyedsayamdost, 2017). This unique SuiA-binding mode suggests that the RRE-like domain is involved in an undetected interaction in which it both recognizes the peptide and delivers it to the active site but at a certain stage in the catalytic cycle releases the precursor peptide.

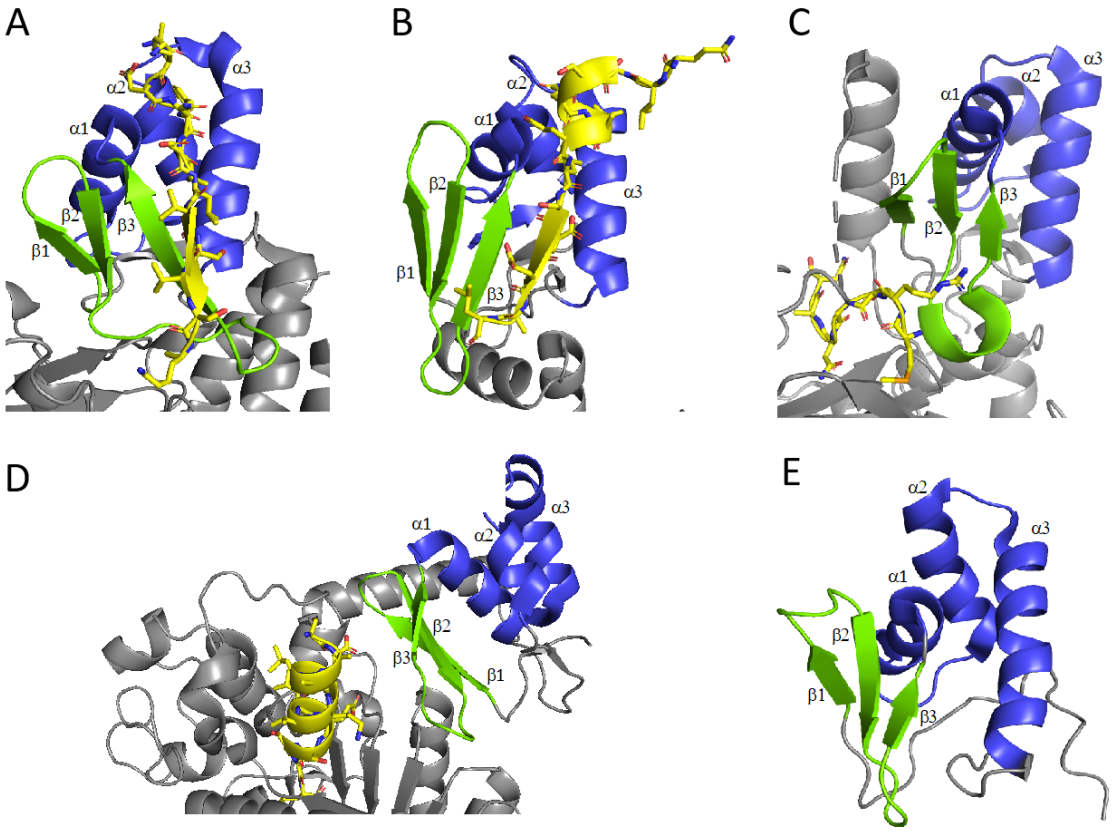

Figure 2.7: RRE of several RiPP maturation enzymes
*Structure of RRE of NisB (**A**, PDB: 4WD9), LynD (**B**, PDB: 4V1T), MccB (**C**, PDB: 3H9J), SuiB (**D**, PDB:5V1T) and structure of the protein PqqD (**E**, PDB: 5SXY). Partial structure of the enzymes are shown in grey. The RRE is composed of β-sheets (green) and α-helices (blue). Yellow indicate the position of the leader domain of the associated precursor peptides.*

It has also been proposed that the leader peptide not only acts as a recognition sequence but might also induce enzyme conformational changes on the maturation enzymes, leading to its catalytic activation or increased affinity of the catalytic domain for the core peptide. This hypothesis is supported by the trans-activity of the leader peptides of some RiPPs. It has been shown that nisin, lacticin, and catenulipeptin, respectively class I,

class II and class III lanthipeptides, are modified by their maturation enzymes when their leader sequence is not contained in the precursor peptide sequence but rather expressed or provided by itself. However, studies on nisin and lacticin also revealed low levels of PTMs incorporation even in the absence of the leader sequence. Therefore, a second model was proposed in which the leader peptide would not induce conformational changes but rather trap the enzyme in the active conformation. In this model, maturation enzymes would exist in multiple evolving conformations, hence the appropriate state for catalytic activity would be in low concentration. Binding of the leader peptide to the active enzyme would form a stable complex, and the concentration of active enzyme would then increase as the concentration of leader peptide increases as well. This trans activity of the leader peptide has been proven for other subclasses of RiPPs such as microcin MccJ25 but not for all subclasses. It is possible that this mechanism is specific of a few classes of RiPPs or that the region needed for optimal enzyme conformation actually covers partial sequence of the leader peptide and of the core peptide. Indeed, in the native biosynthetic pathways of RiPPs the distinction between leader and core peptide only occurs during proteolysis after PTMs incorporation (**Figure 2.6**) (X. Yang & van der Donk, 2013; Ortega & van der Donk, 2016). The role of the leader peptide as an anchor, or an activator for maturation enzymes, provides options for the generation of new RiPPs by its fusion to non-natural core peptides or even by designing hybrid RiPP biosynthetic pathways. In that sense, Burkhart and co-workers built a chimeric leader peptide with elements of recognition for maturation enzymes from different RiPP pathways (**Figure 2.8**), such as a thiazoline modification enzyme associated with either lanthipeptide or sactipeptide modification enzymes. After optimization of a non-natural core peptide and co-expression of the genes encoding the precursor peptide and the two enzymes related to the two different pathways in *E. coli*, both types of PTMs were successfully introduced on the chimeric precursor (Burkhart et al., 2017).

Figure 2.8: Hybrid RiPP biosynthetic pathway strategy for novel RiPPs generation

Figure from Burkhart et al., 2017

The second role proposed for the leader peptide is a protective role for the producer. As a matter of fact, most RiPPs are inactive when attached to their leader peptide and its removal occurs during or after secretion, thus ensuring that the RiPP won't attack the producer cell itself. From that role a third one comes up: the function as a secretion signal (Oman & van der Donk, 2010; Ortega & van der Donk, 2016). In the case of nisin, an extracellular protease and an ABC transporter are encoded in the BGC. Diverse modified and unmodified peptides fused to the leader peptide of the nisin precursor were successfully exported in the extracellular compartment when co-expressed with the nisin transporter in an heterologous system. Therefore, the leader peptide of the nisin precursor indeed harbor a secretion signal (Kuipers et al., 2004).In the nisin biosynthetic pathway, the protease NisP is exported and bound to the cell-wall of the producing bacterial cells. Other class I

lanthipeptides can be cleaved through cytoplasmic proteases or proteases secreted in the extracellular compartment (Montalbán-López et al., 2018). Whereas for lanthipeptides from class I like nisin a protease is encoded in the genetic cluster, no such protease-coding sequence is found for class II. However, the transporters encoded in the cluster harbor a N-terminal peptidase domain. In vitro incubation of the purified lacticin precursor with the N-terminal domain of its ABC transporter (150 out of 691 total amino acid residues) was sufficient to achieve leader peptide removal. Thus, the export and proteolysis of lacticin are coupled and executed by a bi-functional enzyme. The transmembrane domain of the transporter is not required for leader peptide recognition and cleavage. Proteolysis of the leader peptide of the lacticin precursor occurs after two Gly residues. Mutations of these residues prevent the excision of the leader peptide (Furgerson Ihnken et al., 2008). Similar cleavage sites involving a Gly-Gly motif or sometimes a Gly-Ala motif have been identified in other lanthipeptides but also in other RiPPs as well as in class IIb bacteriocins from Gram positive bacteria (see subsection 2.1.3). Therefore, this conserved motif seems to play an important role in proteolytic processing of the precursor. The ABC transporters processing this Gly-Gly motif were found in multiple classes of RiPPs biosynthetic pathways and renamed Peptidase-Containing ATP-binding Cassette (PCAT). Common features of PCAT include 3 distinct domains: a transmembrane domain, a C-terminal nucleotide binding domain achieving ATP hydrolysis and a N-terminal cysteine protease domain cleaving the leader peptide after a Gly-Gly motif. The PCAT transporters form dimers and their overall structure resembles ABC transporters lacking the peptidase domain (Ortega & van der Donk, 2016). Although mutation of the Gly-Gly motif prevents cleavage in many RiPPs, it doesn't affect the incorporation of PTMs on the core peptide by maturation enzymes, suggesting that distinct sequences of the leader peptides are involved in different roles (Oman & van der Donk, 2010). Other motifs necessary for the removal of the peptide leader have been identified. For example, in the class I lanthipeptide epilancin 15X precursor, the excision of the leader peptide is mediated through an Asp-Leu-Asn-Pro-Gln-Ser (Pro: proline, Gln: glutamine, Ser: serine) sequence recognized by the peptidase ElxP. The introduction of this sequence in the NisA precursor allowed the cleavage of NisA by ElxP, whereas wild-type NisA was not processed by ElxP (Ortega et al., 2014). The excision of the leader peptide by proteolysis can be a one step or a multi-steps process. For example, the precursor of lichenicidin, a class II lanthipeptide, is partially cleaved after a Gly-Gly motif by the peptidase domain of a transporter and then the last 6 amino acid residues of the leader peptide are removed after secretion by an extracellular protease (Chen et al., 2019).

2.2.3 Classification

RiPPs are classified according to their PTMs and their related biosynthetic machineries. A brief description of each class of RiPPs is given here and a summary table is included at the end of this subsection. As sactipeptides and ranthipeptides (see subsections 2.2.4 and 2.2.5) will be further discussed they are not included in this subsection.

1. Lanthipeptides: Lanthipeptide, one of the most studied class of RiPPS, stands for lanthionine-containing peptide as these RiPPs carry lanthionine (Lan) and/or 3-methylanthionine (MeLan) residues (**Figure 2.9**). Lan corresponds to two alanine residues bound by a thioether bridge between their β-carbons and MeLan to a Lan carrying an additional methyl group. In lanthipeptides, the thioether crosslinks of Lan and MeLan are formed by the addition of a Cys onto previously dehydrated amino acids, respectively a Ser in 2,3-didehydroalanine (Dha) and a threonine (Thr) in 2,3-didehydrobutyrine (Dhb). In class I lanthipeptides, the formation of Lan and MeLan residues is catalyzed by two enzymes: a dehydratase and a cyclase. For class II to IV, a single bi-functional enzyme, named lanthionine synthetase, carries out the formation of Lan and MeLan. Class II lanthionine synthetases harbor a N-terminal dehydration domain with no homology among the synthetases from the other classes and a C-terminal domain similar with the class I cyclases. Class III and IV are distinctive in their C-terminal cyclase domains but harbor similar phospholyase and kinase domains in the N-terminus both responsible for dehydration. Lanthipeptides can carry dehydrated residues (Dha or Dhb) that are not involved in thioether bridges if the number of Ser and Thr exceed the number of Cys (**Figure 2.9**). Lanthipeptides exhibit antibacterial activity but also antifungal and antiviral activities as well as other types of functions than antimicrobial such as pain relief. Identified antibacterial mode of action of lanthipeptides involves binding to the cell-membrane resulting in pore formation and cell wall synthesis inhibition. Currently, all the identified lanthipeptides are produced by bacteria although putative homologues of lanthipeptide synthetases have been found in the genomes of archaea and eukaryotes including mammals. Lanthipeptide BGCs are found in both Gram positive and negative bacteria (Bierbaum & Sahl, 2009; Arnison et al., 2013; Repka et al., 2017).

2. Linear azol(in)e-containing peptides (LAPs): LAPs harbor thiazol(in)e and (methyl)-oxazol(in)e heterocycles resulting from the cyclization of Cys with the side chains of Ser or Thr (**Figure 2.10**). LAPs can undergo other PTMs including acetylation, methylation, and dehydration (Arnison et al., 2013). This subclass of RiPPs is produced by both Gram negative and positive bacteria. The identified spectra and the modes of action of LAPs differ among them. For example, microcin B17 inhibits DNA synthesis and especially DNA gyrase with a mechanism similar to the quinolone ciprofloxacin (see subsections 1.1.3 and 1.1.4), whereas plantazolicin acts by depolarization and phazolicin as well as klebsazolicin inhibit protein synthesis (Pierrat & Maxwell, 2003; Molohon et al., 2016; Travin et al., 2019).

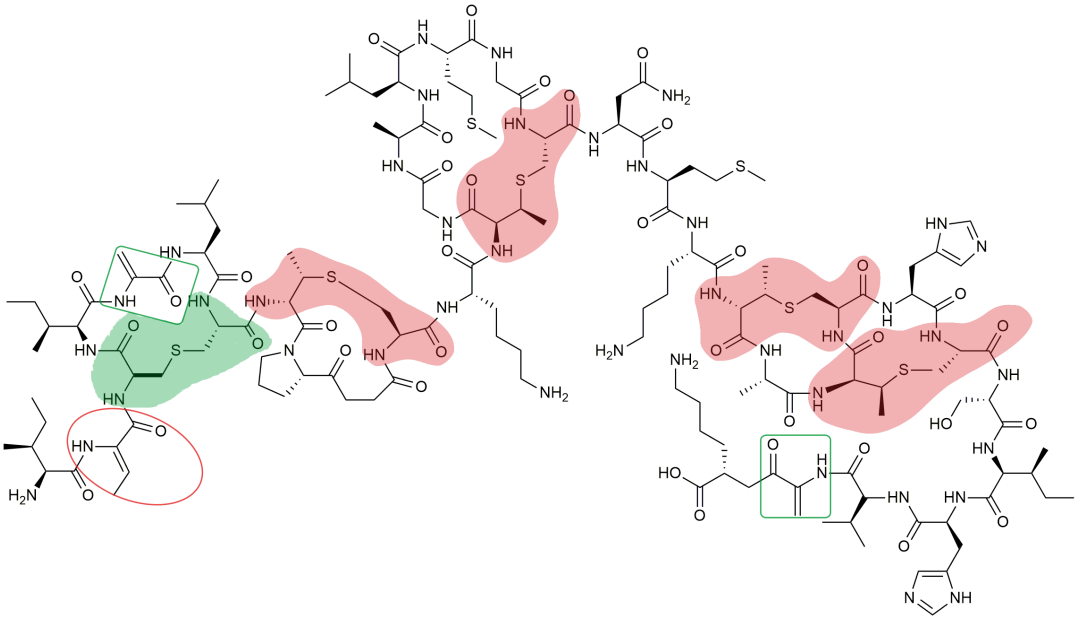

Figure 2.9: Structure of the lanthipeptide nisin A

Lan and MeLan residues are respectively highlighted in green and red while unreactive Dha and Dhb are circled in green and red.

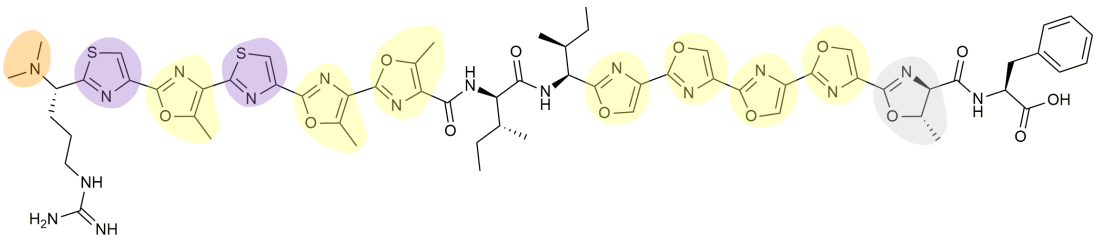

Figure 2.10: Structure of the LAP plantazolicin

N-terminal methylation; thiazole; oxazoles and methyloxazoles; methyloxazoline are highlighted in orange, lilac, light yellow and light grey, respectively.

3. Proteusins: Currently only one family of proteusins, the polytheonamides, has been identified and is produced by the uncultured sponge symbiont *Candidatus* Entotheonella factor. The polytheonamides are the most extensively modified RiPPs as nearly 50 PTMs are performed on their precursors. Their precursor is composed of a large peptide leader and the 48 residues core peptide is modified by multiple types of enzymes, including radical S-adenosylmethionine (SAM) enzymes that is a family also involved in the maturation of other RiPPs such as bottromycins and sactipeptides. Among their many PTMs, polytheonamides contain methylation of carbons and nitrogen atoms and in particular epimerization of 18 amino acid residues as shown on **Figure 2.11** (Helf et al., 2017). The structure of polytheonamide B was revealed by Nuclear Magnetic Resonance (NMR) and consists in a β-helix stabilized by hydrogen bonds between the alternating L- and D-amino acids (Hamada et al., 2010), similar to the structure of the NRP gramicidin D (Arnison et al., 2013). Such as gramicidin D, polytheonamide B has a cytotoxic activity toward mammalian cells. Polytheonamide B inserts in the cell membrane, mimicking transmembrane ion channel proteins, leading to cell depolarization and affects the lysosomal pH gradient after energy-dependent internalization. Treatments of mammalian cells with this RiPP eventually lead to apoptosis. Hence, it could be developed as a drug for cancer treatment (Hayata et al., 2018).

4. Linaridins: Linear dehydrated peptides (or linaridins) are a small subclass of RiPPs with only 3 members isolated produced by *Streptomyces* spp., although dozens of putative linaridin BGCs have been identified in both Gram positive and negative bacteria as well as archaea with genomic tools. The common features of linaridins are the presence of *allo*-isoleucine and Dhb residues (**Figure 2.12**). Additional non proteinogenic residues such as N,N-dimethylalanine, N,N-dimethylisoleucine and S-[(Z)-2-aminovinyl]-D-cysteine (AviCys) can be found in linaridins. The PTMs formation involves an enzyme composed of a N-terminal horizontally transferred transmembrane helix (HTTH) domain and a C- terminal α/β hydrolase fold or two enzymes carrying each of these domains. So far, the described biological activity of these RiPPs include anticancer and narrow-spectrum antibacterial effects but little is known about their mode of action (Claesen & Bibb, 2010; Tietz & Mitchell, 2016; Mo et al., 2017).

5. Bottromycins: This subclass is original in the RiPP classification as the precursor harbor a C-terminal follower peptide instead of a N-terminal leader peptide but with similar functions. The core peptide is only composed of 8 residues whereas the follower is large with 35 to 37 amino acid residues. Additionally a Met is found a the N-terminus of the precursor upstream of the core peptide. PTMs of bottromycins consist in multiple methylation through radical SAM enzymes in pathways similar to proteusins, amidine macrocycle and thiazole heterocycle formations and finally C-terminal decarboxylation (**Figure 2.13**). Both the follower peptide and the N-terminal Met are removed by proteolysis (Arnison et al., 2013; Mann et al., 2016; Schwalen et al., 2017). Bottromycins are produced by *Streptomyces* and active against Gram positive bacteria. They inhibit protein synthesis with a mechanism similar to chloramphenicol (see subsection 1.1.3), i.e. they block the binding of aminoacyl-tRNA to the site A of the 50S ribosome leading to premature termination of the nascent polypeptide chain (Otaka & Kaji, 1976; Arnison et al., 2013).

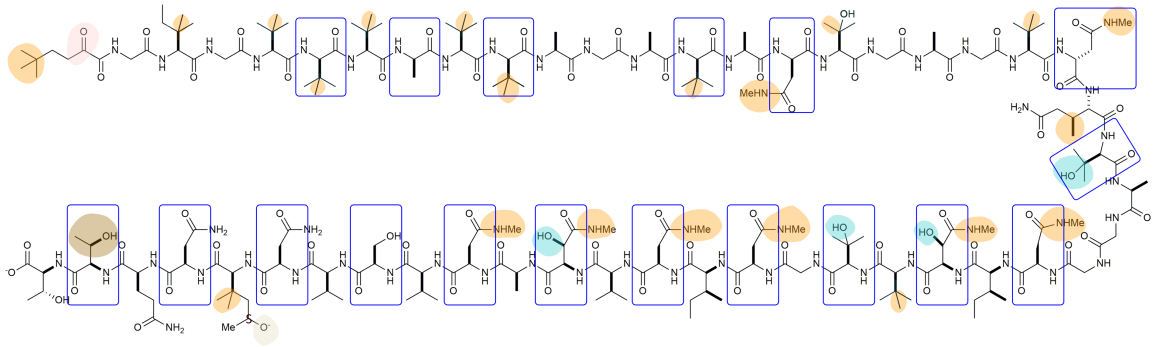

Figure 2.11: Structure of the proteusin polytheonamide B
Methylation, dehydration, hydroxylation, oxidation, allo-threonine are highlighted in orange, light pink, teal, beige and brown, respectively. Dark blue outline indicates epimerization.

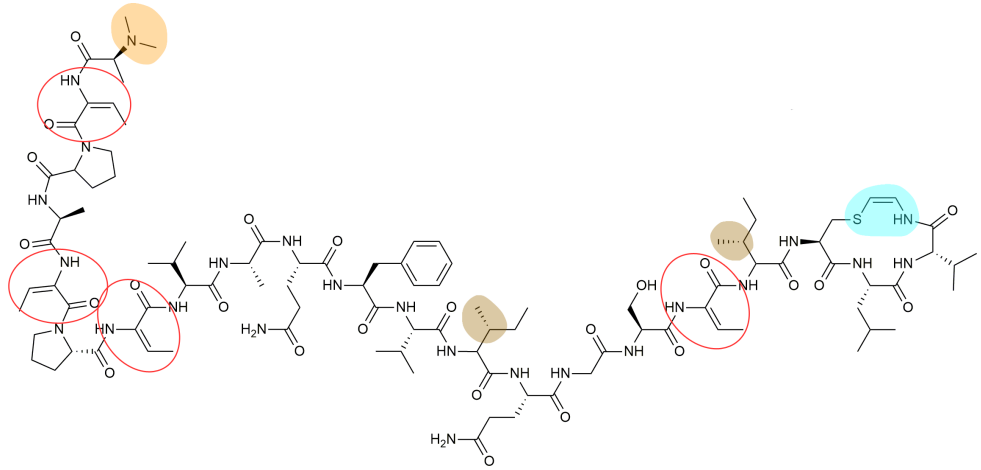

Figure 2.12: Structure of the linaridin cypemycin
N-terminal methylation, allo-*isoleucine, and AviCys residues are highlighted in orange, brown, and light blue, respectively. Red outlines Dhb residues.*

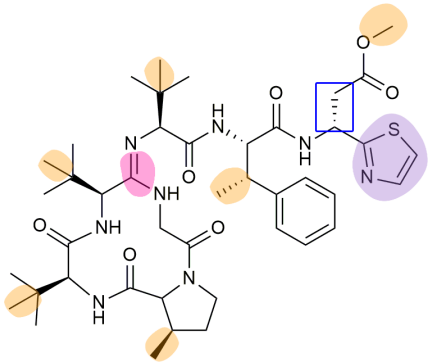

Figure 2.13: Structure of the bottromycin A2
Methylation, macrocyclisation and thiazole are highlighted in orange, pink and lilac, respectively. Dark blue outlines epimerization.

6. Thiopeptides: Thiopeptides or "Thiazolyl peptides" also form a large subclass of RiPPs with more than a hundred members, identified from Gram positive soil and marine bacteria. The common chemical feature of thiopeptides is the presence of a central 6-membered ring containing nitrogen and carrying a least one macrocycle and one tail. The macrocycle and the tail can harbor dehydroamino acids and thiazoles, oxazoles or thiazolines derived from Cys, Ser or Thr. The 6-membered ring is found in different oxidation states, establishing families of thiopeptides. Group a corresponds to a totally reduced piperidine, group b to a 1,2-dehydropiperidine (**Figure 2.14**), group c to a piperidine fused with imidazoline, group d to a trisubstituted pyridine and finally group e to a tetrasubstituted pyridine. Group d is the only family with only one macrocycle, whereas other families harbor two macrocycles. Thiopeptides have a wide-range of biological activities such as anticancer, antifungal, antiplasmodial, antibacterial and immunosuppressive activities. They show potent activity toward Gram positive bacteria but not Gram negative strains, resulting from the inhibition of protein synthesis with specific mechanisms varying according to the size of the macrocycles (Just-Baringo et al., 2014).

7. Microcins: As discussed in subsection 2.1.4, the term microcins regroup unmodified peptides and RiPPs produced by Gram negative bacteria. RiPPs belonging to microcins are active against Gram negative bacteria and in most case specifically against Enterobacteria. They cross the outer membrane of Gram negative bacteria through specific receptors and then the inner membrane through ABC transporter or binding to membrane proteins. Class I encompasses RiPPs with a molecular weight lower than 5 kDa and so far regroups 3 members: MccB17, MccJ25 and MccC. MccB17 and MccJ25 also belong to other RiPP subclasses as their PTMs classify them respectively as LAP and lasso peptides. MccC is the only microcin that is not produced as a precursor with a leader peptide. MccC is a heptapeptide with a covalent C-terminal binding to an adenosine monophosphate with a propylamine group on the phosphate. As a result of their different chemical composition and structure these RiPPs have different mechanisms of action. For example, MccB17 targets DNA gyrase whereas MccJ25 targets RNA polymerase. Class IIb microcins regroup linear peptide carrying siderophore-type PTMs. The siderophore is linked to a Ser-rich C-terminal domain through a glycosylic bond (**Figure 2.15**). These peptides are chromosome-encoded whereas most microcins are encoded on plasmids. Microcins from class IIb can form ion channel or pores in the inner membrane of Gram negative bacteria or target some bacterial membrane proteins and impair their activities (Duquesne et al., 2007; Arnison et al., 2013; Baquero et al., 2019).

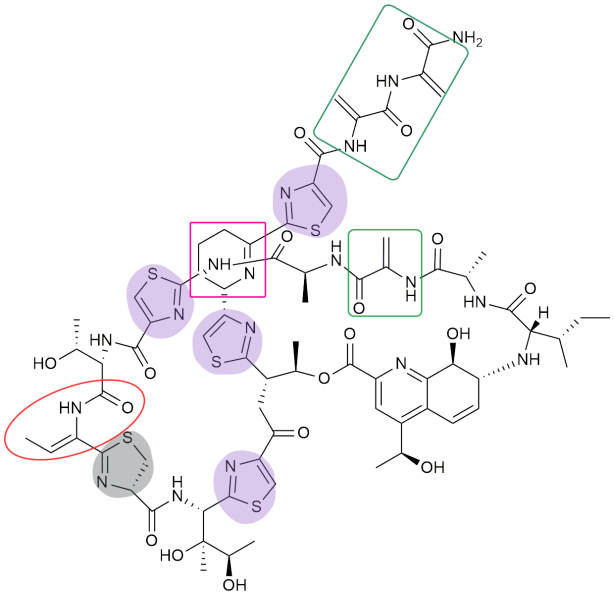

Figure 2.14: Structure of the thiopeptide thiostrepton A
The central dehydropiperidine is outlined by pink whereas green and red outlines Dha and Dub residues, respectively. Thiazoles and thiazolines are respectively highlighted in lilac and dark grey.

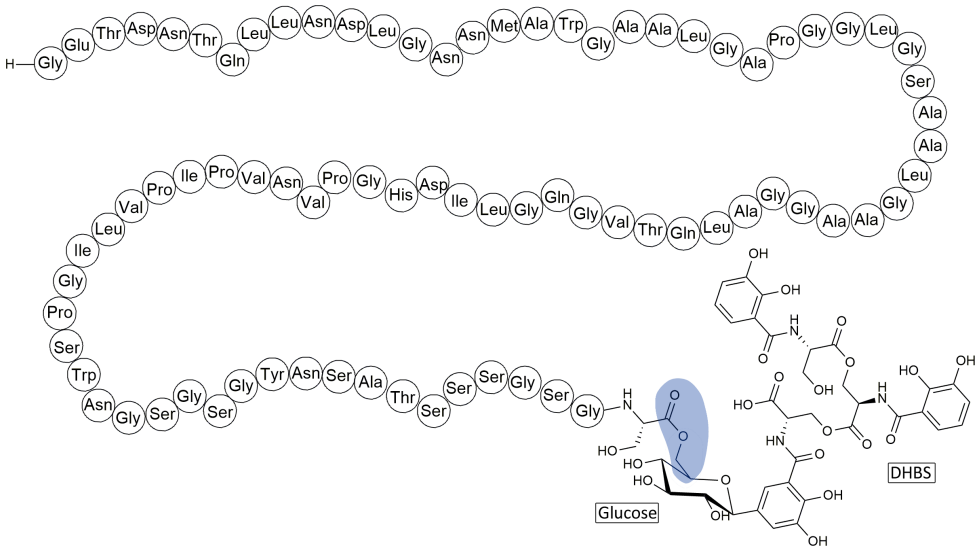

Figure 2.15: Structure of the class IIb microcin E492
Dark blue highlights an ester bond. Additional PTMs are indicated on the figure.

8. Cyanobactins: This subclass of RiPPs is one of the largest, with around 200 members identified, all from cyanobacteria. These RiPPs have a length of 6 to 20 residues. Most of them form a N- to C-terminal macrocycle but some are linear. They all contain a heterocycle at their C-terminus, either a proline or an azol(in)e (thiazole or oxazole) derived from Cys, Ser or Thr (**Figure 2.16**). However, this is the only common chemical feature of cyanobactins, therefore they are defined by their BGCs rather than their structures. Cyanobactins BGCs all harbor a gene encoding a precursor similar to PatE, the precursor of patellamide, and at least one subtilisin-like protease from the PatG family. In addition to the leader peptide, the precursors of cyanobactins carry N- and C-terminal conserved recognition sequences of 4-5 amino acid residues essential for maturation and in particular cyclization by N- to C-termini peptidic linkage. The precursors can be composed of multiple core sequences separated by N- and C-terminal recognition sequences. In that case multiple mature cyanobactins are produced from one precursor. Most cyanobactins display an anticancer activity but some of them also have an antimicrobial activity, mainly towards parasite or virus but also in some cases against selective bacteria (Arnison et al., 2013; Gu et al., 2018).

9. Bacterial head-to-tail cyclized peptides: Bacterial head-to-tail cyclized peptides or circular bacteriocins have already been introduced in subsection 2.1.2 as they correspond to class IIc bacteriocins produced by Gram positive bacteria. These peptides undergo circularization by the formation of a peptide bond between the N- and C-termini after removal of the leader peptide (**Figures 2.2C, 2.17**). They are differentiated from other circular RiPPs like cyanobactins or cyclotides by their large size (between 35 and 70 amino acid residues) and as they are lacking a recognition sequence at the C-terminus of the precursor. The mechanisms behind circularization remain elusive, although it has been hypothesized that a conserved aromatic residues a the C-terminus could play an important role. Their BGCs, that can be carried on plasmids or chromosomes, encode a heavy biosynthetic machinery with up to 10 genes. So far, a dozen of circular bacteriocins have been purified and they were thought to be produced only by Gram positive bacteria. No conserved motif or high sequence homology have been identified from these circular bacteriocins. A phylogenetic analysis identified almost 400 BGCs that could be responsible for the production of 59 unique circular bacteriocins. Though most clusters were indeed found in the genome of Gram positive bacteria and in particular Firmicutes, one of these clusters was found in the genome of the Gram negative bacteria *Novosphingobium* sp. B-7. Bacterial head-to-tail cyclized peptides can be subclassified: class I corresponds to strongly cationic peptides with 4 to 5 helices whereas class II regroups acidic peptides. The circular structure provides to these RiPPs increased resistance to thermal, chemical and proteolytic treatments. They show broad-spectrum activity mainly against Gram positive strains but also against Gram negative bacteria. Identified mechanisms of action of circular bacteriocins consist in cell membrane interaction and pore formation (Arnison et al., 2013; van Heel et al., 2017).

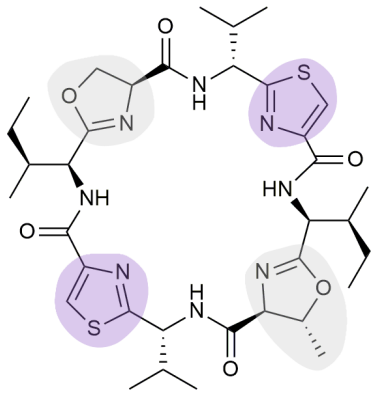

Figure 2.16: Structure of the cyanobactin patellamide A
Thiazoles are highlighted in lilac while oxazolines and methyloxazolines are in light grey.

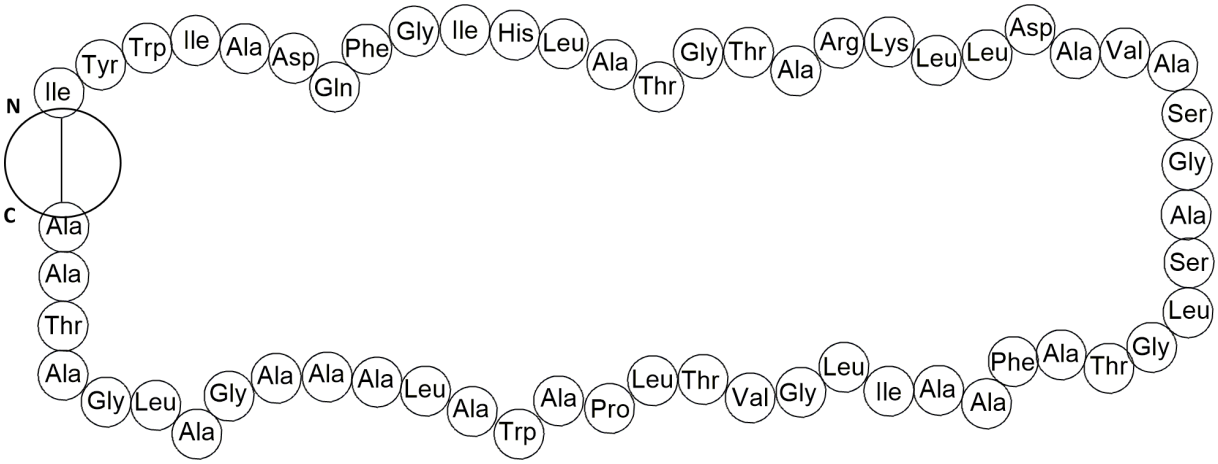

Figure 2.17: Structure of the circular bacteriocin acidocin B
Head-to-tail cyclization by amide bond is indicated by a black circle while N and C designate each termini.

10. Microviridins: Identified microviridins are produced mainly by Cyanobacteria although they might be produced by other families. A phylogenetic analysis spotted more than 170 BGCs in Cyanobacteria but also in Bacteroidetes and in Proteobacteria. Microviridins are tricyclic N-acetylated peptides that harbor an original cage-like structure arising from intramolecular ω-amide and/or ω-ester bonds (**Figure 2.18**). Most microviridins contain lactam or lactone rings. The precursor of microvidins comprises a Pro-Phe-Phe-Ala-Arg-Phe-Leu (Arg: arginine) motif involved in an α-helix structure and in interactions with the maturation enzymes. Additionally, many microviridin precursors harbor a Gly-Gly cleavage motif. Another conserved motif is found in the core sequences: Thr-X-Lys-X-Pro-Ser-Asp (Lys: lysine) that is implicated in cyclization. Based on their precursor sequence microviridins can be divided in 3 classes. Class I regroups precursor consisting in one leader sequence fused to one core sequence. Class II precursors are composed of one leader sequence fused to up to 5 core sequences separated by Gly-Gly motifs or Gly-rich domains or lacking spacers. It is unclear to date if multiple mature RiPPs or one RiPP with repeated cage-like structure are produced from these specific precursors. Multiple RiPPs production from one precursor has been identified in other subclasses such as cyanobactins, orbitides and cyclotides. Class III corresponds to precursors with a length similar to class II, however only one sequence in the C-terminus is found to resemble a core sequence. Rather than acting as antimicrobials, microviridins seem to have a selective activity as serine protease inhibitors, in particular their potent activity was demonstrated against trypsin, chymotrypsin and elastase (Ahmed et al., 2017).

11. Glycocins: So far less than 10 glycocins have been purified from Gram positive bacteria or identified in their genome. These peptides are composed of 37 to 48 amino acids and they all carry one or two monosaccharides linked to the side chain of a Cys, a Ser or a Thr. Additionally glycocins harbor two disulfide bridges (**Figure 2.19**). Rather than homology in core sequences, glycocins exhibit structural similarity consisting in two helices connected by a loop. These RiPPs have an antibacterial activity and while some have a very narrow spectrum, other can be active against both Gram positive and negative bacteria. Glycocins can have a bacteriostatic or bactericidal effect and little is known on their mode of action so far except that it doesn't seem to affect membrane integrity. The monosaccharides are not always essential for antibacterial activity, when they are, glycocins are referred to as "glycoactive" (Norris & Patchett, 2016; Kaunietis et al., 2019).

12. Methanobactins: Methanobactins were first identified from methanotroph Gram negative bacteria. These 11 amino acid residues peptides chelate copper through interactions with two nitrogen heterocycles and adjacent thioamide or enethiol moieties, all derived from modified and conserved Cys (**Figure 2.20**). Most nitrogen heterocycles found in methanobactins correspond to oxazolone rings. These peptides can chelate copper(I) directly or copper(II) after a reduction process with unknown mechanisms. BGCs were identified in other Gram negative bacteria like Proteobacteria but also in Gram positive bacteria like Actinobacteria (Kenney & Rosenzweig, 2018).

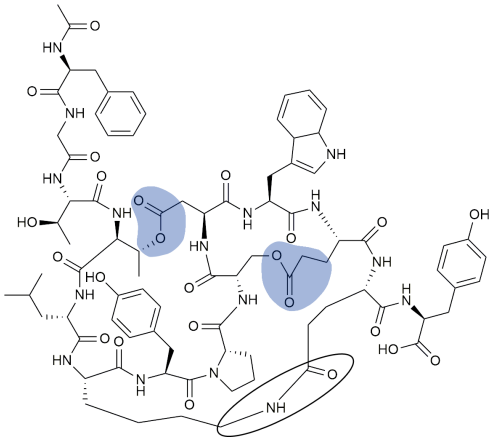

Figure 2.18: Structure of the microviridin B

Ester and amide bonds involving the side chains of amino acids are indicated by dark blue highlight or black outline, respectively.

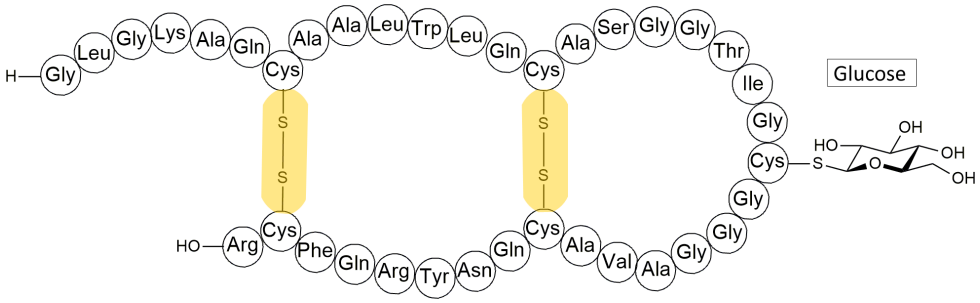

Figure 2.19: Structure of the glycocin sublancin 168

Glycosylation of Cys is indicated directly on the figure while disulfide bonds are highlighted in yellow.

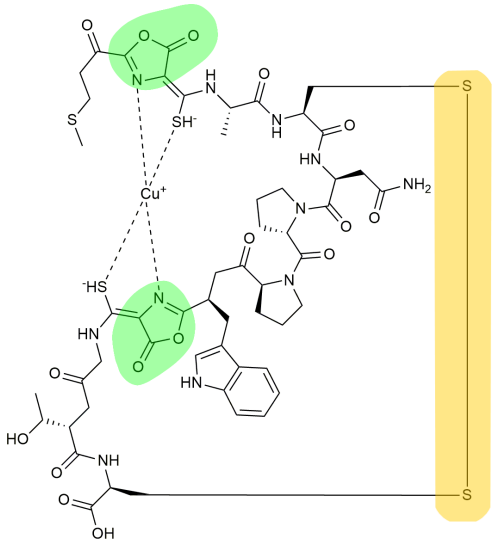

Figure 2.20: Structure of the copper methanobactin produced by *Methylocystis* sp. LW4

Disulfide bonds and oxazolones are indicated in yellow and bright green, respectively.

13. Lasso peptides: These RiPPs are produced by both Gram positive and negative bacteria. So far around 50 members have been identified. They are peptides composed of 15 to 26 amino acid residues harboring a 7 to 9 residues N-terminal macrolactam ring with a C-terminal tail passing through and trapped in the macrolactam ring. This particular structure resembling a lasso confers great stability to chemical, thermal or proteolytic treatments. Lasso peptides are subdivided in 4 classes. Class I regroups peptides harboring two disulfide bonds, one linking the N-terminal Cys to the ring and one linking the ring to the C-terminal tail (**Figure 2.21**). Class II corresponds to peptides with no disulfide bonds and a lasso structure stabilized through steric interactions. Class III and class IV both refer to peptides with one disulfide bond, in class III it is located between the macrolactam ring and the tail whereas it is linking two parts of the C-terminal tail in class IV (Martin-Gómez & Tulla-Puche, 2018). Lasso peptides have different types of biological activities including anticancer, antiviral and antibacterial activities associated with different mechanisms of actions. As cited earlier, for example MccJ25 inhibits the RNA polymerase. Antibacterial lasso peptides can be active against Gram positive or negative bacteria but they usually have a narrow-spectrum regarding the producer strain (Arnison et al., 2013; Kaweewan et al., 2018).

14. Autoinducing peptides: Bacteria live in communities and adapt their gene expression depending on the cell concentration. This process is called Quorum Sensing (QS) and employs different types of molecules for bacteria to communicate between them and detect the surrounding population level. Autoinducing peptides are part of the QS molecules secreted by at least 48 different species of Gram positive bacteria. Their common features comprise a lactone or thiolactone macrocycle ring composed of 5 amino acids and linked to a tail of 2 to 5 amino acids (**Figure 2.22**). The only exception so far has been found in *Enterococcus faecalis* with a 9 residues lactone macrocycle. The amino acid composition of the core sequences is variable. These autoinducing peptides can be involved in intra- or inter-species communications and have been shown to regulate virulence, therefore they could be exploited in bacterial infection treatment (Gordon, 2020). Another type of autoinducing peptides, ComX, is found in various species of *Bacillus* and corresponds to an isoprenylated and cyclic peptide with 6 to 10 amino acids and a conserved Trp (Arnison et al., 2013).

15. Streptides: Streptides have been recently discovered in Streptococcal bacteria, including pathogenic species such as *Streptococcus suis* or *Streptococcus agalactiae*. Only three members have been identified so far: StrA, AgaA and SuiA. The PTM of streptides consists in a cyclization by a carbon-carbon (C-C) linkage between Lys and Trp residues from a Lys-Gly-Asp-Gly-Trp-conserved motif (Trp: tryptophan, **Figure 2.23**). Such as other subclasses of RiPPs like bottromycins or proteusins, the PTM formation is performed by a radical SAM maturase enzyme. NMR investigations clearly established that the Lys-Trp crosslinks in StrA, SuiA and AgaA connect the β-carbon (Cβ) of Lys and the C-7 of Trp in the core peptides. So far, the biological roles of streptides remain to be characterized but they might be involved in intra-species communication. The regulation of their BGCs is under the control of a QS system and they are likely produced at high cell densities by pathogenic Streptococci; a state associated with virulence (Ibrahim et al., 2007; Schramma et al., 2015; Davis et al., 2017; Schramma & Seyedsayamdost, 2017; Bushin et al., 2018).

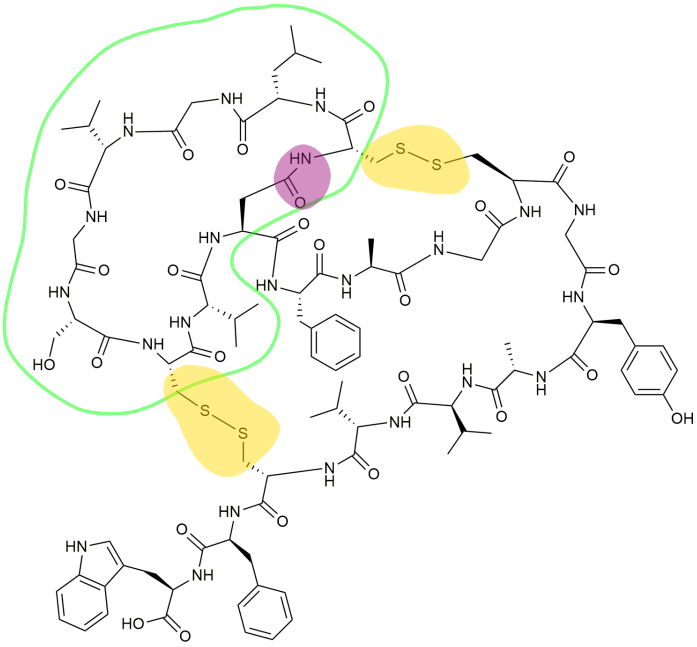

Figure 2.21: Structure of the class I lasso peptide specialicin
Isopeptide and disulfide bonds are highlighted in dark purple and yellow respectively. Bright green outlines the macrolactam ring.

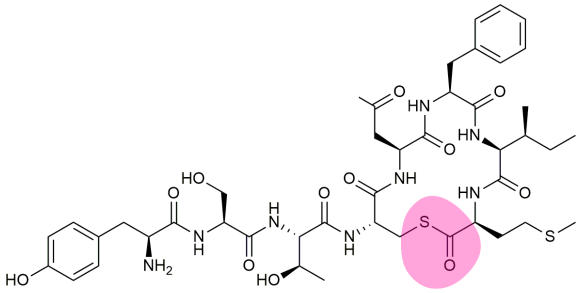

Figure 2.22: Structure of the autoinducing peptide AIP-1
Pink highlights macrocyclization of a cysteine and a methionine to thiolactone.

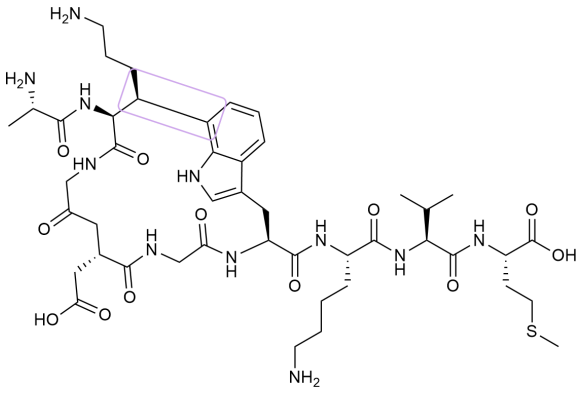

Figure 2.23: Structure of the streptide StrA
Lilac outlines carbon-carbon linkage.

16. Amatoxins and phallotoxins: These fungal RiPPs are produced by several genera of Basidiomycetes, in particular *Amanita* but also *Galerina, Lepiota* and *Conocybe*. They are bicyclic peptides harboring a head-to-tail circularization a well as a tryptathionine resulting from the crosslinking of a Cys and a Trp. Amatoxins are octapeptides (**Figure 2.24A**) whereas phallotoxins are heptapeptides (**Figure 2.24B**). Both their precursors comprise a 10 amino acids leader peptide and a C-terminal recognition sequence. While the core sequences are diverse, the leader and recognition sequences are highly conserved. The core sequences are surrounded by Pro residues targeted by a prolyl protease belonging to the serine protease family for removal of the leader and recognition sequences. The prolyl protease performs both proteolytic cleavage and head-to-tail cyclization by transpeptidation. Amatoxins are actually the agents responsible for the most fatal mushroom poisonings. They act by inhibiting the RNA polymerase II in liver cells, resulting in liver failure and eventually death. Phallotoxins are not as dangerous as they are not active when delivered orally but show toxicity when injected. They have been developed as cytoskeleton dyes as they bind actin (Walton et al., 2010; Luo & Dong, 2019).

17. Borosins: Borosin is one of the most recently discovered subclasses of RiPPs. So far only omphalotin A and its derivatives belong to this family. Although omphalotins have been isolated from the Basidomycetes *Omphalotus olearius* in 1997, until the identification of their BGCs in 2017 they were thought to be NRPs. These peptides composed of 12 amino acids are head-to-tail circularized and harbor 9 to 12 N-methylation (**Figure 2.25**). This recent subclass is rather original from other RiPPs as their precursor is actually fused to the C-terminus of their maturation enzyme which displays homology with SAM-methyltransferase. Like amatoxins, cleavage and cyclization of the precursor involve a prolyl oligopeptidase. In addition to the leader peptide, the precursor harbors a C-terminal recognition sequence. Omphalotins seem to have a selective nematoxic activity (Sterner et al., 1997; Ramm et al., 2017; van der Velden et al., 2017; Luo & Dong, 2019).

18. Dikaritins: Dikaritins are also fungal RiPPs, however unlike amatoxins, phallotoxins and borosins, they are produced by Ascomycetes rather than Basidiomycetes. They are characterized by cyclic structures involving a Tyr residue. Phomopsins have 7 amino acids residues and a 13-membered macrocyclic ring resulting from the ether linkage of the phenyl ring of a Tyr to Ile (Ile: Isoleucine, **Figure 2.26A**). Ustiloxins have a similar ring but are composed of 4 amino acids (**Figure 2.26B**). However, the main difference is that ustiloxins only harbor proteinogenic amino acids whereas phomopsins are composed of dehydroamino acids. Finally asperipins are composed of 6 residues and exhibit a bicyclic structure arising from ether linkages of Tyr side chains and β-carbons (**Figure 2.26C**). The precursors of dikaritins are composed of repeated core sequences surrounded by cleavage recognition motif such as Lys-Arg. Dikaritins have an antimitotic activity and could be used as anticancer drugs (Ding et al., 2016; Nagano et al., 2016; Luo & Dong, 2019).

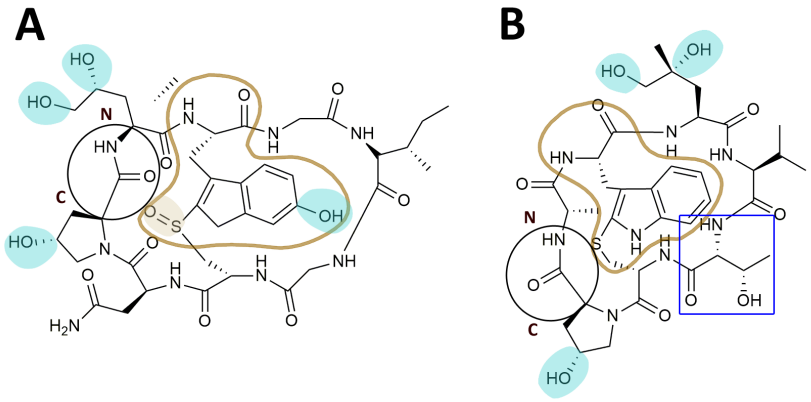

Figure 2.24: Structures of the amatoxin α-amanatin and the phallotoxin phalloidin

A. *α-amanatin.* ***B.*** *phalloidin. Hydroxylation and oxidation are highlighted in teal and beige, respectively. Brown and dark blue outlines represent respectively trypthationine residues and epimerization. Head-to-tail cyclization by amide bond is indicated by a black circle while N and C designate each termini.*

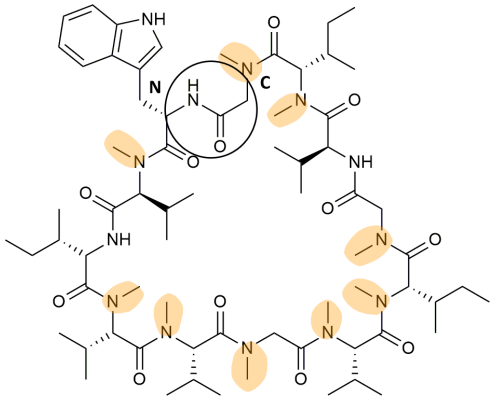

Figure 2.25: Structure of the borosin omphalotin A

Methylation are highlighted in orange. Head-to-tail cyclization by amide bond is indicated by a black circle while N and C designate each termini.

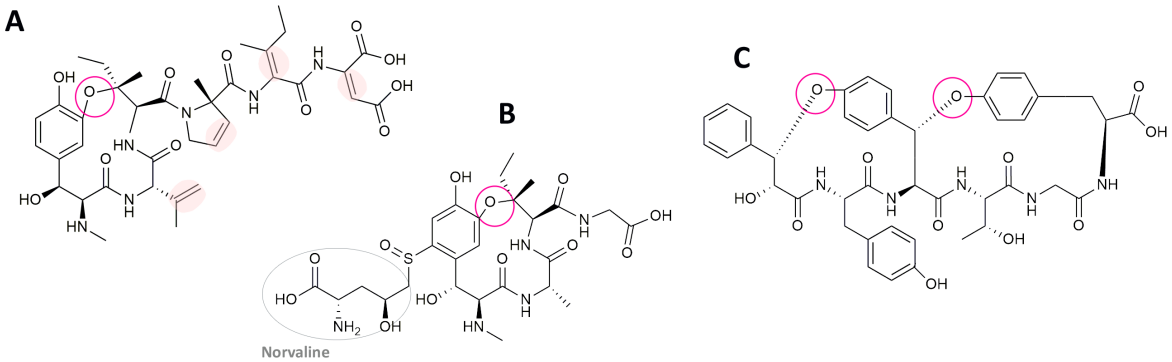

Figure 2.26: Structure of dikaritins

*Structures of phomopsin A (**A**), ustiloxin B (**B**) and asperipin-2a (**C**). Pink outlines ether linkage involving Tyr residues while light pink highlights dehydro-residues. The presence of Norvaline, an additional PTM, is indicated directly on the figure.*

19. Epichloëcyclins: Like dikaritins, epichloëcyclins are produced by Ascomycetes. They were first identified in *Epichloë*, a genus of fungi that can be both symbiont or pathogens of temperate grasses. Phylogenetic analyses revealed that they might be produced by other fungi but restricted to the Clavicipitaceae and Ophiocordycipitaceae families. These peptides of a length up to 12 amino acids residues harbor an oxidative cyclization on a conserved Tyr and a methylation on a Lys (**Figure 2.27**). Their precursor is composed of multiple repeat of core sequences with some amino acids substitutions and conserved motifs, including Lys-Arg cleavage sites. Therefore, a single precursor is processed in multiple RiPPs. Epichloëcyclins biological activities remain to be characterized. It should be noted that production of epichloëcyclins have been identified in symbiotic conditions but not in fungal culture and therefore might be involved in mutualistic effects (Johnson et al., 2015; Luo & Dong, 2019).

20. Cyclotides: This subclass is produced by a wide-range of families of plants such as Rubiaceae, Violaceae, Cucurbitaceae or Fabaceae and hundreds of members have been identified. Cyclotides are composed of around 30 amino acid residues and are characterized by a cyclic cystine knot (CCK) motif and a head-to-tail cyclic backbone. The CCK motif consists in 6 conserved Cys forming 3 disulfide bonds (**Figure 2.28**). This particular structure provides resistance to thermal, chemical and proteolytic treatments. Cyclotides can be subdivided in 3 categories: Möbius, bracelets and linear. Möbius and bracelets differ by a 180° twist in the cyclic backbone due to the presence of a conserved Pro residue. Few linear cyclotides with no head-to-tail cyclic backbone but conserved cyclotide sequence have been identified. The precursor of cyclotides harbor a N-terminal signal sequence that addresses the precursor to the endoplasmic reticulum before maturation, then the leader peptide is composed of two domains: a N-terminal propeptide domain (NTPP) and a N-terminal repeat domain (NTR). A small C-terminal sequence (CTR) can be found in the precursors of some cyclotides. NTR, CTR and the core sequence can be repeated in the precursor. Cyclotides can exert many biological activities including but not only insecticidal, antiviral, anticancer, anthelmintic, immunosuppressive and antibacterial activities. Their main mode of action is the interaction with lipids resulting in membrane disruption (Park et al., 2017).

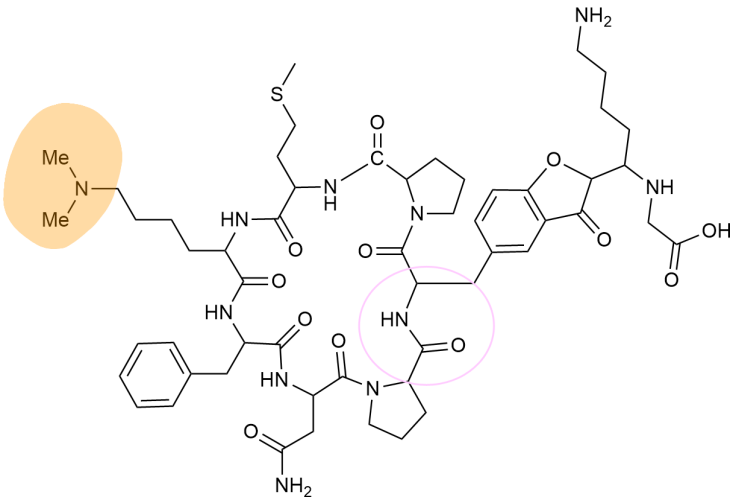

Figure 2.27: Structure of the epichloëcyclin A

Dimethylation of Lys is highlighted in orange while oxydative cyclization is outlined by light pink.

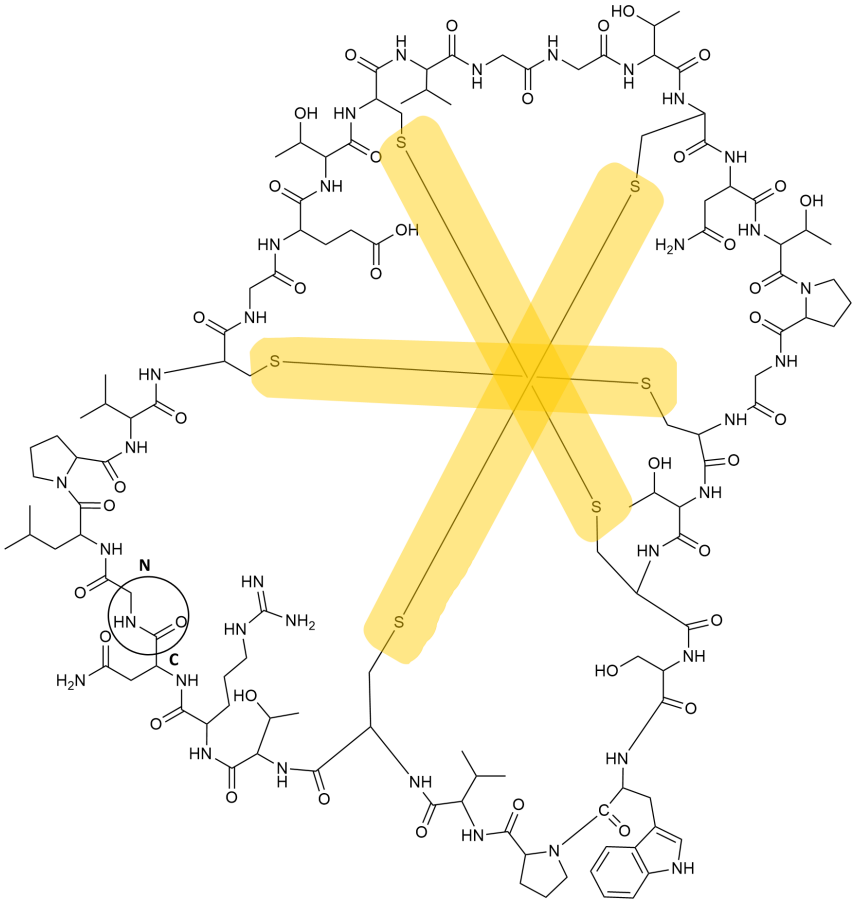

Figure 2.28: Structure of the cyclotide kalata B1

The 6 Cys involved in the cyclic cystine knot (CCK) are linked by 3 disulfide bonds highlighted in yellow. Head-to-tail cyclization by amide bond is indicated by a black circle while N and C designate each termini.

21. Orbitides: Such as cyclotides, these RiPPs are produced by plants and 9 families have been identified yet as orbitides producers such as Caryophyllaceae, Euphorbiaceae, Lamiaceae, Linaceae, Rutaceae. These RiPPs are composed of 5 to 12 amino acid residues and harbor a head-to-tail cyclization (**Figure 2.29**). The amino acid composition in this subclass is original as Cys is the least abundant amino acid, whereas it is often conserved and involved in PTMs in lots of other RiPP subclasses. Orbitides display high contents of hydrophobic amino acids. The precursor might carry a recognition sequence depending on the producer family and such as cyclotides might contain multiple sequences of the core peptide. Hence one single precursor can be processed in multiple cyclic precursor. Orbitides exert many different activities including anticancer, antimalarial, immunosuppressive and antibacterial effects. Regarding the antibacterial activity, some orbitides have been identified as active against exclusively Gram positive or Gram negative bacteria whereas other can target both. Similarly, some orbitides display a very narrow spectrum of action and seem specific to one specie while other are broad-spectrum antimicrobial. Little is known about their mechanisms of action, although some orbitides active against Gram positive bacteria exclusively are known to form pores in the bacterial membrane (Arnison et al., 2013; Ramalho et al., 2018; Luo & Dong, 2019).

22. Conopeptides: These RiPPs are toxins produced in the venom of marine snails. It is estimated that around 500 hundred species of *Conus* are potential producers of conopeptides and hundreds of conopeptides have been identified. These *Conus* toxins differ from venom toxin from other animals as they are smaller, from 10 to 30 residues compared to 30 to 90, and harbor many and diverse PTMs. Identified PTMs that might be incorporated on conopeptide precursors so far include: C-terminal amidation on Gly; N-terminal cyclization on Gln; hydroxylation on Pro, Val, Lys; carboxylation on Glu (Glu: glutamate); sulfation on Tyr; bromination on Trp; oxidation on Cys; glycosylation on Thr; epimerization of Val, Leu, Phe, Trp (**Figure 2.30**). Conopeptides usually describe disulfide-poor peptides (none to 1 disulfide bridge) and conotoxins disulfide-rich peptides (2 or more disulfide bridges). Their precursors harbor an extremely conserved endoplasmic reticulum recognition sequence while the core sequences are diverse. The biosynthetic pathways of most conopeptides remain unclear especially since the biosynthetic genes are not clustered and as the peptides can be produced concomitantly in their mature form with PTMs or without. While many conopeptides still have unknown function, others have been identified as interacting with cell membranes or ion channels and have been developed as neurological drugs (Arnison et al., 2013; Lebbe & Tytgat, 2016; Luo & Dong, 2019).

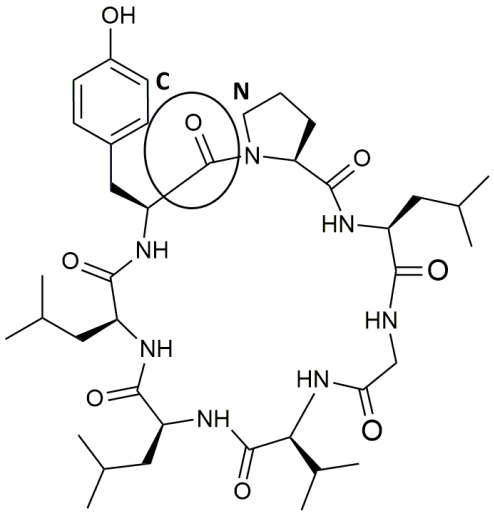

Figure 2.29: Structure of the orbitide pohlianin A

Head-to-tail cyclization by amide bond is indicated by a black circle while N and C designate each termini.

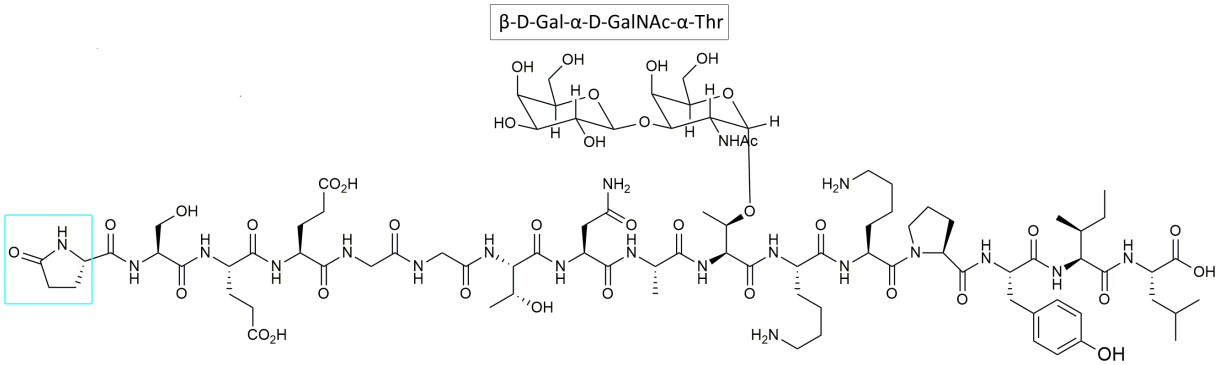

Figure 2.30: Structure of the conopeptide contulakin-G

Light blue outlines cyclization of glutamine to pyroglutamate. Glycosylation is indicated directly on the figure.

Families	Main PTMs	Producers	Identified Activities	Examples
Lanthipeptide	Lan, MeLan residues	Gram + Gram -, eukaryotes?	Antibacterial, antifungal, antiviral, pain relief	Fig. 2.9
LAP	Thiazol(in)e and (methyl)-oxazol(in)e heterocycles	Gram + / -	Antibacterial	Fig. 2.10
Proteusin	Various (including epimerization)	*Candidatus* Entotheonella factor	Anticancer	Fig. 2.11
Linaridin	*Allo*-isoleucine, Dhb residues	*Streptomyces* Other Gram +, Gram -?	Antibacterial Anticancer	Fig. 2.12
Bottromycin	Methylation, amidine macrocyle, thiazole heterocycle	*Streptomyces*	Antibacterial	Fig. 2.13
Thiopeptide	Central 6-membered ring containing nitrogen, at least one macrocycle and one tail	Gram +	Anticancer, antibacterial, antiplasmodial, antifungal, immunosuppressive	Fig. 2.14
Microcin	Various	Gram -	Antibacterial	Fig. 2.15
Cyanobactin	Heterocycle at C-terminus	Cyanobacteria	Anticancer, antiviral, anti-parasite, antibacterial	Fig. 2.16

Families	Main PTMs	Producers	Identified Activities	Examples
Head-to-tail cyclized peptide	Circularization by an amide bond between N- and C-termini	Gram + Gram -?	Antibacterial	Fig. 2.17
Microviridin	Intramolecular ω-amide and/or ω-ester bonds	Cyanobacteria Other Gram -?	Protease inhibitors	Fig. 2.18
Glycocin	Bound to 1 or 2 monosaccharides	Gram +	Antibacterial	Fig. 2.19
Methanobactin	Nitrogen containing heterocycle, thioamide or enethiol moieties	Methanotroph Gram – bacteria Other Gram -, Gram +?	Chelate copper	Fig. 2.20
Lasso peptide	N-terminal macrolactam ring with a C-terminal tail passing through	Gram + / -	Anticancer, antiviral, antibacterial	Fig. 2.21
Autoinducing peptide	Lactone or thiolactone macrocycle ring	Gram +	Bacterial communication	Fig. 2.22
	Isoprenylated and cyclic peptide	*Bacillus spp.*		
Streptide	Carbon-carbon linkage	*Streptococcus spp.*	Bacterial communication?	Fig. 2.23
Sactipeptide	Sulfur-to-α carbon thiother linkage	*Bacillus spp.* Other Gram +, Gram -?	Antibacterial	Fig. 2.31-32
Ranthipeptide	Sulfur-to-β or -γ carbon thiother linkage	Gram +	?	Fig. 2.36-37

Families	Main PTMs	Producers	Identified Activities	Examples
Amatoxin and Phallotoxin	Circularization by an amide bond between N- and C-termini, tryptathionine	Basidiomycetes	Cytoskeleton dye	Fig. 2.24
Borosin	Circularization by an amide bond between N- and C-termini, N-methylation	*Omphatolius olearius*	Nematoxic	Fig. 2.25
Dikaritin	Cyclic structure involving a Tyr residue	Ascomycetes	Anticancer	Fig. 2.26
Epichloëcyclin	Oxidative cyclization on Tyr, methylation on Lys	*Epichloë* Other Ascomycetes?	?	Fig. 2.27
Cyclotide	Cystine Cystic Knot	Various Plants	Insecticidal, antiviral, anticancer, anthelmintic, immunosuppressive, antibacterial	Fig. 2.28
Orbitide	Circularization by an amide bond between N- and C-termini	Various plants	Anticancer, antimalarial, immunosuppressive, antibacterial	Fig. 2.29
Conopeptide	Various	*Conos*	Neurological	Fig. 2.30

2.2.4 Sactipeptides

Sactipeptides are RiPPs containing one or multiple sactionine linkages or sulfur-to-α carbon thiother (sacti) linkages, i.e. crosslinks between the sulfur (S) atom of a Cys and the α-carbon (C_α) of an acceptor amino acid residue (Arnison et al., 2013). In addition to sacti-bridges, sactipeptides can harbor other modifications like head-to-tail linkage by amide bonds or disulfide bridges. So far 5 sactipeptides have been identified: subtilosin A (Kawulka et al., 2003, 2004), the sporulation killing factor (SKF) (Liu et al., 2010), thurincin H (Sit, van Belkum, et al., 2011), thuricin CD (Rea et al., 2010), the latter being composed of the two distinct sactipetides Trn-α and Trn-β and finally huazacin which is also named thuricin Z (Hudson et al., 2019; Mo et al., 2019). Subtilosin A has been isolated from different species of *Bacillus* (Huang et al., 2009). Thuricins and thurincin H are produced by *Bacillus thuringiensis*, a soil microorganism, and SKF by *Bacillus subtilis* which can be found in both soil and human or animal gastro-intestinal tracts. Originally thermocellin (CteA) and Tte1186a were identified as sactipeptides but were very recently reclassified as ranthipeptides, which will be discussed in the next subsection (Hudson et al., 2019; Precord et al., 2019).

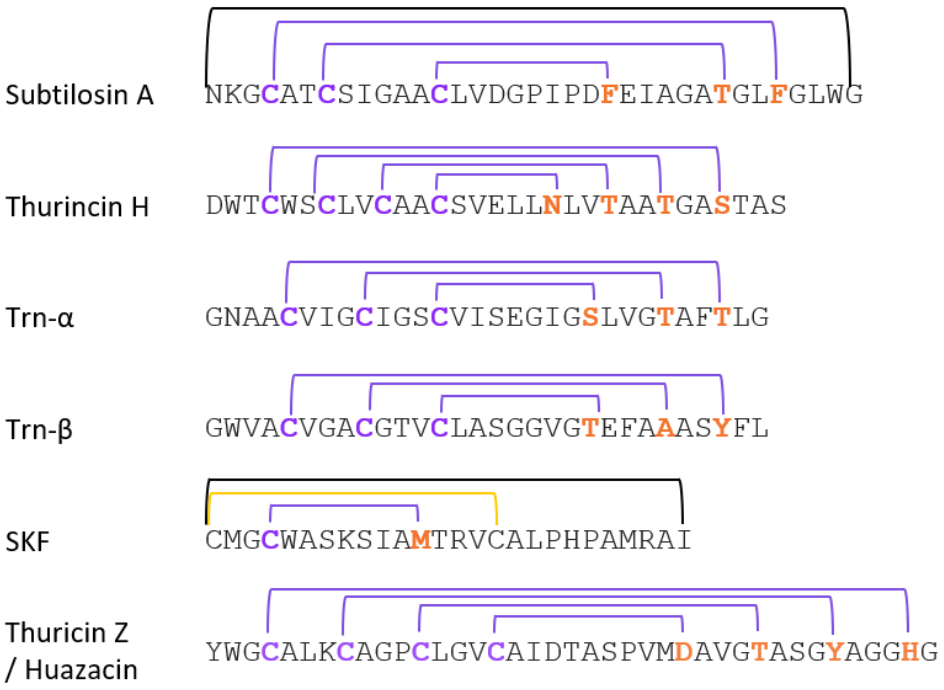

Figure 2.31: Sequences and thioether networks of sactipeptides
Thioether, disulfide bonds and head-to-tail cyclization are indicated respectively in purple, yellow and black lines. Cys are highlighted in purples and amino acid acceptors of the sacti-bonds in orange.

The length of the amino acid core sequence of the known sactipeptides varies as well as the number of sactionine linkages and the presence of other modifications (**Figure 2.31**). SKF is the smallest sactipeptide with 26 amino acids and harbors 1 sactionine linkage, 1 disulfide bond and head-to-tail cyclization. The two peptides of Thuricin CD, Trn-α and Trn-β, are both composed of 30 amino acids with a sequence identity of 40% and display 3 conserved Cys involved in sacti-bridges. The amino acid acceptors of these bridges

differ in their nature in Trn-α and Trn-β but are located at the same positions. Thurincin H is composed of 33 amino acid residues and carries 4 sacti-bridges. Subtilosin A is slightly bigger with 35 amino acids and harbors 3 sactionine linkages as well as head-to-tail cyclization. Finally thuricin Z or huazacin is the largest sactipeptide identified with 39 amino acids and 4 sacti-bridges. Based on the known sactipeptides, a wide-range of amino acid residues can act as acceptors of the thioether bridges. Indeed so far, Phe, Met, Asn, Ala, Tyr, Ser, Asp, His have been identified as partners of Cys in sactionine linkages in one or two sactipeptides. At the exception of SKF, all sactipeptides harbor at least one sactionine linkage involving a Thr. It is worth noting that in all these sactipeptides, the Cys residues are situated in the N-terminal half of the core peptide whereas the acceptor residues are in the C-terminal part. This specific distribution of Cys donors and acceptors folds the sactipeptide backbone in a peculiar hairpin structure maintained by the thioether bridges. The structures of subtilosin A, thurincin H, Trn-α and Trn-β were determined by NMR using ^{13}C-and ^{15}N-labelled peptides (**Figure 2.32**). All these sactipeptides present a net anionic charge at physiological pH with a mostly hydrophobic surface. The amino acid acceptors involved in the thioether bonds holding the helical backbone can adopt L- or D-stereochemistry. The 3 bridges of Trn-α and Trn-β have a LLD stereochemistry while the 3 bridges of subtilosin A have a LDD stereochemistry (Sit, McKay, et al., 2011; Kawulka et al., 2004). In thurincin H the 4 sacti-bridges have a D-stereochemistry (Sit, van Belkum, et al., 2011).

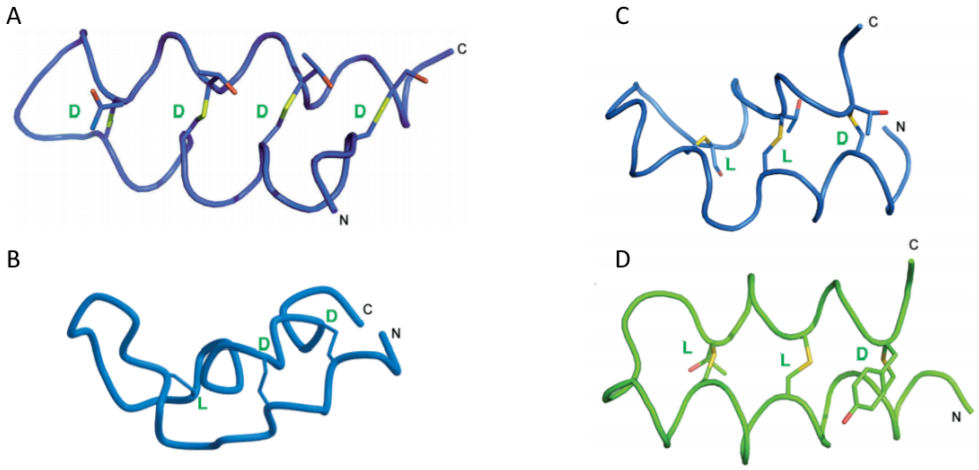

Figure 2.32: Three-dimensional structure of sactipeptides
*Representation of NMR structures of thurincin H (**A**, PDB: 2LBZ), subtilosin A (**B**, PDB: 1PXQ), Trn-α (**C**, PDB: 2L9X) and Trn-β (**D**, PDB: 2LA0). N- and C-termini are indicated as well as L- or D-stereochemistry at the α-carbon. Figure adapted from Sit, van Belkum, et al., 2011 (**A**); Kawulka et al., 2004 (**B**); Sit, McKay, et al., 2011 (**CD**).*

The BGCs of sactipeptides comprise at least genes encoding: a precursor peptide, a maturation enzyme from the radical SAM family and an ABC transporter (**Figure 2.33**). Except for huazacin, a sequence encoding a signal peptidase has also been found in the BGCs of known sactipeptides. Additionally, genes involved in self-immunity and response regulation are present in some of the clusters. The BGC of SKF also contains a putative thioredoxin. In the BGC of subtilosin A and SKF, only one sequence encodes a precursor whereas 2 and 3 sequences encoding identical precursors are found in the BGC of thuricin Z and thurincin H, respectively. For thuricin CD two different sequences

corresponding to Trn-α and Trn-β are found. Sactipeptides' BGCs can contain more than one gene encoding maturation enzymes but in that case it is unclear if one or several enzymes perform the PTMs. In vitro incubation of the precursors of thuricin Z with either ThzC and ThzD, two highly divergent putative maturation enzymes encoded in the BGC of thuricin Z, yielded a precursor with sactionine linkages (Mo et al., 2019). Although both of the enzymes were able to incorporate PTMs in vitro, it is unknown if this is also true in vivo.

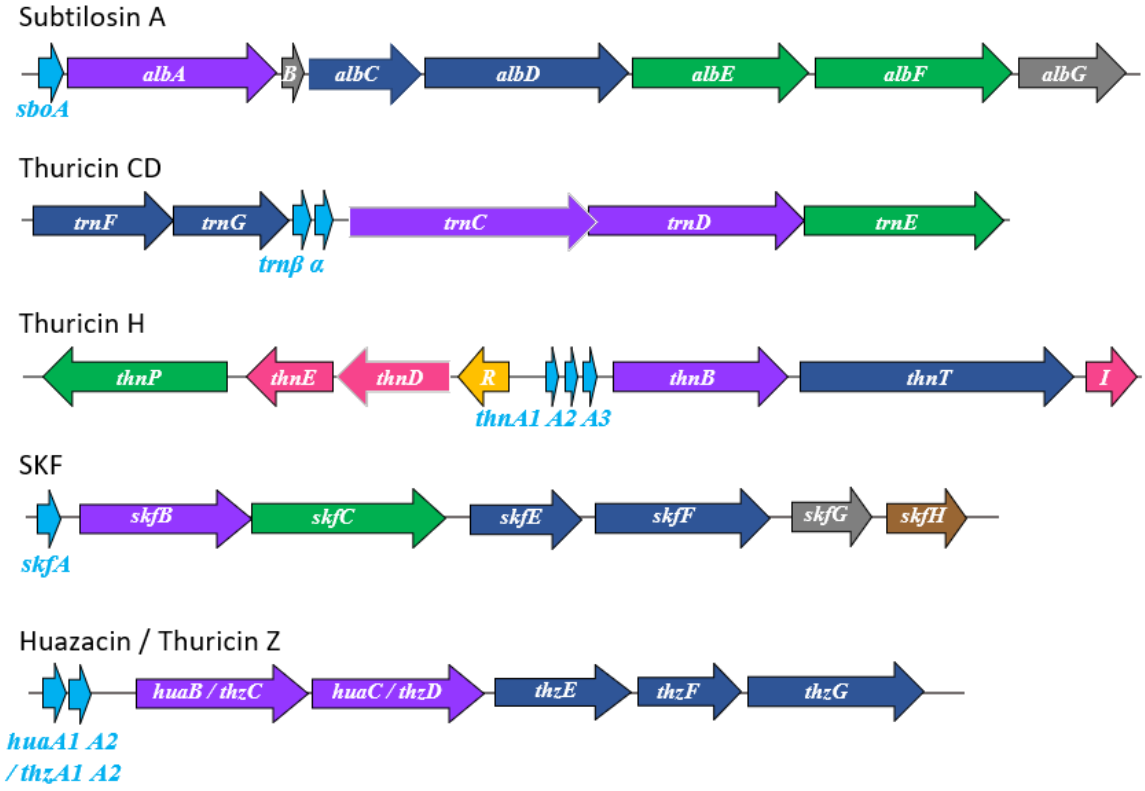

Figure 2.33: Biosynthetic genetic clusters of sactipeptides
Representation of the genes involved in the production of subtilosin A, thuricin CD, thurincin H, SKF and huazacin / thuricin Z. The colors indicate the identified or putative functions of each gene: light blue corresponds to precursor peptides; purple to radical SAM enzymes; dark blue to export systems; green to peptidases; yellow to regulators; pink to immunity systems; brown to thioredoxin; grey indicates unknown function.

The maturation enzymes of sactipeptides are called sactisynthases and belong to the radical SAM family of enzymes (Mahanta et al., 2017). Radical SAM enzymes contain a conserved Cys-X_3-Cys-X_2-Cys motif in which Cys act as ligands for 3 iron (Fe) atoms of a [4Fe-4S] cluster (**Figure 2.34A**). The free 4th Fe of the cluster coordinates the SAM cofactor, which under reduction conditions and electron transfer is cleaved into 5-deoxyadenosyl (5'-Ado•) radical and methionine (**Figure 2.34B**). This 5'-Ado• radical initiates catalysis by abstracting a hydrogen (H) atom on the substrate (Fontecave et al., 2004; Broderick et al., 2014). In particular, in the case of sactisynthases the 5'-Ado• radical extracts a H from the C_α of the acceptor residue, resulting in a substrate radical (**Figure 2.35**) (Flühe & Marahiel, 2013; Bruender & Bandarian, 2016). The exact mechanisms leading to the formation of a sactionine linkage from this substrate radical with

a Cys remain to be characterized to date. In addition to the canonical Cys-X_3-Cys-X_2-Cys motif, sactisynthases are characterized by a Cys-rich C-terminal domain bound to one or two additional [4Fe-4S] clusters, respectively named Twitch or SPASM (Subtilosin A/Pyrroloquinoline quinone/Anaerobic Sulfatase/Mycofactocin maturation enzymes) domains. SPASM domains are constituted by a conserved 7 Cys motif and Twitch domains can be found in different truncated versions of SPASM (Grell et al., 2015). Surprisingly in SkfB, the sactisynthase involved in the biosynthesis of SKF, the Twitch domain has been found to coordinate a [2Fe-2S] cluster rather than a [4Fe-4S] (Grell et al., 2018). Although the precise role of these domains remains unclear in sactipeptides so far, they are essential for thioether bond formation. Mutations of the Cys from the SPASM domain involved in the binding of the auxiliary [4Fe-4S] clusters of AlbA, as well as from the SPASM domain of ThnB and from the Twitch domain of SkfB, prevented the formation of sactionine linkages on the precursor of subtilosin A, thurincin H and SKF, respectively. Despite these mutations, SAM was still cleaved in 5'-Ado•. Hence the 1st [4Fe-4S] cluster performs the reductive cleavage of SAM while the auxiliary clusters are involved in thioether linkage formation (Flühe et al., 2012; Wieckowski et al., 2015; Flühe et al., 2013). The proposed roles for the SPASM or Twitch domain involve electron acceptance by the [4Fe-4S] auxiliary cluster during thioether bond formation of the radical substrate with the S of a Cys that might be coordinated by the auxiliary cluster (**Figure 2.35**) (Flühe & Marahiel, 2013; Benjdia et al., 2016). The core fold of radical SAM enzymes includes a partial TIM barrel $(\beta/\alpha)_6$ with 6 α-helices on the outer surface and 6 parallel β-sheets in the inner face. The canonical Cys-X_3-Cys-X_2-Cys motif is located in the "cluster binding loop" located after α_1 and before β_1 (Grell et al., 2015). The structure of SkfB was resolved by X-ray crystallography and highlighted that SkfB is a modular enzyme composed of N-terminal peptide binding domain, a core with the TIM barrel structure described above and a C-terminal domain including the Twitch domain (Grell et al., 2018).

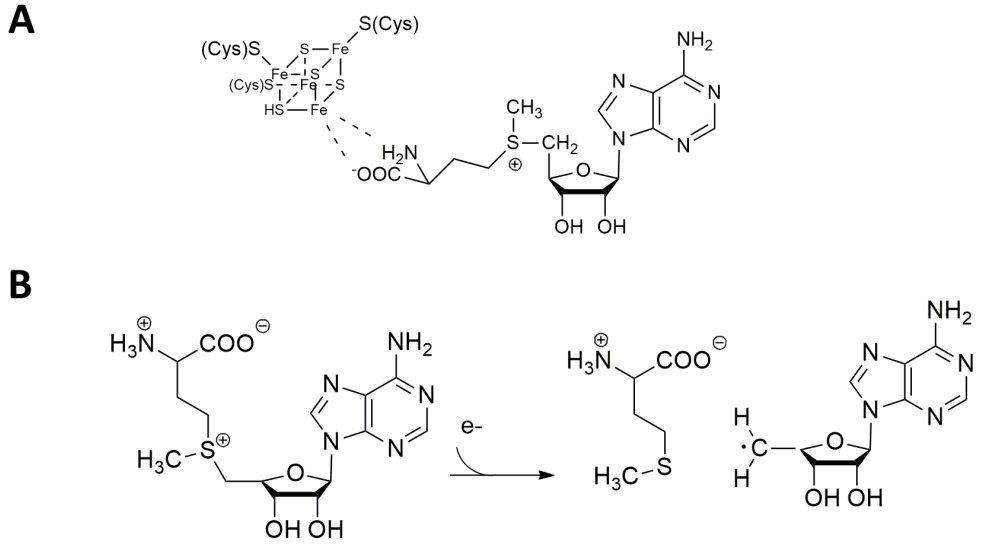

Figure 2.34: Radical SAM-based chemistry

*Coordination of a [4Fe-4S] cluster by 3 Cys and a SAM by the 4th Fe of the [4Fe-4S] cluster (**A**). Reductive cleavage upon electron transfer of SAM in 5'-Ado• (**B**).*

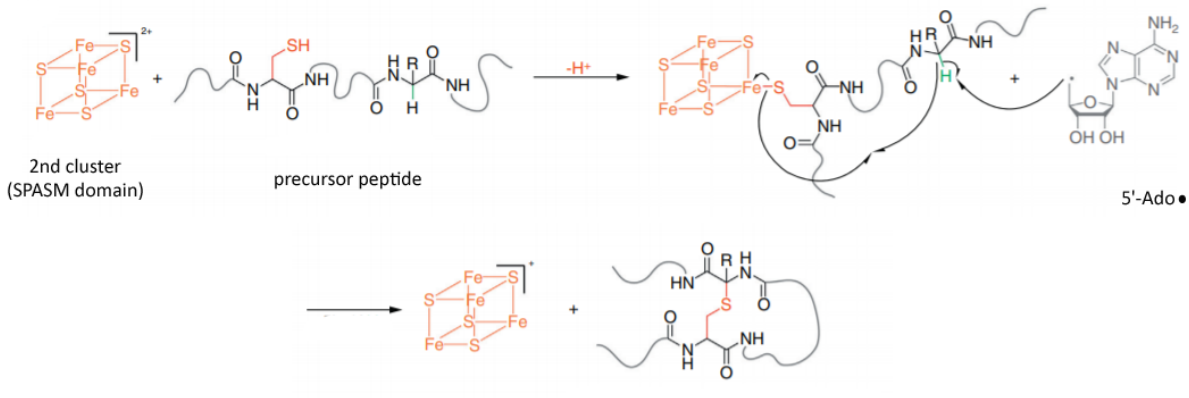

Figure 2.35: Radical based mechanism of thioether formation in sactipeptides
In this proposed mechanism for thioether formation the precursor peptide is linked by a Cys to an auxiliary [4Fe-4S] cluster found in the SPASM domain of the sactisynthase. The 5'-Ado• radical, generated by cleavage of SAM by the first [4Fe-4S] cluster found at the canonical Cys-X_3-Cys-X_2-Cys motif of the sactisynthase, abstracts a H atom from the acceptor amino acid. An electron from the radical acceptor is transferred to the auxiliary [4Fe-4S] cluster during thioether formation. Figure adapted from Flühe and Marahiel, 2013

The role of the leader peptide in sactipeptide maturation has been explored on subtilosin A and SKF. The formation of sactionine linkages on the precursors of these RiPPs by their respective sactisynthases was shown to be prevented in precursors lacking the leader sequence (Flühe et al., 2012, 2013). Therefore, the maturation of sactipeptides seems to be leader-dependent. However it remains unknown if a leader provided by itself, in trans, could be sufficient for the sactisynthases to process leaderless precursors as it has been shown for some RiPPs such as lanthipeptides (cf subsection 2.2.2 Roles of the leader peptide). Moreover, a PqqD-like RRE was identified in ThnB and SkfB, as well as HuaB and HuaC, the sactisynthases involved in the maturation of thurincin H, SKF, thuricin Z / huazacin, respectively (Wieckowski et al., 2015; Grell et al., 2018; Hudson et al., 2019). Deletion of the RRE of ThnB did not impair the ability of ThnB to generate 5'-Ado• radical from SAM but prevented the formation of the sacti-bridges on the precursor of thurincin H, proving its essential role for thurincin H maturation (Wieckowski et al., 2015). In Trn-α and Trn-β, a Gly-Gly proteolytic motif is found at the C-terminus of the leader peptide like in many RiPPs, although unlike these RiPPs the proteolytic cleavage occurs in between the two Gly residues instead of after them (Rea et al., 2010). However, this motif is not found in other sactipeptide precursors in which the cleavage sites involve different amino acid residues. The proteases responsible for leader peptide removal of sactipeptides belong to various families. The BGC of thurincin H encodes a protein with high homology for EpiP, a leader-peptide processing serine protease (Wieckowski et al., 2015) whereas two Zinc-dependent proteases are encoded in the subtilosin A BGC and are thought to be responsible for both leader peptide removal and macrocyclization (Flühe et al., 2012). A putative membrane-bound metalloprotease is also encoded in BGC of SKF, belonging to the Cys-A-A-X (A: an aliphatic amino acid) amino-terminal protease family (González-Pastor et al., 2003). The proteolytic cleavage of the precursors of Trn-α and Trn-β might occur in the cytoplasmic compartment as no signal sequence is found in the peptidase TnrE from the S41-type superfamily (Rea et al., 2010). Finally, the removal of

the leader peptide of huazacin is unexplained so far, as no peptidase is found in its BGC (Mo et al., 2019). In class III lanthipeptides it has been shown than the processing of the leader peptide involves proteases encoded in the genome of the producer that are located outside of the lanthipeptides BGC (Chen et al., 2019), a similar processing of huazacin is a possibility.

Regarding the biological roles of sactipeptides, they all exhibit an antibacterial activity. While subtilosin A has a broad-spectrum of activity against Gram positive and negative bacteria, thuricins CD, Z and thurincin H display narrow-spectra in Gram positive bacteria. The antibacterial activity of SKF appears to be less potent than other sactipeptides and its use as an alternative to antibiotic unlikely. SKF is produced by *B. subtilis* in a cannibalism process occurring when nutriments are limited. In these conditions, to delay the sporulation, *B. subtilis* cells with an active Spo0A protein produce and export SKF while cells with an inactive Spo0A protein are sensitive to SKF and lyse, releasing nutriments (González-Pastor et al., 2003). Although the activity of purified SKF against *B. subtilis* was proven on solid media, still to date no growth inhibition was observed in liquid culture of any type of bacteria (Liu et al., 2010). Subtilosin A is active against Gram positive bacteria including *Enterococcus faecalis, Listeria monocytogenes, Streptococcus pyogenes* and *Porphyromonas gingivalis* as well as some strains of Gram negative bacteria among for example *Klebsiella pneumoniae* or *Shigella sonnei* (Shelburne et al., 2007). The mode of action of subtilosin A involves bacterial membrane interaction. This sactipeptide partially buries itself in the phospholipid bilayers with the Trp-containing edge situated inside the bilayer while its negative charge groups stay outside, resulting in disturbance of the membrane architecture. At high concentration subtilosin A forms pores in the membrane resulting in cytoplasm leakages, although it might have a different and unidentified mode of action at lower but effective concentrations (Thennarasu et al., 2005). In *Gardnerella vaginalis*, it has been shown that subtilosin A causes efflux of intracellular ATP and ions, most likely through transient pores (Noll et al., 2011). In addition to its antibacterial activity, subtilosin A also displays a spermicidal action (Sutyak et al., 2008). Thuricin CD has a narrow-spectrum comprising Clostridia and Bacilli as well as *Listeria monocytogenes* with Minimum Inhibitory Concentrations (MIC) under the micromolar range and for lots of strains inferior to conventional antibiotics (Rea et al., 2010; Mathur et al., 2013; Mathur, Fallico, et al., 2017). The antibacterial activity of thuricin CD seems restricted to Gram positive bacteria and inefficient on Gram negative bacteria. In Gram positive bacteria, most Lactic Acid Bacteria (LAB) and *Bifidobacterium spp.*, which are considered as beneficial for the gut microbiota, are also resistant to thuricin CD. Although Trn-α and Trn-β display antimicrobial activity by themselves, the combination of both results in a synergistic effect with an increased potency by a factor of around 25 (Mathur, Fallico, et al., 2017). Because of its selectivity and potency against Clostridia, thuricin CD could be used as an alternative to antibiotic for the treatment of *C. difficile* infections (CDIs). Indeed, these infections are associated with dysbiosis, therefore selective antibiotics that would not impair the gut microbiota are actively sought. In an ex vivo distal colon model, thuricin CD was shown to be more effective than metronidazole, one of the antibiotic commonly used for the treatment of CDIs, to clear *C. difficile* (Rea et al., 2010). No significant alterations of the microbiota from this model was detected with thuricin CD treatment, whereas treatments with metronidazole or vancomycin, another antibiotic used for CDIs, or the lanthipeptide lacticin 3147 led to drastic remodeling of the different microbial communities populating this ex vivo distal colon model (Rea, Dobson, et al., 2011). Trn-α and Trn-β used alone or in combination have the same lytic action

on bacterial cells which arises from pore formation in the membrane and depolarization of the membrane. Since these sactipeptides have a narrow-spectrum, it is very unlikely that the mechanisms leading to pore formation are similar to those of the lanthipeptide nisin targeting lipid II which is present in most Gram positive bacteria. Thuricin CD most likely target specific receptors located in the membrane or the cell wall before forming pores (Mathur, Fallico, et al., 2017). Such as thuricin CD, thuricin Z has a pore-forming action effective on *Bacillus cereus* and *L. monocytogenes* with respective MIC of 2-8 μM and 4 μM (Mo et al., 2019; Hudson et al., 2019). Hardly any information on the biological activity of thurincin H is available but it seems to have a spectrum of activity similar to thuricin Z, that extends to other species of *Listeria* and *B. subtilis*. Gram negative bacteria as well as some genera of Gram positive bacteria such as *Lactobacillus* seem resistant to thurincin H. It should be noted that these information on the spectrum of action of thurincin H were collected in assays employing the producer strain and not the purified form of thurincin H (Lee et al., 2009). The mode of action of thurincin H remains to be elucidated.

In order to use sactipeptides as alternatives to antibiotics, supplementary information must be gathered on their antibacterial activity but also on their safety and their stability. Subtilosin A and thuricin Z have been shown to be safe for models of vaginal tissues or some human cell lines, respectively (Sutyak et al., 2008; Mo et al., 2019). However, the knowledge on sactipeptide cytotoxicity is limited to these experiments. Similarly, little is known on the sactipeptide stability to chemical, thermal or proteolytic treatments which could restrain their use in the clinic. The supernatant of the producer strain of thuricin CD was shown to keep its antibacterial activity in acidic condition (up to pH2) (Rea et al., 2010). However, purified Trn-β is sensitive to the action of trypsin and pepsin. Thus, thuricin CD can not be administrated orally as Trn-β would be degraded. Trn-α is resistant to the action of digestive enzymes, probably because its aromatic residues that could be used as cleavage sites are protected by sacti-bridges whereas they are located outside of the bridges, near the termini, in Trn-β (Rea et al., 2014).

Currently all known sactipeptides are produced by *Bacillus spp.* However, putative sactipeptide BGCs have been identified by genome mining in other phyla, thus this subclass of RiPPs could expand rapidly. The vast majority of them were found in Firmicutes but putative sactipeptide BGCs were also found in Actinobacteria or even in Gram negative Proteobacteria and Bacteroidetes (Hudson et al., 2019). Another genome mining study found that sactipeptide BGC-like clusters are the second most common RiPP cluster after lanthipeptide in the human gastro-intestinal tract (Walsh et al., 2015). Thuricin CD was isolated from a fecal strain of *B. thuringiensis* (Rea et al., 2010) and the sequence of the precursor of subtilosin A has been identified in metagenomic data from samples collected in the human gut, oral cavity and skin (Zheng et al., 2015). Therefore the human microbiota could be a potential source of sactipeptides. Other strategies to expand the class of sactipeptides employ bioengineering of known sactipeptides. A variant of subtilosin A with Ile instead of Thr at the 6th position was isolated with increased antibacterial potency (Huang et al., 2009). Although this variant exhibits hemolytic activity and thus won't be used in a clinical context, point mutation is an interesting lead for variant generation with novel features or increased potency. In that sense, variants of subtilosin A with Cys at different positions or with different amino acid acceptors or even with the introduction of non-proteinogenic amino acids were produced by co-expression of a bio-engineered gene encoding the precursor of subtilosin A and the gene encoding the sactisynthase AlbA in *E. coli* (Himes et al., 2016).

2.2.5 Ranthipeptides

The ranthipeptide or radical non-α thioether peptide subclass of RiPPs was very recently proposed to classify RiPPs with thioether linkages similar to sactionine but involving the β- or γ-carbon (C_β, C_γ) of the acceptor residue instead of the C_α (**Figure 2.36**) (Hudson et al., 2019; Precord et al., 2019). Ranthipeptides were discovered through the study of SCIFFs which stands for precursor peptides with Six Cysteines In Forty-Five residues. Originally, SCIFFs were identified through genome mining targeting radical SAM enzyme-containing RiPP BGCs. Radical SAM enzymes next to short sequences encoding putative precursors were classified in 5 groups, including a group where the precursors corresponded to putative SCIFFs. This group was the most prevalent in Clostridia (Haft & Basu, 2011). Sequence similarities between the precursor and the sactisynthase of subtilosin A with some putative SCIFF precursors and associated radical SAM enzymes, suggested that SCIFFs could harbor PTMs similar to sactipeptides. One of these SCIFFs, thermocellin CteA encoded in the genome of *Clostridium thermocellum* was modified in vitro after production by heterologous expression in *E. coli* and purification of both the precursor CteA and its associated radical SAM enzyme CteB. A sactionine linkage was identified on this SCIFF that was thus classified as a sactipeptide (Grove et al., 2017). Another SCIFF, Tte1186a, with a sequence similar to CteA was identified from the genome of *Caldanaerobacter subterraneus* subsp. *tengcongensis* and processed by its corresponding radical SAM enzyme in a similar way. Analysis of the maturation of Tte1186a revealed the presence of one thioether linkage at the same position of CteA that was assumed to be a sactionine linkage (Bruender et al., 2016). Tte1186a shows conserved residues with CteA and is therefore part of the thermocellin family. However, no natural SCIFFs were isolated from their producer strains and studied SCIFF were reconstituted in vitro which can sometimes fails to obtain a full maturation (Hudson et al., 2019). Hence, the incorporation of PTMs on SCIFFs and their nature remained speculation. Later another genome mining study identified other putative SCIFFs and their associated radical SAM enzymes. This study revealed that the radical SAM enzymes found in the BGCs of SCIFFs, including thermocellins, are actually more related to the enzyme QhpD than known sactisynthases. QhpD performs PTMs formation on quinohemoprotein amine dehydrogenase (QHNDH). The PTMs of QHNDH consist in 3 thioether linkages essential for QHNDH activity: 2 between Cys and the C_β of Asp and 1 between Cys and the C_γ of Glu. Moreover, it was noted that Asp was a conserved residue in putative SCIFF precursors. Therefore, it was hypothesized that SCIFFs might harbor thioether linkages involving C_β of Asp in particular and C_γ rather than C_α (Hudson et al., 2019). New structural studies were then conducted on CteA. A mature and L-[4-^{13}C,2,3-^{2}H2]-Thr labelled CteA was produced by co-expression of the genes encoding the precursor and the radical SAM maturase CteB in *E. coli*. NMR studies confirmed that CteA harbors a thioether bond between Cys and Thr but also revealed that the linkage involves the C_γ of Thr and not the C_α (Hudson et al., 2019). Although the precise thioether bond of Tte1186a has not been determined yet, because of the high resemblance of Tte1186a to CteA it can be expected to involve the C_γ (**Figure 2.37**).

Another SCIFF identified in this mining study from the genome of *Paenibacillus polymixa* was produced by co-expression of the genes *papA* and *papB* encoding respectively the precursor and the radical SAM enzyme in *E. coli*. PapA has an original sequence as it contains 6 repeats of Cys-X_3-Asp (**Figure 2.37**). Mass spectrometry (MS) analyses of PapA revealed a monoisotopic mass 12 Da lighter than the theoretical mass, which is

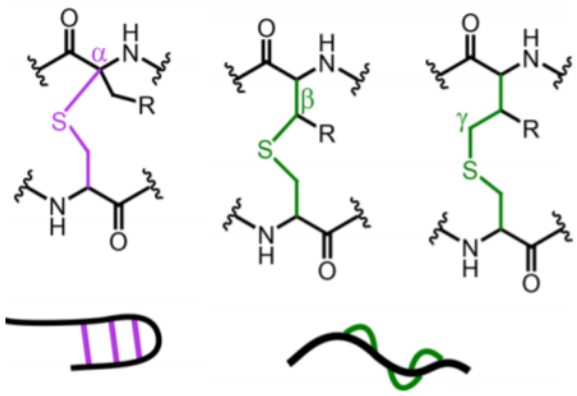

Figure 2.36: Sactipeptide versus ranthipeptide thioether linkages
The top part of the figure represents thioether linkages between a Cys and an amino acid acceptor on its C_α as found in sactipetides (purple) or on its C_β or C_γ as found in ranthipeptides (green). The lower part illustrates the structure resulting from this thioether linkages found in sactipeptides (purple) or ranthipeptides (green) Figure adapted from Hudson et al., 2019

consistent with the formation of 6 thioether linkages as each thioether bridge results in a loss of 2 hydrogen atoms and therefore 2 Da. Tandem Mass spectrometry (MS/MS) analyses of thioether linkages involving C_α or C_β, respectively found in sactipeptides and lanthipeptides, reported that collision-induced dissociation causes the thioether bridges involving a C_α to open whereas those involving C_β stay intact. In the case of PapA, the MS/MS pattern was closer to lanthipeptides than sactipeptides, suggesting that the thioether bonds employ C_β. NMR studies confirmed that the 6 Cys of PapA were bound to the 6 Asp through their C_β. Other variants of PapA were found with conserved 6 repeats of Cys-X_3-Asp and this family of ranthipeptides was named freyrasins (Hudson et al., 2019). Whereas only one Cys of thermocellin CteA is modified, the 6 Cys of freyrasin PapA undergo maturation. Therefore, SCIFFs maturation can involve thioether linkages between C_β or C_γ either on the 6 Cys or on selective Cys. Because of the distribution of Cys and of their amino acid acceptors in freyrasins, they adopt a structure with several loops on the backbone rather than a hairpin structure like sactipeptides (**Figure 2.36**). So far, only one ranthipeptide that does not also belong to the SCIFF family has been identified from the genomes of *Streptococcus orisratti* and *Streptococcus porci*, two commensal bacteria of the oral cavity of rats and pigs, respectively. The synthetic precursor NxxcA was modified in vitro by the associated radical SAM enzyme NxxcB after production by heterologous expression in *E. coli*. MS/MS and NMR analyses showed that NxxcA harbors one thioether bond linking a Cys and the C_β of an Asn. Surprisingly, the thioether bond in this SCIFF involves a Cys situated downstream of the acceptor residue whereas in all the other SCIFFs the Cys are always situated closer to N-terminus than the acceptor residues (**Figure 2.37**) (Caruso et al., 2019). It should be noted that still to date no natural ranthipeptide has been isolated from the producer strain. Although some ranthipeptides have been produced in vivo in *E. coli* rather than reconstituted in vitro, there is currently no proof that the mature ranthipeptides observed in the above-mentioned studies fully correspond to natural products.

Regarding the BGC of ranthipeptides, they all contain genes encoding: one precursor, one radical SAM enzyme also named ranthisynthase and one protein involved in

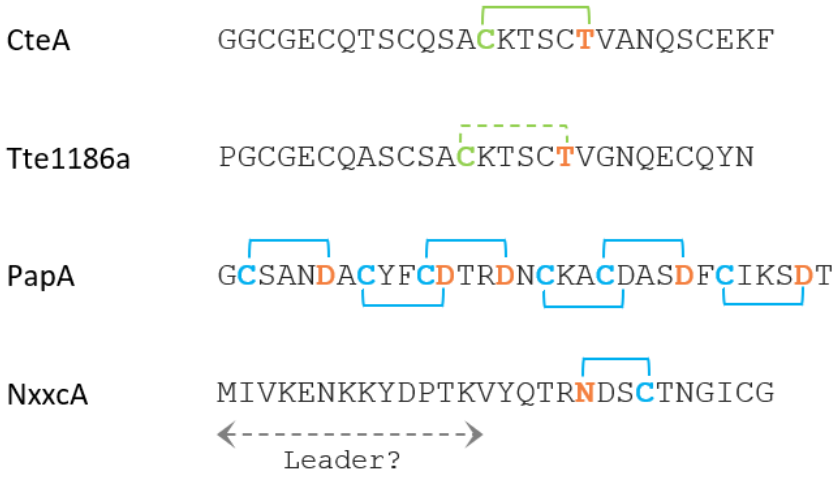

Figure 2.37: Sequences and thioether networks of ranthipeptides
Thioether linkages involving C_β and C_γ are represented in blue and green, respectively. Cys engaged in those bonds are also in blue or green whereas amino acid acceptors are in orange. The green dashed line indicates a thioether bond for which the linkage of S to C_γ has not been confirmed. For NxxcA, the sequence of the full precursor is provided as the partition between the leader and core sequences has not been identified yet whereas only the core sequences are shown for the other ranthipeptides.

export. Except for freyrasins, a 2nd protein for export and one gene with unknown function are found. In the NxxC cluster, a gene corresponding to a peptidase is found as well as two genes involved in regulation.

Like sactisynthases, ranthisynthases are SAM dependent. In vitro reconstitution of modified PapA with PapB occurred only when SAM was added. In PapB the mutation of any Cys from the Cys-X_3-Cys-X_2-Cys motif binding the 1st [4Fe-4S] cluster prevented the formation of 5'-Ado• (Precord et al., 2019). Moreover, all described ranthisynthases harbor a SPASM domain predicted to bind to 2 auxiliary [4Fe-4S] clusters. Therefore, a mechanism similar to sactisynthase in which the [4Fe-4S] bound by the Cys-X_3-Cys-X_2-Cys motif activates SAM in 5'-Ado• and the auxiliary clusters are involved in thioether bond formation can be expected. However, it is unclear how the ranthisynthases select C_β or C_γ rather than C_α for thioether formation. In PapA, the Asp were replaced with Glu. PapB was still able to form thioether bonds on the C_γ instead of the C_β, meaning that the ranthisynthase can tolerate different substrates and that the carbon of the acceptor involved in the thioether bond depends on the amino acid acceptors as observed for QhpD. However, when Asp were mutated in Ala, no PTMs were incorporated by PapB on PapA, so it seems the ranthisynthase has a substrate specificity. Individual mutation of Cys residues of the precursor PapA revealed that each Cys-X_3-Asp repeat is processed independently. In addition, the distance between Cys and the acceptor Asp plays a role in the maturation process as Cys-X_4-Asp repeats were not modified by PapB. Finally, the leader peptide rather than the core sequence seems to be essential for the recognition of the precursor by the ranthisynthase. Indeed, a thioether bond was incorporated by PapB on a precursor composed of the leader peptide of PapA fused to a single Cys-X_3-Asp motif (Precord et al., 2019). Regarding the recognition of the leader peptide by the ranthisynthases, a PqqD-like RRE has been identified in both CteB and PapB. A mutant of PapB lacking this RRE was unable of forming PTMs on PapA in a co-expression heterologous

system. However, when the RRE was also expressed by itself, in trans, in this system, PapA was fully modified (Grove et al., 2017; Precord et al., 2019). Thus, recognition of the precursor by a RRE seems to be essential in the maturation of ranthipeptides too.

No biological activity has been linked to ranthipeptides so far, however they were tested only against few bacteria. They might have a very selective antibacterial activity or a different type of activity. Moreover, as no ranthipeptide has been naturally isolated from bacteria, the forms produced in *E. coli* or in vitro might lack additional processing essential for biological activity. Therefore, further investigations are needed to determinate the functions of ranthipeptides, including screening for other antimicrobial and biological activities (e.g. anti-fungi, anti-inflammatory, anti-proliferative, ...).

2.3 Current clinical application

Ribosomal peptides and proteins offer several advantages as alternatives to antibiotics. First, they display potent antibacterial activity and some of them have mechanisms of action different from conventional antibiotics and therefore could be used to treat infections caused by antibiotic-resistant bacteria. Besides, it seems that bacteriocins and RiPPs have a lower tendency to generate resistance compared to conventional antibiotics, although resistance to these substances have already been observed. Moreover, some of them could be used for the treatment of infections occurring in complex microbial communities without causing dysbiosis as they exhibit high selectivity while other have a broad-spectrum of activity (Dischinger et al., 2014; Mathur, Field, et al., 2017). Another advantage associated with some RiPPs and bacteriocins is their very low toxicity for mammalian cells as they target specific bacterial components. However, this is not true for all bacteriocins and RiPPs that can sometimes display cytotoxicity directed against eukaryotic cells and hemolytic activity (Dischinger et al., 2014). The immune response to bacteriocins and RiPPs remained to be elucidated in most cases and so far some of them have shown low immunogenicity while other have an opposite effect (Dischinger et al., 2014; Vinogradov et al., 2019). Beside their direct action on pathogens, some RiPPs and bacteriocins can also have an indirect action on the infection clearance by modulating the immune response of the host (Mahlapuu et al., 2016).

As mentioned before, one of the major advantages of RiPPs and bacteriocins is that they offer a wide engineering potential and can be synthesized by heterologous expression, although the costs associated to this type of production are usually high and batch-to-batch variation is frequently observed. To overcome these inconvenient, synthetic methods for the production of RiPPs are under development. For example, a method of Solid-Phase Peptide Synthesis (SPPS) and modification named "Deferentially Protected Orthogonal Lanthionine Technology" was patented by the company Oragenics and allowed the consistent and cost-effective production on a large scale of MU1140-S a bioactive synthetic analog of the lanthipeptide mutacin 1140 produced by *Streptococcus mutans* (Mahlapuu et al., 2016; Sandiford, 2015). Moreover, antimicrobial peptides or proteins with a high cost of production could be associated with other antimicrobials or antibiotics that have lower costs of production. This strategy could even the cost of production of the therapeutic agents and offers multiple advantages. First, it has been shown for several RiPPs that they exhibit synergistic effects with antibiotics or other antimicrobials. Moreover, different pathways could be targeted which would reduce the risks of resistance development while increasing the efficacy of the strategy. Finally, using two different agents with

synergistic effects would reduce the needed doses for each agent and therefore decrease their potential secondary effects for mammalian tissues or even allow the uses of molecules that are toxic at high dosages (Arthur et al., 2014; Mathur, Field, et al., 2017).

Along with the cost of production, one of the major inconvenient of RiPPs and bacteriocins is their stability and bioavaibility. Indeed because of their proteinaceous nature, they can be degraded by proteases particularly in blood or by digestive enzymes, which can prevent their administration by the systemic and oral routes respectively. In addition, RiPPs and bacteriocins must stay metabolically active at physiological salt concentrations or pH conditions to be good candidates as alternatives to antibiotics. However, the stability of RiPPs and bacteriocins can be modulated by several strategies including cyclization, chemical modification of the N- or C-termini, incorporation of non-natural amino acids analogs or D-amino acids (Mahlapuu et al., 2016; Vinogradov et al., 2019).

2.3.1 In humans

Although the first RiPP, nisin, was isolated in 1928, the same year as penicillin, there is currently no RiPP approved for the treatment of bacterial or antimicrobial infections in humans. Nisin has been approved as a food preservative first by the Food and Agriculture Organization of the United Nations (FAO) and WHO in 1969, then by the United States Food and Drug Administration (FDA) in 1988 and finally by European Food Safety Authority (EFSA) in 1995. Since then, only the bacteriocin pediocin PA-1 from the class IIa of bacteriocins produced by Gram positive bacteria has also been approved as a food preservative (Silva et al., 2018). As for the medical field, no RiPP or bacteriocin is currently authorized for the treatment of infectious diseases in humans. The therapeutic potential of many RiPPs and bacteriocins has been proven in preclinical studies on animal models for the treatment of various types of bacterial infections and a few molecules are enrolled in clinical trials. Past or ongoing clinical trials on RiPPs and bacteriocins will be discussed in this section. Clinical studies comprise at the minimum 4 phases: (i) in Phase I the safety of the drug is assayed on healthy subjects with multiple doses; (ii) in Phase II the efficacy and side effects of the drug are measured on clinically ill patients; (iii) Phase III is similar to Phase II but concerns a much larger cohort of patients; (iv) Phase IV corresponds to post-marketing surveillance. So far no RiPP or bacteriocin in clinical trials have reached further than Phase II.

Among the clinical trials focusing on RiPPs, several concern the uses of derivatives of the thiopeptide GE2270A. This thiopeptide was originally isolated from *Planobispora rosea* and has a broad-spectrum of activity against Gram positive bacteria including species of *Staphylococcus, Enterococcus, Streptococcus, Clostridium* (Goldstein et al., 1993; LaMarche et al., 2012). GE2270A inhibits protein synthesis by interacting with the Elongation Factor Tu (EF-Tu). The poor solubility of this thiopeptide was an obstacle to its use as an alternative to antibiotic despite its potent antibacterial activity. Several analogs of GE2270A were therefore synthesized, the 4-aminothiazolyl analogs named LFF571 (**Figure 2.38**) was found to have optimal solubility while keeping a potent antibacterial activity and the same target as GE2270A (LaMarche et al., 2012). In particular, LFF571 was shown to be active on more than 500 clinical isolates of *C. difficile* with potency equivalent or greater than metronidazole or vancomycin, the two antibiotics most commonly used for the treatment of CDIs, as well as fidaxomicin, one of the most re-

cently approved antibiotic for the treatment of CDIs (Mullane et al., 2015). The efficacy of LFF571 was also proved pre-clinically on an animal model. Hamsters infected with *C. difficile* were treated with either LFF571 or vancomycin. Compared to untreated animals, the risk of death dropped by 90% with LFF571. Moreover, LFF571 treatment compared to vancomycin showed improved efficacy with lower doses as well as fewer cases of recurrences of CDIs following treatments (Trzasko et al., 2012). A randomized and double-blinded Phase I trial was implemented. Healthy subjects orally received either a single dose or repeated doses every 6 hours for 10 days of LFF571 of 25, 100, 400, 1000 mg while some subjects received placebos. No deaths or serious adverse effects were observed in any conditions. Observed adverse effects consisted in diarrhea or gastrointestinal pain but were as frequent in LFF571 or placebo treated groups (Ting et al., 2012). Therefore, LFF571 can be qualified as a safe drug. Then in a Phase II trial, 72 patients infected with *C. difficile* for the first time or the first recurrence were randomized and orally received either 200 mg of LFF571 or 125 mg of vancomycin 4 times a day during 10 days. The rates of clinical cure at the end of the treatment were of 91% and 78% for LFF571 and vancomycin, respectively. The recurrence of CDIs 30 days after treatment completion was measured by the detection of *C. difficile* toxins and associated with 19% and 25% rates, respectively for patients treated with LFF571 and vancomycin (Mullane et al., 2015). Therefore, LFF571 seems to be a promising alternative to conventional antibiotics for the treatment of CDIs. However, so far no Phase III trial has been reported (Petrosillo et al., 2018) and no information is available on whether the compound is dropped and if so why or whether further clinical investigations are under consideration.

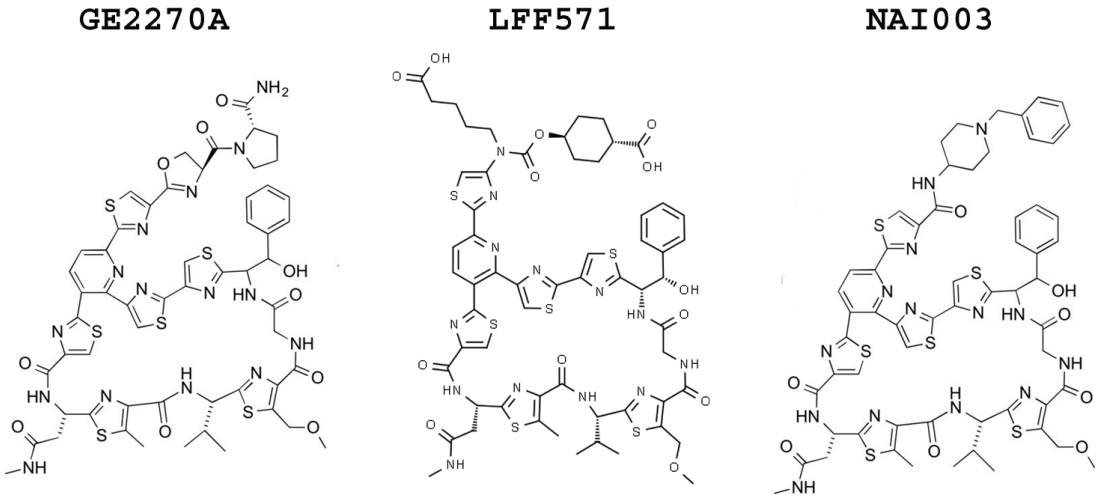

Figure 2.38: Chemical structures of GE2270A and its analogs

Another analog of GE2270A, NAI003 (**Figure 2.38**), displays a reduced spectrum of action. While NAI003 retains the potency of GE2270A against *Propionibacterium* spp. and *Enterococcus faecalis*, it is ineffective against *Staphylococcus* spp. or *Streptococcus* spp., unlike GE2270A. Therefore, its selective activity makes NAI003 a good candidate to inhibit the growth of *Propionibacterium acnes*, that is believed to provoke acne, without affecting the whole skin microbiota although the growth of other species of *Propionibacterium* found in the skin microbiota would most likely be impaired (Fabbretti et al., 2015). A phase II trial was still ongoing in 2019 in which adult men with acne were treated with either a placebo or a topical gel containing 3% NAI003 twice daily for 12 weeks. So

far no result have been reported for the phase II, however a phase III is already planned for 2021-2022 (source:AdisInsight Trials).

Lastly, clinical trials employing a semi-synthetic lanthipeptide have been developed as well. Generation of derivatives of the lanthipeptide deoxyactagardine B produced by *Actinoplanes liguriae* yielded analogs with a positive charge and an increase potency against *C. difficile*. In particular, the 7-aminoheptylamido-deoxyactagardine B analog displays efficacy against *C. difficile* at low concentrations with a potency increased by 4 compared to deoxyactagardine B while other Gram positive bacteria such as *Enterococcus* spp. or *Staphylococcus* spp. are inhibited at higher concentrations. This analog named NVB302 was as efficient as vancomycin to clear CDIs in a in vitro gut model or in animal models. In 2011, a pre-Phase I clinical trial was initiated on healthy subjects receiving NVB302 either in a single dose of 1.5 g or in daily doses of 1 g for 10 days. No adverse effect was observed on these subjects (Crowther et al., 2013; Boakes & Dawson, 2014). A Phase I trial started in 2016, however no results were reported and it was discontinued in 2018 (source:AdisInsight Trials).

So far, no other RiPP or bacteriocin has been the object of clinical trials for the treatment of bacterial infections. Some RiPPs are considered for other medical applications than infectious diseases. For example, the lanthipeptide duramycin entered Phase II trial for the treatment of cystic fibrosis, a genetic disease (Huo et al., 2017). The conopeptides CGX-1160, ACV1 and ziconitide are in Phase I, Phase II or already approved by the FDA for pain management, respectively (Gao et al., 2017).

2.3.2 In poultry

Until now, only one RiPP has been approved by the FDA for the treatment of bacterial infections in livestock. In 1999, the company ImmuCell started the commercialization in the US of Wipe Out®, which corresponds to nisin-containing wipes used before and after milking to prevent mastitis in dairy cows. Mastitis is one of the most common affliction in cows and is linked to bacterial infections caused by a wide range of pathogens, the most frequent being *Streptococcus* spp., *S. aureus, Corynebacterium bovis* and *E. coli* (Dufour et al., 2019). According to the "Dairy 2014" survey of the USDA (United States Department of Agriculture), 21% of dairy cows are treated for mastitis with antibiotics. ImmuCell stopped selling Wipe Out® but the FDA approved the development of another product, Mast Out®, an intramammary nisin-based drug for the treatment of mastitis (ImmuCell, 2016). Currently, ImmuCell is waiting for the FDA approval of Re-Tain™, a syringe pre-filled with nisin, also for the treatment of mastitis. Unlike all the antibiotics currently available for the treatment of mastitis, no trace of nisin was detected with both products in the milk or the meat of the cows after or even during the treatment (ImmuCell, 2016, 2019). Although no other RiPP or bacteriocin is currently approved or under FDA approval for the treatment of bacterial infections in livestock, many assays on the efficacy of RiPPs and bacteriocins are ongoing in different livestock animals. Because poultry is one of the main focus of Adisseo, the private partner of my thesis project, in vivo assays of the efficacy of RiPPs or bacteriocins to clear bacterial infections in poultry will be discussed here.

Research for the uses of ribosomal peptides and proteins to cure infections in poultry focus on two of the main pathogens responsible of these infections: *Clostridium perfringens*

and *E. coli* (Ben Lagha et al., 2017). Additionally, molecules active against *Campylobacter jejuni* are actively sought since *C. jejuni* is responsible of infections in humans often associated with the consumption of contaminated poultry meat (Meunier et al., 2016).

Pediocin A produced by *Pediococcus pentosaceus* FBB61 is a protein of 80 kDa belonging to class III bacteriocins produced by Gram positive bacteria active against *C. perfringens*. The efficacy of pediocin A was assayed on female or male broiler chickens with the filtrated supernatant of FBB61 or a purified form of pediocin A. In any case, preventive treatment led to a significant weight increase of healthy animals but following *C. perfringens* infection no such weight increase was detected between the treated and untreated groups. Moreover, treatment with pediocin A failed to rescue animals from *C. perfringens* infection (Grilli et al., 2009). Based on these 2 studies, it seems that adding pediocin A in feed can increase the weight of healthy animals but in the conditions tested it failed as an alternative to antibiotics to cure a *C. perfringens* infection.

In another study, the purified but unidentified bacteriocin produced by *Lactobacillus plantarum* F1 was used to cure *E. coli* infected broiler chickens. After 7 days of infection, chickens had significantly lost weight compared to healthy animals. On the contrary, chickens that were treated with the bacteriocin produced by *Lactobacillus plantarum* F1 for the last 3 days of the infection exhibited a weight similar to healthy animals. Moreover, both healthy and treated animals had no lesions on the heart, liver and the lung tissues whereas the animals infected but left untreated did. *E. coli* was isolated from the liver, lung and spleen of respectively 60, 48 and 60% of the animals in the infected but untreated group whereas no *E. coli* was detected in healthy broiler chickens. The treatment with the bacteriocin produced by *Lactobacillus plantarum* F1 was successful to reduce the loads of *E. coli* as it was detected in the same compartments of the infected and treated group only in 8, 0 and 4% of cases, respectively. Therefore, the unidentified bacteriocin produced by *L. plantarum* F1 seems to be potent to clear infections of *E. coli* in broiler chickens (Ogunbanwo et al., 2004).

Three different bacteriocins have been assayed to reduce the loads of *C. jejuni* in poultry. The object of the first study was a partially characterized bacteriocin produced by *Paenibacillus polymyxa* NRRL B-30509. This unnamed bacteriocin of 3.9 kDa belongs to the class IIa of bacteriocins produced by Gram positive bacteria. After 7 days of infection with *C. jejuni*, male broiler chickens were treated with this bacteriocin encapsulated in polyvinylpyrrolidone and given in feed for 3 days. The fecal loads of *C. jejuni* were significantly reduced in broiler chickens treated with the bacteriocin (Stern et al., 2005). The 2nd study had the exact same design as the first one but the treatment was done with another class IIa bacteriocin: OR-7. This bacteriocin has a size of 5.1 kDa and is produced by *Lactobacillus salivarius* NRRL B-30514. The outcome of this study was the same as the previous study: the treatment with OR-7 induced a significant decrease of the fecal loads of *C. jejuni* (Stern et al., 2006). Finally, the last bacteriocin that has been assayed in poultry against *C. jejuni* is enterocin E-760, a class IId bacteriocin of 5.4 kDa in the Gram positive classification produced by an unidentified specie of *Enterococcus*. The design of this study was slightly different from the others as no control group of healthy animals was constituted. Instead 4 groups of male broiler chickens were infected with *C. jejuni* and one of them was left untreated whereas the other 3 received increasing doses of enterocin E-760. After the 3 days of treatment, *C. jejuni* couldn't be detected in the cecal contents of the treated animal, even those treated with the lowest dose, whereas detection of *C. jejuni* was validated in untreated animals. Moreover, the efficacy of enterocin E-760 was further proved in naturally *C. jejuni* infected chickens. After the 4 days of

treatments, *C. jejuni* couldn't be detected from the cecal contents of 9 out of 10 treated broiler chickens whereas the cecal contents of all the untreated animals were still carrying *C. jejuni* (Line et al., 2008). Hence, the three different bacteriocins employed in these studies could be considered as alternatives to antibiotics to clear *C. jejuni* infections in broiler chickens.

Chapter 3

RiPPs of *Ruminococcus gnavus* E1

3.1 *Ruminococcus gnavus* E1 vs. *Clostridium perfringens*

R. gnavus is a strictly anaerobic Gram positive bacterium, belonging to the Lachnospiraceae family, the Clostridia class and the Firmicutes phylum. Lachnospiraceae is a predominant family of the Firmicutes in the human colonic microbial community which is the most dense community of the gut. In particular, *R. gnavus* is present in more than 90% of human fecal samples with a median abundance of 0.1% (Sekelja et al., 2011; Crost et al., 2018; Bell et al., 2019). Although increased gut loads of *R. gnavus* have been linked to several types of diseases such as Inflammatory Bowel Disease (IBD) and Crohn's disease (Henke et al., 2019) or even Lupus nephritis (Azzouz et al., 2019), *R. gnavus* might play a protective role against pathogens in a balanced gut microbiome by producing antimicrobial RiPPs.

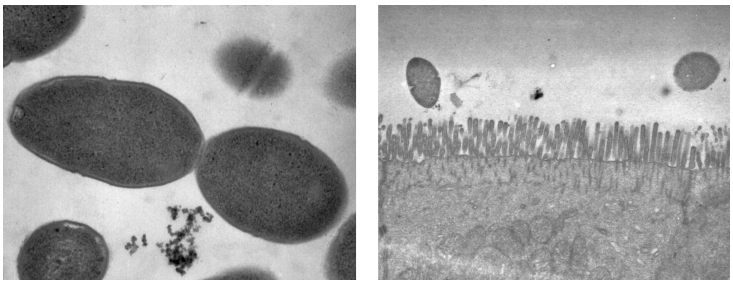

Figure 3.1: *R. gnavus* E1
Transmission electronic microscopy (TEM) of R. gnavus *E1 (left, magnification × 20 000) and the colon of a rat mono-associated with* R. gnavus *E1 (right, magnification × 7 000).*

R. gnavus E1 (**Figure 3.1**) was isolated from a fecal sample of a healthy adult. The first observation of the production of an antimicrobial substance by this strain was brought to light by the colonization of germ-free rats with *R. gnavus* E1 and then infected by serotype A *C. perfringens*. Not only, *C. perfringens* was eliminated faster than a transit marker in these rats but a diffusible substance active against *C. perfringens* was also found in their feces (Ramare et al., 1993). Moreover, inoculation with *R. gnavus* E1 in rats mono-colonized by *C. perfringens* was sufficient to eliminate *C. perfringens* (**Figure**

3.2). Ligation of the pancreatic canal in these rats resulted in the loss of the anti-*C. perfringens* activity in the intestinal tract as well as in the feces. The oral administration of trypsin inhibitors had the same effects. The anti-*C. perfringens* activity was restored as soon as the treatment with trypsin inhibitors stopped or when trypsin was given orally to the rats that underwent pancreatic canal ligation. Moreover, Ramare and co-workers showed that *R. gnavus* E1 produced an anti-*C. perfringens* substance in liquid culture supplemented in trypsin. However, when trypsin was added belatedly in the culture, this anti-*C. perfringens* substance was not produced. Therefore, it seems that trypsin is not acting or not exclusively by activating this substance by proteolysis but rather acts as an inducer or an activator of an inducer. The role of trypsin in the production of this substance is specific as the addition in the liquid culture of other digestive proteases secreted by the pancreas such as chymotrypsin, elastase or carboxypeptidases A or B failed to induce the production of the anti-*C. perfringens* molecule (Ramare et al., 1993).

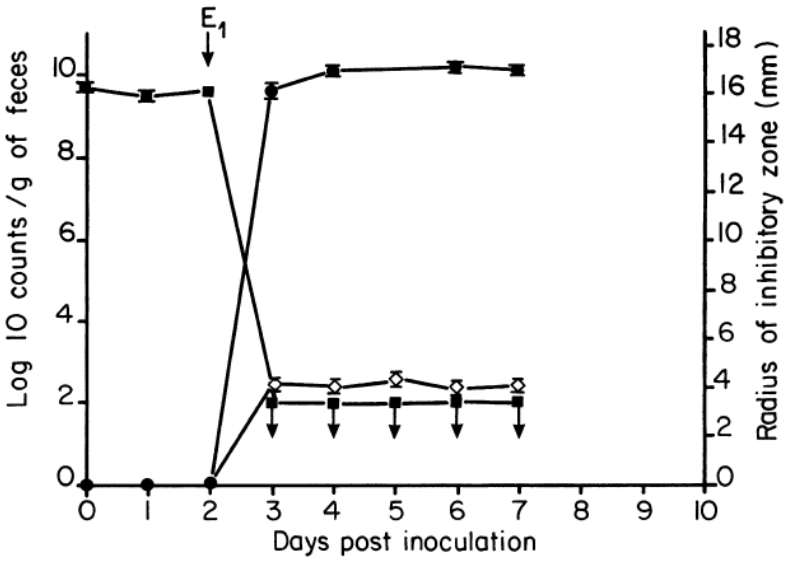

Figure 3.2: Kinetics of elimination of *C. perfringens* CpA in rats feces after inoculation with *R. gnavus* E1

Mono-associated rats with a stable load of C. perfringens *CpA (▪) were inoculated with* R. gnavus *E1 (•). The radius of inhibitory zone against* C. perfringens *CpA around the feces is shown with ⋄. Limit of detection of strains is indicated with ↓. Figure from Ramare et al., 1993.*

3.2 Ruminococcin A

In 2001, Dabard and co-workers identified the anti-*C. perfringens* substance produced by *R. gnavus* E1 ex vivo in liquid culture supplemented with trypsin. They purified from the culture's supernatant an active peptide of 24 amino acids and 2,7 kDa and named it Ruminococcin A (RumA). Mass Spectrometry (MS), Tandem Mass Spectrometry (MS/MS) and Edman degradation revealed a partial sequence and some PTMs of this peptide consisting in the presence of two unreacted Dhb residues. Thanks to the partial

sequence, degenerate oligonucleotides were designed and used to sequence the synthesis gene encoding RumA and get the full sequence of RumA. From the difference in mass between the theoretical sequence and the experimental data and taking into considerations the previous structural data, the authors deduced the presence and position of a Lan and a MeLan rings (**Figure 3.3**). Hence, the peptide was classified as a lanthipeptide (see section 2.1.3. Classification). Dabard and co-workers also showed that RumA has a broad-spectrum activity toward Gram positive bacteria and in particular is active against most enteropathogenic Clostridia (Dabard et al., 2001).

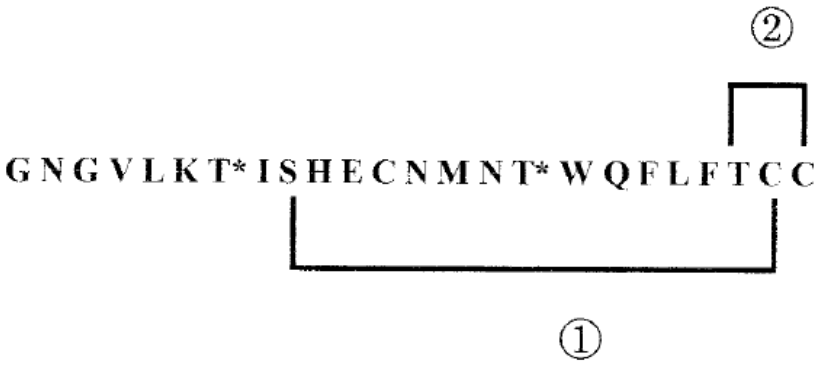

Figure 3.3: Sequence and putative PTMs of RumA
∗ represents Dhb residues, ① and ② indicate respectively the position of the putative Lan and MeLan rings. Figure from Dabard et al., 2001.

After identifying the biosynthesis gene of RumA the entire genetic cluster was sequenced by Gomez and co-workers (Gomez et al., 2002). This 12,8 kb regulon contains 13 ORFs, split in 3 transcriptional units or operons encoding: (i) immunity; (ii) regulation; (iii) synthesis and export (**Figure 3.4**). Genes *rumR2, rumH, rumG, rumE, rumF* are thought to be involved in the immunity of *R. gnavus* E1 to its own lanthipeptide RumA. Two genes seem to regulate the production of RumA: *rumK* and *rumR* show high similarity to genes encoding EnvZ-like sensor histidine kinases and OmpR-like response regulators, respectively. Therefore, RumA's production is most likely regulated by a EnvZ/OmpR-like two-component system, involving an inducer activated by trypsin proteolysis. Indeed, transcription analysis in this study demonstrated that trypsin induces the expression of the genetic cluster of RumA as Ramare and co-workers suspected. In the synthesis and export transcriptional unit, the 3 genes $rumA_1$, $rumA_2$ and $rumA_3$ have a mean identity of 95% in nucleotide sequences and encode the same 47 amino acids precursor. The gene *rumM* encodes a putative protein of 107 kDa showing high similarity with enzymes that catalyze the dehydration and thioether bridge formation on lanthipeptide precursors. Therefore, it seems that RumM has a bifunctional role as dehydratase and cyclase and is the only enzyme required to incorporate PTMs on the RumA precursor, which classifies RumA in the class II lanthipeptide. Downstream *rumM*, a putative ABC transporter is encoded by *rumT*. This transporter is also predicted to be responsible of the cleavage of the leader peptide as it contains a Cys-protease domain in his N-terminal region characteristic of lanthipeptide leader peptide processing. Finally, no known function has been identified for the last gene of this operon, *rumX*.

The regulon of RumA is predicted to be located on a mobile genetic element. Marcille and co-workers isolated 14 strains from adult or children fecal samples exhibiting an anti-*C. perfringens* activity. Out of the strains, 7 harbored *rumA*-like genes with deduced

Figure 3.4: Genetic regulon of RumA
p_1 to p_3 and t_1 to t_4 represent respectively putative transcriptional promoters and terminators. Figure from Gomez et al., 2002.

amino acid sequences identical to RumA or carrying only one different residue. These strains were identified as belonging to the *R. gnavus* specie or to closely related species, namely *Clostridium nexile* and *Ruminococcus hansenii*. Therefore, Marcille and co-workers concluded that the regulon encoding the production of RumA could be present in many more strains and be transferred to several other species in the gut (Marcille et al., 2002).

Recent studies gave more insights on the structure of RumA (Ongey et al., 2018). The genes encoding RumM, the enzyme involved in the maturation of the core peptide of RumA, and the precursor of RumA composed of both leader and core peptide, were expressed in *E. coli*. RumM was sufficient to incorporate PTMs on RumA, consisting in dehydration of threonine and serine and formation of thioether bridges with the sulfur atom of cysteines. Therefore, the bifunctional role of RumM was confirmed as well as the classification of RumA in the class II lanthipeptide. MS and MS/MS analysis confirmed the PTMs found by Dabard and co-workers in 2001. However, an additional MeLan ring was identified. Though these structural studies were done on a biosynthetic RumA produced by heterologous expression instead of the peptide produced by *R. gnavus* E1 and were not confirmed by NMR analysis or crystallography, we can thus consider the following steps for the maturation of RumA by RumM:

1. dehydration of Thr7, 16 and 22 in Dhb and dehydration of Ser9 in Dha;
2. formation of thioether bridges between Dhb7 and Cys12, Dhb22 and Cys24 resulting in MeLan rings, and between Dha9 and Cys23 resulting in a Lan ring.

Removal of the leader peptide and therefore full maturation of RumA into an active form is potentially achieved by the ABC transporter RumT (**Figure 3.5**).

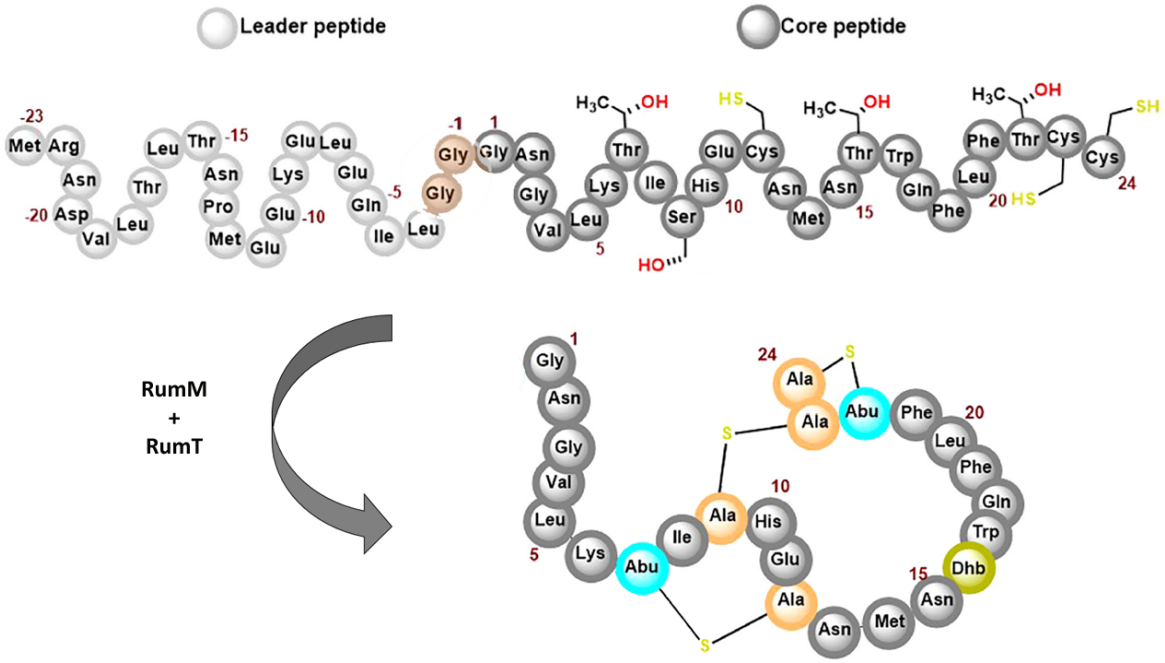

Figure 3.5: Actualized PTMs of RumA

The unmodified sequence of the precursor of RumA is shown at the top. Side chains of Thr or Ser submitted to dehydration and then binding to Cys sulfur atoms are indicated. Fully maturated RumA after PTMs incorporation PTMs by RumM and leader peptide cleavage by RumT is represented at the bottom. Abu-S-Ala = MeLan residue; Ala-S-Ala = Lan residue. Figure adapted from Ongey et al., 2018.

3.3 Ruminococcins C

Transcription analysis revealed that the biosynthesis genes of RumA are not expressed, or at least not above detection limits, in the cecal contents of rats mono-colonized by *R. gnavus* E1 (**Figure 3.6**) (Crost et al., 2011; Pujol et al., 2011), thus suggesting that the anti-*C. perfringens* activity observed in vivo by Ramare and co-workers is 1993 can not be attributed to RumA. Studies on *R. gnavus* E1 were therefore pursued with cecal contents of rats again, instead of liquid cultures, to isolate the substance responsible of the in vivo anti-*C. perfringens* activity.

This substance was identified and named Ruminococcin C (RumC) by Crost and co-workers in 2011. The first attempt to purify RumC from cecal contents of *R. gnavus* E1 mono-associated rats yielded a mixture of 2 peptides characterized by molecular weights of 4324 and 4456 Da and a fraction containing an isolated peptide of 4235 Da. These peptides were partially sequenced by Edman degradation, which allowed the design of degenerate oligonucleotides and then the identification of 5 putative genes encoding the precursors of RumC. The first of these genes is located 8 kb downstream of the last gene of the genetic cluster of RumA (Crost et al., 2011).

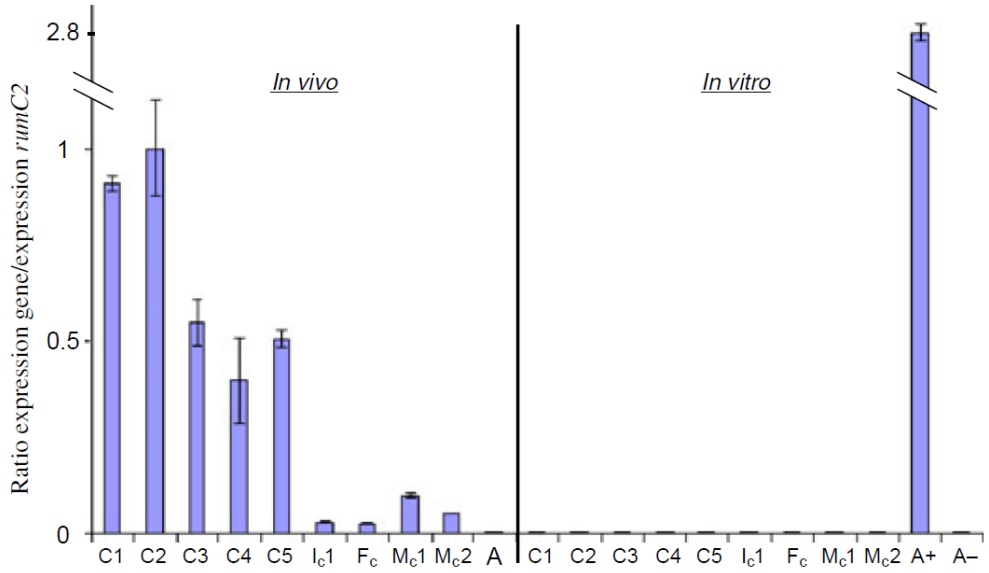

Figure 3.6: Expression of genes from the RumA and RumC regulons
Expression levels of rumC1, rumC2, rumC3, rumC4, rumC5, rumIc1, rumFc, rumMc1, rumMc2 *and* $rumA_{1-3}$ *in the cecal contents of rats mono-associated with* R. gnavus *E1 (in vivo) or in liquid culture of* R. gnavus *E1 (in vitro) supplemented with trypsin (+) or not (-). In the case of the RumC regulon, trypsin supplementation in liquid culture had no impact on gene expression. Figure from Pujol et al., 2011.*

The full regulon of the biosynthesis of RumC was then sequenced and annotated (Pujol et al., 2011). With a size of 15 kb it is composed of 17 ORFs separated in 6 transcriptional units (**Figure 3.7**). Out of these 17 ORFs, 5 encode putative peptides of 63 amino acid residues with sequence identity from 69 to 87% among them, these biosynthesis genes are named *rumC1* to *rumC5*. Thanks to the measured molecular weight of the peptides identified by Crost and co-workers, a partition between the leader peptide and

the core peptide was deduced. This partition was confirmed by the presence of a potential proteolytic cleavage site, namely the lysine or arginine residues in position 19 (**Figure 3.8**). Without their leader peptides, the putative 5 isoforms of RumC exhibit an amino acid sequence identity ranging from 80 to 86% whereas the identity between the precursors is slightly lower from 75 to 86%. By comparison of the measured molecular weights of the isolated peptides and the theoretical weights of the core peptide sequences of the different isoforms, Crost and co-workers deduced that the fraction composed of a mixture of peptides corresponded to RumC1 and RumC4 while the fraction containing one peptide corresponded to RumC5 (**Table 3.1**) (Crost et al., 2011).

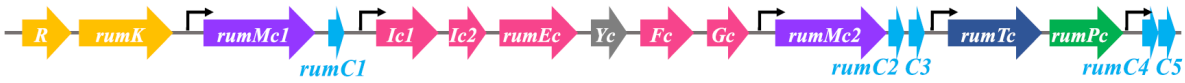

Figure 3.7: Regulon of RumC

Colors indicate the main functions of the genes: yellow=regulation; purple=maturation; light blue=precursor synthesis; pink=immunity; dark blue=secretion; green=peptidase; gray=unknown. ↱ *represents the operons partition.*

The first two ORFs of the RumC regulon, *rumRc* and *rumKc*, encode putative proteins displaying high similarities with OmpR-like regulators and EnvZ-like histine kinase implicated in two-component transcriptional regulation systems, similarly to *rumR* and *rumK* from the RumA regulon. In fact, *rumKc* and *rumK* have 40% identity. Two ORFs with 96% identity encode the putative proteins RumMc1 and RumMc2 containing a domain specific to iron-sulfur (Fe-S) oxydoreductase and were classified as members of the radical S-Adenosyl-Methionine (SAM) enzymes family. This family regroups proteins with [4Fe-4S] clusters coordinated by Cys-X_3-Cys-X_2-Cys motifs. Putative RumMc1 and RumMc2 contain a cysteine rich domain on their C-terminal part and also present homology to other radical SAM enzymes like AlbA and TrnCD, respectively responsible of the maturation of the sactipeptides subtilosin A and thuricin CD. The genes encoding these presumed maturases are adjacent to the synthesis genes: *rumMc1* and *rumMc2* are located directly upstream of *rumC1* and *rumC2-rumC3*, respectively. The 5 ORFs *rumIc1, rumIc2, rumEc, rumFc, rumGc* are predicted as part of the immunity system of *R. gnavus* E1 to RumC. No known function could be attributed to *rumYc*. Finally, RumTc was predicted as an ABC-transporter whereas RumPc was predicted to be a metallopeptidase, both of them are most likely involved in the secretion of RumC. In summary, the 17 ORFs of the RumC regulon are distributed in (i) 3 operons responsible for the biosynthesis of the 5 isoforms of RumC and 3 operons involved in: (ii) regulation, (iii) immunity, (iv) export. In human fecal samples, *rumC*-like genes were found in 10 strains belonging to *R. gnavus* or very closely related (Pujol et al., 2011).

All the genes from the RumC regulon are expressed in vivo in the cecal contents of rats mono-associated with *R. gnavus* E1 (Pujol et al., 2011). Among the 17 ORFs, *rumC1* and *rumC2* show the highest levels of expression (**Figure 3.6**). Surprisingly, *rumC2* and *rumC3* were expressed and *rumC2* even featured the highest level of expression of all the genes from the RumC regulon even though no peptide corresponding to RumC2 and RumC3 were detected in the cecal contents of the *R. gnavus* E1 mono-associated rats (Pujol et al., 2011; Crost et al., 2011). However, it is not possible to tell if those isoforms are not traduced in vivo or if they are degraded in the gut or were degraded along the purification steps. Furthermore, the isoforms might have been lost throughout

the purification. In particular it is conceivable that they have a different activity spectrum than the purified isoforms and are not active against *C. perfringens* which was used as a target to select the purification fractions containing RumCs.

Unlike the genes from the RumA regulon, the genes involved in the production and regulation of RumC are not expressed in liquid culture of *R. gnavus* E1 even when the culture is supplemented with trypsin (**Figure 3.6**) (Pujol et al., 2011). Trypsin was proven to be necessary for the production of RumC in vivo (Ramare et al., 1993) and is an inducer of the production of RumA (Gomez et al., 2002). Trypsin could as well be an inducer of the RumC regulon but there must be another additional inducer produced in the gut that is lacking in the liquid culture of *R. gnavus* E1.

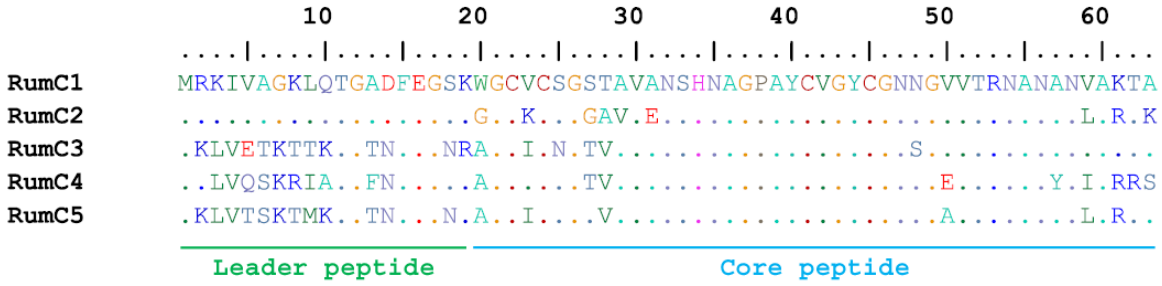

Figure 3.8: Amino acid sequences of the 5 isoforms of RumC

The information withheld in the regulon of RumC suggest that the RumC isoforms could be sactipeptides. Indeed, two putative maturases clustering with sactisynthases are found in this regulon. Moreover, all of the 5 isoforms have 4 cysteines conserved in their core peptide sequences that could be involved in sacti-bridges (**Figure 3.8**). However the structural data gathered by Crost and co-workers on the 3 peptides isolated from cecal contents were not supporting that theory. Interestingly, for these 3 peptides, identified as RumC1, RumC4 and RumC5, there was a loss of 7 Da between the theoretical and the observed weights which suggested that these peptides might undergo PTMs (**Table 3.1**). Edman degradation of these peptides was blocked after the 11th cycle. Interruption of Edman degradation had been observed when Lan or MeLan rings were present or in the case of the sactipeptide subtilosin A at the positions of the sacti-bridges. Therefore, blockage of Edman degradation could have meant that the isoforms of RumC were lanthipeptides or sactipeptides. However, Crost and co-workers followed their studies with alkylation assays and concluded that at least one of the 4 cysteines was free and that the others could be involved in disulfide bonds but not in any kind of mono-sulfide bond (such as Lan, MeLan, or sacti), since all the cysteines could be alkylated after reduction and one without reduction. Therefore, one chemical bond was proposed for RumC: a disulfide bond between 2 cysteines with the 2 others remaining free, although the authors stayed cautious and stated that a thorough characterization of the secondary and tertiary structures of RumC remained to be done (Crost et al., 2011).

Finally we learned from Crost and co-workers that the mixture of RumC1 and RumC4 as well as RumC5 displayed activity against *C. perfringens* as expected with a approximate Minimum Inhibitory Concentration (MIC) of 40 µg/mL, but also against some strains of *Bacillus cereus* and *Listeria monocytogenes*. No activity against Gram negative strains was detected (Crost et al., 2011).

Isoform	Observed	Theoretical
RumC1	4324	4331
RumC4	4456	4463
RumC5	4235	4242

Table 3.1: Molecular weights (Da) of the RumC isoforms isolated from cecal contents of *R. gnavus* E1 mono-associated rats

Chapter 4
Thesis objectives

The aims of my thesis were:

1. to purify the 5 isoforms of RumC and optimize the purification protocol;
2. to characterize the isoforms with a structure-function approach, elucidate their structures and understand the maturation mechanisms;
3. to determine their activity spectra;
4. to study their effects on healthy or *C. perfringens* infected broiler chickens.

As RumC is only produced in vivo when *R. gnavus* E1 is within a host but not in cultures, the chosen strategy to achieve these goals was to colonize germ-free rats with *R. gnavus* E1 and to purify RumC from their gut contents. Working with germ-free rats was made possible thanks to the ANAXEM platform from MICALIS department of the french National Institute for Agricultural Research (INRA) in Jouy-en-Josas. As Crost and co-workers purified 3 of the 5 isoforms of RumC (Crost et al., 2011) and as Pujol and co-workers showed that the gene encoding the 5 isoforms of RumC are expressed in vivo in the rat guts (Pujol et al., 2011), my goal was also to optimize the purification protocol to attempt to isolate the 5 isoforms.

After purification of the RumC isoforms, one of the main objectives was to determine their PTMs using C18-Liquid Chromatography (LC)/MS, MS/MS and NMR and therefore to be able to position RumC in the RiPPs classification. MS analyses were done in collaboration with the EdyP platform of the French Alternative Energies and Atomic Energy Commission (CEA) in Grenoble and NMR in collaboration with the Mediterranean Microbiology Institute (IMM).

Another aim was to characterize the biological activity of the 5 isoforms of RumC against pathogen or commensal bacteria, first using the "inhibition halos" method and then by measuring minimum inhibitory concentrations (MIC) and minimum bactericidal concentration (MBC). The first assay is used in a qualitative manner to identify the sensitive and resistant species to RumC while the second assay allows the quantification of the lowest dose of RumC necessary to inhibit the growth or to kill the sensitive strains.

The last goal of my thesis was to measure the effects of RumC on healthy and *C. perfringens* infected broiler chickens. This model of animal study and infection was chosen for multiple reasons: (i) *R. gnavus* E1 was originally identified as a strain producing active molecules against *C. perfringens*, (ii) *C. perfringens* is one of the main pathogen of broiler chickens and finally (iii) my thesis project was done in collaboration with ISM2 and Adisseo, the latter being a worldwide leading company in nutritional solutions and

additives for animal feed and especially poultry. Adisseo and in particular the CERN department are interested in promoting digestive tract health and understanding the microbial ecology of farming animals. Infection by *C. perfringens*, causing necrotic enteritis, is one of the 3 main causes of death in broiler chickens and sub-clinical infections result in reduction of digestion and therefore loss of weight (Van Immerseel et al., 2004). In 2015, it was estimated that *C. perfringens* infections in poultry were responsible of a economic loss of 6 billions dollars per year worldwide (Wade & Keyburn, 2015). It was also initially considered to assay the effects of RumC on another mono-gastric animal model like mice to confirm the efficiency of RumC to clear infections in multiple models and in order to initiate pre-clinical studies toward human health.

Finally, my thesis is a part of the project RUMBA 2016-2020 ANR-15-CE21-0020, while I was working on the purification of the RumC isoforms from rat cecal contents, our collaborators at the Laboratory of Metal Chemistry and Biology (LCBM) at CEA in Grenoble were studying synthetic or biosynthetic ways of producing RumC. The initial plan was to use a host organism to express the genes encoding RumC and to maturate chemically synthesized peptides in vitro. My part in this project was also to assess the biological activity of these peptides.

The objectives of the project RUMBA 2016-2020 ANR-15-CE21-0020, the strategy chosen to answer them and all the partners involved in this project are summarized on **Figure 4.1**. In particular, I was involved in all the tasks represented in red.

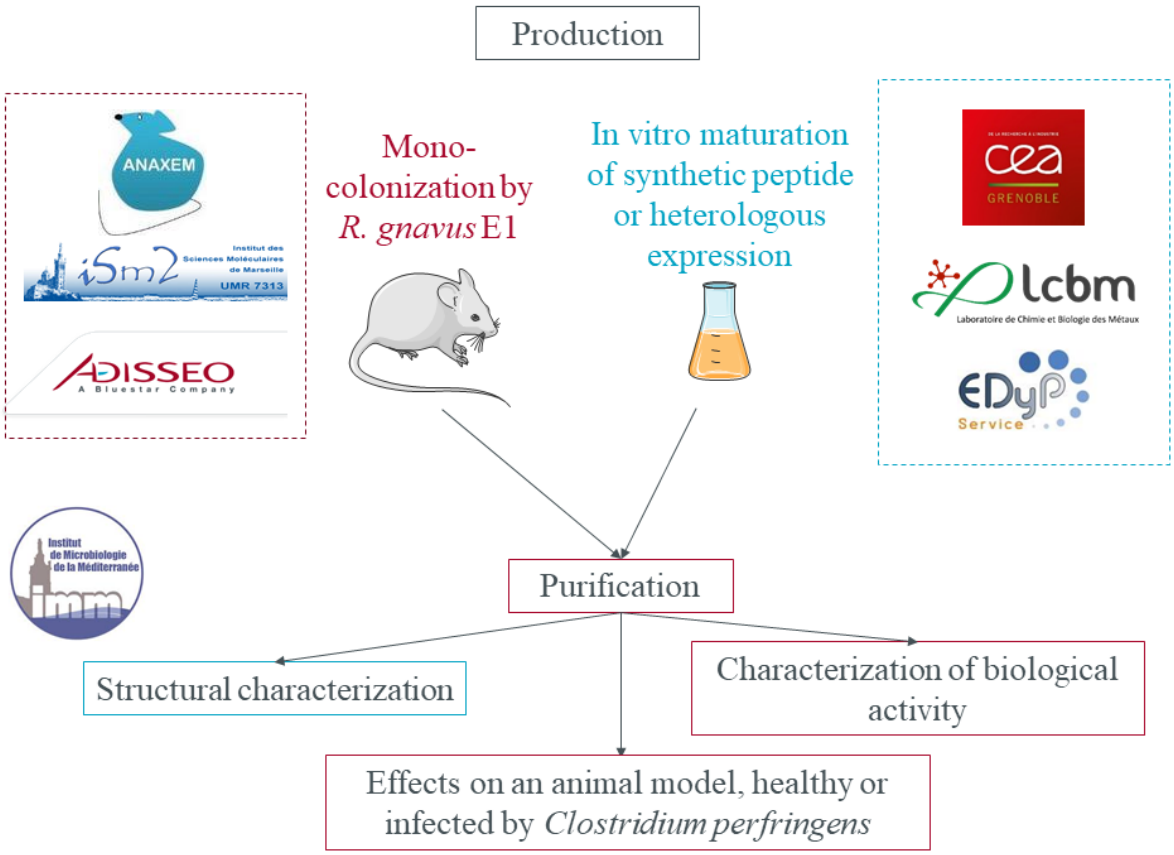

Figure 4.1: Objectives, strategies and partners

Chapter 5

Ruminococcin C, a promising antibiotic produced by a human gut symbiont

5.1 Context

The first step of my project was to purify the 5 isoforms of RumC from cecal contents of rats mono-associated with *R. gnavus* E1 for several reasons. First, Crost and co-workers isolated 3 isoforms, namely RumC1, C4 and C5 (Crost et al., 2011), therefore one of my objectives was to establish if RumC2 and C3 were produced as well and could be isolated. Secondly, another goal was to thoroughly determine the PTMs of the 5 isoforms and hence their classification among RiPPs, since Crost and co-workers only got partial information on the PTMs of the isoforms they purified. Finally, isolation and characterization of RumC1 in particular was crucial to confirm that the synthetic or biosynthetic RumC1 produced by our colleagues of the LCBM had the same PTMs and thus maturation than the peptide produced in vivo in the rats. Based on the protocol developed by Crost and co-workers (**Figure 5.1**), I attempted to develop a new and optimized protocol by modifying the steps that could have limited the purification. The first step was the extraction of the peptides in a liquid fraction from the rat cecal contents. Since it was estimated that the most important loss of RumC happened at that step, I decided to add a protease inhibitor cocktail and to repeat this step several times. Then, 3 types of chromatography were initially used: gel filtration, cation exchange and C-18 reverse phase. We planed to try different combinations of these steps to optimize the purification and reduce it to 2 steps if possible. Along the purification protocol, Crost and co-workers used centrifugal units with a cut-off of 5 kDa to concentrate and desalt their purified fractions. However, when the authors designed this purification protocol they didn't know the molecular weight of the isoforms. Thanks to them, the approximate weight of the isoforms (>4 and <5 kDa) was determined. Therefore, it seemed that they might have lost considerable amounts of peptides using units with a cut-off right above the isoforms molecular weights. It was decided that the steps employing this centrifugal units would be discarded and to look for other means of desalting such as dialysis. Moreover, the new purification protocol was designed to incorporate a step with a filtration unit with a cut-off of 10 kDa, not to concentrate the peptides, but in order to eliminate the bigger molecules and proteins and to avoid a gel filtration chromatography step for that purpose. Instead gel filtration with different columns more appropriate for the separation of peptides would be attempted.

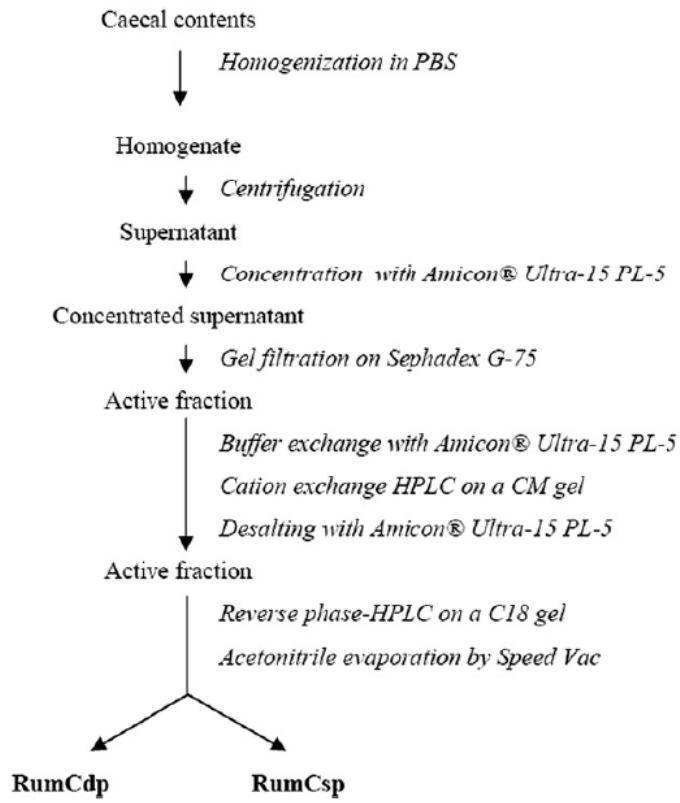

Figure 5.1: Ruminococcin C purification protocol developed by Crost et al., 2011

RumCsp and RumCdp respectively correspond to the isolation of RumC5 and a mixture of RumC1 and RumC4.

Initially, we had plan to determine the spectrum of action of RumC using peptides produced by in vivo in rats as well as in vitro or ex vivo by heterologous expression. I was only involved in the purification of RumC from cecal contents and not in the development of a heterologous system or a synthetic pathway to produce RumC ex vivo or in vitro. These steps were realized at the LCBM and as part of the thesis project of Steve Chiumento. They started to work on the production of RumC1 maturated by RumMc1. It turned out that rather than trying to maturate in vitro a synthetic precursor with a purified enzyme, the most efficient way to produce RumC1 was with the heterologous expression of the genes encoding RumC1, RumMc1 and those necessary for the Fe-S cluster assembly machinery in *E. coli*. This system is described in details in the following paper. Our colleagues from the LCBM provided us with the mature precursor of RumC1. As it still contained the leader peptide I also worked on the in vitro cleavage of the precursor and the purification of the mature core sequence free of the leader peptide. Then I assayed the activity and safety of the mature and cleaved RumC1.

5.2 Published paper

MICROBIOLOGY

Ruminococcin C, a promising antibiotic produced by a human gut symbiont

Steve Chiumento[1]*, Clarisse Roblin[2,3]*, Sylvie Kieffer-Jaquinod[4]*, Sybille Tachon[2], Chloé Leprètre[1], Christian Basset[1], Dwi Aditiyarini[1], Hamza Olleik[2], Cendrine Nicoletti[2], Olivier Bornet[5], Olga Iranzo[2], Marc Maresca[2], Renaud Hardré[2], Michel Fons[6], Thierry Giardina[2], Estelle Devillard[3], Françoise Guerlesquin[5], Yohann Couté[4], Mohamed Atta[1], Josette Perrier[2], Mickael Lafond[2†], Victor Duarte[1†]

A major public health challenge today is the resurgence of microbial infections caused by multidrug-resistant strains. Consequently, novel antimicrobial molecules are actively sought for development. In this context, the human gut microbiome is an under-explored potential trove of valuable natural molecules, such as the ribosomally-synthesized and post-translationally modified peptides (RiPPs). The biological activity of the sactipeptide subclass of RiPPs remains under-characterized. Here, we characterize an antimicrobial sactipeptide, Ruminococcin C1, purified from the caecal contents of rats mono-associated with *Ruminococcus gnavus* E1, a human symbiont. Its heterologous expression and post-translational maturation involving a specific sactisynthase establish a thioether network, which creates a double-hairpin folding. This original structure confers activity against pathogenic *Clostridia* and multidrug-resistant strains but no toxicity towards eukaryotic cells. Therefore, the Ruminococcin C1 should be considered as a valuable candidate for drug development and its producer strain *R. gnavus* E1 as a relevant probiotic for gut health enhancement.

INTRODUCTION

Over the coming decades, it has been estimated that millions of people will succumb to bacterial infections mainly due to the emergence of multidrug-resistant (MDR) strains (*1*, *2*). As a result, we urgently need to discover novel molecules and means to face this major threat. Bacteria constitute a treasure trove of multiple classes of natural antimicrobial compounds, one of which is ribosomally synthesized and posttranslationally modified peptides (RiPPs). RiPPs are biosynthesized from a genetically encoded precursor peptide, generally containing an N-terminal leader sequence and a C-terminal core peptide (*3*). Among these peptides, sactipeptides constitute a subclass of bacteriocins that emerged several years ago (*4*, *5*). Despite spectacular advances made with genomic tools, the sactipeptide subclass is currently limited to only six members (Fig. 1A) (*6*–*12*). Biosynthesis of most of these peptides relies on the expression of a gene cluster encoding at least one peptide precursor, a maturation enzyme named sactisynthase, which places posttranslational modifications, and two proteins, namely, an ABC transporter and a signal peptidase, which are involved in peptide export and signal peptide cleavage, respectively (Fig. 1B) (*13*).

In silico analysis of a 15-kb genomic fragment from the strictly anaerobic *Ruminococcus gnavus* E1 strain, a Gram-positive Firmicutes isolated from the feces of a healthy human, indicated a multi-operonic organization controlled by a two-component regulatory system (i.e., a regulon) (*14*). In addition to the genes involved in regulation, immunity, and export, the *rumC*-regulon includes five open reading frames (ORFs) (*rum*C1 to *rum*C5), which have been suggested to encode sactipeptide precursors (Fig. 1C), two ORFs (*rum*Mc1 and *rum*Mc2) thought to encode sactisynthases (fig. S1A), and one ORF (*rum*Pc) likely to encode Ruminococcin C (RumC) leader peptide-specific metallopeptidase from the M16 family (Fig. 1B) (*15*, *16*). Furthermore, previous works showed that *R. gnavus* E1 produces an anti-*Clostridium* substance in the rat gut in a trypsin-dependent manner (*17*). This substance was later partially purified, identified as RumC isoforms, and shown to be produced exclusively in vivo (*15*, *18*, *19*).

From a chemical maturation standpoint, sactisynthases introduce intramolecular thioether cross-links between cysteine sulfur and the unreactive α-carbon of a partner amino acid by a radical-based mechanism to produce sactipeptides (Fig. 1D) (*20*). All of the sactisynthases characterized so far have been classified in the Radical *S*-adenosyl-L-methionine (SAM) enzymes superfamily (*21*). Although their radical SAM domain is known to be directly involved in the formation of the thioether linkage, they all contain a C-terminal extension called SPASM (Subtilosin A/Pyrroloquinoline quinone/Anaerobic Sulfatase/Mycofactocin maturation enzymes) domain housing additional [4Fe-4S] clusters (*22*), for which the role is still under debate (*12*, *23*–*31*). While the number of sactipeptides is still limited, interesting biological properties have been found regarding their antimicrobial activity and their mode of action (*5*, *8*, *32*–*35*).

Here, we report the in vivo and in vitro production of the RumC1 sactipeptide and its functional and conformational characterizations. We highlight the strong antimicrobial activity against Gram-positive pathogens including MDR strains and the lack of toxic effect toward eukaryotic cells. Therefore, it has a valuable potential for drug development, and its producer strain *R. gnavus* E1 could be used as a powerful probiotic.

[1]Univ. Grenoble Alpes, CEA, CNRS, CBM-UMR5249, 38000 Grenoble, France. [2]Aix-Marseille Univ., CNRS, Centrale Marseille, iSm2, Marseille, France. [3]ADISSEO France SAS, Centre d'Expertise et de Recherche en Nutrition, Commentry, France. [4]Univ. Grenoble Alpes, CEA, INSERM, BGE U1038, 38000 Grenoble, France. [5]LISM, IMM, Aix-Marseille Univ., CNRS, Marseille, France. [6]Unité de Bioénergétique et Ingénierie des Protéines UMR7281, Institut de Microbiologie de la Méditerranée, Aix-Marseille Univ., CNRS, Marseille, France.
*These authors contributed equally to this work.
†Corresponding author. Email: mickael.lafond@univ-amu.fr (M.L.); victor.duarte@cea.fr (V.D.)

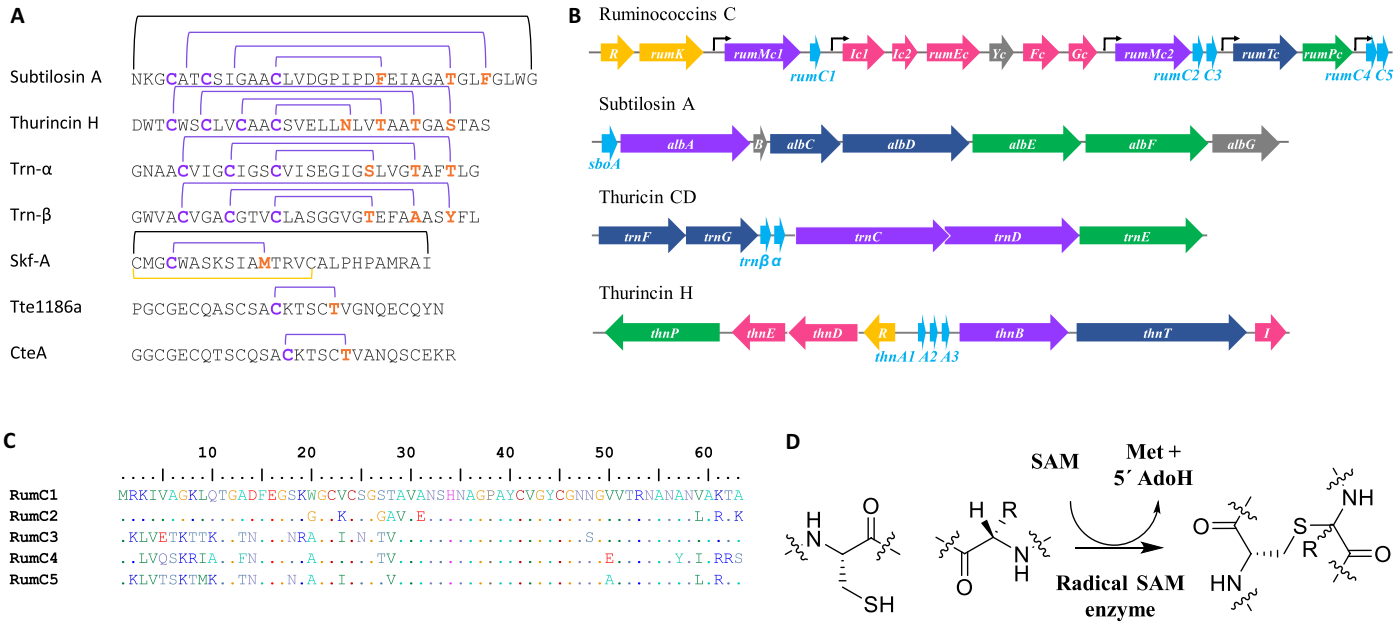

Fig. 1. Biosynthesis of sactipeptides. (**A**) Thioether network in previously described sactipeptides. Thioether bridges, disulfide bridges, and head-to-tail cyclization are indicated by purple, yellow, and black lines, respectively. (**B**) Gene regulon encoding ruminococcins C, subtilosin A, thuricin CD, and thurincin H. Purple, radical SAM enzymes; light blue, precursor peptides; dark blue, transporter systems; green, signal peptidases; yellow, response regulators; pink, immunity systems; and gray, genes of unknown function. (**C**) Alignment of the five RumC peptide isoforms. (**D**) Thioether bond formation in sactipeptides catalyzed by radical SAM enzymes.

RESULTS

In vivo production and purification of RumC1 from *R. gnavus* E1–monoassociated rats

Crost and co-workers (*18*) previously showed that when the digestive tract of axenic rats is colonized with *R. gnavus* E1 strain, the feces obtained and the cecal contents display an anti–*Clostridium perfringens* (anti-*Cp*) activity, which is genetically correlated with the *rumC*-regulon (Fig. 1B) (*15*). Consequently, we began our study by attempting to purify in vivo–produced RumC isoforms. After 12 days of colonization with *R. gnavus* E1, the feces were collected and the cecal contents of monoassociated rats were found to contain an anti-*Cp* substance (Fig. 2A). The expected RumC peptides are 44 amino acid strings after the removal of the supposed N-terminal leader sequence of 19 residues. An ultrafiltration approach based on expected molecular weights was used to enrich peptides of interest in the active fraction (Fig. 2A). The active soluble fraction was then submitted to three consecutives, and optimized chromatographic steps interleaved with desalting steps: cationic exchange, size exclusion, and hydrophobic C18 reversed-phase chromatography. Throughout the subsequent steps, the putative RumC-containing fractions were selected on the basis of an anti-*Cp* assay (Fig. 2A). Nano–liquid chromatography combined with mass spectrometry (LC-MS) analyses revealed a considerable enrichment of the five RumC isoforms in two consecutive fractions of the last purification step (Fig. 2, B and C), which displayed anti-*Cp* activity when combined (Fig. 2A). The masses of the five RumC peptides measured were consistently 8 Da less than their theoretical masses, as shown for in vivo and synthetically produced unmodified RumC1 peptide (Fig. 2, D and F). The iodoacetamide alkylation of the RumC-enriched fraction under reducing conditions failed to alter the observed masses of native RumC1 peptide, suggesting that the four cysteine residues are modified and most likely engaged in intramolecular bonds (Fig. 2E). Unlike the cross-links present in lantibiotics where thioether bridges are formed between the sulfur atom of a cysteine and the β-carbon of a corresponding residue, the thioether linkages in sactipeptides involve the α-carbon (*6*, *7*). This specificity is thought to result in opening of the thioether link during tandem MS (MS/MS) analyses, leading to the formation of a free cysteine and the dehydramino form of the partner amino acid, resulting in a two unit mass decrease (*36*). Higher-energy collisional dissociation–based MS/MS analyses of in vivo–produced RumC1 indicated that residues A12, N16, R34, and K42 are involved in thioether bridges (Fig. 3A and table S1). The same strategy was used to study the four remaining RumC peptides, and they were all found to contain four thioether bridges involving residues at the same positions as those identified in RumC1 (fig. S2).

RumC1 presents a novel thioether network

As thioether bridges open during MS/MS analyses, it is impossible to assign the different cysteine residues to their amino acid partners. Thus, we sought to establish a heterologous expression system allowing site-directed mutagenesis to accurately assign the residues involved in each thioether bridge. Furthermore, the in vitro production of RumC bacteriocins will facilitate future investigations including antimicrobial activity assays, structural, functional, and biophysical studies. Similar to the approach described by Himes and co-workers (*37*) for the production of subtilosin A in *Escherichia coli*, we established a protocol to produce heterologously the mature form of RumC1 (mRumC1), consisting of the leader and core peptide sequences. Here, the genes encoding the radical SAM enzyme RumMc1 and the RumC1 peptide were separately cloned into two different plasmids and co-expressed in the presence of *suf* genes (fig. S3, B and C, top and middle) (*38*). The observed mass of mRumC1 was in good agreement with the presence of four thioether linkages (Fig. 3B). Reductive alkylation of mRumC1 had no effect on its observed molecular

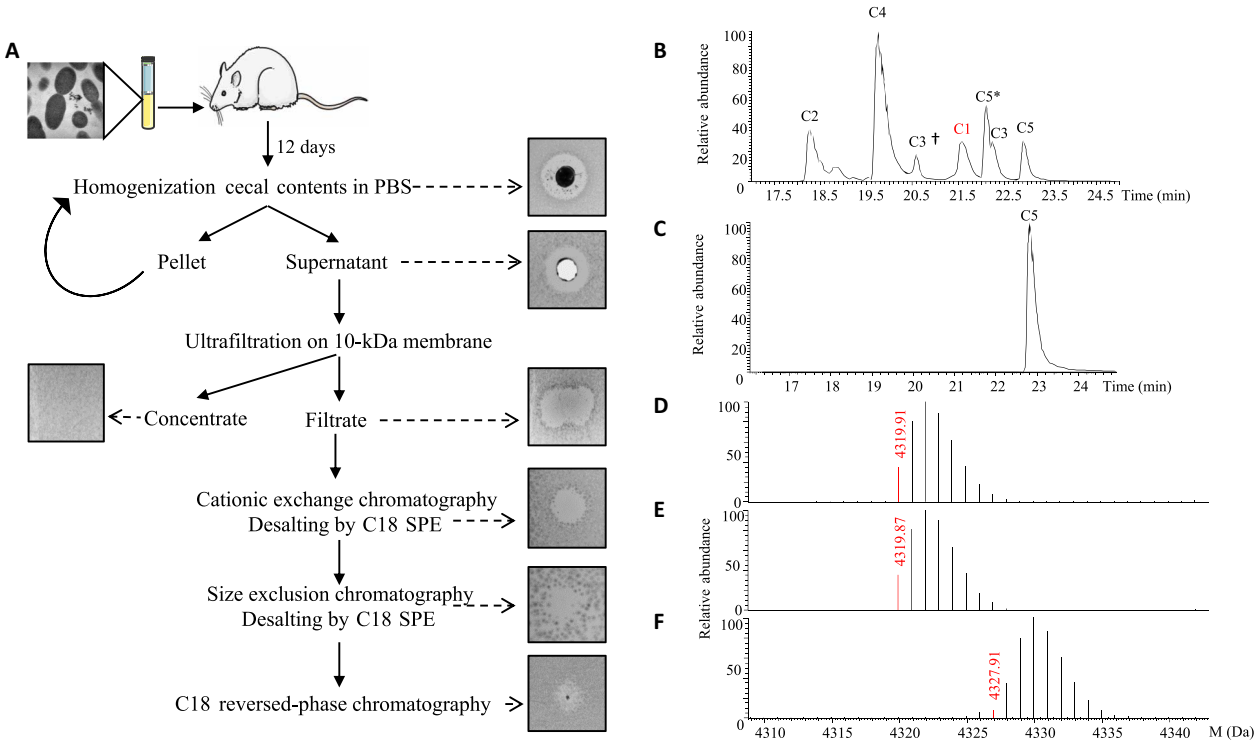

Fig. 2. Purification and characterization of the five RumC isoforms produced in vivo. (**A**) Protocol for extraction from cecal contents to obtain a purified mixture of RumCs. Fractions were selected on the basis of their anti-*Cp* activity throughout the purification steps. PBS, phosphate-buffered saline. (**B** and **C**) LC-MS analyses of the two fractions containing the different RumC (* and † indicate succinimide and deamidated forms of C5 and C3, respectively). RumC5 was present in two consecutive C18 reversed-phase fractions. (**D**) Deconvoluted mass spectrum of RumC1 eluted at 21.6 min in nano–LC-MS analyses. (**E**) Deconvoluted mass spectrum of RumC1 after dithiothreitol (DTT)/iodoacetamide treatment. (**F**) Deconvoluted mass spectrum of synthetic unmodified RumC1.

weight, thus suggesting that the four Cys residues in mRumC1 are involved in posttranslational modifications (Fig. 3C). LC-MS/MS analyses of mRumC1 confirmed the same four partner residues A, N, R, and K, corresponding to A12, N16, R34, and K42 in RumC1 purified from cecal contents (Fig. 3, A and B). In this sample, two peptide fragments, G(-23)-Y21 and A17-A44, were observed, corresponding to the N- and C-terminal parts, respectively, of mRumC1. Both of these fragments were detected with a 4-Da mass decrease (fig. S4, B and C). In good agreement with this observation, the C-terminal peptide, with a similar 4-Da loss of mass, was also detected in the RumC1-containing fraction from the in vivo preparation (fig. S4A). These important results suggest that mature RumC1 contains four thioether bridges, two each in the N- and C-terminal regions.

To identify the residues involved in each thioether bridge, four Cys to Ala mutants were designed: mRumC1-C3A, mRumC1-C5A, mRumC1-C22A, and mRumC1-C26A. All the mutants were produced and purified as described for mRumC1. To detect nonbridged cysteine residues, mutant mRumC1 samples were first treated with iodoacetamide under reducing conditions and then subjected to LC-MS/MS experiments. Analyses of the four single mutants revealed fairly complex peptide mixtures with many peptide fragments bearing alkylated cysteine residues. These data suggest that, during the maturation of mRumC1, the formation of a single thioether linkage may influence how the three other bridges form, making the structure highly labile. Nevertheless, interesting information can be gleaned from the fragmentation patterns of selected peptides present in the mixture. We focused our attention on the residues identified as partners of the four cysteines and for which the mass is either unmodified or presents a loss of 2 Da upon mutation of a single cysteine. MS/MS analysis of the Q(-10)-A20 peptide observed in the mRumC1-C3A mutant showed no mass loss on the N16 residue but a 2-Da decrease on A12. These data indicate that a thioether bridge forms between C5 and A12 and that the bridging partner for C3 is N16 (Fig. 3D, fig. S5A, and table S1). In good agreement, peptide F(-5)-A20 from the mRumC1-C5A mutant contains an unmodified A12 residue (Fig. 3D, fig. S5C, and table S1). In the mRumC1-C22A mutant, the fragmentation of the A17-A44 peptide revealed a 2-Da deficit for R34, whereas K42 was unmodified. These observations suggest that R34 and K42 are the partners of C26 and C22, respectively (Fig. 3D, fig. S5B, and table S1). Together, the MS/MS analyses of both wild-type and mutated mRumC1 peptides allowed us to propose a structural model for mature RumC1 in which the peptide is folded into two distinct structured domains both containing two thioether bridges; the two domains are separated by the strictly conserved AGPAY amino acid sequence present in all five RumC isoforms (Fig. 3E).

To establish the connectivity of the thioether rings, nuclear magnetic resonance (NMR) experiments were performed by using a ^{13}C-, ^{15}N–labeled mRumC1 sample after removal of the N-terminal leader sequence by trypsin. The [^{15}N, ^{1}H] heteronuclear single-quantum coherence (HSQC) spectrum gave well-dispersed peaks, with 39 of 42 backbone NH signals observed. The backbone NH signals for C26, G27, and N28 could not be observed. The sequential assignment was made on the basis of the backbone three-dimensional experiments,

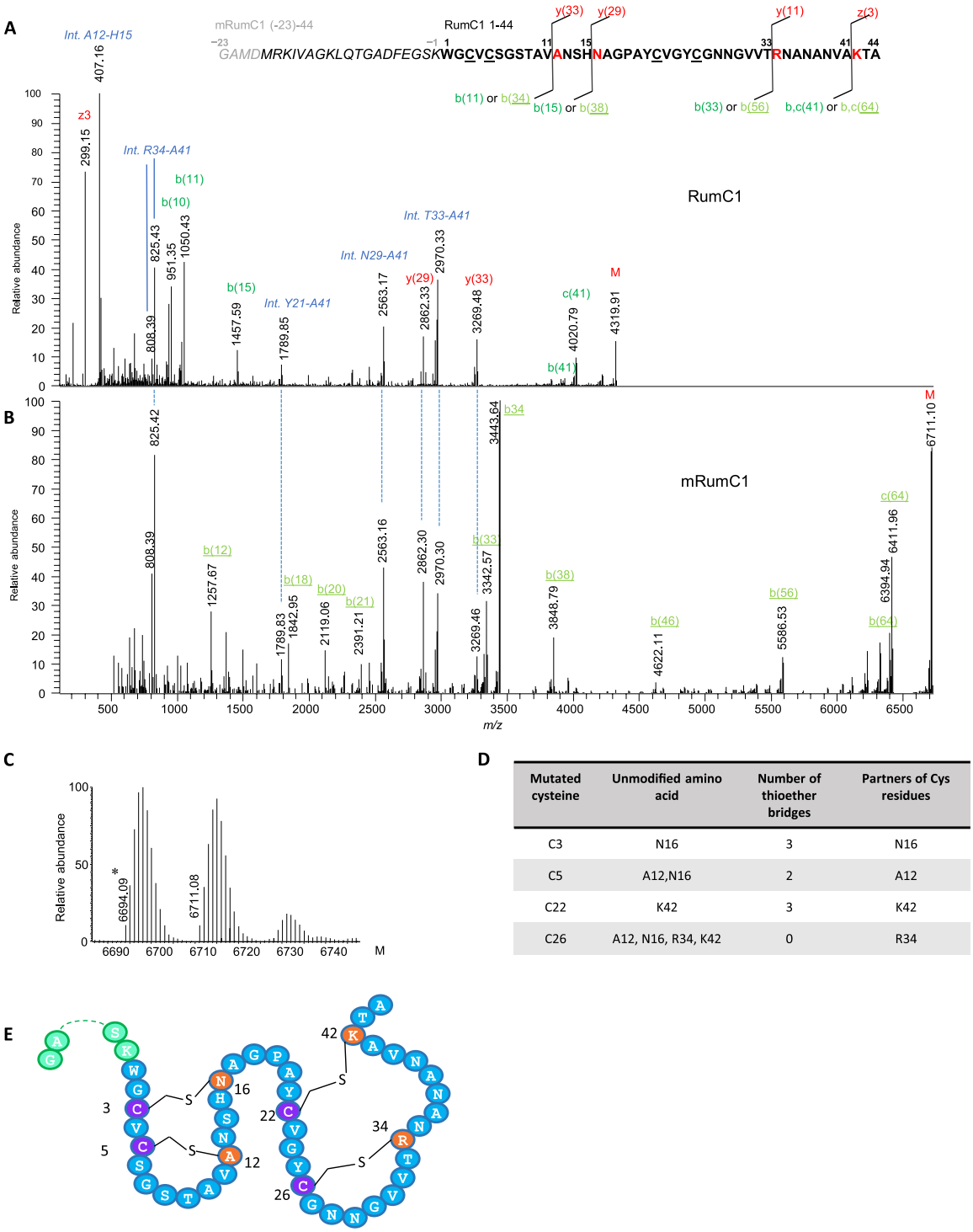

Mutated cysteine	Unmodified amino acid	Number of thioether bridges	Partners of Cys residues
C3	N16	3	N16
C5	A12,N16	2	A12
C22	K42	3	K42
C26	A12, N16, R34, K42	0	R34

Fig. 3. Tandem mass spectra of mature RumC1 peptide from in vivo and in vitro preparations and thioether network (see table S1 for theoretical and observed masses of interest). (**A**) Deconvoluted MS/MS spectrum of in vivo–matured RumC1 (1 to 44, bold sequence) showing prominent y/b and c/z fragments induced by breaking of the amide bonds preceding the residues bound to cysteines in thioether bridges. The very structured peptide produced high-intensity and unusual internal fragments (blue italics), particularly ANSH (A12-H15) and RNANANVA (R34-A41), corresponding to fragments located between two linked residues. (**B**) Deconvoluted MS/MS spectrum of the heterologously matured mRumC1 [containing leader peptide (italics) and four additional GAMD amino acids for cloning purposes (gray italics)], revealing the same characteristic fragmentation pattern. Peaks below 500 Da (identical for the y series of in vivo RumC1) are not shown to improve overall visibility. All masses considered are monoisotopic masses. M (last peak in each spectrum) corresponds to the nonfragmented peptide. (**C**) Deconvoluted MS spectrum of mRumC1 after DTT/iodoalkylation showing no mass increment. Mass of 6694.09 (ammonia loss) corresponds to a succinimide (*) form produced as a by-product of high-temperature reduction of RumC1hm before iodoalkylation. (**D**) Identification of bridging partners. (**E**) Double-hairpin–like structure of mRumC1. Cysteine residues bridged via thioether bonds are shown in purple, and their amino acid partners are indicated in orange.

including HNCACB, CBCA(CO)NH, HNCA, HN(CO)CA, HNCO, and HN(CA)CO. The chemical shifts of the α-carbons of A12, N16, R34, and K42 were found at 72.2, 68.6, 74.5, and 75.5 parts per million (ppm), respectively (fig. S6A). These values are 15 ppm downfield compared to the average value observed for unmodified residues. This is consistent with the influence of an electronegative atom, such as sulfur, being directly attached. Similar chemical shifts were reported for the modified α-carbon atoms in subtilosin A, thurincin H, and thuricin CD (*6*–*9*, *39*). Analyses of the total correlation spectroscopy (TOCSY) and ^{13}C TOCSY-HSQC experiments confirmed that A12, N16, R34, and K42 α-carbons are fully substituted, with no α-protons attached. The atomic connectivity of each thioether linkage was determined by analyzing the nuclear Overhauser effect spectroscopy (NOESY) and ^{15}N NOESY-HSQC data, which show through-space interactions between protons that are close to each other. Nuclear Overhauser effect (NOE) interactions were observed between the β-protons of C3 and the amide proton (HN) of N16, the β-protons of C5 and the HN proton of A12, and the β-protons of C22 and the HN proton of K42 (fig. S6B). These NOE data assigned unambiguously three of the four thioether linkages between C3 and N16, C5 and A12, and C22 and K42. The fourth linkage is not evident to be assigned because of C26 unresolved peak, but only this Cys residue remains to form a thioether bridge with the α-carbon atom of R34 in mRumC1.

Sequential proteolytic cleavage of mRumC1 is required to produce an active form

As we established that in vivo RumC1 and mRumC1 retain the same posttranslational modifications, we performed all subsequent antimicrobial assays using mRumC1. Similar to the chemically synthesized, unmodified form of RumC1, mRumC1 had no anti-*Cp* activity, suggesting that the presence of intramolecular thioether bonds is not sufficient to produce antimicrobial activity (fig. S7A). As a protective strategy for the organisms producing them, RiPPs are in an inactive state until their leader peptide is released as proposed by Yang and van der Donk (*40*). We therefore decided to remove the leader peptide from mRumC1. After checking the up-regulation of the corresponding mRNA by quantitative reverse transcription polymerase chain reaction in the cecal contents (fig. S3A), we cloned the *rumPc* gene encoding the putative leader metallopeptidase identified in the *rumC*-regulon to overproduce and purify the recombinant RumPc protein (fig. S3, B and C, bottom). RumPc-treated mRumC1 (i.e., mRumC1c) remained inactive against *Cp* (fig. S7C, top). Moreover, RP-C18 and LC-MS analyses revealed that mRumC1c retains the FEGSK amino acid motif in its N terminus unlike native RumC1 obtained from rat feces (Figs. 2D and 3A and fig. S7, B and C). Because Ramare and co-workers (*17*) previously reported a trypsin-dependent anti-*Cp* activity in the cecal contents, we next performed proteolytic digestion of mRumC1c by pancreatic trypsin. This sequential treatment led to the complete removal of the leader sequence and generated a mature peptide (i.e., mRumC1cc) identical to in vivo–produced RumC1, as confirmed by high-performance liquid chromatography (HPLC) and MS analyses, which was active against *Cp* (fig. S7, B and C). In good agreement with these results, direct treatment of mRumC1 with pancreatic trypsin led to the complete removal of the leader peptide sequence within 1 hour (fig. S7D). This one-step cleavage was thus subsequently used to prepare active mRumC1cc, currently renamed RumC1 (fig. S7, A, B and C).

Considering these results, the hydrophobicity profile, and the absence of any kind of signal peptide predicting a subcellular localization of RumPc, we can propose an in vivo RumC1 maturation process involving (i) an in situ posttranslational modification of the core peptide by RumMc1 followed by a partial cleavage of the leader peptide by RumPc and (ii) an ex situ cleavage of the five remaining N-terminal amino acids of the leader peptide by pancreatic trypsin, leading to an active bacteriocin released in the gut microbiome. To conclude, the intracellular RumPc cleavage followed by the extracellular trypsin cleavage to produce an active form of a sactipeptide represents a perfect example of mutualism between a symbiont and its host collaborating to generate an antipathogenic molecule as a protective strategy for both.

RumC1 is safe for use against pathogens and MDR bacteria

The antimicrobial spectrum of RumC1 was investigated on a broad range of Gram-positive and Gram-negative bacteria, including pathogens and MDR strains. For these studies, we used RumC1 produced by heterologous expression and activated by trypsin cleavage to determine minimal inhibitory concentrations (MICs; Fig. 4A). To distinguish between a bactericidal and a bacteriostatic effect, we also determined the minimal bacteriostatic concentration (MBC) for each sensitive strain (Fig. 4A). RumC1 was highly effective against a range of pathogenic *Clostridium* species with very low MIC and MBC values. An MBC value of 1.56 μM was observed against *Cp*, which is the third cause of foodborne infections in the United States after Norovirus and *Salmonella* spp. according to the Centers for Disease Control and Prevention (CDC). RumC1 is also effective against *Clostridium difficile* (6.25 μM < MBC < 12.5 μM), one of the main pathogens highlighted in the report published by the CDC in 2013 on "Antibiotic Resistance Threats in the United States" and categorized as an urgent threat for which new antibiotics are needed. Even lower MBC value (0.4 μM) was measured for *Clostridium botulinum*, a pathogen responsible for foodborne botulism (via a preformed toxin), infant botulism (intestinal infection via a toxin-forming *C. botulinum*), and wound botulism. Moreover, RumC1 was also active against a range of Gram-positive organisms such as *Staphylococcus aureus* and MDR strains such as vancomycin-resistant *Enterococcus faecalis*, nisin-resistant *Bacillus subtilis* or methicillin-resistant *S. aureus* (MRSA) at clinically relevant MIC values in the micromolar range of 0.8 to 50 μM. As expected, RumC1was also active against closely phylogenetically related bacteria such as *Clostridium coccoides* with an MIC value of 1.56. Although the antimicrobial assays were performed on a relatively exhaustive panel of bacteria, it seems that RumC1 is not active against Gram-negative bacteria, for which MICs were determined to be >100 μM (Fig. 4A). Last, except for MRSA, the MBC values were identical to the MICs, suggesting that the effect of RumC1 is bactericidal (Fig. 4A).

After assessing the activity spectrum of RumC1, we investigated its mode of action on *Cp* cells. As it is well known that many antimicrobial peptides have a pore-forming effect, we assessed the permeabilization potency of RumC1 following the fluorescent emission of *Cp* cells treated with propidium iodide (PI), a DNA intercalating agent, and the incorporation of the nucleic acid dye SYTOX Green by fluorescence microscopy. Both fluorescent compounds cannot cross undamaged membranes. We used the detergent cetyltrimethylammonium bromide (CTAB) and a well-characterized pore-forming bacteriocin, nisin, as positive controls. Even after 2 hours of treatment, cells exposed to RumC1 showed no PI nor SYTOX Green incorporation, whereas permeabilization with nisin resulted in 59% of the maximum PI incorporation measured with CTAB and caused 97% of the cells to

A

Bacteria	Strain	MIC (μM)	MBC (μM)
Clostridium perfringens	ATCC 13124	1.56	1.56
Clostridium difficile	DSMZ 1296	6.25	6.25–12.5
Clostridium botulinum	DSMZ 1985	0.4	0.4
Staphylococcus aureus	ATCC 6538P	25	25–50
Staphylococcus aureus MRSA[1]	ATCC BAA-1717	50	>100
Enterococcus faecalis VER[2]	DSMZ 13591	12.5	25
Bacillus subtilis	ATCC 6633	0.4	0.4
Bacillus subtilis NR[3]	DSMZ 347	0.8	0.8
Clostridium coccoides	ATCC 29236	1.56–3.13	1.56–3.13

[1]MRSA = methicillin-resistant *Staphylococcus aureus*, [2]VER = vancomycin-resistant, [3]NR = nisin-resistant.

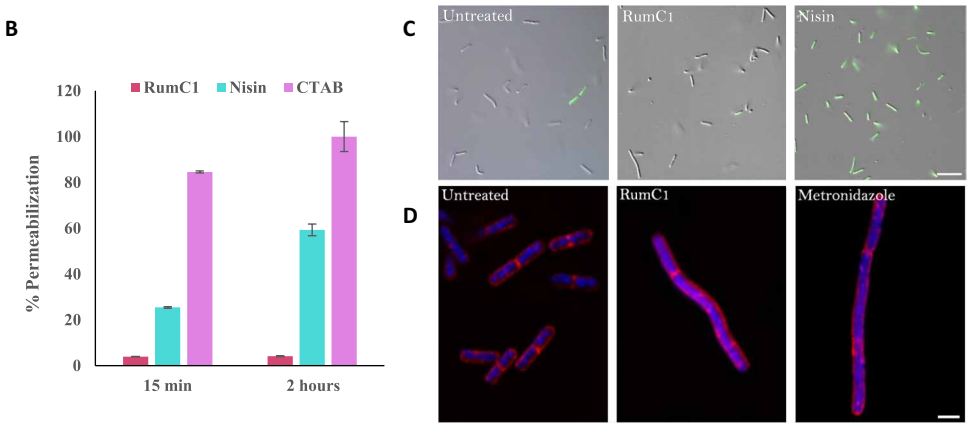

Fig. 4. RumC1 antimicrobial activity. (**A**) Activity spectrum of RumC1 against selected Gram-positive strains. MIC and MBC were >100 μM for the following Gram-negative strains tested: *Salmonella enterica* (CIP 80.39), *E. coli* (ATCC 8739), *E. coli* MR4 (DSMZ 22314), *Pseudomonas aeruginosa* (ATCC 9027), *P. aeruginosa* fluoroquinolone resistant (CIP 107398), *Acinetobacter baumanii* (CIP 103572), *A. baumanii* multiresistant (CIP 110431), and *Klebsiella pneumoniae* MR4 (DSMZ 26371). (**B** and **C**) Membrane permeabilization assay on *Cp* cells treated with RumC1 or nisin based on measurement of PI incorporation (B) or SYTOX Green staining (C). (B) Cells incubated with cetyltrimethylammonium bromide (CTAB) were used as a positive lysis control, and untreated cells were used as a negative control. (C) Cells were treated for 15 min before staining. Scale bar, 10 μm. (**D**) Confocal imaging of control *Cp* cells or *Cp* cells treated with RumC1 or metronidazole. Membranes were stained with FM4-64FX, and DNA was stained with DAPI (4′,6-diamidino-2-phenylindole). RumC1 treatment leads to three morphotypes identical to the ones induced by metronidazole (fig. S9). This figure shows one of these three morphotypes, i.e., one regular cell associated with a cell three to four times longer and with uncondensed DNA throughout the cells with a few spots of highly condensed DNA. Scale bar, 2 μm.

stain positive for SYTOX Green (Fig. 4, B and C). Accordingly, RumC1 is unable to insert into total lipids extracts obtained from *Cp* contrarily to nisin and CTAB (fig. S8). Thus, it appears that, unlike most bacteriocins targeting Gram-positive bacteria, RumC1 does not have a pore-forming action and has most likely an intracellular target. RumC1 can also be expected to be supported by an active membrane transporter to reach the intracellular compartment. Although most peptides acting on intracellular targets are usually active against Gram-negative bacteria and have a much narrower spectrum, some RiPPs such as thiopeptides have a broad spectrum and have been shown to inhibit translation in Gram-positive cells (*41*). We next tried to identify the cellular pathways inhibited by RumC1 through phenotype imaging experiments based on the "bacterial cytological profiling" method (*42*) adapted to anaerobic conditions. Membranes and DNA from *Cp* cells were stained with FM4-64FX and 4′,6-diamidino-2-phenylindole (DAPI), respectively, and confocal images were acquired. Morphological changes on *Cp* cells induced by treatment with RumC1 were compared to the phenotypes induced by conventional antibiotics with well-characterized mechanisms of action. Treatment with RumC1 produced three morphotypes affecting cell length and organization, as well as DNA condensation (Fig. 4D). No morphological similarities were observed in cultures treated either with antibiotics that inhibited transcription or cell wall synthesis or even with those causing loss of membrane potential (fig. S9, A and B). However, when cells were treated with metronidazole, an antibiotic that inhibits nucleic acid synthesis, we observed the three phenotypes identical to those induced by treatment with RumC1. How metronidazole affects nucleic acid synthesis remains unclear. Studies suggest that it could act directly on DNA and disrupt its structure. Some other studies showed that it indirectly inhibits DNA synthesis and repair systems (e.g., mismatch or SOS), possibly by disrupting the cell redox system resulting in ribonucleotide reductase inhibition (*43*). Hence, we hypothesize that RumC1 most likely inhibits nucleic acid synthesis in a metronidazole-like manner.

Antimicrobial efficiency not only must be sufficient to develop a therapeutic molecule but also must be safe for the host. We therefore assayed the cytotoxicity of RumC1 on human cells using two intestinal (Caco2 and T84) and one gastric (N87) cell lines. On the basis of their metabolic activity (via resazurin assays), RumC1 did not affect the viability of these cell lines, even at high concentrations of RumC1 [IC_{50} (median inhibitory concentration), > 200 μM; fig. S10A]. At concentrations of RumC1 up to 200 μM, metabolic activities of Caco2, N87, and T84 cells were at least 90, 80, and 70%, respectively, of the activity measured in untreated cells. Furthermore, RumC1 induced no hemolysis of human erythrocytes even at high concentrations [EC_{50} (median effective concentration), > 200 μM; fig. S10B]. Last, no resistance was induced in serial subcultures of *Cp* exposed daily to RumC1, whereas equivalent treatment with metronidazole led to the emergence of resistant bacteria with up to 500-fold higher MICs (fig. S10C). The high potency of RumC1 against pathogenic strains combined with its lack of effect on eukaryotic cells and the absence

of resistance development makes it a relevant candidate either as therapeutic agent or as food safety agent.

DISCUSSION

Through this study, we were able to (i) develop and optimize a protocol to purify a natural molecule exhibiting antibiotic activity produced by a human intestinal symbiont from cecal contents harvested from *R. gnavus* E1–monoassociated rat and (ii) produce an active recombinant form of this RiPP after maturation and sequential and controlled proteolytic cleavage to remove the leader peptide, in line with the steps naturally occurring in the human gut (Fig. 5). For almost all natural RiPPs, the precursor genes encode an unprocessed peptide bearing an N-terminal leader peptide in addition to the C-terminal core peptide. Although leader peptides have been suggested to play multiple roles during RiPPs biosynthesis, such as acting as a secretion signal or as a recognition pattern for the maturation enzymes, the protective effect of keeping the peptide inactive before secretion remains the most notable (*3*, *44*). Several studies on the broad subclasses of RiPPs, the classes II and III lantibiotics (e.g., cytolysin, plantaricin W, haloduracin, lichenicidin, carnolysin, and flavipeptin or NAI-112, respectively) have reported similarities with a two-step activation process using proteases (*45*–*51*). However, despite the five or six amino acid overhangs remaining after the first proteolytic cleavage in mRumC1c, the GG/ or GA/ recognition motif usually found in lantibiotics is not conserved in the leader peptides of RumC isoforms, in favor of an /FE pattern recognized as a cleavage site by RumPc. Broadly, the different classes of lantibiotics, namely, I, II, and III, involve subtilisin-like serine proteases, papain-like cysteine proteases, and Zn-dependent bifunctional (i.e., endo- and aminopeptidase) proteases, respectively, whereas RumPc is a monofunctional Zn-metallopeptidase with an endo-mode of action recognizing an undescribed motif (/FE) to date. In addition, the second step occurring in the maturation process of RumC1 and leading to an active form involves the human pancreatic trypsin. Consequently, we have identified a two-step cleavage process involving a monofunctional Zn-metallopeptidase from the symbiont (i.e., RumPc) and a serine protease from the host organism (i.e., trypsin) to get an active RiPPs. To our knowledge, nothing equivalent has been reported for the RiPPs, especially for the lantibiotic and sactibiotic subclasses (Fig. 5). Last, through a deep MS study on both the natural isoforms of RumC and recombinant forms, we were able to conclude that maturation of the bacteriocin involves a radical SAM sactisynthase,

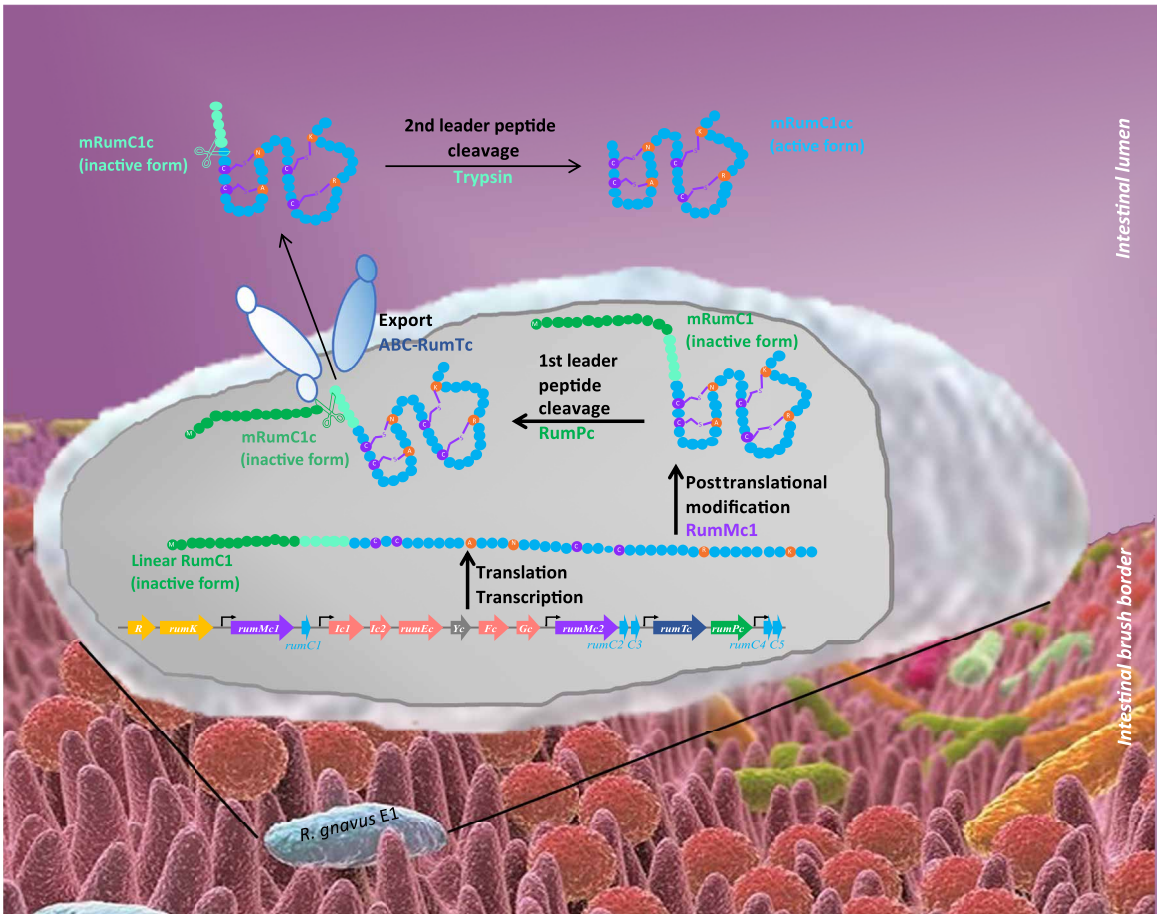

Fig. 5. Proposed mechanism of maturation and activation of RumC1 in the human gut. After induction of the two-component system, conventional transcription, and translation of the gene regulon Ruminococcins C, the intracellular RumC1 maturation process involves (i) an in situ posttranslational modification of the core peptide by RumMc1, leading to the inactive mRumC1; (ii) a partial cleavage of the leader peptide by RumPc, leading to the still inactive mRumC1c; (iii) an export in the intestinal lumen by RumTc; and (iv) an ex situ cleavage of the five remaining N-terminal amino acids of the leader peptide by pancreatic trypsin, leading to an active mRumC1cc (i.e., RumC1).

RumMc, itself capable of generating four thioether bridges resulting in a new folding pattern, which has never yet been described in the literature. The discovery of this new double-hairpin structure leads us to propose a new subclass of sactibiotics.

We thoroughly characterized the bactericidal activity of RumC1 and found that, unlike some bacteriocins (e.g., colicine), which are defined as "narrow-spectrum," RumC1 is active against not only a broad spectrum of Gram-positive bacteria, including phylogenetically *R. gnavus*–related bacteria such as *Cp*, *C. difficile*, and *C. botulinum*, but also more distant bacteria such as *S. aureus*, including MDR strains. Furthermore, our preliminary data suggest a mechanism involving inhibition of nucleic acid synthesis in a metronidazole-like manner, but additional investigation is needed to corroborate this hypothesis. As a result, MICs for RumC1 are in the micromolar range for, e.g., *C. difficile* or *Cp*. Safety assays on several human cell lines revealed no toxicity, and RumC1 does not trigger resistance development unlike many conventional antibiotics. This characteristic is essential when developing new drugs against pathogens considering the rise of MDR strains worldwide. On the basis of all these findings, it is highly relevant to consider RumC for the elaboration of therapeutic strategies, after drug optimization or in combination with other antimicrobial agents or antibiotics, for human or animal health. *Cp* is also a major pathogen affecting poultry, where it causes necrotic enteritis associated with up to 50% mortality (*52*). Consequently, *R. gnavus* E1 or other RumC-like producing bacteria could be considered as natural probiotics and administered for the prevention against Gram-positive pathogens. Otherwise, sactibiotics and other groups of bacteriocins could be helpful in combinatorial therapies with other antimicrobial agents including, e.g., antibiotics to reduce emergence of resistance or to fight clinical pathogens, and RumC1 could be considered in that way (*32*).

Last, from an ecological standpoint, the *R. gnavus* E1 and human partnership constitute a perfect example of mutualism where both host and symbiont work together and need each other to produce an active bacteriocin to fight a common enemy: an opportunistic pathogen for the host and a competitive species for the same ecological environment for the symbiont.

MATERIALS AND METHODS

Animals and sample collection

Animal experiments were performed according to the guidelines of the French Ethics Committee, i.e., agreement no. A78-322-6. Axenic male F344 M rats (6 weeks old) provided by the Germ Free Animals facility ANAXEM (Animalerie Axénique de Micalis) platform [Institut National de la Recherche Agronomique (INRA), UMR 1319 Micalis, France] and maintained on a standard diet during 12 days were inoculated with *R. gnavus* E1 [0.5 ml of late log-phase culture at 10^9 colony-forming units (CFU)/ml] by intragastric route to generate *R. gnavus* E1 monoxenic rats (n = 10). After 5 days, individual fecal samples were collected and bacterial counts were estimated by plating serial dilutions of suspensions. We plated these samples on Brain Heart Infusion agar supplemented with yeast extract (5 g/liter) and hemin (5 mg/liter) (BHI-YH), and on Luria-Bertani (LB) agar, under aerobic and anaerobic conditions, to check for the colonization by *R. gnavus* E1 and possible contamination by other bacteria. The animals were sacrificed 12 days after inoculation, and feces and cecal contents were collected. Samples were frozen in liquid nitrogen before being stored at −80°C until RNA or bacteriocin purification.

Bacteriocin purification

Cecal contents of *R. gnavus* E1 monoxenic rats were diluted in phosphate-buffered saline (PBS) (10 g for 30 ml) supplemented with a protease inhibitor cocktail (cOmplete ULTRA tablets EDTA-free, Roche). The suspension was centrifuged at 10,000*g* for 15 min. Resuspension and centrifugation were repeated twice in half the initial volume of PBS. The three supernatants were pooled and filtered on a polyethersulfone membrane with a 10-kDa cutoff (Merck). The resulting filtrate, containing small molecules including peptides, was submitted to ion exchange chromatography using a Carboxymethyl Sepharose column (GE Healthcare) at 4°C. Elution was performed at 2 ml/min with 20 mM acetate sodium buffer at pH 6.5 under isocratic conditions for 36 min, followed by a linear 0 to 0.5 M sodium chloride gradient for 60 min with a detection at 214 and 280 nm. Elution fractions were desalted by DSC-18-SPE columns (Sigma-Aldrich). Briefly, samples were loaded after dilution (1:1) in 0.1% trifluoroacetic acid (TFA), washed with 0.1% TFA, and eluted in 90% acetonitrile (ACN) and 0.1% TFA before being lyophilized and resuspended in water. Fractions displaying anti-*Cp* activity (as described below) were further purified by size exclusion chromatography using a Superdex 30 Increase column (GE Healthcare). Elution was performed at 4°C at 0.5 ml/min for 120 min under isocratic conditions with PBS, and collected fractions were desalted as described above. Active fractions were then applied to a Jupiter 15-µm C18 300 Å analytical reverse-phase HPLC column (250 mm by 21.2 mm; Phenomenex). Peptides were eluted at 1 ml/min with a 0 to 40% linear gradient of 90% ACN and 0.1% TFA for 30 min before being lyophilized and resuspended in water. The different fractions were maintained at 4°C during all purification steps and stored at −20°C. The protein concentration was estimated either by the Bradford coloration method using a bovine serum albumin standard curve or by measuring the A280 and using the theoretical extinction coefficient of 8480 M^{-1} cm^{-1}.

Bacteriocin activity assays

To track the presence of the bacteriocin along the purification, samples were tested for their antimicrobial activity against *Cp* at each step using the diffusion assay. If needed, samples were concentrated using a Speed-Vac concentrator (Thermo Fisher Scientific). A 10^{-3} dilution of an overnight culture of *Cp* strain [American Type Culture Collection (ATCC) 13124] was spread on BHI-YH agar. After drying for 30 min at room temperature, wells with a diameter of 6 mm were dug with a Pasteur pipette and 100 µl of sample was added per well. Alternatively, 10 µl was spotted directly onto the plate. The presence of inhibition halos around the samples was examined after incubation of the plates at 37°C for 24 hours under anaerobic conditions.

Expression and purification of MBP-RumC1

A synthetic plasmid containing the *E. coli* codon-optimized gene of *R. gnavus* E1 encoding RumC1 (pETM-40-*rumC1*, kanamycin resistant) was obtained from GenScript (Piscataway, NJ), which allows the expression of a MBP (maltose-binding peptide)–tagged peptide. A tobacco etch virus nuclear-inclusion-a endopeptidase (TEV protease) site was inserted in the linker between MBP and RumC1 peptide. pETM40-*rumC1* was used to transform competent *E. coli* BL21 (DE3) cells for expression. The resulting *E. coli* BL21 (DE3) strain was grown in M9 medium containing kanamycin (50 µg/ml), vitamin B1 (0.5 µg/ml), $MgSO_4$ (1 mM), and glucose (4 mg/ml) at 37°C. At an optical density (OD_{600}) of 0.8, the culture was induced using 1 mM isopropyl-β-D-thiogalactopyranoside (IPTG). The temperature was

reduced to 25°C, and the cells were grown for 15 hours under stirring. Cells were then harvested by centrifugation at 4000 rpm for 20 min at 4°C. Cell pellet was suspended in 40 ml of buffer A [50 mM tris (pH 8) and 50 mM NaCl] supplemented with one tablet of a protease inhibitor cocktail (cOmplete, EDTA-free Protease inhibitor cocktail tablets, Roche). Cell pellet was then sonicated, and the lysate was clarified by centrifugation at 40,000 rpm for 40 min at 4°C. The supernatant was collected and passed over Dextrin Sepharose High Performance columns (5 ml; MBPTrap HP, GE Healthcare) coupled to a fast protein liquid chromatography (FPLC) (ÄKTA Purifier 900, ÄKTA FPLC Systems, GE Healthcare). Columns were washed with four column volumes of buffer A. MBP-RumC1 was eluted with buffer B [50 mM tris (pH 8), 50 mM NaCl, and 40 mM maltose]. Fractions containing MBP-RumC1 were pooled and concentrated in a 30,000 molecular weight cutoff (MWCO) filter using Amicon Ultra centrifugal filter devices. The sample was digested by TEV protease for a final TEV protease:MBP-RumC1 ratio of 1:20 (w/w) and incubated for 30 min at room temperature. MBP-tag, TEV protease, and unmodified RumC1 were separated by loading over a HiLoad 16/60 Superdex 75 prep grade column (GE Healthcare) equilibrated in buffer C [50 mM Hepes and 100 mM NaCl (pH 7.5)]. The peptide concentration was estimated by ultraviolet-visible (UV-vis) spectroscopy on a Cary 50 UV-vis spectrophotometer (Varian) by using an extinction coefficient of 8480 M^{-1} cm^{-1} at 280 nm.

Heterologous expression and purification of mature mRumC1

A synthetic plasmid containing the *E. coli* codon-optimized gene of *R. gnavus* E1 encoding RumMc1 (pET-15b-*rumMc1*, ampicillin resistant) was obtained from GenScript. Plasmids pET-15b-*rumMc1*, pETM-40-*rumC1*, and psuf (chloramphenicol resistant) containing *sufABCDSE* genes were used to transform competent *E. coli* BL21 (DE3) cells for expression. The resulting strain was grown in M9 medium containing kanamycin (50 μg/ml), amp (100 μg/ml), chl (34 μg/ml), vitamin B1 (0.5 μg/ml), $FeCl_3$ (50 μM), $MgSO_4$ (1 mM), and glucose (4 mg/ml) at 37°C. At an optical density (OD_{600}) of 0.8, $FeCl_3$ (100 μM) and L-cysteine (300 μM) were added and the culture was induced using 1 mM IPTG. The temperature was reduced to 25°C, and the cells were grown for 15 hours under stirring. Cells were then harvested by centrifugation (4000 rpm for 20 min at 4°C). Mature MBP-mRumC1 was then purified as described above for unmodified RumC1.

RumPc production and purification

A synthetic plasmid containing the *E. coli* codon-optimized synthetic gene of *R. gnavus* encoding RumPc (pET-21a–*rumPc*, ampicillin-resistant) was obtained from GenScript. In silico analysis on the *rumPc*-encoding gene to identify a putative signal peptide was performed by using the SignalP 5.0 server (www.cbs.dtu.dk/services/SignalP/). The plasmid was transformed into thermo-competent BL21 (DE3) *E. coli* cells. Ampicillin-resistant colonies were isolated and subcultured in LB broth. Subcultures were used to inoculate 1 liter of terrific broth (TB) medium supplemented with ampicillin (final concentration, 100 μg/ml). The culture was initiated at OD_{600} = 0.05 in prewarmed medium and incubated at 37°C for 1.5 hours and 28°C for 40 min (until OD_{600} = 0.5). Expression was then induced using 0.5 mM IPTG, and the culture was incubated for 3.5 hours at 28°C. Cells were harvested by centrifugation (5000*g*, 20 min, 4°C) and frozen at −20°C. Cells were lysed in buffer D [50 mM NaH_2PO_4 (pH 7.5) and 150 mM NaCl] using a cell disrupter (Série TS, CellD, Constant Systems). The soluble fraction of the cell lysate was retrieved by centrifugation (14,000*g*, 30 min, 4°C) and filtered at 0.22 μm before being submitted to a 1-ml HisTrap HP purification affinity column (GE Healthcare) according to the manufacturer's instructions. RumPc was eluted using a 0 to 500 mM gradient of imidazole. Pooled fractions containing RumPc (detected by SDS–polyacrylamide gel electrophoresis) were ultrafiltered through a PES (polyethersulfone) 10-kDa MWCO membrane and washed 10 times in buffer C. The protein concentration was estimated by measuring the A280 and using an extinction coefficient of 52,425 M^{-1} cm^{-1}.

mRumC1 leader peptide cleavage

Maturated RumC1 obtained by heterologous coexpression of *rumC1* and *rumMc1* genes in *E. coli* and purified as described above was treated with either RumPc or TPCK (*N*-tosyl-L-phenylalanine chloromethyl ketone)–treated trypsin (Sigma-Aldrich) for 1 hour at 37°C. The molar ratios used were 200:1 for mRumC1:trypsin and 1:5 for mRumC1:RumPc. mRumC1c and mRumC1cc were purified using RP-C18-HPLC with the following gradient: 10 min at 22% followed by 12 min from 22 to 38% of 90% ACN and 0.1% TFA. For the preparation of large amounts of mRumC1cc for biological activity assays, mRumC1 was cleaved with trypsin and purified with the above RP-C18-HPLC conditions on a preparative column (250 mm by 21.2 mm; Phenomenex, Jupiter, 15 μm, 300 Å).

Nano–LC-MS/MS analyses

RumC fractions were generally injected at a concentration of 0.1 μM. Samples were diluted in 5% (v/v) ACN and 0.1% (v/v) TFA and analyzed by online nano–LC-MS/MS (NCS HPLC, Dionex, and Q Exactive HF, Thermo Fisher Scientific). Peptides were sampled on a 300 μm by 5 mm PepMap C18 precolumn and separated on a 75 μm by 250 mm PepMap C18 column (Dionex). The nano-LC method consisted of a 40 min gradient at a flow rate of 300 nl/min, and MS and MS/MS data were acquired using Xcalibur (Thermo Fisher Scientific). Highly sensitive method (by increasing the ion time in the trap to 200 ms) in MS/MS was used to improve the signal to noise of the fragmented large peptides. For the analysis of the maturated forms, combined high collision dissociation energies of 20 to 27 were used to promote the breaking of both weak bonds (thioether bridge) and stronger bonds (amide bonds). Both MS/MS spectra were summed up to give a combined spectrum. Parallel reaction monitoring experiments were also conducted to target the species of interest.

MS data analyses

Data were processed automatically using Mascot Distiller software (version 2.5.1, Matrix Science) followed by Mascot (version 2.6) searches using the sequences of the different peptides of interest as database. None was chosen as enzyme, and the precisions were set at 10 ppm for the peptide precursor and 20 milli mass unit for the fragments. At first instance, many different possibilities of variable modifications were tested to find out on which amino acid was observed in the dehydramino modification (−2H) (*36*). Manual annotations were performed in parallel to Mascot searches to assess the positions of thioether linkages. For final searches, dehydramino (A, N, R, and K), deamidation (NQ), and ammonia loss (N) were set as variable modifications. Qual Browser and Xtract (Thermo Fisher Scientific) were used for the display and the deconvolution of the spectra. All considered experimental masses were monoisotopic and nonprotonated masses.

Antimicrobial activity

All targeted strains were grown at 37°C in LB broth under aerobic conditions (200 rpm), except for Clostridia that were grown in BHI-YH under anaerobic conditions (in a Trexler-type anaerobic chamber, without stirring). Peptides dissolved in sterile distilled water were sterilized 2 min under UV light and added to sterile F-bottom polypropylene 96-well microplates from 100 to 0.1 μM. Twofold series dilutions were performed in cell suspension of each bacterial target, including *Cp*, at 10^{-4} OD_{600} units. For other Clostridia, higher concentrations of bacteria (i.e., cell suspensions at 10^{-3} OD_{600} units) were used. MIC was defined as the lowest concentration of peptide that inhibited the visible growth of bacteria after 24 to 48 hours incubation at 37°C. Cell suspensions were then plated on appropriate solid medium devoid of any antimicrobial agent to evaluate bacterial growth. MBCs were defined as the lowest concentration of peptide that inhibited the visible growth of bacteria after 24 to 48 hours incubation at 37°C on a solid medium. MICs and MBCs were determined three times. Sterility and growth controls were prepared for each assay.

Membrane permeability assay

Permeabilization of the bacterial membrane by RumC1 was measured using the cell-impermeable DNA/RNA probe PI as previously explained (*53*, *54*). A bacterial culture of *Cp* was grown until it reached 10^9 bacteria/ml and then centrifuged for 5 min at 300s. Bacteria pellet was then resuspended in sterile PBS in the original volume. PI (Sigma-Aldrich) was then added to the suspension at a final concentration of 60 μM. One hundred microliters of this suspension was then transferred into 96-well black plate (Greiner Bio-One) and treated with RumC1 or nisin at 5× their MIC values. Water and CTAB diluted at 300 μM final concentration were used as negative and positive controls, respectively. After 15- and 120-min incubations at 37°C under anaerobic conditions, fluorescence was measured (excitation at 530 nm and emission at 590 nm) using a microplate reader (Synergy Mx, BioTek). Results were expressed as the percentage of total permeabilization obtained by treatment with CTAB. All experiments were done in triplicate. For the permeabilization assay with SYTOX Green (Thermo Fisher Scientific), an overnight culture of *Cp* was diluted at 1:100 in BHI-YH and grown at 37°C under anaerobic conditions until OD_{600} = 0.2. Cells were then treated with RumC1 or nisin at 5× their MIC values for 15 min before being stained with SYTOX Green at 0.5 μM. Then, cells were rinsed with Hanks' balanced salt solution +/+ (Gibco) and resuspended in VECTASHIELD (Vector Laboratories, CliniSciences H-1000). Observations were lastly performed with a Leitz DMRB microscope (Leïca), equipped with a Leïca DFC 450C camera.

Study of the mode of action based on phenotype imaging by confocal microscopy

Phenotype observations by confocal microscopy were used to evaluate the mode of action of RumC1, as previously described (*42*) but with some modifications. An overnight culture of *Cp* was diluted at 1:100 in BHI-YH and grown at 37°C under anaerobic conditions until OD_{600nm} = 0.2. Bacteria were then treated with RumC1 or antibiotics with known mechanisms of action (fig. S7) at 5× their MIC values for 2 hours. Then, membranes were stained with FM4-64FX (Thermo Fisher Scientific), and DNA was stained with DAPI (Sigma-Aldrich) at final concentrations of 12 and 2 μg/ml, respectively, for 10 min on ice. Cells were then pelleted (7500 rpm, 30 s) and washed with cold PBS. Cells were fixed with 4% cold paraformaldehyde for 15 min on ice before being washed with cold PBS again. Last, cells were resuspended in VECTASHIELD, and 8 μl was transferred onto microscope glass slides. Images were collected using an IX71 FluoView confocal microscope (Olympus, Rungis, France) for DAPI laser/filter ExWave = "405"/EmWave = "461" and for FM4-64FX laser/filter ExWave = "543"/EmWave = "618."

Cytotoxic assays

The intestinal toxicity of RumC1 was evaluated on human cell lines, with NCI-N87 (ATCC CRL-5822), Caco-2 (ATCC HTB-37), and T84 (ATCC CCL-248) being used as models of human gastric, small intestinal, and colonic epithelial cells, respectively. Cells were cultured in Dulbecco's modified Eagle's medium supplemented with 10% fetal bovine serum, 1% L-glutamine, and 1% streptomycin-penicillin antibiotics (all from Invitrogen). Cells were routinely seeded and grown onto 25-cm^2 flasks maintained in a 5% CO_2 incubator at 37°C. Before cytotoxicity assay, cells grown on 25-cm^2 flasks were detached using trypsin-EDTA solution (Thermo Fisher Scientific), counted using Malassez counting chamber, and seeded into 96-well cell culture plates (Greiner Bio-One) at approximately 104 cells per well. The cells were left to reach confluence for 48 to 72 hours at 37°C in a 5% CO_2 incubator. Plates were then aspirated, and increasing concentrations of RumC1 (final concentrations ranging from 0 to 200 μM) diluted in culture medium were added to the cells for 48 hours at 37°C in a 5% CO_2 incubator. Sterile water was used as a negative control. At the end of the incubation, wells were empty and cell viability was evaluated using a resazurin-based in vitro toxicity assay kit (Sigma-Aldrich) following the manufacturer's instructions (*55*). Briefly, wells were aspirated and filled with 100 μl of diluted resazurin solution obtained by dilution of the resazurin stock solution (1:100) in sterile PBS containing calcium and magnesium [PBS++ (pH 7.4), Thermo Fisher Scientific]. After 4 hours of incubation at 37°C, fluorescence intensity was measured using a microplate reader (Synergy Mx, BioTek) with an excitation wavelength of 530 nm and an emission wavelength of 590 nm. The fluorescence values were normalized by the control and expressed as the percentage of cell viability. All experiments were done in triplicate.

Hemolytic activity assay

The hemolytic activity of RumC1 was evaluated as previously described (*53*, *56*, *57*). Briefly, human erythrocytes (obtained from DivBioScience, NL) were pelleted by centrifugation at 800*g* for 5 min. Cell pellet was then resuspended in sterile PBS and centrifuged at 800*g* for 5 min. This step was repeated three times, and erythrocytes were lastly resuspended in PBS at a concentration of 8%. One hundred microliters were then added per well of sterile 96-well microplates (Greiner Bio-One) containing 100 μl of PBS with increasing concentrations of RumC1 (final concentrations ranging from 0 to 200 μM) obtained by twofold serial dilutions. Sterile water and Triton X-100 diluted in PBS at 0.1% (v/v) were used as negative and positive controls, respectively. After 1 hour at 37°C, the microplates were centrifuged at 800*g* for 5 min. One hundred microliters of cell supernatants was collected and transferred to a new 96-well microplate, and OD_{405nm} was measured using a microplate reader (Synergy Mx, BioTek). Hemolysis caused by RumC1 was expressed as the percentage of total hemolysis given by treatment with Triton X-100 at 0.1%. All experiments were done in triplicate.

Induction of resistance

Cp cells were incubated with RumC1 or metronidazole as described above for MIC determination. After 24 hours of incubation, the well

with the highest concentration of peptide or antibiotic showing visible growth was used to inoculate a new culture that was then treated again. These steps were repeated daily for 30 days to follow MIC changes.

SUPPLEMENTARY MATERIALS

Supplementary material for this article is available at http://advances.sciencemag.org/cgi/content/full/5/9/eaaw9969/DC1

Supplementary Methods

Fig. S1. Multi-alignment of RumMc radical SAM enzymes.

Fig. S2. Tandem mass spectra of RumC2-5 purified from cecal contents.

Fig. S3. Gene expression in the gut of rats monoassociated with *R. gnavus* E1 and heterologous expression and purification of MBP-mRumC1, mRumC1, and RumPc.

Fig. S4. Tandem mass spectra of N- and C-terminal fragments of RumC1 peptide present in in vivo and in vitro samples.

Fig. S5. Tandem mass spectra of mRumC1 mutants from which the residues involved in each thioether bridge were attributed.

Fig. S6. Determination of the connectivity of the thioether linkages in RumC1 by NMR.

Fig. S7. Cleavage of the leader N-terminal peptides of mRumC1 and anti-*Cp* activity assays.

Fig. S8. Evaluation of the ability of RumC1 to insert into bacterial lipids.

Fig. S9. Bacterial cytological profiling against *Cp*.

Fig. S10. Assessing RumC1 safety.

Table S1. Theoretical and experimental spectra lists.

References (*58*, *59*)

REFERENCES AND NOTES

1. A. J. O'Neill, New antibacterial agents for treating infections caused by multi-drug resistant Gram-negative bacteria. *Expert Opin. Investig. Drugs* **17**, 297–302 (2008).
2. J. O'Neill, *Tackling Drug-Resistant Infections Globally: Final Report and Recommendations* (Review on Antimicrobial Resistance, 2016).
3. P. G. Arnison, M. J. Bibb, G. Bierbaum, A. A. Bowers, T. S. Bugni, G. Bulaj, J. A. Camarero, D. J. Campopiano, G. L. Challis, J. Clardy, P. D. Cotter, D. J. Craik, M. Dawson, E. Dittmann, S. Donadio, P. C. Dorrestein, K.-D. Entian, M. A. Fischbach, J. S. Garavelli, U. Göransson, C. W. Gruber, D. H. Haft, T. K. Hemscheidt, C. Hertweck, C. Hill, A. R. Horswill, M. Jaspars, W. L. Kelly, J. P. Klinman, O. P. Kuipers, A. J. Link, W. Liu, M. A. Marahiel, D. A. Mitchell, G. N. Moll, B. S. Moore, R. Müller, S. K. Nair, I. F. Nes, G. E. Norris, B. M. Olivera, H. Onaka, M. L. Patchett, J. Piel, M. J. T. Reaney, S. Rebuffat, R. P. Ross, H.-G. Sahl, E. W. Schmidt, M. E. Selsted, K. Severinov, B. Shen, K. Sivonen, L. Smith, T. Stein, R. D. Süssmuth, J. R. Tagg, G.-L. Tang, A. W. Truman, J. C. Vederas, C. T. Walsh, J. D. Walton, S. C. Wenzel, J. M. Willey, W. A. van der Donk, Ribosomally synthesized and post-translationally modified peptide natural products: Overview and recommendations for a universal nomenclature. *Nat. Prod. Rep.* **30**, 108–160 (2013).
4. M. C. Rea, R. P. Ross, P. D. Cotter, C. Hill, Classification of bacterocins from Gram-positive bacteria, in *Prokaryotic Antimicrobial Peptides: From genes to Applications*, D. Drider, S. Rebuffat, Eds. (Springer, 2011), pp. 29–53.
5. H. Mathur, M. C. Rea, P. D. Cotter, C. Hill, R. P. Ross, The sactibiotic subclass of bacteriocins: An update. *Curr. Protein Pept. Sci.* **16**, 549–558 (2015).
6. K. Kawulka, T. Sprules, R. T. McKay, P. Mercier, C. M. Diaper, P. Zuber, J. C. Vederas, Structure of subtilosin A, an antimicrobial peptide from *Bacillus subtilis* with unusual posttranslational modifications linking cysteine sulfurs to α-carbons of phenylalanine and threonine. *J. Am. Chem. Soc.* **125**, 4726–4727 (2003).
7. K. E. Kawulka, T. Sprules, C. M. Diaper, R. M. Whittal, R. T. McKay, P. Mercier, P. Zuber, J. C. Vederas, Structure of subtilosin A, a cyclic antimicrobial peptide from *Bacillus subtilis* with unusual sulfur to α-carbon cross-links: Formation and reduction of α-thio-α-amino acid derivatives. *Biochemistry* **43**, 3385–3395 (2004).
8. M. C. Rea, C. S. Sit, E. Clayton, P. M. O'Connor, R. M. Whittal, J. Zheng, J. C. Vederas, R. P. Ross, C. Hill, Thuricin CD, a posttranslationally modified bacteriocin with a narrow spectrum of activity against *Clostridium difficile*. *Proc. Natl. Acad. Sci. U.S.A.* **107**, 9352–9357 (2010).
9. C. S. Sit, M. J. van Belkum, R. T. McKay, R. W. Worobo, J. C. Vederas, The 3D solution structure of thurincin H, a bacteriocin with four sulfur to α-carbon crosslinks. *Angew. Chem. Int. Ed. Engl.* **50**, 8718–8721 (2011).
10. W.-T. Liu, Y.-L. Yang, Y. Xu, A. Lamsa, N. M. Haste, J. Y. Yang, J. Ng, D. Gonzalez, C. D. Ellermeier, P. D. Straight, P. A. Pevzner, J. Pogliano, V. Nizet, K. Pogliano, P. C. Dorrestein, Imaging mass spectrometry of intraspecies metabolic exchange revealed the cannibalistic factors of Bacillus subtilis. *Proc. Natl. Acad. Sci. U.S.A.* **107**, 16286–16290 (2010).
11. N. A. Bruender, J. Wilcoxen, R. D. Britt, V. Bandarian, Biochemical and spectroscopic characterization of a radical *S*-adenosyl-L-methionine enzyme involved in the formation of a peptide thioether cross-link. *Biochemistry* **55**, 2122–2134 (2016).
12. T. L. Grove, P. M. Himes, S. Hwang, H. Yumerefendi, J. B. Bonanno, B. Kuhlman, S. C. Almo, A. A. Bowers, Structural insights into thioether bond formation in the biosynthesis of sactipeptides. *J. Am. Chem. Soc.* **139**, 11734–11744 (2017).
13. G. A. Hudson, D. A. Mitchell, RiPP antibiotics: Biosynthesis and engineering potential. *Curr. Opin. Microbiol.* **45**, 61–69 (2018).
14. M. G. Lamarche, B. L. Wanner, S. Crépin, J. Harel, The phosphate regulon and bacterial virulence: A regulatory network connecting phosphate homeostasis and pathogenesis. *FEMS Microbiol. Rev.* **32**, 461–473 (2008).
15. A. Pujol, E. H. Crost, G. Simon, V. Barbe, D. Vallenet, A. Gomez, M. Fons, Characterization and distribution of the gene cluster encoding RumC, an anti-*Clostridium perfringens* bacteriocin produced in the gut. *FEMS Microbiol. Ecol.* **78**, 405–415 (2011).
16. N. D. Rawlings, A. J. Barrett, P. D. Thomas, X. Huang, A. Bateman, R. D. Finn, The MEROPS database of proteolytic enzymes, their substrates and inhibitors in 2017 and a comparison with peptidases in the PANTHER database. *Nucleic Acids Res.* **46**, D624–D632 (2018).
17. F. Ramare, J. Nicoli, J. Dabard, T. Corring, M. Ladire, A. M. Gueugneau, P. Raibaud, Trypsin-dependent production of an antibacterial substance by a human Peptostreptococcus strain in gnotobiotic rats and in vitro. *Appl. Environ. Microbiol.* **59**, 2876–2883 (1993).
18. E. H. Crost, E. H. Ajandouz, C. Villard, P. A. Geraert, A. Puigserver, M. Fons, Ruminococcin C, a new anti-*Clostridium perfringens* bacteriocin produced in the gut by the commensal bacterium *Ruminococcus gnavus* E1. *Biochimie* **93**, 1487–1494 (2011).
19. E. H. Crost, A. Pujol, M. Ladiré, J. Dabard, P. Raibaud, J. P. Carlier, M. Fons, Production of an antibacterial substance in the digestive tract involved in colonization-resistance against *Clostridium perfringens*. *Anaerobe* **16**, 597–603 (2010).
20. L. Flühe, M. A. Marahiel, Radical *S*-adenosylmethionine enzyme catalyzed thioether bond formation in sactipeptide biosynthesis. *Curr. Opin. Chem. Biol.* **17**, 605–612 (2013).
21. J. B. Broderick, B. R. Duffus, K. S. Duschene, E. M. Shepard, Radical *S*-adenosylmethionine enzymes. *Chem. Rev.* **114**, 4229–4317 (2014).
22. T. A. J. Grell, P. J. Goldman, C. L. Drennan, SPASM and twitch domains in *S*-adenosylmethionine (SAM) radical enzymes. *J. Biol. Chem.* **290**, 3964–3971 (2015).
23. L. Flühe, T. A. Knappe, M. J. Gattner, A. Schäfer, O. Burghaus, U. Linne, M. A. Marahiel, The radical SAM enzyme AlbA catalyzes thioether bond formation in subtilosin A. *Nat. Chem. Biol.* **8**, 350–357 (2012).
24. B. M. Wieckowski, J. D. Hegemann, A. Mielcarek, L. Boss, O. Burghaus, M. A. Marahiel, The PqqD homologous domain of the radical SAM enzyme ThnB is required for thioether bond formation during thurincin H maturation. *FEBS Lett.* **589**, 1802–1806 (2015).
25. L. Flühe, O. Burghaus, B. M. Wieckowski, T. W. Giessen, U. Linne, M. A. Marahiel, Two [4Fe-4S] clusters containing radical SAM enzyme SkfB catalyze thioether bond formation during the maturation of the sporulation killing factor. *J. Am. Chem. Soc.* **135**, 959–962 (2013).
26. N. A. Bruender, V. Bandarian, SkfB abstracts a hydrogen atom from Cα on SkfA to initiate thioether cross-link formation. *Biochemistry* **55**, 4131–4134 (2016).
27. L. M. Walker, W. M. Kincannon, V. Bandarian, S. J. Elliott, Deconvoluting the reduction potentials for the three [4Fe-4S] clusters in an AdoMet radical SCIFF maturase. *Biochemistry* **57**, 6050–6053 (2018).
28. W. M. Kincannon, N. A. Bruender, V. Bandarian, A radical clock probe uncouples H atom abstraction from thioether cross-link formation by the radical *S* -adenosyl- l -methionine enzyme SkfB. *Biochemistry* **57**, 4816–4823 (2018).
29. T. A. J. Grell, W. M. Kincannon, N. A. Bruender, E. J. Blaesi, C. Krebs, V. Bandarian, C. L. Drennan, Structural and spectroscopic analyses of the sporulation killing factor biosynthetic enzyme SkfB, a bacterial AdoMet radical sactisynthase. *J. Biol. Chem.* **293**, 17349–17361 (2018).
30. A. Benjdia, C. Balty, O. Berteau, Radical SAM enzymes in the biosynthesis of ribosomally synthesized and post-translationally modified peptides (RiPPs). *Front. Chem.* **5**, 87 (2017).
31. A. Benjdia, A. Guillot, B. Lefranc, H. Vaudry, J. Leprince, O. Berteau, Thioether bond formation by SPASM domain radical SAM enzymes: Cα H-atom abstraction in subtilosin A biosynthesis. *Chem. Commun. Camb. Engl.* **52**, 6249–6252 (2016).
32. H. Mathur, V. Fallico, P. M. O'Connor, M. C. Rea, P. D. Cotter, C. Hill, R. P. Ross, Insights into the mode of action of the sactibiotic thuricin CD. *Front. Microbiol.* **8**, 696 (2017).
33. G. Wang, D. C. Manns, G. K. Guron, J. J. Churey, R. W. Worobo, Large-scale purification, characterization, and spore outgrowth inhibitory effect of thurincin H, a bacteriocin produced by *Bacillus thuringiensis* SF361. *Probiotics Antimicrob. Proteins.* **6**, 105–113 (2014).
34. C. E. Shelburne, F. Y. An, V. Dholpe, A. Ramamoorthy, D. E. Lopatin, M. S. Lantz, The spectrum of antimicrobial activity of the bacteriocin subtilosin A. *J. Antimicrob. Chemother.* **59**, 297–300 (2006).
35. J. E. González-Pastor, E. C. Hobbs, R. Losick, Cannibalism by sporulating bacteria. *Science* **301**, 510–513 (2003).
36. C. T. Lohans, J. C. Vederas, Structural characterization of thioether-bridged bacteriocins. *J. Antibiot.* **67**, 23–30 (2014).

37. P. M. Himes, S. E. Allen, S. Hwang, A. A. Bowers, Production of Sactipeptides in *Escherichia coli*: Probing the substrate promiscuity of subtilosin a biosynthesis. *ACS Chem. Biol.* **11**, 1737–1744 (2016).
38. B. Roche, L. Aussel, B. Ezraty, P. Mandin, B. Py, F. Barras, Iron/sulfur proteins biogenesis in prokaryotes: Formation, regulation and diversity. *Biochim. Biophys. Acta* **1827**, 455–469 (2013).
39. C. S. Sit, R. T. McKay, C. Hill, R. P. Ross, J. C. Vederas, The 3D structure of thuricin CD, a two-component bacteriocin with cysteine sulfur to α-carbon cross-links. *J. Am. Chem. Soc.* **133**, 7680–7683 (2011).
40. X. Yang, W. A. van der Donk, Ribosomally synthesized and post-translationally modified peptide natural products: New insights into the role of leader and core peptides during biosynthesis. *Chem. A Eur. J.* **19**, 7662–7677 (2013).
41. M. C. Bagley, J. W. Dale, E. A. Merritt, X. Xiong, Thiopeptide antibiotics. *Chem. Rev.* **105**, 685–714 (2005).
42. P. Nonejuie, M. Burkart, K. Pogliano, J. Pogliano, Bacterial cytological profiling rapidly identifies the cellular pathways targeted by antibacterial molecules. *Proc. Natl. Acad. Sci. U.S.A.* **110**, 16169–16174 (2013).
43. S. A. Dingsdag, N. Hunter, Metronidazole: An update on metabolism, structure-cytotoxicity and resistance mechanisms. *J. Antimicrob. Chemother.* **73**, 265–279 (2018).
44. T. J. Oman, W. A. van der Donk, Follow the leader: The use of leader peptides to guide natural product biosynthesis. *Nat. Chem. Biol.* **6**, 9–18 (2010).
45. M. C. Booth, C. P. Bogie, H. G. Sahl, R. J. Siezen, K. L. Hatter, M. S. Gilmore, Structural analysis and proteolytic activation of Enterococcus faecalis cytolysin, a novel lantibiotic. *Mol. Microbiol.* **21**, 1175–1184 (1996).
46. A. L. McClerren, L. E. Cooper, C. Quan, P. M. Thomas, N. L. Kelleher, W. A. van der Donk, Discovery and in vitro biosynthesis of haloduracin, a two-component lantibiotic. *Proc. Natl. Acad. Sci. U.S.A.* **103**, 17243–17248 (2006).
47. M. Begley, P. D. Cotter, C. Hill, R. P. Ross, Identification of a novel two-peptide lantibiotic, lichenicidin, following rational genome mining for LanM proteins. *Appl. Environ. Microbiol.* **75**, 5451–5460 (2009).
48. S. Chen, B. Xu, E. Chen, J. Wang, J. Lu, S. Donadio, H. Ge, H. Wang, Zn-dependent bifunctional proteases are responsible for leader peptide processing of class III lanthipeptides. *Proc. Natl. Acad. Sci. U.S.A.* **116**, 2533–2538 (2019).
49. G. H. Völler, B. Krawczyk, P. Ensle, R. D. Süssmuth, Involvement and unusual substrate specificity of a prolyl oligopeptidase in class III lanthipeptide maturation. *J. Am. Chem. Soc.* **135**, 7426–7429 (2013).
50. C. T. Lohans, J. L. Li, J. C. Vederas, Structure and biosynthesis of carnolysin, a homologue of enterococcal cytolysin with D-amino acids. *J. Am. Chem. Soc.* **136**, 13150–13153 (2014).
51. H. Holo, Z. Jeknic, M. Daeschel, S. Stevanovic, I. F. Nes, Plantaricin W from *Lactobacillus plantarum* belongs to a new family of two-peptide lantibiotics. *Microbiology* **147**, 643–651 (2001).
52. F. V. Immerseel, J. D. Buck, F. Pasmans, G. Huyghebaert, F. Haesebrouck, R. Ducatelle, *Clostridium* perfringensin poultry: An emerging threat for animal and public health. *Avian Pathol.* **33**, 537–549 (2004).
53. L. B. Oyama, S. E. Girdwood, A. R. Cookson, N. Fernandez-Fuentes, F. Privé, H. E. Vallin, T. J. Wilkinson, P. N. Golyshin, O. V. Golyshina, R. Mikut, K. Hilpert, J. Richards, M. Wootton, J. E. Edwards, M. Maresca, J. Perrier, F. T. Lundy, Y. Luo, M. Zhou, M. Hess, H. C. Mantovani, C. J. Creevey, S. A. Huws, The rumen microbiome: An underexplored resource for novel antimicrobial discovery. *NPJ Biofilms Microbiomes.* **3**, 33 (2017).
54. E. Di Pasquale, C. Salmi-Smail, J.-M. Brunel, P. Sanchez, J. Fantini, M. Maresca, Biophysical studies of the interaction of squalamine and other cationic amphiphilic molecules with bacterial and eukaryotic membranes: Importance of the distribution coefficient in membrane selectivity. *Chem. Phys. Lipids* **163**, 131–140 (2010).
55. C. Borie, S. Mondal, T. Arif, M. Briand, H. Lingua, F. Dumur, D. Gigmes, P. Stocker, B. Barbarat, V. Robert, C. Nicoletti, D. Olive, M. Maresca, M. Nechab, Enediynes bearing polyfluoroaryl sulfoxide as new antiproliferative agents with dual targeting of microtubules and DNA. *Eur. J. Med. Chem.* **148**, 306–313 (2018).
56. A. Tardy, J.-C. Honoré, J. Tran, D. Siri, V. Delplace, I. Bataille, D. Letourneur, J. Perrier, C. Nicoletti, M. Maresca, C. Lefay, D. Gigmes, J. Nicolas, Y. Guillaneuf, Radical copolymerization of vinyl ethers and cyclic ketene acetals as a versatile platform to design functional polyesters. *Angew. Chem. Int. Ed.* **56**, 16515–16520 (2017).
57. B. T. Benkhaled, S. Hadiouch, H. Olleik, J. Perrier, C. Ysacco, Y. Guillaneuf, D. Gigmes, M. Maresca, C. Lefay, Elaboration of antimicrobial polymeric materials by dispersion of well-defined amphiphilic methacrylic SG1-based copolymers. *Polym. Chem.* **9**, 3127–3141 (2018).
58. K. J. Livak, T. D. Schmittgen, Analysis of relative gene expression data using real-time quantitative PCR and the $2^{-\Delta\Delta CT}$ Method. *Methods* **25**, 402–408 (2001).
59. W. C. Chan, P. D. White, *Fmoc solid phase peptide synthesis: A practical approach* (Oxford University Press, 2000).

Acknowledgments: We would like to thank the people from the AVB platform (iSm2 CNRS, UMR 7313, Marseille) and the "ANAXEM platform" animal facility (Micalis INRA Jouy en Josas, France). We are indebted to S. Rabot (INRA) for providing the axenic and monoassociated rats and A. Balvay for skillful technical assistance. **Funding:** This study was supported by grants from the French National Agency for Research ("Agence Nationale de la Recherche") through the "Projet de Recherche Collaboratif" (RUMBA project, ANR-15-CE21-0020), the "Investissement d'Avenir Infrastructures Nationales en Biologie et Santé" programme (ProFI project, ANR-10-INBS-08), and partial financial support from the Labex ARCANE and CBH-EUR-GS (ANR-17-EURE-0003). We are grateful to Adisseo France company and the Association Nationale Recherche Technologie (ANRT) for funding the doctoral fellowship of C.R. entitled "Bacteriocins RumC, a novel antimicrobial peptide family as alternative to conventional antibiotics." This grant numbered Convention Industrielle de Formation par la RecherchE (CIFRE) no. 2016/0657 runs from 1 March 2017 to 1 March 2020. **Author contributions:** S.C., C.R., C.L., C.B., D.A., O.B., and S.T. performed the in vitro and in vivo assays for RumC1, RumMc1, and RumPc and were involved in interpreting the data and writing the manuscript. S.K.-J. and Y.C. performed the nano–LC-MS/MS characterizations and were involved in writing the manuscript. H.O. and M.M. performed the cytoxicity assays. C.N. performed the confocal microscopy experiments. O.I. and R.H. performed the peptide chemical synthesis. T.G., E.D., F.G., and M.F. were involved in the study design. M.A., M.L., J.P., and V.D. conceptualized the study, designed the experiments, and wrote the manuscript. **Competing interests:** The authors declare that they have no competing interests. **Data and materials availability:** All data needed to evaluate the conclusions in the paper are present in the paper and/or the Supplementary Materials. Additional data related to this paper may be requested from authors.

Submitted 13 February 2019
Accepted 27 August 2019
Published 25 September 2019
10.1126/sciadv.aaw9969

Citation: S. Chiumento, C. Roblin, S. Kieffer-Jaquinod, S. Tachon, C. Leprètre, C. Basset, D. Aditiyarini, H. Olleik, C. Nicoletti, O. Bornet, O. Iranzo, M. Maresca, R. Hardré, M. Fons, T. Giardina, E. Devillard, F. Guerlesquin, Y. Couté, M. Atta, J. Perrier, M. Lafond, V. Duarte, Ruminococcin C, a promising antibiotic produced by a human gut symbiont. *Sci. Adv.* **5**, eaaw9969 (2019).

Ruminococcin C, a promising antibiotic produced by a human gut symbiont

Steve Chiumento, Clarisse Roblin, Sylvie Kieffer-Jaquinod, Sybille Tachon, Chloé Leprètre, Christian Basset, Dwi Aditiyarini, Hamza Olleik, Cendrine Nicoletti, Olivier Bornet, Olga Iranzo, Marc Maresca, Renaud Hardré, Michel Fons, Thierry Giardina, Estelle Devillard, Françoise Guerlesquin, Yohann Couté, Mohamed Atta, Josette Perrier, Mickael Lafond and Victor Duarte

Sci Adv **5** (9), eaaw9969.
DOI: 10.1126/sciadv.aaw9969

Science Advances
AAAS

advances.sciencemag.org/cgi/content/full/5/9/eaaw9969/DC1

Supplementary Materials for

Ruminococcin C, a promising antibiotic produced by a human gut symbiont

Steve Chiumento, Clarisse Roblin, Sylvie Kieffer-Jaquinod, Sybille Tachon, Chloé Leprètre, Christian Basset, Dwi Aditiyarini, Hamza Olleik, Cendrine Nicoletti, Olivier Bornet, Olga Iranzo, Marc Maresca, Renaud Hardré, Michel Fons, Thierry Giardina, Estelle Devillard, Françoise Guerlesquin, Yohann Couté, Mohamed Atta, Josette Perrier, Mickael Lafond*, Victor Duarte*

*Corresponding author. Email: mickael.lafond@univ-amu.fr (M.L.); victor.duarte@cea.fr (V.D.)

Published 25 September 2019, *Sci. Adv.* **5**, eaaw9969 (2019)
DOI: 10.1126/sciadv.aaw9969

The PDF file includes:

Supplementary Methods
Fig. S1. Multi-alignment of RumMc radical SAM enzymes.
Fig. S2. Tandem mass spectra of RumC2-5 purified from cecal contents.
Fig. S3. Gene expression in the gut of rats monoassociated with *R. gnavus* E1 and heterologous expression and purification of MBP-mRumC1, mRumC1, and RumPc.
Fig. S4. Tandem mass spectra of N- and C-terminal fragments of RumC1 peptide present in in vivo and in vitro samples.
Fig. S5. Tandem mass spectra of mRumC1 mutants from which the residues involved in each thioether bridge were attributed.
Fig. S6. Determination of the connectivity of the thioether linkages in RumC1 by NMR.
Fig. S7. Cleavage of the signal and leader N-terminal peptides of mRumC1 and anti-*Cp* activity assays.
Fig. S8. Evaluation of the ability of RumC1 to insert into bacterial lipids.
Fig. S9. Bacterial cytological profiling against *Cp*.
Fig. S10. Assessing RumC1 safety.
References (*58*, *59*)

Other Supplementary Material for this manuscript includes the following:

(available at advances.sciencemag.org/cgi/content/full/5/9/eaaw9969/DC1)

Table S1 (Microsoft Excel format). Theoretical and experimental spectra lists.

A

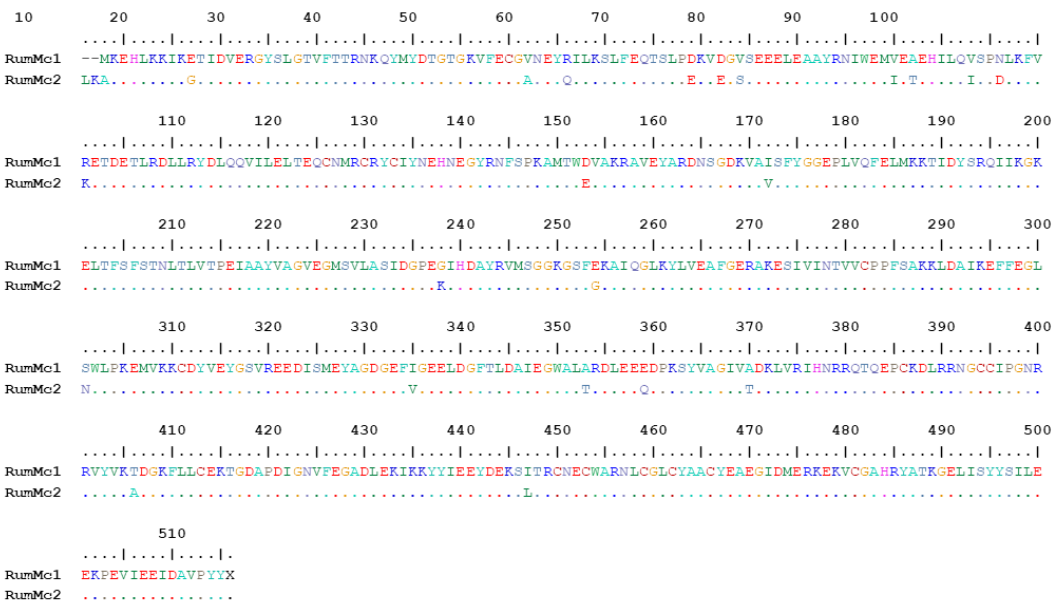

B

Primer Name	Sequence (5'-3')	Target gene	Mutations	Application for
qPCR-rpoB-F	GGGGAAGAACTGGAGAACGTA	*rpoB*		**RT-qPCR**
qPCR-rpoB-R	TTCCATATCAGGAGCGAAATC	*rpoB*		**RT-qPCR**
qPCR-C1-F	GGGATGTGTTTGTAGTGGAAGC	*rumC1*		**RT-qPCR**
qPCR-C1-R	GCCGTTTTTGCGACATTTGC	*rumC1*		**RT-qPCR**
qPCR-C2-F	GGTGGATGTAAATGCAGTGGC	*rumC2*		**RT-qPCR**
qPCR-C2-R	CACTCCGTTGTTTCCACAGTAT	*rumC2*		**RT-qPCR**
qPCR-Mc1-F	AACTGGATGCGATCAAGGAG	*rumMc1*		**RT-qPCR**
qPCR-Mc1-R	AACGTGAAACCGTCCAGTTC	*rumMc1*		**RT-qPCR**
qPCR-Mc2-F	TGTTCTGGCAAGCATAGACG	*rumMc2*		**RT-qPCR**
qPCR-Mc2-R	CACTAAATGGCGGACAGACC	*rumMc2*		**RT-qPCR**
qPCR-Pc-F	GAGACCATCGGAGACGAGTG	*rumPc*		**RT-qPCR**
qPCR-Pc-R	TCACTGTCCGAATTTCTTTCC	*rumPc*		**RT-qPCR**
Mut-C1-C3A-F	CAAGTGGGGTGCCGTGTGCAGCG	*rumC1*	C3A	**Site directed mutagenesis of mRumC1**
Mut-C1-C3A-R	CTGCCCTCGAAGTCCGCA	*rumC1*	C3A	**Site directed mutagenesis of mRumC1**
Mut-C1-C5A-F	GGGTTGCGTGGCCAGCGGTAGCA	*rumC1*	C5A	**Site directed mutagenesis of mRumC1**
Mut-C1-C5A-R	CACTTGCTGCCCTCGAAG	*rumC1*	C5A	**Site directed mutagenesis of mRumC1**
Mut-C1-C22A-F	TCCGGCGTACGCCGTGGGTTATTG	*rumC1*	C22A	**Site directed mutagenesis of mRumC1**
Mut-C1-C22A-R	CCCGCGTTATGGCTGTTC	*rumC1*	C22A	**Site directed mutagenesis of mRumC1**
Mut-C1-C26A-F	CGTGGGTTATGCCGGCAACAACGGTGTGG	*rumC1*	C26A	**Site directed mutagenesis of mRumC1**
Mut-C1-C26A-R	CAGTACGCCGGACCCGCG	*rumC1*	C26A	**Site directed mutagenesis of mRumC1**

Fig. S1. Multi-alignment of RumMc radical SAM enzymes. (A) Alignment of RumMc1 and RumMc2. Conserved residues are marked ".", small and small + hydrophobic (including aromatic -Y) residues are in red, acidic amino acids are in blue, basic amino acids in magenta, hydroxyl + sulfhydryl + amine + G amino acids are green and unusual amino/imino acids are in grey.Alignment of the five RumC peptide isoforms. (**B**) **Primers used in this study.** *All primer sets used for RT-qPCR displayed good efficiency (between 87 and 100%).*

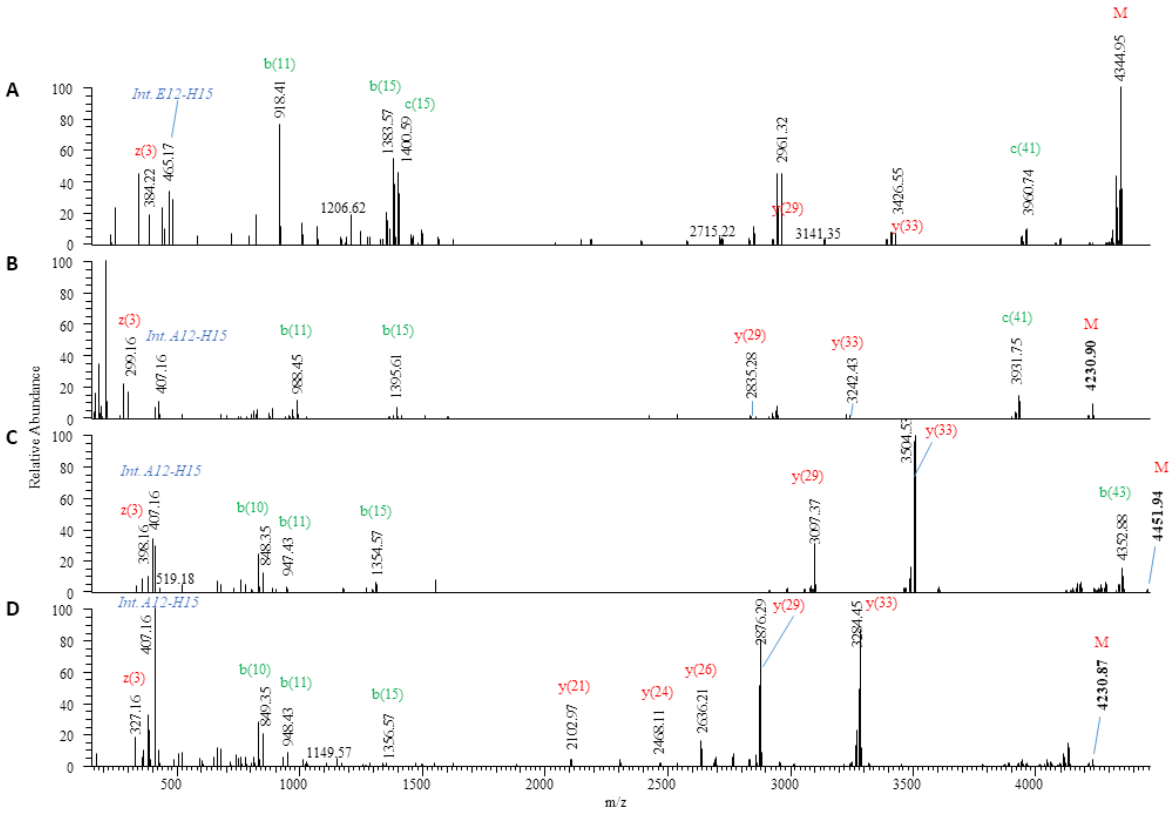

Fig. S2. Tandem mass spectra of RumC2-5 purified from cecal contents. Deconvoluted MS/MS spectra of (**A**) RumC2 peptide eluting at 18' with an m/z = $(1087.24)^{4+}$, (**B**) RumC3 peptide eluting at 22.5' with an m/z = $(1058.728)^{4+}$, (**C**) RumC4 peptide eluting at 20' with an m/z = $(1113.99)^{4+}$, and (**D**) RumC5 peptide eluting at 23' with an m/z = $(1058.722)^{4+}$. As observed for RumC1, these spectra reveal characteristic fragmentation patterns due to the presence of four thioether bonds in each mature peptide.

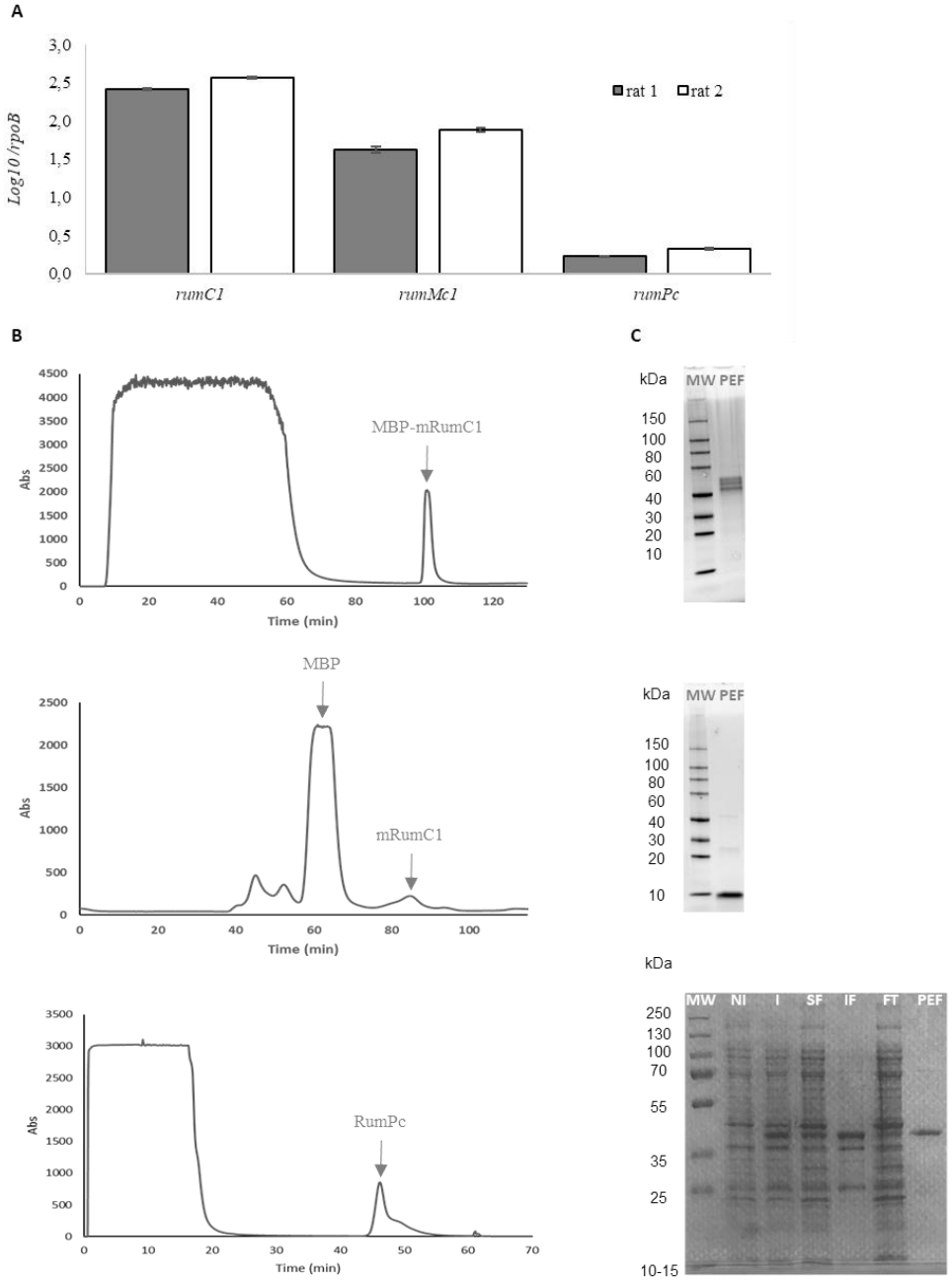

Fig. S3. Gene expression in the gut of rats monoassociated with *R. gnavus* E1 and heterologous expression and purification of MBP-mRumC1, mRumC1, and RumPc. (**A**) mRNA transcripts were purified from caecal contents of rats mono-associated with *R. gnavus* E1. Expression levels were measured for genes encoding the peptide RumC1, the sactisynthase RumMc1 and the peptidase RumPc. Expression levels for the genes of interest were normalised against expression of *rpoB*. (**B**) FPLC chromatograms of overexpressed MBP-mRumC1 (top), mRumC1 (middle) and RumPc (bottom). (**C**) SDS-PAGE analysis of purified MBP-mRumC1 (top), mRumC1 (middle) and RumPc (bottom). NI: Non-induced culture, I: Induced culture, SF: Soluble Fraction, IF: Insouble Fraction, FT: FlowThrough and PEF: Pool of Eluted Fractions.

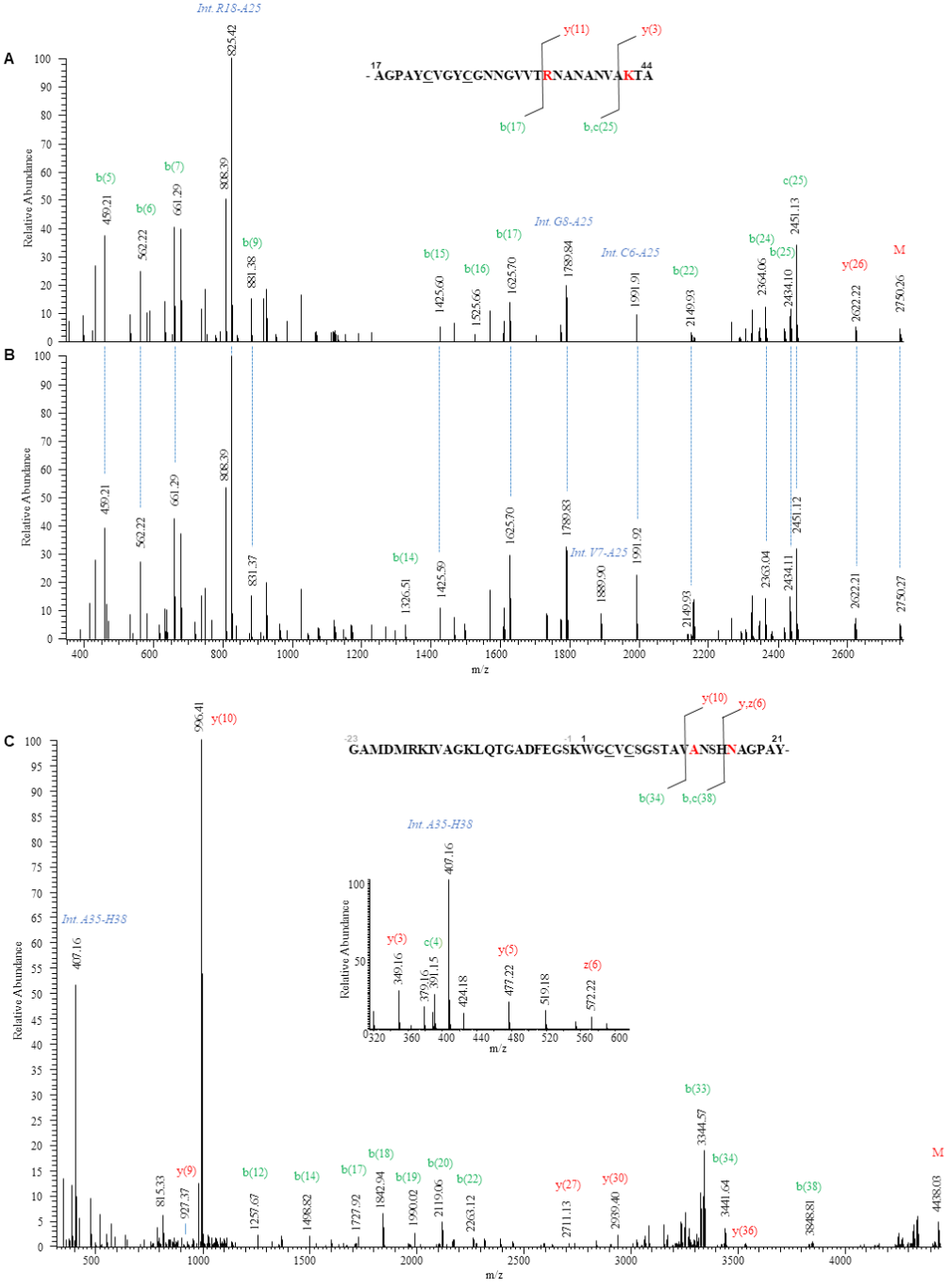

Fig. S4. Tandem mass spectra of N- and C-terminal fragments of RumC1 peptide present in in vivo and in vitro samples. (**A**) Deconvoluted MS/MS spectrum of a C-terminal fragment of the in vivo-produced RumC1 showing a 4-Da mass defect compared to the theoretical mass of the unmodified sequence and exhibiting intense internal fragments and high-intensity b/y fragments before bridged residues R34 and K42. (**B**) Deconvoluted MS/MS spectrum of the same fragment from mRumC1. (**C**) Deconvoluted MS/MS spectrum of an N-terminal fragment of mRumC1 with a 4-Da deficit and specific fragments due to thioether bridges. The inserted spectrum shows the low masses of the same MS/MS spectrum, demonstrating the involvement of A12 and N16 in thioether bridges.

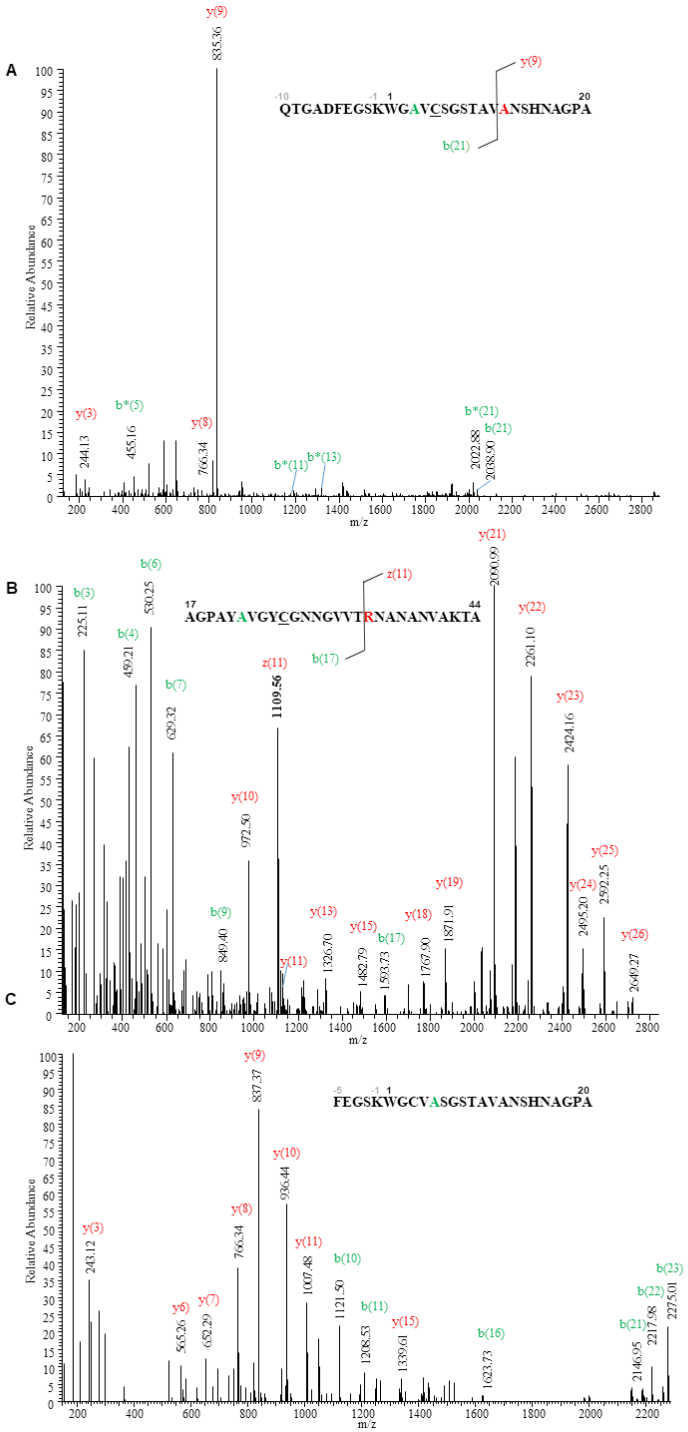

Fig. S5. Tandem mass spectra of mRumC1 mutants from which the residues involved in each thioether bridge were attributed. (see Table S1 for theoretical and observed masses of interest). (**A**) MS/MS spectrum of the Q(-10)-A20 fragment of mRumC1-C3A highlighting the presence of a unique thioether bridge between C5 and A12. The intense y9 fragment highlights the presence of a thioether bridge involving A12. (**B**) MS/MS spectrum of the A17-A44 fragment of mRumC1-C22A highlighting the presence of a unique thioether bridge between C26 and R34. (**C**) MS/MS spectrum of the F(-5)-A20 fragment of mRumC1-C5A revealing alkylation of C3. (b* corresponds to a b fragmentation with a loss of NH3 due to the presence of Q).

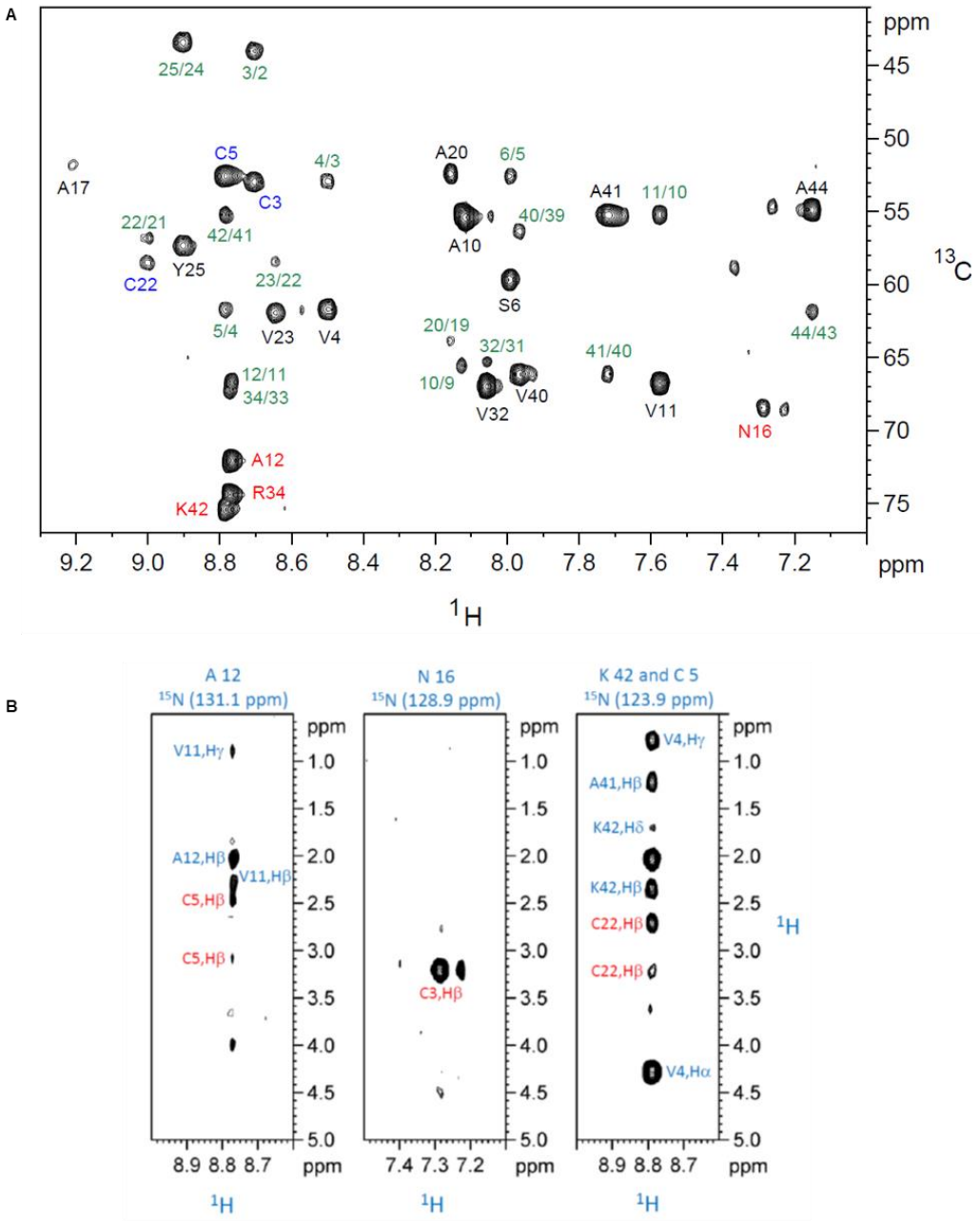

Fig. S6. Determination of the connectivity of the thioether linkages in RumC1 by NMR. (**A**) Superimposition of ^{1}H, ^{13}C planes of the HNCA spectrum showing the correlations between amide proton (HN_i) and α-carbons of its own residue ($C\alpha_i$) and that of the preceding residue ($C\alpha_{i-1}$). The sequential connectivities (HN_i - $C\alpha_{i-1}$) are indicated in green. Amino acids bridged via thioether bonds are shown in red and Cys partners are shown in blue. Note the large downfield shifts at 72.2, 68.6, 74.5 and 75.5 ppm for α-carbons of A12, N16, R34 and K42 residues, respectively. (**B**) Three ^{1}H-^{1}H strip plots from a ^{15}N-NOESY-HSQC experiment taken at the amide ^{15}N and ^{1}H chemical shifts of A12, N16, K42 and C5. The backbone NH signals for K42 and C5 are overlapped. The structural connectivities between the β-protons of Cys and the amide protons of residues involved in a thioether bridge are in red (C5-A12, C3-N16 and C22-K42).

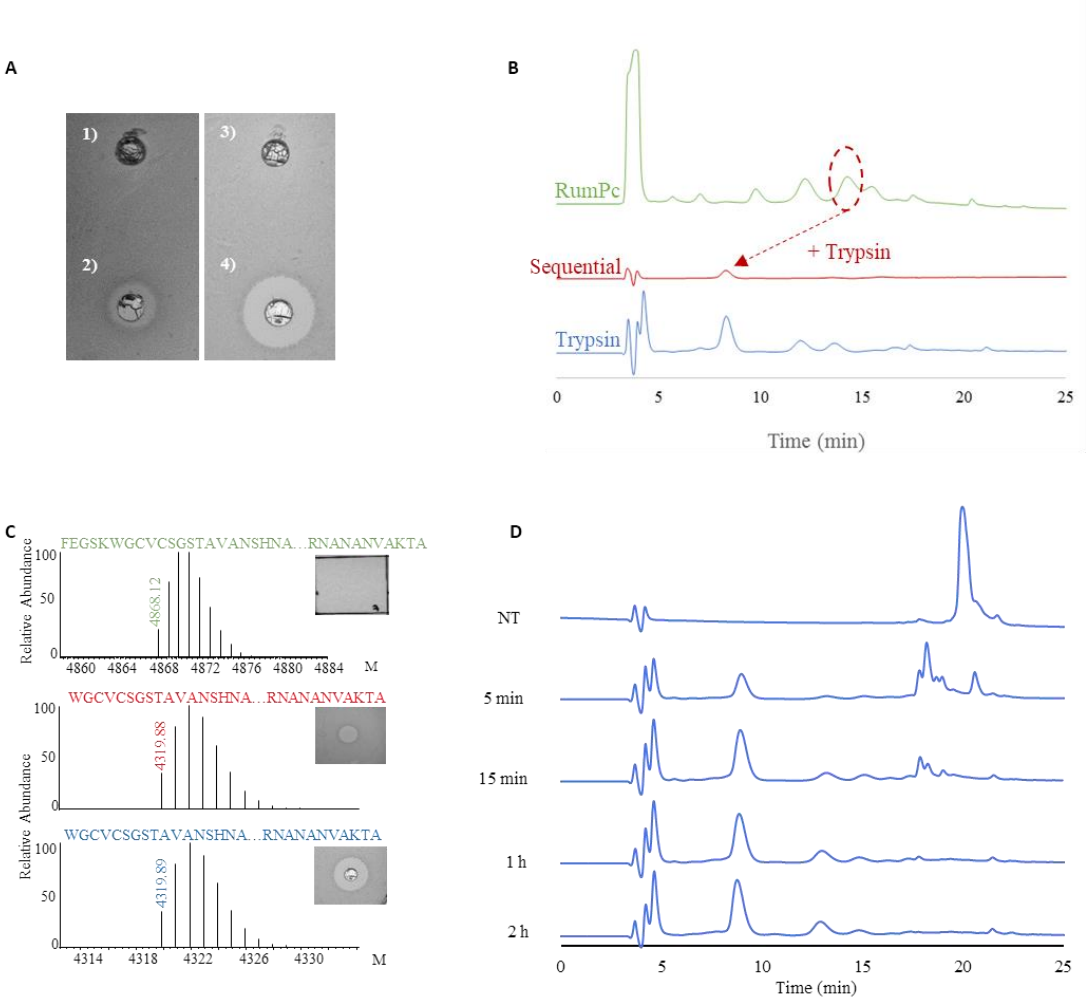

Fig. S7. Cleavage of the signal and leader N-terminal peptides of mRumC1 and anti-*Cp* activity assays. (**A**) Anti-*Cp* activity assays with the different mRumC1 forms, 1: Inactive chemically synthesised unmodified RumC1, 2: Active filtered fraction from the ultrafiltration step used as positive control (see the *in vivo* purification protocol in Fig. 2), 3: Inactive mRumC1, 4: Active mRumC1cc (obtained after cleavage with trypsin). (**B**) RP-C_{18}HPLC chromatograms of mRumC1 cleaved with RumPc, sequentially cleaved with RumPc and trypsin, or cleaved by trypsin only. (**C**) Observed masses of the different cleaved peptide forms and their corresponding anti-*Cp* activity assays (after RumPc cleavage (top), after RumPc followed by trypsin (middle) and after trypsin alone (bottom)). (**D**) RP-C_{18}HPLC chromatograms of a kinetic study for the removal of the leader peptide of mRumC1 (see pic at 20 min) by trypsin leading to the mRumC1cc form (see pic at 9 min), duration of treatment with trypsin is indicated vertically, NT = no treatment. *Peptides were detected at 214 nm in HPLC output*.

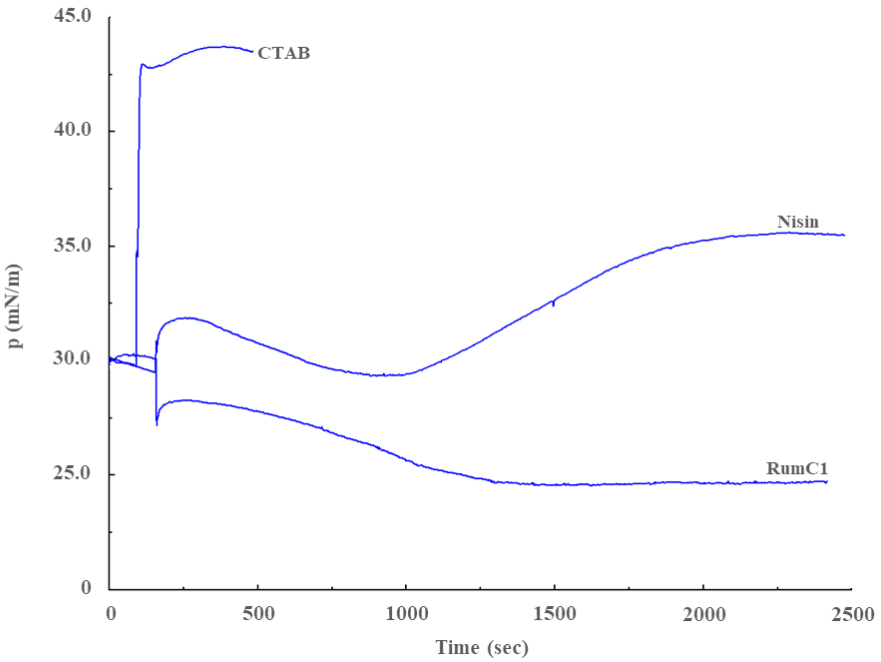

Fig. S8. Evaluation of the ability of RumC1 to insert into bacterial lipids. Total lipids from *C. perfringens* ATCC 13124 were extracted as described in the Supplementary Methods section. Total lipid extract was spread at the air-water interface until the surface pressure (p) reached approximatively 30 mN/m. Tested molecules were then injected into the aqueous sub-phase and the insertion into lipids was followed through the continuous measurement of the surface pressure (p). The detergent cetyl trimethylammonium bromide (CTAB) and the pore-forming antimicrobial peptide Nisin were used as positive controls. CTAB was used at 100 µM whereas Nisin and RumC1 were assayed at 10 x MIC, *i.e.* 7.8 µM and 15.6 µM, respectively. *Graph shown is representative of three independent experiments*.

A

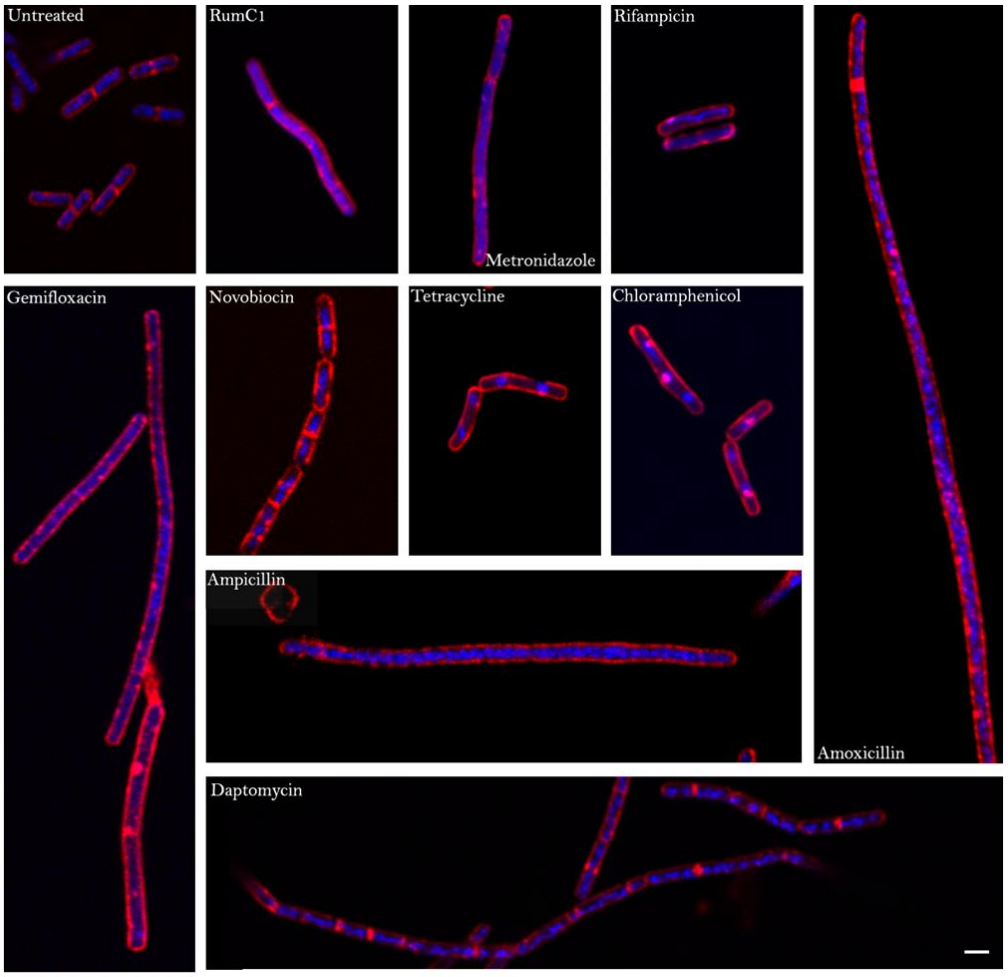

B

Mode of action	Antibiotics	Length	DNA (C/U)	Filament formation (Y/N)
Control		x 1	C	Not more than 2 cells
Inhibition cell wall synthesis	Amoxicillin	x 14-20	C	N
	Ampicillin	x 5-14	C	N
Inhibition DNA synthesis	Novobiocin	x 1	Hyper C	Y
	Gemifloxacin	x 2-9	U	Y and N
Inhibition RNA synthesis	Rifampicin	x 1-2	50 % hyper C / 50 % U	N
Inhibition protein synthesis	Tetracyclin	x 1-2	Hyper C, circular, 1-3 distinct molecules/cell	N
	Chloramphenicol	x 1-4		N
Loss membrane potential	Daptomycin	x 0.25-4	C	Y
Nucleic acid synthesis	Metronidazole	x 1-4	U with few C spots	Y - 2-4 short cells - 1 short + 1 long - 2 shorts + 1 long in the middle

Fig. S9. Bacterial cytological profiling against *Cp*. (**A**) Confocal imaging of untreated and antibiotic-treated Cp cells. Membranes were stained with FM4-64FX and DNA with DAPI. Scale bar = 2 µm. (**B**) Description of the phenotypes observed in a. C=condensed, U=uncondensed, Y=yes, N=no. The Length corresponds to 'x times untreated cell-length'.

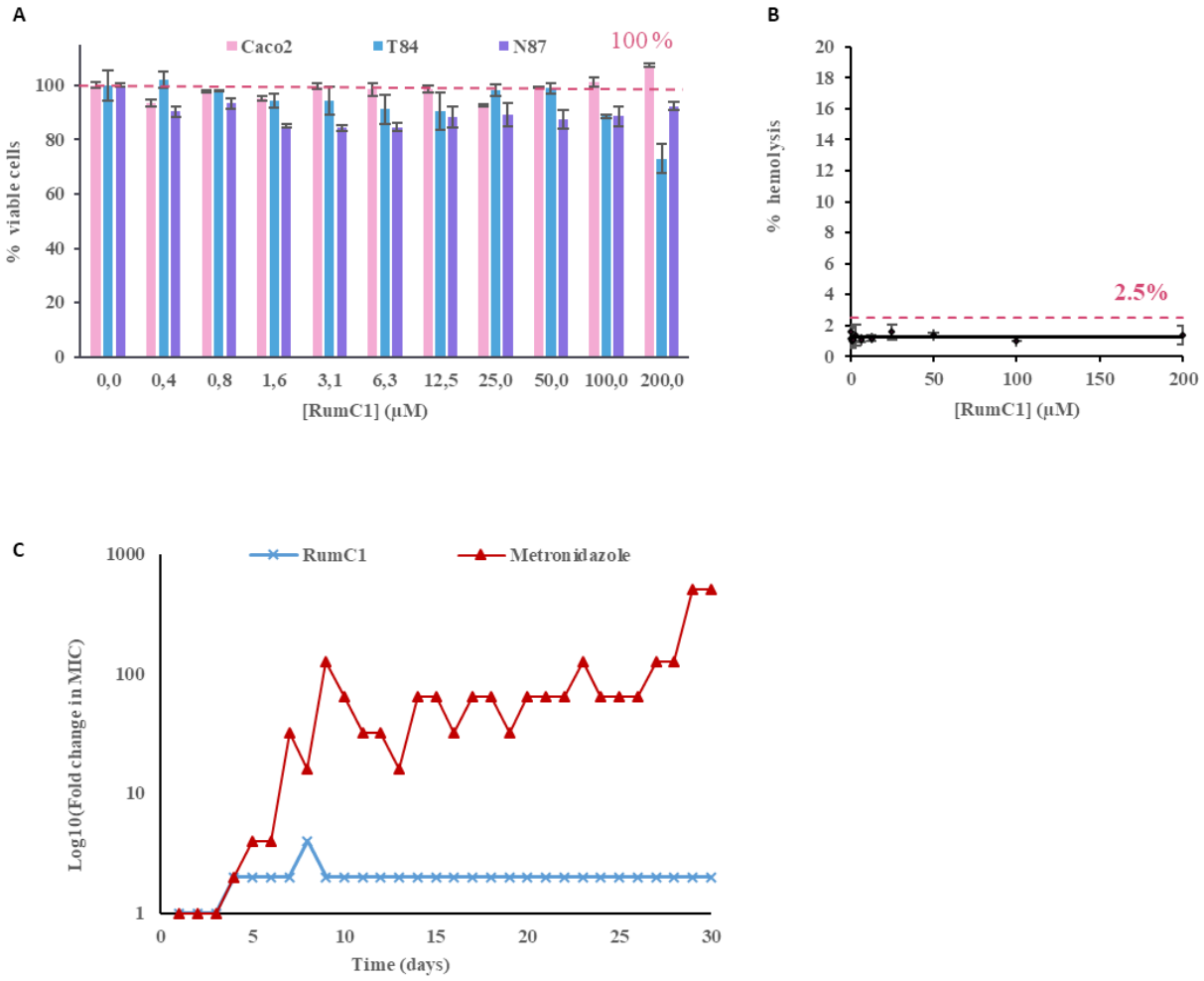

Fig. S10. Assessing RumC1 safety. Human intestinal cell lines (Caco2, T84) and gastric cell lines (N87) (**A**), and human erythrocytes (**B**) were incubated with increasing concentrations of RumC1. (**A**) Cells were incubated with resazurin and conversion into fluorescent resorufin was monitored to determine metabolic activity as an indicator of cell viability, untreated cells were used as a positive control. (**B**) Haemoglobin release was measured to monitor the lytic activity spectrum of RumC1. Cells incubated with CTAB were used as a positive control for maximum lysis, untreated cells were used as negative control. (**C**) Induction of resistance to *Cp*, assessed every day over 30 days treatment with RumC1 (blue) or metronidazole (red).

Supplementary Methods

RNA extractions and real-time PCR

RNA was extracted from the faeces of two *R. gnavus* E1 mono-associated rats collected before and after 12 days of colonization. Faecal samples were thawed in 1 mL RNApro solution containing lysing matrix E (MP Biomedicals). The cells were homogenized in a Fast Prep FP120 cell homogenizer (Thermo Savant) for 2 cycles of 40 s at 6.0 $m.s^{-1}$. RNA was extracted from the aqueous phase by chloroform extraction and ethanol precipitation before being treated twice with DNase I (NEB). No bacterialRNA could be detected in the faeces of rats before colonization. cDNA was generated using the SuperScript VILO kit (Invitrogen, Thermo Fisher Scientific). Real-time PCR amplification was performed using the LightCycler 480 Instrument and SYBR Green I Master (Roche) on 10 ng cDNA per reaction in the presence of 0.5 µM of each forward and reverse primers (Invitrogen) (fig. S1B). PCR amplification was initiated at 95 °C for 10 min, followed by 45 cycles of 9 5 °C for 10 s, 60 °C for 10 s and 72 °C for 10 s. A melting curve was added at the end of the amplification to confirm primer specificity. All reactions were performed in duplicate and repeated five times. Fold change in *R. gnavus* E1 transcript amounts was determined using the 2-ΔCt method (*59*), using *rpoB* as the reference gene.

Peptide synthesis

The linear RumC1 peptide was prepared by solid phase peptide synthesis in an Initiator^{+} Alstra automated microwave assisted synthesizer (Biotage). The peptide was assembled on a Fmoc Ala Wang resin (0.125 mmol scale, 0.53 mmol/g) using standard Fmoc methodologies (*60*). After assembling, the peptide was manually deprotected and cleaved from the resin by treatment with the mixture TFA/TIS/water (%v/v = 95:2.5:2.5) for 2 h at room temperature and under nitrogen. The resin was filtered out and rinsed with TFA. The filtrate and rinses were combined and reduced under a nitrogen stream. Cold diethyl ether was added to precipitate the crude peptide, which was dissolved in the minimum amount of water and lyophilized. The crude peptide was purified by preparative reversed-phase HPLC in a Phenomenex Jupiter column (250 mm × 21.20 mm, 15 µm, 300 Å) using solvent A (99.9% water/0.1 % TFA) and solvent B (90% ACN/9.9% water/0.1 % TFA). The RumC1 peptide was eluted from the column with a linear gradient from 23.5% to 24.5% B at a flow rate of 10 mL/min. Its purity was checked by analytical reversed-phase HPLC (Phenomenex Jupiter column, 250 mm × 4.6 mm, 15 µm, 300 Å) and it was greater than 98%. The peptide was characterized by Electrospray Ionization-Mass spectrometry (ESI-MS) in positive mode using

an online nano-LC−MS/MS (NCS HPLC, Dionex, and Qexactive HF, Thermo Fisher Scientific).

Site directed mutagenesis of mRumC1

Site directed mutagenesis of the *MBP-RumC1* construct was performed following instructions from the Q5 Site-Directed Mutagenesis Kit (New England BioLabs®). The NEBaseChanger tool was used to generate primer sequences (fig. S1B) and annealing temperatures for each Cys to Ala single mutant. Template plasmids were digested using *Dpn*I and were transformed into competent Top10 cells. The mutant plasmids were recovered from cells by using the Wizard® Plus SV Minipreps DNA Purification System (Promega).

Cysteine Alkylation

Ammonium bicarbonate was added to a solution of MBP-mRumC1 (or MBP-mRumC1 mutants) at a concentration of 100 mM. Dithiothreitol was added to this solution at a concentration of 5 mM and subsequently incubated at 55 °C for 35 min. Iodoacetamide was added at a final concentration of 14 mM to alkylate free cysteine and the solution was further incubated at room temperature for 30 min in the dark. To quench unreacted iodoacetamide, dithiothreitol was added to this solution at a concentration of 5 mM and incubating at room temperature for 15 min in the dark. The solution was collected and analysed by LC-MS.

Isotopic labeling of mRumC1

A synthetic plasmid containing the *E. coli* codon-optimized gene of *R. gnavus* E1 encoding RumMc1 (pET-15b-*rumMc1*, ampicillin-resistant) was obtained from Genscript. Plasmids pET-15b-*rumMc1*, pETM-40-*rumC1* and psuf (chloramphenicol-resistant) containing *sufABCDSE* genes were used to transform competent *E. coli* BL21 (DE3) cells. The resulting strain was grown in 3 L of M9 medium containing kan (50 μg/mL), amp (100 μg/mL), chl (34 μg/mL), vitamin B1 (0.5 μg/mL), $MgSO_4$ (1 mM), $FeCl_3$ (50 μM) and glucose (4 mg/mL) at 37 °C. At an optical density (OD_{600}) of 0.25, cells were harvested by centrifugation (4,000 rpm for 20 min at 4°C). The cells were resuspended in 1 L of labeled minimal medium (Na_2HPO_4 6 g/L, KH_2PO_4 3 g/L, $^{15}NH_4Cl$ 1 g/L) containing kan (50 μg/mL), amp (100 μg/mL), chl (34 μg/mL), vitamin B1 (0.5 μg/mL), $MgSO_4$ (1 mM), $FeCl_3$ (50 μM) and labeled glucose-^{13}C (4 mg/mL). The culture was grown at 25°C to an optical density (OD_{600}) of 0.8. $FeCl_3$ (100 μM) and L-cysteine (300 μM) were then added and the culture was induced with 1 mM IPTG. The cells were grown for 15h under stirring and then were harvested by centrifugation (4,000 rpm for 20 min at 4°C). Labeled mRumC1 was purified as described for the unlabeled sample.

NMR of RumC1

NMR experiments were conducted at 27°C, by using a ^{15}N, ^{13}C-labeled RumC1 sample of 0.2 mM in 10 mM phosphate buffer, pH 6.8, in H2O. NMR data were acquired using a Bruker Avance III 600 MHz spectrometer equipped with a cryogenically cooled triple resonance ($^{1}H/^{15}N/^{13}C$) 5 mm probe. The following datasets were performed; 2D: [^{15}N,^{1}H] HSQC and [^{13}C,^{1}H] HSQC; 3D: [^{1}H,^{15}N,^{13}C] HNCACB, CBCA(CO)NH, HNCA, HN(CO)CA, HNCO, HN(CA)CO, ^{15}N-NOESY-HSQC (mixing time of 150 ms) and ^{13}C-TOCSY-HSQC (spin lock of 80 ms).

Lipid insertion assay

Lipid insertion was measured using reconstituted lipid monolayer at the air-water interface as previously described (*54, 58*). Total lipids were extracted from 3 mL of an overnight culture of *C. perfringens* ATCC 13124 as previously described (*58*). Extracted total lipids were dried, resolubilized in chloroform:methanol (2:1, v:v) and store at -20 °C under nitrogen. For lipid insertion assay, total lipid extract was spread using a 50 µL Hamilton's syringe at the surface of 700 µL of sterile PBS creating a lipid monolayer at the air-water interface. Lipids were added until the surface pressure reached approximatively 30 mN/m, this surface pressure corresponding to a lipid packing density theoretically equivalent to that of the outer leaflet of the cell membrane (*54*). Lipid insertion of tested molecules was evaluated by injecting them directly into the 700 µL sub-phase of PBS under the lipid monolayer (pH 7.4, volume 800 µL) using a 10 µL Hamilton syringe. Tested molecules were: i) the detergent Cetyl trimethylammonium bromide (CTAB) (at a final concentration of 100 µM), ii) the pore-forming antimicrobial peptide Nisin (at a final concentration of 7.8 µM, corresponding to 10-times its MIC) and iii) RumC1 (at a final concentration of 15.6 µM, corresponding to 10-times its MIC). The variation of the surface pressure caused by the insertion of the molecules into the lipid monolayer was then continuously monitored using a fully automated microtensiometer (µTROUGH SX, Kibron Inc., Helsinki, Finland) until reaching equilibrium.

5.3 Summary and comments

The first objective of my thesis project (see Chapter 4) was to isolate the 5 isoforms of RumC. The purification protocol, from cecal contents of rats mono-associated with *R. gnavus* E1, that I developed successfully yielded the 5 isoforms of RumC free of contaminants. Previously, Crost and co-workers obtained only 3 isoforms (RumC1, C4 and C5) on the first attempt to isolate RumC from cecal contents (Crost et al., 2011). Therefore, a doubt remained on whether RumC2 and C3 were produced as well in vivo. Here, we showed that they are indeed synthesized by *R. gnavus* E1 in mono-colonized rats. The previous purification protocol included 3 chromatography steps (Crost et al., 2011), although I tried to reduce these steps to 2 by varying their order and the columns employed for each step, eventually I still had to use ion exchange, size exclusion and reverse-phase chromatography to isolate the RumC isoforms. However, compared to the protocol designed by Crost and co-workers I inverted the size exclusion and ion exchange steps (**Figure 5.1**). The size exclusion steps in the Crost's protocol aimed at isolating the active molecules in their size range. Since the approximate molecular weights of the isoforms were known when I started this new protocol, molecules that were not peptides (i.e. > 10 kDa) were excluded by filtration on a membrane. The chromatography size exclusion step was then later performed with a column specific for peptides to refine the purification. Therefore, instead of reducing the number of chromatography steps to optimize the protocol developed by Crost and co-workers, I used the same steps but with phases more appropriate to peptides and I added at the beginning of the purification protocol a filtration step to select only peptides before the chromatographies.

The trickiest part of the development of this protocol was to find an appropriate way for desalting the purified fractions along the chromatography steps. Indeed, the ion exchange and size exclusion chromatography steps both employed salt-containing buffers for elution. After fraction collection, I had to concentrate them using a Speed Vac rotator before assessing their anti-*C. perfringens* activity in order to determinate which one contained the active isoforms. If salts were not extracted from the purification fractions, after concentration, I obtained false positives as the high salts concentrations were sufficient to inhibit the growth of *C. perfringens*. I tried to physically separate the salts from the liquid fractions as they would precipitate during Speed Vac rotator concentration. This technique was efficient after the 1st step of chromatography but after the 2nd step no activity could be found in any fractions with this desalting technique. This was probably due to a co-precipitation of salts with peptides eventually leading to loss of activity. Then, I tried desalting with a centrifugal unit with a cut-off of 2 kDa and dialysis with a membrane cut-off of 1 kDa. Desalting with these two techniques was successful on the fractions obtained before the chromatography steps but again no anti-*C. perfringens* activity could be found from the fractions resulting from the different chromatographies. At that time I already had some active RumC1 produced by heterologous expression by LCBM. The anti-*C. perfringens* activity was lost when RumC1 was subjected to dialysis or centrifugation with the 2 kDa membrane, which meant that RumC1 was able to cross these membranes. Thus, we hypothesized that the isoforms had a very compact tridimensional structure since their molecular weight above 4 kDa should prevent them from crossing a 1 kDa or 2 kDa cut-off membrane. These membranes probably retained most of the isoforms in the early fraction from the in vivo purification protocol as they might aggregate with other molecules. Accordingly during the size exclusion step, we noticed later that the active fraction was eluted with a retention time corresponding to smaller peptides. However,

we did not get concrete proof of that hypothesis until later and the full resolution of the structure of RumC1 by NMR which will be presented in the next chapter. Surprisingly, Crost and co-workers used membranes with a 5 kDa cut-off to concentrate or desalt their purified fractions (Crost et al., 2011). In the first steps they might have retained the RumC isoforms thanks to aggregation, however it is still unclear how they were able to isolate some isoforms at the end of the purification protocol. As it became clear that I wouldn't be able to separate the isoforms and the salts based on their size I decided to try solid phase extraction using a C-18 reverse-phase. After loading the samples on the solid reverse-phase, salts were eluted with water whereas all the molecules able to perform hydrophobic interactions were eluted after with acetonitrile. Samples were then lyophilized to evaporate the acetonitrile which also abolished the need for concentration steps. This technique successfully desalted the purified fraction and permitted the identification of the active fraction after the ion exchange and size exclusion chromatographies.

After purification of the isoforms, C18-LC/MS and MS/MS analyses were performed by Sylvie Kieffer-Jaquinod from the EdyP plateform of CEA to determine their PTMs. Based on the results of alkylation assays, Crost and co-workers suggested that 2 Cys of RumC were linked by a disulfide bond and that the 2 others stayed free (Crost et al., 2011). These observations remain mysteries for our team, as no alkylation of any Cys was observed even under reductive condition, thus suggesting that the 4 Cys were engaged in mono-sulfide bonds. The same observations were made on RumC1 produced by heterologous expression by the LCBM. Moreover MS/MS analyses showed that the 5 isoforms all harbor 4 sacti-bridges. Strikingly, the amino acid acceptor of the sacti-bridges are located at the same positions on the 5 isoforms. These studies confirmed the affiliation of the 5 RumC isoforms in the sactipeptide subclass. Moreover, these analyses established that the heterologous expression system designed by the LCBM and in particular by Steve Chiumento was successful to yield a mature RumC1 carrying the same PTMs as the peptide produced by *R. gnavus* E1 in a mammalian host. Additionally, the heterologous expression system allowed the production of mutants of RumC1 consisting in the replacement of each Cys involved in the sacti-bridges by Ala and therefore allowed the determination by MS/MS of the Cys partners and thus the bridges position (i.e. Cys3-Asn16; Cys5-Ala12; Cys22-Lys42; Cys26-Arg34). Three of these bridges and the associated partners were confirmed by NMR. The bridges positions induce a double hairpin shaped structure whereas all known sactipeptides harbor a single hairpin structure. Therefore thanks to these mutational studies, we were able to claim that at least RumC1 belongs to a new subclass of sactipeptides. The resolution of the PTMs introduced in the RumC isoforms as well as the identification of the double hairpin structure partially answer the 2nd objective of my thesis which concerns the structure and maturation of RumC, although full completion of this objective will be presented in the next chapter.

Initially we had planed to assess the biological activities of RumC using the rat cecal contents and the novel purification protocol. However, as the amount of RumC resulting from the in vivo production is very limited and as the LCBM developed a biosynthetic production of RumC1 providing us with consequent amounts of mature peptide, we decided to focus the biological activity study on RumC1. First, I had to achieve the full maturation of RumC1 by removing the leader peptide from the mature precursor. Sybille Tachon, a post-doctoral fellow involved in the Rumba project, produced RumPc, the peptidase found in the RumC regulon, in *E. coli*. I used the purified protein to cleave the mature RumC1 precursor. Surprisingly, these studies showed that 5 amino acid residues of the leader peptide are left after the cleavage with RumPc. These 5 amino acids are then

removed by trypsin which was known to be essential for RumC production (Ramare et al., 1993). Therefore, both RumPc and mammalian trypsin are required to fully remove the leader peptide of RumC1, revealing a beautiful demonstration of mutualism between host and symbiont. Previously, trypsin was thought to be an inducer of the RumC regulon as it is for the RumA regulon, as its inhibition would result in a loss of anti-*C. perfringens* activity in the fecal samples of *R. gnavus* E1 mono-associated rats (see Chapter 3) (Ramare et al., 1993; Gomez et al., 2002; Pujol et al., 2011). In the case of RumC1, we showed that trypsin cleaves the precursor in an active form free of the leader peptide. Therefore, the absence of trypsin production or its inhibition in vivo would result in the production of partially mature and inactive peptides undetectable with the type of anti-*C. perfringens* assays used by Ramare and co-workers in 1993. Trypsin might be an inducer of the two-component regulation system of the RumC regulon but could also act only on the maturation of RumC.

Then, after purifying RumC1 fully mature and free of leader peptide, I quantified its antibacterial activity. Crost and co-workers evaluated the MIC of RumC5 and the mixture of RumC1 and RumC4 against *C. perfringens* at 40 µg/mL (Crost et al., 2011). I determined a MIC in the micromolar range for RumC1 against *C. perfringens* (around 7 µg/mL), the difference in MIC might arise from optimized purification and quantification. Indeed in the previous study, the authors explained that the absorbance at 280 nm of the fractions containing RumC5 and the mixture of RumC1 and RumC4 were too low to calculate concentrations and therefore they used an estimated concentration determined after Edman's degradation. Here, we had enough biosynthetic RumC1 to be able to quantify the solution's concentration with the classical protein dosage method based on absorbance at 280 nm. I also performed the screening of bacterial targets of RumC1 and showed that it was active against a broad spectrum of Gram positive bacteria but not against Gram negative bacteria. Therefore, I partially completed the 3rd objective of my project, although we decided to take further steps to characterize the biological activities of RumC1 which will be presented in the next 3 chapters. I also initiated studies of the mode of action of RumC1, which was not originally planed in my thesis project objectives. These studies revealed that RumC1 does not have a pore-forming action unlike many antimicrobial peptides and seems to have an intracellular target which inhibition affects the synthesis of nucleic acids. More information on the mode of actions of RumC1 will be provided in chapters 6 and 8. Finally, I worked with Hamza Olleik and Marc Maresca from ISM2, on the evaluation of the safety of RumC1. We showed that RumC1 is not only active against pathogens including resistant strains but seems also safe as a therapeutic agent for human health.

During the editing process of our article, another paper was also published on the heterologous expression of RumC1 (Balty et al., 2019). However this paper does not cover the purification of the RumC isoforms produced directly by *R. gnavus* E1. Although they used an expression system different from the one developed by the LCBM, they also obtained maturation of RumC1 consisting in 4 sacti-bridges when co-expressed with RumMc1 in *E. coli*. They also obtained low amounts of maturated RumC2 when co-expressed with RumMc2 and, like our team, came to the conclusion that RumC2 and RumC1 harbor sacti-bridges involving the conserved Cys and residues located at the same positions. Mutagenesis of the Cys of RumC2 also led them to the conclusion that RumC2 has a double hairpin structure. Therefore, not only RumC1 but also RumC2 belong to the new subclass of sactipeptides, which suggests that the other isoforms probably belong to this subclass too and have a similar double hairpin structure. Balty and co-workers also initiated a char-

acterization of the biological activity of RumC1. They used trypsin to remove the leader peptide of RumC1 with the rational that this type of proteolytic process is "likely to occur in the digestive tract where RumC exerts its physiological activity". However, they did not consider that the RumPc peptidase encoded in the RumC regulon in *R. gnavus* E1 might be responsible for the leader peptide removal. Although the conclusions from our consortium and Balty and co-workers were rather similar on the heterologous expression and maturation of RumC, our data on biological activity are divergent. In Balty's work, the activity against *C. perfringens* was not quantified and only two MICs have been provided with higher concentrations than ours by a factor of 6 and 15, for *E. faecalis* and *B. subtilis*, respectively. The authors wrote that the MICs might be overestimated because of contamination of RumC1 by traces of the maturation enzyme. It is unclear why MIC determination were not performed with purified fraction. Moreover they detected no inhibition of *S. aureus* with RumC1 at 70 µM whereas we showed growth inhibition at 25 µM and even inhibition of MRSA at 50 µM. Finally the authors suggest that RumC1 could shape the human microbiota by targeting Gram positive and negative bacteria. However they only show the induction of a lag phase in the growth of *E. coli* with a concentration of RumC1 of 70 µM, a concentration that is unlikely to happen in the human microbiota. They suggest an activity towards Gram negative bacteria when the activity of RumC1 was monitored only on one strain of one specie of Gram negative bacteria. In our study we assayed the ability of RumC1 to inhibit the growth of 8 strains belonging to 5 species of Gram negative bacteria and found no growth inhibition of all these strains with concentrations up to 100 µM. Finally, another discrepancy of our consortium with the work published by Balty *et al.* concerns the stereochemistry of the sacti-bridges but this part will be discussed in the next chapter.

Chapter 6

The unusual structure of Ruminococcin C1 antimicrobial peptide confers clinical properties

6.1 Context

In the previous publication, our team showed that RumC1 could be produced by heterologous expression in *E. coli* with the same PTMs as RumC1 produced by *R. gnavus* E1 in a mammalian host, consisting in four sacti-bridges. Moreover, we demonstrated that unlike the 5 previously characterized sactipeptides, RumC1 has an original double-hairpin structure. In the next study, we decided to take a step further and elucidate the three-dimensional structure of RumC1 by NMR. As sactipeptides can harbor intramolecular thioether linkages with D- or L-strereochemistry (see subsection 2.2.4 Sactipeptides) we also planed to investigate the stereochemistry of the sacti-bridges in RumC1. For these structural studies, a ^{13}C-and ^{15}N-labelled mature RumC1 was produced by heterologous expression at the LCBM and in particular by Steve Chiumento. Then, as I developed the protocol for leader peptide removal, I performed the cleavage and last purification step of this mature and labelled RumC1 before 3D-NMR analyses which were done at IMM by Olivier Bornet and Matthieu Nouailler. In addition, the [4Fe-4S] clusters of the RumMc1 sactisynthase were further characterized by EPR and Mössbauer spectroscopies. Moreover, the role and necessity of the leader peptide in the maturation process were also investigated. These tasks were performed at LCBM with the help of the EdyP platform.

Regarding the biological activities of RumC1, we showed in the previous study that RumC1 is active against Gram positive bacteria on collection strains and could be used as an alternative to antibiotics. We followed our investigations in a preclinical context to further explore this potential and hopefully bear out the clinical application of RumC1. First, we assayed the potency of RumC1 against Gram positive clinical pathogens. The MICs were determined by Katy Jeannot with the clinical isolates collected at the University Hospital of Besançon. Similarly, after showing that RumC1 is safe for human cell lines, we decided to investigate its effects on human tissues coming from clinical biopsies. That part of the project was realized with Marc Maresca and Cendrine Nicoletti on samples collected from patients treated at Laveran Hospital in Marseille. Finally, I double-checked the primary function of RumC1 as an antibiotic by investigating its ability to kill bacteria in a mammalian context, i.e. in the presence of an epithelium. Another line of research investigated in the following study concerns the stability of RumC1. Indeed, the poor stability

of bacteriocins and RiPPs is currently one of the major obstacles regarding their use in a clinical context. Therefore I measured its stability to thermal, chemical and proteolytic treatments to determine if RumC1 could be subjected to manufacturing processes and tolerate the physiological conditions encountered in typical drug administration routes.

Originally we had planned to expose the antibacterial mode of action of RumC1 in a third publication, that would also cover its efficacy in an animal model and its potential other biological roles. However, during the revision process of the following paper, we decided to include some information about the mode of action of RumC1 that would further demonstrate the interest for RumC1 in a clinical context. The studies on the mode of action of RumC1 presented in this publication were done at ISM2 and at the Laboratory of Microbiology and Molecular Genetics (LMGM) at University Paul Sabatier in Toulouse. These studies were realized by Hamza Olleik, Marc Maresca, Mickael Lafond and myself.

6.2 Accepted paper

The following publication has been accepted in P.N.A.S. on June 2020, 22nd.

The unusual structure of Ruminococcin C1 antimicrobial peptide confers clinical properties

Clarisse Roblin[1,2†], Steve Chiumento[3†], Olivier Bornet[4*], Matthieu Nouailler[5], Christina S. Müller[6], Katy Jeannot[7,8], Christian Basset[3], Sylvie Kieffer-Jaquinod[9], Yohann Couté[9], Stéphane Torelli[3], Laurent Le Pape[3], Volker Schünemann[6], Hamza Olleik[1], Bruno De La Villeon[10], Philippe Sockeel[10], Eric Di Pasquale[11], Cendrine Nicoletti[1], Nicolas Vidal[12], Leonora Poljak[13], Olga Iranzo[1], Thierry Giardina[1], Michel Fons[14], Estelle Devillard[2], Patrice Polard[13], Marc Maresca[1], Josette Perrier[1], Mohamed Atta[3], Françoise Guerlesquin[5], Mickael Lafond[1*], Victor Duarte[3*]

[1]Aix-Marseille Univ, CNRS, Centrale Marseille, iSm2, 13013, Marseille, France.

[2]ADISSEO France SAS, Centre d'Expertise et de Recherche en Nutrition, 03600, Commentry, France.

[3]Univ. Grenoble Alpes, CEA, IRIG, CBM, CNRS UMR5249, 38054, Grenoble, France.

[4]NMR platform, Institut de Microbiologie de la Méditerranée, CNRS, Aix-Marseille Université, 13009, Marseille, France.

[5]Laboratoire d'Ingénierie des Systèmes Macromoléculaires, UMR7255, Institut de Microbiologie de la Méditerranée, CNRS, Aix-Marseille Université, 13009, Marseille, France.

[6]Fachbreich Physik, Technische Universität Kaiserslautern, Erwin-Schrödinger-Str. 56, 67663, Kaiserslautern, Germany.

[7]Centre National de Référence de la Résistance aux Antibiotiques, Laboratoire de Bactériologie, Centre Hospitalier Universitaire de Besançon, 25030, Besançon, France.

[8]UMR 6249 Chrono-Environnement, UFR Santé, Université de Bourgogne-Franche-Comté, 25030, Besançon, France.

[9]Univ. Grenoble Alpes, CEA, Inserm, IRIG, BGE, 38054, Grenoble, France.

[10]Departement of Digestive, Endocrine and Metabolic Surgery, Hôpital Laveran, Military Health Service, 13013 Marseille, France.

[11]Aix Marseille Univ, Faculté de Médecine, Institut de NeuroPhysioPathologie, 13397 Marseille, France.

[12]Yelen Analytics, 10 bd tempête, 13820 Ensues la Redonne, France.

[13]Laboratoire de Microbiologie et de Génétique Moléculaires, Centre de Biologie Intégrative, Université de Toulouse, CNRS, UPS, Toulouse, France.

[14]Laboratoire de Bioénergétique et Ingénierie des protéines, UMR 7281, Institut de Microbiologie de la Méditerranée, CNRS, Aix-Marseille Université, 13009, Marseille, France.

* Correspondence to: bornet@imm.cnrs.fr; mickael.lafond@univ-amu.fr; victor.duarte@cea.fr

† The following authors contributed equally to this work: Clarisse Roblin & Steve Chiumento

Radical SAM enzyme, RiPP, sactipeptide, *Ruminococcus gnavus*, antibiotic

The emergence of superbugs developing resistance to antibiotics and the resurgence of microbial infections have led scientists to start an antimicrobial arms race. In this context, we have previously identified an active RiPP, the Ruminococcin C1, naturally produced by *Ruminococcus gnavus* E1, a symbiont of the healthy human intestinal microbiota. This RiPP, subclassified as a sactipeptide, requires the host digestive system to become active against pathogenic Clostridia and multidrug resistant strains. Here, we report its unique compact structure on the basis of four intramolecular thioether bridges with reversed stereochemistry introduced post-translationally by a specific radical-SAM sactisynthase. This structure confers to the Ruminococcin C1 important clinical properties including stability to digestive conditions and physicochemical treatments, a higher affinity for bacteria than simulated intestinal epithelium, a valuable activity at therapeutic doses on a range of clinical pathogens, mediated by energy resources disruption and finally safety for human gut tissues.

Significance

Since the discovery of penicillin, humans have widely developed and used antibiotics to protect themselves from microbial infections. However, the intensive use of these compounds has led to the emergence of pathogens resistant to all classes of antibiotics. This major public health threat has led scientists to find new molecules with different structures and modes of action to overcome resistance phenomena. A promising alternative concerns bacteriocins secreted by certain bacteria. Of a peptidic nature, their ribosomal synthesis differentiates them from conventional antibiotics. The recently identified RumC1 antimicrobial peptide presents a remarkable bactericidal activity for multi-drug resistant strains. Added to this efficacy, RumC1 is not toxic against a number of human cell lines and is safe for human gut tissues.

INTRODUCTION

Ribosomally synthesized and Post-translationally modified Peptides (RiPPs) are an important group of compounds that have stimulated research interest, notably as natural antimicrobial agents with bacteriocins (1). During RiPPs biogenesis, a precursor peptide composed of at least a leader and a core sequence is synthesized by the ribosome. The core peptide is modified by tailoring enzymes and then the leader sequence is cleaved by one or two peptidases to produce the final active product (1–4). Among the RiPPs, sactipeptides (Sulfur-to-alpha carbon thioether cross-linked peptides) are a subgroup that has emerged in recent years (5–7). Despite spectacular soaring made with genomic tools, the sactipeptide subclass is currently limited to only seven members. They include subtilosin A (SboA) (8, 9), thurincin H (10), the sporulation killing factor (SkfA) (11), thuricin CD that consists of two peptides, Trn-α and Trn-β (12), thuricin Z or huazacin (13, 14) and the recently characterized Ruminococcin C1 (RumC1) (15, 16).

The precise mechanistic details of sactipeptide cross-link formation are not fully understood. However, from a chemical point of view, the thioether bonds in these natural products are distinct from those of the well-studied lanthipeptides, such as nisin, in which they are formed between a Cys residue and a β-carbon of a dehydrated Thr/Ser residue (17). In contrast to the two-step redox neutral mechanism used for the maturation of lanthipeptides, radical-SAM sactisynthase enzymes introduce chemically equivalent thioether bonds by a one-step radical-based mechanism (5–7). The enzymes within this superfamily contain the canonical $CysX_3CysX_2Cys$ motif, that binds the radical-SAM $[4Fe\text{-}4S]^{2+/1+}$ cluster (referred to as the RS cluster), in which the fourth, unique iron, is used to bind S-adenosylmethionine (SAM) cofactor (18). In its reduced state, the $[4Fe\text{-}4S]^{1+}$ cluster catalyzes the reductive cleavage of SAM to generate a 5′-deoxyadenosyl radical (5'-Ado•). This radical abstracts a H- atom from the cognate substrate to initiate catalysis (18). In the case of the characterized radical-SAM enzymes involved in the sactipeptide biosynthesis, H-atom abstraction was shown to occur from the α-carbon of the acceptor residue (5–7). A survey of available structural and functional data indicate that all radical-SAM enzymes involved in the sactipeptides biosynthesis contain a C-terminal extension appended to the radical-SAM domain called SPASM/Twitch domain that houses additional [4Fe-4S] clusters (19, 20). In contrast to the Twitch domains, which bind only one additional cluster, SPASM domains present a conserved cysteine-rich motif that coordinates two additional iron-sulfur clusters. The role of these clusters

remains to be clarified, but it was suggested that they possibly interact with the substrate during catalysis or may also be implicated in electrons transfer (5–7, 21).

Among the seven sactipeptides reported to date, four are structurally characterized (SboA, thurincin H, Trn-α and Trn-β) and all of them have been purified from the genus *Bacillus*. SboA is a cyclic peptide with three thioether bridges involving two phenylalanines and one threonine. Trn-α, Trn-β and thurincin H are not cyclic, they present three and four thioether bridges, respectively. One common feature of SboA, Trn-α, Trn-β and thurincin H is that they all present Cys residues in the N-terminal half and the corresponding partners at the C-terminal part, a property that folds the peptide in a single hairpin-shaped form with the hydrophobic residues facing outwards as showed by the available structures (8–10, 12, 22). Sequence analysis of the last identified sactipeptide, namely RumC1, suggests a new fold. Indeed, one pair of cysteines is located at the N-terminal part of the sequence while the other one is in the C-terminal end (Fig. 1A). Recent data on the characterization of mature RumC1 by mass spectrometry, strongly suggests that the thioether network folds the peptide in a double hairpin like structure that differs from the currently reported ones (16). Furthermore, sactipeptides and by extension antimicrobial peptides (including RiPPs but not only) have emerged as a potential trove of new weapons and alternatives to conventional antibiotics to fight multidrug-resistant (MDR) bacteria. However, their clinical use remains a challenge due to high cost of production, sensitivity to physiological or manufacturing conditions, as well as toxicity for human tissues (23, 24). In this context, we previously showed that RumC1 has a potent activity against Gram positive bacteria and is harmless for human cells (16). Obviously, the next step was to study RumC1 in a clinical context and to address the above-mentioned reasons that prevent antimicrobial peptides from being considered for pharmaceutical development.

In this work, we sought to determine the three-dimensional structure of RumC1. The rapid and large-scale production of ^{13}C- and ^{15}N-labelled mature RumC1, by heterologous expression in *Escherichia coli* (16, 25), allowed extensive nuclear magnetic resonance (NMR) analyses to solve the structure of RumC1 and to propose the thioether network stereochemistry. In the meantime, combined EPR and Mössbauer spectroscopies enabled us to characterize the Fe-S clusters in RumMc1 sactisynthase. Finally, we point out that the fold of RumC1 confers resistance to physical, chemical and digestive constraints, features essential for consideration in pharmaceuticals. The clinical properties of RumC1 also covers activity against clinical pathogens, including resistant

strains, maintained in a mammalian environment and mediated through energy resources depletion, without any impact to human tissues.

Results

RumC1 sactipeptide displays a double hairpin-like structure. The two-dimensional [^{1}H, ^{15}N] HSQC spectrum of RumC1 is well-resolved with 39 peptide amide peaks out of 42 expected, thus attesting for the folding of the protein (fig. S1). No NH peaks were observed for residues C26, G27 and N28, probably due to fast amide exchange with the solvent and/or high flexibility of the region. We assigned the backbone carbon, nitrogen and proton resonances using a combined strategy of sequential residue correlations based on HNCACB, CBCA(CO)NH, HNCA, HN(CO)CA, HNCO, HN(CA)CO triple resonance experiments, and through-space nOe connectivities using 2D [^{1}H, ^{1}H] NOESY, 3D [^{1}H, ^{15}N, ^{1}H] and 3D [^{1}H, ^{13}C, ^{1}H] NOESY experiments. NMR studies of Subtilosin A, Thuricin CD and Thurincin H, by Vederas *et. al.* have shown that cysteine sulfur to α-carbon thioether linkages induce a 10 to 15 ppm downfield shift for the α-carbon atoms of bridged residues (8–10, 12, 22). Moreover, through-space nOe interactions were observed between the β-protons of cysteines and the amide proton (NH) of modified residues (8–10, 12, 22). In the same manner, we have demonstrated that RumC1 contains four sulfur to α-carbon thioether cross-links between Cys3 and Asn16, Cys5 and Ala12, Cys22 and Lys42, and Cys26 and Arg34 (16). Since there are four thioether bridges, each can adopt one of the two possible configurations at the α-carbon atom (L or D). Consequently, 16 stereoisomers must be considered to establish the three-dimensional structure of RumC1. Calculations for all 16 stereoisomers were carried out using the CYANA software and seven rounds performed on each stereoisomer using the same NMR restraints file (26). The structural statistics and constraint violations (table S1) allowed to identify the stereoisomer with the D stereochemistry at Ala12 (α-S), Asn16 (α-S), Arg34 (α-S) and Lys42 (α-S) as a representative structure given: i) the absence of thioether bridge constraint violations, ii) the great number of nOe connectivities used in the structure calculation, iii) the lowest average target function value and a low root mean square deviation (*rmsd*). To improve the structure of the DDDD stereoisomer, an additional refinement step by returning to the NOESY spectra to eliminate the ambiguities found during the structure calculation by the CYANA software was added. The resulting structural statistics of the 20 conformers for the DDDD isomer of RumC1 are summarized in table S2. The backbones of the 20 lowest target function value conformers for the DDDD isomer

of RumC1 superimpose quite well with a *rmsd* value of 0.81 Å for the backbone (Fig. 1B). The three-dimensional structure of RumC1 is thus composed on both sides by two α-helices and in the middle by a 2-stranded parallel β-sheet fragment and the whole stiffened by four cysteine sulfur to α-carbon thioether cross-links (Fig. 1C).

The electrostatic surface potentials present an overall positive charge (Fig. 1D) and the surface hydrophobicity of the DDDD stereoisomer shows a majority of hydrophilic residues (Fig. 1E). The compact three-dimensional solution structure of RumC1 reveals a new sactipeptide fold and by extension a new antimicrobial peptide fold (fig. S2A). Four sulfur to α-carbon thioether bridges with a DDDD stereochemistry have been already reported for thurincin H (10). However, the presence of an additional 2-stranded parallel β-sheet fragment in the middle of RumC1 induces a new fold, thus resulting in a different location of the thioether crosslinks (fig. S2, B-E) (9, 10, 22).

Expression, purification and characterization of the RumMc1 sactisynthase. RumMc1 is predicted to contain accessory Fe-S clusters, in addition to the RS cluster, thus we decided to co-express the *rumMc1* gene with the pDB1282 plasmid, which encodes for a set of proteins involved in iron-sulfur cluster biogenesis (IscS, IscU, IscA, HscB, HscA and Fdx) (27). After the final step of anaerobic purification, the purity was evaluated by SDS-PAGE to be over 95% (fig. S3). As expected, the holo-RumMc1 protein was dark brown in color and the iron titration revealed, on average, ten metal centers per monomer. In good agreement, the UV-vis spectrum of holo-RumMc1 suggests the presence of [4Fe-4S] clusters (Fig. 2A, solid line). Mössbauer spectroscopy on ^{57}Fe-enriched oxidized holo-RumMc1was then used to deeply investigate the nature of the Fe-S clusters. The experimental spectrum recorded at T = 77 K (dashed line) could be simulated (red line) with three components **1**, **2** and **3** in a 2:1:1 ratio (Fig. 2B). **1** and **2** are characterized by similar isomer shifts (δ) with $\delta = 0.42$ mms^{-1} for **1** and $\delta = 0.44$ mms^{-1} for **2** while the quadrupole splitting (ΔE_q) varies with $\Delta E_q = 0.98$ mms^{-1} for **1** and $\Delta E_q = 1.30$ mms^{-1} for **2**. These values are in a typical range for $Fe^{2,5+}$ ions in a diamagnetic $[4Fe\text{-}4S]^{2+}$ cluster (28–30). This is supported by simulations of the spectra recorded at T = 4.2 K in external fields of B = 0.1 T and B = 5 T (fig. S4, A and B) based on the spin Hamilton formalism assuming a total spin of S = 0. The 2:1 ratio suggests that holo-RumMc1 contains three $[4Fe\text{-}4S]^{2+}$ clusters. This is supported by the sequence alignment of RumMc1 with other related proteins that contain conserved cysteine residues localized at the C-terminal half of the protein (fig. S5). Hence, we can conclude that **1** represents 8 $Fe^{2,5+}$ ions in the

same tetrahedral sulfur environment belonging to two $[4Fe\text{-}4S]^{2+}$ clusters while **2** corresponds to four indistinguishable $Fe^{2,5+}$ ions present in the single $[4Fe\text{-}4S]^{2+}$ cluster supposed to contain the SAM-binding iron site (RS-cluster). The difference in ΔE_q between **1** and **2** points to a slightly different distribution of electron density. **3** is characterized by $\delta = 0.33$ mms^{-1} and $\Delta E_q = 0.49$ mms^{-1} typical for Fe^{3+} high spin (S = 5/2) in a tetrahedral sulfur environment (28). This component was adequately simulated (fig. S4A, with an external magnetic field) by combining contributions from three distinct, but antiferromagnetically coupled Fe^{3+} centers, thus resulting in a global S = 1/2 spin state as described for a paramagnetic $[3Fe\text{-}4S]^{1+}$ cluster (31, 32). The respective hyperfine parameters are characteristic for $[3Fe\text{-}4S]^{1+}$ clusters (fig. S4B) (31, 32). Upon addition of dithionite on the holo-RumMc1, the absorption decreased over the entire 310-420 nm range as expected for the conversion of the S = 0 $[4Fe\text{-}4S]^{2+}$ chromophore to the S = 1/2 $[4Fe\text{-}4S]^{1+}$ level (Fig. 2A, dashed line). This reduced form has been investigated by X-band EPR spectroscopy in order to gain insights into the individual features of the three [4Fe-4S] clusters involved. The experimental EPR spectrum of holo-RumMc1 is extremely rich, suggesting the presence of multiple S = 1/2 $[4Fe\text{-}4S]^{1+}$ clusters (fig. 2C, black line). It was satisfactorily simulated considering the three following sets of g-tensors [2.034, 1.913, 1.870] (**A**), [2.050, 1.937, 1.902] (**B**) and [2.074, 1.932, 1.885] (**C**) (Fig. 2, C and E). Addition of the natural SAM cofactor then induced a substantial change in the spectrum that was well simulated with four sets of g-tensors [2.034, 1.910, 1.860] (**A**), [2.049, 1.937, 1.904] (**B**), [2.073, 1.932, 1.885] (**C**) and [2.076, 1.930, 1.852] (**A'**) instead of three (Fig. 2, D and E). As the contribution of **A** has to be lowered to achieve a reliable simulation, these experiments support that **A** originates from the RS cluster while **B** and **C** rely to two additional clusters. The new component **A'** was assigned to the amount of the RS cluster, which is bond to the SAM as previously described (33).

Efficient maturation of RumC1: both the leader and the core sequences are crucial. Here we sought to gain insights into the features of RumC1 that are required for its efficient maturation by RumMc1. It is established that the post-translational modification of RiPPs is an event that is dependent on the presence of the leader peptide (2). For example, in the case of the sactipeptide subclass, Marahiel and co-workers have shown that AlbA failed to transform a variant of the SboA peptide without its leader sequence in a mature sactipeptide (34). We investigated the maturation of RumC1 by the way of an *in vitro* assay in the presence of RumMc1, the SAM cofactor and

dithionite as an external electron source. These experiments were performed with a full-length RumC1 precursor peptide, a leader less variant of 44 amino acids (RumC1-44) and a third condition in which the leader sequence and the core peptide were dissociated but both present in the solution (RumC1-44-LS). The reaction mixtures were analyzed by LC-MS to detect the formation of thioether bonds within the three substrates (fig. S6). Since the full maturation of RumC1 leads to the formation of four thioether bonds, the percentages of maturation (fig. S6A) account for the species that present a loss of 8 Da in mass compared to the unmodified substrate. The data clearly indicate that only the RumC1 peptide is fully modified, both RumC1-44 and RumC1-44-LS led to less than one and ten percent of species with four thioether linkages, respectively (fig. S6, A and B). It has to be noted that attempts to yield mature peptides form the latter two substrates lead mainly to a mixture of peptides harboring partial maturation with 2 and 3 thioether bonds (fig. S6, C and D). In good agreement with the lack of maturation of RumC1-44 during the *in vitro* enzymatic assay, we also observed that no mature peptide is obtained when this leader less form of RumC1 is produced *in vivo* using the heterologous expression and maturation protocol in *E. coli* (fig. S7A).

In contrast to the sactipeptides identified so far, the thioether connectivity in RumC1 folds the peptide in a double hairpin like structure. Sequence alignments of the five RumC isoforms shows a strictly conserved Gly18/Pro19 motif in the loop region between the two hairpins (16). We therefore sought to determine whether this motif is necessary for inducing a turn in the sequence and allowing the peptide maturation by RumMc1. For this, we replaced the Gly18/Pro19 motif by Ala18/Ala19. LC-MS analysis of the heterologously expressed Ala18/Ala19 RumC1 variant clearly demonstrate the lack of maturation thus suggesting that the loop alteration in RumC1 may disturb substrate-enzyme interactions that are crucial for the formation of the thioether network (fig. S7B). As reported by Grove and coworkers for CteA (21), these results suggest that the binding of RumC1 by RumMc1 involves determinants from both the leader and the core sequences.

The compact structure confers a high stability to RumC1. Studies have proven the potent activity of sactipeptides (12, 35), however there is a lack of evidence showing that they possess the physiochemical properties necessary for *in vivo* administration and, from an applied point of view, for pharmaceutical development (35). Consequently, we assayed the tolerance of RumC1 to such

properties. RumC1 showed no loss of activity when exposed to acidic or basic pH from 2 to 11 (Fig. 3A). Furthermore, RumC1 was resistant to 70 and 100°C for up to 1 hour and more than 15 minutes respectively, meaning that RumC1 possesses the intrinsic thermal resistance that are required for drug formulation processes (Fig. 3B). Because of their sensitivities to enzymatic digestion or to physiological salts concentrations and blood enzymes, the administration of antimicrobial peptides by oral route and/or systemic injection is limited. Interestingly, the activity of RumC1 wasn't impaired by salts concentrations higher than 150 mM for NaCl and 2 mM for $MgCl_2$ (Fig. 3C), which are considered as physiological saline conditions. Likewise, incubation in human serum at 37°C up to 24 hours did not affect the activity of RumC1 (Fig. 3D). RumC1 was finally treated with pepsin at pH 2.5 for 2 hours at 37°C, and with pancreatin at pH 6.5 for 5 hours at 37°C in order to mimic the human gastric and intestinal compartments, respectively. RumC1 showed no loss of activity and its integrity was revealed by MS analysis after these treatments whereas the lanthipeptide nisin used as a positive control for pancreatin activity showed reduced antimicrobial potency (Fig. 3E, fig. S8, A and B). Pepsin activity was confirmed as well by hydrolysis of Bovine Serum Albumine (BSA) (fig. S8A). Therefore, the thioether network leading to a compact structure of RumC1 confers to the sactipeptide high resistance to physico-chemical treatments and to the physiological but harsh conditions encountered in blood or in the digestive tract after systemic or oral administration.

RumC1 is able to act on a simulated infected intestinal epithelium. Many studies on antimicrobial peptides show their direct activity on bacterial cultures, without considering their efficiency in a mammalian environment, such as an infected epithelium. Indeed, antimicrobial peptides can act on bacteria but can also insert into eukaryotic cells or merely bind to their surface (24, 36), which could cause a partial loss of activity against extracellular pathogens. On the contrary, some peptides have higher affinity for bacterial cells than host cells (37). Therefore, we assayed the potency of RumC1 against *Bacillus cereus*, an aerotolerant human intestinal opportunistic pathogen, on simulated gut epitheliums using Caco2 and T84 cells as models of human small intestinal and colonic epithelium, respectively. *B. cereus* was able to grow on untreated monolayers of Caco2 and T84 whereas treatment with RumC1 was effective to clear the infection (fig. S9). The MIC of RumC1 against *B. cereus* was measured in the eukaryotic cell line culture medium in the presence or the absence of human intestinal cells. The MIC value did not

increase in the presence of intestinal cells when RumC1 was added 30 min before, concomitantly or 30 min after the bacterial cells (Fig. 4A). Indeed, no loss of activity was detected as well when *B. cereus* was allowed to colonize the epithelium for 30 min before adding RumC1 (Fig. 4A). Therefore, it appears that RumC1 has a preferential affinity for bacterial cells rather than host cells. Finally, these results suggest that the physiological environment of the two cell lines did not affect significantly the activity of RumC1.

RumC1 displays a potent activity against Gram-positive pathogenic clinical isolates. We previously showed that RumC1 is active against a broad range of Gram-positive bacteria including resistant and multi-resistant strains (16), but focusing only on collection strains. In order to evaluate the potentiality of RumC1 being considered for pharmaceutical development, we investigated its activity against Gram-positive strains isolated in a clinical context from humans or animals (i.e. broiler chickens). As RumC1 was first identified for its anti- *Clostridium perfringens* activity (16, 38, 39), we measured for the first time the MIC of the sactipeptide against a large panel of *C. perfringens* clinical isolates (Fig. 4B). RumC1 was active under the micromolar range (between 0.4 and 0.8 µM) on all the ten strains tested. In comparison with the reference molecules, usually used to eradicate *C. perfringens*, RumC1 showed a higher activity than metronidazole (12 to 23 µM) and an activity similar to vancomycin (0.2 to 0.4 µM). Interestingly, in a livestock context, RumC1 was not only active against the CP24 *C. perfringens* strain isolated from a healthy broiler chicken, but also against strains isolated from animals suffering from dysbiosis or necrotic enteritis, respectively CP56 and CP60 (40). In addition, RumC was also active against *C. perfringens* strains isolated from humans suffering from bacteremia (*n=6*) (Fig. 4B).

Then, we studied the effect of RumC1 on another main intestinal pathogen from the *Clostridium* genus, *Clostridium difficile*. RumC1 showed activity against collection and clinical strains of *C. difficile* with lower MIC (0.3 to 0.6 µM) than two of the most common antibiotics used for *C. difficile* intestinal infections (CDI), i.e. metronidazole (1.5 µM) and vancomycin (0.3 to 0.7 µM) (Fig. 4B). Moreover, RumC1 is also efficient at the micromolar range against other intestinal pathogens (clinical and collection strains) of main importance such as *Listeria monocytogenes*, *B. cereus*, *Enterococcus faecalis* and *Enterococcus faecium* including strains resistant to amoxicillin and/or vancomycin (Fig. 4B). Beside its activity against pathogens causing gut infections, RumC1 is also active against a clinical *Streptococcus pneumoniae* strain at a low

MIC (0.3 µM), a pathogen responsible of multiple types of infection (including respiratory tract infection, meningitis and septicemia) (Fig. 4B).

The killing mechanism of RumC1 involves energy resource shortage. Unlike many bacteriocins RumC1 does not have a pore forming action (16), we therefore investigated its effects on the main macromolecules synthesis pathways usually targeted by antibiotics. *C. perfringens* cells were exposed to RumC1 and the synthesis of DNA, RNA, proteins and peptidoglycan were followed by measuring the incorporation of radio-labelled precursors. Remarkably, RumC1 was able to inhibit the synthesis pathways of the four macromolecules with efficacies similar to conventional antibiotics targeting each of these pathways (Fig. 5A). As these synthesis pathways are all energy-dependent, we assayed the potency of RumC1 to break such energy resources. Thus, we measured by bioluminescent assay the ATP released by *C. perfringens* cells in the extracellular medium, and then lysed cells to derive the intracellular ATP content (Fig 5B). Upon treatment with RumC1 for 15 min, outer ATP was not increased compared to cells untreated whereas inner ATP decreased in a dose-dependent manner. Treatment with nisin, a pore-forming bacteriocin led to drastic increase of outer ATP whereas metronidazole does not impact ATP synthesis pathway. Since the synthesis of DNA, RNA, proteins and peptidoglycan accounts for the consumption of approximately 70 % of the total ATP content of bacteria, their observed inhibition is likely linked to ATP depletion and therefore the specificity of RumC1 could be related to an inhibition of the ATP synthesis pathway (41).

Integrity of human tissues treated with RumC1. We previously reported that RumC1 was a safe new antimicrobial peptide because of its lack of *in vitro* toxicity on gastric and intestinal cell lines culture (16). To further characterize the safety of RumC1, we assayed the toxicity of the sactipeptide *ex vivo*, directly on human ileocecal tissues. Intestinal explants were isolated from unaffected area of ileocecal resection from two patients diagnosed with intestinal carcinoma and were incubated with RumC1 at 100 µM or the detergent CTAB at 300 µM for 4 hours. Control and RumC1 exposed human intestinal explants displayed normal tissue organization with normal crypt and villosity lengths and no sign of epithelial desquamation or erosion, in accordance with data we obtained previously *in vitro* on human intestinal cell lines. Conversely, exposure to CTAB, used

as positive control of tissue damages, caused important lesions to the human intestinal epithelium with cell desquamation and shortening of the crypts and villosities (Fig. 6).

Discussion

In this study, we elucidated the three-dimensional structure of mature Ruminococcin C1 from *Ruminococcus gnavus* E1. NMR experiments clearly showed that the thioether network of RumC1, involving four sulfur to α-carbon bridges, folds the peptide into a double hairpin-like motif, which differs from the currently reported structures within the sactipeptide family. By extension, the fold not described so far includes two-stranded parallel β-sheet into the core enclosed between two parallel α-helixes. In contrast to a recent report by Berteau *et al.*, where the residues involved in the thioether bridges were identified to be L-configurated, after hydrolysis and derivatization (15), here we found that the stereoisomers that fits best with the NMR data featured D-configurations at Ala12, Asn16, Arg34 and Lys42. RumC1 has a global positive charge at physiological pH and displays a constrained and rigid backbone structure that presents a mostly hydrophilic surface unlike sactipeptides with known structure presenting mostly hydrophobic surface. These sactipeptides, like most of the bacteriocins that target Gram-positive strains, have a pore-forming mode of action. Despite an overall cationic charge, RumC1 is unable to insert into lipids extracts most likely due to its hydrophilic surface and exerts probably an intracellular mode of action reaching one or more specific targets by active transport.

The double hairpin-like structure of RumC1 provides stability to pH and high-temperatures, which could facilitate pharmaceutical manufacturing processes. We also showed that RumC1 is resistant to digestive proteolytic conditions, most likely because the sites of cleavage are protected by the four thioether bonds and the tridimensional folding of the peptide. Many RiPPs including sactipeptides, such as Subtilosin A and Thuricin CD, are not resistant to both pepsin and pancreatic proteases (42, 43), implying that the original folding of RumC1 offers additional protection. Moreover, RumC1 is also resistant to physiological salts conditions as well as to human serum, which can both be detrimental for an exogenous compound. Based on these considerations, we followed our investigations of RumC1 in a preclinical context. The first step was to ensure that RumC1 could cure infections in the mammalian environment. Therefore, we treated with RumC1 a *B. cereus* infected simulated epitheliums. RumC1 remained active at very low doses, exactly at the same level as the MIC obtained in the absence of eukaryotic cells. This observation confirms

the stronger affinity of RumC1 for bacterial versus host cells, and the specific primary function of RumC1 as antibiotic compound. Then we checked that RumC1 has potent activity on Gram-positive clinical pathogens and not only on collections strains. RumC1 showed strong activity under the micromolar range toward *Clostridia* pathogens from both human and animal origins. The measured MICs are equivalent to vancomycin, one of the reference antibiotics used in therapy against these pathogens, and lower than metronidazole, another reference antibiotic known to generate resistance (16). Therefore, the use of RumC1 to treat infections caused by *C. perfringens* or *C. difficile* should be considered. Indeed, from a livestock point of view, *C. perfringens* can cause necrotic enteritis, which is one of the most common infection in broiler chickens with mortality rates as high as 50% and resulting in dehydration, lesions on intestinal mucosa or other organs like the liver, spleen, heart or kidneys (44). On the other hand, *C. difficile* is a major human pathogen causing nosocomial infections, community-associated diarrhea and is responsible of 250,000 intestinal infections per year in the US, associated with a mortality rate of 15 to 20%. In 2019, *C. difficile* has been classified by the Centre for Diseases Control and Prevention as an urgent threat for which new antimicrobials are needed (45, 46). In the same line, RumC1 is active against amoxicillin and vancomycin resistant *E. faecium*, registered on all priority lists of human pathogens for which new antimicrobials are urgently needed. It is registered by the CDC as a serious concern that requires prompt action and by the WHO on the "antibiotic-resistant priority pathogens" as high concern. *E. faecium* is also pointed by the Infectious Diseases Society of America (IDSA) across the "ESKAPE pathogens" list of bacteria, which includes *Enterococcus faecium, Staphylococcus aureus, Klebsiella pneumoniae, Acinetobacter baumannii, Pseudomonas aeruginosa* and *Enterobacter* spp., (47) for its ability to escape the effects of the commonly used antibiotics through evolutionarily developed mechanisms of resistance (48). *E. faecium*, characterized by drug resistance mechanisms, commonly causes life-threatening nosocomial infections amongst critically ill and immunocompromised individuals. Consequently, it is important to note that RumC1 is particularly active against this pathogen with a MIC of 1,2 µM, thus it could be considered as a potential therapeutic solution. In the case of *S. pneumoniae*, with a prevalence of 1.2 million of infections per year in the US, leading to its inclusion into the CDC and the WHO lists of priority pathogens, the use of RumC1 with a MIC of 300 nM may also be relevant. It should be noted that RumC1 is a broad-spectrum anti-Gram-positive molecule directed against resistant anaerobic and aerobic clinical pathogens, which is rare in the antibiotics market with a few exceptions such as

vancomycin, thus enhancing its clinical potential. Moreover, we showed that RumC1 inhibits the synthesis of macromolecules including DNA, RNA, proteins or peptidoglycan and the production of ATP. At this stage, since the main biosynthetic pathways are inhibited, it is conceivable that RumC1 applies its antimicrobial activity intracellularly through a non-specific mechanism, or conversely, targeting specifically ATP synthases and thus disrupting all necessary energy resources, such as bedaquiline, the only antibiotic currently on the market targeting ATP synthases but used only for the treatment of infections caused by Mycobacterium (49). Otherwise, we have previously identified that the phenotype induced by RumC1 treatment resembles the one induced by metronidazole in *C. perfringens* (16). However, we have shown here that metronidazole only inhibits DNA synthesis and, to a lesser extent, protein synthesis. Metronidazole is known to impact DNA synthesis and repair systems, and most likely inhibits the activity of the strictly ATP-dependent ribonucleotide reductase by modulating the redox state of cells, but its precise mechanism remains elusive (50). Here we suggest that the phenotypic similarities induced by RumC1 and metronidazole might arise from a DNA synthesis inhibition and possibly other common events, although they certainly do not share the same mechanism. Therefore, further in-depth investigations are needed to resolve the potentially unique intracellular mode of action of RumC1. Finally, we followed our preclinical studies by assessing the safety of RumC1 on gut tissues directly sourced from patients. RumC1 did not induce epithelial lesions at a dose about a hundred times higher than the effective antimicrobial dose. This observation could be expected as humans have been exposed to RumC1 through evolution as this peptide is produced by a symbiotic bacterium present in the gut microbiota of healthy adults. Overall, RumC1 encompass properties essential for a drug candidate to cure intestinal infections, especially since i) it can be administrated by oral route, ii) it is active in the intestinal epithelium environment, iii) RumC1 shows activity at therapeutic doses against clinical intestinal resistant pathogens, and finally iv) since it is safe for gut tissues. Only few AMPs meet all the conditions that are necessary for reaching the marketing step, i.e. respecting the conditions of stability, presenting activity under physiological conditions (including in the presence of eukaryotic cells), owning antimicrobial effect against clinical pathogens at very low doses including resistant or MDR, and finally retaining safety for human cells and tissues. It is interesting to note that RumC1 fulfils all these conditions, except one remaining bottleneck for the industrial scale use, which concerns the cost of production. RumC-

like synthetic molecule development could be addressed to solve this concern and highlight the great potential of this original sactipeptide.

Materials and Methods

Detailed descriptions of materials and methods, including expression, purification of (^{13}C, ^{15}N)-labelled mature RumC1, NMR studies, structure calculations, EPR and Mössbauer analyses of RumMc1, stability assays of RumC1 and MIC determinations are given in *SI Appendix*.

Supporting Information

Supplementary figures Fig. S1 to Fig. S9 as well as Tables S1 and S2 are provided in *SI Appendix*.

Data Availability

All data needed to evaluate the conclusions in the paper are present in the paper and the *SI Appendix*. All of the peak lists and the complete ^{1}H, ^{13}C and ^{15}N backbone and side chain chemical shift assignments of RumC1 have been deposited into the Biological Magnetic Resonance Databank (http://www.bmrb.wisc.edu) under ascension code 50027. Coordinates of the twenty conformations of DDDD stereoisomer of RumC1 have been deposited into the PDB under ascension code 6T33.

ACKNOWLEDGMENTS. We would like to thank Pr. Richard Ducatelle and Pr. Filip Van Immerseel from UGent for providing us with clinical isolates of *C. perfringens* from broiler chickens. We would also like to thank Pr. Lhousseine Touqui for scientific advising. Finally, we would like to thank the people from the AVB platform (iSm2 CNRS UMR 7313, Marseille). This study was supported by grants from the French National Agency for Research ("Agence Nationale de la Recherche") through the "Projet de Recherche Collaboratif" (*RUMBA project,* ANR-15-CE21-0020), the "Investissement d'Avenir Infrastructures Nationales en Biologie et Santé" programme (*ProFI project*, ANR-10-INBS-08) and partial financial support from the Labex ARCANE and CBH-EUR-GS (ANR-17-EURE-0003). We are grateful to Adisseo France company and the Association Nationale Recherche Technologie (ANRT) for funding the doctoral fellowship of C.R. entitled "Bacteriocins RumC, a novel antimicrobial peptide family as alternative to conventional antibiotics." This grant numbered *Convention Industrielle de Formation par la*

RecherchE (CIFRE) no. 2016/0657 runs from 1 March 2017 to 1 March 2020. VS and CSM. acknowledge the support of the German Science Foundation (DFG) within SPP 1927 (SCHU 1251/17-1, 2).

Author contributions: CR, SC, KJ and CB performed the *in vitro* assays for RumC1, RumMc1 and were involved in interpreting the data and writing the manuscript; OB and MN performed the RumC1 structural analysis by RMN; CSM and VS performed the Mössbauer analyses on RumMc1 and wrote the corresponding parts; ST and LLP performed the EPR analysis on RumMc1; SKJ and YC performed nanoLC-MS/MS characterizations; BDLV, PS, EDP, MM and CN performed the chirurgical biopsy, the human explant treatment, the cytotoxicity assays and the microscopy analysis; HO, NV and LP were involved in biosynthetic pathways and ATP assays; OI performed the peptide chemical synthesis; TG, MF and ED were involved in study design; PP, JP, MA, FG, ML and VD conceptualized the study, designed experiments, interpreted the data and wrote the manuscript.

Competing interests: The authors declare that they have no competing interests.

References

1. P. G. Arnison, *et al.*, Ribosomally synthesized and post-translationally modified peptide natural products: overview and recommendations for a universal nomenclature. *Nat. Prod. Rep.* **30**, 108–160 (2013).

2. T. J. Oman, W. A. van der Donk, Follow the leader: the use of leader peptides to guide natural product biosynthesis. *Nat. Chem. Biol.* **6**, 9–18 (2010).

3. G. A. Hudson, D. A. Mitchell, RiPP antibiotics: biosynthesis and engineering potential. *Curr. Opin. Microbiol.* **45**, 61–69 (2018).

4. J. R. Chekan, C. Ongpipattanakul, S. K. Nair, Steric complementarity directs sequence promiscuous leader binding in RiPP biosynthesis. *Proc. Natl. Acad. Sci.* **116**, 24049–24055 (2019).

5. N. Mahanta, G. A. Hudson, D. A. Mitchell, Radical S-Adenosylmethionine Enzymes Involved in RiPP Biosynthesis. *Biochemistry* **56**, 5229–5244 (2017).

6. A. Benjdia, C. Balty, O. Berteau, Radical SAM Enzymes in the Biosynthesis of Ribosomally Synthesized and Post-translationally Modified Peptides (RiPPs). *Front. Chem.* **5**, 87 (2017).

7. L. Flühe, M. A. Marahiel, Radical S-adenosylmethionine enzyme catalyzed thioether bond formation in sactipeptide biosynthesis. *Curr. Opin. Chem. Biol.* **17**, 605–612 (2013).

8. K. Kawulka, *et al.*, Structure of Subtilosin A, an Antimicrobial Peptide from *Bacillus subtilis* with Unusual Posttranslational Modifications Linking Cysteine Sulfurs to α-Carbons of Phenylalanine and Threonine. *J. Am. Chem. Soc.* **125**, 4726–4727 (2003).

9. K. E. Kawulka, *et al.*, Structure of subtilosin A, a cyclic antimicrobial peptide from *Bacillus subtilis* with unusual sulfur to alpha-carbon cross-links: formation and reduction of alpha-thio-alpha-amino acid derivatives. *Biochemistry* **43**, 3385–3395 (2004).

10. C. S. Sit, M. J. van Belkum, R. T. McKay, R. W. Worobo, J. C. Vederas, The 3D Solution Structure of Thurincin H, a Bacteriocin with Four Sulfur to α-Carbon Crosslinks. *Angew. Chem. Int. Ed.* **50**, 8718–8721 (2011).

11. W.-T. Liu, *et al.*, Imaging mass spectrometry of intraspecies metabolic exchange revealed the cannibalistic factors of *Bacillus subtilis*. *Proc. Natl. Acad. Sci.* **107**, 16286–16290 (2010).

12. M. C. Rea, *et al.*, Thuricin CD, a posttranslationally modified bacteriocin with a narrow spectrum of activity against *Clostridium difficile*. *Proc. Natl. Acad. Sci. U. S. A.* **107**, 9352–9357 (2010).

13. T. Mo, *et al.*, Thuricin Z: A Narrow-Spectrum Sactibiotic that Targets the Cell Membrane. *Angew. Chem. Int. Ed Engl.* **58**, 18793–18797 (2019).

14. G. A. Hudson, *et al.*, Bioinformatic Mapping of Radical S-Adenosylmethionine-Dependent Ribosomally Synthesized and Post-Translationally Modified Peptides Identifies New Cα, Cβ, and Cγ-Linked Thioether-Containing Peptides. *J. Am. Chem. Soc.* **141**, 8228–8238 (2019).

15. C. Balty, *et al.*, Ruminococcin C, an anti-clostridial sactipeptide produced by a prominent member of the human microbiota *Ruminococcus gnavus*. *J. Biol. Chem.* **294**, 14512–14525 (2019).

16. S. Chiumento, *et al.*, Ruminococcin C, a promising antibiotic produced by a human gut symbiont. *Sci. Adv.* **5**, eaaw9969 (2019).

17. P. J. Knerr, W. A. van der Donk, Discovery, biosynthesis, and engineering of lantipeptides. *Annu. Rev. Biochem.* **81**, 479–505 (2012).

18. J. B. Broderick, B. R. Duffus, K. S. Duschene, E. M. Shepard, Radical S-Adenosylmethionine Enzymes. *Chem. Rev.* **114**, 4229–4317 (2014).

19. T. A. J. Grell, P. J. Goldman, C. L. Drennan, SPASM and Twitch Domains in *S* -Adenosylmethionine (SAM) Radical Enzymes. *J. Biol. Chem.* **290**, 3964–3971 (2015).

20. J. A. Latham, I. Barr, J. P. Klinman, At the confluence of ribosomally synthesized peptide modification and radical S-adenosylmethionine (SAM) enzymology. *J. Biol. Chem.* **292**, 16397–16405 (2017).

21. T. L. Grove, *et al.*, Structural Insights into Thioether Bond Formation in the Biosynthesis of Sactipeptides. *J. Am. Chem. Soc.* **139**, 11734–11744 (2017).

22. C. S. Sit, R. T. McKay, C. Hill, R. P. Ross, J. C. Vederas, The 3D structure of thuricin CD, a two-component bacteriocin with cysteine sulfur to α-carbon cross-links. *J. Am. Chem. Soc.* **133**, 7680–7683 (2011).

23. M. Mahlapuu, J. Håkansson, L. Ringstad, C. Björn, Antimicrobial Peptides: An Emerging Category of Therapeutic Agents. *Front. Cell. Infect. Microbiol.* **6** (2016).

24. W. Aoki, M. Ueda, Characterization of Antimicrobial Peptides toward the Development of Novel Antibiotics. *Pharm. Basel Switz.* **6**, 1055–1081 (2013).

25. P. M. Himes, S. E. Allen, S. Hwang, A. A. Bowers, Production of Sactipeptides in Escherichia coli: Probing the Substrate Promiscuity of Subtilosin A Biosynthesis. *ACS Chem. Biol.* **11**, 1737–1744 (2016).

26. P. Güntert, C. Mumenthaler, K. Wüthrich, Torsion angle dynamics for NMR structure calculation with the new program DYANA. *J. Mol. Biol.* **273**, 283–298 (1997).

27. R. M. Cicchillo, *et al.*, Lipoyl synthase requires two equivalents of S-adenosyl-L-methionine to synthesize one equivalent of lipoic acid. *Biochemistry* **43**, 6378–6386 (2004).

28. M.-E. Pandelia, N. D. Lanz, S. J. Booker, C. Krebs, Mössbauer spectroscopy of Fe/S proteins. *Biochim. Biophys. Acta* **1853**, 1395–1405 (2015).

29. P. Middleton, D. P. E. Dickson, C. E. Johnson, J. D. Rush, Interpretation of the Mössbauer Spectra of the Four-Iron Ferredoxin from *Bacillus stearothermophilus*. *Eur. J. Biochem.* **88**, 135–141 (1978).

30. G. Layer, *et al.*, Radical S-Adenosylmethionine Enzyme Coproporphyrinogen III Oxidase HemN. *J. Biol. Chem.* **280**, 29038–29046 (2005).

31. B. H. Huynh, *et al.*, On the active sites of the [NiFe] hydrogenase from *Desulfovibrio gigas.* Mössbauer and redox-titration studies. *J. Biol. Chem.* **262**, 795–800 (1987).

32. M. Teixeira, *et al.*, Redox intermediates of *Desulfovibrio gigas* [NiFe] hydrogenase generated under hydrogen. Mössbauer and EPR characterization of the metal centers. *J. Biol. Chem.* **264**, 16435–16450 (1989).

33. N. A. Bruender, J. Wilcoxen, R. D. Britt, V. Bandarian, Biochemical and Spectroscopic Characterization of a Radical S-Adenosyl-L-methionine Enzyme Involved in the Formation of a Peptide Thioether Cross-Link. *Biochemistry* **55**, 2122–2134 (2016).

34. L. Flühe, *et al.*, The radical SAM enzyme AlbA catalyzes thioether bond formation in subtilosin A. *Nat. Chem. Biol.* **8**, 350–357 (2012).

35. H. Mathur, M. C. Rea, P. D. Cotter, C. Hill, R. P. Ross, The sactibiotic subclass of bacteriocins: an update. *Curr. Protein Pept. Sci.* **16**, 549–558 (2015).

36. K. Takeshima, A. Chikushi, K.-K. Lee, S. Yonehara, K. Matsuzaki, Translocation of Analogues of the Antimicrobial Peptides Magainin and Buforin across Human Cell Membranes. *J. Biol. Chem.* **278**, 1310–1315 (2003).

37. M. M. Welling, A. Paulusma-Annema, H. S. Balter, E. K. J. Pauwels, P. H. Nibbering, Technetium-99m labelled antimicrobial peptides discriminate between bacterial infections and sterile inflammations. *Eur. J. Nucl. Med.* **27**, 292–301 (2000).

38. F. Ramare, *et al.*, Trypsin-dependent production of an antibacterial substance by a human Peptostreptococcus strain in gnotobiotic rats and in vitro. *Appl. Environ. Microbiol.* **59**, 2876–2883 (1993).

39. E. H. Crost, *et al.*, Ruminococcin C, a new anti-Clostridium perfringens bacteriocin produced in the gut by the commensal bacterium *Ruminococcus gnavus* E1. *Biochimie* **93**, 1487–1494 (2011).

40. A. R. Gholamiandekhordi, R. Ducatelle, M. Heyndrickx, F. Haesebrouck, F. Van Immerseel, Molecular and phenotypical characterization of *Clostridium perfringens* isolates from poultry flocks with different disease status. *Vet. Microbiol.* **113**, 143–152 (2006).

41. J. M. Stokes, A. J. Lopatkin, M. A. Lobritz, J. J. Collins, Bacterial Metabolism and Antibiotic Efficacy. *Cell Metab.* **30**, 251–259 (2019).

42. K. E. Sutyak, R. E. Wirawan, A. A. Aroutcheva, M. L. Chikindas, Isolation of the *Bacillus subtilis* antimicrobial peptide subtilosin from the dairy product-derived *Bacillus amyloliquefaciens*. *J. Appl. Microbiol.* **104**, 1067–1074 (2008).

43. M. C. Rea, *et al.*, Bioavailability of the anti-clostridial bacteriocin thuricin CD in gastrointestinal tract. *Microbiology*, **160**, 439–445 (2014).

44. F. V. Immerseel, *et al.*, *Clostridium perfringens* in poultry: an emerging threat for animal and public health. *Avian Pathol.* **33**, 537–549 (2004).

45. , Antibiotic Resistance Threats in the United States, 2019. 148 (2019).

46. W. K. Smits, D. Lyras, D. B. Lacy, M. H. Wilcox, E. J. Kuijper, *Clostridium difficile* infection. *Nat. Rev. Dis. Primer* **2**, 16020 (2016).

47. L. B. Rice, Progress and Challenges in Implementing the Research on ESKAPE Pathogens. *Infect. Control Hosp. Epidemiol.* **31**, S7–S10 (2010).

48. V. Cattoir, J.-C. Giard, Antibiotic resistance in *Enterococcus faecium* clinical isolates. *Expert Rev. Anti Infect. Ther.* **12**, 239–248 (2014).

49. K. Andries, *et al.*, A Diarylquinoline Drug Active on the ATP Synthase of *Mycobacterium tuberculosis*. *Science* **307**, 223–227 (2005).

50. S. A. Dingsdag, N. Hunter, Metronidazole: an update on metabolism, structure–cytotoxicity and resistance mechanisms. *J. Antimicrob. Chemother.* **73**, 265–279 (2018).

Figure legends

Fig. 1. Sequence and three-dimensional structure of Ruminococcin C1. (A) Sequence of RumC1 containing leader peptide (italics) and core peptide (RumC1-44), cysteine residues are underlined. **(B)** Backbone overlay of the 20 lowest target function value conformers for the DDDD stereoisomer of RumC1. **(C)** Cartoon backbone representation of the three-dimensional solution structure of RumC1 with the D stereochemistry at Ala12 (α-S), Asn16 (α-S), Arg34 (α-S) and Lys42 (α-S). Cysteine sulfur to α-carbon thioether cross-links are colored in orange and the position are indicated. **(D)** Electrostatic surface potential of RumC1, where blue indicates positive charge and red indicates negative charge. **(E)** Surface hydrophobicity of RumC1, where yellow represents hydrophobic residues and white represents hydrophilic residues.

Fig. 2. Spectroscopic characterizations of holo-RumMc1. (A) UV-vis spectrum of holo-RumMc1 in the absence (solid trace) or the presence of dithionite (dashed trace). **(B)** Mössbauer spectrum of holo-RumMc1 taken at T = 77 K with the simulation (red solid line) representing the sum of the subcomponents **1**, **2** and **3** (black lines). **1** and **2** are simulated in a ratio of 2:1 and represent two diamagnetic $[4Fe4S]^{2+}$ clusters. One $[4Fe\text{-}4S]^{2+}$ cluster is supposed to bind SAM. **3** was assigned to Fe^{3+} ions present in a $[3Fe\text{-}4S]^{1+}$ cluster in a S = 1/2 state. The respective Mössbauer parameters obtained from the simulation of the spectra at 77 K are summarized below the spectrum. **(C)** X-band CW EPR spectra of dithionite-reduced holo-RumMc1. The black line represents the experimental spectrum, while the red trace is the simulated spectrum by using three components A, B and C. **(D)** X-band CW EPR spectra of dithionite-reduced holo-RumMc1 in the presence of SAM. The black trace represents the experimental spectrum, while the red trace is the simulated spectrum by using four components A, B, C and A'. **(E)** g-values of components A, B, C and A' used to simulate the experimental EPR spectra.

Fig. 3. **Stability of RumC1. (A)** RumC1 was exposed to a range of pH for 1 hour, (**B**) to high temperatures up to 1 hour, (**C**) to human serum up to 24 hours, before measuring its MIC. (**D**) MIC of RumC1 was determined in MH medium supplemented with NaCl or $MgCl_2$. (**A to D**) All MICs were determined against *C. perfringens.* Residual antimicrobial activity was calculated based on the MIC of untreated RumC1. (**E**) Stability of RumC1 in conditions mimicking the GI tract. MIC of RumC1 against *C. perfringens* was determined after exposure to digestive enzymes. Nisin was used as a positive control of pancreatin activity. Residual antimicrobial activity was calculated

based on the MIC of untreated bacteriocins. [a] Residual antimicrobial activity were measured in this study.[b] Published by Jarvis and Mahoney, 1969.

Fig. 4. Antimicrobial activity of RumC1. (A) Activity assays of RumC1 on *Bacillus cereus* grown in eukaryotic cell culture medium in the absence or the presence of a simulated intestinal epithelium. Small and colic intestine compartments were simulated by Caco2 and T84 culture cells monolayer respectively, whereas RumC1 was added before (30 min), concomitantly and after infection (30 min) with $5x10^5$ CFU/mL *B. cereus* culture. **(B)** Activity spectrum of RumC1 against laboratory and clinical Gram-positive pathogens. Collection strains and clinical isolates are indicated. The table includes MIC of conventional antibiotics commonly used for clinical treatment and considered here as references (i.e. metronidazole, vancomycin and amoxicillin). Acquired resistance to antibiotics were determined following the EUCAST 2019 clinical breakpoint tables and are indicated by "R", whereas "i.r." refers to "intrinsic resistance", and * to the laboratory isolate references.

Fig. 5. Antibacterial mode of action of RumC1. (A, B) Cells of *C. perfringens* in early log phase were either treated with RumC1, control antibiotics, metronidazole, nisin or left untreated. Each experiment was done in independent triplicates. **(A)** After 15 min of treatment at 5xMIC, *C. perfringens* cells were incubated with radio-labelled precursors of DNA, RNA, proteins and peptidoglycan for 45 min. The synthesis of each pathway was measured by radioactivity counts. Gemifloxacin, rifampicin, tetracycline and vancomycin were used as controls antibiotics for the inhibition of DNA, RNA, proteins and peptidoglycan, respectively. Radio-labelled precursor incorporation is expressed as a percentage of maximum incorporation determined with the untreated condition. **(B)** After 15 min of treatment, the ATP present in the extracellular media (outer ATP) was measured by bioluminescence, then cells were lysed and the ATP content in the extracellular media was measured again. The inner ATP content was deduced from the difference between ATP content in the extracellular media before and after cell lysis. Cells were treated with 2.5x, 5x and 10xMIC for each condition. Relative Light Units (RLU) are expressed as percentages normalized by the value of the inner ATP content of untreated cells.

Fig. 6. **Histological analysis of human intestinal tissue treated with RumC1.** Human intestinal explants were left untreated or treated with RumC1 (100 µM) or CTAB (300 µM) for 4 h before H&E staining and microscopic observations as described in the Materials and Methods section. Images are representative of overall observed effects. Scale bar = 50 µm.

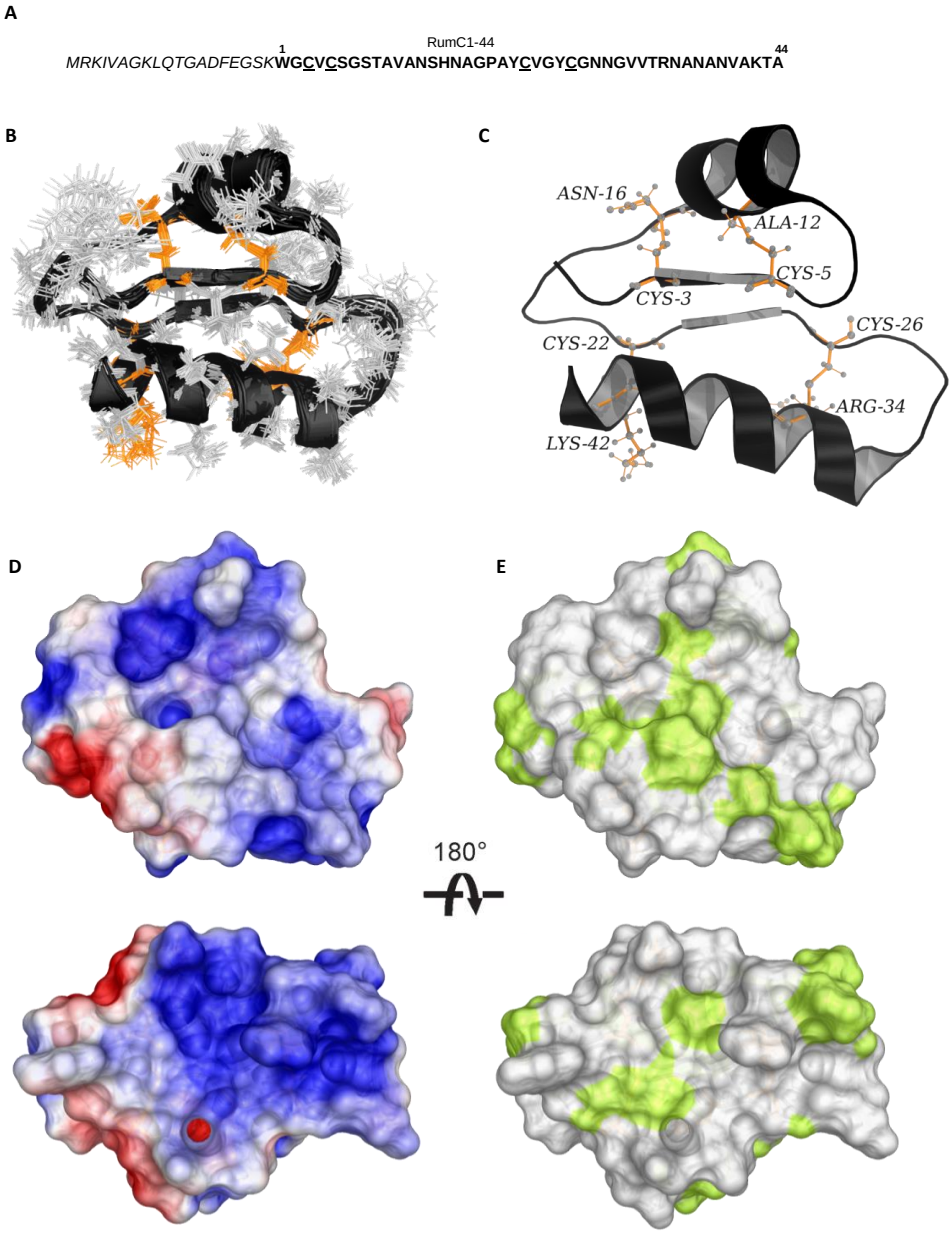

Fig. 1. Sequence and three-dimensional NMR structure of Ruminococcin C1. (A) Sequence of RumC1 containing leader peptide (italics) and core peptide (RumC1-44), cysteine residues are underlined. **(B)** Backbone overlay of the 20 lowest target function value conformers for the DDDD stereoisomer of RumC1. **(C)** Cartoon backbone representation of the three-dimensional solution structure of RumC1 with the D stereochemistry at Ala12 (α-S), Asn16 (α-S), Arg34 (α-S) and Lys42 (α-S). Cysteine sulfur to α-carbon thioether cross-links are colored in orange and the position are indicated. **(D)** Electrostatic surface potential of RumC1, where blue indicates positive charge and red indicates negative charge. **(E)** Surface hydrophobicity of RumC1, where yellow represents hydrophobic residues and white represents hydrophilic residues.

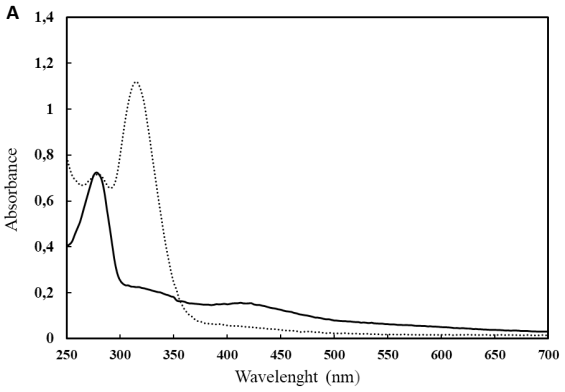

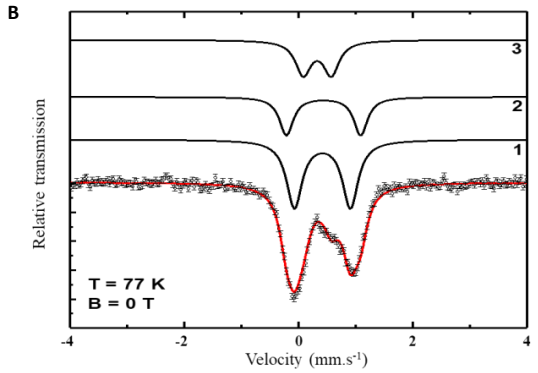

	1	2	3
δ (mms^{-1})	0.42 (± 0.01)	0.44 (± 0.01)	0.33 (± 0.02)
ΔE_q (mms^{-1})	0.98 (± 0.02)	1.30 (± 0.02)	0.49 (± 0.02)
Γ (mms^{-1})	0.33 (± 0.01)	0.29 (± 0.01)	0.33 (± 0.02)
Area (%)	50 (± 1)	25 (± 1)	25 (± 1)

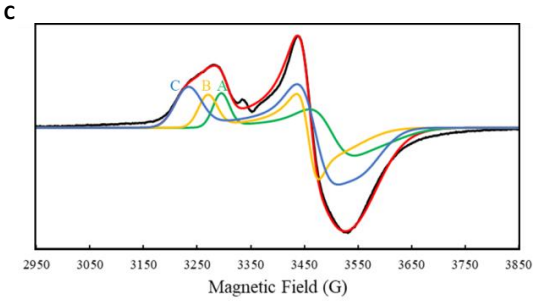

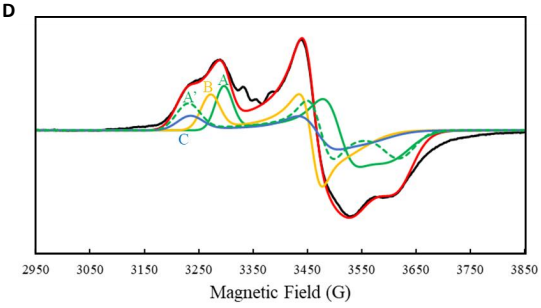

E

Proteins	SAM	A g_x g_y g_z	B g_x g_y g_z	C g_x g_y g_z	A' g_x g_y G_z
RumMc1	-	2,034(2) 1,913(2) 1,870(4)	2,050(2) 1,937(2) 1,902(4)	2,074(2) 1,932(2) 1,885(4)	
RumMc1	+	2,034(2) 1,910(2) 1,860(4)	2,049(2) 1,937(2) 1,904(4)	2,073(2) 1,932(2) 1,885(4)	2,076(2) 1,930(2) 1,852(3)

Fig. 2. Spectroscopic characterizations of holo-RumMc1. (A) UV-vis spectrum of holo-RumMc1 in the absence (solid trace) or the presence of dithionite (dashed trace). **(B)** Mössbauer spectrum of holo-RumMc1 taken at T = 77 K with the simulation (red solid line) representing the sum of the subcomponents **1**, **2** and **3** (black lines). **1** and **2** are simulated in a ratio of 2:1 and represent two diamagnetic $[4Fe4S]^{2+}$ clusters. One $[4Fe4S]^{2+}$ cluster is supposed to bind SAM. **3** was assigned to Fe^{3+} ions present in a $[3Fe4S]^{1+}$ cluster in a S = 1/2 state. The respective Mössbauer parameters obtained from the simulation of the spectra at 77 K are summarized below the spectrum. **(C)** X-band CW EPR spectra of dithionite-reduced holo-RumMc1. The black line represents the experimental spectrum, while the red trace is the simulated spectrum by using three components A, B and C. **(D)** X-band CW EPR spectra of dithionite-reduced holo-RumMc1 in the presence of SAM. The black trace represents the experimental spectrum, while the red trace is the simulated spectrum by using four components A, B, C and A'. **(E)** g-values of components A, B, C and A' used to simulate the experimental EPR spectra.

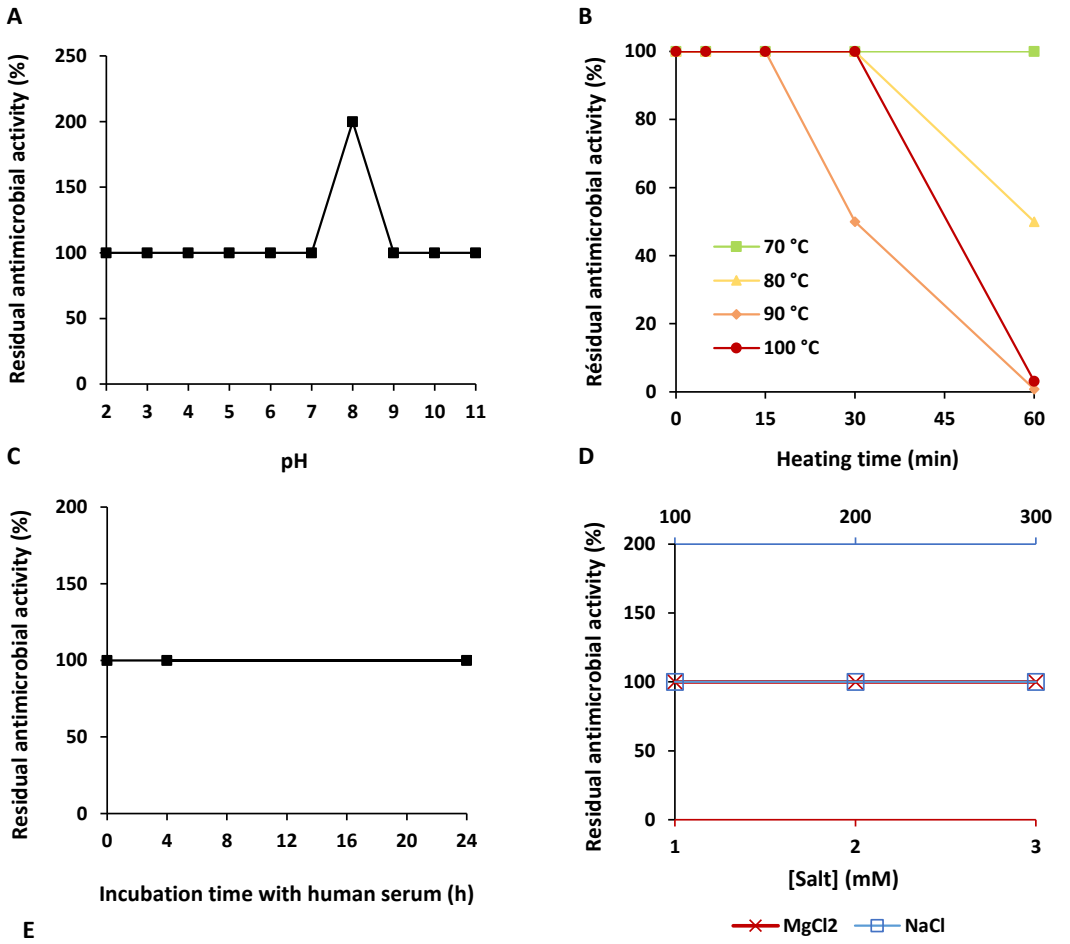

E

Simulated digestive compartment	Enzymes	pH	Temperature (°C)	Time (h)	Residual antimicrobial activity (%)	
					RumC1	Nisin
Stomac	Pepsin	2.5	37	2	100[a]	100[b]
Intestin	Pancreatin	6.5	37	5	100[a]	12.5[a]

Fig. 3. **Stability of RumC1. (A)** RumC1 was exposed to a range of pH for 1 hour, (**B**) to high temperatures up to 1 hour, (**C**) to human serum up to 24 hours, before measuring its MIC. (**D**) MIC of RumC1 was determined in MH medium supplemented with NaCl or $MgCl_2$. (**A to D**) All MICs were determined against *C. perfringens*. Residual antimicrobial activity was calculated based on the MIC of untreated RumC1. (**E**) Stability of RumC1 in conditions mimicking the GI tract. MIC of RumC1 against *C. perfringens* was determined after exposure to digestive enzymes. Nisin was used as a positive control of pancreatin activity. Residual antimicrobial activity was calculated based on the MIC of untreated bacteriocins. [a] Residual antimicrobial activity were measured in this study.[b] Published by Jarvis and Mahoney, 1969.

A

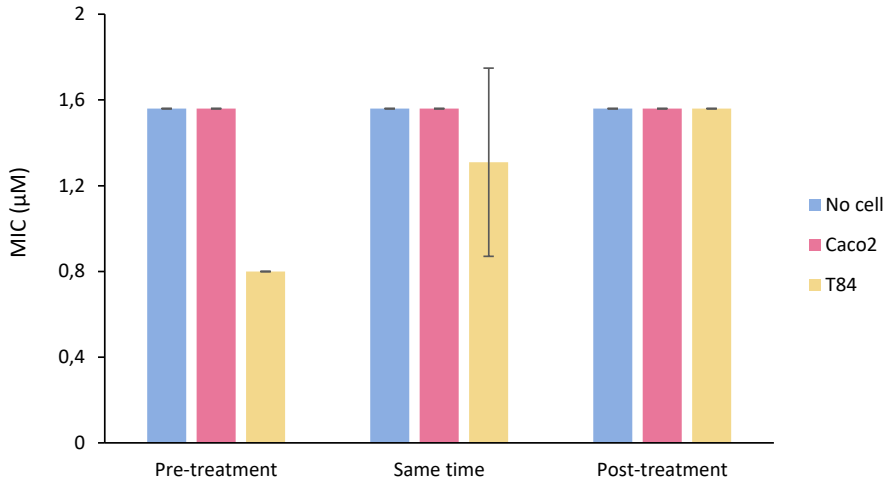

B

Organism	Source	Clinical isolate	Strain number	RumC1 MIC (µM)	Conventional antibiotics MIC (µM)		
					Metronidazole	Vancomycin	Amoxicillin
Clostridium perfringens	Laboratory	/	ATCC 13124	**0.8**	12	0.2	2.2
	Broilers	"	CP24*	**0.4**	12	0.2	2.2
	"	"	CP56*	**0.8**	12	0.2	2.2
	"	"	CP60*	**0.4**	12	0.2	2.2
	Human	Haemoculture	1*	**0.6**	23	0.4	≤ 0.3
	"	"	2*	**0.6**	23	0.4	≤ 0.3
	"	"	1600366478*	**0.6**	12	0.2	0.3
	"	"	1500022151*	**0.6**	12	0.2	0.7
	"	"	1600114439*	**0.6**	12	0.2	0.7
	"	"	1600096289*	**0.6**	12	0.2	0.7
Clostridium difficile	Laboratory	/	ATCC 700057	**0.6**	1.5	0.7	i.r.
	Human	Sacrum tissue	1600597867*	**0.3**	1.5	0.3	i.r.
Listeria monocytogenes	Human	Haemoculture	1*	**0.8**	i.r.	0.7	≤ 0.3
Bacillus cereus	Laboratory	/	CIP 5257	**1.6**	i.r.	0.7	i.r.
	Human	Haemoculture	1900276321*	**1.2**	i.r.	R	11
Streptococcus pneumoniae	Laboratory	/	ATCC 49619	**0.6**	i.r.	≤ 0.1	0.2
	Human	Haemoculture	1900304262*	**0.3**	i.r.	≤ 0.1	0.2
Enterococcus faecalis	Laboratory	/	JH2-2	**2.5**	i.r.	0.7	0.7
	Human	Haemoculture	1900302094*	**2.5**	i.r.	1.4	0.7
Enterococcus faecium	Laboratory	/	BM4147	**1.2**	i.r.	R	R
	Human	Haemoculture	1900300992*	**1.2**	i.r.	0.7	11

Fig. 4. Antimicrobial activity of RumC1. (A) Activity assays of RumC1 on *Bacillus cereus* grown in eukaryotic cell culture medium in the absence or the presence of a simulated intestinal epithelium. Small and colic intestine compartments were simulated by Caco2 and T84 culture cells monolayer respectively, whereas RumC1 was added before (30 min), concomitantly and after infection (30 min) with $5x10^5$ CFU/mL *B. cereus* culture. **(B)** Activity spectrum of RumC1 against laboratory and clinical Gram-positive pathogens. Collection strains and clinical isolates are indicated. The table includes MIC of conventional antibiotics commonly used for clinical treatment and considered here as references (i.e. metronidazole, vancomycin and amoxicillin). Acquired resistance to antibiotics were determined following the EUCAST 2019 clinical breakpoint tables and are indicated by "R", whereas "i.r." refers to "intrinsic resistance", and * to the laboratory isolate references.

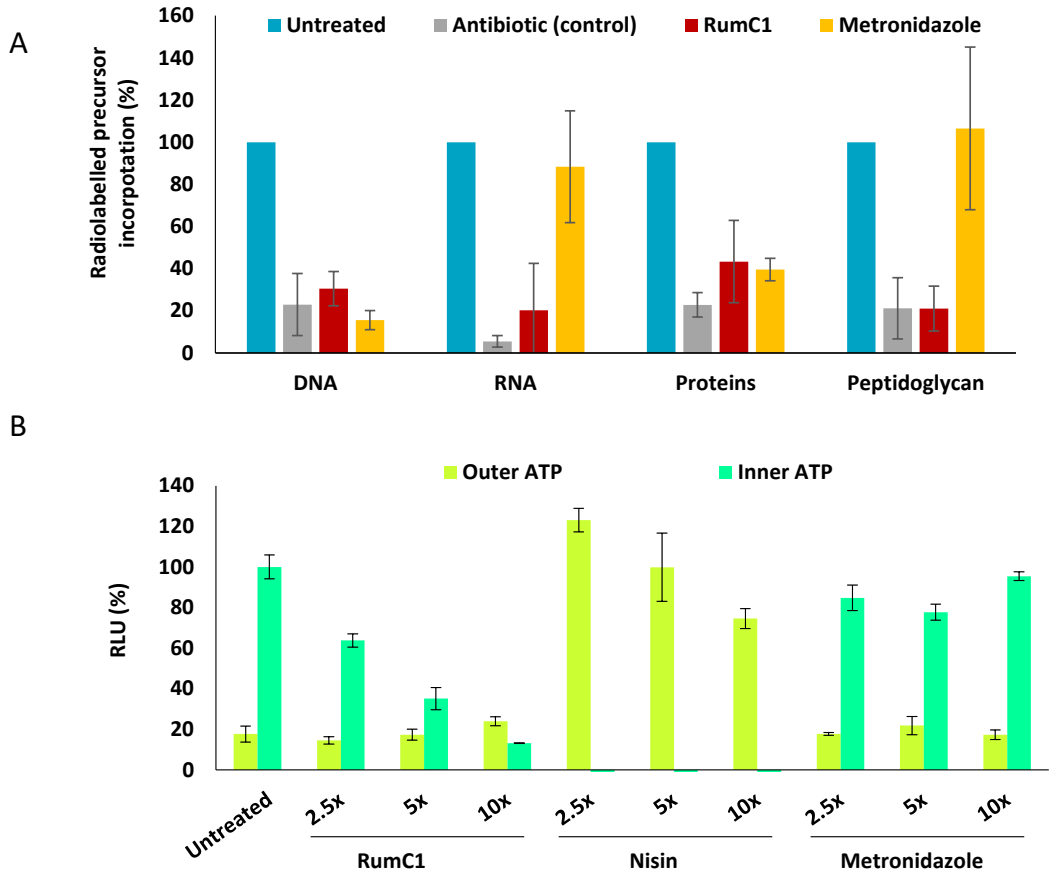

Fig. 5. Antibacterial mode of action of RumC1. (A,B) Cells of *C. perfringens* in early log phase were either treated with RumC1, control antibiotics, metronidazole, nisin or left untreated. Each experiment was done in independent triplicates. **(A)** After 15 min of treatment at 5xMIC, *C. perfringens* cells were incubated with radio-labelled precursors of DNA, RNA, proteins and peptidoglycan for 45 min. The synthesis of each pathway was measured by radioactivity counts. Gemifloxacin, rifampicin, tetracycline and vancomycin were used as controls antibiotics for the inhibition of DNA, RNA, proteins and peptidoglycan, respectively. Radio-labelled precursor incorporation is expressed as a percentage of maximum incorporation determined with the untreated condition. **(B)** After 15 min of treatment, the ATP present in the extracellular media (outer ATP) was measured by bioluminescence, then cells were lysed and the ATP content in the extracellular media was measured again. The inner ATP content was deduced from the difference between ATP content in the extracellular media before and after cell lysis. Cells were treated with 2.5x, 5x and 10xMIC for each condition. Relative Light Units (RLU) are expressed as percentages normalized by the value of the inner ATP content of untreated cells.

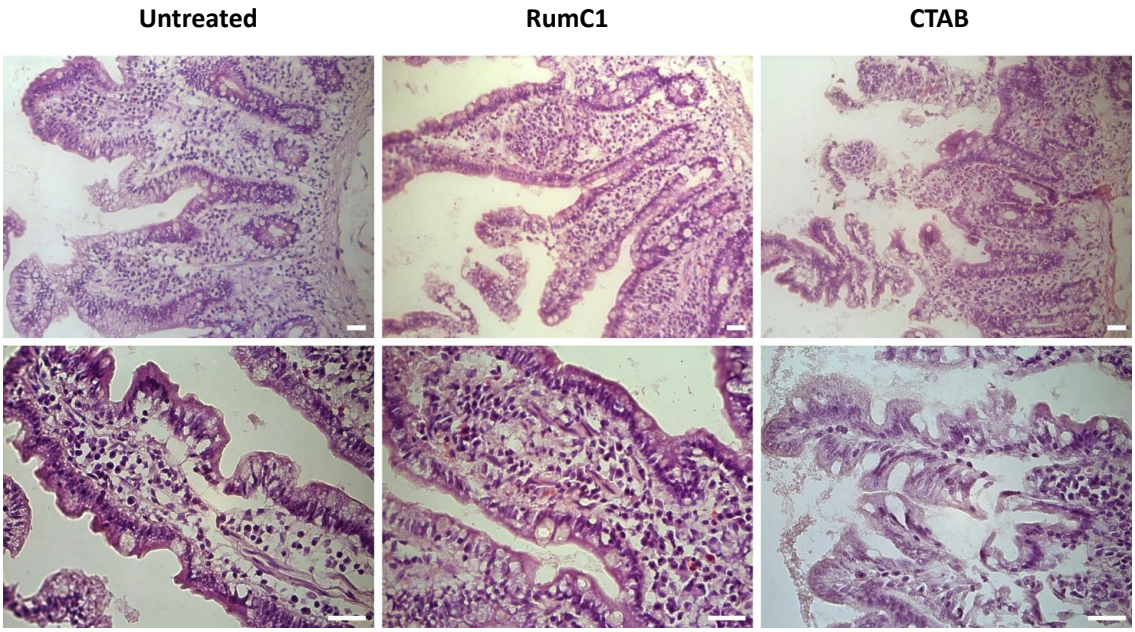

Fig. 6. **Histological analysis of human intestinal tissue treated with RumC1.** Human intestinal explants were left untreated or treated with RumC1 (100 µM) or CTAB (300 µM) for 4 h before H&E staining and microscopic observations as described in the Materials and Methods section. Images are representative of overall observed effects. Scale bar = 50 µm.

Supporting Information for

The unusual structure of Ruminococcin C1 antimicrobial peptide confers clinical properties

Clarisse Roblin[†], Steve Chiumento[†], Olivier Bornet*, Matthieu Nouailler, Christina S. Müller, Katy Jeannot, Christian Basset, Sylvie Kieffer-Jaquinod, Yohann Couté, Stéphane Torelli, Laurent Le Pape, Volker Schünemann, Hamza Olleik, Bruno De La Villeon, Philippe Sockeel, Eric Di Pasquale, Cendrine Nicoletti, Nicolas Vidal, Leonora Poljak, Olga Iranzo, Thierry Giardina, Michel Fons, Estelle Devillard, Patrice Polard, Marc Maresca, Josette Perrier, Mohamed Atta, Françoise Guerlesquin, Mickael Lafond*, Victor Duarte*

* Correspondence to: bornet@imm.cnrs.fr; mickael.lafond@univ-amu.fr; victor.duarte@cea.fr
† The following authors contributed equally to this work: Clarisse Roblin & Steve Chiumento

This PDF fil includes:

Figures S1 to S9

Tables S1 and S2

SI Materials and Methods

SI References

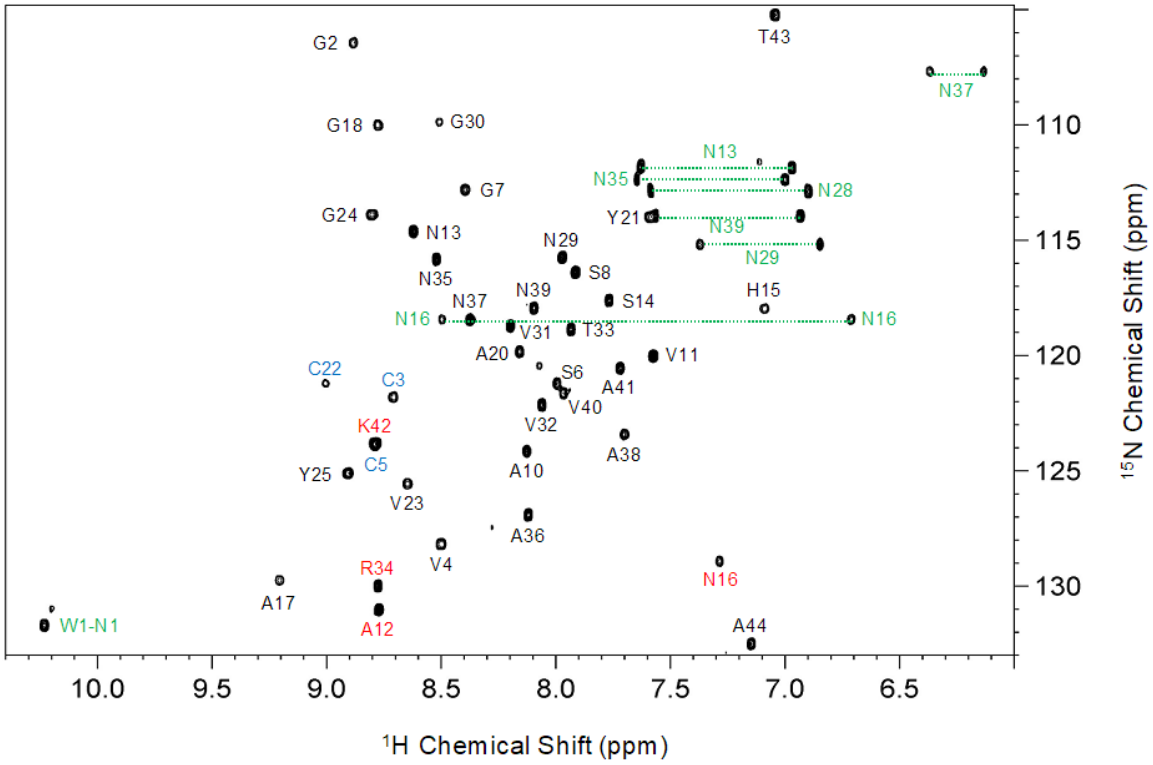

Fig. S1. Two-dimensional [^{1}H, ^{15}N] HSQC spectrum of RumC1. The number and the respective single letter code of amino acids are indicated at each assigned backbone NH cross-peak. Peaks corresponding to asparagine side chain amides are connected with a dotted horizontal line. The tryptophan indole NH group is labeled (W1-N1). Acquisition was done on a Bruker Avance III 600MHz spectrometer equipped with a cryogenically cooled 5 mm TCI probe head. Data was collected with a 0.2 mM sample concentration of ^{13}C and ^{15}N-isotopically enriched RumC1 in 10 mM phosphate buffer, pH 6.8 in 90% H_2O/ 10% D_2O at 27°C.

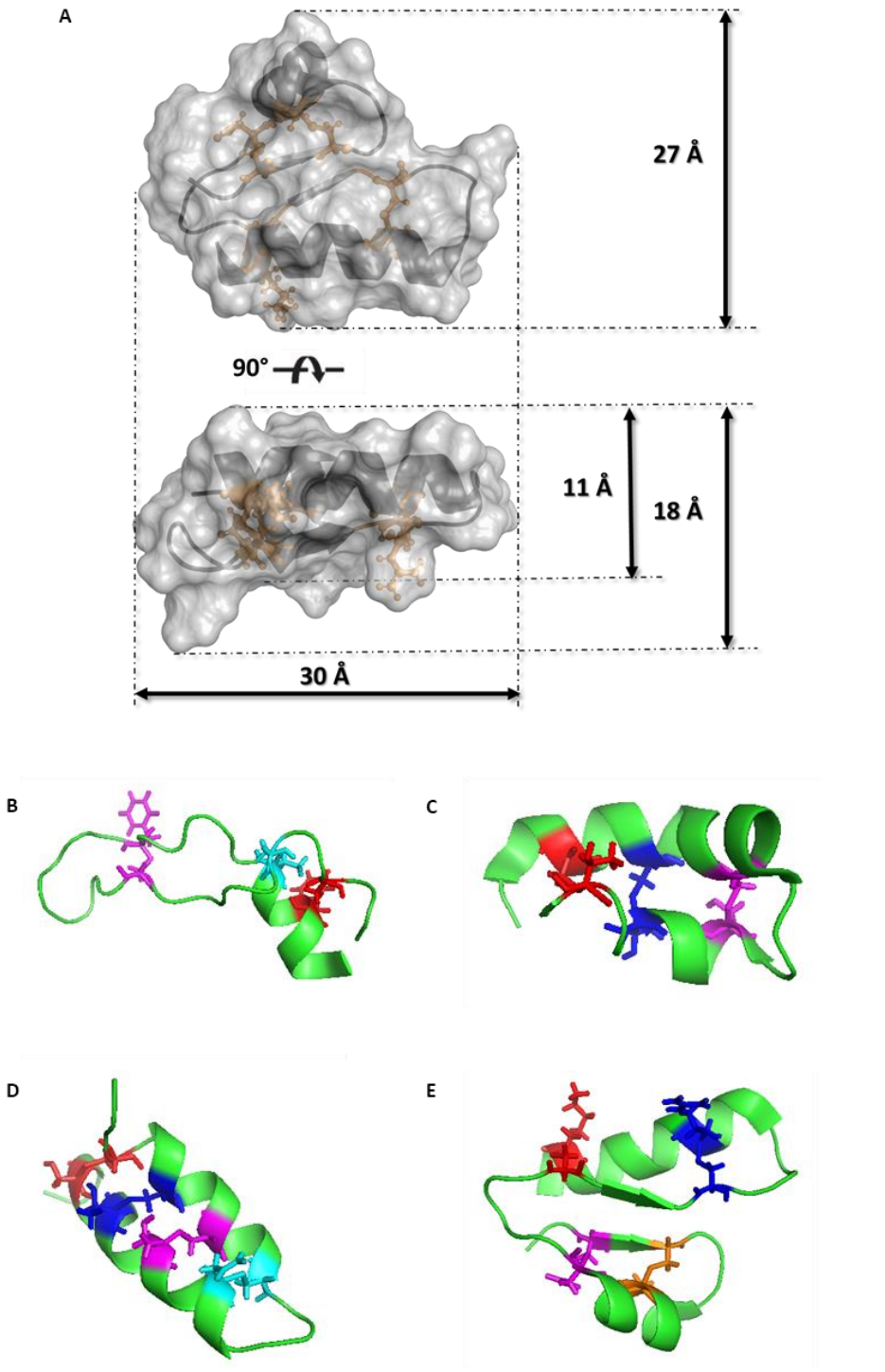

Fig. S2. Dimensions of the NMR structure of RumC1. Comparison of sactipeptides structures. (A) Dimensions of the NMR structure of the DDDD stereoisomer of RumC1. NMR Structures of: **(B)** Subtilosin A, **(C)** Thuricin CD, **(D)** Thurincin H and **(E)** RumC1. Stereoisomers at the α-carbons are LDD, LLD, DDDD and DDDD for subtilosin A, thuricin CD, thurincin H and RumC1, respectively. The Protein Data Bank codes for Subtilosin A, Thuricin CD , Thurincin H and RumC1 are 1PXQ, 2L9X, 2LBZ and 6T33, respectively.

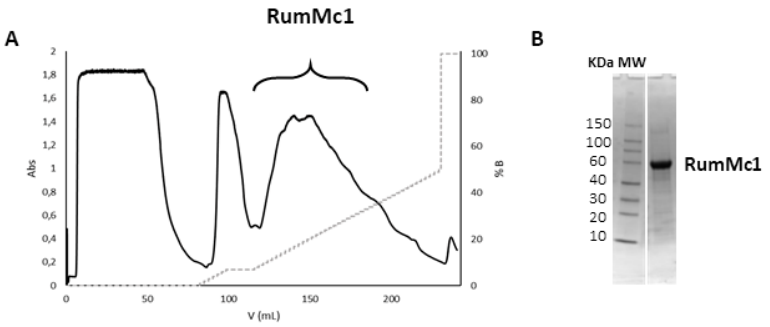

Fig. S3. Anaerobic purification of RumMc1. (A) FPLC chromatogram of overexpressed RumMc1 on a nickel-charge IMAC column. %B is the % of a 50 mM HEPES, pH 7,5, 300 mM NaCl, 500 mM imidazole buffer solution. **(B)** SDS-PAGE analysis of purified RumMc1

A

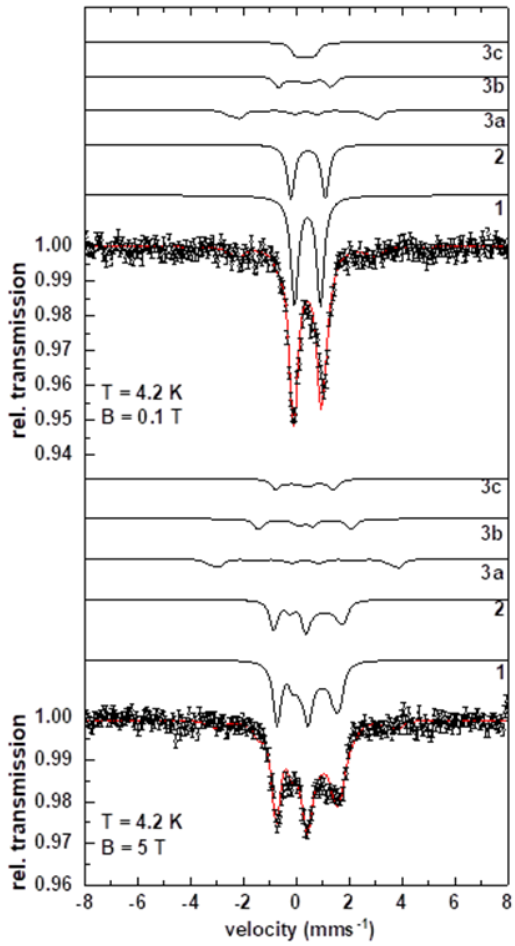

B

	1	2	3a	3b	3c
δ (mm/s)	0.42 (±0.02)	0.44 (±0.02)	0.33 (±0.03)	0.33 (±0.03)	0.33 (±0.03)
ΔE_Q (mm/s)	0.98 (±0.02)	1.30 (±0.02)	0.49 (±0.03)	0.49 (±0.03)	0.49 (±0.03)
Γ (mm/s)	0.35 (±0.02)	0.33 (±0.02)	0.33 (±0.03)	0.33 (±0.03)	0.33 (±0.03)
η	1 (-0.4)	1 (-0.4)	0 (+0.5)	0 (+0.5)	0 (+0.5)
$A_{xyz}/\mu_N g_N$ (T)	(0/0/0)	(0/0/0)	(36/28/32)[1]	(11/11/11)[1]	(2.5/2.5/2.5)[1]
Area (%)	50	25	8.33	8.33	8.33

Fig. S4. Field dependent spectra of RumMc1. (A) Mössbauer spectra of RumMc1 with the simulation (red solid line) representing the sum of the subcomponents **1**, **2** and **3** (black lines). Component **1** and **2** are simulated in a ratio of 2:1 and represent two diamagnetic $[4Fe4S]^{2+}$ clusters. Component **3** is divided into three subcomponents **3a**, **3b** and **3c** that represent three Fe^{3+} high spin ions antiferromagnetically coupled to a total spin of S = 1/2 as present in a $[3Fe4S]^{1+}$ cluster. **(B)** Mössbauer parameters obtained from the simulation of the field dependent spectra of RumMc1. [1] Values for $A_{xyz}/\mu_N g_N$ were taken from B. H. Huynh *et al*. (1).

Fig. S5. Alignment of selected radical-SAM enzymes with RumMc1. Alignment of anSME (anaerobic Sulfatase Maturating Enzyme), AlbA, and RumMc1. Conserved residues are marked "*" and cysteine residues are highlighted in green.

A

	RumC1	RumC1-44	RumC1-44-LS
% maturation	90%	< 1%	< 10%

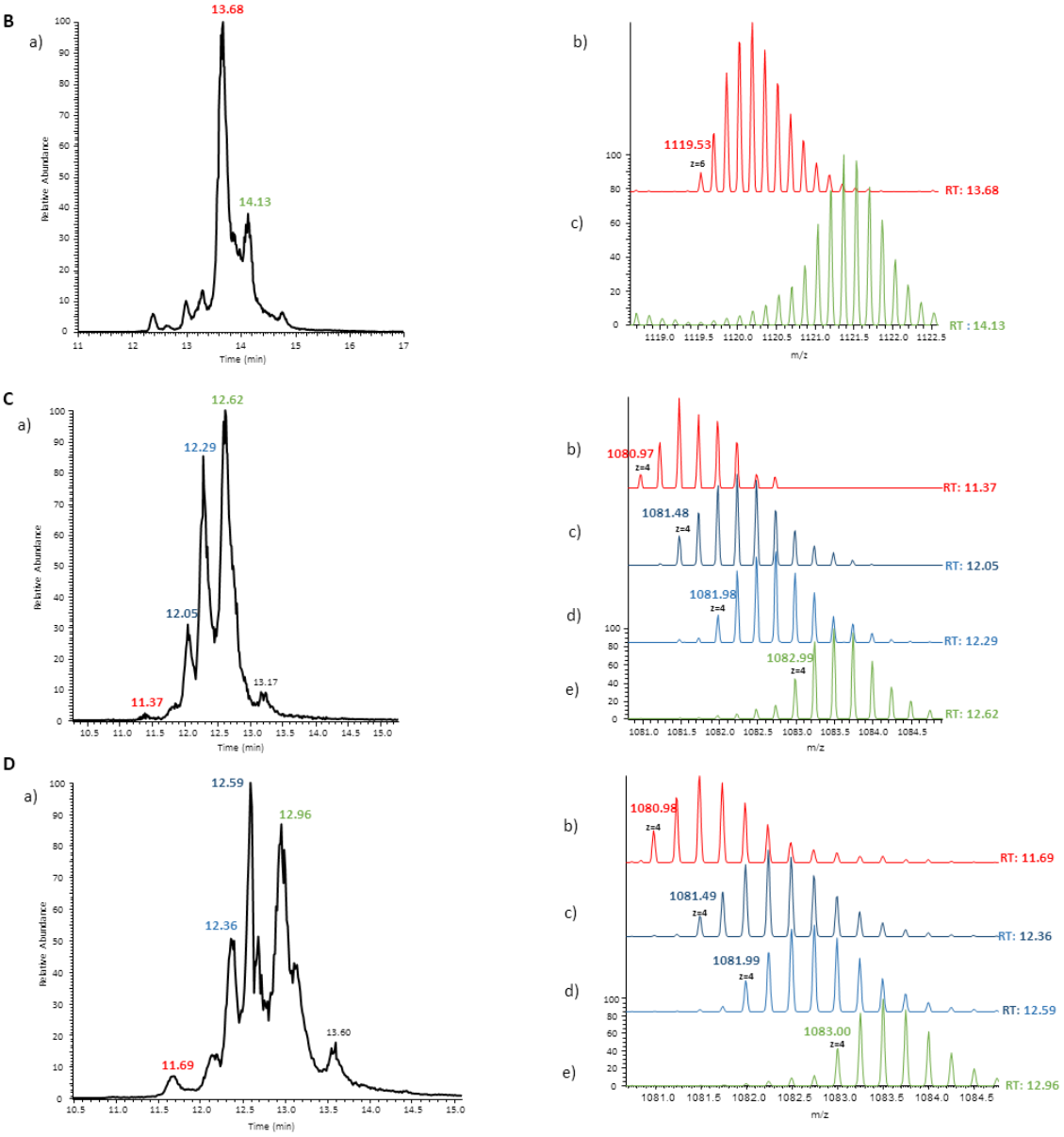

Fig. S6. LC-MS analyses of leader peptide-dependent maturation of RumC1. (A) Percentage of the full maturation for the different constructions. **(B)** Maturation of RumC1: (a) LC-MS trace of *in vitro* matured RumC1. Zoom-in spectra at RT = 13.68 (b) and RT = 14.13 (c) for m/z corresponding to RumC1. (b) A major ion $[M+6H]^{6+}$ = 1119.5 Da corresponds to the fully maturated form containing 4 thioether bonds. (c) A mixture of unmaturated forms containing no, one or two disulfide bonds are observed. **(C)** Maturation of RumC1-44: (a) LC-MS trace of *in vitro* matured RumC1-44. Zoom-in spectra at RT = 11.37 (b), RT = 12.05 (c), RT = 12.29 (d), and RT = 12.62 (e) for m/z corresponding to RumC1-44. (b) A major ion $[M+4H]^{4+}$ = 1081 Da corresponds to the fully maturated form containing 4 thioether bonds. (c) A major ion $[M+4H]^{4+}$ = 1081.5 Da corresponds to a species containing 3 thioether bridges. (d) A major ion $[M+4H]^{4+}$ = 1082 Da corresponds to a species with 2 thioether bridges. (e) A major ion $[M+4H]^{4+}$ = 1083 Da corresponds to the non maturated form of RumC1-44. **(D)** Maturation of RumC1-44-LS: (a) LC-MS trace of *in vitro* matured RumC1-44-LS. Zoom-in spectra at RT = 11.69 (b), RT = 12.36 (c), RT = 12.59 (d), and RT = 12.96 (e) for m/z corresponding to RumC1-44-LS. (b) A major ion $[M+4H]^{4+}$ = 1081 Da corresponds to the fully maturated form containing 4 thioether bonds. (c) A major ion $[M+4H]^{4+}$ = 1081.5 Da corresponds to a species containing 3 thioether bridges. (d) A major ion $[M+4H]^{4+}$ = 1082 Da corresponds to a species with 2 thioether bridges. (e) A major ion $[M+4H]^{4+}$ = 1083 Da corresponds to the non maturated form of RumC1-44-LS.

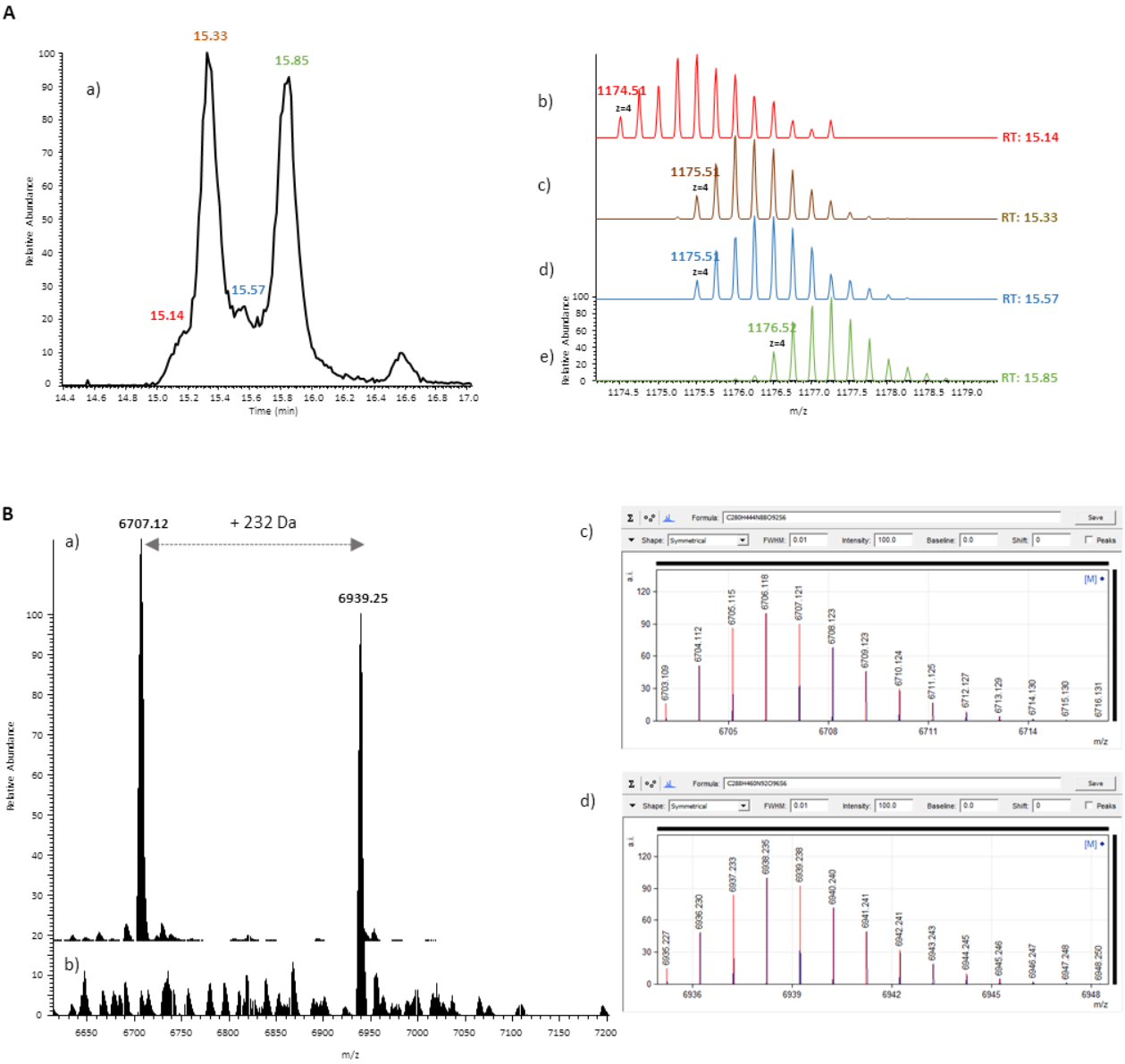

Fig. S7. Analysis of *in vivo* maturation of RumC1-44 and RumC1-Ala18/Ala19 variant. (A) LC-MS analysis of *in vivo* maturated RumC1-44. (a) LC-MS trace of *in vivo* matured RumC1-44. Zoom-in spectra at RT = 15.14 (b), RT = 15.33 (c), RT = 15.57 (d) and RT = 15.85 (e) for m/z corresponding to RumC1-44. (b) A major ion $[M+4H]^{4+}$ = 1174.5 Da corresponds to the fully maturated form containing 4 thioether bonds. (c) and (d) A major ion $[M+4H]^{4+}$ = 1175.5 Da corresponds to species with respectively 2 disulfide bridges and 2 thioether bridges, according to their corresponding MS/MS spectra. (e) A major ion $[M+4H]^{4+}$ = 1176.5 Da corresponds to the non maturated form of RumC1-44. **(B)** MS Analysis of *in vivo* maturated RumC1-Ala18/Ala19. (a) The deconvoluted mass obtained for the main species is 6707.1 and corresponds to a species containing 2 disulfide bridges. (b) After DTT reduction and iodoacetamide alkylation, the mass is shifted to 6939.2 corresponding to RumC1-Ala18/Ala19 alkylated 4 times (mass increased by 232 Da corresponding to 4 alkylations and 2 disulfide bridge reductions). (c) and (d) Simulated MS profiles of RumC1-Ala18/Ala19 with disulfide bonds and fully alkylated cysteines, respectively.

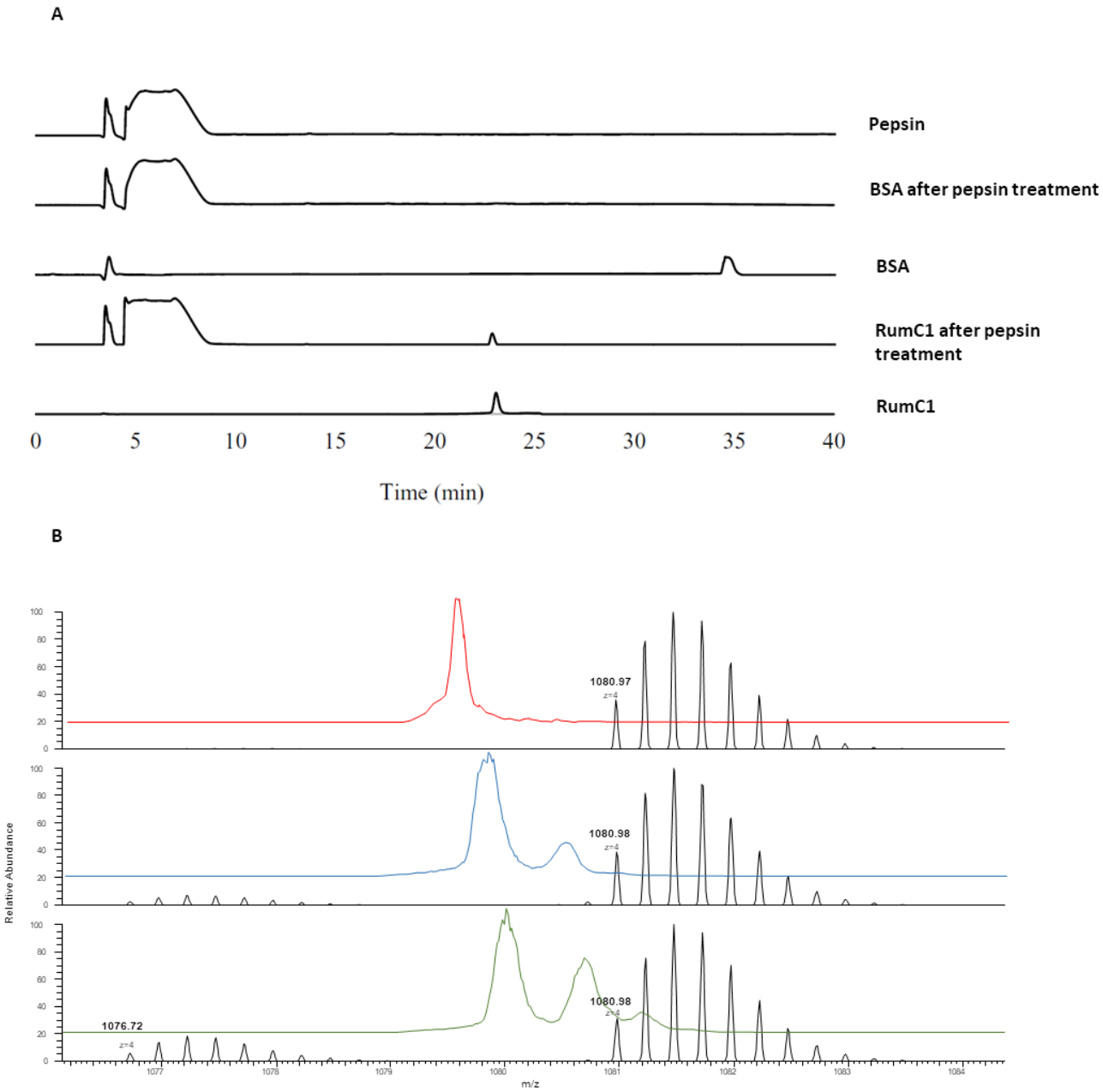

Fig. S8. Chromatographic and spectroscopic analyses to evaluate RumC1 integrity. (A) Chromatogram of RP-C18-HPLC of RumC1, or BSA used as control, treated with pepsin and in conditions simulating the stomach (pH 2,5 37°C 2h). **(B)** LC-MS profiles and MS spectra of RumC1 (top, red) submitted to pepsin (middle, blue) or pancreatic conditions (bottom, green). No change on RumC1 was observed after digestion except the presence of a light amino loss species due to heating (-NH3).

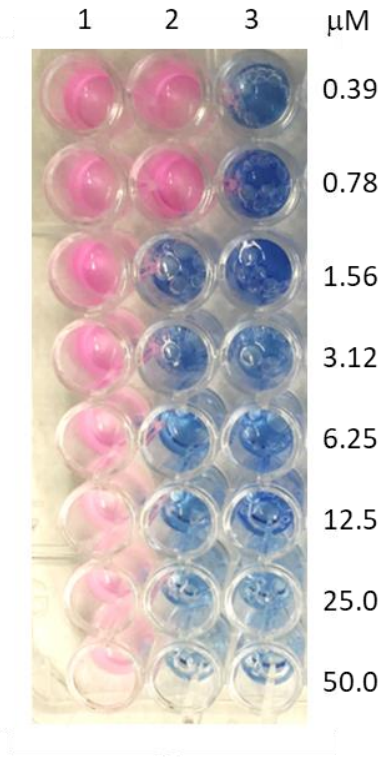

Fig. S9. **Evaluation of RumC1 activity on simulated intestinal epithelium infected by *Bacillus cereus*.** After 24h of incubation, suspension of *B. cereus* grown on Caco-2 and T84 cells were transferred to new 96 well plates free of eukaryotic cells. Resazurin was added to determine the viability of the bacterial cells. Briefly, resazurin is a blue dye that is reduced in pink resorufin in the presence of metabolically active cells. An example of untreated *B. cereus* grown on Caco-2 cells is shown in column 1, whereas the column 2 corresponds to *B. cereus* grown on Caco-2 cells with increasing concentrations of RumC1 and column 3 represents uninfected and untreated Caco-2 cells.

Table S1. Comparison of statistics generated by the 16 stereoisomers of RumC1. Assigned NOEs represent total number of off-diagonal NOE assignments used by CYANA to perform the structure calculation.

Table entry	Isomers	Thioether bond violations	Assigned NOEs	RMSD (Angstroms)	CYANA average target function value
1	LLLL	3	374	2.5 ± 0.4	0.7
2	LLLD	3	385	1.9 ± 0.8	2.0
3	LLDL	2	400	1.3 ± 0.5	1.3
4	LLDD	2	371	2.7 ± 0.4	3.8
5	LDLL	3	399	1.4 ± 0.5	1.2
6	LDLD	4	404	1.2 ± 0.3	1.5
7	LDDL	3	398	1.1 ± 0.3	0.7
8	LDDD	1	399	1.4 ± 0.2	0.6
9	DLLL	3	405	1.6 ± 0.3	1.1
10	DLLD	4	430	1.5 ± 0.2	0.7
11	DLDL	8	406	2.3 ± 0.4	2.9
12	DLDD	6	377	2.5 ± 0.6	5.3
13	DDLL	3	405	1.5 ± 0.5	1.3
14	DDLD	2	404	1.3 ± 0.2	0.7
15	DDDL	1	394	1.2 ± 0.2	0.3
16	DDDD	0	417	0.9 ± 0.2	0.1

Table S2. Structure calculation statistics for the DDDD stereoisomer of RumC1. Statistics for structure calculation refers to all the twenty structures.

Final NMR restraints in the DDDD structure calculation		
Short-range ($\|i-j\|=1$)	317	
Medium-range ($1<\|i-j\|<5$)	99	
Long-range ($\|i-j\|\geq 5$)	80	
Total nOe distance restraints	496	
Hydrogen bonds	50	
Thioether Bridge distance restraints	8	
Dihedral angle restraints	46	
Total restraints	600	13.6 restraints/residu
Residual violations		
CYANA target function	0.36 +/- 1.08	
NOE upper distance constrain violation		
Number > 0.1 Å in at least 1 structure	7	
Dihedral angle constrain violations		
Number > 0.1°	0	
Van der Waals violations		
Number > 0.1 Å	0	
Average structural RMSD to the mean coordinates (Å)		
All backbone atoms	0.81 +/- 0.50	
All heavy atoms	1.19 +/- 0.54	
Ramachandran statistics, % of all residues		
Most favored regions	84.1	
Additional allowed regions	15.4	
Generously allowed regions	0.4	
Disallowed regions	0	

SI Materials and Methods

Heterologous expression and purification of (^{13}C, ^{15}N)-labelled mature RumC1. A synthetic plasmid containing the *E. coli* codon-optimized gene of *R. gnavus* E1 encoding RumMc1 (pET-15b-*rumMc1*, ampicillin-resistant) was obtained from Genscript. Plasmids pET-15b-*rumMc1*, pETM-40-*rumC1* and psuf (chloramphenicol-resistant) containing *sufABCDSE* genes were used to transform competent *E. coli* BL21 (DE3) cells for expression. The resulting strain was grown in 3 L of M9 medium containing kan (50 μg/mL), amp (100 μg/mL), chl (34 μg/mL), vitamin B1 (0.5 μg/mL), $MgSO_4$ (1 mM), $FeCl_3$ (50 μM) and glucose (4 mg/mL) at 37 °C. At an optical density (OD_{600}) of 0.25, cells were harvested by centrifugation (4,000 rpm for 20 min at 4°C). The cells were resuspended in 1 L of labeled minimal medium (Na_2HPO_4 6 g/L, KH_2PO_4 3 g/L, $^{15}NH_4Cl$ 1 g/L) containing kan (50 μg/mL), amp (100 μg/mL), chl (34 μg/mL), vitamin B1 (0.5 μg/mL), $MgSO_4$ (1 mM), $FeCl_3$ (50 μM) and labeled glucose-^{13}C (4 mg/mL). The culture was grown at 25°C to an optical density (OD_{600}) of 0.8. $FeCl_3$ (100 μM) and L-cysteine (300 μM) were then added and the culture was induced with 1 mM IPTG. The cells were grown for 15h under stirring and then were harvested by centrifugation (4,000 rpm for 20 min at 4°C). Labelled MBP-RumC1 was purified as described for the MBP-RumC1 (2). (^{13}C, ^{15}N)-labelled mature RumC1 was obtained after cleavage of the MBP tag by using TEV and purified as previously reported (2). Leader peptide cleavage was performed with trypsin as described by Chiumento *et al.*, (2). Briefly, labelled RumC1was treated with TPCK (N-tosyl-L-phenylalanine chloromethyl ketone)–treated trypsin (Sigma-Aldrich) for 1 hour at 37°C at a molar ratio of 200:1 (RumC1:trypsin). Then RumC1 was purified using RP-C18-HPLC with the following gradient: 10 min at 22% followed by 12 min from 22 to 38% of 90% ACN and 0.1% TFA, on a preparative column (250 mm by 21.2 mm; Phenomenex, Jupiter, 15 μm, 300 Å).

NMR spectroscopy of RumC1. The NMR sample used for sequential assignment of ^{13}C-^{15}N-labeled RumC1 was approximately 0.2 mM in 10 mM phosphate buffer, 90% H_2O/10% D_2O at pH 6.8. All NMR data were collected at 27°C using a Bruker Avance III 600 MHz NMR spectrometer equipped with a TCI 5 mm cryoprobe. The following datasets were performed; 2D: [^{15}N,^{1}H] HSQC and [^{13}C,^{1}H] HSQC; 3D: [^{1}H,^{15}N,^{13}C] HNCACB, CBCA(CO)NH, HNCA, HN(CO)CA, HNCO, HN(CA)CO, ^{13}C-TOCSY-HSQC (spin lock of 80 ms) and (H)CCH-TOCSY. Backbone resonances

were assigned from triple resonance spectra and were extended to give side chain assignments using (H)CCH-TOCSY and ^{13}C-TOCSY-HSQC. ^{1}H assignments for aromatic side chains and asparagines side chain amides were made using 2D [^{1}H, ^{1}H] TOCSY and NOESY (mixing time of 150 ms) spectra. Spectra were processed with Topspin 3.5 and analyzed with CcpNmr Analysis software (3). All of the peak lists and the complete ^{1}H, ^{13}C and ^{15}N backbone and side chain chemical shift assignments have been deposited into the Biological Magnetic Resonance Databank (http://www.bmrb.wisc.edu) under ascension code 50027.

Structure Calculations. For the structure calculations, a 2D [^{1}H, ^{1}H] NOESY was acquired with a mixing time of 150 ms, using a 2 mM unlabeled RumC1 sample in 10 mM phosphate buffer, 90% H_2O/ 10% D_2O, pH 6.8 at 27°C, performed on the Bruker Avance III 600 MHz spectrometer. The structures of the 16 stereoisomers were calculated with CYANA 2.1 (4), using NOE restraints measured from the 2D [^{1}H, ^{1}H] NOESY, 3D [^{1}H, ^{15}N, ^{1}H] NOESY, 3D [^{1}H, ^{13}C, ^{1}H] NOESY experiments and angle restraints obtained from the TALOS+ server (5). The NOEs were calibrated within CYANA according to their intensities. The same nOe peaks list and angle restraints were used for the structure calculations of each stereoisomer, following the same procedure as previously described by John Vederas and co-workers (6–8). Twenty lowest target function value conformations were generated for each of the 16 stereoisomers. Coordinates of the twenty conformations of DDDD stereoisomer of RumC1 have been deposited into the Protein Data Bank under ascension code 6T33.

Expression of RumMc1. We obtained a commercially supplied codon-optimized synthetic plasmid of *Ruminococcus gnavus* RumMc1 (pET-28a–*rumMc1*, kanamycin-resistant) from Genscript. Vectors pET-28a-*rumMc1* and pDB1282 (ampicillin-resistant), which carries the *isc* operon required for proper assembly of the Fe-S clusters in RumMc1, were subsequently co-transformed into chemically-competent BL21 (DE3) *E. coli* cells. A 500 mL sterile culture erlenmeyer containing 100 mL Luria Bertani medium (LB) supplemented with kan (50 μg/mL), amp (100 μg/mL) was inoculated with a single colony of BL21 (DE3) cells carrying pET-28a-*rumMc1* and pDB1282. The 100 mL culture was grown overnight at 37 °C, 200 rpm and used to inoculate 10 liters M9 minimal medium on a fermenter. The minimal medium was prepared by supplementing M9 Minimal Salts (Sigma) with a final concentration of 20 mM glucose, 2 mM

MgSO4, 50 µg/mL kan, 100 µg/mL amp) and 50 µM $FeCl_3$. The fermenter culture was grown at 37 °C, 200 rpm to an OD_{600} nm ~ 0.3-04 and then supplemented with a final concentration of 50 µM $FeCl_3$, 300 µM L-Cys, and 13.3 mM L-arabinose. At an (OD_{600}) of 1.2, the culture was cooled at 24°C, supplemented with a final concentration of 1 mM IPTG and grown for 15h under stirring. The cells were harvested by centrifugation (4,000 rpm for 20 min at 4°C).

Purification of RumMc1. The purification protocol was carried out under strictly anaerobic conditions. The cell pellet was suspended in 40 mL of buffer A (50 mM HEPES, pH 7.5, 300 mM NaCl), sonicated and lysate clarified by centrifugation at 40,000 rpm at 4 °C for 40 min. The supernatant was collected and passed over nickel-charge IMAC column (HisTrap^{TM} HP 5mL GE Healthcare). Columns were washed with 4 volumes of buffer A. RumMc1 was eluted from nickel-charge IMAC columns with a gradient of 0-50% of buffer B (50 mM HEPES, pH 7.5, 300 mM NaCl, 500 mM imidazole). Fractions containing RumMc1were pooled and concentrated in a 30,000 MWCO filter in an Amicon® Ultra centrifugal filter devices. To eliminate imidazole and salts, sample was passed on NAP^{TM} Column, NAP-25 equilibrated in buffer C (HEPES 50mM, NaCl 100 mM pH 7.5). Anaerobic UV-visible spectra were recorded on an Uvikon XL100 spectrophotometer (Bio-Tek instruments) connected by optical fibers to the cuvette holder in the anaerobic chamber. The protein concentration was estimated by UV-visible spectroscopy by using an extinction coefficient at 280 nm of 73266 $M^{-1}.cm^{-1}$. Iron content of RumMc1 samples were measured according to the Fish method (ref). The calibration curve was obtained by measuring iron standards with iron content form 2 to 30 nmol.

Site directed mutagenesis of *rumC1* and heterologous expression of RumC1 variant. Site directed mutagenesis of the *MBP-rumC1* construct was performed to produce the Ala18/Ala19 variant of RumC1. Mutagenesis was done by following the instructions from the Q5 Site-Directed Mutagenesis Kit (New England BioLabs®). The NEBaseChanger tool was used to generate the 2 primer sequences (5'-CCATAACGCGGCTGCGGCGTACTGCG, 5'-CTGTTCGCAACCGCGGTG) and annealing temperatures. Template plasmids were digested using DpnI and were transformed into competent Top10 cells. The mutant plasmids were recovered from cells by using the Wizard® Plus SV Minipreps DNA Purification System (Promega).

Production and purification of RumC1-Ala18/Ala19 variant were performed as previously described for RumC1 (2).

Leader-peptide chemical synthesis

Chemicals

The N-fluorenylmethoxycarbonyl (Fmoc)-protected amino acids, rink amide MBHA resin (100 - 200 mesh) and 2-(1H-Benzotriazole-1-yl)-1,1,3,3-tetramethyluronium hexafluorophosphate (HBTU) were obtained from Novabiochem; N,N-diisopropylethylamine (DIEA), trifluoroacetic acid (TFA), anisole, thioanisole, 1,2-ethandithiol, acetic anhydride, piperidine and triethylamine (TEA) were from Sigma-Aldrich. All the other chemicals and solvents (N,N-dimethylformamide (DMF), diethyl ether, dichloromethane (DCM), acetonitrile (ACN) and N-methyl-2-pyrrolidone (NMP) were from different commercial sources (highest available grade) and used without further purification.

Peptide synthesis

The leader sequence of RumC1 peptide (H_2N-MRKIVAGKLQTGADFEGSK-NH_2) was prepared by solid phase peptide synthesis in an Initiator$^+$ Alstra automated microwave assisted synthesizer (Biotage). The peptide was assembled on a rink amide MBHA resin (0.25 mmol scale, 0.59 mmol/g) using standard Fmoc methodologies (9). Namely, the amino acids (4 equiv) were coupled using HBTU (3.9 equiv) as coupling agent, DIEA as base (8 equiv) and DMF as solvent. The removal of the Fmoc protecting groups was always done by treating the resin with 20% piperidine in DMF solution. After assembling, the peptide was manually deprotected and cleaved from the resin by treatment with the mixture TFA/thioanisole/anisole/1,2-ethandithiol (%v/v = 90:5:3:2) for 2 h at room temperature and under nitrogen. The resin was filtered out and rinsed with TFA. The filtrate and rinses were combined, reduced under a nitrogen stream and slowly added to cold diethyl ether with magnetic stirring to precipitate the crude peptide. The suspension was transferred to a centrifuge to recover the peptide which was washed with cold diethyl ether and centrifuged again. This step was repeated several times and finally the crude peptide was dissolved in the minimum amount of water and lyophilized. The crude peptide was purified by preparative reversed-phase HPLC in a Phenomenex Jupiter column (250 mm × 21.20 mm, 15 μm, 300 Å) using solvent A (99.9% water/0.1 % TFA) and solvent B (90% ACN/9.9% water/0.1 % TFA). The leader sequence of RumC1 peptide was eluted with a linear gradient from 15% to 35% B in 30 min at a flow rate

of 10 mL/min (R_t = 14 min). Its purity was checked by analytical reversed-phase HPLC (Phenomenex Jupiter column, 250 mm × 4.6 mm, 15 µm, 300 Å) and it was greater than 95%. The peptide was characterized by Electrospray Ionization-Mass spectrometry (ESI-MS) in positive mode using a Waters Synapt G2 HDMS (Manchester, UK) equipped with an ESI source employing the following parameters: ESI capillary voltage: +2.8 kV; extraction cone voltage: +20 V; desolvation gas (N2) flow: 100 $L.h^{-1}$; source temperature: 35 °C. Sample solutions were introduced in the ionization source at a 10 $\mu L.min^{-1}$ flow rate using a syringe pump.

***In Vitro* Enzyme Assay.** The *in vitro* enzymatic assays were performed in 100 µl of 100 mM HEPES, pH 7.5, in the presence of 100 µM of the desired peptide substrate, 25 µM of RumMc1 protein, 0.25 mM SAM and 1 mM dithionite. The assays were carried out at 37 °C during 3h under anaerobic conditions. The reactions were stopped by air exposure and were flash frozen in liquid nitrogen.

EPR and Mössbauer spectroscopies. EPR and Mössbauer samples (400 µM) were prepared and flash frozen under anaerobic conditions. When needed, cluster reduction was achieved in 1 hour by addition of 10 mM dithionite. Samples in the presence of SAM were prepared with 3 mM SAM. EPR spectra were recorded on a Bruker EMX spectrometer operating at X-band frequency equipped with an Oxford instrument ESR 900 flow cryostat. Spectra were recorded with a microwave frequency 9.65 GHz under saturated (10K, 39dB, modulation amplitude 10 G) and non-saturated (6K, 13dB, modulation amplitude 10 G) conditions for the g = 2 region. Simulations were performed using Easy Spin toolbox for matLAB. Mössbauer spectra were recorded in transmission mode with a conventional Mössbauer spectrometer which was operated in the constant acceleration mode in conjunction with a multi-channel analyzer in the time-scale mode (WissEl GmbH). The spectrometer was calibrated against α-iron at room temperature. Experiments at 77 K were conducted using a flow cryostat (Optistat^{DN}, Oxford Instruments). Field-dependent Mössbauer spectra were obtained with a helium closed-cycle cryostat (CRYO Industries of America, Inc.) equipped with a superconducting magnet (10). The magnetic field was aligned parallel to the γ-ray beam. The spectral data were transferred from the multi-channel analyzer to a PC for further analysis employing the public domain program Vinda (11) running on an Excel 2003® platform. Analysis of the spectra was performed by least-squares fits using Lorentzian line shapes with the

linewidth Γ. Field-dependent spectra were simulated by means of the spin Hamilton formalism (12).

Nano-LC−MS/MS Analyses. RumC1 samples were generally injected at a concentration of 0.1 μM. Samples were diluted in 5% (v/v) acetonitrile and 0.1% (v/v) trifluoroacetic acid and analysed by online nano-LC−MS/MS (NCS HPLC, Dionex, and Qexactive HF, Thermo Fisher Scientific). Peptides were sampled on a 300 μm × 5 mm PepMap C18 precolumn and separated on a 75 μm × 250 mm C18 column (PepMap, Dionex). The nano-LC method consisted of a 40 min gradient at a flow rate of 300 nL/min, and MS and MS/MS data were acquired using Xcalibur (Thermo Fisher Scientific). In order to improve the quality of the MS/MS spectra we performed parallel reaction monitoring (PRM) experiments to characterize RumC1 species. According to our previous characterization of RumC1 (Chiumento et al., 2019), we decided to focus these analyses on the highest m/z ions for the long (with leader peptide) and short (without leader peptide) peptides (respectively m/z = 1120 (6^+) and m/z = 1083 (4^+)). The m/z window was open at 4 units in order to consider modified species. The collision energy was set to 27.
The MS interpretations were done on the basis of previously annotated spectra and specific fragmentation pattern of thioether bridges using HCD (2). Mascot (version 2.6) was also used for the confirmation of the modifications, as previously described (2).

Stability assays. Stability of RumC1 was evaluated after incubation varying pH, temperatures, and in human serum. RumC1 was incubated in phosphate-buffered saline (PBS) at pH range from 2 to 11 at a volume ratio of 1:1 for 1 hour at room temperature. In a second assay RumC1 was incubated at temperatures of 70, 80, 90 and 100 °C for 5, 15, 30 or 60 minutes before being cooled on ice. Finally, RumC1 was incubated in human serum (Sigma Aldrich) at a volume ratio of 1:1 for 4 or 24 hours at 37°C with stirring (180 rpm). After each of this treatment, Minimal Inhibitory Concentrations (MIC) were determined against *Clostridium perfringens* ATCC13124 in Brain Heart Infusion broth supplemented with yeast extract (5 g/L) and hemin (5 mg/L) (BHI-YH) as described (2). MIC of untreated RumC1 was used to set the maximum of antimicrobial activity and calculate the residual activity of each treated RumC1. Stability and activity of RumC1 was also measured in physiological and higher concentration of salts: MIC of RumC1 was determined as above but the BHI-YH medium was replaced with Mueller Hinton (MH) broth supplemented in

either NaCl at 100, 200, and 300 mM or in $MgCl_2$ at 1, 2 and 3 mM. For the stability to salts assays, MIC of untreated RumC1 in MH broth was used as the maximum of antimicrobial activity.

Simulated gastro-intestinal digestion of RumC1. RumC1 was treated with pepsin (Sigma-Aldrich) with a molecular ratio of 1:2.5 (RumC1:pepsin) at 37°C in sodium acetate 50 mM pH 2.5 for 2 hours with stirring (180 rpm) to mimic the digestive conditions occurring in the human stomach. To stop the enzymatic reaction of pepsin, $NaHCO_3$ 1M was added until pH 7 was reached. To simulate the intestinal compartment, RumC1 was incubated with pancreatin (Sigma-Aldrich) with a molecular ratio of 1:5 (RumC1:pancreatin) at 37°C in sodium acetate 50 mM pH 6.5 for 5 hours with stirring (180 rpm). Then Phenylmethanesulfonyl fluoride (PMSF, Sigma-Aldrich) was added to a final concentration of 0.1 mM to inhibit the action of pancreatin. MIC of treated RumC1 was determined against *C. perfringens* ATCC13124 in BHI-YH as described (2) after controlling that the enzymes in the above conditions without RumC1 showed no anti-*C. perfringens* activity. MIC of untreated RumC1 was used to set the maximum of antimicrobial activity and calculate the residual activity of each treated RumC1. Furthermore, RumC1 was detected by RP-C18-HPLC using an analytical column Jupiter 15-µm C18 300 Å (250 mm by 21.2 mm; Phenomenex). Elution was performed at 1 ml/min with a 0 to 40% linear gradient of 90% ACN and 0.1% TFA for 30 min. Finally, mass spectrometry analysis were conducted to compare the molecular masses of digested RumC1 and untreated RumC1. As it has been reported that the bacteriocin nisin is digested by pancreatin but not by pepsin (13), nisin (from Sigma-Aldrich) was used as a positive control of the enzymatic activity of pancreatin only. To validate pepsin activity, Bovine Albumine Serum (BSA, Sigma-Aldrich) was used as a positive control.

Antimicrobial activity on human intestinal epithelium models. Caco-2 (ATCC HTB-37) and T84 (ATCC CCL-248) cells were being used as models of small intestinal and colonic epithelial cells, respectively. Cells were cultured in Dulbecco's modified essential medium (DMEM) supplemented with 10 % foetal calf serum (FCS), 1 % L-glutamine and 1 % Streptomycin-Penicillin antibiotics (all from Invitrogen). Cells were routinely seeded and grown onto 25 cm^2 flasks maintained in a 5 % CO_2 incubator at 37 °C. To test the influence of human intestinal epithelial cells on RumC1 activity, cells grown on 25 cm^2 flasks were detached using trypsin–EDTA solution (from Thermo Fisher Scientific), counted using Mallasez counting chamber and

seeded into 96-well cell culture plates (Greiner bio-one) at approximately 10^4 cells per well. Cells were grown for 7-10 days until differentiation. The culture medium was then replaced twice with DMEM supplemented with 10% FCS but free of phenol red and of antibiotics 24h and 48h to make sure any trace of antibiotics was removed prior to the infection with *B. cereus.* A suspension of *B. cereus* DSM31 was prepared in the same media at a final concentration of 5.10^5 CFU/mL and added or not to Caco-2 and T84 monolayers. RumC1 was added 30 min before or at the same time or after the bacterial cells. Microplates were incubated for 24h at 37°C with 5% CO_2. Minimum inhibitory concentration (MIC) was defined as the lowest concentration of peptide that inhibited the growth of bacteria. Independent triplicate were made and sterility and growth controls were prepared for each assay.

MIC determination. Strains tested were acquired from commercial collections (the American Type Culture Collection (ATCC), www.atcc.org; the Collection de l'Institut Pasteur (CIP), www.pasteur.fr), from a laboratory collection (Centre National de Référence de la résistance aux antibiotiques, www.cnr-resistance-antibiotiques.fr) or from clinical sampling. *C. perfringens* CP24, 56, 60 were isolated from chickens and provided by UGent (14). Human clinical strains were mostly isolated from bloodstream infections, and in bone and joint infection at the University hospital of Besançon (France). The MIC were determined by broth microdilution for fastidious organisms (*Streptococcus pneumoniae*, *Listeria monocytogenes*, and *Bacillus cereus*), and non-fastidious organisms (*Enterococcus* species) by independent triplicates according to the EUCAST 2019 recommendations except for the Clostridia (15). Briefly, a bacterial suspension of Clostridia was grown in anaerobic conditions (in a Trexler-type anaerobic chamber without stirring) and adjusted in MH broth supplemented with 5% lysed horse blood and 20 mg/L β-nicotinamide adenine dinucleotide at 5.10^6 UCF/mL. Ninety microliters of cell suspension were transferred in a sterile F-bottom polypropylene 96-well microplates. Thus, ten microliters of sterile RumC1 or antibiotics used as control from 100 to 0.1 µM by two-fold serial dilutions were added to the bacterial suspension to obtain a final concentration of 5.10^5 CFU/mL. Microplates were incubated 48h at 37°C in anaerobic conditions. MIC was defined as the lowest concentration of peptide that inhibited the growth of bacteria after 48h incubation at 37°C. Sterility and growth controls were prepared for each assay.

Macromolecules synthesis studies. *C. perfringens* ATCC 13124 was grown in BHI-YH broth (2) in airtight jars in the presence of anerobic atmosphere generation bags (Sigma-Aldrich) without stirring at 37°C until $OD_{600\ nm}$ reached 0.2. Then RumC1 or metronidazole or antibiotics with known mechanisms of action were added at 5xMIC. The antibiotics gemifloxacin, rifampicin, tetracycline and vancomycin were used as controls for the inhibition of DNA, RNA, protein and peptidoglycan synthesis, respectively. After 15 min of incubation at 37°C in anaerobic conditions, samples were labelled with [methyl-3H]thymidine or [5,6-3H]uridine or L-[4,5-3H(N)]-leucine or D-[1-3H] HCl glucosamine (all from Hartmann Analytic) at 10 µCi/mL to follow the synthesis of DNA, RNA, proteins and peptidoglycan respectively. After 45 min of incubation at 37°C in anaerobic conditions, bacterial cells were lysed and the macromolecules were precipitated with ice cold trichloroacetic acid (TCA, Sigma-Aldrich) at a final concentration of 20%; samples were kept on ice for an hour. Then the precipitates were filtered on Whatman glass microfiber filters pre-soaked in ice cold TCA 5%. After washing the filters with ice cold TCA 5% twice and then ice cold absolute ethanol once, they were soaked in 10 mL of scintillation liquid (Ultima Gold, PerkinElmer). Radioactivity was measured by liquid scintillation counting (TriCarb2800, PerkinElmer). As each condition displayed different growth rates, the radioactivity counts were normalized by the $OD_{600\ nm}$ of the samples. Results were expressed as a percentage of total macromolecule synthesis that was measured for each macromolecule with untreated cells. All experiments were done in independent triplicates.

ATP bioluminescent assays. *C. perfringens* ATCC 13124 was grown in BHI-YH broth (2) in anaerobic conditions (in a Trexler-type anaerobic chamber without stirring) at 37°C until $OD_{600\ nm}$ reached 0.4. Then *C. perfringens* cells were distributed in white polystyrene Nunc™ 96-well plate (ThermoFisher Scientific) and RumC1, metronidazole or nisin were added at 2.5, 5 or 10xMIC. After 15 min of incubation in the same conditions, 100 µL of cells were mixed with 10 µL of luciferin-luciferase reagent (Yelen Analytics) prepared in IMI-Yelen Buffer (Yelen Analytics). The mix was homogenized and incubated 30 s before reading of the emitted photon using a microplate reader (Synergy Mx, BioTek). Then, 10 µL of lysis reagent (Yelen Analytics) was added to the mixture, homogenized and incubated 1 min before a new reading of the emitted photon. The intensity of the bioluminescent light was expressed as relative light units (RLU) which is proportional to extracellular ATP concentration (16). The inner ATP concentration was derived

from the difference in ATP concentration in the extracellular media before and after cell lysis. Results were expressed as a percentage of total inner ATP concentration that was measured with untreated cells. All experiments were done in independent triplicates.

***Ex-vivo* evaluation of the RumC1 innocuity using human intestinal explants**. In order to evaluate the innocuity of RumC1 peptide for the human gut, *ex-vivo* experiments were performed using human explants as previously described (17). Human intestinal tissues, corresponding to ileocecal area, were obtained from patients undergoing surgery at the unit of gastrointestinal surgery, Hospital Laveran (Marseille, France), according to a collaborative "clinical transfer" project. The procedure was approved by the French ethic committee (CODECOH n° DC-2019-3402). All patients agreed for the use of their tissues for research purposes. Diagnoses leading to surgery were intestinal carcinoma. Samples were taken from macroscopically unaffected area as identified by the surgeons. After resection, the tissues were placed in ice-cold oxygenated sterile DMEM solution containing 1% (w/v) streptomycin/penicillin solution and 50 µg/mL gentamycin and were directly transferred to the laboratory within 15 min. Intestinal tissues were extensively washed and maintained in ice-cold culture media. Tissues were cleaned under binocular microscope from vascular vessels and conjunctive tissue using forceps. Intestinal explants (diameter of 0.5 cm^2) were then isolated from the cleaned resections using surgical punch, the complete procedure being complete in less than 2 h after the resections were obtained from the surgery unit. Finally, the explants were washed 3 times with culture media without antibiotics and transferred into 24-well plates before being incubated at 37°C during 4 h with RumC1 peptide diluted in DMEM media at 100 µM. In parallel, explants were left untreated (negative controls) or were incubated with the 300 µM of detergent cetyl trimethylammonium bromide (CTAB) used as positive control of tissue damages. After incubation, the explants were collected, washed three times with PBS^{2+} and fixed overnight at 4°C with PFA diluted at 4% (v/v) in PBS. The next day, intestinal explants were washed twice with PBS and included in inclusion medium (TFM - EMS), in transverse position to allow cutting respecting the crypt-villosity axis using cryostat (Leica CM3050). Four sections of 5 µm thickness were obtained per explant and each section being separated from the next by 100 µm in order to cover all the tissue. Explants were then stained using hematoxylin and eosin (H&E) staining protocol. Briefly, samples were incubated for 8 min in hematoxylin (from Sigma-Aldrich) and then allowed to stain by incubation with water for 2 min.

Then explants were incubated for 1 min in eosin (from Sigma-Aldrich) and then in water for 1 min. This was followed by incubation of explants with ethanol at concentration of 70% then 95% and finally 100% for 2 min each. After blotting excess ethanol, intestinal explants were incubated for 15 min with xylene and mounted with coverslip using Eukitt mounting media (EMS, Hatfield, PA, USA). Finally, explants were left overnight to dry before examination of tissue organization under the microscope (Leitz DMRB microscope (Leïca) equipped with Leïca DFC 450C camera) (18).

SI References

1. B. H. Huynh, *et al.*, On the active sites of the [NiFe] hydrogenase from Desulfovibrio gigas. Mössbauer and redox-titration studies. *J. Biol. Chem.* **262**, 795–800 (1987).

2. S. Chiumento, *et al.*, Ruminococcin C, a promising antibiotic produced by a human gut symbiont. *Sci. Adv.* **5**, eaaw9969 (2019).

3. W. F. Vranken, *et al.*, The CCPN data model for NMR spectroscopy: development of a software pipeline. *Proteins* **59**, 687–696 (2005).

4. P. Güntert, C. Mumenthaler, K. Wüthrich, Torsion angle dynamics for NMR structure calculation with the new program DYANA. *J. Mol. Biol.* **273**, 283–298 (1997).

5. G. Cornilescu, F. Delaglio, A. Bax, Protein backbone angle restraints from searching a database for chemical shift and sequence homology. *J. Biomol. NMR* **13**, 289–302 (1999).

6. K. E. Kawulka, *et al.*, Structure of subtilosin A, a cyclic antimicrobial peptide from Bacillus subtilis with unusual sulfur to alpha-carbon cross-links: formation and reduction of alpha-thio-alpha-amino acid derivatives. *Biochemistry* **43**, 3385–3395 (2004).

7. C. S. Sit, M. J. van Belkum, R. T. McKay, R. W. Worobo, J. C. Vederas, The 3D Solution Structure of Thurincin H, a Bacteriocin with Four Sulfur to α-Carbon Crosslinks. *Angew. Chem. Int. Ed.* **50**, 8718–8721 (2011).

8. C. S. Sit, R. T. McKay, C. Hill, R. P. Ross, J. C. Vederas, The 3D structure of thuricin CD, a two-component bacteriocin with cysteine sulfur to α-carbon cross-links. *J. Am. Chem. Soc.* **133**, 7680–7683 (2011).

9. W. C. Chan, P. D. White, Eds., *Fmoc solid phase peptide synthesis: a practical approach* (Oxford University Press, 2000).

10. A. Janoschka, G. Svenconis, V. Schünemann, A closed cycle-cryostat for high-field Mössbauer spectroscopy. *J. Phys. Conf. Ser.* **217**, 012005 (2010).

11. H. P. Gunnlaugsson, Spreadsheet based analysis of Mössbauer spectra. *Hyperfine Interact.* **237**, 79 (2016).

12. V. Schünemann, H. Winkler, Structure and dynamics of biomolecules studied by Mössbauer spectroscopy. *Rep. Prog. Phys.* **63**, 263–353 (2000).

13. B. Jarvis, R. R. Mahoney, Inactivation of Nisin by Alpha-Chymotrypsin. *J. Dairy Sci.* **52**, 1448–1450 (1969).

14. A. R. Gholamiandekhordi, R. Ducatelle, M. Heyndrickx, F. Haesebrouck, F. Van Immerseel, Molecular and phenotypical characterization of Clostridium perfringens isolates from poultry flocks with different disease status. *Vet. Microbiol.* **113**, 143–152 (2006).

15. , v_9.0_Breakpoint_Tables.pdf (December 12, 2019).

16. E. W. Chappelle, G. V. Levin, Use of the firefly bioluminescent reaction for rapid detection and counting of bacteria. *Biochem. Med.* **2**, 41–52 (1968).

17. E. H. Ajandouz, *et al.*, Hydrolytic Fate of 3/15-Acetyldeoxynivalenol in Humans: Specific Deacetylation by the Small Intestine and Liver Revealed Using in Vitro and ex Vivo Approaches. *Toxins* **8** (2016).

18. H. Olleik, *et al.*, Temporin-SHa and Its Analogs as Potential Candidates for the Treatment of Helicobacter pylori. *Biomolecules* **9**, 598 (2019).

6.3 Summary and comments

In the first publication, we proposed that RumC1 belongs to a new subclass of sactipeptide because it displays a double hairpin structure rather than a single hairpin structure like previously described sactipeptides. A concomitant and independent study observed the same double hairpin structure in RumC2 (Balty et al., 2019). However, our first study only confirmed 3 out of the 4 bridges by 3D-NMR and the 2nd study only reported a structural model based on site directed mutagenesis experiments and mass analysis. Here, we confirmed the Cys-amino acid acceptor tandems involved in 4 sacti-bridges on a fully mature RumC1 by 3D-NMR establishing a double hairpin shaped structure and we gave the fully-resolved three-dimensional structure of RumC1. As RumC1 carries 4 thioether bridges and the amino acid acceptors of these bridges can follow a natural L-conformation or D-reverse conformation, there are 16 theoretical stereoisomers. Based on structural analysis and constraint violations, the stereoisomer that fits the best the NMR data is the DDDD stereoisomer. Such conformation has already been observed in the case of the sactipeptide thuricin H (cf Subsection 2.2.4 Sactipeptides). Previously, Balty and co-workers reported a LLLL conformation for RumC1, however this conclusion arose from hydrolysis and derivatization but was not supported by any structural data (Balty et al., 2019). Based on our NMR data, a LLLL stereoisomer is associated with constraint violations on 3 out of the 4 thioether bridges and is therefore one of the most unlikely stereoisomer.

The resolved three-dimensional structure of RumC1 revealed an undescribed fold so far consisting in two α-helices separated by a loop containing two stranded paralled β-sheets. Each α-helix is folded facing one β-sheet by the thioether linkages. The presence of β-sheets is a novel feature in sactipeptides. Unlike the 4 sactipeptides for which the structure was resolved (i.e. subtilosin A, thuricin H, Trn-α, Trn-β, cf Subsection 2.2.4 Sactipeptides), RumC1 displays an overall positive charge and a surface mainly composed of hydrophylic residues. On the contrary, the previously described sactipeptides exhibit a negative charge and a hydrophobic surface. We previously showed that RumC1 does not have a pore-forming action unlike these sactipeptides, which might be explained by the difference of surface hydrophobicity. All the NMR analyses were done at IMM by Oliver Bornet, Matthieu Nouailler and Françoise Guerlesquin on a mature and labelled peptide produced at LCBM in particular by Steve Chiumento. The resolution of the structure of RumC1 completed the 2nd objective set for my thesis project although my involvement on these experiments was limited to the leader peptide removal and final purification of the labelled RumC1 before NMR.

Another aspect of this publication focuses on the maturation process, these studies were also done at LCBM. The sactisynthase RumMc1, like known sactisynthases, harbors a SPASM domain. Mössbauer and EPR spectroscopies revealed that the [4Fe-4S]2+ cluster coordinated by the canonical Cys-X_3-Cys-X_2-Cys radical SAM enzyme motif binds SAM and that the SPASM domain coordinates two auxiliary [4Fe-4S]2+ clusters. So far, studies on previously described sactisynthases showed that they are unable to form PTMs on the sactipeptide precursor in the absence of the leader peptide. This was confirmed by maturation attempts of RumC1 by RumMc1 in vitro or by heterologous expression in *E. coli*. For the first time, the leader peptide of a sactipeptide was provided in trans in vitro. In these conditions, only 10% of the leaderless precursors of RumC1 were fully processed. Therefore it seems that the leader peptide is essential for recognition by the sactisynthase. Another element essential for maturation was located outside of the leader

peptide. A conserved Gly18-Pro19 motif was identified in the 5 RumC isoforms in between the two hairpin domains. RumMc1 failed to perform PTMs on the RumC1 precursor when this motif was mutated, demonstrating the crucial role of this motif in the maturation process.

As mentioned in the sactipeptides subsection, little is known about their stability to thermal, chemical and proteolytic treatments which I assayed on RumC1. I showed that RumC1 is resistant to treatments with the digestive enzymes and the conditions encountered in both the gastric and intestinal compartments. The latter property was not surprising as RumC1 is naturally produced by *R. gnavus* E1 in the host intestine. However since *R. gnavus* E1 does not colonize the stomach it was possible that RumC1 would be degraded in the conditions mimicking this compartment. In addition to its resistance to digestive enzymes, RumC1 also remained active after treatment with enzymes contained in human serum. Thus, RumC1 could be administrated by both oral and systemic routes. The stability of RumC1 to proteases can be explained by the fact that the potential cleavage sites are protected by the sacti-bridges. RumC1 was not only stable at the acidic conditions encountered in the stomach but also at basic pH. Moreover, RumC1 was still active after treatment at high temperatures (up to 1 hour for 70°C and 15 minutes for 100°C). The stability of RumC1 to temperature was further investigated by circular dichroïsm at Synchotron Soleil. The results of these experiments were not included in the presented publication as they were obtained after the submission. Information on protein secondary structures can be obtained by circular dichroïsm signals at wavelength between 190 and 240 nm (Miles & Wallace, 2016). The spectra of RumC1 was obtained at 25°C and then at increasing temperature by 10°C. We can see on **Figure 6.1**, that the secondary structures of RumC1 start collapsing at 45°C resulting in a shift of the spectra. However, when the temperature reached 95°C and was brought down to 25°C, the spectra recovered around 80% of the initial absorbance observed before heating, meaning than most of the secondary structures were recovered. It is expected that the thioether bridges remain stable during heating, thus enabling the refolding of RumC1 after cooling. Indeed, since the formation of sacti-bridges involves a very specific radical-based mechanism, it is highly unlikely that the sacti-bridges could be reformed without the sactisynthase if they would open during the heating phase, and thus that RumC1 would recover its secondary structure. The capacity of RumC1 to refold after exposure to high temperatures may explain its activity even after treatment at these temperatures.

Another poorly described feature of sactipeptides is their safety toward humans. After showing the safety of RumC1 on human gastric and intestinal cell lines, we showed here for the first time the direct effect of a sactipeptide on a human biopsy. The lack of lesions on the human intestinal tissue treated with high doses of RumC1 provided another proof of its interest as an antibiotic. In addition I also showed that RumC1 is active in a mammalian environment, which is an important feature for alternatives to antibiotics that is not often demonstrated.

In the dramatic context of antibiotic resistance, we showed that RumC1 is active, under or in the micromolar range, against resistant and MDR clinical pathogens such as *Clostridium difficile* and *Enterococcus faecium*, both listed as priority targets by the WHO and the CDC for which new antimicrobials are urgently needed. The activity of RumC1 was determined on an extensive panel of pathogens. Although the activity of the other isoforms of RumC remains to be characterized, the extensive characterization of RumC1 answers to the 3rd objective of my project which was the determination of the activity spectrum of RumC. Overall, beside having a potent antibacterial activity and being safe

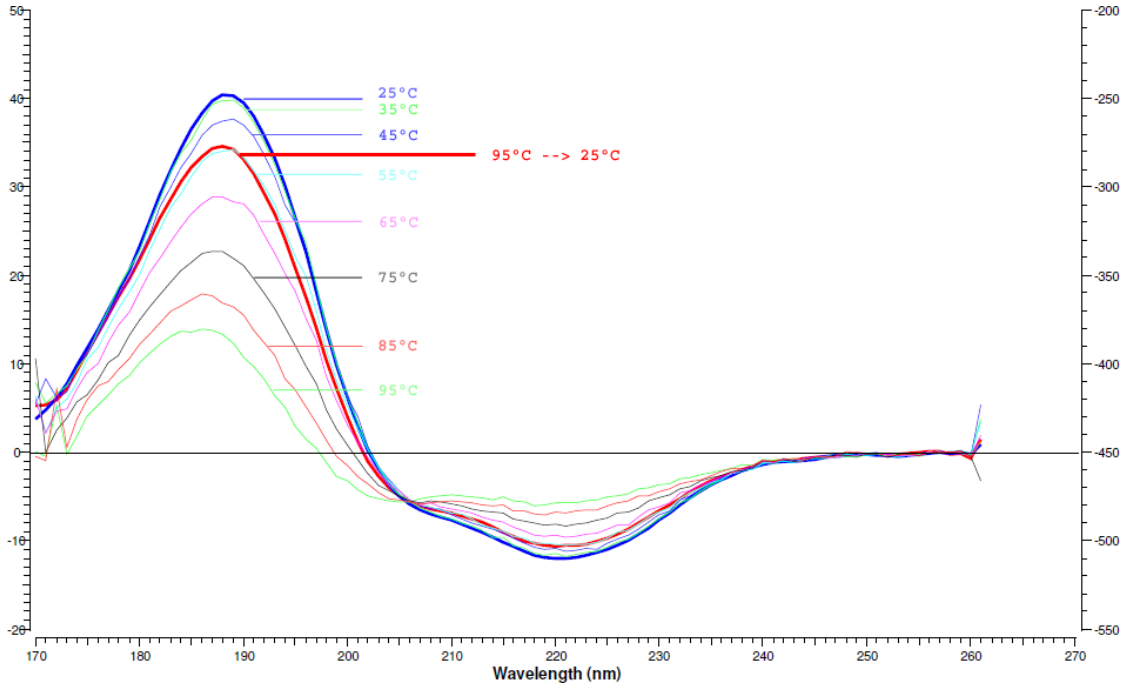

Figure 6.1: Spectra of thermal denaturation of RumC1

for humans, RumC1 meets most of the conditions necessary for reaching the clinical and marketing steps that are often limiting the development of RiPPs.

Finally, we showed that RumC1 has an intriguing mode of action. By following the incorporation of radiolabelled precursors of the synthesis of DNA, RNA, proteins and peptidoglycan in *C. perfringens*, we showed that RumC1 inhibits the synthesis pathways of all of these macromolecules. These studies were done at the Laboratoire de Microbiologie et Génétique Moléculaire (LMGM) in Toulouse where Hamza Olleik, Marc Maresca and I had access to facilities with abilitation for radioactivity manipulation. As a fluorescent precursor (3-[(7-Nitro-2,1,3-benzoxadiazol-4-yl)amino]-D-alanine, NADA) of the peptidoglycan synthesis was also available, we confirmed the inhibition of the peptidoglycan synthesis by fluorescent microscopy with the help of Nathalie Campo, at LMGM in Toulouse as well (**Figure 6.2**). The inhibition of the production of these macromolecules is most likely a consequence of the inhibition of ATP synthesis that is also observed in *C. perfringens* cells treated with RumC1 as their production is ATP-dependent. The studies on the ATP synthesis were done with Mickael Lafond. Additional studies are required to decipher the precise mechanism of RumC1 leading to the inhibition of ATP synthesis. It is conceivable that RumC1 directly targets ATP synthases although further studies are necessary to conclude on the precise mechanism of action of RumC1 and its target. Currently, there is only one antibiotic (i.e. bedaquiline) on the market that inhibits ATP synthases. Because of its very narrow-spectrum, its use is restricted to infections caused by Mycobacterium. Hence, a novel antibiotic active against a wide range of Gram positive pathogens that targets ATP synthases could be useful to treat infections caused by strains that have developed resistance to antibiotics targeting other synthesis pathways.

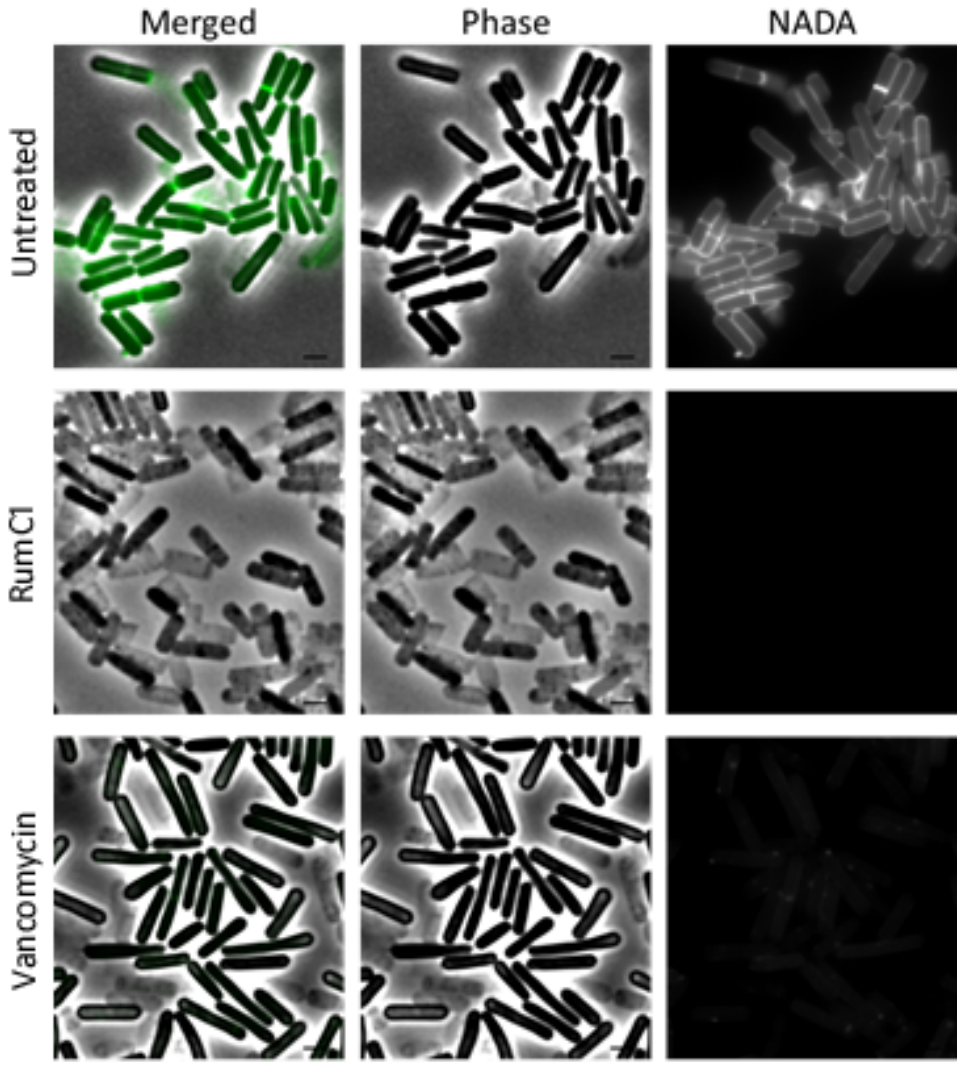

Figure 6.2: Incorporation of a fluorescent precursor of peptidoglycan
C. perfringens *cells in early log phase were treated with either RumC1 or vancomycin at 5xMIC or left untreated. Cells were incubated in anaerobic conditions at 37°C for 30 min before adding the fluorescent precursor NADA. After another 30 min of incubation cells were washed with PBS and seeded on an agar medium mounted on microscopy slides.*

Chapter 7

Ruminococcin C1, a multifunctional antibacterial sactipeptide

7.1 Context

In the first and second publications, we have exposed the therapeutic potential of RumC1 based on (i) its ability to kill Gram positive pathogens in the micromolar range, including in the presence of a mammalian tissue; (ii) its safety for human cell lines and primary tissues; (iii) its low propensity for resistance generation and (iv) its stability to physiological or manufacturing conditions. However, an ultimate assay to prove the therapeutic potential of RumC1 as an alternative to antibiotics remained to be done, consisting in the evaluation of its efficacy to rescue an animal model from a bacterial infection. Initially, we had planed to study the effects of RumC1 on broiler chickens as their health is one of the main concerns of the private partner of the ANR RUMBA project, Adisseo. Because *C. perfringens* is a major gut pathogen affecting chickens, causing billions of dollars of loss worldwide each year, this specie was selected as the infecting agent. However, although an efficient biosynthetic mean of production of RumC1 has been developed with the heterologous expression system in *E. coli* by the LCBM, we are not currently able to produce enough RumC1 to treat infected chickens. Hence, a much smaller animal model was chosen, i.e. mice.

Because *C. perfringens* is an intestinal pathogen, we first attempted to establish a *C. perfringens* gut colonization in mice. However, no such colonization was obtained in conventional mice as their gut microbiome seems to offer a natural barrier protection against this pathogen. Therefore, we decided to infect mice in the peritoneal cavity and to also deliver the treatment intraperitoneally as this model of infection has been widely used for decades as a standard for antibiotic research (Frimodt-Møller, 1993). These in vivo studies were done in collaboration with Cédric Jacqueline from Atlangram and Nantes University. However, the mouse peritonitis model has several limitations when it comes to the study of intestinal infections. One of them regards the natural gut environment that is not reproduced in the peritoneal compartment, i.e. the pH and enzymatic conditions. However, we already showed in the previous publication that RumC1 is active in the intestinal environment (Roblin et al., 2020). Unlike the peritoneal cavity, the gut hosts a complex microbiome. Therefore, another limitation of the chosen model is the assessment of the efficacy of RumC1 on isolated *C. perfringens* cells rather than in a complex microbial community composed of other bacteria that could absorb RumC1. Thus, we decided to also assess the efficacy of RumC1 to kill *C. perfringens* in a microbial community. As

we learned that the natural mice intestinal microbiome is resistant to colonization by *C. perfringens* and as our initial subject of study was the intestinal infection of *C. perfringens* in chickens, we decided to used cecal contents of broiler chickens as sources of microbiota. Adisseo and in particular the CERN has developed a high expertise in the analysis of intestinal health and microbial communities of chickens. The experiments on cecal contents of chickens were done in their facilities by Eric Pinloche and myself.

As seen in section 2.2, RiPPs may have multiple types of biological activities. Hence, we decided to investigate in this study a wide scope of applications. All these assays were done in Marseille at ISM2. First, regarding the antimicrobial action of RumC1, I studied its ability to inhibit biofilm formation or to disrupt biofilm. We also explored a potential antifungal activity of RumC1 with Hamza Olleik and Elise Courvoisier-Dezord. Then, we focused on the effects on the human host. We assayed the potency of RumC1 to stop the proliferation of cancer cell lines or to promote an anti-inflammatory effect with Marc Maresca. Finally, Cendrine Nicoletti and I studied the impact of RumC1 on the rate of cell migration in a wound healing context.

7.2 Publication in preparation

{Publication in preparation}

Ruminococcin C1, a multifunctional antibacterial sactipeptide

Clarisse Roblin[1,2], Steve Chiumento[3], Cédric Jacqueline[4], Hamza Olleik[1], Elise Courvoisier-Dezord[1], Agnès Armouric[1], Christian Basset[3], Louis Dru[1,3], Cendrine Nicoletti[1], Eric Pinloche[2], Florine Ecale[5], Alexandre Crépin[5], Marc Maresca[1], Mohamed Atta[3], Victor Duarte[3], Estelle Devillard[2], Josette Perrier[1], Mickael Lafond[1]*

[1]Aix-Marseille Univ, CNRS, Centrale Marseille, iSm2, 13013, Marseille, France.

[2]ADISSEO France SAS, Centre d'Expertise et de Recherche en Nutrition, 03600, Commentry, France.

[3]Univ. Grenoble Alpes, CEA, IRIG, CBM, CNRS UMR5249, 38054, Grenoble, France.

[4]EA3826, IRS2 Nantes-Biotech, Université de Nantes, 44200, Nantes, France.

[5]Univ. Poitiers. Écologie et Biologie des Interactions, CNRS UMR7267, Équipe Microbiologie de l'Eau, 86073, Poitiers, France

* Correspondence to: mickael.lafond@univ-amu.fr

Keywords: Antibiotics, RiPP, Sactipeptide, *Ruminococcus gnavus*, Peritonitis infection, Microbiome.

The world is on the verge of a major antibiotic crisis as the emergence of antibiotic resistant bacteria is increasing and as very few novel antibiotics have been introduced in the clinic since the 1960s. In this context, scientists have been exploring alternatives to antibiotics such as, Ribosomally synthesized and Post-translationally modified Peptides (RiPPs). Previously, the highly potent in vitro antibacterial activity and safety on human cells and tissues of the Ruminococcin C1, one of these RiPPs belonging to the sactipeptide subclass, has been demonstrated. Here, we show that the Ruminococcin C1 is efficient to protect challenged mice from *Clostridium perfringens*, with a lower dose than the conventional antibiotic vancomycin. Moreover, the Ruminococcin C1 is also effective against this pathogen in a complex microbial community with modest impact on the overall community. Finally, this sactipeptide exhibits other biological activities that could be beneficial for human health or for other fields of applications. Overall, this study highlights the new properties of Ruminococcin C1, beyond its now well-known antimicrobial scope, extending its therapeutic interest.

INTRODUCTION

According to the World Health Organization (WHO), antibiotic resistance is one of the biggest threats to Public Health and food safety worldwide. Development of resistance is promoted by exposure to antibiotics. Indeed, antibiotic exposure creates a selective pressure: bacteria with an acquired or intrinsic resistance have an advantage for survival and for spreading on sensitive bacteria (*1-3*). As most antibiotics come from natural origins and in particular from microorganisms, bacteria have been exposed to them and started developing resistance long before their discovery by humans (*4*). However, the industrialization of antibiotics has accelerated this phenomenon and every introduction of a new antibiotic in the clinic has been followed by the emergence of resistant bacteria a couple years later or sometimes even the same year. Some bacteria have evolved so much in the last decades that they became resistant to several classes of antibiotics or to all of them, they are respectively designated as Multi-Drug or Pan-Drug Resistant (MDR and PDR) bacteria (*5*)**.** Currently, in the United-States, it is estimated that almost 100,000 deaths are caused each year because of antibiotic-resistant pathogen-associated hospital-acquired infections (HAIs, *6*) and thought to drastically increase up to 10 million worldwide by 2050, making antimicrobial resistance the first cause of death (*7*). Moreover, the total economic loss that can be credited to antibiotic resistance in the US is estimated at 55 billion of dollars a year (*6*). Effective antibiotics are needed not only for the treatment of reported infections, but also for many medical procedures such as common surgeries that could be lethal in case of postoperative infections (*8*). Furthermore, procedures that require or provoke depression of the immune system such as organs transplantation or chemotherapy could be too dangerous to perform if no effective antibiotics are available. Therefore, the rise of resistance is expected to lead to the return to "the Dark Ages of Medicine" which designate the era of medicine before antibiotic discovery. As only two classes of antibiotics, the lipopeptides and the diarrylquinolines, have been introduced to the clinic since the 1960s (*9-10*), it is urgent to find new antibiotics that could reach the clinic and fight MDR or PDR bacteria.

In that context, several alternatives to antibiotic treatment such as phage therapy, immunotherapy, or microbiota transplantation are under investigation to overcome the antibiotic resistance crisis (*11*). Among these alternatives, Ribosomally synthesized and Post-translationally modified Peptides (RiPPs) constitute a potential trove of active molecules. RiPPs are produced by organisms from the 3 domains of Life (archaea, prokaryotes and eukaryotes) and exert multiple types of biological activities including antibacterial and antimicrobial

activities but also insecticidal, nematoxic and anti-cancer effects among others. Although RiPPs share a common biosynthesis pathway consisting in the mRNA-dependent synthesis of a precursor peptide that undergo post-translational modifications (PTMs) on a core sequence before being excised from a leader sequence, the PTMs carried by RiPPs and their structures are highly diverse, determining their classification (*12-13*).

Recently, we have characterized such a RiPP, the Ruminococcin C1 (RumC1), produced by the bacterial strain E1 of one of the prominent members of the human gut microbiome, *Ruminococcus gnavus* (*14-16*). This RiPP belongs to the sactipeptide subclass as it carries four sulfur-to-alpha carbon thioether cross-links, leading to a previously undescribed and highly compact three-dimensional structure, conferring to RumC1 high resistance to physiological conditions encountered during systemic or oral administration (*16-17*). RumC1 displays potent in vitro activity towards Gram-positive pathogens, including clinical isolates and antibiotic-resistant strains (*16-17*). Moreover, RumC1 retained its activity in the presence of a simulated and infected intestinal epithelium and was shown to be safe both in vitro on human cells lines and ex vivo on intestinal tissues (*16-17*). To our knowledge, this original sactipeptide gathers more clinical properties than any other described members of this subclass of RiPPs.

Taking into account all these essential clinical properties, we decided to take this study a step further and validate the potency of RumC1 as a drug-lead in vivo in an infected animal model. Indeed, we show that RumC1 is at least as efficient as the conventional antibiotic vancomycin to clear a peritoneal *Clostridium perfringens* infection in mice with a dose 20-fold lower. Moreover, RumC1 successfully kills *C. perfringens* in the context of a complex microbial intestinal community, while having a limited action on the distribution of the rest of the microbiome. Then, we investigated the other typical biological activities found in RiPPs and more broadly antimicrobial peptides such anti-biofilm, antifungal and anti-cancer activities. Here, we show that RumC1 could be used to reduce biofilms of Gram-positive bacteria or as a highly selective antifungal agent. Finally, in addition to its antibacterial role, RumC1 could have beneficial effects on the host due to anti-inflammatory and wound healing potentials.

RESULTS

RumC1 is effective to clear a *C. perfringens* infection in vivo.

Previously, we showed that RumC1 is active against Gram-positive pathogens in vitro, on laboratory strains as well as on clinical isolates (*16-17*). In particular, RumC1 is active under the micromolar range against multiple strains of *C. perfringens* with MICs similar to the conventional antibiotic vancomycin (*17*), commonly used for the treatment of gut infections caused by Clostridia. Here, we compared the efficacy of RumC1 and vancomycin to protect mice from a *C. perfringens* infection. Mice were infected with the clinical isolate *C. perfringens* CP24 by intraperitoneal injection and then received either Phosphate-Buffered Saline (PBS), vancomycin or RumC1 delivered intraperitoneally at 0.5, 1 and 4 h post-infection (hpi). In the control group that received PBS, the infection was lethal for all the mice 6 hpi (**Fig. 1A**). Preliminary studies revealed that administrating vancomycin at 110 mg/kg led to mice dying starting at 24 hpi (**Fig. S1**). Therefore, vancomycin was delivered at a higher dose of 200 mg/kg for each injection. Three groups of mice treated with RumC1 were constituted with doses injected three times of 0.1, 1 and 10 mg/kg. Strikingly, RumC1 at 10 mg/kg was sufficient to protect 100% of treated mice whereas treatment with vancomycin at 200 mg/kg led to the survival of 85% of treated mice (**Fig. 1A**). On the contrary, RumC1 at 0.1 mg/kg had no impact on the survival of mice whereas no mice treated with 1 mg/kg lived longer than 28 hpi. Moreover, between the two groups that survived until the end of the study (48 hpi), i.e. mice treated with either RumC1 at 10 mg/kg or vancomycin at 200 mg/kg, mice that received RumC1 notably exhibited lower scores of impaired health and physical conditions (**Fig. 1B, S2**) and less weight loss (**Fig. 1C**). Bacterial loads of *C. perfringens* contained in the peritoneal cavity or in the spleen of mice at the time of death were determined by plating and colonies counting **(Fig. 1D-E)**. The mice treated with the low doses of RumC1, i.e. 0.1 or 1 mg/kg, displayed reduced contents of *C. perfringens* in the peritoneal cavity compared to control mice but barely any reduction in the spleen. On the contrary, no *C. perfringens* was detected in the peritoneal cavity of mice that received the high dose of RumC1 of 10 mg/kg and loads of the pathogens were drastically reduced in the spleen. Regarding, now, the treatment with vancomycin, no *C. perfringens* was detected in the spleen, but one out of 7 mice still had high bacterial contents in the peritoneal cavity. Overall, taking into accounts the survival, weight, health of mice as well as the bacterial cell counts, RumC1 was at least as efficient as vancomycin to cure mice from a *C. perfringens* infection, with a lower dose.

RumC1 is effective to kill *C. perfringens* in a complex microbial community with minimal perturbation for the community.

After showing that RumC1 was efficient to protect mice from a lethal *C. perfringens* infection and since we have previously demonstrated that RumC1 is active against a broad spectrum of Gram-positive bacteria (*16-17*), we wanted to investigate if RumC1 could effectively kill *C. perfringens* in the context of a complex and diverse natural microbiota. As *C. perfringens* CP24 was isolated from a broiler chicken (*18*), we used cecal contents of broiler chickens as a source of intestinal microbiota. These cecal contents were supplemented or not with *C. perfringens* CP24 and treated with RumC1 at a dose equivalent to 5xMIC of CP24 or not, before being incubated in anaerobic conditions at 39°C for 24 h. The composition of the microbiota was then determined by 16S rRNA sequencing. A sequence corresponding to the 16S rRNA gene of *C. perfringens* CP24 was detected only in the cecal contents supplemented with this strain and without RumC1 at a relative abundance of 0.06% **(Fig. 2A)**. Therefore, *C. perfringens* CP24 is able to colonize a natural intestinal chicken microbiota and RumC1 effectively inhibited this colonization. Then, we analyzed the rest of the distribution of the microbiota **(Fig. 2B)**. Overall, RumC1 had limited effects on the distribution of the microbiota and more than 75% of the main microbial members (relative abundance > 0.1%) were conserved compared to untreated cecal contents. The main differences consist in the major reduction of *Clostridium* from the cluster XIVb from 8% of relative abundance to 0.5% and a counterpart increase in Gram-negative bacteria, in particular *Escherichia* and *Shigella.* Gram-negative *Desulfovibrio* and *Hydrogenoanaerobacterium* were majorly increased in the RumC1-treated cecal contents but relatively stayed in low abundance in the overall community. The cluster XIVb of *Clostridium* is composed of 6 species: *C. propionicum, C. neopropionicum, C. lentocellum, Epulopiscium sp, C. colinum, C. piliforme* (*19*). These last two species are respectively responsible of ulcerative enteritis in chicken and Tyzzer's disease. Interestingly, other *Clostridium* clusters such as clusters IV and XIVa were not impacted by RumC1. In human, these two clusters associated with *Bacteroides* compose 98% of the commensal intestinal microbiota (*20*).

RumC1 disrupts biofilms.

In microbial populations, bacteria can exist in a planktonic mode of growth, meaning that they are isolated cells, or they can evolve in biofilm. In biofilm, bacterial cells are adjacent

and compose a complex community embedded in an extracellular matrix. It has been estimated that 80% of bacterial infections are caused by bacterial cells in a biofilm mode of growth. The extracellular matrix consisting of DNA, exopolysaccharides and proteins provides protection to bacterial cells and bacteria are 10 to 1,000 times more resistant to antibiotics in biofilm than in their planktonic mode of growth (*21*). Therefore, prevention of biofilm formation and disruption of pre-formed biofilms are desirable traits for alternatives to antibiotics. Based on the previously demonstrated ability of RumC1 to kill *B. subtilis* ATCC 6633 with a MIC/MBC of 0.4 µM (*16)*, we assayed here the potency of RumC1 to prevent biofilm of this strain in Calgary Biofilm Devices (CBD, *22*). On these devices, pegs are embedded in the lids of 96-well plates which allow the growth of a biofilm on the surface of the pegs soaking in bacterial cell suspensions. RumC1 was unable to prevent biofilm formation at concentrations lower than the MIC. At higher concentrations, biofilm was prevented as expected as the growth of planktonic cells in the suspension was inhibited as well **(Fig. 3A)**. In a second assay, *B. subtilis* was grown in biofilm for 48 h before adding RumC1. Incubation with RumC1 for 24 h at 1xMIC induced a slight biofilm disruption. Less than 50% of the pre-formed biofilm was left after incubation with RumC1 at 2xMIC or higher concentrations **(Fig. 3B)**. Therefore, RumC1 does not have a preventive effect on biofilm formation at sub-inhibitory concentrations but is effective to degrade already formed biofilms.

RumC1 exhibits a selective antifungal activity.

As many RiPPs exhibit several distinct biological activities, and in particular diverse antimicrobial effects (*12*), we investigated the antifungal activity of RumC1 on a panel composed of Ascomycetes and Basidiomycetes. No growth inhibition was detected on the strains of Ascomycetes studied (i.e MIC > 100 µM). The activity of RumC1 was assayed on two strains of Basidiomycetes, *Coniophora puteana* BFRM 497 and *Heterobasidion annosum* BRFM 524. Similarly to the selected Ascomycetes, no activity was detected against the first specie of Basidiomycetes. However, growth of *H. annosum* was inhibited in the presence of RumC1 at 12.5 µM **(Fig. 4)**. *H. annosum* is one of the most studied forest fungi as this pathogen, responsible of conifer diseases, is responsible for the highest economic lost in the forest industry in the Northern hemisphere (*23-24*). Therefore, RumC1 seems to exert a highly selective antifungal activity.

RumC1 has beneficial effects for the human host.

Since RumC1 is produced by the human gut symbiont *R. gnavus* E1 (*14-16*), we also investigated the activities that RumC1 could exert on the human host. First, the anti-inflammatory effect of RumC1 was assayed using the reporter cell line HeLa eLUCidate TLR4/IL-8. This cell line stably expresses at the membrane the Toll-like receptor (TLR) 4. TLRs are involved in the recognition and response to bacterial infections, and in particular TLR4 is activated through binding to lipopolysaccharide (LPS). Activation of TLR4 induces the production of pro-inflammatory cytokines such as IL-1, IL-6, IL-8, IL-10, IL-12 and TNFα (*25-26*). In the HeLa eLUCidate TLR4/IL-8 cell line, the expression of the Renilla luciferase reporter gene is under the control of the IL-8 promoter. Therefore, the detection of luciferase luminescence is directly linked to the induction of the inflammatory signaling mediated through LPS exposure. Here, we incubated this cell line with purified LPS of *Escherichia coli* and *Pseudomonas aeruginosa*. Then, cells were treated with increasing concentrations of RumC1 or left untreated as controls which were used to calculate the maxima of inflammatory responses. An inhibition of 50% of the inflammatory response was recorded with RumC1 at 25 and 50 µM, respectively in the case of the induction by the LPS of *E. coli* or *P. aeruginosa* **(Fig. 5A)**. To discriminate between a general pro-inflammatory effect or a specific inhibition of the inflammation mediated by LPS and thus by microbial infections, we also investigated the basal inflammatory status (in the absence of a pro-inflammatory stimulus) and the inflammatory response to IL-1β. IL-1β is another pro-inflammatory cytokine causing activation of the NF-κB signaling pathway which regulates the transcription of many genes involved in inflammatory response, including IL-8 (*27*). Without stimulus, the endogenous inflammatory response dropped by 40% in the presence of RumC1 at 50 µM. At the same concentration, the inflammatory pathway stimulated by IL-1β was inhibited by 82% **(Fig. 5A)**, suggesting therefore that RumC1 acts as a general anti-inflammatory molecule.

Secondly, we assayed the potency of RumC1 to inhibit the proliferation of cancer cell lines. Pancreas and prostate human cancer cell lines, respectively MIAPaCa2 and PC-3 were incubated with increasing concentration of RumC1 and their proliferation was followed. Endothelial HUVEC primary cells were also included in the assay, because of their high proliferative rates during angiogenesis. After 24 h of incubation with RumC1 a slight inhibition of proliferation was observed on the 3 cell models but under 10-20% of the maximum proliferation rate measured on untreated cells (**Fig 5B**). Moreover, this low inhibition was not

dose-dependent. Therefore, it seems that RumC1 does not act as anti-proliferative agent, at least on these specific human cell models.

Finally, we investigated the impact of RumC1 on wound healing. The human skin cell line HaCaT was grown in inserts creating a gap within a cell monolayer. The insert was then removed and cells were incubated with increasing concentrations of RumC1 before monitoring daily the migration of cells to fill the gap. After 4 days of incubation in culture medium supplemented with 1% of Fetal Bovine Serum (FBS), untreated cells filled around 20% of the initial gap. HaCaT cells treated with RumC1 exhibited an increase in migration in a dose-dependent manner. Indeed, cells treated with RumC1 filled the initial gap by 54 and 72% when incubated in the presence of 1 or 10 µM, respectively (**Fig. 5C, S3**). As a positive control, HaCaT cells were incubated in culture medium supplemented with 10% FBS after gap creation. After 4 days, gaps were filled by 83 to 98%, independently of RumC1 addition (**Fig. 5C, S4**). Thus, in conditions limiting cell growth, RumC1 speeds the migration and proliferation of this keratinocyte cell line and could have a positive impact on wound healing process.

DISCUSSION

In this study, we showed that RumC1 is not only active against Gram-positive pathogens in culture media or on a simulated epithelium in vitro, but also in vivo on an infected animal model. Considering the MIC of RumC1 and vancomycin against *C. perfringens* CP24 (1.56 µM and 0.8 µM in Brain-Heart Infusion media, respectively) and taking into account the average peritoneal cavity volume, RumC1 was able to protect 100% of the mice challenged with *C. perfringens* at a dose corresponding to around 11x$MIC_{in\ vitro}$ whereas vancomycin only protected 85% of mice at a corresponding dose of 1,470x$MIC_{in\ vitro}$. Thus, RumC1 displays high potency against *C. perfringens* in vivo in a mammalian organism. We previously showed that RumC1 is safe for mammalian tissues. Here, we demonstrate that RumC1 at an effective antibacterial dose is very well tolerated by an animal model. Indeed, mice treated with RumC1 exhibited modest weight loss and the lowest scores of impaired health and physical conditions.

Additionally, RumC1 was able to kill *C. perfringens* in a complex chicken intestinal microbial community. While the rest of the community was partially affected by RumC1, being active against broad-spectrum Gram-positive bacteria, most of the distribution of the community was not impaired. In particular, human intestinal commensal that are Gram-positive bacteria had the same distribution in the control and RumC1-treated microbiota. Because we

previously showed that RumC1 (i) is naturally produced in the gut, (ii) is active against Gram-positive pathogens, (iii) is safe for human intestinal tissues, (iv) is active in the physiological gut conditions, (v) could be delivered orally (*16*-*17*) and we now demonstrated through this study that RumC1 (vi) is efficient to cure a microbial infection in an animal model, (vii) is effective to kill a pathogen colonizing an intestinal microbial community and finally (viii) has moderate impact on said community and especially on human commensal intestinal strains, RumC1 seems to be a well-suited alternative to antibiotics to treat gastro-intestinal infections.

The human gut hosts a highly complex microbiota and dysregulation of this community can lead to dysbiosis and trigger or worsen intestinal infections. In particular, antibiotic exposure can cause drastic changes in the microbial distribution and disrupt the gut barrier (*28*). Therefore, antibiotics with modest impact on the gut microbiome that could prevent dysbiosis would be highly useful. One of the major examples of this complex relationship between dysbiosis, bacterial infections and antibiotics is the infection by *Clostridium difficile* (CDI). Extreme gut colonization by *C. difficile* can occur in individuals who suffer from dysbiosis, for example after a heavy treatment with broad-spectrum antibiotics. As a result, CDIs are the most frequent nosocomial infections in the US (*29*). Treatments with vancomycin, one of the most prescribed antibiotics for CDIs, often fail or result in relapses (*30*) and have been shown to provoke drastic alterations in microbiota and in particular to decrease commensal *Firmicutes* and *Bacteroidetes* (*31*-*32*). We previously demonstrated the high in vitro potency of RumC1 against *C. difficile* (*17*). Because RumC1 seems to be safe for commensal *Clostridium* belonging to the clusters IV and XIVa and *Bacteroides*, composing 98% of the commensal intestinal human microbiota, further studies on the efficacy of RumC1 for the treatment of CDIs should be considered.

Independently, RumC1 could be considered in other fields than bacterial infections. Indeed, we showed here that RumC1 also displays a highly selective antifungal activity against a forest pathogenic fungus. Further in-depth studies of RumC1's fungal spectrum could reveal if other fungi affecting human, animals or the environment could be eliminated by RumC1, and large-scale production investigation should be considered before.

In addition to its antibacterial activity RumC1 displays a general anti-inflammatory effect that could be beneficial for the host, in particular in the context of a gastro-intestinal infections. Indeed, gut inflammation has been associated to several chronic intestinal diseases such as Crohn's disease that are often linked to dysbiosis and can be triggered by several factors including antibiotic exposure or infection (*33*-*35*). Thus, an antibacterial activity associated to

an anti-inflammatory activity is a desirable trait for an alternative to antibiotics for the treatment of gastro-intestinal infections. Blooms of Enterobacteriaceae, including *Escherichia coli*, have also been linked to inflammatory and chronic intestinal diseases (*33*). RumC1, by inhibiting and killing Gram-positive bacteria, favors the growth of *Escherichia spp.* However, the blooms of Enterobacteriaceae appears to be a consequence of inflammation rather than a cause in chronic intestinal diseases (*33*). Moreover, as seen before the growth of *Clostridium* from clusters IV and XIVa was not impacted by RumC1 and these clusters with *Bacteroides* account for around 98% of the human intestinal microbiota and are known to be essential players in the gut homeostasis (*20*). Therefore, intestinal inflammation following RumC1 treatment is unlikely to happen and RumC1 could actually help to reduce an inflammatory state of the host while clearing an intestinal infection.

As RumC1 displays a wide spectrum of action against Gram-positive pathogens and other clinical properties such as anti-biofilm or wound healing activities, infections occurring in other compartments could be considered as well. For example, we previously showed that RumC1 displays in vitro a high potency against *Streptococcus pneumoniae* (*17*) which is responsible of nasopharyngeal infections, involving biofilm formation (*36*). RumC1 could be a candidate for in vivo clearance of infections caused by this pathogen. Moreover, antimicrobial molecules with wound healing properties are actively searched as non-healing wounds are often colonized by bacteria such as *Enterococcus faecalis*, another pathogen highly sensitive to RumC1 (*37, 17*). It is estimated that 50% of chronic wounds, such as those encountered by people suffering from diabetes, are associated with bacterial biofilms. Molecules that promote skin cell migration and proliferation while inhibiting bacterial growth, especially in a biofilm mode of growth, and reducing inflammatory response are attractive for wound healing therapies (*37*). However, the in vivo efficacy of RumC1 against other Gram-positive pathogens remains to be studied in the future to be validated as a drug-lead to enter in clinical phase.

MATERIALS AND METHODS

In vivo efficacy of RumC1.

Six-week-old pathogen-free RjOrl:SWISS female mice (weight, 20-24 g) were obtained from Janvier Labs; these non-isogenic (outbred) mice, used frequently in bacterial infection models, reflect the heterogeneity of the mouse population better than inbred mice. Mice were housed in cages, given food and water *ad libitum*, and allowed to adapt to their new environment for 4 days before any procedures were initiated. Immunocompetent mice were infected intraperitoneally with 600 µL of appropriately diluted cell suspensions corresponding to the LD_{100} for *C. perfringens* CP24 isolate. Drugs were prepared in sterile PBS and administered by intraperitoneal injections (200 µL) at 0.5, 1 and 4 hpi. Animals were randomly assigned to either no treatment (control, PBS, n=7), vancomycin at 200 mg/kg (n=7), and RumC1 at 0.1 mg/kg (n=5), 1 mg/kg (n=5) or 10 mg/kg (n=6). Survival rates were recorded at 1, 4, 6, and 24 hpi, and three times daily on subsequent days until the end of the 2-day observation period. Percentage body weight change and scoring system for assessment of disease severity (according to the criteria listed on **Fig. S2**) for each animal was recorded daily. All surviving mice were euthanized 48 hpi. For each animal, spleen was removed, weighed, and homogenized in 1 mL of saline buffer (Mixer Mill MM400) and peritoneal fluid (5x 1mL, PBS) was collected. Both spleen homogenates and peritoneal fluids were used for quantitative cultures on *C. perfringens* selective media CP ChromoSelect Agar (Sigma) for 24 h at 37°C under anaerobic conditions. Viable counts were expressed as mean (± SD) $\log_{10}$CFU per gram of organ or per mL of peritoneal fluids. Mice judged by experienced animal technicians to be experiencing pain or serious distress received buprenorphine (0.1 mg/kg, s.c. b.i.d., sufficient to cover the nocturnal period) over the course of the experiment. Signs of unrelieved suffering triggered the humane endpoint of euthanasia by CO_2 inhalation. Normally distributed data were analyzed using analysis of variance to compare the effects between the different groups, followed by a Bonferroni test to compare the treated groups 2 by 2 (GraphPad Prism Software, version 6.0).

Fermentation of chicken cecal contents.

All experiments were conducted according to the European Union Guidelines of Animal Care and legislation governing the ethical treatment of animals, and investigators were certified by the French government to conduct animal experiments. The Center for Expertise and Research in Nutrition facilities are in accordance with the agreement no. C 03 159 4 of 6 November 2008, relative to experimentation on vertebrate living animals (European regulation 24/11/86 86/609

CEE; Ministerial decree of 19 April 1988). Twelve 14-days old broilers chickens were euthanized and their cecal contents were collected and pooled. Cecal chicken microbial fermentation was performed in Hungate tubes in anaerobic buffer prepared according to Davies et al. (2001). The anaerobic buffer is composed of 5 solutions (A, B, C, D and E) prepared individually: solution A (per Liter: 5.7 g Na2HPO4, 6,2g KH2PO4 and 0,6g MgSO4-7H2O), solution B (per Liter: 4 g NH4HCO3 and 35 g NaHCO3), solution C (per 10mL: 132 mg CaCl2-2H2O, 100 mg MnCl2-4H2O, and 80 mg FeCl3-6H2O), solution D (per Liter: 0.1 % resazurine) and solution E (per 100mL: 4ml de NaOH 1M, 625mg de Na2S). The anaerobic buffer was assembled in anaerobic condition the day of the experiment (gazed with a mixture of CO2 and N2): 0,01 % of solution A, 25,3% of solution B, 25,3% of solution C, 0,1 % of solution C, 49,29% of ultra-pure water (18,2mΩ) and autoclaved in the presence of 0,5g/L of L-cystein (reducing agent). On the day of the experiment, the buffer for further reduced by adding 4% (*v/v*) of solution E before adding the cecal inoculum (final pH: 7.5 and Eh: -150mV). The cecal content was mixed (5% *w/v*) with the anaerobic buffer and 10 mL of the slurry was transferred in Hungate tubes. *Clostridium perfringens* CP24 was inoculated in cecal fermentation medium at 10^6 CFUs/mL. RumC1 was diluted in anaerobic buffer and added to the fermentation tube to obtain a final concentration of 5xMIC of CP24, i.e. 7.8 µM. The fermentation was then performed in water bath under constant agitation (200 rpm) at 39°C during 24h. Then, DNA was extracted for taxonomic analyses.

Taxonomic analyses.

Sequencing of 16s was done on Illumina platform at GenoScreen using the Metabiote kit on the V3-V4 16s hypervariable region. Briefly, DNA was extracted, normalized and the multiplex library (30 samples using unique indexes) were prepared for Illumina Myseq Paire-end 2x300 bases. Quality control of the sequencing was performed using a mock community (15 bacterial and 2 archaeal strains) including in the sequencing run. The primer and index were identified (100% homology) and removed to create demultiplexed fastq files. The fastq files were quality trimmed at Q30 at the end of the read, the reads were then paired assembled with minimum 30bp alignment at 97% homology using Qiime. The demultiplexed, quality trimmed and assembled read were then clustered using DADA2 software. The dada2 package infers exact amplicon sequence variants (ASVs) from high-throughput amplicon sequencing data, replacing the coarser and less accurate OTU clustering approach. The dada2 pipeline takes as input demultiplexed fastq files, and outputs the sequence variants and their sample-wise abundances after removing substitution and chimera errors. Taxonomic classification is done via a native

implementation of the RDP naive Bayesian classifier. The normalized ASV table (normalized to the lower number of sequence/sample) is then analyzed using Phyloseq (phyloseq object containing ASV table, taxonomic assignment and environmental data), vegan and other Bioconductor package under R environment to generate PcoA plots, diversity indexes, graphs… Statistical analysis was performed using linear models and the P values were adjusted to account for multi-variable testing using fdr method (false discovery rate) for the phylum and genera tables.

Antibiofilm formation assay

B. subtilis ATCC 6633 was grown in Luria-Bertani (LB) broth at 30°C with agitation at 180 rpm until OD_{600nm} reached 0.2-0.3. Cells were then diluted to 10^5 CFU/mL in Tryptic Soy Broth (TSB) and 150 µL of cell suspension were added per well of the Calgary Biofilm Device (CBD, *22*). Sterile RumC1 was added at a maximum concentration of 0.8 µM (i.e 2xMIC) and 2-fold series dilutions were performed in cell suspension. As it has been demonstrated that an edge effect affects the biofilm formation, all the edges of the plates were filled with TSB and used as sterility and negative controls (*38*). After 48 h of incubation at 30°C with agitation reduced to 110 rpm, the lid of the CBD was removed and the pegs were rinsed twice in PBS and then fixed in methanol for 15 min. Pegs were rinsed with PBS once more and then air-dried before being stained with Crystal violet (CV) at 0.2% for 15 min. Pegs were rinsed with PBS twice before being air-dried and then destained in methanol for 15 min before being discarded. Absorbance at 570nm was measured to evaluate biofilm formation. All the rinsing, staining and destaining steps were done in 96-well plates with a volume of 200 µL per well in order for the biofilm to be totally soaked. All experiments were done in independent triplicates, and measurements were acquired on at least two wells for each condition and for each replicate.

Antibiofilm disruption assay

Suspension of *B. subtilis* ATCC 6633 cells were prepared as described above and CBD were filled with 150 µL of cell suspension without addition of RumC1 and taking into account the edge effect previously mentioned. After 48 h of growth at 30°C and with an agitation of 110 rpm, the lid of the CBD was transferred in a new 96-well plate containing fresh TSB media supplemented with RumC1 from 6.4 µM to 0.2 µM (8xMIC and 0.25xMIC, respectively) or not. Wells were filled with 200 µL to make sure the pegs were totally soaked. Then, after 24 h of incubation in the same condition, pegs were rinsed, fixed, stained and destained as described

above. A volume of 300 µL was used per well. Absorbance at 570nm was measured to evaluate biofilm formation and disruption. All experiments were done in independent triplicates, and measurements were acquired on at least two wells for each condition and for each replicate.

Antifungal assay

All targeted strains were grown Potato Dextrose (PD) agar, at 25°C. Fungi suspensions were prepared by scraping spores NaCl 0,85% + 100 µl/L Tween 80 and were diluted to 2.10^4 spores/mL in appropriate broth (RPMI with MOPS or PD for ascomycetes and basidiomycetes, respectively) after counting by microscopy with a calibrated cell. Sterile RumC1 was added to fungi suspension in polypropylene 96-well microplates from 100 to 0.1 µM by 2-fold serial dilutions. Fungi were left for several days to grow at room temperature. MIC was defined as the lowest concentration of peptide inhibiting visible growth. Sterility and growth controls were included in each assay. MICs were determined in independent triplicates.

Evaluation of the anti-inflammatory activity

Anti-inflammatory activity of RumC1 was evaluated using the commercial eLUCidate™ HeLa, TLR4/IL8 reporter cells (Genlantis). This reporter cell line corresponds to a stably transfected HeLa cells which express human TLR4 (i.e. the receptor of LPS) as well as Renilla luciferase reporter gene under the transcriptional control of the IL-8 promoter, making them a valuable model to detect activation of IL-8 expression by LPS but also by other stimuli causing NFkB activation such as IL-1. Cells are routinely grown on 75 cm 2 flasks at 37°C with 5% CO_2 in DMEM supplemented with 10% FBS, 1% Pen/Strep and selection antimitotic agents, i.e. Puromycin (at 3 µg/mL), Blasticidin (at 5 µg/mL) and G418 (at 500 µg/mL) (all from Sigma). To evaluate the anti-inflammatory effect RumC1, eLUCidate™ HeLa cells were detached from 75 cm^2 flasks using Trypsin-EDTA solution (Thermo-Fisher), counted using Malassez counting chamber and seeded into 96-well cell culture plates (Greiner bio-one) at approximately 50,000 cells per well following manufacturer's instructions. The next day, wells were emptied and cells were left untreated (negative controls) or were treated with 100 µl of culture medium containing 10 ng/mL of LPS extracted from *P. aeruginosa* or *E. coli* (Invivogen) or 10 ng/mL of human recombinant IL-1 beta (Peprotech) in the presence of increasing concentrations of RumC1 (from 0 to 100 µM, serial 1:2 dilutions). Well-known anti-inflammatory molecules (i.e. Pyrrolidine dithiocarbamate (PDTC) and Epigallocatechin Gallate (EGCG)) as well as well-known blocker of LPS (i.e. polymyxin B) were used as positive controls (all from Sigma). Importantly, all steps were performed using non-pyrogenic plastics and RNase/DNase

molecular biology tips to limit the risk of presence of trace of LPS. After 6 h incubation at 37°C with 5% CO_2 , wells were emptied and the cells were lysed during 10 min at 4°C with 70 µL of ice-cold PBS containing 1% Triton X-100. Fifty µL of cell lysates were then transferred into white 96-well luminescence plates (Dominique Dutscher) already containing 100 µL of Renilla luciferase substrate (Yelen). Luminescence signals of the wells were immediately measured using microplate reader (Biotek, Synergy Mx).

Antiproliferative assay

Antiproliferative assays were done on the human cancer cell lines PC-3 (*ATCC*® CRL-1435™) and MIAPaCa2 (*ATCC*® CRL-1420™), originating from human prostate and pancreatic cancer, respectively. The vascular endothelial primary cells HUVEC (Sigma) were also included in the assay. PC-3 and MIAPaCa2 cells were cultured in Dulbecco's modified Eagle's medium (DMEM) supplemented with 10% heat-inactivated fetal calf serum and 1% antibiotics (all from Thermofisher) whereas HUVEC cells were grown in defined all-in-one ready to use endothelial cell growth medium (Sigma). Cells were routinely grown on 25 cm^2 flasks and maintained in a 5% CO_2 incubator at 37°C in a 95% humidified atmosphere containing 5% CO_2. Antiproliferative effect of RumC1 was evaluated as previously described (*39*). Briefly, human normal and cancer cells grown on 25 cm^2 flasks were detached using trypsin-EDTA solution (Thermofisher). Cells were diluted in appropriate culture medium and seeded into 96-well cell culture plates (Greiner bio-one) at approximately 2,000 cells per well. After 4 h to allow cell attachment, cells were then treated with increasing concentration of RumC1 diluted in appropriate medium. After 24 h, medium was aspirated and number of viable cells was measured using resazurin assay as previously described (*39*).

Wound Healing assay

The HaCaT keratinocyte cell line (obtained from Creative Bioarray) was cultured in Dulbecco's modified Eagle's medium (DMEM) supplemented with 10% fetal bovine serum (FBS) and 1% antibiotics (all from Thermofisher). Cells were routinely grown on 25 cm^2 flasks and maintained in a 5% CO_2 incubator at 37 °C in a 95% humidified atmosphere containing 5% CO_2. Cells grown on 25 cm^2 flasks were detached using trypsin-EDTA solution (Thermofisher). Cells were then diluted in culture medium and seeded into silicone Culture-Insert 2 well in 24 wells-plate (Ibidi) developed for wound healing assay at approximately 200,000 cells per plate well. After cells reached confluence, inserts were removed to create a gap and wells were washed 3 times with culture medium free of FBS and antibiotics. Cells were then treated with

RumC1 or left untreated in culture medium supplemented with 1% FBS. Cells incubated with culture medium supplemented with 10% FBS were used as a positive control. Nomarsky interference contrast images were acquired daily.

BIBLIOGRAPHY

1. Martínez, J. L. Effect of antibiotics on bacterial populations: a multi-hierachical selection process. *F1000Res* **6**, (2017).
2. Richardson, L. A. Understanding and Overcoming Antibiotic Resistance. *PLOS Biology* **2017**, *15* (8), e2003775.
3. Murray, A. K.; Zhang, L.; Yin, X.; Zhang, T.; Buckling, A.; Snape, J.; Gaze, W. H. Novel Insights into Selection for Antibiotic Resistance in Complex Microbial Communities. *mBio.* **2018**, *9* (4).
4. Aminov, R. I. A Brief History of the Antibiotic Era: Lessons Learned and Challenges for the Future. *Front. Microbiol.* **2010**, *1*.
5. Ventola, C. L. The Antibiotic Resistance Crisis. *P. T.* **2015**, *40* (4), 277–283.
6. Aslam, B.; Wang, W.; Arshad, M. I.; Khurshid, M.; Muzammil, S.; Rasool, M. H.; Nisar, M. A.; Alvi, R. F.; Aslam, M. A.; Qamar, M. U.; Salamat, M. K. F.; Baloch, Z. Antibiotic Resistance: A Rundown of a Global Crisis. *Infect. Drug. Resist.* **2018**, *11*, 1645–1658.
7. O'Neill, J. Tackling Drug-Resistant Infections Globally: Final Report and Recommendations (Review on Antimicrobial Resistance, **2016**).
8. Dadgostar, P. Antimicrobial Resistance: Implications and Costs. *Infect Drug Resist* **2019**, *12*, 3903–3910.
9. Lewis, K. Platforms for Antibiotic Discovery. *Nat. Rev. Drug. Discov.* **2013**, *12* (5), 371–387.
10. Aminov, R. History of Antimicrobial Drug Discovery: Major Classes and Health Impact. *Biochem. Pharmacol.* **2017**, *133*, 4–19.
11. Ghosh, C.; Sarkar, P.; Issa, R.; Haldar, J. Alternatives to Conventional Antibiotics in the Era of Antimicrobial Resistance. *Trends Microbiol.* **2019**, *27* (4), 323–338.
12. Arnison, P. G.; Bibb, M. J.; Bierbaum, G.; Bowers, A. A.; Bugni, T. S.; Bulaj, G.; Camarero, J. A.; Campopiano, D. J.; Challis, G. L.; Clardy, J.; Cotter, P. D.; Craik, D. J.; Dawson, M.; Dittmann, E.; Donadio, S.; Dorrestein, P. C.; Entian, K.-D.; Fischbach, M. A.; Garavelli, J. S.; Göransson, U.; Gruber, C. W.; Haft, D. H.; Hemscheidt, T. K.; Hertweck, C.; Hill, C.; Horswill, A. R.; Jaspars, M.; Kelly, W. L.; Klinman, J. P.; Kuipers, O. P.; Link, A. J.; Liu, W.; Marahiel, M. A.; Mitchell, D. A.; Moll, G. N.; Moore, B. S.; Müller, R.; Nair, S. K.; Nes, I. F.; Norris, G. E.; Olivera, B. M.; Onaka, H.; Patchett, M. L.; Piel, J.; Reaney, M. J. T.; Rebuffat, S.; Ross, R. P.; Sahl, H.-G.; Schmidt, E. W.; Selsted, M. E.; Severinov, K.; Shen, B.; Sivonen, K.; Smith, L.; Stein, T.; Süssmuth, R. D.; Tagg, J. R.; Tang, G.-L.; Truman, A. W.; Vederas, J. C.; Walsh, C. T.; Walton, J. D.; Wenzel, S. C.; Willey, J. M.; van der Donk, W. A. Ribosomally Synthesized and Post-Translationally Modified Peptide Natural Products: Overview and Recommendations for a Universal Nomenclature. *Nat Prod Rep* **2013**, *30* (1), 108–160.
13. Luo; Dong. Recent Advances in the Discovery and Biosynthetic Study of Eukaryotic RiPP Natural Products. *Molecules* **2019**, *24* (8), 1541.
14. Ramare, F.; Nicoli, J.; Dabard, J.; Corring, T.; Ladire, M.; Gueugneau, A. M.; Raibaud, P. Trypsin-Dependent Production of an Antibacterial Substance by a Human Peptostreptococcus Strain in Gnotobiotic Rats and in Vitro. *Appl. Environ. Microbiol.* **1993**, *59* (9), 2876–2883.
15. Crost, E. H.; Ajandouz, E. H.; Villard, C.; Geraert, P. A.; Puigserver, A.; Fons, M. Ruminococcin C, a New Anti-Clostridium Perfringens Bacteriocin Produced in the Gut by the Commensal Bacterium Ruminococcus Gnavus E1. *Biochimie* **2011**, *93* (9), 1487–1494.

16. Chiumento, S.; Roblin, C.; Kieffer-Jaquinod, S.; Tachon, S.; Leprètre, C.; Basset, C.; Aditiyarini, D.; Olleik, H.; Nicoletti, C.; Bornet, O.; Iranzo, O.; Maresca, M.; Hardré, R.; Fons, M.; Giardina, T.; Devillard, E.; Guerlesquin, F.; Couté, Y.; Atta, M.; Perrier, J.; Lafond, M.; Duarte, V. Ruminococcin C, a Promising Antibiotic Produced by a Human Gut Symbiont. *Sci. Adv.* **2019**, *5* (9), eaaw9969.
17. Roblin, C.; Chiumento, S.; Bornet, O.; Nouailler, M.; Müller, C.; Jeannot, K.; Basset, C.; Kieffer-Jaquinod, S.; Couté, Y.; Torelli, S.; Le Pape, L.; Schüneman, V.; Olleik, H.; De La Villeon, B.; Sockeel, P.; Di Pasquale, E.; Nicoletti, C.; Vidal, N.; Poljak, L.; Iranzo, O.; Giardina, T.; Fons, M.; Devillard, E.; Polard, P.; Maresca, M.; Perrier, J.; Atta, M.; Guerlesquin, F.; Lafond, M.; Duarte, V. The Unusual Structure of Ruminococcin C1 Antimicrobial Peptide Confers Clinical Properties. *P.N.A.S.* **2020**.
18. Gholamiandekhordi, A. R.; Ducatelle, R.; Heyndrickx, M.; Haesebrouck, F.; Van Immerseel, F. Molecular and Phenotypical Characterization of Clostridium Perfringens Isolates from Poultry Flocks with Different Disease Status. *Vet. Microbiol*. **2006**, *113* (1–2), 143–152.
19. Collins, M. D.; Lawson, P. A.; Willems, A.; Cordoba, J. J.; Fernandez-Garayzabal, J.; Garcia, P.; Cai, J.; Hippe, H.; Farrow, J. A. The Phylogeny of the Genus Clostridium: Proposal of Five New Genera and Eleven New Species Combinations. *Int. J. Syst. Bacteriol.* **1994**, *44* (4), 812–826.
20. Lopetuso, L. R.; Scaldaferri, F.; Petito, V.; Gasbarrini, A. Commensal Clostridia: Leading Players in the Maintenance of Gut Homeostasis. *Gut Pathogens* **2013**, *5* (1), 23.
21. Galdiero, E.; Lombardi, L.; Falanga, A.; Libralato, G.; Guida, M.; Carotenuto, R. Biofilms: Novel Strategies Based on Antimicrobial Peptides. *Pharmaceutics* **2019**, *11* (7).
22. Ceri, H.; Olson, M. E.; Stremick, C.; Read, R. R.; Morck, D.; Buret, A. The Calgary Biofilm Device: New Technology for Rapid Determination of Antibiotic Susceptibilities of Bacterial Biofilms. *J Clin Microbiol* **1999**, *37* (6), 1771–1776.
23. Asiegbu, F. O.; Adomas, A.; Stenlid, J. Conifer Root and Butt Rot Caused by Heterobasidion Annosum; *Molecular Plant Pathology* **2005**, *6* (4), 395–409.
24. Garbelotto, M.; Gonthier, P. Biology, Epidemiology, and Control of Heterobasidion Species Worldwide. *Annu Rev Phytopathol* **2013**, *51*, 39–59.
25. Drexler, S. K.; Foxwell, B. M. The Role of Toll-like Receptors in Chronic Inflammation. *Int. J. Biochem. Cell Biol.* **2010**, *42* (4), 506–518.
26. Krutzik, S. R.; Sieling, P. A.; Modlin, R. L. The Role of Toll-like Receptors in Host Defense against Microbial Infection. *Curr. Opin. Immunol*. **2001**, *13* (1), 104–108.
27. Liu, T.; Zhang, L.; Joo, D.; Sun, S.-C. NF-KB Signaling in Inflammation. *Signal Transduction and Targeted Therapy* **2017**, *2* (1), 1–9.
28. Iacob, S.; Iacob, D. G. Infectious Threats, the Intestinal Barrier, and Its Trojan Horse: Dysbiosis. *Front. Microbiol.* **2019**, *10*.
29. Nowak, A.; Hedenstierna, M.; Ursing, J.; Lidman, C.; Nowak, P. Efficacy of Routine Fecal Microbiota Transplantation for Treatment of Recurrent Clostridium Difficile Infection: A Retrospective Cohort Study. *Int J Microbiol* **2019**, *2019*, 7395127.
30. Cunha, B. A.; Sessa, J.; Blum, S. Enhanced Efficacy of High Dose Oral Vancomycin Therapy in Clostridium Difficile Diarrhea for Hospitalized Adults Not Responsive to Conventional Oral Vancomycin Therapy: Antibiotic Stewardship Implications. *J Clin Med* **2018**, *7* (4).

31. Rea, M. C.; Dobson, A.; O'Sullivan, O.; Crispie, F.; Fouhy, F.; Cotter, P. D.; Shanahan, F.; Kiely, B.; Hill, C.; Ross, R. P. Effect of Broad- and Narrow-Spectrum Antimicrobials on Clostridium Difficile and Microbial Diversity in a Model of the Distal Colon. *Proc. Natl. Acad. Sci. U.S.A.* **2011**, *108 Suppl 1*, 4639–4644.
32. Sun, L.; Zhang, X.; Zhang, Y.; Zheng, K.; Xiang, Q.; Chen, N.; Chen, Z.; Zhang, N.; Zhu, J.; He, Q. Antibiotic-Induced Disruption of Gut Microbiota Alters Local Metabolomes and Immune Responses. *Front. Cell. Infect. Microbiol.* **2019**, *9*.
33. Zeng, M. Y.; Inohara, N.; Nuñez, G. Mechanisms of Inflammation-Driven Bacterial Dysbiosis in the Gut. *Mucosal Immunology* **2017**, *10* (1), 18–26.
34. Guan, Q. A Comprehensive Review and Update on the Pathogenesis of Inflammatory Bowel Disease. *J Immunol Res* **2019**, *2019*.
35. Lobionda, S.; Sittipo, P.; Kwon, H. Y.; Lee, Y. K. The Role of Gut Microbiota in Intestinal Inflammation with Respect to Diet and Extrinsic Stressors. *Microorganisms* **2019**, *7* (8).
36. Chao, Y.; Marks, L. R.; Pettigrew, M. M.; Hakansson, A. P. Streptococcus Pneumoniae Biofilm Formation and Dispersion during Colonization and Disease. *Front Cell Infect Microbiol* **2015**, *4*.
37. Gomes, A.; Teixeira, C.; Ferraz, R.; Prudêncio, C.; Gomes, P. Wound-Healing Peptides for Treatment of Chronic Diabetic Foot Ulcers and Other Infected Skin Injuries. *Molecules* **2017**, *22* (10).
38. Shukla, S. K.; Rao, T. S. An Improved Crystal Violet Assay for Biofilm Quantification in 96-Well Microtitre Plate. *bioRxiv* **2017**, 100214.
39. Borie, C.; Mondal, S.; Arif, T.; Briand, M.; Lingua, H.; Dumur, F.; Gigmes, D.; Stocker, P.; Barbarat, B.; Robert, V.; Nicoletti, C.; Olive, D.; Maresca, M.; Nechab, M. Enediynes Bearing Polyfluoroaryl Sulfoxide as New Antiproliferative Agents with Dual Targeting of Microtubules and DNA. *Eur. J. Med. Chem.* **2018**, *148*, 306–313.

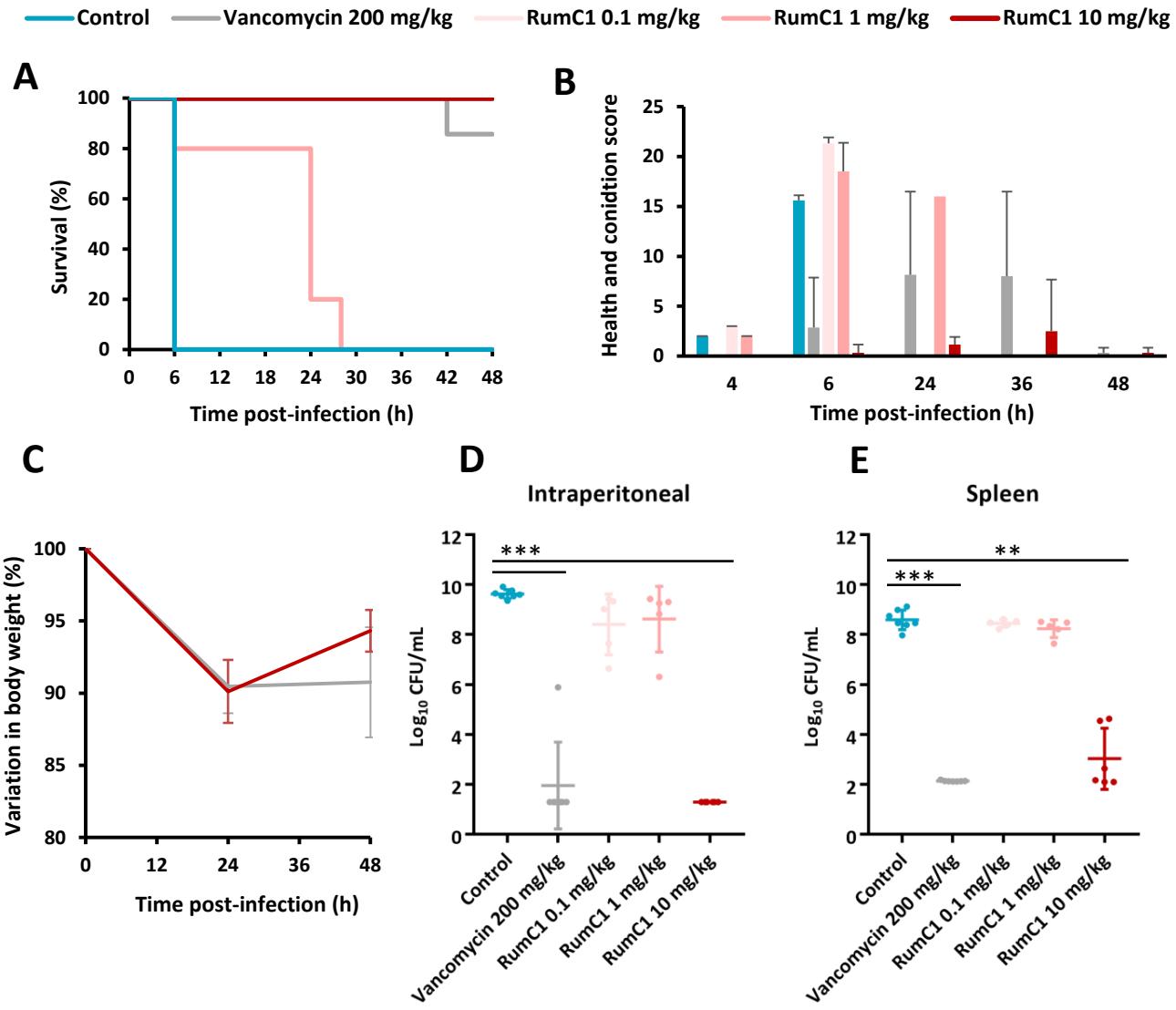

Fig. 1. In vivo antibacterial efficacy of RumC1. Mice were challenged intraperitoneally with *C. perfringens* CP24. After 0.5, 1 and 4 hours post-infection (hpi), vancomycin and RumC1 were injected intraperitoneally at 200 mg/kg or 0.1, 1 and 10 mg/kg, respectively, or PBS was injected (control). The groups were composed of 5 to 7 animals. **(A)** The survival of mice was followed over 48 h. Survival of mice that received RumC1 at 0.1 mg/kg does not appear on the figure as their survival had the same evolution as control mice. **(B)** The health and condition of mice was measured over time. High scores are representative of impaired health and physical condition. Criteria measured and observed to determinate this score are listed on **Fig S2**. **(C)** The weight of mice that were still alive at 24 and 48 hpi was measured. **(D-E)** *C. perfringens* loads found in the intraperitoneal cavity **(D)** or in the spleen **(E)** were measured by plating at time of death or at the end of the study for surviving mice (i.e. 48 hpi). Normally distributed data were analyzed using analysis of variance to compare the effects between the different groups, followed by a Bonferroni test to compare the treated groups 2 by 2 .

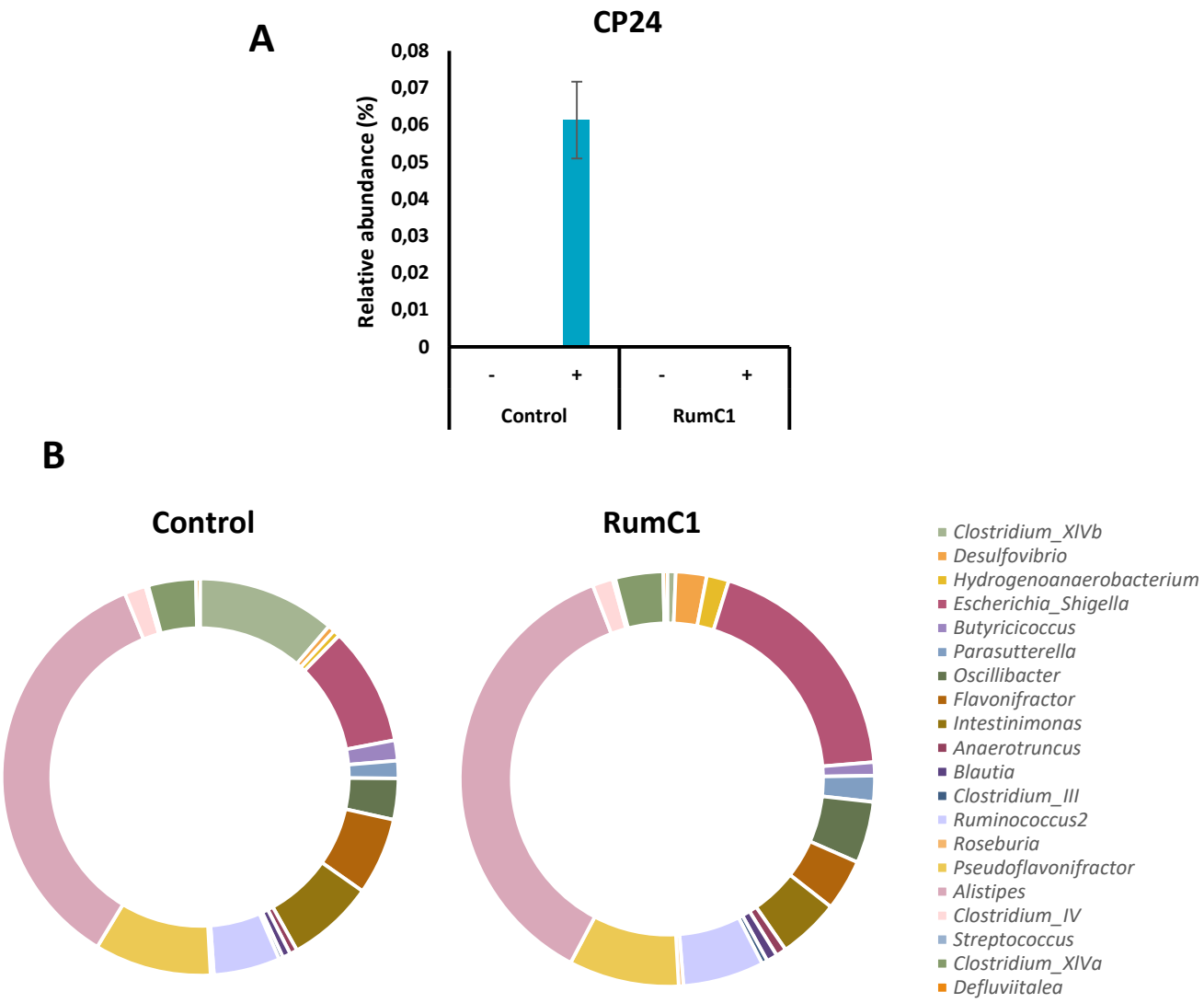

Fig. 2. Clearance of *C. perfringens* by RumC1 in a complex microbial community. Cecal contents of broilers chickens were supplemented with *C. perfringens* Cp24 at 10^6 CFU/mL (+) or not (-) and with RumC1 at 5xMIC of *C. perfringens* CP24 or left untreated (control). Microbial fermentation was then performed in anaerobic conditions for 24 h at 39°C. The composition of the microbiota from each condition was obtained by 16S rRNA sequencing. Each treatment was done on 5 replicates. **(A)** Detection of the 16S rRNA gene sequence of Cp24 and relative abundance in the microbial community. **(B)** Major genera and clusters composing the microbial communities with relative abundance > 0.1%.

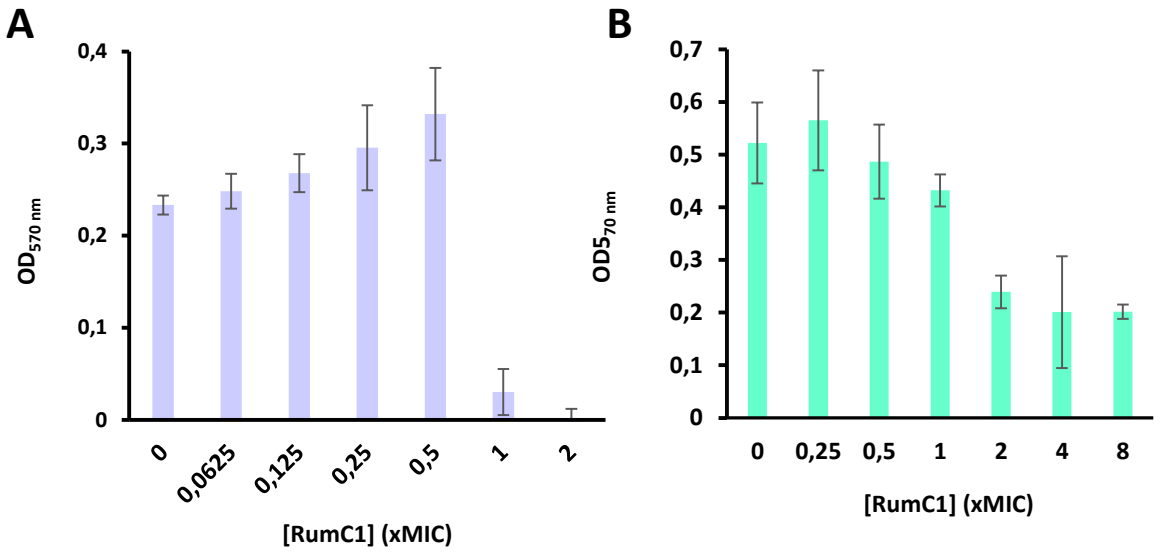

Fig. 3. Anti-biofilm activity of RumC1. Inhibition of biofilm formation **(A)** or disruption of biofilm **(B)** was evaluating on B. subtilis ATCC 6633. This strain was grown in Calgary Biofilm device in TSB for 48 h in the presence **(A)** or in the absence **(B)** of RumC1. **(B)** After 48 h of growth, the pegs from the Calgary Biofilm device were transferred to a new 96-wells plate containing fresh media supplemented with RumC1 and incubated for another additional 24 h. **(A-B)** Biofilm formation on pegs from the Calgary Biofilm device was evaluated with Crystal Violet staining as described in the Material and Methods section. Each experiment was repeated in independent triplicates.

Division	Fungi	Strain	MIC (µM)
Basidiomycetes	***Heterobasidion annosum***	**BRFM 524**	**12.5**
	Coniophora puteana	BRFM 497	> 100
Ascomycetes	*Aspergillus niger*	ATCC 9142	> 100
	Fusarium verticillioides	DSMZ 62264	> 100
	Stachybotrys chartarum	DSMZ 2144	> 100
	Microdochium bolleyi	DSM 62073	> 100
	Penicillium verrucosum	DSM 12639	> 100

Fig. 4. In vitro antifungal activity of RumC1. Activity spectrum of RumC1 against selected Ascomycetes and Basiodiomycetes strains. MIC determination were done in independent triplicates.

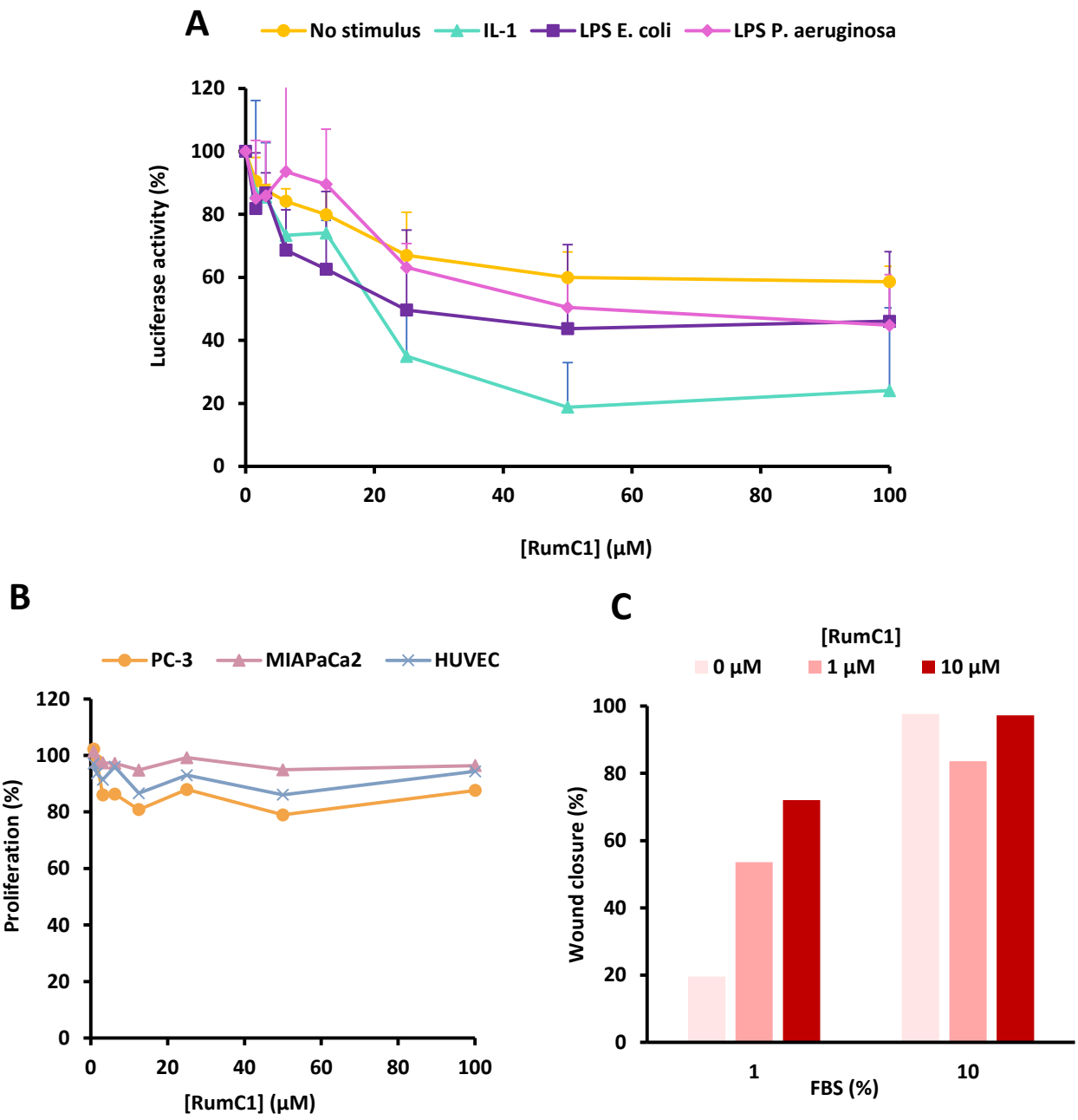

Fig. 5. Host beneficial activities of RumC1. (A) Evaluation of the anti-inflammatory effect of RumC1. HeLa eLUCidate TLR4/IL-8 cells were incubated with IL-1β, LPS from *E. coli or P. aeruginosa* or without any pro-inflammatory stimulus and then treated with increasing concentrations of RumC1. Luciferase luminescence, induced by pro-inflammatory transcription factors, was measured. **(B)** The cell lines PC-3 and MIAPaca2 as well as the primary vascular cells HUVEC were incubated with resazurin and conversion into fluorescent resorufin was monitored to determine their proliferation in the absence or presence of increasing concentration of RumC1. **(A-B)** Results are expressed as the percentage of maximum response measured without RumC1. **(C)** Percentage of gap closure during a Wound Healing assay on HaCaT cells in the absence or the presence of RumC1. Percentages of closure were measured 4 days after the gap formation and treatment. FBS at 10% was used as a positive control. **(A-C)** All experiments were done in independent triplicates (NB: measurement on triplicates are still ongoing for the wound healing assay).

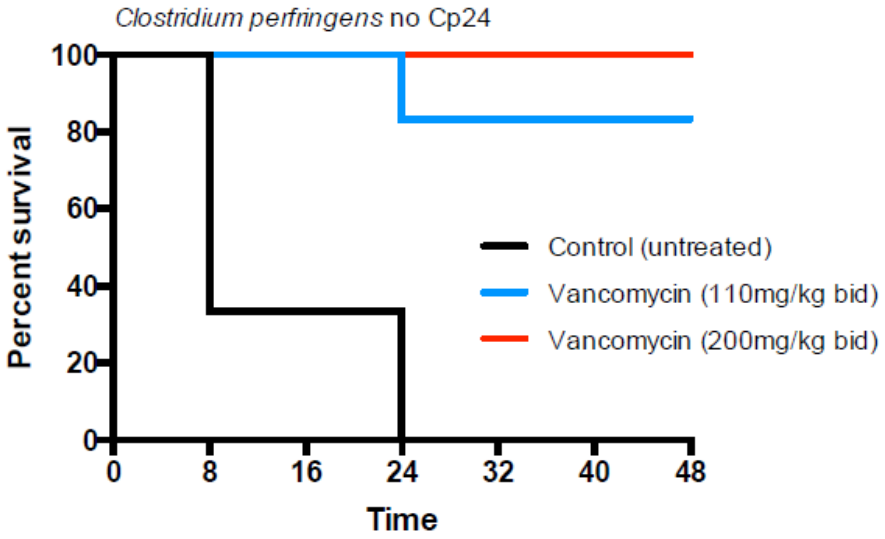

Fig. S1. In vivo efficacy of vancomycin. In preliminary in vivo studies, mice were challenged with *C. perfringens* CP24 delivered by intra-peritoneal injection and treated with vancomycin injected in the peritoneal cavity twice daily (bid). Survival was followed.

Hair	Normal, stiff	0
	Bristly	1
General morphology	Normal	0
	Abdominal swelling	1
	Arched back	2
Weight Loss	< 10% of initial weight	0
	Between 10% and 20% of initial weight	1
	> 20% of initial weight	2
Eye lids	Opened	0
	Half-opened	1
	Closed	2
Tears	None	0
	Normal looking/red	1
	Eye glued/wounded	2
Mucosa/ears colors	Normal, pink	0
	Lighter color	1
	Yellow or blue	2
Agressivity	None	0
	High (repeated biting)	1
Social behavior	United	0
	Isolated	1
Activities/games	Normal behavior	0
	Reduced activity	1
	Stereotypy	2
Breathing	Normal	0
	Faster or slower	1
	Loud/difficult/suffocation	2
Score		

Fig. S2. Health and physical condition score grid.

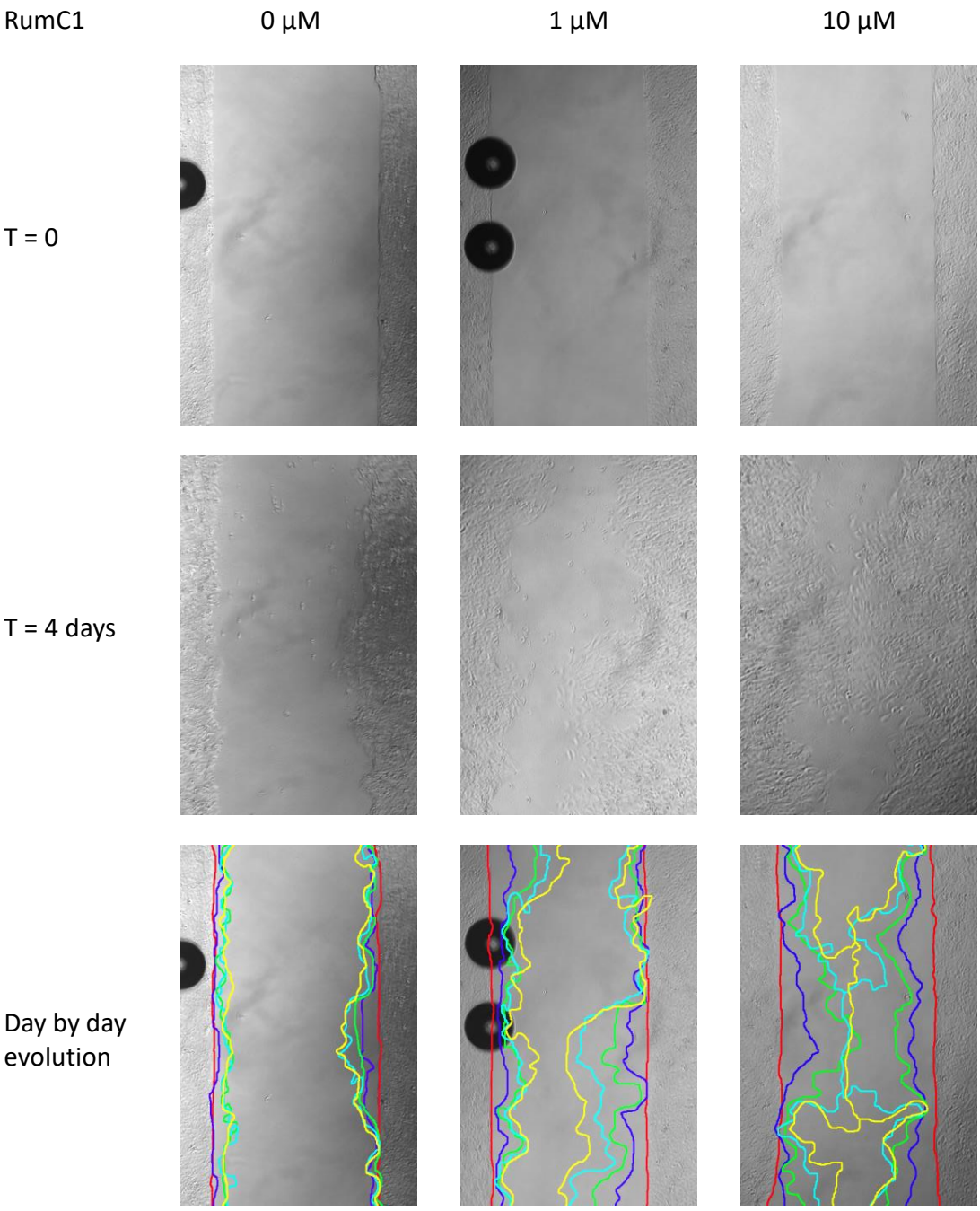

Fig. S3. Migration of HaCaT cells in 1% FBS. On the first day of the experiment, a gap was formed in a HaCaT monolayer cell culture and cells were incubated with or without RumC1 in DMEM, FBS 1%. Gap closure was followed by microscopy everyday and is represented by colored lines: red=day 0, dark blue=day 1, green= day 2, light blue= day 3, yellow=day 4.

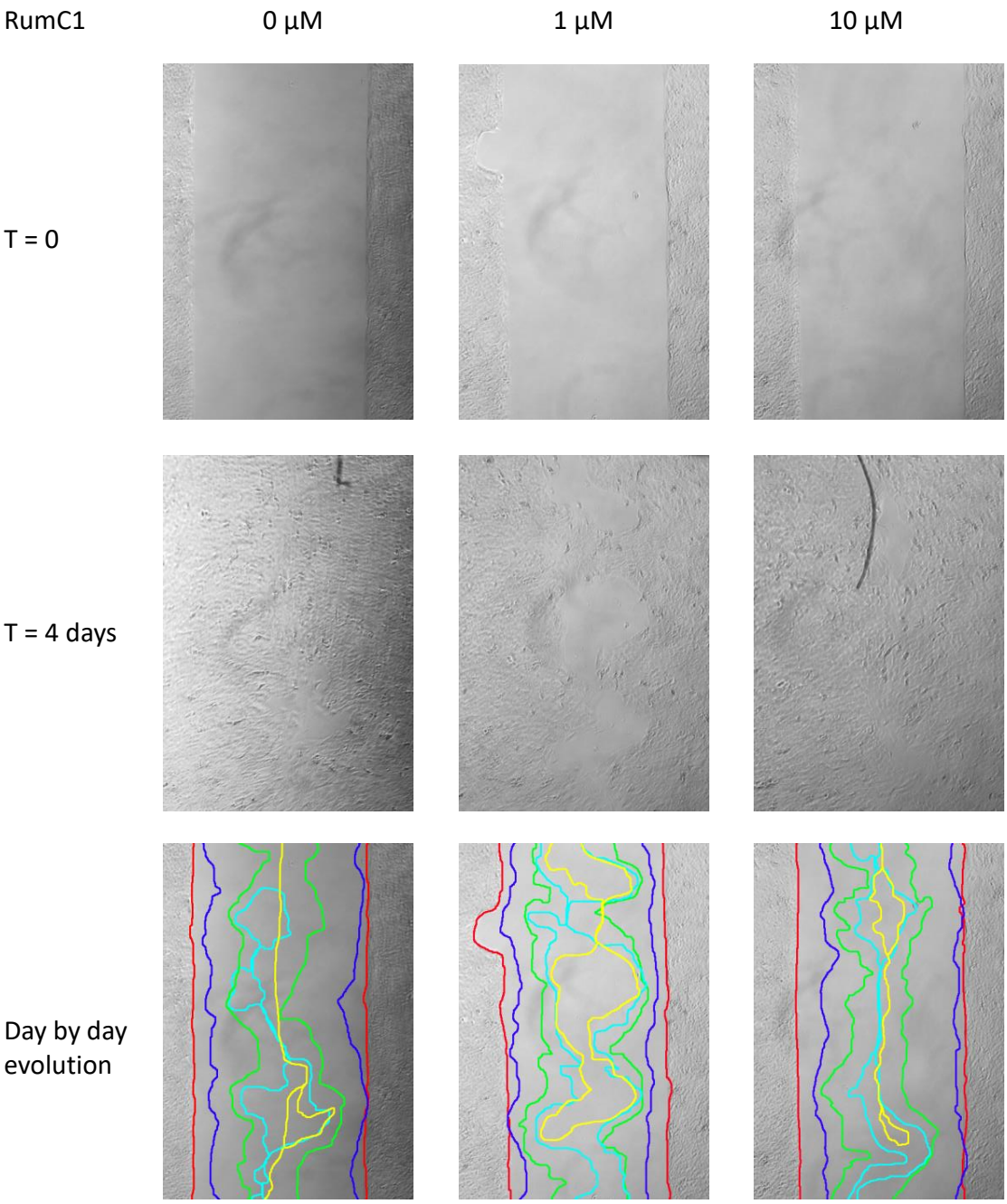

Fig. S4. Migration of HaCaT cells in 10% FBS. On the first day of the experiment, a gap was formed in a HaCaT monolayer cell culture and cells were incubated with or without RumC1 in DMEM, FBS 10%. Gap closure was followed by microscopy everyday and is represented by colored lines: red=day 0, dark blue=day 1, green= day 2, light blue= day 3, yellow=day 4.

7.3 Summary and comments

In the first two publications we demonstrated the interesting properties of RumC1 as an alternative to antibiotics in vitro. Here, we confirmed in vivo that RumC1 could be used for the treatment of bacterial infections. Notably, RumC1 is at least as efficient, if not more, as the conventional antibiotic vancomycin with a dose 20 times lower. It is conceivable that vancomycin diffuses and is eliminating by mice faster than RumC1 explaining this difference in minimal efficient dosage. Additionally, RumC1 might be more effective than vancomycin as it kills *C. perfringens* faster in vitro. The data on the time-killing of these two antimicrobials will be presented in the next chapter.

The peritoneal infection model harbors limitations as the *C. perfringens* infection is not reproduced in physiological conditions. Indeed, *C. perfringens* infections occur in the gut compartment. However, we previously showed that RumC1 stays active in the physico-chemical and biological conditions encountered in the GI tract. Moreover, in this study we demonstrated that RumC1 is able to kill *C. perfringens* in a complex intestinal microbial community. Interestingly, RumC1 targeted other Clostridia than the exogenous *C. perfringens* in this community but had no impact on *Clostridium* from the cluster IV and XIVa which are composed of major human intestinal commensals involved in gut homeostasis. One of the major inconvenient of broad-spectrum conventional antibiotics, such as vancomycin, is that they induce dysbiosis and affect commensal strains which can lead to an increase in susceptibility to intestinal infections, a compromised gut homeostasis and a deregulated metabolism (Francino, 2016). Thus, in addition to its efficacy at lower doses, RumC1's modest impact on the microbial community is another major advantage over the conventional antibiotic vancomycin for the treatment of infections caused by pathogenic Clostridia.

So far, the only other studies on the in vivo efficacy of sactipeptides concern Thuricin CD. This two-component sactipeptide has a narrower spectrum than RumC1 and in particular is active against *C. difficile*. First, Thuricin CD was shown to be as effective as vancomycin to clear a *C. difficile* infection in a distal colon ex vivo model and to cause no significant perturbation of the human microbiota used in the model whereas vancomycin provoked drastic remodelling (Rea, Dobson, et al., 2011). Then the authors of these studies attempted to show in an animal model that Thuricin CD could clear a *C. difficile* infection. *C. difficile* was delivered in the mouse colon via the rectum. Thuricin CD was then administrated via the same route 15 min later. After 6 h of infection, *C. difficile* was undetected in the colon of 6 out of the 9 mice treated whereas it was undetected only in 3 out of 10 untreated mice. However, 12 h post-infection no *C. difficile* was detected in any conditions, probably because the natural colon microbiota of the mice prevented a colonization by this pathogen. Thus, although Thuricin CD apparently accelerated the elimination of *C. difficile*, there is no proof that it would be efficient to clear a stable and lethal infection. Moreover Trn-β, one of the two sactipeptides composing Thuricin CD, is degraded in the enzymatic conditions found in the GI tract (Rea et al., 2014). Therefore, to date, RumC1 is the member of the sactipeptide subclass that shows the most promising clinical features.

In addition to its efficacy in vivo, we also demonstrated that RumC1 has other interesting biological roles. Indeed, it disrupts biofilm which can prevent the action of antibiotics by protecting the bacteria. Moreover, RumC1 has beneficial actions on the human host such as anti-inflammatory or wound healing effects. Finally, we showed that RumC1 has a highly selective anti-fungal activity. To our knowledge this is the first time a sactipeptide

is shown to have another antimicrobial activity than antibacterial. Further studies could reveal if RumC1 is active against other microorganisms such as parasites or viruses. Currently, the activity of RumC1 against SARS-CoV-2 is assayed by the team of Nicolas Lévêque in the Centre Hostpitalier Universitaire (CHU) of Poitiers.

To conclude, through this study, I completed the 4th and last objective of my thesis which concerned the in vivo activity of RumC1. The initial precise objective was to study the impact of RumC1 in healthy and *C. perfringens* infected broiler chickens. As explained in the Context subsection of this chapter, administrating RumC1 to bigger animals than mice is not conceivable presently. Thus, we had to adapt and switch the animal model. We did not administrated RumC1 in the peritoneal mouse model on healthy animals as planned on chickens since the goal of this experiments was to evaluate the perturbation induced by RumC1 on the intestinal microbiota. Instead, we studied these effects on an ex vivo chicken intestinal microbiota. In the previous three chapters of results, I exposed all the promising clinical features of RumC1. One major obstacle for the further clinical development of this sactipeptide and in particular its study in bigger animal models remains and concerns the cost of production. In order to implement more pre-clinical assays on RumC1 and eventually move to clinical assays, a cost-effective mean of production of RumC1 must be developed. A possible option would be to chemically synthesize RumC1 and perform simpler chemical bonds than sacti-bridges that would mimic the overall structure of RumC1. Another lead is to identify the molecular target of RumC1 which would allow the design of smaller biomimetic molecules. Our team have the intention to continue the work on RumC1 in both directions. During my project, I had the opportunity to work on preliminary experiments on the identification of the molecular target and this work will be presented in the next and final results chapter.

Chapter 8

Mechanism of antibacterial action of Ruminococcin C1

8.1 Context

After showing that RumC1 displays potent antibacterial activity in vitro, we demonstrated that RumC1 is active in vivo in an animal model and has interesting clinical properties. Another desirable trait for an alternative to antibiotics is a novel mechanism of action to fight strains that have developed resistance to the mechanisms of conventional antibiotics. Thus, we initiated the study of the antibacterial mechanism of action of RumC1. Moreover, as stated in the last chapter, the identification of the precise molecular target could help to overcome the production cost challenge of RumC1. Indeed, if the molecular target and its interaction with RumC1 are deciphered, smaller biomimetic molecules could be assayed as alternatives to antibiotics.

Previously, we demonstrated that unlike most RiPPs and bacteriocins targeting Gram positive bacteria, RumC1 does not have a pore-forming mode of action. Moreover, we showed that RumC1 inhibits ATP synthesis and, most likely as a consequence, the ATP-dependent synthesis pathways of macromolecules such as DNA, RNA, proteins and peptidoglycan (see Chapters 5 and 6). Here, we further characterized the mode of action of RumC1.

8.2 Preliminary data

RumC1 has a lytical action on dividing cells.

First, we assayed the ability of RumC1 to kill *C. perfringens* cells either in log or stationary phase. RumC1 was able to kill more than 99% of the cells in log phase initially present in the culture in an hour and no surviving cells were detected after 6 h of treatment. The killing mechanism of RumC1 appeared to be a little bit slower than the antibiotic metronidazole but faster than vancomycin (**Figure 1A**). On the contrary, no killing was observed even after 48 h on cells in stationary phase (**Figure 1B**). The concentration of RumC1 was increased from 5xMIC to 10xMIC, still no change of the survival of *C. perfringens* cells in stationary phase was detected. The pore-forming lanthipeptide nisin was able to kill *C. perfringens* in stationary phase with no surviving cell detected in less than an hour of treatment. On the contrary, metronidazole and vancomycin, two

antibiotics with intracellular targets, failed to kill *C. perfringens* in stationary phase at 5xMIC. Therefore, RumC1 acts with a mode of action closer to the two antibiotics than the pore-forming lanthipeptide nisin.

Nonetheless, the mechanism of action of RumC1 eventually induces cell lysis. Indeed, permeabilization of *C. perfringens* was followed by measuring the incorporation of the DNA dye SYTOX green, which is only able to cross the bacterial membranes if they are damaged. *C. perfringens* cells in early log phase were treated with nisin or RumC1 at 5xMIC and were visualized by fluorescence microscopy. Whereas the maximum fluorescence intensity was detected after 10 min of treatment with nisin and then decreased with time as DNA leaked outside of permeabilized cells, fluorescent cells were detected starting at 30 min of incubation with RumC1 and fluorescence intensity per cell surface significantly increased with time exposure (**Figures 2, S1**). Permeabilization of *C. perfringens* cells was confirmed with a second method. *C. perfringens* was again treated with nisin or RumC1 at 5xMIC or the detergent cetyltrimethylammonium bromide (CTAB) and stained with propidium iodide (PI), another DNA dye unable to enter cells with intact membrane. Whereas SYTOX green was detected by fluorescent microscopy, fluorescent intensity of propidium iodide was measured using a microplate reader (**Figure S2**). In this second method, cells are incubated in a 96-well plate and are not washed after treatment with the antimicrobials. Therefore, PI bound to DNA inside or outside of the cells is detected on the contrary to the first method in which cells stained with SYTOX green are washed and only DNA that is still inside the cells membrane is detected. An increase in PI staining was measured for RumC1 after 60 min of incubation. However, even after 2 h of treatment the relative PI fluorescence stayed low (around 13%). In this second method, relative PI staining is measured based on the maximum staining detected with CTAB, whereas the fluorescent microscopy method gives an absolute answer to whether cells have incorporated the fluorescent dye or not. Therefore the two methods are complementary and revealed that RumC1 does permeabilize *C. perfringens* cells after 30 min of incubation but with a very low signal compared to the positive control. It is possible in the case of RumC1 that the lytical action co-occurs with DNA degradation, explaining the low PI relative signal.

Because treatment with RumC1 seemed to lead to cell lysis, we observed the impact of RumC1 on cells integrity by flow cytometry. Flow cytometry gives information on the diameter and granularity of analyzed cells. *C. perfringens* cells in early log phase were treated at 5xMIC. After 15 min of incubation with RumC1, a shift toward smaller particles was denoted with flow cytometry, compared to untreated cells, which drastically increased with time. After an hour of treatment with RumC1, the population of *C. perfringens* cells was not plotted in an homogeneous populations anymore but rather as a mixture of particles from an extended range of volumes (**Figure S3**), confirming the lytical action of RumC1 on dividing cells.

To conclude, unlike nisin the primary action of RumC1 is not pore formation but it leads to cell lysis. In the 2nd publication we showed that RumC1 at the same concentration inhibits 65% of ATP synthesis after only 15 min of incubation (Roblin *et al.*, 2020), hence it is likely that in the cascade of events of the mode of action of RumC1, ATP synthesis inhibition occurs quickly and before cell lysis.

RumC1 does not induce membrane depolarization.

As mentioned above, RumC1 causes energy shortage and in particular reduction in

ATP contents in *C. perfringens*. As ATP reduction has been linked to membrane depolarization in some cases such as the action of the antimicrobial peptide gramicidin-G (Pavithrra & Rajasekaran, 2020), we evaluated the action of RumC1 on membrane depolarization of *C. perfringens*. For these experiments gramicidin-G was used as a control. *C. perfringens* cells in early log phase were incubated with RumC1, gramicidin-G at 5xMIC or left untreated before being stained with $DiBAC_4(3)$, a potential-sensitive probe that only enters into depolarized cells, and PI. Cells were then analyzed by flow cytometry (**Figure 3**). After 15 min, cells treated with gramicidin-G displayed an increase in green fluorescence proportional to $DiBAC_4(3)$ incorporation but PI was excluded as seen by the low red fluorescence intensity. Therefore, *C. perfringens* cells were depolarized but not lysed. In RumC1-treated cells, an increase in green fluorescence was denoted as well, though lower than in the case of gramicidin-G. However, it coincided with a important increase in red fluorescence, meaning that the cells were starting to lyse. Moreover, dose-dependent experiments showed that increasing concentrations of RumC1 resulted in increasing red fluorescence but equal green fluorescence whereas the opposite results were obtained with gramicidin-G (**Figure S4**). Therefore, RumC1 does not seem to cause membrane depolarization and reduction in ATP contents must come from another mechanism.

RumC1 has a membrane-bound target.

To get insight into the interaction of RumC1 with bacterial cells, RumC1 was covalently labelled with the fluorescent dye Alexa Fluor 488 (AF488) at its N-terminus. After verifying that the labelled RumC1 was still active against *C. perfringens*, cells in early log phase were treated with AF488-RumC1 at a concentration corresponding to 1xMIC. Samples were collected at 15, 30, 60 and 90 min, washed to eliminate the excess of AF488-RumC1 and then fixed. Membranes were stained with FM4-64Fx and DNA with DAPI. Images were then acquired by confocal microscopy (**Figure 4**). At any duration of treatment, some AF488-RumC1 seems to be located inside the cells. However, intense fluorescent spots are located at the cell membrane. In particular, spots of RumC1 are found at the cell poles or at the septums of dividing cells. Over time, AF488-RumC1 accumulates at the cell membrane and corresponding green fluorescence intensity increases.

Then, we repeated these experiments but this time cells were visualized by 3D-Structured Illumination Microscopy (3D-SIM) to observe the interaction between AF488-RumC1 and *C. perfringens* cells at a super-resolution level (**Figure 5**). This second microscopy technique confirmed the previous observation: while some AF488-RumC1 can be detected inside the cells, most labelled peptide is located on the entire surface of the membrane with some spots of accumulation, in particular at the septums of dividing cells. Some cells have incorporated high contents of AF488-RumC1 but in those cells, no DNA was detected, indicating that they probably have already undergone lysis.

To confirm the interaction of RumC1 with bacterial cells, we incubated another Gram-positive pathogen sensitive to RumC1, i.e. *Streptococcus pneumoniae*, with AF488-RumC1. After a short time of incubation of 2 min, *S. pneumoniae* cells in early log phase were visualized by wide-field fluorescent microscopy. In these experiments, bacterial cells were also stained with Hydroxycoumarin-amino-D-alanine (HADA), a fluorescent precursor of the peptidoglycan synthesis (**Figure S5**). During cell division, in *S. pneumoniae*, the peptidoglycan is synthesized from the septal ring at mid-cell toward the periphery (Sham et al., 2012). AF488-RumC1 is located directly upstream of the novel synthesis of

peptidoglycan in *S. pneumoniae* dividing cells.

Independently, because RumC1 is only effective on cells in log phase and not in stationary phase, we also incubated *C. perfringens* cells in stationary phase with AF488-RumC1 before acquiring images by confocal microscopy to distinguish if the lack of action of RumC1 arises from a target that wouldn't be express, or active in non-dividing cells, or the impossibility for RumC1 to enter these cells. *C. perfringens* cells in stationary phase were thus incubated with AF488-RumC1 at 1xMIC and cells were visualized by confocal microscopy as explained above (**Figure S6**). Unlike cells in log phase, not all of the cells in stationary phase were stained by AF488-RumC1. However, some of them exhibited a few spots of AF488-RumC1 with low fluorescent intensity. These spots were co-localized with accumulation of red fluorescence and therefore membrane.

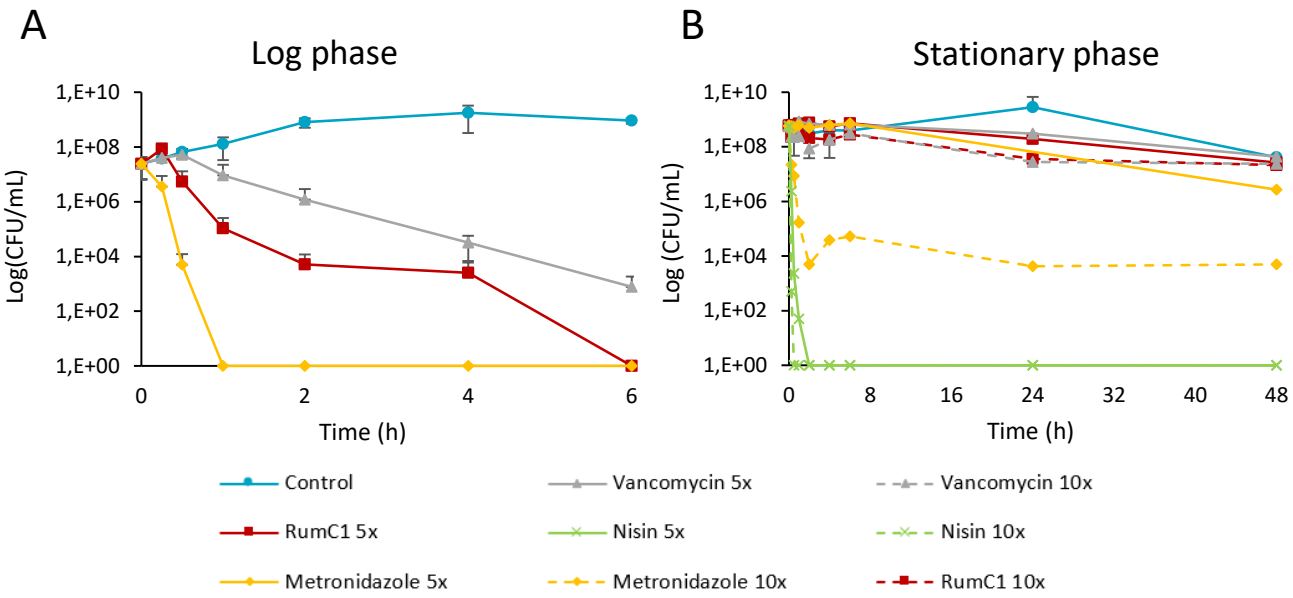

Fig. 1. Killing kinetics of *C. perfringens* by RumC1. Cells of *C. perfringens* ATCC 13124 in early log phase **(A)** or stationary phase **(B)** were treated with RumC1, vancomycin, metronidazole and nisin at 5x or 10xMIC or left untreated. After 15 or 30 min, 1, 2, 4, 6 h **(A)** and additionally 24 and 48 h **(B)**, 20 µL of each cell suspensions were collected and serial dilutions were plated on BHI-YH agar free of antibiotics. After 24h of growth in anaerobic conditions at 37°C, colonies that grew on the plates were counted. Each conditions was independently repeated twice **(A)** or once when two concentrations of each antimicrobial were assayed **(B)**.

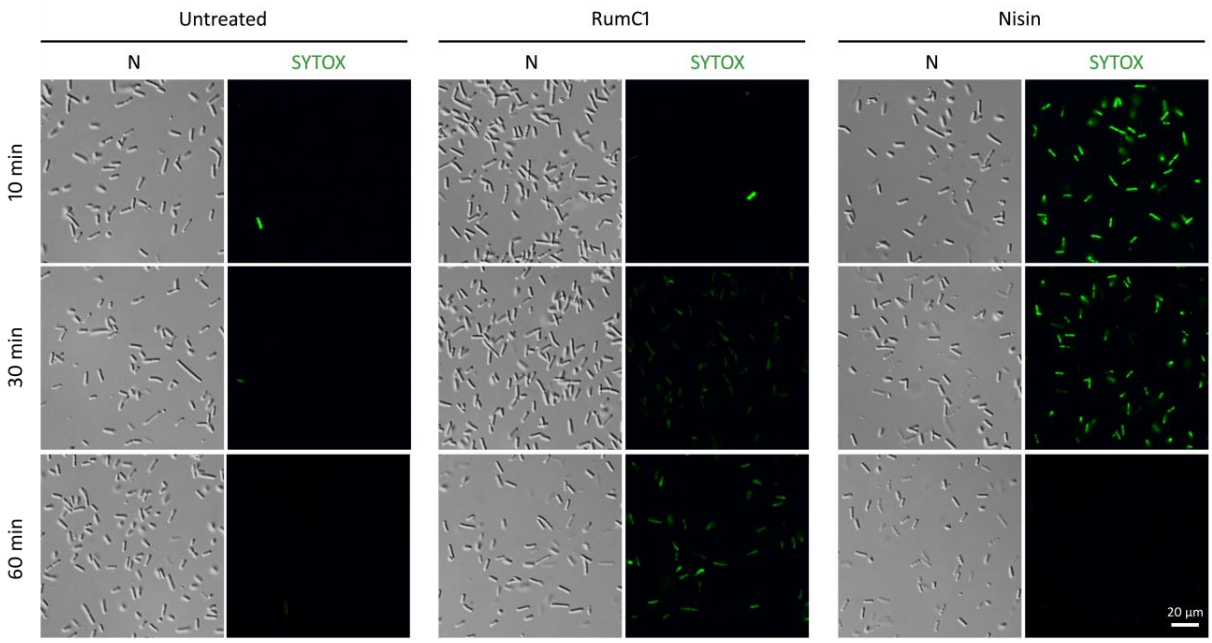

Fig. 2. Kinetics of *C. perfringens* permeabilization by RumC1. *C. perfringens* ATCC 13124 was incubated with RumC1 or nisin at 5xMIC or left untreated. After 10, 30 or 60 min of incubation in anaerobic conditions at 37°C, cells were stained with Sytox green. This dye stains DNA but is unable to cross undamaged membranes. Images of Nomarski interference contrast (N) and fluorescent signal (SYTOX) were acquired. Representative data of independent triplicates are shown.

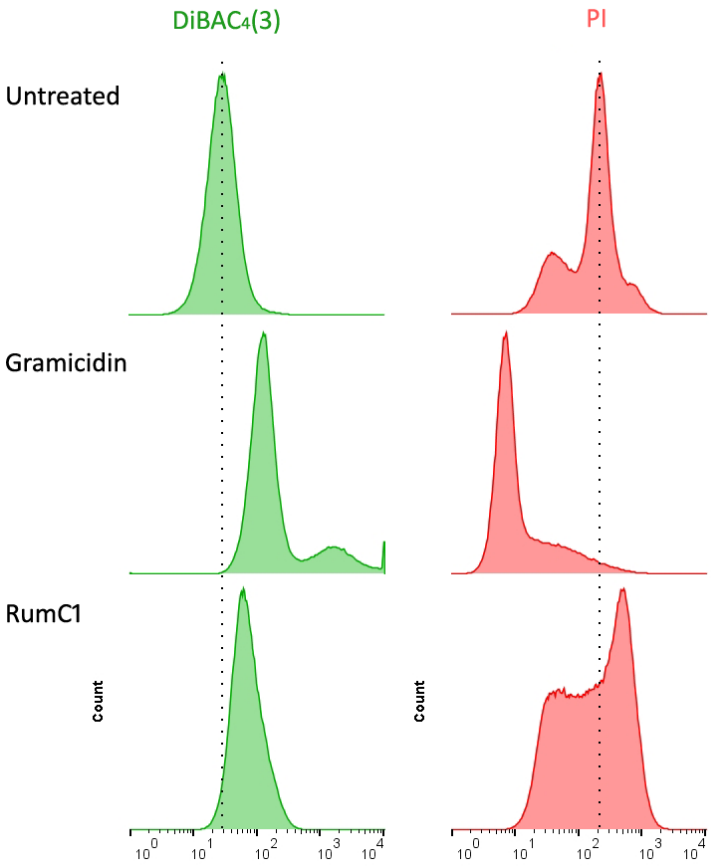

Fig. 3. Impact of RumC1 on *C. perfringens* membrane potential. *C. perfringens* ATCC 13124 was incubated with RumC1 or gramicidin at 5xMIC or left untreated. After 15 min of incubation in anaerobic conditions at 37°C, cells were stained with $DiBAC_4(3)$ and propidium iodide (PI). Green and red corresponding fluorescent signals were acquired through flow cytometry. The X axis represents the fluorescence intensity while the Y axis shows the associated number of events. Representative data of independent triplicates are shown.

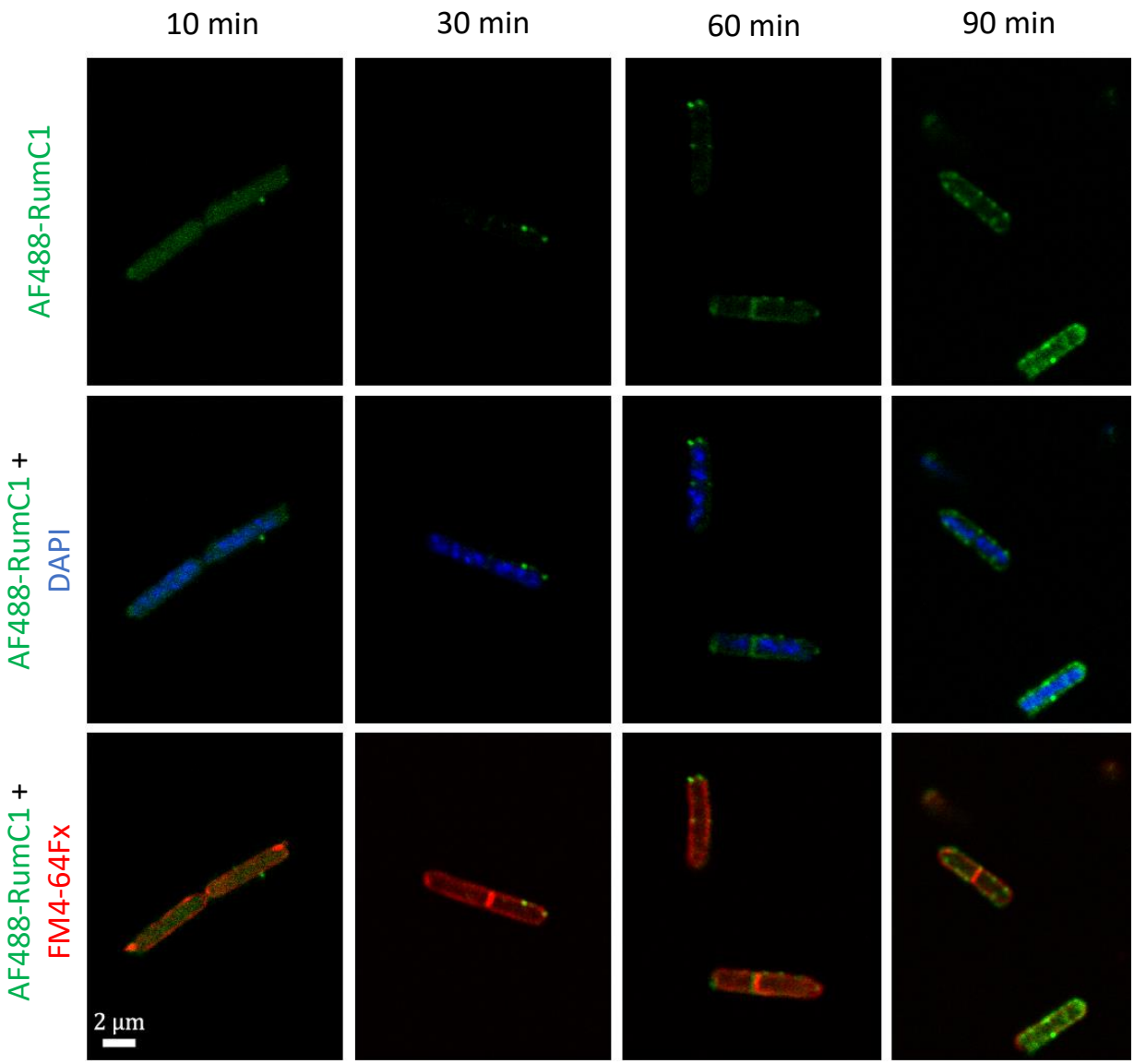

Fig. 4. Localization of RumC1 in *C. perfringens* cells by confocal microscopy. *C. perfringens* ATCC 13124 in early log phase was incubated with AF488-RumC1 at 1xMIC. After 10, 30, 60 or 90 min of incubation in anaerobic conditions at 37°C, cells were washed and then fixed. Membranes were stained with FM4-64Fx and DNA with DAPI. Representative data of independent triplicates are shown.

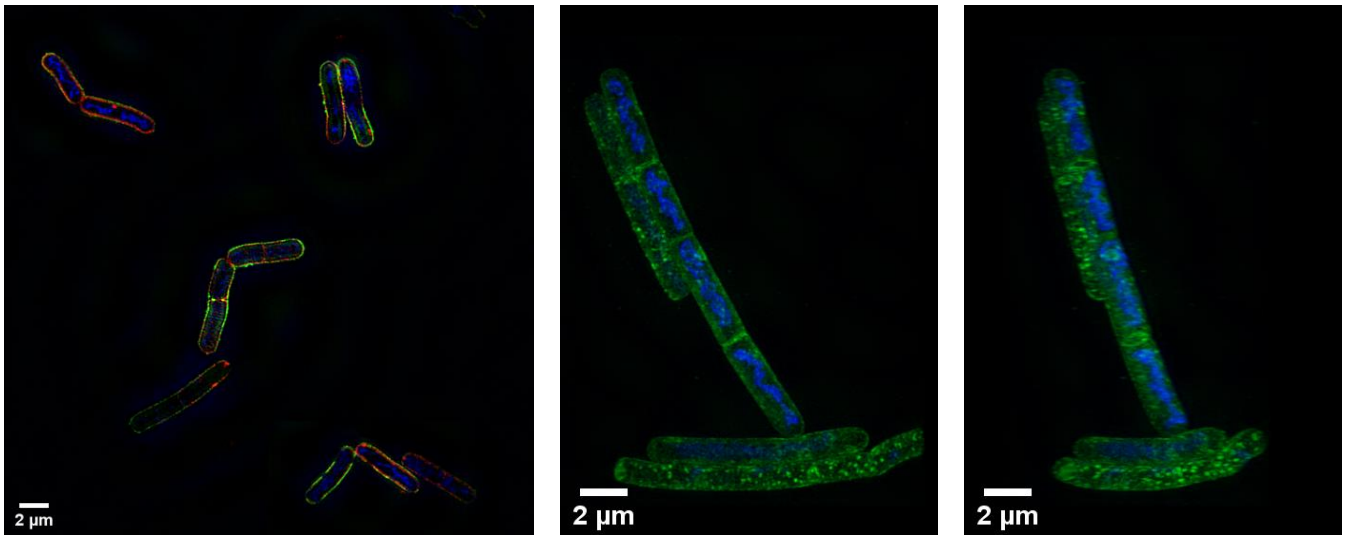

Fig. 5. Localization of RumC1 in *C. perfringens* cells by 3D-SIM. *C. perfringens* ATCC 13124 in early log phase was incubated with AF488-RumC1 at 1xMIC. After 60 of incubation in anaerobic conditions at 37°C, cells were washed and then fixed. Membranes were stained with FM4-64Fx and DNA with DAPI.

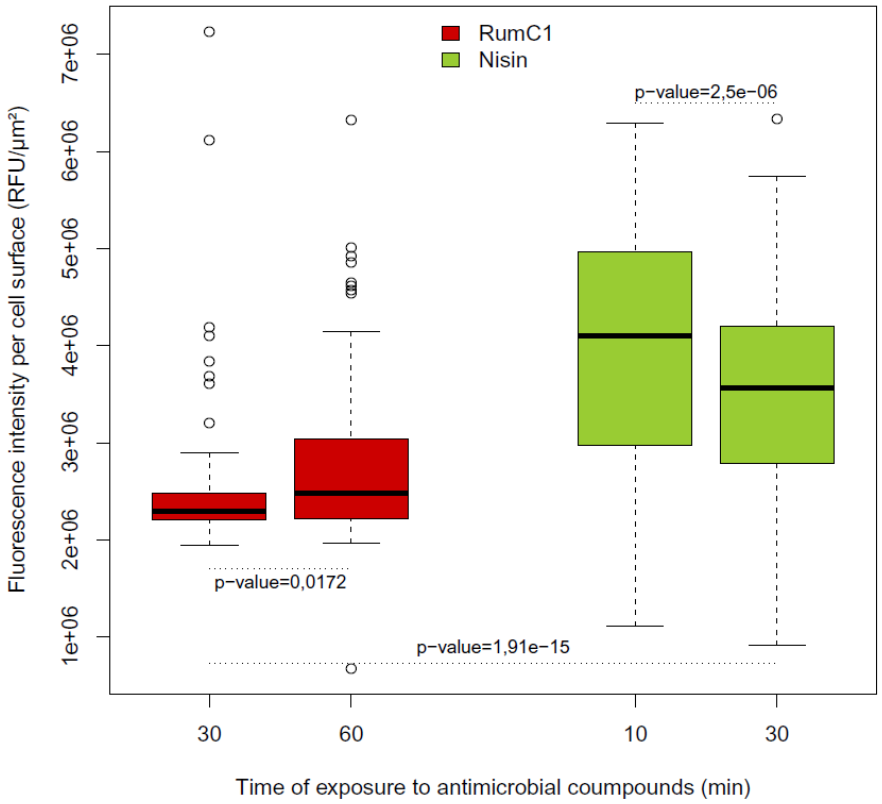

Fig. S1. Quantification of Sytox green incorporation. *C. perfringens* ATCC 13124 was incubated with RumC1 or nisin at 5xMIC or left untreated. After 10, 30 or 60 min of incubation in anaerobic conditions at 37°C, cells were stained with Sytox green. This dye stains DNA but is unable to cross undamaged membranes. The fluorescent signal per cell surface was quantified on a mean of 200 hundred cells from different fields and statistically analyzed by Mann-Whitney-Wilcoxon test. P-values are indicated on the figure.

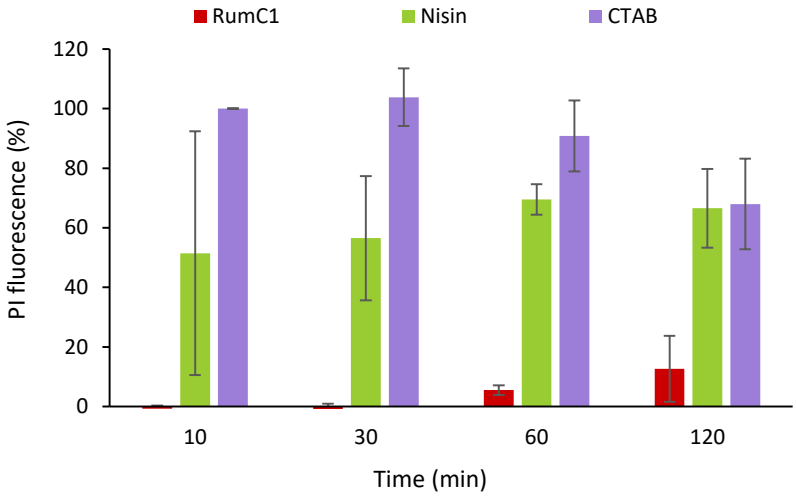

Fig. S2. Kinetics of propidium iodide incorporation. *C. perfringens* was incubated with RumC1 or nisin at 5xMIC. After 10, 30 or 60 min of incubation in anaerobic conditions at 37°C, cells were stained with propidium iodide and fluorescent signal (excitation at 535 nm, emission at 617 nm) was acquired. Propidium iodide stains DNA but is unable to cross undamaged membranes. Cells incubated with cetyltrimethylammonium bromide (CTAB) were used as a positive lysis control and untreated cells were used as a negative control. Experiments were done in independent triplicates.

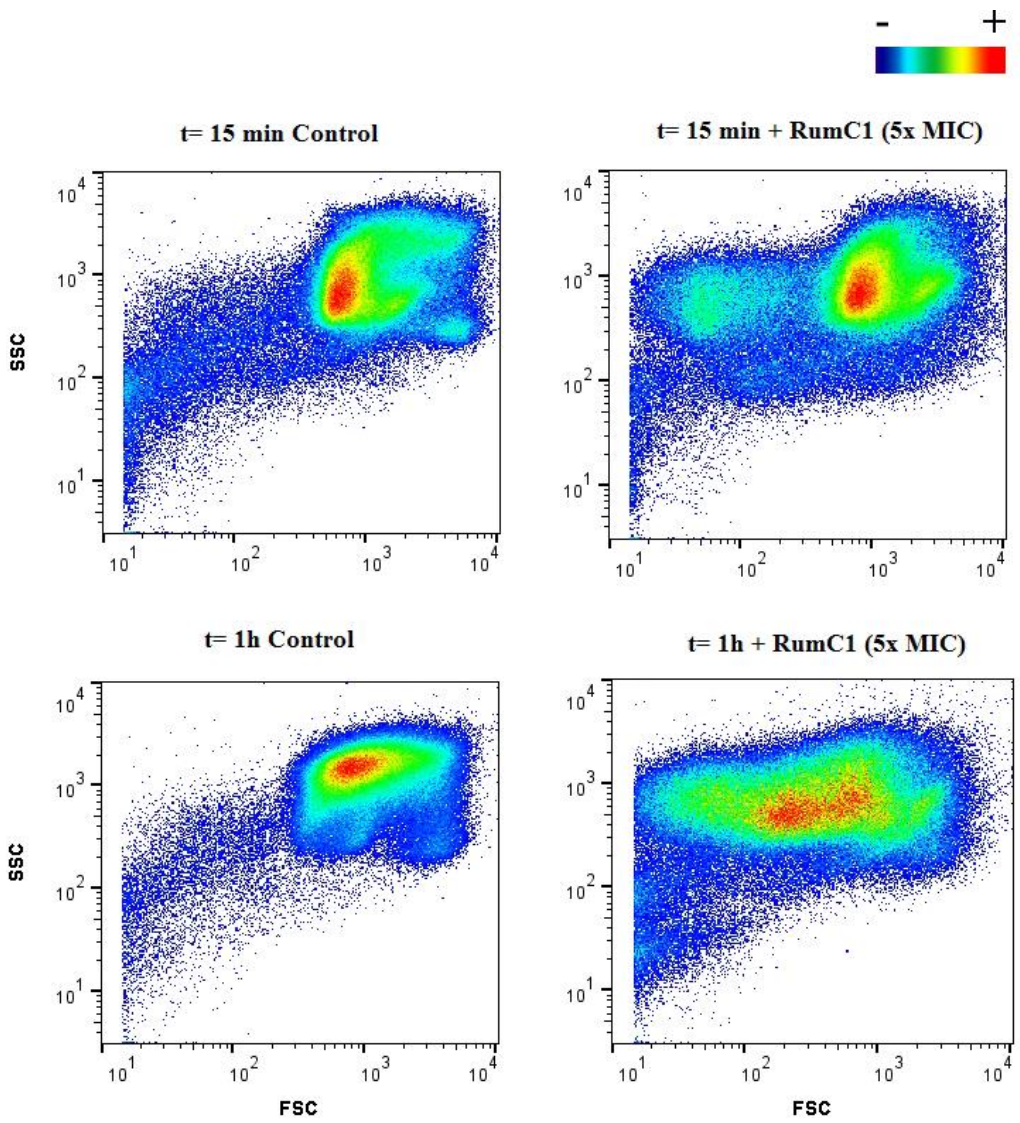

Fig. S3. Impact of RumC1 on *C. perfringens* cells integrity. *C. perfringen*s ATCC 13124 was incubated with RumC1 at 5xMIC or left untreated. After 15 min or 1 hour of incubation in anaerobic conditions at 37°C, cells were analyzed by flow cytometry. Forward Scatter (FSC) intensity is proportional to the cells diameter whereas Side Scatter (SSC) intensity depends on the cells granularity. Distribution of collected events (500 000 for each condition) is given in a color-code indicated at the top of the figure. Representative data of independent triplicates are shown.

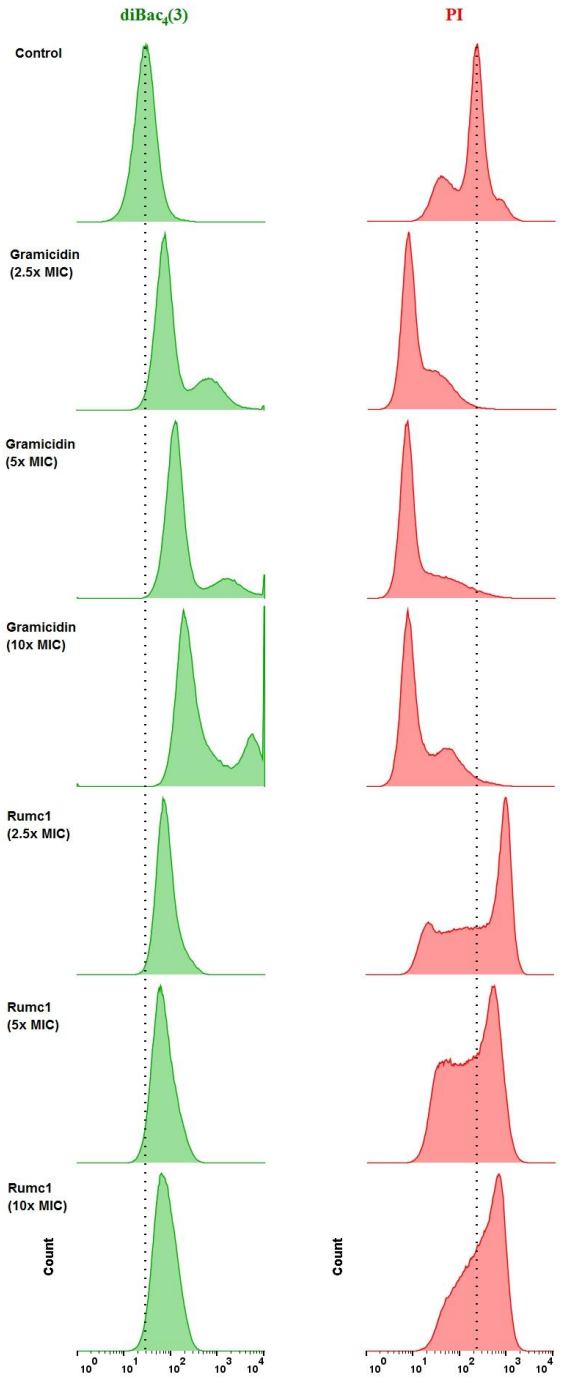

Fig. S4. Dose-dependent impact of RumC1 on *C. perfringens* membrane potential. *C. perfringens* ATCC 13124 was incubated with RumC1 or gramicidin at 2.5, 5 or 10xMIC or left untreated. After 15 min of incubation in anaerobic conditions at 37°C, cells were stained with DiBAC$_4$(3) and propidium iodide (PI). Green and red corresponding fluorescent signals were acquired through flow cytometry. The X axis represents the fluorescence intensity while the Y axis shows the associated number of events. Representative data of independent triplicates are shown.

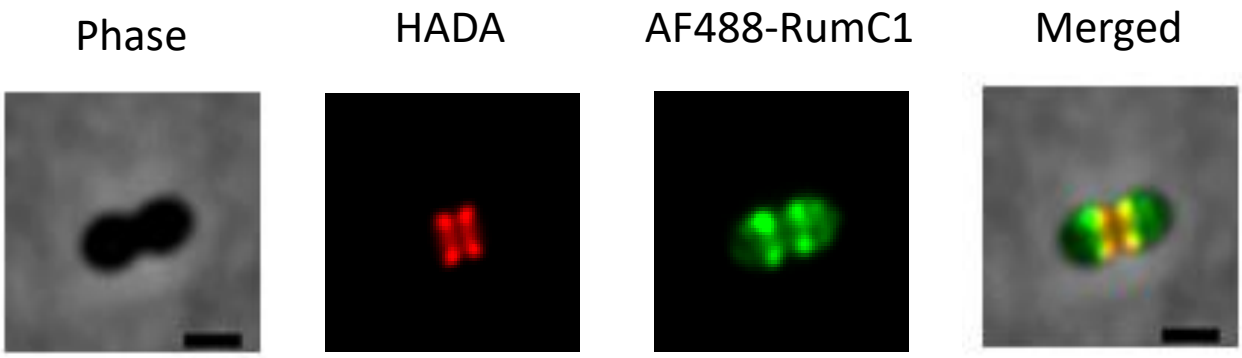

Fig. S5. Localization of RumC1 in *S. pneumoniae* cells by wide-field fluorescent microscopy. *S. pneumoniae* R1501 in early log phase was incubated with AF488-RumC1 at 1xMIC. After 2 min of incubation, cells were washed. Nascent peptidoglycan was stained with HADA.

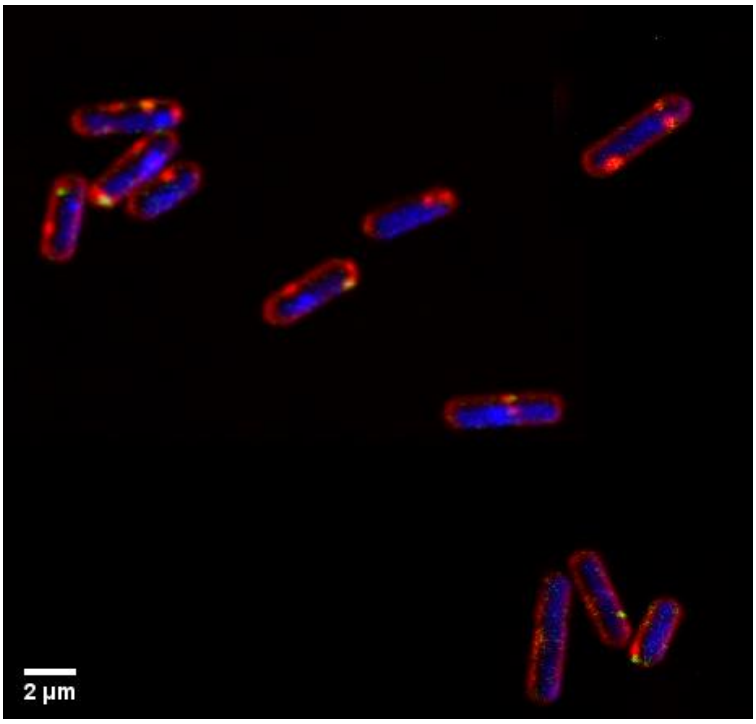

Fig. S6. Localization of RumC1 in *C. perfringens* cells in stationary phase by confocal microscopy. *C. perfringens* ATCC 13124 in stationary phase was incubated with AF488-RumC1 at 1xMIC. After 60 min of incubation in anaerobic conditions at 37°C, cells were washed and then fixed. Membranes were stained with FM4-64Fx and DNA with DAPI.

8.3 Material and Methods

Time-kill kinetics assay

C. perfringens ATCC 13124 was grown in BHI-YH in anaerobic conditions at 37°C overnight. For the studies on log phase cells, the overnight culture was diluted to 1:100 in BHI-YH and grown until OD_{600} reached 0.3 before being treated with RumC1, nisin, vancomycin, or metronidazole at 5xMIC. For the studies on stationary phase cells, the overnight culture was treated directly with the same antimicrobials at 5 or 10xMIC. In both cases, untreated cells were used as a control of natural growth and death. Cells were incubated in anaerobic conditions. At 15, 30 min, 1, 2, 4, 6, 24, 48 h, 20 µL of each cell suspension were collected and serial diluted. Dilutions were plated on BHI-YH agar and after 24 h of growth in anaerobic conditions at 37°C, colonies were counted to determine the CFU/mL. For the log phase studies, each conditions was repeated twice independently. For the stationary phase studies, each antimicrobial was studied once at the two concentrations.

Permeabilization assay by SYTOX green incorporation

An overnight culture of *C. perfringens* ATCC 13124 was diluted at 1:100 in BHI-YH and grown at 37°C under anaerobic conditions until OD_{600} reached 0.3. Cells were then treated with RumC1 or nisin at 5× their MIC values for 10, 30 or 60 min or left untreated before being stained with SYTOX Green (Thermo Fisher Scientific) at 0.5 µM. Then, cells were rinsed with Hanks' balanced salt solution +/+ (Gibco) and resuspended in VECTASHIELD (Vector Laboratories, CliniSciences H-1000). Observations were lastly performed with a Leitz DMRB microscope (Leïca), equipped with a Leïca DFC 450C camera. Fluorescence per cell surface was calculated with the software Fiji on a mean of 200 cells per condition. Fluorescence per cell surface was statistically analyzed by Mann-Whitney-Wilcoxon using the software R.

Permeabilization assay by PI incorporation

An overnight culture of *C. perfringens* ATCC 13124 was diluted at 1:100 in BHI-YH and grown at 37°C under anaerobic conditions until OD_{600} reached 0.3. Cells were then pelleted for 5 min at 3,500 rpm before being resuspended in sterile Phosphate-Buffered Saline (PBS) in their original volume. PI (Sigma-Aldrich) was then added to the suspension at a final concentration of 40 µM. One hundred microliters of this suspension were then transferred into a 96-well black plate (Greiner Bio-One) and treated with RumC1 or nisin at 5× their MIC values. Water and CTAB diluted at 300 µM final concentration were used as negative and positive controls, respectively. After 10, 30, 60 and 120 min of incubation at 37°C under anaerobic conditions, fluorescence was measured (excitation at 530 nm and emission at 617 nm) using a microplate reader (Synergy Mx, BioTek). Results were expressed as the percentage of total permeabilization obtained by treatment with CTAB. All experiments were done in independent triplicate.

Flow cytometry

An overnight culture of *C. perfringens* ATCC 13124 was diluted at 1:100 in BHI-YH and grown at 37°C under anaerobic conditions until OD_{600} reached 0.3. Cells were then treated with RumC1 or gramicidin at 2.5x, 5x and 10x their MIC values for 15 or 60 min or left untreated. Cells were then pelleted and diluted in an appropriate volume of PBS before being analyzed by flow cytometry on a Bio-Rad S3E cells sorter. The blue laser (488nm, 100mW) was used for forward (FSC), side scatter (SSC) and excitation of the $DiBAC_4(3)$ probe (1.9 µM) whereas the yellow-green laser (561 nm, 100 mW) was used for

excitation of the DNA binding propidium iodide (PI, 40 µM). Signals were collected using the emission filters FL1 (525/30 nm) and FL4 (655/LP), respectively. Samples were run in the low pressure mode at about 10,000 particles/s. The threshold on FSC was about 0.16% and the voltages of the photomultipliers 362, 308, 724 and 622 volts for FSC, SSC, FL1 and FL4, respectively. The density plots obtained (small angle scattering FSC versus wide angle scattering SSC signal) were first gated on the population of cells, filtered to remove the multiple events and finally gated for $DiBAC_4(3)$ (FL1) and PI (FL4) intensity signals. Populations of 500,000 events were used and analyzed statistically. Measurements were carried out at least three times with bacteria from different cultures. Results were analysed and plotted using FlowJO v10.6.

Fluorescent labelling of RumC1

Lyophilized AF488 (Thermo Fisher Scientific) was resuspended in 20% DMSO at 12 mM. RumC1 was then mixed with AF488 at a ratio of 1:5 (w/w) in $NaHCO_3$ 0.15 M pH 8.3. The coupling was performed at room temperature for 1 h in the dark. Then conjugated AF488-RumC1 was purified by RP-C18-HPLC. RumC1 was detected at 214 and 280 nm, while AF488 was detected at 500 nm. AF488-RumC1 was then lyophilized and resuspended in water.

Localization of RumC1 by fluorescent microscopy

C. perfringens ATCC 13124 cells in log or stationary phases were prepared as described for the time-kill kinetics assays. Cells were then treated with AF488-RumC1 at a concentration corresponding to 1xMIC of *C. perfringens* in log phase and incubated in anaerobic conditions at 37°C. Untreated cells as well as cells incubated with AF488 alone were used as controls. After 10, 30, 60 or 90 min, cells were washed with Hanks' balanced salt solution +/+ (Gibco). Cells were stained with DAPI (Sigma) at a final concentration of 2 µg/mL and with FM4-64Fx (Thermo Fisher Scientific) at a final concentration of 12 µg/mL. Cells were then fixed with PFA 4% (Sigma) for 15 min before being rinsed again and then resuspended in VECTASHIELD (Vector Laboratories, CliniSciences H-1000). For confocal studies, 8 µL were then transferred onto microscope glass slides. Images were collected using Confocal Olympus FV1000 microscope. For 3D-SIM, 1 µL of cells was transferred on pads composed of 20% Luria-Bertani broth, 1% agarose. Images were collected using an Structured Illumination Microscopy (SIM) DeltaVision OMX SR.

S. pneumoniae R1501 was grown at 37°C until OD_{550} reached 0.3 in Todd-Hewitt medium supplemented with 0.5% Yeast Extract (THY). Then, cells were treated with AF488-RumC1 at 1xMIC and HADA (Kuru et al., 2012) at 50 µM for 2 min before being rinsed with PBS. Cells were spotted on a microscope slide containing pads with THY medium. Phase contrast and fluorescence microscopy were performed with an automated inverted epifluorescence microscope Nikon Ti-E/B.

8.4 Summary and comments

We already concluded in our first publication that RumC1 does not have a pore-forming mechanisms of action (Chiumento *et al.*, 2019). The selective killing of RumC1 toward dividing cells, unlike nisin, corroborates this postulate. In this first publication, data presented no increase in PI signal over time after treatment with RumC1 on *C. perfringens* cells. However, although the experiment was similar, *C. perfringens* in stationary phase were used instead of cells in log phase and as seen above RumC1 is not active against cells in stationary phase. Moreover we also studied the incorporation of SYTOX green after a short incubation time (i.e. 15 min) with RumC1 or nisin and observed no incorporation of the green fluorescent dye in RumC1-treated log phase cells in opposition to nisin-treated cells. Therefore the lytical action of RumC1 was undetected. Here, through several methods (i.e. fluorescent microscopy, fluorescent spectroscopy and flow cytometry), the lytical action of RumC1 is demonstrated.

The cell lysis is not the direct antibacterial action of RumC1 but rather appears to be a consequence of the activity of RumC1 involving first ATP synthesis inhibition. The data gathered on RumC1 are not sufficient so far to conclude if DNA, RNA, proteins and peptidoglycan synthesis inhibitions occur before or after cell lysis in the timeline of event. Additional studies are also required to confirm or infirm DNA degradation in RumC1-treated cells. Inhibition of ATP synthesis by RumC1 is not induced by depolarization. However, it remains unknown if RumC1 directly targets ATP synthases or causes ATP depletion by another mechanism. In order to answer this question, the molecular target of RumC1 must be identified.

In that sense, I labelled RumC1 with a fluorescent dye to observe its cellular localization. In *C. perfringens* cells in log or stationary phase, RumC1 seems to be bound to the membrane. However, we showed in the first publication that RumC1 is unable to insert in lipids extract from *C. perfringens* and thus in its membrane (Chiumento *et al.,* 2019). Therefore RumC1 might target (i) the peptidoglycan or (ii) proteins inserted in the membrane or the peptidoglycan. Images acquired on *S. pneumoniae* and *C. perfringens* in stationary phase suggest that RumC1 could enter at sites of peptidoglycan synthesis. These preliminary data reveal an intriguing mode of action of RumC1, possibly undescribed to date. Many questions remain regarding the precise molecular target and cascade of events leading to ATP synthesis inhibition, macromolecules synthesis inhibition and cell lysis.

I was in charge of all the experiments described in this chapter. The flow cytometry experiments were done with Gael Brasseur from the Bacterial Chemistry Laboratory in Marseille. Cendrine Nicoletti from ISM2 was involved in SYTOX green assays. Nathalie Campo from LMGM in Toulouse was responsible of the culture and microscopy on *S. pneumoniae*. Finally 3D-SIM images were acquired with the help of Hugo Le Guenno from the microscopy platform at IMM in Marseille.

During the last months of my thesis project, I attempted some pull-down assays with RumC1 bound to sepharose beads and incubated with cell extracts of *C. perfringens*, in order to identify a molecular target. These first experiments were not concluding. It is possible that the binding site of RumC1 was not free or that the spacing between RumC1 molecules on the beads did not allow the interaction with the target. Thus, different techniques of pull-downs are considered for the future studies on the mechanisms of action of RumC1. As (i) RumC1 can be successfully labelled by AF488, (ii) AF488-RumC1 retains activity, (iii) antibodies targeting AF488 are available, a possible strategy could be

an immunoprecipitation after incubation of AF488-RumC1 with cell extracts. Another strategy could be the direct isolation of AF488-RumC1 bound to its target via native-gel electrolysis or gel filtration and detection thanks to the fluorescence of AF488. Additionnally, Nathalie Campo with Mathieu Bergé from LMGM are working on the identification of *S. pneumoniae* mutants resistant to RumC1 that could give an insight on the molecular target(s). Finally, a more precise localization of RumC1 in *C. perfringens* cells is studied by Cendrine Nicoletti by TEM using AF488-RumC1, antibodies anti-AF488 and secondary antibodies coupled do gold particles.

Chapter 9

General conclusion and perspectives

Antibiotics have emerged as "magic bullets" at the beginning of the XXth century. Nowadays, they are so common in our everyday life that we have forgotten what bacterial infections would imply without them and what medicine would look like without them. However, antibiotics should be dealt with very carefully. Antibiotics resistance is rising worldwide while their consumption keeps increasing. In the light of the recent events, as the world is shaken by a global viral pandemic, more than ever the need for functional antibiotics appears to be crucial. On one hand many patients infected with SARS-CoV-2 received unnecessary antibiotic treatments, increasing the risk of antimicrobial resistance development in the hospital setting. On the other hand, viral infections are often associated with secondary bacterial infections (Murray, 2020). As our world might be facing more viral pandemics, it is crucial that we keep a supply of active antibiotics and that we use them carefully. Moreover, antibiotic resistance is not a fast spreading pandemic like the one caused by SARS-CoV-2 but is still a pandemic, more insidious, moving at a slow pace but surely, an "invisible pandemic" as characterized by WHO. Another lesson from the Covid-19 pandemic is that microorganisms know no borders, antibiotics should be regulated and sanitation promoted to prevent spreading of infections worldwide to slow down the antibiotic crisis. One can hope that the current viral pandemic will be the opportunity to acknowledge the other health care threatening crises and to take actions to resolve them. In the mean time, finding new ways for accurate diagnosis and new antimicrobial molecules are two fields in which research can be developed to fight the antibiotic resistance crisis.

For decades, antibiotics were isolated from soil microorganisms but eventually this source dried up. Recently, research on the human microbiome and in particular the gut microbiome has blossomed (Cani, 2018). The gut microbiome is a highly diverse and complex community, composed of microorganisms that produce antimicrobials, such as soil microorganisms, as self-defense weapons for the competition for their environmental niche. However, this niche remains under-explored so far. During my thesis project, I had the opportunity to characterize one of such antimicrobials, the Ruminococcin C. The Ruminococcin C, produced by the human gut symbiont *R. gnavus* E1 in 5 isoforms, belongs to the RiPP classification. In particular, RumCs fall in the sactipeptide subclass. Through this thesis project, and more broadly the ANR RUMBA project, we have demonstrated that RumCs and in particular RumC1 are remarkably original in this subclass. First, they are the only sactipeptides isolated so far that are not produced by *Bacillus* spp. Instead, RumCs are produced in the human gut as a result of a mutualism action between the symbiont *R. gnavus* E1 and its host. Indeed, we showed that the full processing of RumC1 into an active form requires the action of both organisms. Secondly, RumC1 displays a

previously undescribed double hairpin structure, expected to be found in other RumCs, and arising from the distribution of Cys in both the N- and C-termini of the core sequence. Genome mining studies have been engaged to find more sactipeptides (Hudson et al., 2019). However, these studies have been focused on the identification of putative precursors encoding Cys in the N-terminal half of the core sequence, as found in other members of the sactipeptide subclass. New (meta-)genome mining studies based on the sequence and Cys distribution of RumCs could potentially lead to the identification of new sactipeptides. The overall structure of RumC1 is original as well as, unlike other members of the sactipeptide subclass, the surface of RumC1 is mostly hydrophilic and positively charged. From that structure might arise another particularity: RumC1 does not have a pore-forming action and seems to have a membrane-bound target or to directly target the peptidoglycan. Although the precise molecular target of RumC1 remains to be identified, we initiated the characterization of an original mode of action implying ATP synthesis inhibition as well as macromolecules synthesis inhibition and leading to cell lysis. The complex and compact structure of RumC1 is also associated with a high stability to physico-chemical and biological treatments, unidentified in the sactipeptide subclass, yet. We have demonstrated that RumC1 is a multifunctional peptide with a considerable scope of biological activities on both prokaryotes and eukaryotes. Indeed, RumC1 displays potent antibacterial activity in vitro, in bacteria growing in planktonic or biofilm mode of growth, as well as efficiency to protect an animal model from a lethal bacterial infection. In addition RumC1 exerts a selective antifungal activity. Finally, RumC1 might promote human health by positively acting on the inflammatory response or the wound healing process. So far, no other sactipeptide has been described with such extended functions.

The objectives of my thesis project were to :

1. purify the isoforms of RumC from cecal contents;
2. characterize their structures;
3. determine their activity spectra;
4. study their effects on healthy or *C. perfringens* infected broiler chickens.

Globally, these 4 objectives were fulfilled. The 5 isoforms of RumC were indeed purified from cecal contents of rats mono-associated with *R. gnavus* E1. For each of them, the PTMs involving Cys and amino acid acceptors bound by thioether bridges on their Cα were identified. However, as the amount of each isoform isolated from the in vivo purification is not sufficient for 3D-NMR studies and since RumC1 was first chosen for the development of a system of heterologous expression in *E. coli*, the three-dimensional structure of RumC was only resolved on RumC1. In a similar way, the antibacterial activity spectrum was also only determined on RumC1. Our partners at the LCBM have been working on the production of the other isoforms by heterologous expression. The studies of the activity spectra of these isoforms is expected to be performed in the near future. *R. gnavus* E1 has maintained in its genome 5 slightly divergent genes encoding precursors and we have shown that they are all produced in vivo. It would be interesting to study if they have different functions or properties or if they can act in synergy like the two sactipeptides composing Thuricin CD. Another lead for future studies concerns synergy as well, but with other antimicrobials and in particular with antibiotics. Indeed, as the costs of antimicrobial peptides and in particular RiPPs remain high, a possible

strategy to use these potent molecules could be to associate them to conventional antibiotics characterized by a lower cost of production. This strategy could help the prevention of antimicrobial resistance development as two concomitant and different mechanisms of action would be imposed to the bacteria. Moreover, as exposed recently by Mathur *et al.* (2017), some antimicrobial peptides have positive synergistic effects with antibiotics. These studies on the synergy between RumC1 and antibiotics were supposed to be initiated by a Master 1 student during an internship. However, due to the lock-down they have to be rescheduled. The last objective was to study the efficacy of RumC1 in broiler chickens, as explained before because of scale-limitations in the production of RumC1, we had to switch the animal model. Nonetheless, the efficacy of RumC1 was proven in vivo. One of the challenges for the future, presently limiting the consideration of RumC1 for clinical studies, regards the cost-effective production of RumC1 on a large scale. A possible lead is the generation of biomimetic molecules, either reproducing the entire structure of RumC1 but with different chemical bonds, or only the active antibacterial domain. For that second option to be explored, the molecular target must be identified and this task is one of the priorities in the future studies of RumC1. Finally during my project, I went beyond the initial objectives by studying other functions of RumC1. As we have shown that RumC1 can have other antimicrobial activities such as an antifungal activity, the activity spectrum of RumC1 against other microorganisms could be explored in the future. In that sense, the activity of RumC1 is currently assayed against SARS-CoV-2. To conclude, during this thesis project I participated in the elucidation of the many therapeutical properties of RumC1 and further studies should be implemented to keep deciphering its potential as a drug-lead.

References

Ahmed, M. N., Reyna-González, E., Schmid, B., Wiebach, V., Süssmuth, R. D., Dittmann, E., & Fewer, D. P. (2017). Phylogenomic Analysis of the Microviridin Biosynthetic Pathway Coupled with Targeted Chemo-Enzymatic Synthesis Yields Potent Protease Inhibitors. *ACS chemical biology*, *12*(6), 1538–1546.

Alanis, A. J. (2005). Resistance to Antibiotics: Are We in the Post-Antibiotic Era? *Archives of Medical Research*, *36*(6), 697–705.

Alvarez-Sieiro, P., Montalbán-López, M., Mu, D., & Kuipers, O. P. (2016). Bacteriocins of lactic acid bacteria: extending the family. *Applied Microbiology and Biotechnology*, *100*(7), 2939–2951.

Aminov, R. (2010). A Brief History of the Antibiotic Era: Lessons Learned and Challenges for the Future. *Frontiers in Microbiology*, *1*.

Aminov, R. (2017). History of antimicrobial drug discovery: Major classes and health impact. *Biochemical Pharmacology*, *133*, 4–19.

Arnison, P. G., Bibb, M. J., Bierbaum, G., Bowers, A. A., Bugni, T. S., Bulaj, G., Camarero, J. A., Campopiano, D. J., Challis, G. L., Clardy, J., Cotter, P. D., Craik, D. J., Dawson, M., Dittmann, E., Donadio, S., Dorrestein, P. C., Entian, K.-D., Fischbach, M. A., Garavelli, J. S., Göransson, U., Gruber, C. W., Haft, D. H., Hemscheidt, T. K., Hertweck, C., Hill, C., Horswill, A. R., Jaspars, M., Kelly, W. L., Klinman, J. P., Kuipers, O. P., Link, A. J., Liu, W., Marahiel, M. A., Mitchell, D. A., Moll, G. N., Moore, B. S., Müller, R., Nair, S. K., Nes, I. F., Norris, G. E., Olivera, B. M., Onaka, H., Patchett, M. L., Piel, J., Reaney, M. J. T., Rebuffat, S., Ross, R. P., Sahl, H.-G., Schmidt, E. W., Selsted, M. E., Severinov, K., Shen, B., Sivonen, K., Smith, L., Stein, T., Süssmuth, R. D., Tagg, J. R., Tang, G.-L., Truman, A. W., Vederas, J. C., Walsh, C. T., Walton, J. D., Wenzel, S. C., Willey, J. M., & van der Donk, W. A. (2013). Ribosomally synthesized and post-translationally modified peptide natural products: overview and recommendations for a universal nomenclature. *Natural product reports*, *30*(1), 108–160.

Arthur, T. D., Cavera, V. L., & Chikindas, M. L. (2014). On bacteriocin delivery systems and potential applications. *Future Microbiology*, *9*(2), 235–248.

Asahara, T., Nomoto, K., Shimizu, K., Watanuki, M., & Tanaka, R. (2001). Increased resistance of mice to Salmonella enterica serovar Typhimurium infection by synbiotic administration of Bifidobacteria and transgalactosylated oligosaccharides. *Journal of Applied Microbiology*, *91*(6), 985–996.

Aslam, B., Wang, W., Arshad, M. I., Khurshid, M., Muzammil, S., Rasool, M. H., Nisar, M. A., Alvi, R. F., Aslam, M. A., Qamar, M. U., Salamat, M. K. F., & Baloch, Z. (2018). Antibiotic resistance: a rundown of a global crisis. *Infection and Drug Resistance*, *11*, 1645–1658.

Azzouz, D., Omarbekova, A., Heguy, A., Schwudke, D., Gisch, N., Rovin, B. H., Caricchio,

R., Buyon, J. P., Alekseyenko, A. V., & Silverman, G. J. (2019). Lupus nephritis is linked to disease-activity associated expansions and immunity to a gut commensal. *Annals of the Rheumatic Diseases*, *78*(7), 947–956.

Balty, C., Guillot, A., Fradale, L., Brewee, C., Boulay, M., Kubiak, X., Benjdia, A., & Berteau, O. (2019). Ruminococcin C, an anti-clostridial sactipeptide produced by a prominent member of the human microbiota Ruminococcus gnavus. *Journal of Biological Chemistry*, jbc.RA119.009416.

Baquero, F., Lanza, V. F., Baquero, M.-R., del Campo, R., & Bravo-Vázquez, D. A. (2019). Microcins in Enterobacteriaceae: Peptide Antimicrobials in the Eco-Active Intestinal Chemosphere. *Frontiers in Microbiology*, *10*.

Barry, C. E. (2011). Lessons from Seven Decades of Antituberculosis Drug Discovery. *Current topics in medicinal chemistry*, *11*(10), 1216–1225.

Bartholomae, M., Buivydas, A., Viel, J. H., Montalbán-López, M., & Kuipers, O. P. (2017). Major gene-regulatory mechanisms operating in ribosomally synthesized and post-translationally modified peptide (RiPP) biosynthesis. *Molecular Microbiology*, *106*(2), 186–206.

Bastos, M. d. C. d. F., Coutinho, B. G., & Coelho, M. L. V. (2010). Lysostaphin: A Staphylococcal Bacteriolysin with Potential Clinical Applications. *Pharmaceuticals*, *3*(4), 1139–1161.

Batson, S., de Chiara, C., Majce, V., Lloyd, A. J., Gobec, S., Rea, D., Fülöp, V., Thoroughgood, C. W., Simmons, K. J., Dowson, C. G., Fishwick, C. W. G., de Carvalho, L. P. S., & Roper, D. I. (2017). Inhibition of D-Ala:D-Ala ligase through a phosphorylated form of the antibiotic D-cycloserine. *Nature Communications*, *8*(1), 1–7.

Belkum, M. J. v., Martin-Visscher, L. A., & Vederas, J. C. (2011). Structure and genetics of circular bacteriocins. *Trends in Microbiology*, *19*(8), 411–418.

Bell, A., Brunt, J., Crost, E., Vaux, L., Nepravishta, R., Owen, C. D., Latousakis, D., Xiao, A., Li, W., Chen, X., Walsh, M. A., Claesen, J., Angulo, J., Thomas, G. H., & Juge, N. (2019). Elucidation of a sialic acid metabolism pathway in mucus-foraging Ruminococcus gnavus unravels mechanisms of bacterial adaptation to the gut. *Nature Microbiology*, *4*(12), 2393–2404.

Benjdia, A., Guillot, A., Lefranc, B., Vaudry, H., Leprince, J., & Berteau, O. (2016). Thioether bond formation by SPASM domain radical SAM enzymes: C H-atom abstraction in subtilosin A biosynthesis. *Chemical Communications*, *52*(37), 6249–6252.

Ben Lagha, A., Haas, B., Gottschalk, M., & Grenier, D. (2017). Antimicrobial potential of bacteriocins in poultry and swine production. *Veterinary Research*, *48*(1), 22.

Bentley, R., & Bennett, J. W. (2003). What Is an Antibiotic? Revisited. *Advances in Applied Microbiology*, *52*, 303–331.

Bierbaum, G., & Sahl, H.-G. (2009). Lantibiotics: mode of action, biosynthesis and bioengineering. *Current Pharmaceutical Biotechnology*, *10*(1), 2–18.

Biliński, J., Grzesiowski, P., Muszyński, J., Wróblewska, M., Mądry, K., Robak, K., Dzieciątkowski, T., Wiktor-Jedrzejczak, W., & Basak, G. W. (2016). Fecal Microbiota Transplantation Inhibits Multidrug-Resistant Gut Pathogens: Preliminary Report Performed in an Immunocompromised Host. *Archivum Immunologiae Et Therapiae Experimentalis*, *64*(3), 255–258.

Binda, E., Marinelli, F., & Marcone, G. L. (2014). Old and New Glycopeptide Antibiotics: Action and Resistance. *Antibiotics*, *3*(4), 572–594.

Bionda, N., Pitteloud, J.-P., & Cudic, P. (2013). Cyclic lipodepsipeptides: a new class

of antibacterial agents in the battle against resistant bacteria. *Future medicinal chemistry*, *5*(11).

Bisacchi, G. S. (2015). Origins of the Quinolone Class of Antibacterials: An Expanded "Discovery Story": Miniperspective. *Journal of Medicinal Chemistry*, *58*(12), 4874–4882.

Bitzan, M. (2009). Treatment options for HUS secondary to Escherichia coli O157:H7. *Kidney International. Supplement*(112), S62–66.

Blanco, P., Hernando-Amado, S., Reales-Calderon, J. A., Corona, F., Lira, F., Alcalde-Rico, M., Bernardini, A., Sanchez, M. B., & Martinez, J. L. (2016). Bacterial Multidrug Efflux Pumps: Much More Than Antibiotic Resistance Determinants. *Microorganisms*, *4*(1).

Boakes, S., & Dawson, M. J. (2014). Discovery and Development of NVB302, a Semisynthetic Antibiotic for Treatment of Clostridium difficile Infection. In *Natural Products* (pp. 455–468). John Wiley & Sons, Ltd.

Bonfiglio, G., & Furneri, P. M. (2001). Novel streptogramin antibiotics. *Expert Opinion on Investigational Drugs*, *10*(2), 185–198.

Bozdogan, B., & Appelbaum, P. C. (2004). Oxazolidinones: activity, mode of action, and mechanism of resistance. *International Journal of Antimicrobial Agents*, *23*(2), 113–119.

Briers, Y., Walmagh, M., Grymonprez, B., Biebl, M., Pirnay, J.-P., Defraine, V., Michiels, J., Cenens, W., Aertsen, A., Miller, S., & Lavigne, R. (2014). Art-175 is a highly efficient antibacterial against multidrug-resistant strains and persisters of Pseudomonas aeruginosa. *Antimicrobial Agents and Chemotherapy*, *58*(7), 3774–3784.

Broderick, J. B., Duffus, B. R., Duschene, K. S., & Shepard, E. M. (2014). Radical S-Adenosylmethionine Enzymes. *Chemical Reviews*, *114*(8), 4229–4317.

Bruender, N. A., & Bandarian, V. (2016). SkfB Abstracts a Hydrogen Atom from C on SkfA To Initiate Thioether Cross-Link Formation. *Biochemistry*, *55*(30), 4131–4134.

Bruender, N. A., Wilcoxen, J., Britt, R. D., & Bandarian, V. (2016). Biochemical and Spectroscopic Characterization of a Radical S-Adenosyl-L-methionine Enzyme Involved in the Formation of a Peptide Thioether Cross-Link. *Biochemistry*, *55*(14), 2122–2134.

Burkhart, B. J., Hudson, G. A., Dunbar, K. L., & Mitchell, D. A. (2015). A prevalent peptide-binding domain guides ribosomal natural product biosynthesis. *Nature Chemical Biology*, *11*(8), 564–570.

Burkhart, B. J., Kakkar, N., Hudson, G. A., van der Donk, W. A., & Mitchell, D. A. (2017). Chimeric Leader Peptides for the Generation of Non-Natural Hybrid RiPP Products. *ACS central science*, *3*(6), 629–638.

Bushin, L. B., Clark, K. A., Pelczer, I., & Seyedsayamdost, M. R. (2018). Charting an Unexplored Streptococcal Biosynthetic Landscape Reveals a Unique Peptide Cyclization Motif. *Journal of the American Chemical Society*, *140*(50), 17674–17684.

Bédard, F., Hammami, R., Zirah, S., Rebuffat, S., Fliss, I., & Biron, E. (2018). Synthesis, antimicrobial activity and conformational analysis of the class IIa bacteriocin pediocin PA-1 and analogs thereof. *Scientific Reports*, *8*(1), 1–13. (Number: 1 Publisher: Nature Publishing Group)

Caflisch, K. M., Suh, G. A., & Patel, R. (2019). Biological challenges of phage therapy and proposed solutions: a literature review. *Expert Review of Anti-infective Therapy*, *17*(12), 1011–1041.

Calcuttawala, F., Hariharan, C., Pazhani, G. P., Ghosh, S., & Ramamurthy, T. (2015). Activity Spectrum of Colicins Produced by Shigella sonnei and Genetic Mechanism of Colicin Resistance in Conspecific S. sonnei Strains and Escherichia coli. *Antimicrobial Agents and Chemotherapy*, *59*(1), 152–158.

Cani, P. D. (2018). Human gut microbiome: hopes, threats and promises. *Gut*, *67*(9), 1716–1725.

Caruso, A., Bushin, L. B., Clark, K. A., Martinie, R. J., & Seyedsayamdost, M. R. (2019). Radical Approach to Enzymatic -Thioether Bond Formation. *Journal of the American Chemical Society*, *141*(2), 990–997.

Cascales, E., Buchanan, S. K., Duché, D., Kleanthous, C., Lloubès, R., Postle, K., Riley, M., Slatin, S., & Cavard, D. (2007). Colicin Biology. *Microbiology and Molecular Biology Reviews*, *71*(1), 158–229.

Centers for Disease Control and Prevention (CDC). (2013). Vital signs: carbapenem-resistant Enterobacteriaceae. *MMWR. Morbidity and mortality weekly report*, *62*(9), 165–170.

Chanishvili, N. (2012). Phage therapy–history from Twort and d'Herelle through Soviet experience to current approaches. *Advances in Virus Research*, *83*, 3–40.

Chekan, J. R., Ongpipattanakul, C., & Nair, S. K. (2019). Steric complementarity directs sequence promiscuous leader binding in RiPP biosynthesis. *Proceedings of the National Academy of Sciences*, *116*(48), 24049–24055.

Chen, S., Xu, B., Chen, E., Wang, J., Lu, J., Donadio, S., Ge, H., & Wang, H. (2019). Zn-dependent bifunctional proteases are responsible for leader peptide processing of class III lanthipeptides. *Proceedings of the National Academy of Sciences*, *116*(7), 2533–2538.

Chokshi, A., Sifri, Z., Cennimo, D., & Horng, H. (2019). Global Contributors to Antibiotic Resistance. *Journal of Global Infectious Diseases*, *11*(1), 36–42.

Chopra, I. (1998). Over-expression of target genes as a mechanism of antibiotic resistance in bacteria. *The Journal of Antimicrobial Chemotherapy*, *41*(6), 584–588.

Chopra, I., & Roberts, M. (2001). Tetracycline antibiotics: mode of action, applications, molecular biology, and epidemiology of bacterial resistance. *Microbiology and molecular biology reviews: MMBR*, *65*(2), 232–260 ; second page, table of contents.

Claesen, J., & Bibb, M. (2010). Genome mining and genetic analysis of cypemycin biosynthesis reveal an unusual class of posttranslationally modified peptides. *Proceedings of the National Academy of Sciences of the United States of America*, *107*(37), 16297–16302.

Coates, A., Hu, Y., Bax, R., & Page, C. (2002). The future challenges facing the development of new antimicrobial drugs. *Nature Reviews. Drug Discovery*, *1*(11), 895–910.

Cotter, P. D., Ross, R. P., & Hill, C. (2013). Bacteriocins - a viable alternative to antibiotics? *Nature Reviews. Microbiology*, *11*(2), 95–105.

Cox, G., & Wright, G. D. (2013). Intrinsic antibiotic resistance: Mechanisms, origins, challenges and solutions. *International Journal of Medical Microbiology*, *303*(6), 287–292.

Crost, E. H., Ajandouz, E. H., Villard, C., Geraert, P. A., Puigserver, A., & Fons, M. (2011). Ruminococcin C, a new anti-Clostridium perfringens bacteriocin produced in the gut by the commensal bacterium Ruminococcus gnavus E1. *Biochimie*, *93*(9), 1487–1494.

Crost, E. H., Le Gall, G., Laverde-Gomez, J. A., Mukhopadhya, I., Flint, H. J., & Juge,

N. (2018). Mechanistic Insights Into the Cross-Feeding of Ruminococcus gnavus and Ruminococcus bromii on Host and Dietary Carbohydrates. *Frontiers in Microbiology*, *9*.

Crowther, G. S., Baines, S. D., Todhunter, S. L., Freeman, J., Chilton, C. H., & Wilcox, M. H. (2013). Evaluation of NVB302 versus vancomycin activity in an in vitro human gut model of Clostridium difficile infection. *The Journal of Antimicrobial Chemotherapy*, *68*(1), 168–176.

Cui, Y., Zhang, C., Wang, Y., Shi, J., Zhang, L., Ding, Z., Qu, X., & Cui, H. (2012). Class IIa Bacteriocins: Diversity and New Developments. *International Journal of Molecular Sciences*, *13*(12), 16668–16707.

Dabard, J., Bridonneau, C., Phillipe, C., Anglade, P., Molle, D., Nardi, M., Ladiré, M., Girardin, H., Marcille, F., Gomez, A., & Fons, M. (2001). Ruminococcin A, a new lantibiotic produced by a Ruminococcus gnavus strain isolated from human feces. *Applied and Environmental Microbiology*, *67*(9), 4111–4118.

Dabrowska, K., Switała-Jelen, K., Opolski, A., Weber-Dabrowska, B., & Gorski, A. (2005). Bacteriophage penetration in vertebrates. *Journal of Applied Microbiology*, *98*(1), 7–13.

Dadgostar, P. (2019). Antimicrobial Resistance: Implications and Costs. *Infection and Drug Resistance*, *12*, 3903–3910.

Davis, K. M., Schramma, K. R., Hansen, W. A., Bacik, J. P., Khare, S. D., Seyedsayamdost, M. R., & Ando, N. (2017). Structures of the peptide-modifying radical SAM enzyme SuiB elucidate the basis of substrate recognition. *Proceedings of the National Academy of Sciences*, *114*(39), 10420–10425.

Delcour, J., Ferain, T., Deghorain, M., Palumbo, E., & Hols, P. (1999). The biosynthesis and functionality of the cell-wall of lactic acid bacteria. *Antonie Van Leeuwenhoek*, *76*(1-4), 159–184.

Ding, W., Liu, W.-Q., Jia, Y., Li, Y., van der Donk, W. A., & Zhang, Q. (2016). Biosynthetic investigation of phomopsins reveals a widespread pathway for ribosomal natural products in Ascomycetes. *Proceedings of the National Academy of Sciences of the United States of America*, *113*(13), 3521–3526.

Dinos, G. P. (2017). The macrolide antibiotic renaissance. *British Journal of Pharmacology*, *174*(18), 2967–2983.

Dinos, G. P., Athanassopoulos, C. M., Missiri, D. A., Giannopoulou, P. C., Vlachogiannis, I. A., Papadopoulos, G. E., Papaioannou, D., & Kalpaxis, D. L. (2016). Chloramphenicol Derivatives as Antibacterial and Anticancer Agents: Historic Problems and Current Solutions. *Antibiotics*, *5*(2).

Dischinger, J., Basi Chipalu, S., & Bierbaum, G. (2014). Lantibiotics: promising candidates for future applications in health care. *International journal of medical microbiology: IJMM*, *304*(1), 51–62.

Dufour, S., Labrie, J., & Jacques, M. (2019). The Mastitis Pathogens Culture Collection. *Microbiology Resource Announcements*, *8*(15).

Duquesne, S., Destoumieux-Garzón, D., Peduzzi, J., & Rebuffat, S. (2007). Microcins, gene-encoded antibacterial peptides from enterobacteria. *Natural Product Reports*, *24*(4), 708–734.

Edgar, R., Friedman, N., Molshanski-Mor, S., & Qimron, U. (2012). Reversing Bacterial Resistance to Antibiotics by Phage-Mediated Delivery of Dominant Sensitive Genes. *Applied and Environmental Microbiology*, *78*(3), 744–751.

Ekblad, B., Kyriakou, P. K., Oppegård, C., Nissen-Meyer, J., Kaznessis, Y. N., & Kris-

tiansen, P. E. (2016). Structure-Function Analysis of the Two-Peptide Bacteriocin Plantaricin EF. *Biochemistry*, *55*(36), 5106–5116.

Evans, R. L., Latham, J. A., Xia, Y., Klinman, J. P., & Wilmot, C. M. (2017). Nuclear Magnetic Resonance Structure and Binding Studies of PqqD, a Chaperone Required in the Biosynthesis of the Bacterial Dehydrogenase Cofactor Pyrroloquinoline Quinone. *Biochemistry*, *56*(21), 2735–2746.

Fabbretti, A., He, C.-G., Gaspari, E., Maffioli, S., Brandi, L., Spurio, R., Sosio, M., Jabes, D., & Donadio, S. (2015). A Derivative of the Thiopeptide GE2270A Highly Selective against Propionibacterium acnes. *Antimicrobial Agents and Chemotherapy*, *59*(8), 4560–4568.

Feeds, National Research Council (US) Committee to Study the Human Health Effects of Subtherapeutic Antibiotic Use in Animal (Ed.). (1980). *Antibiotics In Animal Feeds*. National Academies Press (US).

Fernández-Villa, D., Aguilar, M. R., & Rojo, L. (2019). Folic Acid Antagonists: Antimicrobial and Immunomodulating Mechanisms and Applications. *International Journal of Molecular Sciences*, *20*(20).

Fleming, A. (1945). Penicillin. *Nobel lecture*.

Floss, H. G., & Yu, T.-W. (2005). Rifamycin-mode of action, resistance, and biosynthesis. *Chemical Reviews*, *105*(2), 621–632.

Flühe, L., Burghaus, O., Wieckowski, B. M., Giessen, T. W., Linne, U., & Marahiel, M. A. (2013). Two [4Fe-4S] clusters containing radical SAM enzyme SkfB catalyze thioether bond formation during the maturation of the sporulation killing factor. *Journal of the American Chemical Society*, *135*(3), 959–962.

Flühe, L., Knappe, T. A., Gattner, M. J., Schäfer, A., Burghaus, O., Linne, U., & Marahiel, M. A. (2012). The radical SAM enzyme AlbA catalyzes thioether bond formation in subtilosin A. *Nature Chemical Biology*, *8*(4), 350–357.

Flühe, L., & Marahiel, M. A. (2013). Radical S-adenosylmethionine enzyme catalyzed thioether bond formation in sactipeptide biosynthesis. *Current Opinion in Chemical Biology*, *17*(4), 605–612.

Fontecave, M., Atta, M., & Mulliez, E. (2004). S-adenosylmethionine: nothing goes to waste. *Trends in Biochemical Sciences*, *29*(5), 243–249.

Francino, M. P. (2016). Antibiotics and the Human Gut Microbiome: Dysbioses and Accumulation of Resistances. *Frontiers in Microbiology*, *6*.

Frimodt-Møller, N. (1993). The mouse peritonitis model: present and future use. *The Journal of Antimicrobial Chemotherapy*, *31 Suppl D*, 55–60.

Fruciano, D. E., & Bourne, S. (2007). Phage as an antimicrobial agent: d'Herelle's heretical theories and their role in the decline of phage prophylaxis in the West. *The Canadian Journal of Infectious Diseases & Medical Microbiology = Journal Canadien Des Maladies Infectieuses Et De La Microbiologie Medicale*, *18*(1), 19–26.

Furgerson Ihnken, L. A., Chatterjee, C., & van der Donk, W. A. (2008). In vitro reconstitution and substrate specificity of a lantibiotic protease. *Biochemistry*, *47*(28), 7352–7363.

Gao, B., Peng, C., Yang, J., Yi, Y., Zhang, J., & Shi, Q. (2017). Cone Snails: A Big Store of Conotoxins for Novel Drug Discovery. *Toxins*, *9*(12).

Ghosh, C., Sarkar, P., Issa, R., & Haldar, J. (2019). Alternatives to Conventional Antibiotics in the Era of Antimicrobial Resistance. *Trends in Microbiology*, *27*(4), 323–338.

Ghoul, M., & Mitri, S. (2016). The Ecology and Evolution of Microbial Competition. *Trends in Microbiology*, *24*(10), 833–845.

Goldstein, B. P., Berti, M., Ripamonti, F., Resconi, A., Scotti, R., & Denaro, M. (1993). In vitro antimicrobial activity of a new antibiotic, MDL 62,879 (GE2270 A). *Antimicrobial Agents and Chemotherapy*, *37*(4), 741–745.

Gomez, A., Ladiré, M., Marcille, F., & Fons, M. (2002). Trypsin mediates growth phase-dependent transcriptional tegulation of genes involved in biosynthesis of ruminococcin A, a lantibiotic produced by a Ruminococcus gnavus strain from a human intestinal microbiota. *Journal of Bacteriology*, *184*(1), 18–28.

Gondil, V. S., Harjai, K., & Chhibber, S. (2020). Endolysins as emerging alternative therapeutic agents to counter drug-resistant infections. *International Journal of Antimicrobial Agents*, *55*(2), 105844.

González-Pastor, J. E., Hobbs, E. C., & Losick, R. (2003). Cannibalism by sporulating bacteria. *Science (New York, N.Y.)*, *301*(5632), 510–513.

Gordon, C. P. (2020). Synthetic strategies to access staphylococcus auto-inducing peptides as quorum sensing modulators. *Organic & Biomolecular Chemistry*, *18*(3), 379–390.

Gould, K. (2016). Antibiotics: from prehistory to the present day. *Journal of Antimicrobial Chemotherapy*, *71*(3), 572–575.

Grell, T. A. J., Goldman, P. J., & Drennan, C. L. (2015). SPASM and Twitch Domains in S-Adenosylmethionine (SAM) Radical Enzymes. *The Journal of Biological Chemistry*, *290*(7), 3964–3971.

Grell, T. A. J., Kincannon, W. M., Bruender, N. A., Blaesi, E. J., Krebs, C., Bandarian, V., & Drennan, C. L. (2018). Structural and spectroscopic analyses of the sporulation killing factor biosynthetic enzyme SkfB, a bacterial AdoMet radical sactisynthase. *The Journal of Biological Chemistry*, *293*(45), 17349–17361.

Grilli, E., Messina, M. R., Catelli, E., Morlacchini, M., & Piva, A. (2009). Pediocin A improves growth performance of broilers challenged with Clostridium perfringens. *Poultry Science*, *88*(10), 2152–2158.

Grove, T. L., Himes, P. M., Hwang, S., Yumerefendi, H., Bonanno, J. B., Kuhlman, B., Almo, S. C., & Bowers, A. A. (2017). Structural Insights into Thioether Bond Formation in the Biosynthesis of Sactipeptides. *Journal of the American Chemical Society*, *139*(34), 11734–11744.

Gu, W., Dong, S.-H., Sarkar, S., Nair, S. K., & Schmidt, E. W. (2018). The biochemistry and structural biology of cyanobactin biosynthetic enzymes. *Methods in enzymology*, *604*, 113–163.

Guillemont, J., Meyer, C., Poncelet, A., Bourdrez, X., & Andries, K. (2011). Diarylquinolines, synthesis pathways and quantitative structure–activity relationship studies leading to the discovery of TMC207. *Future Medicinal Chemistry*, *3*(11), 1345–1360.

Haft, D. H. (2009). A strain-variable bacteriocin in Bacillus anthracis and Bacillus cereus with repeated Cys-Xaa-Xaa motifs. *Biology Direct*, *4*, 15.

Haft, D. H., & Basu, M. K. (2011). Biological Systems Discovery In Silico: Radical S-Adenosylmethionine Protein Families and Their Target Peptides for Posttranslational Modification. *Journal of Bacteriology*, *193*(11), 2745–2755.

Hamada, T., Matsunaga, S., Fujiwara, M., Fujita, K., Hirota, H., Schmucki, R., Güntert, P., & Fusetani, N. (2010). Solution Structure of Polytheonamide B, a Highly Cytotoxic Nonribosomal Polypeptide from Marine Sponge. *Journal of the American Chemical Society*, *132*(37), 12941–12945.

Hammami, R., Zouhir, A., Ben Hamida, J., & Fliss, I. (2007). BACTIBASE: a new web-accessible database for bacteriocin characterization. *BMC microbiology*, *7*, 89.

Hayata, A., Itoh, H., & Inoue, M. (2018). Solid-Phase Total Synthesis and Dual Mechanism of Action of the Channel-Forming 48-mer Peptide Polytheonamide B. *Journal of the American Chemical Society*, *140*(33), 10602–10611.

Helf, M. J., Jud, A., & Piel, J. (2017). Enzyme from an Uncultivated Sponge Bacterium Catalyzes S-Methylation in a Ribosomal Peptide. *ChemBioChem*, *18*(5), 444–450.

Henke, M. T., Kenny, D. J., Cassilly, C. D., Vlamakis, H., Xavier, R. J., & Clardy, J. (2019). Ruminococcus gnavus, a member of the human gut microbiome associated with Crohn's disease, produces an inflammatory polysaccharide. *Proceedings of the National Academy of Sciences*, *116*(26), 12672–12677.

Himes, P. M., Allen, S. E., Hwang, S., & Bowers, A. A. (2016). Production of Sactipeptides in Escherichia coli: Probing the Substrate Promiscuity of Subtilosin A Biosynthesis. *ACS Chemical Biology*, *11*(6), 1737–1744.

Huang, T., Geng, H., Miyyapuram, V. R., Sit, C. S., Vederas, J. C., & Nakano, M. M. (2009). Isolation of a Variant of Subtilosin A with Hemolytic Activity. *Journal of Bacteriology*, *191*(18), 5690–5696.

Hudson, G. A., Burkhart, B. J., DiCaprio, A. J., Schwalen, C. J., Kille, B., Pogorelov, T. V., & Mitchell, D. A. (2019). Bioinformatic Mapping of Radical S-Adenosylmethionine-Dependent Ribosomally Synthesized and Post-Translationally Modified Peptides Identifies New C, C, and C-Linked Thioether-Containing Peptides. *Journal of the American Chemical Society*, *141*(20), 8228–8238.

Huh, H., Wong, S., St. Jean, J., & Slavcev, R. (2019). Bacteriophage interactions with mammalian tissue: Therapeutic applications. *Advanced Drug Delivery Reviews*, *145*, 4–17.

Huo, L., Ökesli, A., Zhao, M., & van der Donk, W. A. (2017). Insights into the Biosynthesis of Duramycin. *Applied and Environmental Microbiology*, *83*(3).

Ibrahim, M., Guillot, A., Wessner, F., Algaron, F., Besset, C., Courtin, P., Gardan, R., & Monnet, V. (2007). Control of the Transcription of a Short Gene Encoding a Cyclic Peptide in Streptococcus thermophilus: a New Quorum-Sensing System? *Journal of Bacteriology*, *189*(24), 8844–8854.

ImmuCell. (2016). United states securities and exchange commission washington, d.c. 20549 form 10-k annual report pursuant to section 13 or 15(d) of the securities exchange act of 1934.

ImmuCell. (2019). United states securities and exchange commission washington, d.c. 20549 form 10-k annual report pursuant to section 13 or 15(d) of the securities exchange act of 1934.

Jack, R. W., Tagg, J. R., & Ray, B. (1995). Bacteriocins of gram-positive bacteria. *Microbiological Reviews*, *59*(2), 171–200.

Jacoby, G. A. (2005). Mechanisms of Resistance to Quinolones. *Clinical Infectious Diseases*, *41*(Supplement_2), S120–S126.

Jin, X., Kightlinger, W., Kwon, Y.-C., & Hong, S. H. (2018). Rapid production and characterization of antimicrobial colicins using Escherichia coli-based cell-free protein synthesis. *Synthetic Biology*, *3*(1).

Johnson, R. D., Lane, G. A., Koulman, A., Cao, M., Fraser, K., Fleetwood, D. J., Voisey, C. R., Dyer, J. M., Pratt, J., Christensen, M., Simpson, W. R., Bryan, G. T., & Johnson, L. J. (2015). A novel family of cyclic oligopeptides derived from ribosomal peptide synthesis of an in planta-induced gene, gigA, in Epichloë endophytes of

grasses. *Fungal genetics and biology: FG & B*, *85*, 14–24.

Just-Baringo, X., Albericio, F., & Álvarez, M. (2014). Thiopeptide Antibiotics: Retrospective and Recent Advances. *Marine Drugs*, *12*(1), 317–351.

Kaunietis, A., Buivydas, A., Čitavičius, D. J., & Kuipers, O. P. (2019). Heterologous biosynthesis and characterization of a glycocin from a thermophilic bacterium. *Nature Communications*, *10*(1), 1–12.

Kaweewan, I., Hemmi, H., Komaki, H., Harada, S., & Kodani, S. (2018). Isolation and structure determination of a new lasso peptide specialicin based on genome mining. *Bioorganic & Medicinal Chemistry*, *26*(23), 6050–6055.

Kawulka, K., Sprules, T., Diaper, C., Whittal, R., McKay, R., Mercier, P., Zuber, P., & Vederas, J. (2004). Structure of subtilosin A, a cyclic antimicrobial peptide from Bacillus subtilis with unusual sulfur to alpha-carbon cross-links: formation and reduction of alpha-thio-alpha-amino acid derivatives. *Biochemistry*, *43*(12), 3385–3395.

Kawulka, K., Sprules, T., McKay, R. T., Mercier, P., Diaper, C. M., Zuber, P., & Vederas, J. C. (2003). Structure of subtilosin A, an antimicrobial peptide from Bacillus subtilis with unusual posttranslational modifications linking cysteine sulfurs to alpha-carbons of phenylalanine and threonine. *Journal of the American Chemical Society*, *125*(16), 4726–4727.

Kenney, G. E., & Rosenzweig, A. C. (2018). Methanobactins: Maintaining copper homeostasis in methanotrophs and beyond. *The Journal of Biological Chemistry*, *293*(13), 4606–4615.

Kim, K. O., & Gluck, M. (2019). Fecal Microbiota Transplantation: An Update on Clinical Practice. *Clinical Endoscopy*, *52*(2), 137–143.

Kittilä, T., Mollo, A., Charkoudian, L. K., & Cryle, M. J. (2016). New Structural Data Reveal the Motion of Carrier Proteins in Nonribosomal Peptide Synthesis. *Angewandte Chemie (International Ed. in English)*, *55*(34), 9834–9840.

Klein, T., Eckhard, U., Dufour, A., Solis, N., & Overall, C. M. (2018). Proteolytic Cleavage—Mechanisms, Function, and "Omic" Approaches for a Near-Ubiquitous Posttranslational Modification. *Chemical Reviews*, *118*(3), 1137–1168.

Koehnke, J., Mann, G., Bent, A. F., Ludewig, H., Shirran, S., Botting, C., Lebl, T., Houssen, W., Jaspars, M., & Naismith, J. H. (2015). Structural analysis of leader peptide binding enables leader-free cyanobactin processing. *Nature Chemical Biology*, *11*(8), 558–563.

Krause, K. M., Serio, A. W., Kane, T. R., & Connolly, L. E. (2016). Aminoglycosides: An Overview. *Cold Spring Harbor Perspectives in Medicine*, *6*(6).

Krautz-Peterson, G., Chapman-Bonofiglio, S., Boisvert, K., Feng, H., Herman, I. M., Tzipori, S., & Sheoran, A. S. (2008). Intracellular neutralization of shiga toxin 2 by an a subunit-specific human monoclonal antibody. *Infection and Immunity*, *76*(5), 1931–1939.

Kuipers, A., de Boef, E., Rink, R., Fekken, S., Kluskens, L. D., Driessen, A. J. M., Leenhouts, K., Kuipers, O. P., & Moll, G. N. (2004). NisT, the transporter of the lantibiotic nisin, can transport fully modified, dehydrated, and unmodified prenisin and fusions of the leader peptide with non-lantibiotic peptides. *The Journal of Biological Chemistry*, *279*(21), 22176–22182.

Kuru, E., Hughes, H. V., Brown, P. J., Hall, E., Tekkam, S., Cava, F., de Pedro, M. A., Brun, Y. V., & VanNieuwenhze, M. S. (2012). InSitu probing of newly synthesized peptidoglycan in live bacteria with fluorescent D-amino acids. *Angewandte Chemie*

(International Ed. in English), *51*(50), 12519–12523.

LaMarche, M. J., Leeds, J. A., Amaral, A., Brewer, J. T., Bushell, S. M., Deng, G., Dewhurst, J. M., Ding, J., Dzink-Fox, J., Gamber, G., Jain, A., Lee, K., Lee, L., Lister, T., McKenney, D., Mullin, S., Osborne, C., Palestrant, D., Patane, M. A., Rann, E. M., Sachdeva, M., Shao, J., Tiamfook, S., Trzasko, A., Whitehead, L., Yifru, A., Yu, D., Yan, W., & Zhu, Q. (2012). Discovery of LFF571: an investigational agent for Clostridium difficile infection. *Journal of Medicinal Chemistry*, *55*(5), 2376–2387.

LaRocca, T. J., Katona, L. I., Thanassi, D. G., & Benach, J. L. (2008). Bactericidal Action of a Complement-Independent Antibody against Relapsing Fever Borrelia Resides in Its Variable Region. *The Journal of Immunology*, *180*(9), 6222–6228.

Lawley, T. D., Clare, S., Walker, A. W., Stares, M. D., Connor, T. R., Raisen, C., Goulding, D., Rad, R., Schreiber, F., Brandt, C., Deakin, L. J., Pickard, D. J., Duncan, S. H., Flint, H. J., Clark, T. G., Parkhill, J., & Dougan, G. (2012). Targeted Restoration of the Intestinal Microbiota with a Simple, Defined Bacteriotherapy Resolves Relapsing Clostridium difficile Disease in Mice. *PLoS Pathogens*, *8*(10).

Laws, M., Shaaban, A., & Rahman, K. M. (2019). Antibiotic resistance breakers: current approaches and future directions. *FEMS Microbiology Reviews*, *43*(5), 490–516.

Lebbe, E. K. M., & Tytgat, J. (2016). In the picture: disulfide-poor conopeptides, a class of pharmacologically interesting compounds. *Journal of Venomous Animals and Toxins including Tropical Diseases*, *22*(1), 30.

Lee, H., Churey, J. J., & Worobo, R. W. (2009). Biosynthesis and transcriptional analysis of thurincin H, a tandem repeated bacteriocin genetic locus, produced by Bacillus thuringiensis SF361. *FEMS Microbiology Letters*, *299*(2), 205–213.

Lewis, K. (2013). Platforms for antibiotic discovery. *Nature Reviews Drug Discovery*, *12*(5), 371–387.

Li, B., Sher, D., Kelly, L., Shi, Y., Huang, K., Knerr, P. J., Joewono, I., Rusch, D., Chisholm, S. W., & van der Donk, W. A. (2010). Catalytic promiscuity in the biosynthesis of cyclic peptide secondary metabolites in planktonic marine cyanobacteria. *Proceedings of the National Academy of Sciences of the United States of America*, *107*(23), 10430–10435.

Lin, D. M., Koskella, B., & Lin, H. C. (2017). Phage therapy: An alternative to antibiotics in the age of multi-drug resistance. *World Journal of Gastrointestinal Pharmacology and Therapeutics*, *8*(3), 162–173.

Line, J. E., Svetoch, E. A., Eruslanov, B. V., Perelygin, V. V., Mitsevich, E. V., Mitsevich, I. P., Levchuk, V. P., Svetoch, O. E., Seal, B. S., Siragusa, G. R., & Stern, N. J. (2008). Isolation and Purification of Enterocin E-760 with Broad Antimicrobial Activity against Gram-Positive and Gram-Negative Bacteria. *Antimicrobial Agents and Chemotherapy*, *52*(3), 1094–1100.

Link, A. J. (2015). Leading the Way to RiPPs. *Nature chemical biology*, *11*(8), 551–552.

Liu, W.-T., Yang, Y.-L., Xu, Y., Lamsa, A., Haste, N. M., Yang, J. Y., Ng, J., Gonzalez, D., Ellermeier, C. D., Straight, P. D., Pevzner, P. A., Pogliano, J., Nizet, V., Pogliano, K., & Dorrestein, P. C. (2010). Imaging mass spectrometry of intraspecies metabolic exchange revealed the cannibalistic factors of Bacillus subtilis. *Proceedings of the National Academy of Sciences of the United States of America*, *107*(37), 16286–16290.

Llanes, C., Hocquet, D., Vogne, C., Benali-Baitich, D., Neuwirth, C., & Plésiat, P. (2004). Clinical Strains of Pseudomonas aeruginosa Overproducing MexAB-OprM

and MexXY Efflux Pumps Simultaneously. *Antimicrobial Agents and Chemotherapy*, *48*(5), 1797–1802.

Lood, R., Winer, B. Y., Pelzek, A. J., Diez-Martinez, R., Thandar, M., Euler, C. W., Schuch, R., & Fischetti, V. A. (2015). Novel phage lysin capable of killing the multidrug-resistant gram-negative bacterium Acinetobacter baumannii in a mouse bacteremia model. *Antimicrobial Agents and Chemotherapy*, *59*(4), 1983–1991.

Luo, S., & Dong, S.-H. (2019). Recent Advances in the Discovery and Biosynthetic Study of Eukaryotic RiPP Natural Products. *Molecules*, *24*(8).

Mach, B., Reich, E., & Tatum, E. L. (1963). Separation of the Biosynthesis of the Antibiotic Polypeptide Tyrocidine from Protein Biosynthesis. *Proceedings of the National Academy of Sciences*, *50*(1), 175–181.

Mahanta, N., Hudson, G. A., & Mitchell, D. A. (2017). Radical SAM enzymes involved in RiPP biosynthesis. *Biochemistry*, *56*(40), 5229–5244.

Mahlapuu, M., Håkansson, J., Ringstad, L., & Björn, C. (2016). Antimicrobial Peptides: An Emerging Category of Therapeutic Agents. *Frontiers in Cellular and Infection Microbiology*, *6*.

Mai, V., Ukhanova, M., Reinhard, M. K., Li, M., & Sulakvelidze, A. (2015). Bacteriophage administration significantly reduces Shigella colonization and shedding by Shigella-challenged mice without deleterious side effects and distortions in the gut microbiota. *Bacteriophage*, *5*(4), e1088124.

Mann, G., Huo, L., Adam, S., Nardone, B., Vendome, J., Westwood, N. J., Müller, R., & Koehnke, J. (2016). Structure and Substrate Recognition of the Bottromycin Maturation Enzyme BotP. *Chembiochem: A European Journal of Chemical Biology*, *17*(23), 2286–2292.

Marcille, F., Gomez, A., Joubert, P., Ladiré, M., Veau, G., Clara, A., Gavini, F., Willems, A., & Fons, M. (2002). Distribution of genes encoding the trypsin-dependent lantibiotic ruminococcin A among bacteria isolated from human fecal microbiota. *Applied and Environmental Microbiology*, *68*(7), 3424–3431.

Maron, D. F., Smith, T. J. S., & Nachman, K. E. (2013). Restrictions on antimicrobial use in food animal production: an international regulatory and economic survey. *Globalization and Health*, *9*, 48.

Martin-Gómez, H., & Tulla-Puche, J. (2018). Lasso peptides: chemical approaches and structural elucidation. *Organic & Biomolecular Chemistry*, *16*(28), 5065–5080.

Martínez-Núñez, M. A., & López, V. E. L. y. (2016). Nonribosomal peptides synthetases and their applications in industry. *Sustainable Chemical Processes*, *4*(1), 13.

Mast, Y., & Wohlleben, W. (2014). Streptogramins – Two are better than one! *International Journal of Medical Microbiology*, *304*(1), 44–50.

Mathur, H., Fallico, V., O'Connor, P. M., Rea, M. C., Cotter, P. D., Hill, C., & Ross, R. P. (2017). Insights into the Mode of Action of the Sactibiotic Thuricin CD. *Frontiers in Microbiology*, *8*, 696.

Mathur, H., Field, D., Rea, M. C., Cotter, P. D., Hill, C., & Ross, R. P. (2017). Bacteriocin-Antimicrobial Synergy: A Medical and Food Perspective. *Frontiers in Microbiology*, *8*.

Mathur, H., O'Connor, P. M., Hill, C., Cotter, P. D., & Ross, R. P. (2013). Analysis of Anti-Clostridium difficile Activity of Thuricin CD, Vancomycin, Metronidazole, Ramoplanin, and Actagardine, both Singly and in Paired Combinations. *Antimicrobial Agents and Chemotherapy*, *57*(6), 2882–2886.

Mavaro, A., Abts, A., Bakkes, P. J., Moll, G. N., Driessen, A. J. M., Smits, S. H. J.,

& Schmitt, L. (2011). Substrate recognition and specificity of the NisB protein, the lantibiotic dehydratase involved in nisin biosynthesis. *The Journal of Biological Chemistry*, *286*(35), 30552–30560.

McCallin, S., Sacher, J. C., Zheng, J., & Chan, B. K. (2019). Current State of Compassionate Phage Therapy. *Viruses*, *11*(4).

McEwen, S. A., & Collignon, P. J. (2018). Antimicrobial Resistance: a One Health Perspective. *Microbiology Spectrum*, *6*(2).

Meunier, M., Guyard-Nicodème, M., Dory, D., & Chemaly, M. (2016). Control strategies against Campylobacter at the poultry production level: biosecurity measures, feed additives and vaccination. *Journal of Applied Microbiology*, *120*(5), 1139–1173.

Miles, J., & Wallace, A. (2016). Circular dichroism spectroscopy of membrane proteins. *Chemical Society Reviews*, *45*(18), 4859–4872.

Mo, T., Ji, X., Yuan, W., Mandalapu, D., Wang, F., Zhong, Y., Li, F., Chen, Q., Ding, W., Deng, Z., Yu, S., & Zhang, Q. (2019). ThuricinZ: A Narrow-Spectrum Sactibiotic that Targets the Cell Membrane. *Angewandte Chemie (International Ed. in English)*, *58*(52), 18793–18797.

Mo, T., Liu, W.-Q., Ji, W., Zhao, J., Chen, T., Ding, W., Yu, S., & Zhang, Q. (2017). Biosynthetic Insights into Linaridin Natural Products from Genome Mining and Precursor Peptide Mutagenesis. *ACS Chemical Biology*, *12*(6), 1484–1488.

Mohr, K. I., Volz, C., Jansen, R., Wray, V., Hoffmann, J., Bernecker, S., Wink, J., Gerth, K., Stadler, M., & Müller, R. (2015). Pinensins: the first antifungal lantibiotics. *Angewandte Chemie (International Ed. in English)*, *54*(38), 11254–11258.

Moll, G. N., Kuipers, A., & Rink, R. (2010). Microbial engineering of dehydro-amino acids and lanthionines in non-lantibiotic peptides. *Antonie Van Leeuwenhoek*, *97*(4), 319–333.

Molohon, K. J., Blair, P. M., Park, S., Doroghazi, J. R., Maxson, T., Hershfield, J. R., Flatt, K. M., Schroeder, N. E., Ha, T., & Mitchell, D. A. (2016). Plantazolicin is an ultra-narrow spectrum antibiotic that targets the Bacillus anthracis membrane. *ACS infectious diseases*, *2*(3), 207–220.

Montalbán-López, M., Deng, J., van Heel, A. J., & Kuipers, O. P. (2018). Specificity and Application of the Lantibiotic Protease NisP. *Frontiers in Microbiology*, *9*.

Mullane, K., Lee, C., Bressler, A., Buitrago, M., Weiss, K., Dabovic, K., Praestgaard, J., Leeds, J. A., Blais, J., & Pertel, P. (2015). Multicenter, randomized clinical trial to compare the safety and efficacy of LFF571 and vancomycin for Clostridium difficile infections. *Antimicrobial Agents and Chemotherapy*, *59*(3), 1435–1440.

Munita, J. M., & Arias, C. A. (2016). Mechanisms of Antibiotic Resistance. *Microbiology spectrum*, *4*(2).

Murray, A. K. (2020). The Novel Coronavirus COVID-19 Outbreak: Global Implications for Antimicrobial Resistance. *Frontiers in Microbiology*, *11*.

Nagano, N., Umemura, M., Izumikawa, M., Kawano, J., Ishii, T., Kikuchi, M., Tomii, K., Kumagai, T., Yoshimi, A., Machida, M., Abe, K., Shin-ya, K., & Asai, K. (2016). Class of cyclic ribosomal peptide synthetic genes in filamentous fungi. *Fungal Genetics and Biology*, *86*, 58–70.

Nikaido, H. (2003). Molecular basis of bacterial outer membrane permeability revisited. *Microbiology and molecular biology reviews: MMBR*, *67*(4), 593–656.

Nissen-Meyer, J., Oppegård, C., Rogne, P., Haugen, H. S., & Kristiansen, P. E. (2010). Structure and Mode-of-Action of the Two-Peptide (Class-IIb) Bacteriocins. *Probiotics and Antimicrobial Proteins*, *2*(1), 52–60.

Noll, K. S., Sinko, P. J., & Chikindas, M. L. (2011). Elucidation of the Molecular Mechanisms of Action of the Natural Antimicrobial Peptide Subtilosin Against the Bacterial Vaginosis-associated Pathogen Gardnerella vaginalis. *Probiotics and Antimicrobial Proteins*, *3*(1), 41–47.

Norris, G. E., & Patchett, M. L. (2016). The glycocins: in a class of their own. *Current Opinion in Structural Biology*, *40*, 112–119.

Nowak, A., Hedenstierna, M., Ursing, J., Lidman, C., & Nowak, P. (2019). Efficacy of Routine Fecal Microbiota Transplantation for Treatment of Recurrent Clostridium difficile Infection: A Retrospective Cohort Study. *International Journal of Microbiology*, *2019*.

Ogunbanwo, S. T., Sanni, A. I., & Onilude, A. A. (2004). Influence of bacteriocin in the control of Escherichia coli infection of broiler chickens in Nigeria. *World Journal of Microbiology and Biotechnology*, *20*(1), 51–56.

Okano, A., Isley, N. A., & Boger, D. L. (2017). Total Syntheses of Vancomycin Related Glycopeptide Antibiotics and Key Analogues. *Chemical reviews*, *117*(18), 11952–11993.

Oman, T. J., & van der Donk, W. A. (2010). Follow the leader: the use of leader peptides to guide natural product biosynthesis. *Nature Chemical Biology*, *6*(1), 9–18.

O'Neill, j. (2016). Tackling drug-resistant infections globally: Final report and recommendations. *Review on Antimicrobial Resistance*.

Ongey, E. L., Giessmann, R. T., Fons, M., Rappsilber, J., Adrian, L., & Neubauer, P. (2018). Heterologous Biosynthesis, Modifications and Structural Characterization of Ruminococcin-A, a Lanthipeptide From the Gut Bacterium Ruminococcus gnavus E1, in Escherichia coli. *Frontiers in Microbiology*, *9*, 1688.

Ortega, M. A., Hao, Y., Zhang, Q., Walker, M. C., van der Donk, W. A., & Nair, S. K. (2015). Structure and mechanism of the tRNA-dependent lantibiotic dehydratase NisB. *Nature*, *517*(7535), 509–512.

Ortega, M. A., & van der Donk, W. A. (2016). New Insights into the Biosynthetic Logic of Ribosomally Synthesized and Post-translationally Modified Peptide Natural Products. *Cell Chemical Biology*, *23*(1), 31–44.

Ortega, M. A., Velásquez, J. E., Garg, N., Zhang, Q., Joyce, R. E., Nair, S. K., & van der Donk, W. A. (2014). Substrate specificity of the lanthipeptide peptidase ElxP and the oxidoreductase ElxO. *ACS chemical biology*, *9*(8), 1718–1725.

Otaka, T., & Kaji, A. (1976). Mode of action of bottromycin A2. Release of aminoacyl- or peptidyl-tRNA from ribosomes. *The Journal of Biological Chemistry*, *251*(8), 2299–2306.

Palmer, A. C., & Kishony, R. (2014). Opposing effects of target overexpression reveal drug mechanisms. *Nature communications*, *5*, 4296.

Pandit, N., Singla, R. K., & Shrivastava, B. (2012). Current Updates on Oxazolidinone and Its Significance. *International Journal of Medicinal Chemistry*.

Park, S., Yoo, K.-O., Marcussen, T., Backlund, A., Jacobsson, E., Rosengren, K. J., Doo, I., & Göransson, U. (2017). Cyclotide Evolution: Insights from the Analyses of Their Precursor Sequences, Structures and Distribution in Violets (Viola). *Frontiers in Plant Science*, *8*.

Patel, R., & DuPont, H. L. (2015). New Approaches for Bacteriotherapy: Prebiotics, New-Generation Probiotics, and Synbiotics. *Clinical Infectious Diseases: An Official Publication of the Infectious Diseases Society of America*, *60*(Suppl 2), S108.

Pavithrra, G., & Rajasekaran, R. (2020). Gramicidin Peptide to Combat Antibiotic

Resistance: A Review. *International Journal of Peptide Research and Therapeutics*, *26*(1), 191–199.

Perez, R. H., Zendo, T., & Sonomoto, K. (2018). Circular and Leaderless Bacteriocins: Biosynthesis, Mode of Action, Applications, and Prospects. *Frontiers in Microbiology*, *9*.

Petrosillo, N., Granata, G., & Cataldo, M. A. (2018). Novel Antimicrobials for the Treatment of Clostridium difficile Infection. *Frontiers in Medicine*, *5*.

Pham, T. D. M., Ziora, Z. M., & Blaskovich, M. A. T. (2019). Quinolone antibiotics. *MedChemComm*, *10*(10), 1719–1739.

Pierrat, O. A., & Maxwell, A. (2003). The action of the bacterial toxin microcin B17. Insight into the cleavage-religation reaction of DNA gyrase. *The Journal of Biological Chemistry*, *278*(37), 35016–35023.

Poole, K. (2004). Resistance to beta-lactam antibiotics. *Cellular and molecular life sciences: CMLS*, *61*(17), 2200–2223.

Precord, T. W., Mahanta, N., & Mitchell, D. A. (2019). Reconstitution and Substrate Specificity of the Thioether-Forming Radical S-Adenosylmethionine Enzyme in Freyrasin Biosynthesis. *ACS Chemical Biology*, *14*(9), 1981–1989.

Principi, N., Silvestri, E., & Esposito, S. (2019). Advantages and Limitations of Bacteriophages for the Treatment of Bacterial Infections. *Frontiers in Pharmacology*, *10*.

Prosser, G. A., & de Carvalho, L. P. S. (2013). Metabolomics Reveal d-Alanine:d-Alanine Ligase As the Target of d-Cycloserine in Mycobacterium tuberculosis. *ACS Medicinal Chemistry Letters*, *4*(12), 1233–1237.

Pujol, A., Crost, E. H., Simon, G., Barbe, V., Vallenet, D., Gomez, A., & Fons, M. (2011). Characterization and distribution of the gene cluster encoding RumC, an anti-Clostridium perfringens bacteriocin produced in the gut. *FEMS Microbiology Ecology*, *78*(2), 405–415.

Ramalho, S. D., Pinto, M. E. F., Ferreira, D., & Bolzani, V. S. (2018). Biologically Active Orbitides from the Euphorbiaceae Family. *Planta Medica*, *84*(9-10), 558–567.

Ramare, F., Nicoli, J., Dabard, J., Corring, T., Ladire, M., Gueugneau, A. M., & Raibaud, P. (1993). Trypsin-dependent production of an antibacterial substance by a human Peptostreptococcus strain in gnotobiotic rats and in vitro. *Applied and Environmental Microbiology*, *59*(9), 2876–2883.

Ramm, S., Krawczyk, B., Mühlenweg, A., Poch, A., Mösker, E., & Süssmuth, R. D. (2017). A Self-Sacrificing N-Methyltransferase Is the Precursor of the Fungal Natural Product Omphalotin. *Angewandte Chemie (International Ed. in English)*, *56*(33), 9994–9997.

Rea, M. C., Alemayehu, D., Casey, P. G., O'Connor, P. M., Lawlor, P. G., Walsh, M., Shanahan, F., Kiely, B., Ross, R. P., & Hill, C. (2014). Bioavailability of the anticlostridial bacteriocin thuricin CD in gastrointestinal tract. *Microbiology (Reading, England)*, *160*(Pt 2), 439–445.

Rea, M. C., Dobson, A., O'Sullivan, O., Crispie, F., Fouhy, F., Cotter, P. D., Shanahan, F., Kiely, B., Hill, C., & Ross, R. P. (2011). Effect of broad- and narrow-spectrum antimicrobials on Clostridium difficile and microbial diversity in a model of the distal colon. *Proceedings of the National Academy of Sciences of the United States of America*, *108*(Suppl 1), 4639–4644.

Rea, M. C., Ross, R. P., Cotter, P. D., & Hill, C. (2011). Classification of Bacteriocins from Gram-Positive Bacteria. In *Prokaryotic Antimicrobial Peptides* (pp. 29–53).

Springer, New York, NY.

Rea, M. C., Sit, C. S., Clayton, E., O'Connor, P. M., Whittal, R. M., Zheng, J., Vederas, J. C., Ross, R. P., & Hill, C. (2010). Thuricin CD, a posttranslationally modified bacteriocin with a narrow spectrum of activity against Clostridium difficile. *Proceedings of the National Academy of Sciences of the United States of America*, *107*(20), 9352–9357.

Rebuffat, S. (2011). Bacteriocins from Gram-Negative Bacteria: A Classification? In D. Drider & S. Rebuffat (Eds.), *Prokaryotic Antimicrobial Peptides: From Genes to Applications* (pp. 55–72). New York, NY: Springer.

Regni, C. A., Roush, R. F., Miller, D. J., Nourse, A., Walsh, C. T., & Schulman, B. A. (2009). How the MccB bacterial ancestor of ubiquitin E1 initiates biosynthesis of the microcin C7 antibiotic. *The EMBO journal*, *28*(13), 1953–1964.

Repka, L. M., Chekan, J. R., Nair, S. K., & van der Donk, W. A. (2017). Mechanistic Understanding of Lanthipeptide Biosynthetic Enzymes. *Chemical Reviews*, *117*(8), 5457–5520.

Roach, D. R., & Donovan, D. M. (2015). Antimicrobial bacteriophage-derived proteins and therapeutic applications. *Bacteriophage*, *5*(3), e1062590.

Roblin, C., Chiumento, S., Bornet, O., Nouailler, M., Müller, C., Jeannot, K., Basset, C., Kieffer-Jaquinod, S., Couté, Y., Torelli, S., Le Pape, L., Schüneman, V., Olleik, H., De La Villeon, B., Sockeel, P., Di Pasquale, E., Nicoletti, C., Vidal, N., Poljak, L., Iranzo, O., Giardina, T., Fons, M., Devillard, E., Polard, P., Maresca, M., Perrier, J., Atta, M., Guerlesquin, F., Lafond, M., & Duarte, v. (2020). The unusual structure of ruminococcin c1 antimicrobial peptide confers clinical properties. *P.N.A.S.*

Rodríguez-Rubio, L., Gutiérrez, D., Donovan, D. M., Martínez, B., Rodríguez, A., & García, P. (2016). Phage lytic proteins: biotechnological applications beyond clinical antimicrobials. *Critical Reviews in Biotechnology*, *36*(3), 542–552.

Rogers, L. D., & Overall, C. M. (2013). Proteolytic Post-translational Modification of Proteins: Proteomic Tools and Methodology. *Molecular & Cellular Proteomics : MCP*, *12*(12), 3532–3542.

Romero-Calle, D., Guimarães Benevides, R., Góes-Neto, A., & Billington, C. (2019). Bacteriophages as Alternatives to Antibiotics in Clinical Care. *Antibiotics*, *8*(3).

Saha, S., Tomaro-Duchesneau, C., Tabrizian, M., & Prakash, S. (2012). Probiotics as oral health biotherapeutics. *Expert Opinion on Biological Therapy*, *12*(9), 1207–1220.

Salfinger, M., & Migliori, G. B. (2015). Bedaquiline: 10 years later, the drug susceptibility testing protocol is still pending. *European Respiratory Journal*, *45*(2), 317–321.

Salmond, G. P. C., & Fineran, P. C. (2015). A century of the phage: past, present and future. *Nature Reviews Microbiology*, *13*(12), 777–786.

Sandiford, S. K. (2015). Perspectives on lantibiotic discovery – where have we failed and what improvements are required? *Expert Opinion on Drug Discovery*.

Sang, Y., & Blecha, F. (2008). Antimicrobial peptides and bacteriocins: alternatives to traditional antibiotics. *Animal Health Research Reviews*, *9*(2), 227–235.

Sawa, T., Kinoshita, M., Inoue, K., Ohara, J., & Moriyama, K. (2019). Immunoglobulin for Treating Bacterial Infections: One More Mechanism of Action. *Antibodies (Basel, Switzerland)*, *8*(4).

Saylor, C., Dadachova, E., & Casadevall, A. (2009). Monoclonal antibody-based therapies for microbial diseases. *Vaccine*, *27*, G38–G46.

Schatz, A., Bugle, E., & Waksman, S. A. (1944). Streptomycin, a Substance Exhibiting Antibiotic Activity Against Gram-Positive and Gram-Negative Bacteria. *Proceed-*

ings of the Society for Experimental Biology and Medicine, *55*(1), 66–69.

Schmelcher, M., Shen, Y., Nelson, D. C., Eugster, M. R., Eichenseher, F., Hanke, D. C., Loessner, M. J., Dong, S., Pritchard, D. G., Lee, J. C., Becker, S. C., Foster-Frey, J., & Donovan, D. M. (2015). Evolutionarily distinct bacteriophage endolysins featuring conserved peptidoglycan cleavage sites protect mice from MRSA infection. *The Journal of Antimicrobial Chemotherapy*, *70*(5), 1453–1465.

Schramma, K. R., Bushin, L. B., & Seyedsayamdost, M. R. (2015). Structure and biosynthesis of a macrocyclic peptide containing an unprecedented lysine-to-tryptophan crosslink. *Nature Chemistry*, *7*(5), 431–437.

Schramma, K. R., & Seyedsayamdost, M. R. (2017). Lysine-Tryptophan-Crosslinked Peptides Produced by Radical SAM Enzymes in Pathogenic Streptococci. *ACS Chemical Biology*, *12*(4), 922–927.

Schwalen, C. J., Hudson, G. A., Kosol, S., Mahanta, N., Challis, G. L., & Mitchell, D. A. (2017). *In Vitro Biosynthetic Studies of Bottromycin Expand the Enzymatic Capabilities of the YcaO Superfamily* [rapid-communication].

Seed, K. D. (2015). Battling Phages: How Bacteria Defend against Viral Attack. *PLoS pathogens*, *11*(6), e1004847.

Sekelja, M., Berget, I., Næs, T., & Rudi, K. (2011). Unveiling an abundant core microbiota in the human adult colon by a phylogroup-independent searching approach. *The ISME Journal*, *5*(3), 519–531.

Sham, L.-T., Tsui, H.-C. T., Land, A. D., Barendt, S. M., & Winkler, M. E. (2012). Recent Advances in Pneumococcal Peptidoglycan Biosynthesis Suggest New Vaccine and Antimicrobial Targets. *Current Opinion in Microbiology*, *15*(2), 194–203.

Shelburne, C. E., An, F. Y., Dholpe, V., Ramamoorthy, A., Lopatin, D. E., & Lantz, M. S. (2007). The spectrum of antimicrobial activity of the bacteriocin subtilosin A. *Journal of Antimicrobial Chemotherapy*, *59*(2), 297–300.

Sillankorva, S., Pereira, M. O., & Henriques, M. (2019). Editorial: Antibiotic Alternatives and Combinational Therapies for Bacterial Infections. *Frontiers in Microbiology*, *9*.

Silva, C. C. G., Silva, S. P. M., & Ribeiro, S. C. (2018). Application of Bacteriocins and Protective Cultures in Dairy Food Preservation. *Frontiers in Microbiology*, *9*.

Singh, S. B., Young, K., & Silver, L. L. (2017). What is an "ideal" antibiotic? Discovery challenges and path forward. *Biochemical Pharmacology*, *133*, 63–73.

Sit, C. S., McKay, R. T., Hill, C., Ross, R. P., & Vederas, J. C. (2011). The 3D Structure of Thuricin CD, a Two-Component Bacteriocin with Cysteine Sulfur to -Carbon Cross-links. *Journal of the American Chemical Society*, *133*(20), 7680–7683.

Sit, C. S., van Belkum, M. J., McKay, R. T., Worobo, R. W., & Vederas, J. C. (2011). The 3D solution structure of thurincin H, a bacteriocin with four sulfur to -carbon crosslinks. *Angewandte Chemie (International Ed. in English)*, *50*(37), 8718–8721.

Sonu, Parveen, B. R., Praveen, S., & Pal, H. (2017). A short review on sulphonamides with antimicrobial activity. *International Journal of Pharmaceutical Chemistry*, *7*(5), 70–73.

Spížek, J., & Řezanka, T. (2017). Lincosamides: Chemical structure, biosynthesis, mechanism of action, resistance, and applications. *Biochemical Pharmacology*, *133*, 20–28.

Stern, N. J., Svetoch, E. A., Eruslanov, B. V., Kovalev, Y. N., Volodina, L. I., Perelygin, V. V., Mitsevich, E. V., Mitsevich, I. P., & Levchuk, V. P. (2005). Paenibacillus polymyxa purified bacteriocin to control Campylobacter jejuni in chickens. *Journal of Food Protection*, *68*(7), 1450–1453.

Stern, N. J., Svetoch, E. A., Eruslanov, B. V., Perelygin, V. V., Mitsevich, E. V., Mit-

sevich, I. P., Pokhilenko, V. D., Levchuk, V. P., Svetoch, O. E., & Seal, B. S. (2006). Isolation of a Lactobacillus salivarius Strain and Purification of Its Bacteriocin, Which Is Inhibitory to Campylobacter jejuni in the Chicken Gastrointestinal System. *Antimicrobial Agents and Chemotherapy*, *50*(9), 3111–3116.

Sterner, O., Etzel, W., Mayer, A., & Anke, H. (1997). Omphalotin, A New Cyclic Peptide with Potent Nematicidal Activity from Omphalotus Olearius II. Isolation and Structure Determination. *Natural Product Letters*, *10*(1), 33–38.

Sutyak, K. E., Anderson, R. A., Dover, S. E., Feathergill, K. A., Aroutcheva, A. A., Faro, S., & Chikindas, M. L. (2008). Spermicidal activity of the safe natural antimicrobial peptide subtilosin. *Infectious Diseases in Obstetrics and Gynecology*, *2008*, 540758.

Süssmuth, R. D., & Mainz, A. (2017). Nonribosomal Peptide Synthesis—Principles and Prospects. *Angewandte Chemie International Edition*, *56*(14), 3770–3821.

Tagg, J. R., Dajani, A. S., & Wannamaker, L. W. (1976). Bacteriocins of gram-positive bacteria. *Bacteriological Reviews*, *40*(3), 722–756.

Tang, W., & van der Donk, W. A. (2012). Structural Characterization of Four Prochlorosins: A Novel Class of Lantipeptides Produced by Planktonic Marine Cyanobacteria. *Biochemistry*, *51*(21), 4271–4279.

Tariq, S., Rizvi, S. F. A., & Anwar, U. (2018). Tetracycline: Classification, Structure Activity Relationship and Mechanism of Action as a Theranostic Agent for Infectious Lesions-A Mini Review. *Biomedical Journal of Scientific & Technical Research*, *7*(2), 001-010.

Thennarasu, S., Lee, D.-K., Poon, A., Kawulka, K. E., Vederas, J. C., & Ramamoorthy, A. (2005). Membrane permeabilization, orientation, and antimicrobial mechanism of subtilosin A. *Chemistry and Physics of Lipids*, *137*(1-2), 38–51.

Theuretzbacher, U., Bush, K., Harbarth, S., Paul, M., Rex, J. H., Tacconelli, E., & Thwaites, G. E. (2020). Critical analysis of antibacterial agents in clinical development. *Nature Reviews Microbiology*, 1–13.

Theuretzbacher, U., Outterson, K., Engel, A., & Karlén, A. (2020). The global preclinical antibacterial pipeline. *Nature Reviews Microbiology*, *18*(5), 275–285. (Number: 5 Publisher: Nature Publishing Group)

Tietz, J. I., & Mitchell, D. A. (2016). Using Genomics for Natural Product Structure Elucidation. *Current Topics in Medicinal Chemistry*, *16*(15), 1645–1694.

Tillotson, G. S. (1996). Quinolones: structure-activity relationships and future predictions. *Journal of Medical Microbiology*, *44*(5), 320–324.

Ting, L. S. L., Praestgaard, J., Grunenberg, N., Yang, J. C., Leeds, J. A., & Pertel, P. (2012). A first-in-human, randomized, double-blind, placebo-controlled, single- and multiple-ascending oral dose study to assess the safety and tolerability of LFF571 in healthy volunteers. *Antimicrobial Agents and Chemotherapy*, *56*(11), 5946–5951.

Tossavainen, H., Raulinaitis, V., Kauppinen, L., Pentikäinen, U., Maaheimo, H., & Permi, P. (2018). Structural and Functional Insights Into Lysostaphin–Substrate Interaction. *Frontiers in Molecular Biosciences*, *5*.

Travin, D. Y., Watson, Z. L., Metelev, M., Ward, F. R., Osterman, I. A., Khven, I. M., Khabibullina, N. F., Serebryakova, M., Mergaert, P., Polikanov, Y. S., Cate, J. H. D., & Severinov, K. (2019). Structure of ribosome-bound azole-modified peptide phazolicin rationalizes its species-specific mode of bacterial translation inhibition. *Nature Communications*, *10*(1), 1–11.

Trevors, J. (1999). Evolution of gene transfer in bacteria. *World Journal of Microbiology and Biotechnology*, *15*(1), 1–6.

Truman, A. W. (2016). Cyclisation mechanisms in the biosynthesis of ribosomally synthesised and post-translationally modified peptides. *Beilstein Journal of Organic Chemistry*, *12*(1), 1250–1268.

Trzasko, A., Leeds, J. A., Praestgaard, J., Lamarche, M. J., & McKenney, D. (2012). Efficacy of LFF571 in a hamster model of Clostridium difficile infection. *Antimicrobial Agents and Chemotherapy*, *56*(8), 4459–4462.

Ubeda, C., Bucci, V., Caballero, S., Djukovic, A., Toussaint, N. C., Equinda, M., Lipuma, L., Ling, L., Gobourne, A., No, D., Taur, Y., Jenq, R. R., van den Brink, M. R. M., Xavier, J. B., & Pamer, E. G. (2013). Intestinal microbiota containing Barnesiella species cures vancomycin-resistant Enterococcus faecium colonization. *Infection and Immunity*, *81*(3), 965–973.

Van Boeckel, T. P., Brower, C., Gilbert, M., Grenfell, B. T., Levin, S. A., Robinson, T. P., Teillant, A., & Laxminarayan, R. (2015). Global trends in antimicrobial use in food animals. *Proceedings of the National Academy of Sciences of the United States of America*, *112*(18), 5649-5654.

van der Velden, N. S., Kälin, N., Helf, M. J., Piel, J., Freeman, M. F., & Künzler, M. (2017). Autocatalytic backbone N-methylation in a family of ribosomal peptide natural products. *Nature Chemical Biology*, *13*(8), 833–835.

Van Epps, H. L. (2006). René Dubos: unearthing antibiotics. *Journal of Experimental Medicine*, *203*(2), 259–259.

van Heel, A. J., Montalban-Lopez, M., Oliveau, Q., & Kuipers, O. P. (2017). Genome-guided identification of novel head-to-tail cyclized antimicrobial peptides, exemplified by the discovery of pumilarin. *Microbial Genomics*, *3*(10).

Van Immerseel, F., De Buck, J., Pasmans, F., Huyghebaert, G., Haesebrouck, F., & Ducatelle, R. (2004). Clostridium perfringens in poultry: an emerging threat for animal and public health. *Avian Pathology: Journal of the W.V.P.A*, *33*(6), 537–549.

Ventola, C. L. (2015). The Antibiotic Resistance Crisis. *Pharmacy and Therapeutics*, *40*(4), 277–283.

Verna, E. C., & Lucak, S. (2010). Use of probiotics in gastrointestinal disorders: what to recommend? *Therapeutic Advances in Gastroenterology*, *3*(5), 307–319.

Vinogradov, A. A., Yin, Y., & Suga, H. (2019). Macrocyclic Peptides as Drug Candidates: Recent Progress and Remaining Challenges. *Journal of the American Chemical Society*, *141*(10), 4167–4181.

Wade, B., & Keyburn, A. (2015). The true cost of necrotic enteritis. *PoultryWorld*, *31*, 5.

Waksman, S. (1947). What is an antibiotic or an antibiotic substance? *Mycologia*.

Walsh, C. J., Guinane, C. M., Hill, C., Ross, R. P., O'Toole, P. W., & Cotter, P. D. (2015). In silico identification of bacteriocin gene clusters in the gastrointestinal tract, based on the Human Microbiome Project's reference genome database. *BMC Microbiology*, *15*.

Walton, J. D., Hallen-Adams, H. E., & Luo, H. (2010). Ribosomal biosynthesis of the cyclic peptide toxins of Amanita mushrooms. *Biopolymers*, *94*(5), 659–664.

Wang, Z., He, Y., & Zheng, Y. (2019). Probiotics for the Treatment of Bacterial Vaginosis: A Meta-Analysis. *International Journal of Environmental Research and Public Health*, *16*(20).

Watanabe, K., Rude, M. A., Walsh, C. T., & Khosla, C. (2003). Engineered biosynthesis of an ansamycin polyketide precursor in Escherichia coli. *Proceedings of the National*

Academy of Sciences of the United States of America, *100*(17), 9774–9778.

Wehrli, W. (1977). Ansamycins chemistry, biosynthesis and biological activity. *Springer*, 21–49.

Weisman, L. E., Fischer, G. W., Thackray, H. M., Johnson, K. E., Schuman, R. F., Mandy, G. T., Stratton, B. E., Adams, K. M., Kramer, W. G., & Mond, J. J. (2009). Safety and pharmacokinetics of a chimerized anti-lipoteichoic acid monoclonal antibody in healthy adults. *International Immunopharmacology*, *9*(5), 639–644.

Weisman, L. E., Thackray, H. M., Garcia-Prats, J. A., Nesin, M., Schneider, J. H., Fretz, J., Kokai-Kun, J. F., Mond, J. J., Kramer, W. G., & Fischer, G. W. (2009). Phase 1/2 Double-Blind, Placebo-Controlled, Dose Escalation, Safety, and Pharmacokinetic Study of Pagibaximab (BSYX-A110), an Antistaphylococcal Monoclonal Antibody for the Prevention of Staphylococcal Bloodstream Infections, in Very-Low-Birth-Weight Neonates. *Antimicrobial Agents and Chemotherapy*, *53*(7), 2879–2886.

Wenzel, M., Rautenbach, M., Vosloo, J. A., Siersma, T., Aisenbrey, C. H. M., Zaitseva, E., Laubscher, W. E., van Rensburg, W., Behrends, J. C., Bechinger, B., & Hamoen, L. W. (2018). The Multifaceted Antibacterial Mechanisms of the Pioneering Peptide Antibiotics Tyrocidine and Gramicidin S. *mBio*, *9*(5).

WHO. (2015). Global action plan on antimicrobial resistance. *World Health Organization*.

Wieckowski, B. M., Hegemann, J. D., Mielcarek, A., Boss, L., Burghaus, O., & Marahiel, M. A. (2015). The PqqD homologous domain of the radical SAM enzyme ThnB is required for thioether bond formation during thurincin H maturation. *FEBS letters*, *589*(15), 1802–1806.

Winn, M., K. Fyans, J., Zhuo, Y., & Micklefield, J. (2016). Recent advances in engineering nonribosomal peptide assembly lines. *Natural Product Reports*, *33*(2), 317–347.

Xia, G., Kohler, T., & Peschel, A. (2010). The wall teichoic acid and lipoteichoic acid polymers of Staphylococcus aureus. *International journal of medical microbiology: IJMM*, *300*(2-3), 148–154.

Yacoby, I., Bar, H., & Benhar, I. (2007). Targeted Drug-Carrying Bacteriophages as Antibacterial Nanomedicines. *Antimicrobial Agents and Chemotherapy*, *51*(6), 2156–2163.

Yang, S.-C., Lin, C.-H., Sung, C. T., & Fang, J.-Y. (2014). Antibacterial activities of bacteriocins: application in foods and pharmaceuticals. *Frontiers in Microbiology*, *5*.

Yang, X., & van der Donk, W. A. (2013). Ribosomally synthesized and post-translationally modified peptide natural products: new insights into the role of leader and core peptides during biosynthesis. *Chemistry (Weinheim an Der Bergstrasse, Germany)*, *19*(24), 7662–7677.

Yuan, J., Zhang, Z.-Z., Chen, X.-Z., Yang, W., & Huan, L.-D. (2004). Site-directed mutagenesis of the hinge region of nisinZ and properties of nisinZ mutants. *Applied Microbiology and Biotechnology*, *64*(6), 806–815.

Zakharov, S. D., & Cramer, W. A. (2002). Colicin crystal structures: pathways and mechanisms for colicin insertion into membranes. *Biochimica et Biophysica Acta (BBA) - Biomembranes*, *1565*(2), 333–346.

Zanders, E. D. (2015). *Human Drug Targets: A Compendium for Pharmaceutical Discovery*. John Wiley & Sons.

Zeng, D., Debabov, D., Hartsell, T. L., Cano, R. J., Adams, S., Schuyler, J. A., McMillan, R., & Pace, J. L. (2016). Approved Glycopeptide Antibacterial Drugs: Mechanism

of Action and Resistance. *Cold Spring Harbor Perspectives in Medicine*, *6*(12).

Zhanel, G. G., Walkty, A. J., & Karlowsky, J. A. (2015). Fidaxomicin: A novel agent for the treatment of Clostridium difficile infection. *The Canadian Journal of Infectious Diseases & Medical Microbiology*, *26*(6), 305–312.

Zhang, L.-j., & Gallo, R. L. (2016). Antimicrobial peptides. *Current Biology*, *26*(1), R14–R19.

Zhang, Q., Yang, X., Wang, H., & van der Donk, W. A. (2014). High divergence of the precursor peptides in combinatorial lanthipeptide biosynthesis. *ACS chemical biology*, *9*(11), 2686–2694.

Zheng, J., Gänzle, M. G., Lin, X. B., Ruan, L., & Sun, M. (2015). Diversity and dynamics of bacteriocins from human microbiome. *Environmental Microbiology*, *17*(6), 2133–2143.

Appendix 1: Book soon to be published

PEPTIDE AND PROTEIN ENGINEERING FOR BIOTECHNOLOGICAL AND THERAPEUTICAL APPLICATIONS

Temporary table of content.

1. “Biohybrid Catalysts Harboring a Synthetic Metal Complex within a Barrel Protein”
   Akira Onoda, Takashi Hayashi
   Japan

2. "Recombinant Production and Purification of Cysteine-rich Domains: the Case of the Death Receptors Involved In Cancer Treatment"
   Antoine Baudin, Antoine Loquet, Sophie Lecomte, Benoît Odaert
   France

3. “Chemistry for a better life: elaborating artificial metalloenzymes for eco-compatible chemical synthesis procedures and therapeutical applications“
   Jean-Pierre Mahy, Wadih Ghattas, Ricoux Rémy, Frédéric Avenir
   France

4. “Conformational control of short peptides with metal coordination”
   M. Eugenio Vázquez
   Spain

5. “Antimicrobial Ribosomally synthesized and Post-translationally modified Peptides as a source of alternatives to antibiotics: a focus on the sactipeptides and ranthipeptides subclasses”
   Clarisse Roblin, Pierre Rousselot-Pailley, Victor Duarte, Josette Perrier & Mickael Lafond
   France

6. “How to bridge scales between molecular and kinetic modelling”
   Juergen Pleiss and Henrique Carvalho
   Germany

7 “Peptide-based artificial metalloenzymes by design”
   Angela Lombardi
   University of Napoli “Federico II”
   Italy

8 « Cis-Amide Stabilizing Proline Analogs - Synthesis and Applications »
   Isita Banerjee, Indranil Duttagupta, Abhishek Gupta and Surajit Sinha
   India

9 “Peptide-based nanomaterials for theranostic applications”
   Prof. Cristina Satriano
   University of Catania
   Italy

10 “Peptide nanotubes as dynamic materials”
Prof. Juan Granja, Federica Novelli
Spain

11 “Metal ion binding peptides and proteins: from simple molecular probes to whole cell-based biosensors for the detection of (toxic) metal ions”
Ria Balogh, Levente Szekeres, Bela Gyurcsik, Attila Jancso
University of Szeged
Hungary

12 “Antimicrobial peptides.”
Josette Perrier/Marc Maresca
France

Chapter 5

Antimicrobial Ribosomally synthesized and Post-translationally modified Peptides as a source of alternatives to antibiotics: a focus on the sactipeptides and ranthipeptides subclasses

Clarisse Roblin, Pierre Rousselot-Pailley, Victor Duarte, Josette Perrier & Mickael Lafond

Abstract

The resurgence of microbial infections associated with the increasing emergence of antibiotic resistant strains and the lack of new antibiotics have escalated quickly to become one of the major threats in Public Health nowadays. In that context, new molecules with antibacterial activity are actively searched. Ribosomally synthesized and Post-translationally modified Peptides (RiPPs) are a potential trove of such alternatives to antibiotics. In this chapter, we review the common chemical and biosynthesis features of RiPPs offering bio-engineering potentials. Then, we give a brief description of each class of RiPPs known to date before presenting into further details two subclasses of RiPPs: sactipeptides and ranthipeptides. They share common features consisting in the incorporation of thioether bonds by radical SAM enzyme. The distinction between these two subclasses lies in the position of the carbon of the acceptor residue involved in the thioether bond: Cα for sactipeptides and Cβ or Cγ for ranthipeptides. Sactipeptides constitute a small but growing subclass of RiPPs displaying potent antibacterial activity and with identified clinical properties for some members. On the other hand, ranthipeptides are the most recently characterized RiPPs and their biological roles remain to be characterized so far.

Keywords: Antibiotics, RiPPs, sactipeptides, ranthipeptides, radical SAM enzyme

Appendix 2: Patent FR 19 01896 - Fungal cyclic peptides as antibacterial agents active against *Clostridium perfringens*

During my thesis I had the opportunity to work on another project on antimicrobial peptides developed at ISM2 by Marc Maresca and Hamza Olleik. These peptides are non-ribosomal fungal cyclic peptides. In particular, I was involved in the studies on Destruxin A and B, which have a very narrow-spectrum. Indeed, to date the only identified bacterial specie sensitive to Destruxin A and B is *C. perfringens*. These peptides are commercially available so our team didn't have to work on the production and purification and their structures was already known but the characterization of the biological activity was very similar to RumC which is why I was involved in this project as well.

Description

Titre de l'invention : Utilisation de peptides cycliques fongiques de type destruxine comme agents antibactériens actifs contre Clostridium perfringens

[0001] La présente invention concerne le domaine de la prévention ou du traitement des infections bactériennes, notamment par *Clostridium perfringens*.

[0002] *Clostridium perfringens* est responsable d'infections intestinales chez l'Homme ainsi que chez l'animal. Chez l'Homme, *Clostridium perfringens* est responsable de toxi-infections alimentaires. Clostridium perfringens est ainsi l'une des causes les plus courantes d'intoxication alimentaire aux États-Unis et au Canada (Johnson, E. A., Summanen, P., & Finegold, S. M. (2007). Clostridium. In P. R. Murray (Ed.), Manual of Clinical Microbiology (9th ed., pp. 889-910). Washington, D.C. : ASM Press). En France, *Clostridium perfringens* occupe le 4e rang en nombre de foyers (2006- 2007) et le 1er (2006) ou le 3e rang (2007) (Tableau 3) en nombre de cas parmi les causes identifiées dans le cadre de la déclaration obligatoire (DO) des toxi-infections alimentaires collectives (TIAC) (source ANSES, https://www.anses.fr/fr/system/files/MIC2010sa0235Fi.pdf). Chez les animaux d'élevage, *Clostridium perfringens* infecte principalement les porcs et les volailles avec des conséquences économiques (baisse de rendement, mortalité et coût du traitement) et sanitaires (transmission à l'Homme). Dans les élevages de volailles, il peut causer dans sa forme clinique une mortalité très anormalement élevée (jusqu'à 50% de l'élevage) et dans sa forme sub-clinique une infection par *Clostridium perfringens* se traduit généralement par des pertes économiques importantes puisque les performances des animaux sont largement diminuées.

[0003] Il est désirable de mettre au point des compositions permettant d'agir spécifiquement contre cette souche afin de ne pas entrainer de modifications de la flore intestinale.

[0004] Les destruxines sont des peptides cycliques fongiques de type cyclohexadepsipeptides produits par divers champignons principalement du genre *Metarhizium anisopliae* mais aussi des genres *Metarhizium brunneum, Beauveria felina, Ophiocordyceps coccidiicola, Alternaria brassice, Alternaria linicola* et *Aschersonis sp*.

[0005] Il existe diverses destruxines (35 molécules identifiées à ce jour) regroupées en 7 séries (séries A, B, C, D, E, F et G) (Pedras et al. Phytochemistry 2002, 59, 579-96).

[0006] Elles sont formées de cinq acides aminés (de conformation spatiale S) et d'un acide alpha-hydroxylé (de conformation spatiale R). Les destruxines des différentes séries diffèrent selon le type d'acides aminés, le type d'acide alpha-hydroxylé et/ou sur la présence ou non de N-méthylation des acides aminés. Ces molécules sont connues

pour avoir diverses activités biologiques (Wang et al., Molecules 2018, 23, 169; doi:10.3390) telles que des activités insecticides, cytotoxiques, immunosuppresive, antiproliférative, antivirale (Pedras et al., Phytochemistry, 2002, 59, 579-96 et Wang et al., Molecules 2018, 23, 169; doi:10.3390) et certaines demandes de brevet auraient allégué une activité contre l'ostéoporose (CN101433214B, CN106810601A, WO2002064155A1). Néanmoins, leur effet antibactérien n'a jamais été rapporté (Wang et al., Molecules 2018, 23, 169; doi:10.3390). L'activité contre la bactérie *Helicobacter pylori* rapportée (Kao et al., Process. Biochem. 2015, 50, 134-139) ne correspond pas à une activité antibactérienne mais à une activité d'inhibition de la vacuolisation causée par *H pylori* dans les cellules gastriques.

[0007] De façon inattendue, il a maintenant été démontré que les destruxines présentent une activité contre *Clostridium perfringens.* De plus, à l'inverse d'autres peptides cycliques fongiques (Enniatines A, A1, B, B1 et Beauvericine notamment qui ont un spectre d'action large avec une activité antibactérienne sur plusieurs bactéries Gram+), les destruxines ont montré une sélectivité d'action contre *Clostridium perfringens*. Cette activité sélective des destruxines permet d'envisager leur utilisation pour le traitement et/ou la prévention des infections liées à *Clostridium perfringens* notamment les infections intestinales chez l'Homme et l'animal d'élevage, dont le poulet.

[0008] Selon un premier objet, la présente invention concerne une composition comprenant au moins une destruxine pour traiter et/ou prévenir les infections par *Clostridium perfringens*.

[0009] Selon un mode de réalisation, la destruxine est choisie parmi les destruxines des séries A, B, C, D, E, F ou G de champignon, ou leurs dérivés.

[0010] On entend par « destruxines » des peptides cycliques de type cyclohexadepsipeptide, tels que ceux produits par les champignons du genre *Metarhizium anisopliae, Metarhizium brunneum, Beauveria felina, Ophiocordyceps coccidiicola, Alternaria brassice, Alternaria linicola* et *Aschersonis sp*.

[0011] On peut notamment citer les destruxines des séries A, B, C, D, E, F et G décrites par Pedras et al. Phytochemistry, 2002, 59, 579-96, et notamment les destruxines :

- Série A : Dx A, A_1, A_2, A_3, A_4, A_5, A_4 chlorohydrin, desmethylDx A, dihydroDx A ;
- Série B : B, B_1, B_2, desmethylDx B, Desmethyl Dx B_2, homoDx, protoDx, hydroxyDx B, hydroxyhomoDx B, beta-D-Glucopyranosyl-hydroxyDx B ;
- Série C : C, C_2, desmethylDx C ;
- Série D : D, D_1, D_2
- Série E : E, E_1, E_2, E chlorhydrin, E_2 chlorohydrin, E diol, E_1 diol ;
- Série F : F ;
- PseudoDx A , PseudoDx B .

[0012] Selon un mode de réalisation particulier, on peut notamment citer les destruxines A, B, C, D, E, F ou G et leurs dérivés (dont les sources sont notamment indiquées dans Pedras et al, *supra*)notamment les destruxine A et B. Les destruxines A et B sont disponibles commercialement (Sigma-Aldrich ou A2S, pureté>98%).

[0013] Une destruxine selon l'invention inclut les destruxines pré-citées, ainsi que leurs dérivés, notamment définis par la formule générale (I) ci-dessous.

[0014] La destruxine pour l'application antibactérienne de l'invention est une destruxine fonctionnelle.

[0015] Par "destruxine fonctionnelle" ou "destruxine à activité fonctionnelle", on entend une destruxine présentant une activité susceptible de prévenir et ou traiter une infection bactérienne. On peut déterminer si une protéine est fonctionnelle, par toute méthode connue, par exemple par un essai in vitro de détermination de l'activité antibactérienne (CMI, tel que décrit dans l'exemple 1).

[0016] La destruxine selon l'invention peut être d'origine fongique ou de synthèse, de préférence d'origine fongique.

[0017] L'expression "destruxine d'origine fongique" inclut la destruxine de champignon telle que celles définies ci-avant ou un dérivé de celle-ci.

[0018] A titre de destruxine selon l'invention, on peut notamment citer les composés de formule (I) :

[Chem.1]

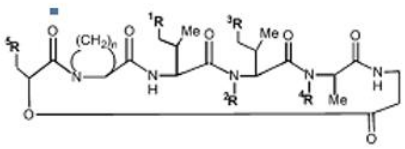

[0019] (I)

[0020] Dans laquelle

[0021] ^{1}R représente un atome d'hydrogène, un groupe C1-C6 alkyle ou un groupe aralkyle ;

[0022] ^{2}R, ^{3}R, ^{4}R identiques ou différents représentent indépendamment un atome d'hydrogène ou un groupe C1-C6 alkyle ;

[0023] ^{5}R représente un groupe choisi parmi les groupes C2-C6 alkènyle et C1-C6 alkyle éventuellement substitués par un ou plusieurs substituants choisis parmi les atomes d'halogène, les groupes hydroxy (OH), carboxy (COOH), -glycosyle, et les groupes hétérocycliques de 3 à 6 membres comprenant un ou plusieurs hétéroatomes choisis parmi N, O et S ;

[0024] Et plus particulièrement:

[0025] ^{1}R représente un atome d'hydrogène, un groupe méthyle ou un groupe benzyle ;

[0026] ^{2}R, ^{3}R, ^{4}R identiques ou différents représentent indépendamment un atome d'hydrogène ou un groupe méthyle ;

[0027] ^{5}R représente un groupe choisi parmi –CH=CH_2, -CHOHCH_2Cl, CH=CH_2, -$CHMe_2$, -$COHMe_2$, -C(O-beta-D-glycosyl)Me_2, -$CHMeCH_2OH$, -CHMeCOOH, [Chem2] 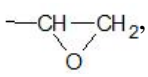 , -CHOHCH_2Cl, -$CHOHCH_2OH$, -CHOHMe, -$CHMe_2$.

[0028] Selon la présente invention, les radicaux Alkyle représentent des radicaux hydrocarbonés saturés, en chaîne droite ou ramifiée, de 1 à 6 atomes de carbone, tels que les radicaux méthyle, éthyle, propyle, butyle, pentyle, hexyle, isopropyle, tert-butyl, 2-méthylbutyle, 2-méthylpentyle, 1-méthylpentyle.

[0029] Parmi les atomes d'Halogène, on cite plus particulièrement les atomes de fluor, de chlore, de brome et d'iode, de préférence le fluor.

[0030] Les radicaux Alkényle représentent des radicaux hydrocarbonés de 2 à 6 atomes de carbone, en chaîne droite ou ramifiée, et comprenant une ou plusieurs insaturations éthyléniques. Parmi les radicaux Alkènyle, on peut notamment citer les radicaux allyle ou vinyle.

[0031] Le terme aralkyle désigne les groupes AlkyleAryle où alkyle est défini comme ci-avant et aryle désigne un système aromatique hydrocarboné, mono ou bicyclique de 6 à 10 atomes de carbone. Parmi les radicaux -AlkyleAryle, on peut notamment citer le radical benzyle ou phénétyle.

[0032] La composition de l'invention peut comprendre une destruxine sous forme pure en mélange, ou sous forme d'un champignon produisant une destruxine, ou un extrait de celui-ci, tel qu'un broyat ou un surnageant de culture de celui-ci, notamment un extrait comprenant une destruxine, ou leurs mélanges.

[0033] Wang et al. (*supra*) décrit notamment différentes destruxines et les champignons les produisant (pages 14 et 15). A titre de champignon produisant une destruxine, on peut citer les espèces *Metarrhizium, Beauveria, Ophiocordyceps, Alternaria* et *Aschersoni* et notamment les genres *Metarrhizium anisopliae, Metarhizium brunneum, Beauveria felina, Ophiocordyceps coccidiicola, Alternaria brassicae, Alternaria linicola, Ophiocordyceps coccidiicola, Alternaria brassicae et Aschersonis sp ;* notamment *Beauveria felina* , *Metarrhizium anisopliae,Metarhizium brunneum* , Ophiocordyceps sp., *Alternaria alternata, Alternaria brassicae, Alternaria linicola* ; et leurs mélanges, ou les extrait de ceux-ci, et/ou les surnageant de culture de ceux-ci.

[0034] Certains de ces genres sont disponibles commercialement ou disponibles auprès d'organismes de dépôt : *Beauveria felina* et *Metarhizium anisopliae* sont notamment disponibles commercialement, chez DSMZ et ATCC, par exemple sous les références DSM 4678 et ATCC® 60335™ ou DSM 1490

[0035] Certains de ces genres sont disponibles commercialement ou disponibles auprès d'organismes de dépôt. Ils sont notamment disponibles commercialement, chez DSMZ et ATCC, par exemple *Beauveria felina* sous la référence DSM 4678 ; *Metarrhizium*

anisopliae sous la référence ATCC® 60335™, DSM 1490 et DSM 21704 ; *Metarhizium brunneum* sous la référence ATCC® 90448™ ; Ophiocordyceps sp. sous la référence ATCC® 24400™; *Alternaria alternata* sous la référence ATCC® 13963, ATCC® 66981, DSM-12633, DSM-62006, DSM-62010 ou DSM-1102; *Alternaria brassicae* sous la référence ATCC® 58169, ATCC® 38713 ou ATCC® 34642 ; *Alternaria linicola* sous la référence ATCC® 201065, ATCC® 11802 ou ATCC® 201658.

[0036] On entend par « surnageant » de culture ou sécrétome, le milieu de culture dans lequel a été cultivé le champignon, après séparation dudit champignon.

[0037] Selon la présente invention, les composés de formule (I) présentent une activité anti-bactérienne spécifique contre *Clostridium perfringens.*

[0038] Les composés de formule (I) sont donc utiles dans le traitement et/ou la prévention des infections liées à *Clostridium perfringens*.

[0039] Les compositions selon l'invention peuvent être utilisées en thérapie humaine ou vétérinaire afin de traiter une infection causée par *Clostridium perfringens*, ou à titre de complément alimentaire pour animaux afin de prévenir l'infection par *Clostridium perfringens*.

[0040] De façon avantageuse et contrairement aux antibiotiques tel que le métronidazole classiquement utilisé pour traiter les infections par *Clostridium perfringens*, l'administration de destruxine n'induit pas de sélection de bactéries résistantes (voir Figure 1).

[0041] *Clostridium perfringens* comprend ou consiste en la séquence ATCC®13124™ déposée auprès de l'*ATCC.* Par exemple, *Clostridium perfringens* peut comprendre ou consister en une séquence présentant un degré d'identité d'au moins 80% à ladite séquence ATCC®13124™, disponible commercialement, notamment au moins 85% d'identité, de préférence au moins 90% d'identité, et plus particulièrement au moins 95%, au moins 96%, au moins 97%, au moins 98% ou au moins 99% d'identité, étant entendu que ladite séquence de *Clostridium perfringens* est fonctionnelle.

[0042] Selon un autre objet, la présente invention concerne donc une composition pharmaceutique comprenant une destruxine selon l'invention avec un excipient pharmaceutiquement acceptable.

[0043] De préférence, ladite composition contient une quantité efficace du composé selon l'invention. De préférence, ladite composition est administrée à un patient ou un animal qui en a besoin.

[0044] La présente invention concerne également une destruxine selon l'invention pour le traitement et/ou la prévention d'infections bactériennes liées à *Clostridium perfringens,* telles que les infections intestinales, notamment les entérites nécrotiques.

[0045] Les compositions pharmaceutiques selon l'invention peuvent être présentées sous des formes destinées à l'administration par voie parentérale ou orale.

[0046] Elles seront donc présentées sous forme de solutés ou de suspensions injectables ou flacons multi-doses, sous forme de comprimés nus ou enrobés, de dragées, de capsules, de gélules, de pilules, de cachets, de poudres, de suppositoires ou de capsules rectales, de solutions ou de suspensions.

[0047] Les excipients qui conviennent pour de telles administrations sont les dérivés de la cellulose ou de la cellulose microcristalline, les carbonates alcalino-terreux, le phosphate de magnésium, les amidons, les amidons modifiés, le lactose pour les formes solides.

[0048] Pour l'usage parentéral, l'eau, les solutés aqueux, le sérum physiologique, les solutés isotoniques sont les véhicules les plus commodément utilisés.

[0049] La posologie peut varier dans les limites importantes (0,5 mg à 1000 mg) en fonction de l'indication thérapeutique et de la voie d'administration, ainsi que de l'âge et du poids du sujet.

[0050] Selon un autre objet, la présente invention concerne également les compositions alimentaires comprenant une destruxine selon l'invention. Lesdites compositions conviennent particulièrement à l'alimentation des animaux d'élevage tels que le porc ou les volailles ou tout autre animal d'élevage susceptible d'être infecté par *Clostridium perfringens*.

[0051] Selon un autre objet, la présente invention concerne également l'utilisation d'une destruxine à titre d'additif alimentaire pour les animaux d'élevage dont le porc et les volailles pour le traitement et/ou la prévention des infections bactériennes par une infection par la souche *Clostridium perfringens*.

[0052] Les exemples suivants illustrent l'invention, sans toutefois la limiter. Les produits de départs utilisés sont des produits connus ou préparés selon des modes opératoires connus.

Brève description des dessins

[0053] [fig.1]

La Figure 1 illustre l'évaluation de l'induction de résistance chez Clostridium perfringens par les destruxines A ou B et le métronidazole. L'apparition de mutants résistants a été évaluée en présence de destruxines A ou B ou de métronidazole comme indiqué dans le texte.

[0054] [fig.2]

La Figure 2 illustre l'évaluation de l'effet perméabilisant des destruxines sur Clostridium perfringens. Clostridium perfringens a été exposée pendant 2h aux destruxines A ou B, à la nisine, à l'enniatine A1 ou au CTAB à une dose correspondant à 5 fois leur CMI. La perméabilisation de la membrane bactérienne a été mesurée à l'aide d'iodure de propidium comme expliqué dans le texte. La perméabilisation est

exprimée en pourcentage, le CTAB servant de contrôle positif et donnant 100 % de perméabilisation. Les valeurs portées dans le graphique correspondent aux moyennes +/- écart-type.

[0055] [fig.3]

La Figure 3 représente la détermination de la pression critique d'insertion des destruxines dans une monocouche formée de lipides extraits de Clostridium perfringens. Les pressions critiques d'insertion des destruxines A et B, de la nisine, de l'enniatine A1 et du CTAB ont été mesurées comme indiqué dans le texte à une dose correspondant à 5 fois leur CMI.

[0056] [fig.4]

La Figure 4 illustre la détermination de la capacité d'insertion des destruxines dans une monocouche formée de lipides extraits de Clostridium perfringens et présentant une pression initiale de surface correspondant à la membrane des bactéries. L'insertion des destruxines A et B, de la nisine, de l'enniatine A1 et du CTAB dans une monocouche lipidique mimant la membrane de Clostridium perfringens a été mesuré comme indiqué dans le texte à une dose correspondant à 5 fois leur CMI. Les valeurs portées dans le graphique correspondent à la moyenne +/- écart-type.

[0057] [fig.5]

La Figure 5 représente le phénotype morphologique de la bactérie Clostridium perfringens (ATCC 13124) incubée avec différents antibiotiques conventionnels de mécanisme d'action connu. Clostridium perfringens (ATCC 13124) a été exposé à divers antibiotiques conventionnels agissant sur la synthèse de macromolécules indiquée dans le graphique ou à la destruxine A (à une dose correspondant à 5 fois leur CMI). Après 2h d'exposition, les bactéries ont été marquées comme indiqué dans le texte avant observation au microscope à fluorescence des phénotypes obtenus.

[0058] Exemples

[0059] **I- Exemple 1 : Evaluation de l'activité antibactérienne**

[0060] *Matériels et Méthodes :*

[0061] L'activité antimicrobienne des destruxines A et B a été évalué sur divers souches de bactéries et champignons commerciales listées dans le Tableau 2 et obtenues chez ATCC, DSMZ ou l'institut Pasteur (CIP). L'activité antimicrobienne a été mesurée par détermination de la Concentration Minimale Inhibitrice ou CMI suivant les instructions du *National Committee of Clinical Laboratory Standards* (NCCLS, 1997) et tel que décrit dans les publications suivantes : Oyama et al., Nature Biofilms and Microbiomes, 2017, 3, 33; Benkhaled et al., Polym. Chem., 2018, 9, 3127-3141; Olleik et al., Eur J Med Chem, 2019, 165, 133-141.

[0062] La détermination de la CMI se fait par exposition des bactéries ou champignons à des doses croissantes de destruxines A ou B ou d'antibiotiques de références obtenues par

dilution en cascade au ½ de ces molécules dans le milieu de culture.

[0063] Brièvement, chaque souche bactérienne ou fongique a été cultivée sur boite de Pétri contenant le milieu de culture spécifique de la souche étudiée. Une colonie a été prélevée et utilisée pour ensemencer 3 ml de milieu de culture. Après incubation à 37°C sous agitation (200 rotations par minutes (rpm)) durant 16h, la densité optique (DO) a été lue à 600 nm afin d'estimer la densité bactérienne. La suspension bactérienne a alors été diluée au 1/100 dans 3 ml de milieu de culture avant incubation à 37°C sous agitation à 200 rpm pendant 2-3h jusqu'à obtenir une DO_{600nm} de 0.6.

[0064] Les bactéries ont alors été diluées afin d'atteindre une densité de 10^{E5} bactéries par millilitre (10^{E5} bactéries/ml). Pour les souches fongiques, la densité utilisée a été de 10^{E3} cellules par ml pour *Candida albicans* et 10^{E4} conidies par mil pour les autres champignons. 100 µl de cette suspension bactérienne ont alors été ajoutés à des puits d'une plaque de 96 puits en polypropylène (Greiner BioOne) contenants déjà 100 µl de destruxines A ou B ou d'antibiotiques de référence dilués en cascade au ½ dans du milieu de culture. Les plaques 96 puits ont ensuite été incubées selon la souche testée dans les conditions de température et de temps indiquées dans le Tableau 2.

[0065] Dans le cas des souches anaérobies (dont toutes les souches de *Clostridium*), la CMI a été mesurée en utilisant une chambre anaérobie (Coy Laboratory Products, Grass Lake, MI).

[0066] Pour les souches micro-anaérobies (*H. pylori* et *E. faecalis*) la CMI a été mesurée en utilisant les systèmes micro-anaérobiques BD GasPack.

[0067] En fin d'incubation, la DO_{600nm} a été lue à l'aide d'un lecteur de microplaque (Synergy Mx, Biotek), la CMI correspondant à la plus faible concentration de destruxines A ou B ou d'antibiotique de référence capable d'inhiber l'augmentation de DO_{600nm} causée par la croissance bactérienne ou fongique. Le test a été répété 3 fois de manière indépendante (n=3).

[0068] La Concentration Minimale Bactéricide (CMB) correspondant à la plus faible concentration entraînant la mort de plus de 99.9 % des bactéries ou champignons a également été mesurée. La CMB a été mesurée en étalant sur boite de Pétri de 10 µl du contenu des puits des plaques 96 puits utilisées lors de la mesure de la CMI. Après incubation dans les conditions propres à chaque souche et listées dans le Tableau 2, le nombre de colonies bactériennes/fongiques a été déterminé. Les concentrations d'antibiotique donnant une seule colonie ou pas de colonie ont été considérées comme étant les CMB.

[0069] L'induction de résistance a également été évaluée comme décrit dans les publications suivantes : Oyama et al., Nature Biofilms and Microbiomes, 2017, 3, 33; Benkhaled et al., Polym. Chem., 2018, 9, 3127-3141. Pour cela, la bactérie *Clostridium perfringens* (ATCC13124) a été exposée à la destruxine A, à la destruxine B ou au métronidazole

durant 18 jours consécutifs. Chaque jour, la CMI a été mesurée comme indiqué précédemment. Le dernier puits où une croissance bactérienne a eu lieu (correspondant donc à la CMI divisée par deux) a été utilisé pour préparer l'inoculum permettant de mesurer la CMI le jour suivant.

[0070] **Table 2 : Souches testées et conditions de culture utilisées.**

[0071] LB : milieu Luria-Bertoni ; MH : milieu Mueller-Hinton ; BHI : milieu Brain Heart Infusion ; TS : milieu Tryptocasein Soja ; PD : Potato Dextrose ; RPMI : Roswell Park Memorial Institute medium ; Middlebrook 7H9 et 7H10: milieu sélectif des Mycobacterium.

[Tableaux1]

		Souches	Milieu de culture	Milieu utilisé pour le test de CMI	T° de la CMI	Temps d'incubation
Gram(-)	Aérobie	*Acinetobacter baumannii* (CIP 110431)	LB	MH	37	16-24
		Citrobacter farmeri (ATCC 51633)	LB	MH	37	16-24
		Citrobacter rodentium (ATCC 51116)	LB	MH	37	16-24
		Escherichia coli (ATCC 8739)	LB	MH	37	16-24
		Klebsiella pneumoniae (DSM 26371)	LB	MH	37	16-24
		Klebsiella variicola (DSM 15968)	LB	MH	37	16-24
		Pseudomonas aeruginosa (CIP 107398)	LB	MH	37	16-24
		Salmonella enterica (CIP 80.39)	LB	MH	37	16-24
		Shigella flexneri (ATCC 12022)	LB	MH	37	16-24
	Anaérobie	*Bacteroides thetaiotaomicron* (DSM 2255)	BHI	BHI	37	16-24
		Helicobacter pylori (ATCC 43504)	BHI	MH	37	24

Gram(+)	Aérobie	*Arthrobacter gandavensis* (DSM 2447)	LB	MH	37	48
		Bacillus subtilis (DSM 347)	LB	MH	37	16-24
		Bacillus cereus (DSM 31)	LB	MH	37	16-24
		Lactococcus lactis (DSM 20481)	LB	MH	37	16-24
		Listeria monocytogenes (DSM 20600)	BHI	BHI	37	16-24
		Micrococcus luteus (DSM 20030)	TS	TSB	37	16-24
		Staphylococcus aureus MRSA USA300 (ATCC BAA-1717)	LB	MH	37	16-24
		Staphylococcus aureus (ATCC 6538P)	LB	MH	37	16-24
	Anaérobie	*Clostridium botulinum* (DSM 1985)	BHI	BHI	37	24 – 48
		Clostridium coccoides (DSM 935)	BHI	BHI	37	24 – 48
		Clostridium difficile (DSM 1296)	BHI	BHI	37	24 – 48
		Clostridium nexile (DSM 1787)	BHI	BHI	37	24 – 48
		Clostridium perfringens (ATCC 13124)	BHI	LB	37	24 – 48
		Clostridium propionicum (DSM 6251)	BHI	BHI	37	48 - 72
		Enterococcus faecalis (DSM 13591)	LB	MH	37	16-24
		Lactobacillus acidophilus (DSM 20079)	BHI	BHI	37	24 – 48
		Propionibacterium	BHI	BHI	37	24 -

		acnes (ATCC 6919)				48
		Streptococcus pyogenes (DSM 20565)	BHI	BHI	37	24 – 48
Streptococcus thermophilus (ATCC LMD-9)	BHI	BHI	37	24 – 48		
Mycobacterium	Aérobie	*Mycobacterium smegmatis*(ATCC 700084)	Middlebrook 7H10	Middlebrook 7H9	37	48 – 72
Champignons	Aérobie	*Aspergillus flavus* (DSM 1959)	PD	RMPI	RT	48 – 72
		Aspergillus niger (ATCC 9142)	PD	RMPI	RT	48
		Aspergillus ochraceus (DSM 824)	PD	RMPI	RT	48 – 72
		Candida albicans (DSM 10697)	PD	RMPI	35	24
		Fusarium graminearum (DSM 1095)	PD	RMPI	RT	48 – 72
		Fusarium oxysporum (DSM 62316)	PD	RMPI	RT	48 – 72
		Fusarium verticillioides (DSM 62264)	PD	RMPI	RT	48 - 72
		Penicillium verrucosum (DSM 12639)	PD	RMPI	RT	48 – 72

[0072] *Résultats :*

[0073] Les activités antimicrobiennes de la destruxine A, de la destruxine B et d'antibiotiques de références utilisés pour comparaison sont données dans les Tableaux 3 à 6.

[0074] **Tableau 3: Valeurs des CMI de la DesA, DesB, Bafilomycine A1 et Bafilomycine B obtenues sur diverses souches bactériennes et fongiques testées. Les CMI sont**

exprimées en micromolaire ou µM (micromole par litre).

[Tableaux2]

		Souches	CMI Des A	CMI DesB	CMI Bafilo A1	CMI Bafilo B
Gram (-)	Aérobie	*Acinetobacter baumannii* (CIP 110431)	>100	>100	>100	>100
		Citrobacter farmeri (ATCC 51633)	>100	>100	100	>100
		Citrobacter rodentium (ATCC 51116)	>100	>100	>100	>100
		Escherichia coli (ATCC 8739)	>100	>100	25	>100
		Klebsiella pneumoniae (DSMZ 26371)	>100	>100	100	>100
		Klebsiella variicola (DSM 15968)	>100	>100	>100	>100
		Pseudomonas aeruginosa (CIP 107398)	>100	>100	>100	>100
		Salmonella enterica (CIP 80.39)	>100	>100	>100	>100
		Shigella flexneri (ATCC 12022)	>100	>100	>100	>100
	Anaérobie	*Bacteroides thetaiotaomicron* (DSM 2255)	>100	>100	>100	>100
		Helicobacter pylori (ATCC 43504)	>100	>100	>100	>100

Gram (+)	Aérobie	*Arthrobacter gandavensis* (DSM 2447)	>100	>100	3	3
		Bacillus cereus (DSM 31)	>100	>100	12.5	25
		Bacillus subtilis (DSM 347)	>100	>100	100	20
		Lactococcus lactis (DSM 20481)	>100	>100	50	50
		Listeria monocytogenes (DSM 20600)	>100	>100	25	50
		Micrococcus luteus (DSM 20030)	>100	>100	25	25
		Staphylococcus aureus MRSA USA300 (ATCC BAA-1717)	>100	>100	>100	20
		Staphylococcus aureus (ATCC 6538P)	>100	>100	12.5	10
	Anaérobie	*Clostridium botulinum* (DSM 1985)	>100	>100	6.25	30
		Clostridium coccoides (DSM 935)	>100	>100	>100	30
		Clostridium difficile (DSM 1296)	>100	>100	>100	>100
		Clostridium nexile (DSM 1787)	>100	>100	50	60
		Clostridium perfringens (ATCC 13124)	1.5	3	25	10
		Clostridium propionicum (DSM 6251)	>100	>100	25	25
		Enterococcus faecalis	>100	>100	>100	40

		(DSMZ 13591)				
		Lactobacillus acidophilus (DSM 20079)	>100	>100	33	10
		Propionibacterium acnes (ATCC 6919)	>100	>100	50	60
		Streptococcus pyogenes (DSM 20565)	>100	>100	66	20
Streptococcus thermophilus (ATCC LMD-9)	>100	>100	25	30		
Mycobacterium	Aérobie	*Mycobacterium smegmatis*(ATCC 700084)	>100	>100	>100	>100
Champignons	Aérobie	*Aspergillus flavus* (DSM 1959)	>100	>100	3.25	3.25
		Aspergillus niger (ATCC 9142)	>100	>100	>100	100
		Aspergillus ochraceus (DSM 824)	>100	>100	>100	6.25
		Candida albicans (DSM 10697)	>100	>100	>100	100
		Fusarium graminearum (DSM 1095)	>100	>100	6.25	25
		Fusarium oxysporum (DSM 62316)	>100	>100	>100	50
		Fusarium verticillioides (DSM 62264)	>100	>100	50	50
		Penicillium verrucosum (DSM 12639)	>100	>100	6.25	6.25

[0075] L'analyse des résultats du Tableau 3 montre que :

- Parmi toutes les souches bactériennes et fongiques testées, seule la souche *Clostridium perfringens* (ATCC 13124) est sensible à la destruxine A et la destruxine B avec de très bonne valeur de CMI (respectivement 1.5 et 3 µmol/l) démontrant la sélectivité des destruxines A et B contre la souche *Clostridium perfringens* (ATCC 13124).
- La bafilomycine A1 et la bafilomycine B, deux antibiotiques ayant la même cible moléculaire que les destruxines dans les cellules eucaryotes (la V-ATPase) ne sont pas sélectives de *Clostridium perfringens* et sont ainsi actives contre de nombreuses souches bactériennes et fongiques indiquées dans le Tableau 3.

[0076] **Tableau 4 : Valeurs des CMI de la DesA, DesB, Bafilomycine A1, B1 et du métronidazole obtenues sur diverses souches bactériennes anaérobies. Les CMI sont exprimées en micromolaire ou µM (micromole par litre).**

[Tableaux3]

Souche	CMI DesA	CMI DesB	CMI Bafilo A1	CMI Bafilo B	CMI Métro-nidazole
Bacteroides thetaioataomicron (DSM 2255)	>100	>100	>100	>100	2.34
Clostridium botulinum (DSM 1985)	>100	>100	6.25	30	0.29
Clostridium coccoides (DSM 935)	>100	>100	>100	30	0.29
Clostridium difficile (DSM 1296)	>100	>100	>100	>100	1.17
Clostridium nexile (DSM 1787)	>100	>100	50	60	2.34
Clostridium perfringens (ATCC 13124)	1.5	3	25	10	9.37
Clostridium propionicum (DSM 6251)	>100	>100	25	25	1.17
Enterococcus faecalis (DSM 13591)	>100	>100	>100	40	>1500
Helicobacter pylori (ATCC 21031)	>100	>100	>100	>100	>1500
Lactobacillus acidophilus (DSM 20079)	>100	>100	33	10	>1500
Propionibacterium acnes (ATCC	>100	>100	50	60	1500

6919)					
Streptococcus pyogenes (DSM 20565)	>100	>100	66	20	>1500
Streptococcus thermophilus (ATCC LMD-9)	>100	>100	25	30	1500

[0077] Les données du Tableau 4 confirment que :

- Parmi toutes les souches bactériennes anaérobies testées, seule la souche *Clostridium perfringens* (ATCC 13124) est sensible à la destruxine A et la destruxine B avec de très bonne valeur de CMI (respectivement 1.5 et 3 µmol/l) démontrant la sélectivité des destruxines A et B contre cette souche.
- De manière importante, toutes les autres souches de *Clostridium* testées (autre que *Clostridium perfringens*) sont insensibles aux destruxines A et B (CMI > 100 µM).
- Les données du Tableau 4 confirment que, contrairement aux destruxines, le métronidazole, un antibiotique conventionnel actif sur de nombreuses bactéries anaérobies Gram+ et Gram-, n'est pas sélectif de *Clostridium perfringens* et est actif sur toutes les souches de *Clostridium* testés dans le Tableau 4.

[0078] **Tableau 5 : Valeurs des CMI de divers antibiotiques conventionnels et des destruxines A et B contre la souche *Clostridium perfringens* (ATCC13124). Les CMI sont exprimées en micromolaire ou µM (micromole par litre) et en mg/l (milligramme par litre).**

[Tableaux4]

Antibiotique	**CMI (µM)**	**CMI (mg/l)**
Bafilomycin A1	25	15.5
Bafilomycin B1	10	8.15
Chloramphénicole	12.5	4.03
Daptomycine	8	12.96
Destruxine A	1.5	0.86
Destruxine B	3	1.78
Enniatine A1	6.25	4.16
Fosfomycine	125	22.75
Métronidazole	9.37	1.60
Tétracycline	11.7	5.20

[0079] L'analyse des résultats du Tableau 5 montre que les CMI de la destruxine A et de la destruxine B obtenues sur la souche *Clostridium perfringens* (ATCC 13124) sont proches ou inférieures à celles d'antibiotiques conventionnels utilisés pour traiter les infections bactériennes. De manière importante, les CMI de la destruxine A (1.5 µM ou 0.86 mg/l) et de la destruxine B (3 µM ou 1.78 mg/l) sont nettement inférieures à celle du métronidazole (9.37 µM ou 1.6 mg/l), l'antibiotique conventionnel classiquement utilisé dans le traitement des infections intestinales causées par *Clostridium perfringens*.

[0080] **Tableau 6 : Comparaison des valeurs de CMI des destruxines A et B et de l'enniatine A1 contre divers souches bactériennes et fongiques.** Les CMI sont exprimées en micromolaire ou µM (micromole par litre).

[Tableaux5]

	Destruxine A	**Destruxine B**	**Enniatine A1**
Bacillus subtilis (DSM 347)	>100	>100	25
Clostridium perfringens (ATCC 13124)	1.5	3	6.25
Enterococcus faecalis (DSM 13591)	>100	>100	6.25
Escherichia coli (ATCC 8739)	>100	>100	>100
Pseudomonas aeruginosa (CIP 107398)	>100	>100	>100
Staphylococcus aureus (ATCC 6538P)	>100	>100	25
Candida albicans (DSM 10697)	>100	>100	3.125

[0081] Les données du Tableau 6 montrent que l'enniatine A1, un peptide cyclique fongique appartenant à la famille des depsipeptides comme les destruxines, ne présente pas la sélectivité étroite des destruxines contre le *Clostridium perfringens* puisque l'enniatine A1 est active contre diverses souches Gram+ et la levure *Candida albicans* comme indiqué dans le Tableau 6. Ceci démontre que les propriétés antimicrobiennes des destruxines, particulièrement leur sélectivité contre *Clostridium perfringens* ne sont pas partagées par d'autres membres de la même famille de peptide, les depsipeptides fongiques.

[0082] **Tableau 7 : Valeurs des CMI de la destruxine A et de la destruxine B contre divers souches cliniques de *Clostridium perfringens* isolées de patients humains ou d'animaux. Les CMI sont exprimées en micromolaire ou µM (micromole par litre).**

[Tableaux6]

Souche	**CMI DesA**	**CMI DesB**
Humaine 779269	0.75	3
Humaine 779790	1.5	3
Humaine 779794	1.5	3
Humaine 779809	1.5	3
Humaine 664408	1.5	3
Humaine 256313	1.5	3
Humaine 597867	1.5	3
Humaine 22151	1.5	3
Humaine 366478	1.5	3
Humaine 96289	1.5	3
Animal 24	0.75	3
Animal 56	3	3
Animal 60	1.5	1.5

[0083] L'analyse des résultats du Tableau 7 montre que la destruxine A et la destruxine B possèdent des CMI sur souches cliniques de *Clostridium perfringens* (isolées de patients ou d'animaux infectés) proches ou inférieures à celles obtenues sur la souche *Clostridium perfringens* (ATCC 13124). Ainsi, les destruxines A et B ont la même activité, voir sont plus actives sur les souches isolées de patients ou d'animaux que sur la souche ATCC de référence, démontrant leur possible utilisation dans le traitement des humains et animaux infectés par *Clostridium perfringens* ou dans le traitement préventif des infections par *Clostridium perfringens* des animaux d'élevage dont le porc et les volailles.

[0084] Les concentrations minimales bactéricides de la destruxine A et de la destruxine B ont été déterminées sur la souche *Clostridium perfringens* (ATCC 13124) et sur les souches cliniques de *Clostridium perfringens* isolées de patients ou d'animaux. Dans tous les cas, les valeurs de CMB sont identiques aux valeurs de CMI obtenues, démontrant que les destruxines A et B ont une action bactériolytique sur *Clostridium perfringens*.

[0085] De manière très importante, l'évaluation de l'induction de résistance chez la bactérie *Clostrium perfringens* (ATCC 13124) exposée aux destruxines A ou B ou au métronidazole durant 18 jours montre que (Figure 1):

– les CMI des destruxine A et B n'évoluent pas ou peu (avec un doublement de

la valeur de la CMI) durant les 18 jours consécutifs de contact

– A l'inverse, le métronidazole entraine rapidement l'apparition de résistance avec une augmentation importante de sa CMI : multiplication de la CMI par 10 après 7 jours de contact et multiplication par 50-100 après 9 jours de contact.

[0086] Ceci démontre que, contrairement à un antibiotique conventionnel tel que le métronidazole, les destruxines A et B n'entraînent pas l'apparition et/ou la sélection de mutants de *Clostridium perfringens* résistant à leur action.

[0087] En conclusion des tests d'activité antimicrobienne des destruxines A et B, il apparait que :

– Contrairement aux antibiotiques conventionnels, dont le métronidazole, les destruxines A et B ont une action extrêmement sélective, ne présentant d'activité que contre les souches commerciales et cliniques de *Clostridium perfringens* avec une CMI / CMB très faible (0.75-3 µM). Cette sélectivité très étroite est un atout majeur des destruxines car, contrairement aux antibiotiques conventionnels qui perturbent fortement la flore commensale intestinale, l'utilisation des destruxines n'entrainera pas de dysbiose intestinale. Ceci pourrait également permettre un traitement préventif des animaux d'élevage dont le porc et les volailles par les destruxines pour prévenir l'infection par *Clostridium perfringens* sans risquer de perturber la flore commensale bénéfique des animaux.

– La sélectivité des destruxines A et B contre *Clostridium perfringens* n'est pas présente chez d'autres membres de la famille de depsipeptides fongiques dont l'enniatine A1 démontrant que tous les membres de la famille des depsipeptides n'ont pas les mêmes activités antimicrobiennes.

– Contrairement aux antibiotiques conventionnels, tel le métronidazole, l'exposition répétée aux destruxines A et B ne conduit pas à l'apparition de souches résistantes. De plus, ces résultats montrent que les destruxines sont actives contre la souche de *Clostridium perfringens* (ATCC13124) rendue résistante au métronidazole. Ces deux observations renforcent l'intérêt thérapeutique et/ou préventif des destruxines dans le contexte actuel d'augmentation constante du nombre de souches bactériennes résistantes ou multi-résistantes aux antibiotiques conventionnels.

[0088] **II- Exemple 2 : Evaluation de l'innocuité et du passage transépithélial des destruxines A et B à l'aide de cellules intestinales humaines et animales**

[0089] *Matériels et Méthodes :*

[0090] L'innocuité des dextruxines a été d'abord mesurée par un test d'hémolyse réalisé sur globules rouges humains comme publié dans le papier Oyama et al., Nature Biofilms

and Microbiomes, 2017, 3, 33. Des globules rouges obtenus chez Divbioscience (Pays Bas) ont été lavés 3 fois dans du tampon phosphate (PBS, pH 7) puis dilués à 8 % (volume : volume) dans du PBS. 100 µl de cette suspension cellulaire ont été ajoutés dans des plaques 96 puits puis 100 µl de PBS contenant des doses croissantes de destruxines A ou B ont été ajoutés dans chaque puits. Après 1h d'incubation à 37°C, les plaques ont été centrifugées à 800 g pendant 5 min. 100 µl de surnageant ont alors été transférés dans une nouvelle plaque 96 puits avant lecture de la densité optique à 405 nm. Le pourcentage d'hémolyse causé par les destruxines a été quantifié en utilisant le Triton-X100 (Sigma Aldrich) comme contrôle positif donnant 100 % d'hémolyse.

[0091] L'innocuité et l'absorption intestinale des destruxines ont également été évaluée à l'aide de cellules intestinales humaines mimant l'intestin grêle (cellules Caco-2 (ATCC HTB-37) ou le colon (cellules T84 (ATCC CCL-248) et de cellules d'intestin grêle de porc (DSM ACC701). Les cellules ont été cultivées en routine dans du milieu Dulbecco's Modified Eagle Medium supplémenté avec 10 % (volume : volume) de sérum de veau fétal. Les cellules ont été ensemencées en flasques de 25 cm2 et maintenues à 37°C dans un incubateur à CO2 avec changement de milieu tous les deux jours et passage lorsque les cellules atteignaient 80-90% de confluence.

[0092] Pour les tests d'innocuité, les cellules les cellules Caco-2, T84 ou IPEC-J2 ont été trypsinisées et ensemencées en plaques de 96 puits. Une fois confluentes, les cellules ont été exposées à des doses croissantes de destruxines A ou B ou d'autres molécules durant 48h. Après 48h d'incubation, la viabilité cellulaire a été mesurée à l'aide du kit de dosage de la toxicité de Sigma-Aldrich basé sur la résazurine (réf TOX8-1KT). Après 4h d'incubation avec le réactif du kit, la viabilité cellulaire a été mesurée par lecture de la fluorescence des puits (excitation à 530 nm / émission à 590 nm). La concentration causant 50% de mortalité cellulaire (IC50) a été calculée graphiquement à l'aide du logiciel GraphPad® Prism 7 software. L'analyse statistique des données a été faite par le test-t et le test ANOVA du logiciel.

[0093] Pour les tests d'absorption intestinale, les cellules Caco-2, T84 ou IPEC-J2 ont été ensemencées sur des inserts de culture Greiner de 1 cm2 de diamètre et de porosité 0.4 µm. Après 21 jours de culture, l'étanchéité de l'épithélium intestinal a été confirmée par mesure de la résistance électrique transépithéliale à l'aide d'un voltohmètre (EVOM de Millipore). Le passage transépithélial (apical vers basal) et l'accumulation intracellulaire des divers antibiotiques (destruxines A ou B, bafilomycine A1, métronidazole, enniatine A1) ont été mesurés après ajout dans le compartiment apical (correspondant à la lumière intestinale) de 100 µM de composé dilué dans du PBS contenant du calcium et du magnésium (PBS++). Après 4h d'incubation à 37°C, la résistance électrique transépithéliale a été mesurée à l'aide d'un voltohmètre (EVOM de Millipore) et les milieux apical, basal et intracellulaire ont été collectés et analysés par

chromatographie HPLC afin de quantifier la teneur en antibiotique.

[0094] *Résultats :*

[0095] Le test d'hémolyse (Tableau 8) montre que les destruxines A et B (comme la bafilomycine A1 et le métronidazole) n'induisent aucune hémolyse, même pour des doses de 100 µM (0 % d'hémolyse à 100 µM). A l'inverse, en accord avec sa toxicité déjà connue et rapportée dans la littérature, l'enniatine A1 qui appartient pourtant à la même famille de peptides cycliques fongiques (les depsipeptides) entraîne une hémolyse des globules rouges humains avec 51 % d'hémolyse observé à 100 µM d'enniatine A1.

[0096] L'évaluation de la toxicité des destruxines A et B sur les cellules intestinales humaines (Caco-2 et T84) et de porc (IPEC-J2) (Tableau 9) montre que, comme le métronidazole, les destruxines ne sont pas toxiques même à 100 µM vis-à-vis de ces cellules. A l'inverse, comme rapporté dans la littérature, l'enniatine A1 est toxique vis-à-vis de ces cellules intestinales. De la même façon, la bafilomycine A1 est toxique contre toutes les cellules intestinales testées avec des IC50 comprises entre 1.8 et 11.8 µM.

[0097] **Tableau 8 : Evaluation de l'effet hémolytique des destruxines A et B, de l'enniatine A1, de la bafilomycine A1 ou du métronidazole vis-à-vis des globules rouges humains.** Les valeurs portées dans le tableau indiquent le pourcentage d'hémolyse observée après 1h de contact avec 100 µM d'antibiotique.

[Tableaux7]

	Destruxine A	Destruxine B	Enniatine A1	Bafilomycine A1	Métronidazole
Pourcentage d'hémolyse	0 +/- 0	0 +/- 0	51 +/- 12	0 +/- 0	0 +/- 0

[0098] **Tableau 9 : Evaluation de la toxicité des destruxines A et B, de l'enniatine A1, de la bafilomycine A1 ou du métronidazole vis-à-vis des cellules intestinales humaines et porcines.** Les valeurs portées dans le tableau correspondent aux IC50 exprimées en µmol/l (µM) (moyenne +/- écart-type).

[Tableaux8]

	Caco-2 (mimant l'intestin grêle humain)	T84 (mimant le colon humain)	IPEC-J2 (mimant l'intestin grêle de porc)
Destruxine A	>100	>100	>100
Destruxine B	>100	>100	>100
Enniatine A1	3.1 +/- 0.5	4.5 +/- 1.2	5.1 +/- 0.6
Bafilomycine A1	11.8 +/- 2.0	9.9 +/- 0.9	1.8 +/- 1.9
Métronidazole	>1500	>1500	>1500

[0099] Sur la base des données de toxicité, on peut conclure que, comme le métronidazole (antibiotique conventionnel de référence utilisé pour traiter les infections intestinales causées par *Clostridium perfringens*, les destruxines A et B ne sont pas hémolytiques et ne causent pas de toxicité à l'encontre des cellules humaines et porcines aux doses actives contre *Clostridium perfringens*. Sur la base de la CMI et des IC50 de la destruxine A et B, le facteur de sécurité (calculé en divisant l'IC50 obtenue dans le test de toxicité par la CMI obtenue avec le *Clostridium perfringens* (ATCC 13124)) est d'au moins 66. A l'inverse, la bafilomycine A1 et l'enniatine A1 présentent une toxicité à faible dose contre les cellules humaines et porcines (de 1.8 à 11.8 µM pour la bafilomycine A1 et de 3.1 à XX µM pour l'enniatine A1). Les CMI contre *Clostridium perfringens* (ATCC 13124) étant de 25 µM pour la bafilomycine A1 et de 6.25 µM pour l'enniatine A1, à l'inverse des destruxines ou du métronidazole, ces molécules ne présentent pas de facteurs de sécurité (facteur de sécurité inférieur à 1 pour la bafilomycine A1 et pour l'enniatine A1).

[0100] L'absence de toxicité des destruxines A et B les distingue donc également de l'enniatine A1, un autre peptide cyclique fongique de type depsipeptides à action antibactérienne qui lui est très toxique.

[0101] L'évaluation du transport transépithélial et de l'accumulation intracellulaire des destruxines A et B à l'aide de cellules épithéliales humaines ou porcines (Tableau 10) montre que l'absorption intestinale des destruxines A et B même au bout de 4h d'incubation est faible et comprise entre 0.2 et 3.3 % de la dose initiale. De la même manière, l'accumulation intracellulaire des destruxines A et B au bout de 4h est faible et comprise entre 3.0 et 20.4 % de la dose initiale. Ceci diffère de l'enniatine A1 et de

la bafilomycine A1 qui s'accumulent dans les cellules intestinales (de 19.5 à 77.4 % de la dose initiale) en lien avec leur forte toxicité.

[0102] **Tableau 10 : Evaluation à l'aide de cellules épithéliales intestinales humaines et porcines du passage transépithélial et de l'accumulation intracellulaire des destruxines A et B, de l'enniatine A1, de la bafilomycine A1 et du métronidazole.**

[0103] Les valeurs indiquées dans le tableau ont été mesurées par HPLC après 4h d'incubation avec les cellules et correspondent au pourcentage de la dose initialement ajoutée aux cellules dans le compartiment apical.

[Tableaux9]

	Caco-2 (mimant l'intestin grêle humain)				
	Destruxine A	Destruxine B	Enniatine A1	Bafilomycine A1	Métronidazole
Fraction apicale	88.3	92.4	58.7	0.1	80.2
Fraction basale	2.3	2.5	1.95	22.5	12.9
Fraction intracellulaire	9.2	5.5	43.2	77.4	12.7

[Tableaux10]

	T84 (mimant le colon humain)				
	Destruxine A	Destruxine B	Enniatine A1	Bafilomycine A1	Métronidazole
Fraction apicale	87.6	81.6	80.5	2.5	71.3
Fraction basale	3.3	2.0	2.0	30.5	9.7
Fraction intracellulaire	15.1	20.4	19.5	68.0	19.0

[Tableaux11]

	IPEC-J2 (mimant l'intestin grêle de porc)				
	Destruxine A	Destruxine B	Enniatine A1	Bafilomycine A1	Métronidazole
Fraction apicale	88.6	95.5	45.7	0.1	84.0
Fraction basale	0.2	1.5	1.3	28.1	7.1
Fraction intracellulaire	11.1	3.0	53.0	71.8	8.9

[0104] L'intégrité tissulaire après 4h d'exposition aux destruxines A ou B a été évaluée par mesure de la résistance électrique transépithéliale des cellules intestinales humaines ou porcine cultivées sur inserts à l'aide d'un appareil de type EVOM (Tableau 11). Les données montrent que les destruxines, comme le métronidazole, affectent peu ou pas la résistance électrique transépithéliale (diminution comprise entre 2 et 17 % pour les destruxines et entre 0 et 34 % pour le métronidazole) indiquant que ces molécules causent peu ou pas d'atteinte de l'intégrité intestinale. A l'inverse, l'enniatine A1 et la bafilomycine A1 entrainent de fortes diminutions de la résistance électrique transépithéliale (diminution comprise entre 67 et 83 % pour l'enniatine A1 et 61 et 75 % pour la bafilomycine A1), indiquant une atteinte importante de l'intégrité tissulaire intestinale.

[0105] **Tableau 11 : Evaluation à l'aide de cellules épithéliales intestinales humaines et porcines de l'atteinte tissulaire causée par les destruxines A et B, de l'enniatine A1, de la bafilomycine A1 et du métronidazole.**

[0106] Les cellules intestinales humaines et porcines cultivées sur inserts ont été exposées pendant 4h à 100 µM de chaque molécule ajoutée dans le compartiment apical des inserts. Après 4h, l'intégrité tissulaire a été évaluée par mesure de la résistance électrique transépithéliale. Les valeurs sont en ohm.cm2 (moyennes +/- écart-type).

[Tableaux12]

	Contrôle	Destruxine A	Destruxine B	Enniatine A1	Bafilomycine A1	Métronidazole
Caco-2	293 +/- 7.5	281 +/- 13.3	282 +/- 15.0	95 +/- 20.6	112 +/- 16.5	252 +/- 13.7
T84	449 +/- 35.2	373 +/- 21.7	377 +/- 10.4	122 +/- 11.3	118 +/- 10.4	293 +/- 12.3
IPEC-J2	786 +/- 12.5	768 +/- 41.3	763 +/- 21.2	128 +/- 3.2	191 +/- 62.2	875 +/- 203

[0107] En conclusion, il apparait que :

– Les destruxines A et B sont non hémolytiques et peu ou pas toxiques vis-à-vis des cellules intestinales humaines et porcines testées
– L'accumulation intracellulaire et le passage transépithélial des destruxines A et B est faible, ce qui est une bonne chose. En effet, suite à leur ingestion les destruxines A et B resteront majoritairement dans la lumière intestinale ce qui est un avantage pour leur utilisation dans le traitement topique et/ou la prévention des infections intestinales causées par *Clostridium perfringens*.

[0108] **III- Exemple 3 : Identification du mécanisme d'action des destruxines A et B**

[0109] *Matériels et Méthodes :*

[0110] Le mécanisme d'action des destruxines A et B a été étudié par divers techniques. La plupart des peptides antimicrobiens (PAM) rapportés dans la littérature sont connus pour s'insérer dans la membrane bactérienne formant des pores et causant une perméabilisation / lyse de la membrane bactérienne. La capacité des destruxines A et B à perméabiliser la membrane de *Clostridium perfringens* (ATCC 13124) a donc été évaluée. La nisine, un PAM connu pour perméabiliser la membrane bactérienne a été utilisé en contrôle positif de perméabilisation. La capacité de l'enniatine A1 à former des pores a aussi été évaluée. L'évaluation de la perméabilisation se fait à l'aide de l'iodure de propidium, une molécule qui devient fluorescente une fois qu'elle rentre en contact avec de l'ADN (Oyama et al., Nature Biofilms and Microbiomes, 2017, 3, 33). La membrane bactérienne étant imperméable à l'iodure de propidium, celui ne peut rentrer en contact avec de l'ADN que si la membrane est perméabilisée. Le principe du test est le suivant. Une culture liquid de *Clostridium perfringens* (ATCC 13124) est centrifugée à 3000 rpm pendant 5 min. Le culot bactérien est alors resuspendu dans du PBS à une concentration de 10^{E9} bactéries / ml. De l'iodure de propidium (Sigma Aldrich) est ensuite ajouté à cette suspension bactérienne à une concentration finale de 60 µM. 100 µl de cette suspension sont ensuite ajoutés dans des puits d'une plaque 96

puits noire pour fluorescence (Greiner) contenant 100 µl de molécules à tester diluées dans du PBS à une concentration correspondant à 5 fois leur CMI. Après 120 min d'incubation à 37°C en condition anaérobie, la fluorescence des puits a été lue à l'aide d'un lecteur de microplaques fluorescence (excitation à 530 nm et émission à 590 nm). La perméabilisation de la membrane bactérienne de *Clostridium perfringens* (ATCC 13124) a été exprimée en pourcentage, le CTAB servant de référence et donnant 100 % de perméabilisation.

[0111] La capacité des destruxines A et B à s'insérer dans les lipides membranaires de *Clostridium perfringens* a également été étudiée par la technique des monocouches lipidiques ou balance de Langmuir (Oyama et al., Nature Biofilms and Microbiomes, 2017, 3, 33). Les lipides membranaires totaux de *Clostridium perfringens* (ATCC 13124) ont été extrait selon la technique de Folch (Oyama et al., Nature Biofilms and Microbiomes, 2017, 3, 33). Ces lipides ont été déposés à l'aide d'une seringue Hamilton à la surface d'une goutte de PBS formant une monocouche lipidique à l'interface PBS-air. Durant le test, la température est maintenue à 20 +/- 0.2 °C. Le film lipidique formé comprime une sonde positionnée à la surface du PBS entrainant une augmentation de la pression de surface mesurée à l'aide d'un microtensiomètre de surface (µTROUGH SX, Kibron Inc). Les lipides sont ainsi ajoutés jusqu'à atteindre la pression de surface souhaitée nommée pression de surface initiale (Pi dont l'unité est mN/m). Une fois la pression de surface stabilisée, les antibiotiques à tester sont injectées dans la sous-phase de PBS à l'aide d'une autre seringue Hamilton. Si l'antibiotique injecté est capable de s'insérer dans le film lipidique, il s'ensuit une augmentation de la pression de surface jusqu'à atteindre une valeur maximale correspondant à la pression de surface maximale (Pmax en mN/m). La variation de surface causée par l'insertion de l'antibiotique testé (deltaP en mN/m) est calculée en soustrayant Pi à Pmax (DeltaP = Pmax – Pi). L'affinité d'un antibiotique pour le film lipidique est évaluée par mesure de la pression critique d'insertion (Pc). Pc correspond à la pression de surface initiale qui ne permet pas l'insertion de l'antibiotique. Ainsi, plus la valeur de Pc est élevée et plus l'antibiotique peut s'insérer dans le film lipidique. Pc est déterminée graphiquement en mesurant la DeltaP causée par l'insertion de l'antibiotique à différentes valeurs de Pi (approximativement 10, 15, 20, 25 et 30 mN/m). Après avoir rapporté les points obtenus dans un graphique de type DeltaP (portée sur l'axe des Y) en fonction de Pi (portée sur l'axe des X), Pc est déterminé à partir de l'équation de la droite obtenue quand Y (DeltaP) = 0. Dans certaines expériences, pour mimer la situation physiologique, la DeltaP causée par l'insertion de l'antibiotique dans le film lipidique est mesurée pour une pression de surface Pi fixée à 30 +/- 0.5 mN/m, la pression de la membrane lipidique d'une bactérie entière étant théoriquement de cet ordre (Oyama et al., Nature Biofilms and

Microbiomes, 2017, 3, 33).

[0112] Le mécanisme d'action des destruxines A et B sur *Clostridium perfringens* (ATCC 13124) a aussi été étudié par microscopie comme précédemment expliqué (Nonejuie et al., PNAS October 1, 2013 110 (40) 16169-16174). Une suspension bactérienne de *Clostridium perfringens* (ATCC 13124) a été diluée au 1/100 et cultivée à 37°C en condition anaérobie jusqu'à atteindre une densité optique à 600 nm de 0.2. Les bactéries ont ensuite été traitées pendant 2h avec les destruxines A ou B ou avec divers antibiotiques conventionnels dont on connait la cible moléculaire. La dose d'antibiotique utilisée correspond à 5 fois leur CMI. Après 2h d'incubation, la membrane bactérienne a été marquée 10 min dans la glace à l'aide de la molécule fluorescente rouge FM4-64FX (de ThermoFisher, utilisée à 12 µg/ml) et l'ADN bactérien avec la molécule fluorescente bleu DAPI (de Sigma Aldrich, utilisée à 2 µg/ml). Les bactéries ont ensuite été centrifugées à 7 500 rpm pendant 30 sec et lavées avec de PBS. Les bactéries sont ensuite fixées à l'aide d'une solution de paraformaldéhyde à 4% pendant 15 min dans la glace avant d'être une nouvelle fois centrifugées et lavées avec du PBS. Finalement, les bactéries sont reprises dans du liquide de montage Vectashield (Vector Laboratories) et déposées entre lame et lamelle avant observation au microscope confocal à l'aide des filtres spécifiques à FM4-64FX et au DAPI (Olympus, Rungis, France).

[0113] *Résultats :*

[0114] L'effet perméabilisant sur *Clostridium perfringens* (ATCC 13124) des destruxines A et B a été évalué à l'aide de l'iodure de propidium et est illustré dans la Figure 2. Alors que la nisine et l'enniantine A1 causent une perméabilisation de l'ordre de 50-60 % de *Clostridium perfringens* (ATCC 13124), les destruxines sont sans effet, ne causant aucune perméabilisation.

[0115] La technique des monocouches lipidiques a ensuite été utilisée pour confirmer l'absence d'insertion des destruxines A et B dans la membrane de *Clostridium perfringens* (Figures 3 et 4). La détermination de la pression critique d'insertion (Pc) (Figure 3 et Tableau 12) montre que les destruxines A et B s'insérent très faiblement dans une monocouche lipidiques formée à partir de lipides totaux extraits de *Clostridium perfringens* (ATCC 13124) avec une valeur de Pc 26.9 et 27.1 mN/m pour la destruxine A et la destruxine B. Ceci signifie que les destruxines A et B ne peuvent pas s'insérer dans la membrane de *Clostridium perfringens* dont la pression de surface théorique est de 30 mN/m, comme montré dans la Figure 4 et en accord avec les données de perméabilisation (Figure 2). A l'inverse, l'enniatine A1, la nisine et le CTAB présentent tous les trois des Pc supérieures à 30 mN/m (40.1, 36.9 et 46.8 mN/m, respectivement) indiquant qu'ils peuvent donc s'insérer dans une monocouche lipidique formée de lipides de *Clostridium perfringens* à la pression initiale de 30 mN/

m (Figure 4), en accord avec leur capacité à perméabiliser la bactérie (Figure 2).

[0116] **Tableau 12 : Détermination de la pression critique d'insertion des destruxines A et B, de l'enniatine A1, de la nisine et du CTAB.**

[0117] Les pressions critiques d'insertion (Pc) des différentes molécules injectées à 5 fois leur CMI ont été déterminées à partir de la Figure 3.

[Tableaux13]

	Destruxine A	Destruxine B	Enniatine A1	Nisine	CTAB
Pc (en mN/m)	26.9	27.1	40.1	36.9	46.8

[0118] Les résultats de l'étude du mécanisme d'action des destruxines A et B sur *Clostridium perfringens* (ATCC 13124) sont portés dans la Figure 5. La microscopie montre que les destruxines agissent comme le chloramphénicol en provoquant une hypercondensation de l'ADN bactérien. Ceci suggère que, comme le chloramphénicol, les destruxines agissent en inhibant la synthèse protéique, un mécanisme d'action original pour un PAM.

[0119] En conclusion :

[0120] Ayant montré l'activité sélective des destruxines A et B sur *Clostrium perfringens*, les raisons de cette sélectivité ont été investiguées. Classiquement, les peptides antimicrobiens (PAM) sont peu ou pas sélectifs, agissant soit sur toutes les bactéries Gram+ et Gram-, soit que sur les bactéries Gram+ ou Gram-, soit sur un ensemble de bactéries proches phylogénétiquement. Les destruxines A et B sont donc très originaux puisqu'ils n'agissent que sur *Clostrium perfringens* (souches cliniques et ATCC) sans agir sur des bactéries proches phylogénétiquement comme les autres souches de *Clostridium* testés dans les Tableaux 3 et 4. La sélectivité des destruxines A et B contre *Clostrium perfringens* provient de leur mécanisme d'action original.

[0121] Ainsi, alors que la majorité des PAM déjà connus agissent en perméabilisant la membrane des bactéries, les destruxines A et B ne perméabilisent pas la membrane bactérienne de *Clostridium perfringens* (Figure 2). De même, alors que la majorité des PAM sont capables de s'insérer dans les lipides bactériens (activité suivie par la technique des monocouches lipidiques), les destruxines A et B ne pénètrent pas un film de lipides bactériens (Figures 3 et 4).

[0122] Des tests par microscopie ont permis de déterminer le mécanisme d'action de ces molécules expliquant leur action spécifique contre les bactéries du genre *Clostrium perfringens*. Il semble qu'une inhibition de la synthèse d'ADN et/ou de la paroi bactérienne (peptidoglycane) soit en cause (Figure 5). L'existence d'une cible spécifique restant à identifier et présente uniquement dans *Clostrium perfringens* explique cer-

tainement la sélectivité des destruxines A et B contre *Clostrium perfringens*. De manière importante, l'absence de perméabilisation membranaire et d'insertion dans les lipides des destruxines A et B les distinguent des autres peptides cycliques fongiques à action antibactérienne testés tel que l'enniatine A1 qui est capable de s'insérer dans les lipides et de perméabiliser la membrane bactérienne (Figures 2, 3 et 4). Cette différence de mécanisme d'action entre les destruxines A et B et l'enniatine A1 explique la différence de sélectivité de ces molécules, une action de type perméabilisation membranaire n'étant pas ou peu sélective comme le montre l'action non sélective de l'enniatine A1 qui est active contre *Clostridium perfringens* mais aussi contre d'autres bactéries Gram+ et contre *Candida albicans* comme illustrée dans le Tableau 6.

[0123] **IV- Exemple 4 : Evaluation de l'activité antibactérienne et de l'innocuité de surnageant (sécrétomes) de champignons producteurs de destruxines**.

[0124] *Matériels et Méthodes :*

[0125] Afin de tester les effets antimicrobiens d'extrait de champignons producteurs de destruxines, la moisissure *Beauveria felina* (DSM 4678) a été utilisée. Les sécrétomes de cette moisissure ont été obtenu après inoculation de milieu de culture dextrosé à la pomme de terre ou Potato Dextrose (PD) par le champignon et culture à 25°C pendant 2 semaines sous agitation (200 rpm). Les sécrétomes obtenus ont été centrifugés à 3000 rpm pendant 5 min puis stérilisés par filtration sur filtre de 0.2 µm. Les sécrétomes stériles ont ensuite été utilisés pour réaliser des tests antimicrobiens comme détaillé dans l'exemple 1 par dilution au 1 / 2 à partir des sécrétomes purs.

[0126] *Résultats :*

[0127] L'activité antimicrobienne des sécrétomes de *Beauveria felina* (DSM 4678) a été évaluée sur certaines souches bactériennes Gram+ et Gram- comme illustrées dans le Tableau 13.

[0128] **Tableau 13 : Détermination de l'activité antimicrobienne du sécrétome obtenu à partir de la moisissure *Beauveria felina* (DSM 4678).**

[0129] L'activité antimicrobienne des sécrétomes de *Beauveria felina* (DSM 4678) a été testée sur divers souches Gram+ et Gram- par dilution en cascade. L'activité est exprimée en pourcentage de sécrétome dilué présentant une activité.

[Tableaux13]

Souches bactériennes	Pourcentage d'extrait le plus faible présentant une activité antimicrobienne contre la souche testée
Clostridium perfringens (ATCC 13124)	6.25 %
Bacillus cereus (DSM 31)	6.25 %
Staphylococcus aureus (ATCC 6538P)	12.5 %
Escherichia coli (ATCC 8739)	>50 %
Klebsiella pneumoniae (DSM 26371)	>50 %
Pseudomonas aeruginosa (CIP 107398)	>50 %
Salmonella enterica (CIP 80.39)	>50 %

[0130] Les données du Tableau 13 montrent que les sécrétomes de *Beauveria felina* (DSM 4678) sont bien actifs contre *Clostridium perfringens* (ATCC 13124) mais également contre d'autres souches Gram+ pathogènes tel que *Bacillus cereus* (DSM 31) et *Staphylococcus aureus* (ATCC 6538P). Ceci suggère que les sécrétomes contiennent d'autres molécules, en plus des destruxines A et B, qui sont actives contre les bactéries Gram+. Même si la perte de sélectivité contre *Clostridium perfringens* est préjudiciable, le fait que les sécrétomes de *Beauveria felina* (DSM 4678) soient actifs contre divers pathogènes Gram+ infectant les animaux et les humains est un point positif. L'utilisation de fractions plus purifiées du sécrétome, enrichies en destruxines, devrait permettre de retrouver la sélectivité contre *Clostridium perfringens*.

[0131] BILAN

[0132] Les résultats ci-dessus démontrent donc une activité ultra sélective des destruxines A et B à l'encontre des bactéries du genre *Clostrium perfringens* responsable d'infections intestinales chez l'Homme et l'animal d'élevage dont le porc et les volailles.

[0133] Du fait de l'absence de toxicité des destruxines A et B aux doses antibactériennes, l'utilisation des destruxines A et B est envisageable dans le traitement des infections humaines par *Clostridium perfringens* mais également dans le traitement de l'infection intestinale par *Clostridium perfringens* des animaux d'élevage, dont le porc et les volailles.

[0134] Le fait que les sécrétomes de *Beauveria felina* (DSM 4678) soient actifs contre *Clostridium perfringens* permet de proposer également d'utiliser des extraits plus ou moins purifiés de ce champignon ou d'autres champignons producteurs de destruxines (tel que *Metarrhizium, Beauveria, Ophiocordyceps, Alternaria* et *Aschersoni* et notamment les genres *Metarrhizium anisopliae, Metarhizium brunneum, Beauveria*

felina, Ophiocordyceps coccidiicola, Alternaria brassicae, Alternaria linicola, Aschersonis sp, Ophiocordyceps coccidiicola, Alternaria brassice et Aschersonis sp) afin de prévenir l'infection des animaux d'élevage (dont le porc et les volailles) par *Clostridium perfringens*.

[0135] .

Revendications

[Revendication 1] Composition comprenant au moins une destruxine pour traiter et/ou prévenir les infections par *Clostridium perfringens*.

[Revendication 2] Composition selon la revendication 1 telle que la destruxine est choisie parmi les destruxines des séries A, B, C, D, E, F ou G de champignon, ou leurs dérivés.

[Revendication 3] Composition selon l'une quelconque des revendications précédentes telle que la destruxine répond à la formule (I) :

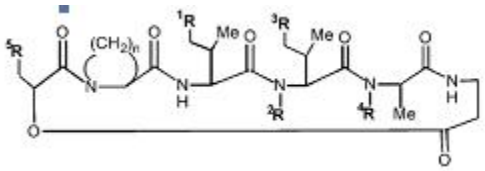

(I)

Dans laquelle

^{1}R représente un atome d'hydrogène, un groupe C1-C6 alkyle ou un groupe aralkyle ;

^{2}R, ^{3}R, ^{4}R identiques ou différents représentent indépendamment un atome d'hydrogène ou un groupe C1-C6 alkyle ;

^{5}R représente un groupe choisi parmi les groupes C2-C6 alkènyle et C1-C6 alkyle éventuellement substitués par un ou plusieurs substituants choisis parmi les atomes d'halogène, les groupes hydroxy (OH), carboxy (COOH), -glycosyle, et les groupes hétérocycliques de 3 à 6 membres comprenant un ou plusieurs hétéroatomes choisis parmi N, O et S.

[Revendication 4] Composition selon l'une quelconque des revendications précédentes telle qu'elle comprend un champignon produisant une destruxine, ou un extrait de celui-ci, tel qu'un broyat ou surnageant de culture de celui-ci.

[Revendication 5] Composition selon la revendication 4 telle que ledit champignon est choisi parmi les genres *Metarrhizium anisopliae, Metarhizium brunneum, Beauveria felina, Ophiocordyceps coccidiicola, Alternaria brassice, Alternaria linicola, Aschersonis sp, Ophiocordyceps coccidiicola, Alternaria brassice et Aschersonis sp*

ou un extrait de ceux-ci, et/ou le surnageant de culture de ceux-ci.

[Revendication 6] Composition selon l'une quelconque des revendications précédentes telle qu'il s'agit d'un complément alimentaire pour les animaux d'élevage dont le porc et les volailles.

[Revendication 7] Composition selon l'une quelconque des revendications 1 à 6 telle qu'il

s'agit d'une composition pharmaceutique humaine ou vétérinaire à visée antibiotique comprenant en outre un ou plusieurs excipients pharmaceutiquement acceptables.

[Revendication 8] Une destruxine ou un champignon produisant une destruxine, ou un extrait de celui-ci, tels que définis selon l'une quelconque des revendications 1) 5 pour son utilisation en thérapeutique humaine ou vétérinaire pour le traitement des infections bactériennes par une infection par la souche *Clostridium perfringens*.

[Revendication 9] La destruxine ou un champignon produisant une destruxine, ou un extrait de celui-ci, pour son utilisation selon la revendication 8 telle que la destruxine est définie selon l'une quelconque des revendications 1 ou 5.

[Revendication 10] La destruxine ou un champignon produisant une destruxine, ou un extrait de celui-ci, pour son utilisation selon l'une quelconque des revendications 8 à 9 telle que l'infection est une infection intestinale telle que l'entérite nécrotique.

[Revendication 11] Utilisation d'une destruxine ou un champignon produisant une destruxine, ou un extrait de celui-ci tels que définis selon l'une quelconque des revendications 1 à 5, à titre d'additif alimentaire pour les animaux d'élevage tels que le porc et les volailles, pour le traitement et/ou la prévention des infections bactériennes par une infection par la souche *Clostridium perfringens*.

Abrégé

Utilisation de peptides cycliques fongiques de type destruxine comme agents anti-bactériens actifs contre *Clostridium perfringens*

La présente invention concerne l'utilisation d'une destruxine ou leurs dérivés pour prévenir ou lutter contre *Clostridium perfringens*, en thérapie humaine ou vétérinaire, ou en nutrition animale.

Figure pour l'abrégé : aucune

[Fig. 1]

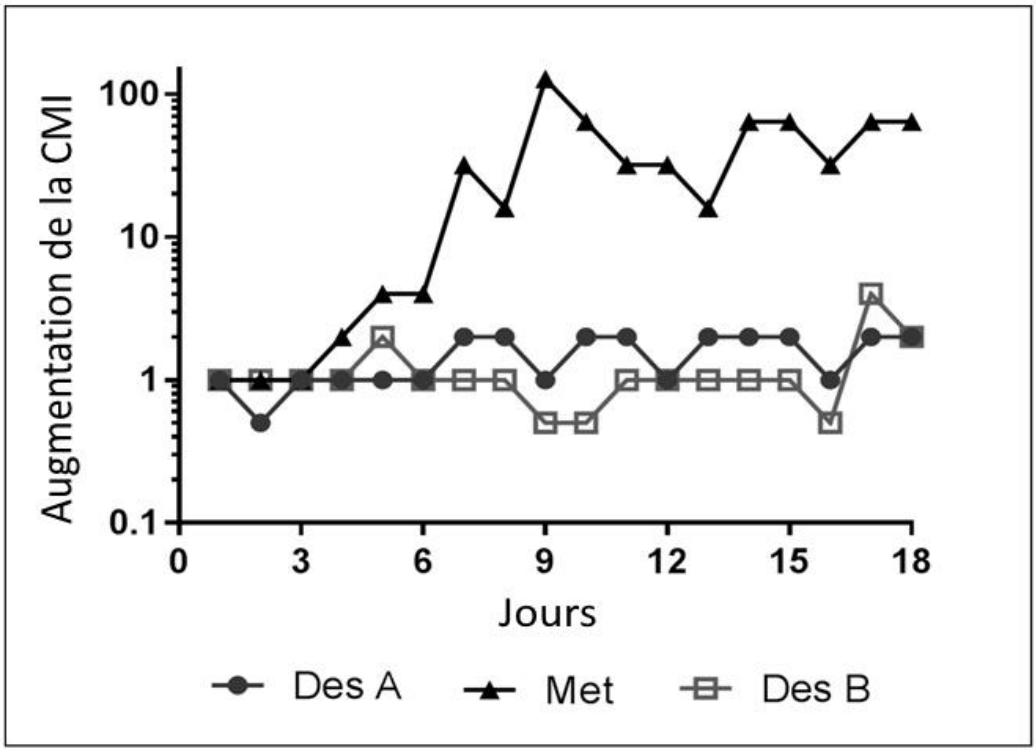
Augmentation de la CMI
100
10
1
0.1
0
3
6
9
12
15
18
Jours
Des A
Met
Des B

[Fig. 2]

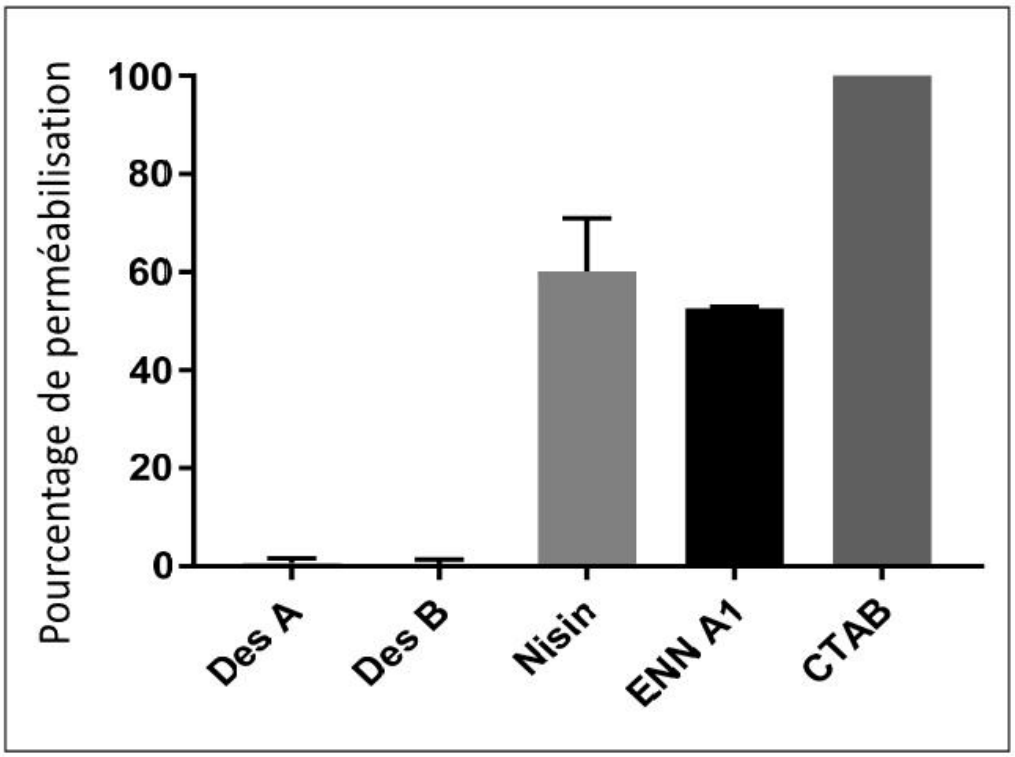
Pourcentage de perméabilisation
100
80
60
40
20
0
Des A
Des B
Nisin
ENN A1
CTAB

[Fig. 3]

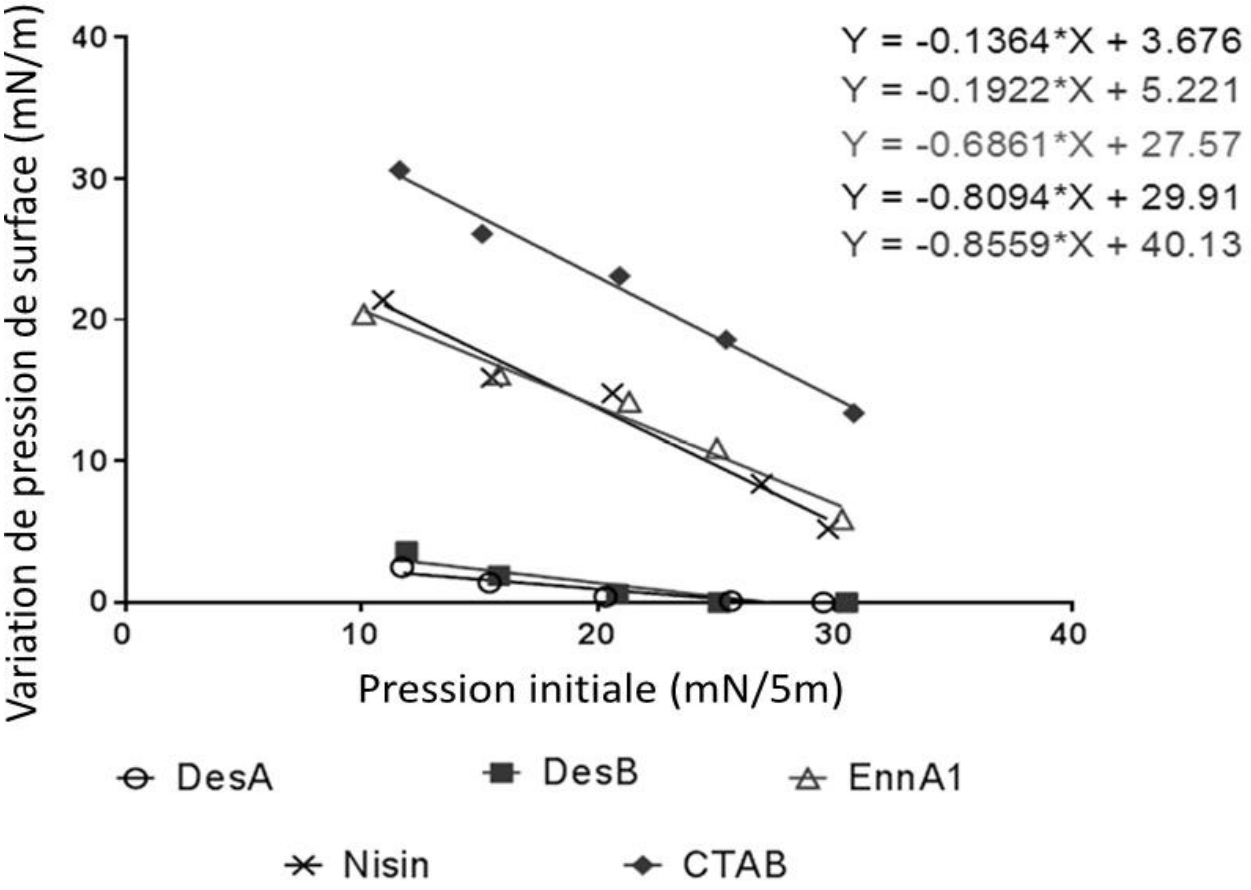
Y = -0.1364*X + 3.676
Y = -0.1922*X + 5.221
Y = -0.6861*X + 27.57
Y = -0.8094*X + 29.91
Y = -0.8559*X + 40.13
Variation de pression de surface (mN/m)
Pression initiale (mN/5m)
0
10
20
30
40
DesA
DesB
EnnA1
Nisin
CTAB

[Fig. 4]

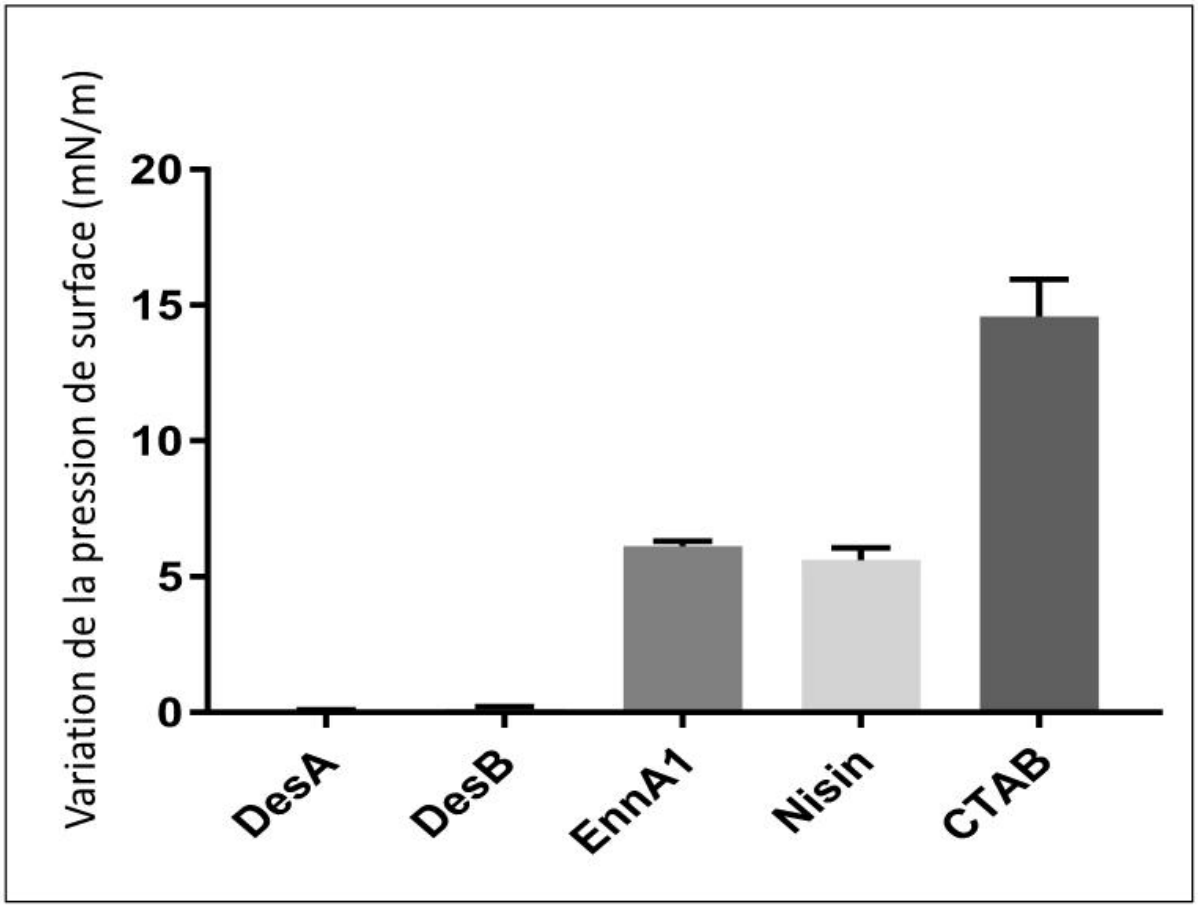
Variation de la pression de surface (mN/m)
20
15
10
5
0
DesA
DesB
EnnA1
Nisin
CTAB

[Fig. 5]

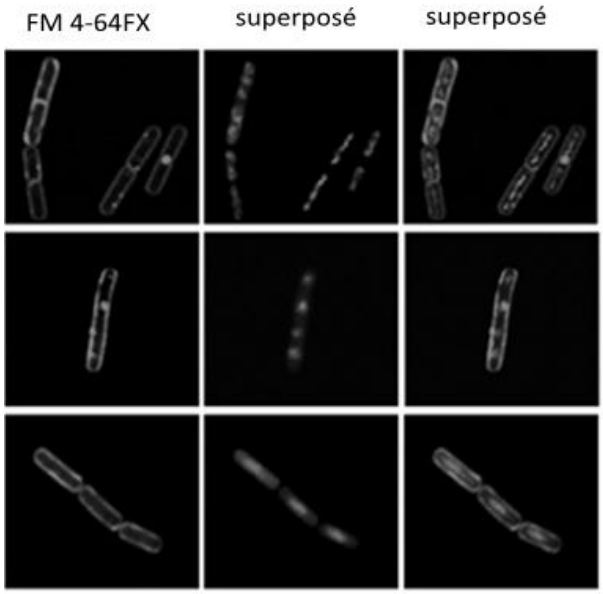

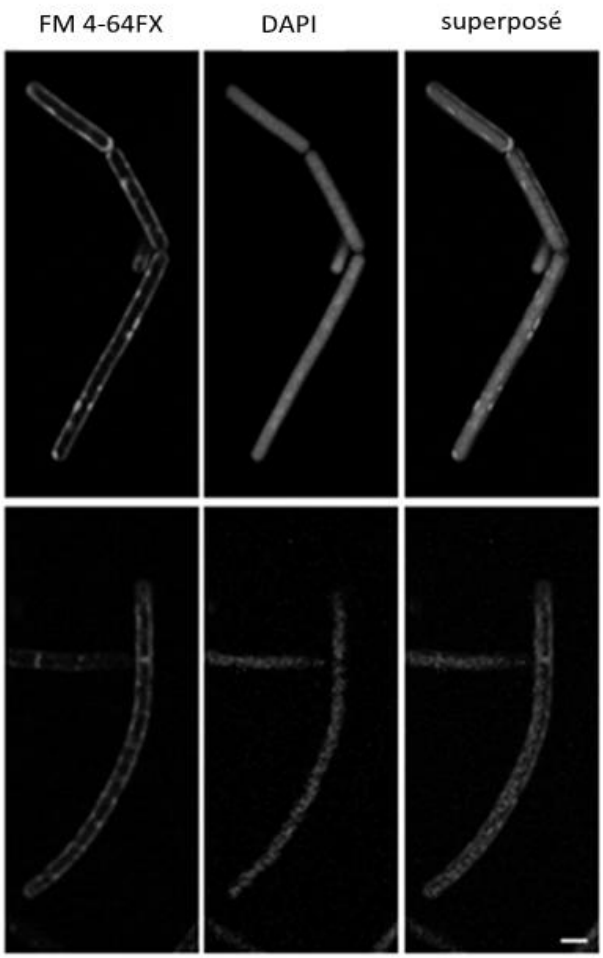

Antibiotique	Synthèse inhibée (cible)
Amoxicilline	Peptidoglycane
Chloramphénicol	Protéines
Gemifloxacine	ADN
Métronidazole	ADN / ARN

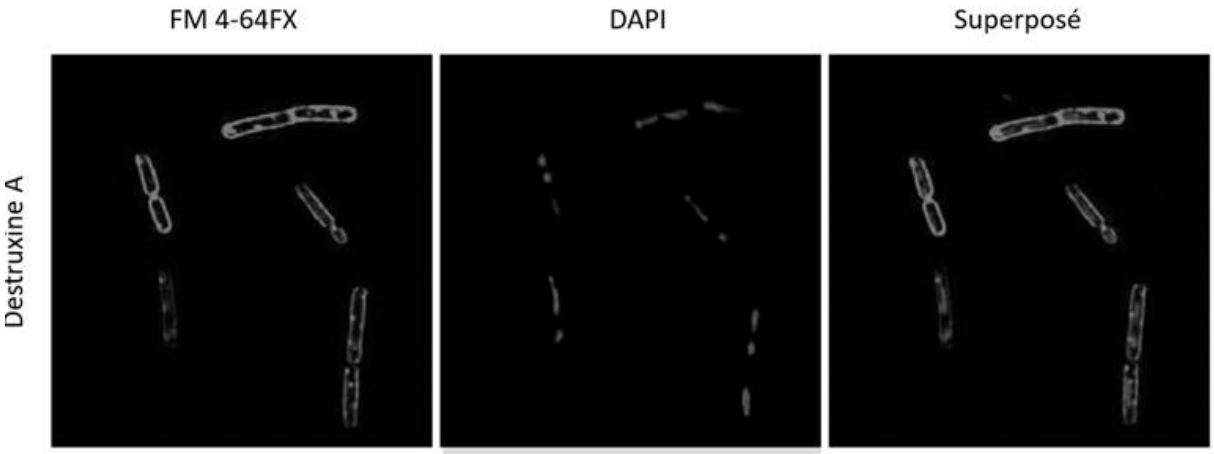

Abstract

The resurgence of microbial infections associated with the increasing emergence of antibiotic resistant strains and the lack of new antibiotics have escalated quickly to become one of the major threats in Public Health nowadays. In that context, new molecules with antibacterial activity are actively searched. Ribosomally synthesized and Post-translationally modified Peptides (RiPPs) are a potential trove of such alternatives to antibiotics. One of the prominent members of the human gut microbiome, *Ruminococcus gnavus*, produces various antibacterial RiPPs designated as Ruminococcins. The focus of my thesis project was the Ruminococcin C (RumC) which is synthesized in the form of several variants by the strain E1, exclusively in the context of symbiosis within an animal host. During this project, a purification protocol to extract the various isoforms of RumC from cecal contents of *R. gnavus* E1 mono-associated rats was developed. On one hand, their mass spectroscopic characterization classified them as sactipeptides as all the isoforms exhibit four thioether bridges linking the sulfur atom of a cysteine to the alpha carbon of an acceptor amino acid residue. Mutagenesis analysis and structural resolution of the RumC1 isoform revealed that it belongs to a new family of sactipeptides with a previously undescribed three-dimensional structure. On the other hand, the biological characterization of RumC1 demonstrated its promising potential as a therapeutic agent. First, RumC1 shows potent activity towards Gram-positive pathogens including multi-drug resistant clinical strains in vitro. Secondly, treatment with RumC1 successfully rescued mice infected with *Clostridium perfringens* from a lethal infection. Finally, RumC1 displays drug-like features such as resistance to proteolytic, physical, and chemical treatments; safety for human tissues; low propensity for resistance selection and higher affinity for bacterial than eukaryotic cells. It is worth noting that the lack of these drug-like features is often limiting the clinical development of RiPPs. Hence, RumC1 appears to be a good candidate for drug development as alternatives to antibiotics. Preliminary results on the mode of action of RumC1 revealed that it inhibits ATP synthesis and - most likely as a consequence - the synthesis of DNA, RNA, proteins and peptidoglycan. Currently, investigations are ongoing to identify the precise molecular target of RumC1 which could support and enhance the development of a therapeutic agent.

Keywords: RiPPs, sactipeptides, bacteriocins, antibiotics, *Ruminococcus gnavus* E1, human gut microbiome.

Résumé

La recrudescence des maladies infectieuses associée à l'émergence croissante de souches résistantes aux antibiotiques et au manque de nouveaux antibiotiques s'est rapidement intensifiée au point de devenir une des menaces majeures de Santé Publique. Dans ce contexte, de nouvelles molécules avec des activités antimicrobiennes sont activement recherchées. Les peptides synthétisés par voie ribosomale et modifiés post-traductionnellement (RiPPs) constituent un vaste réservoir d'alternatives potentielles aux antibiotiques. Un des membres proéminents du microbiote intestinal humain, *Ruminococcus gnavus*, produit divers RiPPs antibactériens nommés Ruminococcines. Mon projet de thèse a porté sur les Ruminococcines C (RumC) qui sont synthétisées sous formes de plusieurs isoformes par la souche E1, et ce uniquement dans un contexte symbiotique avec un hôte animal. Au cours de ce projet, un protocole d'extraction des différentes isoformes de RumC a été établi à partir de contenus caecaux de rats mono-colonisés par *R. gnavus* E1. D'un côté, leur caractérisation par spectrométrie de masse a permis de les classifier comme sactipeptides puisque toutes les isoformes ont montré la présence de quatre ponts thioéther entre l'atome de souffre d'une cystéine et le carbone alpha d'un acide aminé accepteur. Des analyses de mutagénèse et structurale de RumC1 ont de plus révélé une structure tridimensionnelle inédite, attribuant cette isoforme a une nouvelle famille de sactipeptides. D'un autre côté, la caractérisation biologique de RumC1 a démontré son potentiel prometteur en tant qu'agent thérapeutique. En effet, RumC1 possède in vitro une forte activité antibiotique contre des pathogènes à Gram-positif, y compris contre des souches cliniques multi-résistantes. De plus, le traitement avec RumC1 de souris infectées, sur un modèle de péritonite létale à *Clostridium perfringens*, a montré son efficacité d'éradication du pathogène. Enfin, RumC1 présente des caractéristiques propres et indispensables aux développements de médicaments comme la résistance à des traitements protéolytique ou physico-chimique ; une absence de toxicité sur tissus humains ; une faible propension à générer de la résistance ; et une affinité supérieure pour les cellules procaryotes qu'eucaryotes. Il est à noter que l'absence des ces propriétés est souvent une des limitations du développement clinique des RiPPs. Par conséquent, RumC1 semble être un bon candidat pour le développement d'alternatives aux antibiotiques. Des résultats préliminaires sur le mode d'action de RumC1 ont montré qu'elle inhibe la synthèse d'ATP et – probablement par conséquence – d'ADN, d'ARN, de protéines et du peptidoglycane. L'identification de la cible moléculaire précise de RumC1 est en cours, ce qui permettrait de promouvoir et perfectionner le développement d'un agent thérapeutique.

Mots clés : RiPPs, sactipeptides, bactériocines, antibiotiques, *Ruminococcus gnavus* E1, microbiote intestinal humain.